ELECTRICAL PROPERTIES OF OXIDE GLASSES CONTAINING IRON AND MANGANESE

A Thesis Presented

for the Degree

of

Doctor of Philosophy

by

David Robert Thomas Warner

Department of Metallurgy and Materials Science
Imperial College of Science and Technology
The University of London

November 1981

ABSTRACT

Dc and ac conductivity measurements have been made between 293 - 773 K on calcium aluminosilicate glasses containing up to 20%MnO and 10%Fe_2O_3, and the dc conductivity behaviour analysed using the small polaron model. To investigate the effect of glass former on the conductivity, barium borate glasses containing manganese were also prepared. The glasses were characterised by chemical analysis and optical absorption spectroscopy to establish the redox ratio and site coordination of the transition metal ions. Some glasses were also studied using electronic paramagnetic resonance spectroscopy.

When the mean transition metal interionic spacing was <8 Å, the conditions for small polaron hopping were satisfied, although many glasses exhibited a change in slope of the log ρ/T - $1/T$ plot between 400 - 540 K. This has been explained by postulating conduction between ions in similar coordination sites at lower temperatures and different sites at higher temperatures, which introduces a structural differences term ($\sim$0.13eV) into the activation energy. The dc activation energy of the concentrated manganese glasses was >1.0eV compared to <0.7eV for equivalent iron glasses and their resistivities were consequently higher. This reflects the greater polaron binding energy on the d^5 state Mn^{2+} ion compared to the d^6 state Fe^{2+} ion.

Mixed iron-manganese glasses were prepared and analysis showed that Mn^{3+} and Fe^{2+} did not coexist in these glasses. The conductivity was similar in magnitude to that expected for the element present in two oxidation states but the presence of the third transition metal ion caused an interaction which reduced both the resistivity and activation energy. Ionic interactions were also suggested by the spectroscopic measurements.

Both manganese and iron oxides were found to be effective nucleating agents for the crystallization of the silicate glasses. The dc and ac conductivities of the glass-ceramics have been explained in terms of the microstructure and composition of the crystalline and glassy phases.

CONTENTS

TABLES

FIGURES

FIGURES (Contd.)

FIGURES (Contd.)

FIGURES (Contd.)

FIGURES (Contd.)

PLATES

PLATES (Contd)

LIST OF PHYSICAL CONSTANTS

c	velocity of light	3.00×10^{8} m s^{-1}
e	electronic charge	1.60×10^{-19} C
ε_o	permittivity of vacuum	8.85×10^{-12} F m^{-1}
h	Planck's constant	6.62×10^{-34} J s
$\hbar$	$h/2\pi$	1.05×10^{-34} J s
k	Boltzmann's constant	1.38×10^{-23} J K^{-1}
m	electron mass	9.11×10^{-31} kg
N	Avogadro's number	6.02×10^{26} moles/kg mole

INTRODUCTION

In recent years, as part of the general interest in the electrical properties of non-crystalline materials, considerable attention has been focussed on the electronic properties of oxide glasses containing transition metal ions. However, although oxide glasses were the first amorphous materials in which electronic conduction was observed[1], the present understanding of conduction mechanisms in such materials is much less well developed than for other classes of amorphous semiconductors such as amorphous silicon and the chalcogenide glasses which were discovered later. In particular, the knowledge of the electronic band structure of multicomponent oxide glasses is very primitive when compared to that of crystalline and other amorphous materials.

It is now well established that glasses containing transition metal ions in different oxidation states can show electronic conductivity to an extent which depends upon the concentration of the transition metal ions and a number of other factors. The dependence of the conductivity on temperature and other basic glass parameters is usually explained using an equation developed by Mott and this will be the basis of the present study. The Mott equation was developed from a consideration of small polaron hopping in oxide glasses. A small polaron model is appropriate because the electron is considered to interact strongly with the surrounding ions thereby producing a pseudo particle which is called a polaron. In practice, however, several deviations from the predictions of the Mott equation have been observed by various authors and the relevance of these in explaining the results of this study will be discussed.

The investigation reported in this thesis has concentrated on several features of the conduction process in transition metal oxide glasses which have not received much attention by other workers in the field. Most of the previous work has been conducted on phosphate and borate glass forming systems with little study to date of silicate glasses. The present study has been devoted almost entirely to silicate systems although some borate glasses have also been included which has enabled the effect of base glass composition and glass former on the conductivity to be observed.

Among the transition metal oxide glasses, those containing vanadium and iron have received most attention followed by titanium and copper. Less work has been performed on manganese glasses so these

have formed the major part of this study. Manganese glasses are of interest since they are one member of a group of transition metal oxide glasses in which the reduced ion is the major oxidation state and for which very high resistivities have been reported previously. To contrast the behaviour of manganese glasses with those for which the oxidised transition metal ion is predominant, some iron glasses with an identical base glass composition to one used for the manganese glasses have also been studied.

Another feature of this work is that glasses containing small concentrations (<10%) of manganese and iron have been included. Generally transition metal concentrations have been in excess of 20% and the threshold concentration at which electronic conductivity becomes appreciable has often not been observed.

Finally, if two or more different transition metal elements each with multivalent oxidation states co-exist in a glass there is no reason in principle why conduction should not proceed between ions of different elements. This feature has also received relatively little attention and so has been included in this study by preparing mixed manganese-iron glasses.

For each glass electrical measurements, both ac and dc, have been supplemented by a number of chemical and physical techniques to elucidate the conduction process; chemical analysis has been performed to determine the redox ratio of the transition metal element and further information on the site symmetry and coordination of the individual transition metal ions has been gained by both optical and electronic paramagnetic resonance spectroscopy.

Another aspect of the addition of transition metal oxides to silicate glasses is the production of the group of materials known as glass-ceramics by controlled crystallization of the glass. The changes accompanying the growth of crystalline phases might be expected to exert a considerable influence on the electrical properties of the material. For this reason the changes in conductivity following heat treatment of the glasses have also been studied.

The content of the thesis is as follows. The first chapter is concerned with the theory related to the experiments; the phenomenon of glass formation and the crystallization of glasses to form glass-ceramics is discussed first, followed by sections devoted to the theory of optical spectroscopy and electron paramagnetic resonance and their

application to oxide glasses. Finally in that chapter a detailed review of electronic conduction in oxide glasses containing transition metal ions is presented. The second chapter is concerned with the production of the glasses and glass-ceramics and the principal experimental techniques which have been applied to characterise them. The experimental results are given in the third chapter along with some limited discussion to clarify the findings, whilst the main body of discussion is given in chapter four. The conclusions of the study are presented in chapter five.

CHAPTER I

THEORY

1.1 Glass Formation and Crystallization

1.1.1 Glass Formation

Glass formation is a widespread phenomenon, for materials from each of the four main categories of bonding (covalent, ionic, metallic and molecular) can be formed in the amorphous state. However, many materials cannot be prepared in this state by the traditional method of cooling a melt, therefore more novel techniques must be utilised. Some examples of these are listed in Table 1.1.

For some materials, the properties of the amorphous state are similar, irrespective of the method of preparation, but in many cases this is not so. Therefore it has become customary in the literature to distinguish between the terms glassy, non-crystalline, vitreous and amorphous, according to the technique used for preparation. Different authors, however, are not always consistent and the argument is largely one of semantics. A convenient viewpoint is that the words non-crystalline or amorphous should be used interchangeably as generic terms, reserving glassy or vitreous for the special case of materials produced by cooling a melt. Glasses are therefore continuous with the liquid phase and will always have a glass transformation temperature (T_g), whereas this is not necessarily so for all amorphous materials.

The two principal characteristics of the amorphous state are:

(a) the absence of long range order and therefore of definable symmetry, although a high degree of short range order is preserved, and,

(b) an excess of free energy, or chemical potential, frozen into the system compared to the thermodynamically stable phase of the same composition.

Amorphous materials are therefore in a state of metastable equilibrium and will tend to relax to a state of stable equilibrium given a sufficient period of time. For common silicate glasses this relaxation takes of the order of a few minutes at the glass transformation temperature, but many hundreds of years at room temperature.

The question of why only certain materials can be formed in the glassy state has still not been satisfactorily resolved. As inferred above, bond type and crystal symmetry do not give any means of classifying materials as glass formers, though these ideas have been important historically and are included in the discussion of theories of glass formation which follows.

1.1.2 Theories of Glass Formation [2]

These theories fall into one of three general models: structural, thermodynamic and kinetic.

1.1.2.1 Structural Theories

Structural theories explain glass formation as some feature of the material in either the solid state, or both the solid and liquid states. Historically the greatest debate about the structure of glass has been between supporters of the rival crystallite and random network theories, previously considered mutually exclusive. The crystallite view, originated by Lebedeff and propagated by the Russian school, held that glass consisted of very small randomly arranged crystallites. Multicomponent glasses, such as those in the present study, would have different kinds of crystallite corresponding to different compounds in the phase diagram and thus would be heterogeneous. The opposite view, proposed by Zachariasen, postulated a totally homogeneous random network with no structural unit repeated in three dimensions at regular intervals. This was later supported by the X-ray analysis of Warren who showed from the breadth of the main diffraction maximum that the size of any crystallite would be just one unit cell and that these must be held together with material of similar density and composition. The nature of this inter-crystallite material was never adequately explained by the advocates of the crystallite hypothesis.

Thus the random network hypothesis was accepted, along with Zachariasen's four 'rules' to determine potential glass forming oxides. These rules were based on the idea that the interatomic forces in crystals and glasses of the same composition must be similar, but that the disordered glassy structure leads to an internal energy surplus over the corresponding crystal. The smaller this energy difference, the greater the resistance to crystallization. These rules have some success in predicting network formers, network

modifiers and intermediates in oxide glasses, but are not generally applicable. Furthermore the application to oxide glasses is limited to compositions rich in network formers, because for compositions with higher modifier to network ratios than 1:1 the structure is thought to consist of discrete anions e.g. ortho- and pyro-silicates, as in the crystalline silicates.

Other authors e.g. Masson[3], have also proposed that discrete anions are present in the solid glass by considering the structure of the liquid melts, especially silicates and phosphates. The possible anions are found by applying polymerization theory to the self-condensation of monomers e.g. orthosilicate ions in the case of silicates, to calculate ionic distribution and average chain length. These approaches are attractive but cannot be used for compositions rich in network former as expressions cannot be formulated, at present, for network or cyclic structures.

Structural theories of glass formation therefore have a limited application to oxide glasses but their main failing is that they do not give any insights into the relative ease of glass formation. For estimates of this, thermodynamic quantities such as energy and entropy have been suggested to be important.

1.1.2.2 Thermodynamic Theories

Many theories have attempted to relate bond strength to the ease of glass formation.

Sun[4] correlated glass forming tendency and the average dissociation energy of the bonds in the material and suggested rules to determine the possibility of glass formation. This concept was later developed by Rawson[4] who took into account the energy available at the melting temperature to break the bonds.

Stanworth[4] proposed a link between electronegativity values and glass forming tendency, however the correlation can at best be described as poor. Other theories of this type include Dietzel's field strength criterion and Winter's p electron criterion.

With the range of glass formation including all types of interatomic bonding these simple approaches are bound to fail. They have limited success for oxide glasses in predicting the important glass-forming oxides which, to be fair, is all that they attempt to explain. However, materials such as antimony oxide are predicted to

rank in glass forming ability alongside silica, which is clearly incorrect.

Gibbs[2] has developed an entropy approach and proposed that the fall of the configurational entropy of liquids with decreasing temperature results in decreased molecular mobility. At the freezing point, if crystallization occurs, the configurational entropy will fall to zero, but for a supercooled liquid it has been shown to decrease slowly with temperature, leading to a small excess entropy at the glass transformation temperature. This excess entropy concept has been used by Gibbs to predict the value of T_g of some copolymers and also viscosity-temperature relationships near T_g. Again the approach can be criticized in that it cannot predict the relative glass forming tendency of materials.

1.1.2.3 Kinetic Theories

The most satisfactory and widely applicable theories of glass formation are those that treat it as a kinetic phenomenon. To obtain a glass it is necessary to cool the melt to a temperature below the glass transformation temperature without observable crystallization taking place. This requires prevention of both the nucleation and growth processes. The theory of these processes will be considered in some detail below (section 1.1.3) where it will be shown that both nucleation and growth rates pass through a maximum as the temperature is lowered below the melting point. Crystallization can therefore be prevented by quickly cooling through these maxima to a temperature at which the translational motion of the atoms is so restricted that the atomic rearrangements necessary to produce crystals are impossible. Therefore the question is no longer what feature of the material allows a glass to be formed, but rather how quickly must the material be cooled to obtain a glass. Kinetic theories attempt to calculate the minimum cooling rates needed for glass formation i.e. to avoid detectable nucleation and growth.

Dietzel[2] defined 'glassiness' as the reciprocal of the crystal growth rate (U) and tried to relate this to material properties such as viscosity, liquidus temperature and change of composition on crystallization. These parameters were found to be important but no direct relationships could be established.

As an alternative approach, Turnbull[2] has used the nucleation rate (I_v). He argued that for a liquid with low viscosity a single

nucleation event could lead to crystallization, so even this must be avoided. Therefore the cooling rate necessary to avoid nucleation can be used to rank materials in glass forming ability. However, the calculated cooling rates were rather different to experimental values, which was not surprising considering the viscosity at the liquidus temperature was assumed to be quite low (10^{-2} Poise). The approach has some value for metallic systems, where viscosities are low, but viscosities of oxide glasses are relatively high so they can tolerate more than one nucleation event without crystallizing.

One of the most recent and valuable approaches is to consider both nucleation and growth rates and construct time-temperature-transformation (TTT) curves for the production of a barely detectable fraction of crystal. Uhlmann[2] has assumed a volume fraction (V_c/V) of 10^{-6} to be just discernable. The time (t) taken to reach this value is calculated at a range of temperatures from the experimental or computed nucleation and growth rates, using the classical Johnson-Mehl treatment:

$$\frac{V_c}{V} \simeq \frac{\pi}{3} I_v U^3 t^4 \qquad (1.1.1)$$

In the first approximation, any transient time required to establish the steady state nucleation frequency is neglected and uniform homogeneous nucleation is assumed. If the nucleation rate is unknown, which is quite likely, several reasonable values are assumed and the results compared with experiment.

Once the TTT curve has been drawn, the critical cooling rate needed to preclude crystallization is given by the cooling rate which just bypasses the nose of the curve.

Using this model the important factors affecting glass formation were determined as:

(a) a high viscosity at the liquidus temperature,

(b) a viscosity which increases markedly with undercooling;

and for materials with similar viscosity-temperature relationships glass formation is favoured by:

(c) a low liquidus temperature: and in complex systems,

(d) a large redistribution of material being required for crystallization.

Many of these factors had already been identified by other authors

without quantitative calculations.

The model can be further refined by calculating continuous cooling (CT) curves and this has been performed for some complex silicate lunar samples, using both calculated and experimentally determined nucleation rates. The latter showed excellent agreement with classical nucleation theory which is surprising for such a complex material.

Further modifications include the possibility of heterogeneous nucleation and taking account of the size of body obtainable in the glassy state using a given cooling rate. Calculations indicate that only heterogeneities with contact angles of less than 80^0 are effective catalysts at small undercoolings.

The maximum quench rate attainable in the laboratory is currently about 10^{10} K s^{-1}, thus materials with critical cooling rates higher than this cannot at present be prepared in the glassy state. Other methods, such as those listed in Table 1.1, must therefore be used to obtain the non-crystalline state for these materials.

1.1.3 Crystallization of Glasses

The section above has been concerned with the avoidance of crystallization. In this section the factors influencing crystallization will be examined leading to the idea of the controlled crystallization of glasses to form the class of materials known as glass-ceramics.

The process of crystallization consists of two stages. Nuclei must first be formed by a nucleation process and these nuclei must subsequently grow to form crystals.

Two nucleation mechanisms are normally considered: homogeneous and heterogeneous. In the latter case, nuclei may occur in the form of impurity particles, minute fragments of crystals which have not completely melted or dissolved and even the walls of the container may provide a suitable site. With homogeneous nucleation, nuclei are generated within the melt itself and this case will be considered first.

1.1.3.1 Homogeneous Nucleation

In any melt thermal fluctuations will result in clusters of atoms, ions or molecules which will have similar configurations to

that of the crystalline phase. Above the melting point these clusters do not grow because the free energy of the crystalline phase is greater than that of the liquid. As the liquid is cooled below the melting point the clusters increase in stability; the free energy of the system is lowered by crystallization, but opposing this is an increase in free energy as the result of the crystal-liquid interface which is formed.

The work required to form a spherical embryo of the new phase with radius r is:

$$W = 4\pi r^2 \sigma + (4/3)\pi r^3 \quad \Delta G_v \qquad (1.1.2)$$

where σ is the interfacial energy and ΔG_v the free energy change per unit volume for the phase transition.

Using this equation the critical radius (r*) for a stable nucleus is obtained from the condition:

$$\frac{\partial W}{\partial r} = 0$$

which gives:

$$r^* = -\frac{2\sigma}{\Delta G_v} \qquad (1.1.3)$$

Clusters up to r* in size are referred to as subcritical embryos and those with sizes equal to or greater than r* are called critical or supercritical nuclei respectively. Critical nuclei will grow spontaneously because the increase in size is accompanied by a decrease in free energy.

The corresponding value of W is equal to ΔG^*, the free energy of formation of a critical nucleus where:

$$\Delta G^* = \frac{16\pi \sigma^3}{3 (\Delta G_v)^2} \qquad (1.1.4)$$

Assuming the number of embryos is much smaller than the total number of molecules and a Boltzmann distribution is obeyed, the nucleation rate (I) is given by:

$$I = A \exp (- \Delta G^* / kT) \qquad (1.1.5)$$

This describes the thermodynamic barrier to nucleation.

The rate of formation of critical nuclei depends upon the growth rate of the embryos, as the nucleus is too large to result from a single fluctuation within the melt. The embryos are assumed to grow by unimolecular steps and eventually, if the growth rate is not too

high, a steady state equilibrium of critical nuclei is established. This creates a kinetic barrier to nucleation, represented by A above, accounting for the rate at which the structure of the material is changed from the liquid to the crystalline state by diffusion across the interface. The value of A is given by:

$$A = n\nu \exp(-\Delta G_D / kT) \qquad (1.1.6)$$

where $\nu = kT/h$ is the molecular jump frequency, ΔG_D is the activation energy for transport across the interface and n the number of molecules/cm^3.

The total expression for a one component system is therefore given by the Turnbull-Fisher equation[5]:

$$I = \frac{nkT}{h} \exp(-\Delta G_D / kT) \exp(-\Delta G^* / kT) \qquad (1.1.7)$$

The temperature dependence of the nucleation rate is of great importance.

At low temperatures, the kinetic barrier to nucleation increases as the diffusivities of the components decrease. At higher temperatures ΔG^* rapidly approaches zero as the undercooling is decreased. This can be illustrated for a nucleus with the same composition as that of the melt by substituting:

$$\Delta G_v = (\Delta H_v / T_m).\ \Delta T$$

into the equation for ΔG^* giving:

$$\Delta G^* = \frac{16\pi\ \sigma^3 T_m^2}{3\ (\Delta H_v)^2 (\Delta T)^2} \qquad (1.1.8)$$

where T_m is the melting temperature and ΔH_v the change in enthalpy per unit volume.

Therefore:

$$\Delta G^* \propto 1 / \Delta T^2 \qquad (1.1.8a)$$

The dependence of the nucleation rate on the undercooling ΔT is shown in Figure 1.1.

For multicomponent systems equation 1.1.7 must be modified by the following:

(a) the mole fraction of the nucleating component must be included;

(b) the free energy change on crystallization, ΔG_v, will depend on the composition of the nucleating component:

Suppose N_2 moles of a crystalline phase with composition z nucleate leaving N_1 moles of liquid phase with composition y, then the change in free energy, neglecting any surface energy changes, is:

$$\Delta G_v = N_1 G_y + N_2 G_z - (N_1+N_2)\, G_x \qquad (1.1.9)$$

assuming $N_2 << N_1$ and x is the composition of the original liquid. Therefore:

$$\Delta G_v = N_1 (G_y - G_x) + N_2 (G_z - G_x) \qquad (1.1.10)$$

This may be calculated from a free energy diagram of the system.

(c) The dependence of the interfacial energy on the chemical composition gradient must be included, and,

(d) The kinetic term must account for long range diffusion of the nucleating component to replenish the surrounding liquid.

In practice, homogeneous nucleation is observed in relatively few systems so additions of a nucleating agent are often made. Without homogeneously formed nuclei, nucleation often takes place on heterogeneities within the melt.

1.1.3.2 Heterogeneous Nucleation

In the case of heterogeneous nucleation the thermodynamic barrier is lowered by a factor which depends on the degree of wetting of the nucleation substrate. The activation energy therefore becomes:

$$\Delta G^*(\text{het}) = \Delta G^*(\text{hom}) \times f(\theta) \qquad (1.1.11)$$

where:

$$f(\theta) = (2+\cos\theta)(1-\cos\theta)^2 / 4$$

θ is the contact angle and $\cos\theta = (\sigma_{\alpha s} - \sigma_{\beta s})/\sigma_{\alpha\beta}$ (see Figure 1.2)

A low contact angle, i.e. good wetting of the substrate, is therefore desirable.

The complete expression for the rate of heterogeneous nucleation (I_s) must also take into account the effective area of the substrate with suitable sites for nucleation. Therefore:

$$I_s = K_s \exp\{-(\Delta G_D + \Delta G^*_{(\text{het})}) / kT\} \qquad (1.1.12)$$

The factor K_s may be difficult to calculate in practical situations.

An alternative approach relates the potency of the nucleus to the

degree of similarity between its crystal structure and that of the phase being nucleated. This is basically the phenomenon of epitaxial growth, in which crystals form on the surface of a foreign crystal with a definite orientation. Generally the criterion for this to occur is that the disregistry between similar low index planes of the nucleus and the precipitating crystal should not exceed a figure of between 10-20%. For effective nucleation the degree of disregistry should be less than 15%; with increasing mismatch of the crystal lattices greater degrees of supercooling will be required before nucleation can take place.

1.1.3.3 Deviations from Classical Nucleation Theory

The description so far has briefly outlined classical nucleation theory which is based upon a number of assumptions. In practice modifications to the theory must be considered.

In the classical theory, embryos are treated as bulk material and the free energy of crystallization does not depend upon the size of the embryo. Also the embryo-glass interface is assumed to be sharp, with a well defined interfacial energy.

In real systems, the first phase to crystallise may not be the one expected from thermodynamic considerations, so the free energy change on forming a nucleus may be difficult to estimate. It may also depend on the radius of the embryo. For silicate glasses the molecular species involved in nucleation is often not known and the concept of an interface between a small cluster of molecules and the network, ring or chain structure of the glass breaks down. Thus the interface is not necessarily sharp and as the radius of the cluster becomes of the same order as the range of intermolecular forces, the interfacial tension will become a function of size.

Even if the problems of the physical interpretation of the nucleation phenomenon are ignored, the mathematical theory developed above assumes that the embryos obey the Boltzmann distribution, which is not quite true, and no account has been taken of transient times (τ) required to establish the steady state nucleation frequency. The effect of a transient on the time dependence of the nucleation frequency can be expressed by:

$$I_t = I \exp(t/\tau) \qquad (1.1.13)$$

where I_t is the nucleation frequency at time t. The variation of the number of nuclei per unit volume with time is shown in Figure 1.3.

A final consideration is that the nucleation process may be modified by liquid/liquid phase separation which will be discussed in the section below.

In conclusion, therefore, the classical theory must be modified to describe nucleation in practical systems, although a complete description is hampered by a lack of experimental data. However, as this work is not explicitly concerned with the kinetics of nucleation, these problems will not be discussed in any further detail.

1.1.3.4 Liquid-Liquid Phase Separation[6]

Separation of the liquid into two liquid phases often precedes the nucleation of a crystalline phase. Crystallization is then favoured either because the interface can act as a preferential site for nucleation or one of the separated phases can nucleate homogeneously because the molecular groups have a higher mobility than in the parent liquid.

Phase separation can take place by one of two distinct mechanisms: nucleation and growth or spinodal decomposition.

Two regions can be distinguished in the free energy diagram shown in Figure 1.4b. In region N, small variations in composition lead to an increase in the free energy of the system since $\delta^2G/\delta c^2$ is positive. The melt is stable against these. In region S, however, this is not so since $\delta^2G/\delta c^2$ is negative and the system is unstable with respect to small compositional fluctuations as its free energy is decreased. For phase separation of compositions in region N, critical nuclei must be formed by overcoming a thermodynamic barrier and these must subsequently grow. The overall nucleation is large in degree but small in extent and obeys the classical nucleation equations derived above.

In region S, however, there is no thermodynamic barrier and a large number of small compositional fluctuations are formed spontaneously which subsequently grow in degree, i.e. the gradient of the variation increases with time and the distinction between the phases becomes clearer. This is termed spinodal decomposition as it occurs within the spinodal curve (Figure 1.4a).

The early stage of spinodal decomposition therefore gives a highly interconnected two-phase morphology, whilst nucleation and growth would be expected to yield discrete second phase particles within a continuous matrix. It was thought originally that the morphology, as observed by electron microscopy, gave an indication of the mechanism of separation, however, this is not the case. Discrete particles grown by a nucleation and growth mechanism in contact with each other can coalesce by viscous sintering yielding an interconnected morphology. Similarly, an interconnected structure can reduce its free energy by a coarsening process either retaining connectivity, or by necking off and spherodising thus giving discrete particles.

1.1.3.5 Crystal Growth

Once a steady state equilibrium of nuclei has been established, the subsequent crystallization is dependent upon the crystal growth rate. This is controlled by the rate at which species arrive at the interface and attach themselves to the crystal. Three possible rate determining steps can be identified:

(a) Long range diffusion of the crystallizing species to the interface. This gives a time dependent growth rate. Short range diffusion around the interface will only affect the crystal morphology. In practice, long range diffusion is rarely the rate controlling step.

(b) As new crystal is generated, latent heat is evolved. If this is not removed by conduction, the resulting temperature gradient will affect the morphology of the crystal phase. If the undercooling of the melt is less than that required for the maximum growth rate, the temperature increase at the interface will reduce the local undercooling, and hence the growth rate, until the rate of production of latent heat is equal to the rate of heat removal.

(c) Finally, the interfacial reaction may be rate controlling. This is the most common situation and gives a time dependent crystal growth rate as does (b) above.

The classical mathematical analysis of crystal growth sets up expressions for both the rate of attachment of species from the liquid to the crystal and also the reverse process. Three possible mechanisms of surface attachment are usually identified:

(a) Normal or continuous growth. This is expected for interfaces

which are rough on the atomic scale where species can attach onto any site.

(b) Surface growth, usually found for smooth surfaces, and,

(c) Growth onto screw dislocations intersecting the surface.

Considering Figure 1.5 and a normal growth mechanism, the number of species transferring from the liquid to the crystal per unit time is given by:

$$x_{lc} = s\nu_0 \exp\ (-\Delta G_D' / kT) \qquad (1.1.14)$$

where s is the number of molecules in the liquid facing the crystal across the interface and ν_0 is the jump attempt frequency.

Similarly for species detachment:

$$x_{cl} = s\nu_0 \exp\ \{-(\Delta G_D' + v\Delta G_v)/ kT\} \qquad (1.1.14a)$$

Therefore the net transfer from liquid to crystal is given by:

$$x_{lc} - x_{cl} = s\nu_o \exp\ (-\Delta G_D' / kT)\ \{1 - \exp\ (-v\Delta G_v/kT)\} \qquad (1.1.15)$$

where ΔG_v is the change in free energy per unit volume and v is the volume per molecule.

This results in a growth rate (U) of:

$$U = \lambda\nu_o \exp\ (-\Delta G_D' / kT)\ \{1 - \exp\ (-v\Delta G_v/ kT)\} \qquad (1.1.16)$$

where λ is the jump distance.

In general the value of $\Delta G_D'$ is unknown thus an approximation must be made. Hillig and Turnbull[7] defined an effective diffusion coefficient (D) for transport across the interface:

$$D = D_o \exp\ (-\Delta G_D' / kT) = \nu_o\lambda^2 \exp\ (-\Delta G_D' / kT) \qquad (1.1.17)$$

The Hillig-Turnbull equation for the growth rate is therefore:

$$U = (D/\lambda)\ \{1 - \exp\ (-v\Delta G_v / kT)\} \cdot f \qquad (1.1.18)$$

where f is the active site fraction which is introduced to account for the fact that not all sites are available for growth i.e. the normal growth model does not always apply.

According to Wagstaff[8] a further approximation can be made to estimate ΔG_v:

$$\Delta G_v \simeq \Delta T \cdot \Delta S_v = \Delta T\ \Delta H_v / T_m \qquad (1.1.19)$$

where $\Delta T = T_L - T$ and ΔH_v is the latent heat of crystallization per unit volume.

To calculate a value for D, it is often assumed for simplicity that the activation process for diffusion across the interface is similar to that for viscous flow, so the Stokes-Einstein equation can be used. This assumption is only likely to be valid for simple systems. Therefore:

$$D = \frac{k\,T}{3\pi\lambda\eta} \qquad (1.1.20)$$

where η is the viscosity.

Having made these approximations, two limiting cases are usually considered:

(a) At small undercoolings $v\Delta G_v << kT$, therefore:

$$\frac{v\Delta T\ \Delta H_v}{T_L} << kT \text{ and writing: } v\Delta G_v = \frac{\Delta G_m}{N} = \frac{\Delta H_m\ \Delta T}{T_L N}$$

where the subscript m refers to molar quantities, gives:

$$U = \frac{\Delta H_m\ f\ k}{3\pi\lambda^2 kNT_L} \cdot \frac{1}{\eta} \cdot \Delta T = \frac{\text{constant}}{\eta}\ \Delta T \qquad (1.1.21)$$

Therefore the growth rate is proportional to the degree of undercooling.

(b) Similarly for large undercoolings:

$$v\Delta G_v >> kT \quad \text{and,}$$

$$\ln U \propto 1/T \qquad (1.1.22)$$

A schematic plot of growth rate against temperature is shown in Figure 1.6.

For more complex systems, growth occurs by lateral mechanisms i.e. surface nucleation or screw dislocation. In the former case a two dimensional nucleus forms at any site on the surface of the crystal. It is then more favourable energetically on smooth surfaces for the next atomic or molecular species to bond to this nucleus and this process is continued. Each layer is nucleated separately and then grows over the whole surface.

Such a mechanism is not observed in silicate or other crystals where screw dislocations are present. The intersection of a screw dislocation with the surface causes a unimolecular step at which new species can join. As screw dislocations are shaped in a continuous

Archimedian spiral this process can continue to generate new crystal material through a self-perpetuating source of steps.

The mechanism of growth operating can be determined by calculating the reduced growth rate (U_R) and investigating its dependence on the undercooling ΔT:

$$U_R = \frac{U\ \eta}{\{1-\exp(-\frac{\Delta H_m \Delta T}{kNT_L T})\}} = \frac{kT}{3\pi\lambda^2}\ .\ f \qquad (1.1.23)$$

U_R is primarily a measure of the fraction of sites on the crystal surface for molecular attachment and can be used to calculate f.

It can be shown[9] that for:

(a) Normal growth; a plot of U_R against ΔT is a line with zero slope. Silica and germania provide good examples.

(b) Surface nucleation; a plot of log U_R against ΔT is a straight line e.g. $CaMgSi_2O_6$ pyroxenoid.

(c) Screw dislocation; a plot of U_R against ΔT is a straight line e.g. sodium trisilicate.

Finally, consideration is given to two common growth morphologies found in crystallized glasses: spherulitic and dendritic, as these have both been observed in the present study.

Spherulitic and dendritic forms of growth are competitive and the one observed depends upon the degree of undercooling. Both form when the composition of the growing crystal phase differs from the overall composition of the melt thus necessitating diffusion of the crystallizing component to the interface. The tip of a growing fibrous crystal has the greatest accessible volume from which components can be drawn, therefore fibrous growth is favoured. Keith and Padden[10] have shown that the width of this accessible volume is given by D/U, therefore by considering the change of U with temperature it is easily shown that D/U decreases with decreasing crystallization temperature and the separation between fibres also decreases.

At high undercoolings, spherulitic growth is favoured. Perturbations on the surface of a fast growing fibrous crystal will branch from the main crystal at a low angle, the value of which depends on the interference of the diffusion fields of adjacent branches. Eventually the growth becomes radial and the characteristic spherulitic

morphology is formed.

At smaller undercoolings dendrite formation takes place and in this case the branching occurs at favoured angles to the original fibre. The main branches in turn may have sub-branches, often realigned to the original fibre thus producing parallel growth. The growth rate is highly anisotropic as the sides of the fibres are more depleted of crystallizing component than the tip.

The discussion above has not included the effect of latent heat of crystallization on crystal morphology because normally the growth rate in glass-ceramic systems is very small, so there is no significant temperature rise at the interface.

1.1.4 Glass-Ceramics

Normally uncontrolled crystallization, or devitrification, of a glass is undesirable because the product is invariably weak as a result of the coarse microstructure. Frequently only crystal growth inwards from the surface is obtained. However, additions can be made to the glass to facilitate the production of a large number of internal nuclei. These can then grow to produce a fine-grained glass-ceramic material which has improved physical properties compared to the parent glass. These additions, known as nucleating agents, include metals, fluorides, sulphides and oxides.

The theories of the nucleation and growth rates have shown that both go through a maximum as the temperature is decreased below the liquidus. In general these maxima are separated by a few hundred degrees so the heat treatment process to produce a glass-ceramic is usually in two stages. A typical schedule is shown in Figure 1.7.

The nucleation temperature selected is usually one at which the rate is highest and this can be determined by experiment. Similarly a high growth rate is preferred although other constraints must be considered including:

(a) the temperature must not be so high that the glass becomes fluid and slumps under its own weight and,

(b) if the crystal growth rate is too high cracking can occur. This is because the crystals set up stresses as the result of the difference in density between the phases, which the remaining glass cannot relax.

Finally, the heating and cooling rates indicated on Figure 1.7 are chosen to avoid cracking of the sample.

1.1.4.1 Nucleation Mechanisms Excluding Transition Metal Oxides

As mentioned above, certain metals, fluorides, sulphides and oxides will effect nucleation when added to a glass.

Typically metals act by forming a uniform dispersion of particles, with colloidal dimensions, throughout the volume of the glass. The metals which can be used are those which have a simple compound (oxide or chloride) that will readily dissociate in the glass either with the application of heat or by using a reducing agent. The metal atoms then aggregate to form particles which can act as heterogeneous sites for nucleation of the principal crystalline phases. Typical examples include: copper, silver, gold and the platinum group metals, e.g.

(a) $2Cu^{+} + Sn^{2+} \rightarrow Sn^{4+} + 2Cu^{0}$

Copper is added as Cu_2O with SnO as the reducing agent. The glass is quenched and then reheated whereupon:

$$Cu^{0} \rightarrow Cu \text{ (crystals)}$$

This mechanism is the basis of 'striking' copper ruby glasses.

(b) Platinum is added as the chloride which dissociates on melting and the atoms form colloidal particles on cooling.

The mechanism of sulphide nucleation by, for example, CdS or CdS + CdSe is similar. The sulphides dissolve in the molten glass but on reheating to the upper annealing temperature after quenching, striking occurs.

The mechanism of fluoride nucleating agents is not so clear. Fluorides are sparingly soluble in oxide glasses at the melting temperature and will precipitate on cooling. This is the mechanism used to produce fluoride opal glasses. These precipitates may also be used to nucleate glass-ceramics. On the other hand, Rogers[11] has reported the existence of liquid in liquid phase separation in specimens of Na_2O-CaO-Al_2O_3-SiO_2-NaF glass after a nucleation only heat treatment. However, the scale of the subsequent spherulitic growth was two or more orders of magnitude greater than that of the phase separation, indicating that the relationship between nucleation and phase separation was complex.

Of all the possible nucleating agents, oxides, particularly titania and phosphorus pentoxide, have the greatest practical use in commercial glass-ceramic compositions. The mechanism for TiO_2

will be discussed in the section devoted to transition metal (TM) oxides which follows. P_2O_5 is known to encourage phase separation in some systems but in practice either metallic phosphate precipitates or surface energy effects are probably responsible for increasing the nucleation rate.

1.1.4.2 Crystallization of Glasses Containing TM Oxides

The way in which TiO_2 encourages nucleation is not well understood and may depend on the composition of the system involved. Three possible mechanisms have been proposed.

Originally it was thought[12] that rutile precipitated on cooling, however this is unlikely as TiO_2 is not predicted to be a stable phase by the equilibrium phase diagram. Maurer[13] has proposed that titanates could be formed in $MgO-Al_2O_3-SiO_2-TiO_2$ compositions by phase separation of the glass and crystallization of a TiO_2 rich phase. However, Barry[14] did not find any evidence of phase separation in $Li_2O-Al_2O_3-SiO_2$ compositions. Lithium titanate was detected but it was thought that it had crystallized with the major phases and played no part in their nucleation. Barry suggested that TiO_2 lowered the surface energy between liquid and crystalline phases, thus lowering the activation energy barrier to nucleation, since $W^* \propto \sigma^3$. The mechanism involved redistribution of non-bridging oxygen ions by Ti^{4+} ions to the periphery of completely bridged network regions to form the nuclei.

One of the greatest impetuses of the work to enhance crystallization in glasses using TM oxides, has been the desire to convert waste materials, such as blast-furnace slags and oil shales, to useful glass-ceramic products. This has been pioneered in the USSR with the production of Slag-sitalls and is also receiving attention in the UK with Slag-ceram. Blast-furnace slags contain significant proportions of iron so the behaviour of iron oxides as nucleating agents is of interest. The effect of chromium and vanadium oxides has also been studied but manganese oxides have received little attention.

Rogers and Williamson[15] investigated the crystallization of glasses with compositions in the $CaO-MgO-Al_2O_3-SiO_2$ system with additions of iron oxide. The valence state of the iron was found to be an important factor since only glasses containing ferric ion showed any tendency to nucleate and grow crystals internally. A plot of the number of crystals per unit volume against the reciprocal of

the temperature gave an estimate of the activation energy for the kinetic barrier to nucleation of between 100 - 120kcal/mole. The authors suggested that this was too large to be accounted for by cationic diffusion and represented a major form of reconstruction during nucleation, of the kind found during viscous flow. Activation energies measured for the latter process for similar glasses had similar values[16].

The nucleating species was thought to be $MgAl_2O_4$[17], with some replacement of Al^{3+} by Fe^{3+}. Both $MgAl_2O_4$ and $MgFe_2O_4$ have a normal spinel structure and the Al^{3+} or Fe^{3+} ions are in six-fold coordination. It was proposed that formation of the spinel was favoured by additions of ferric ion, because ferric ion tends to occupy four-fold sites, therefore upsetting the balance of Al^{3+} between four and six-fold sites towards octahedral coordination. Six-fold coordinated Al^{3+} can then form spinel by interaction with the relatively more mobile Mg^{2+} cations.

Ferrous ion has been found to influence the rate of crystal growth[18]; the growth rate being proportional to the square of the ferrous ion concentration. Electron probe microanalysis showed an increase in the iron concentration at the crystal-glass interface due to the rejection of iron from the growing diopside crystals. It was proposed that an increase in ferrous ion lowered the viscosity of the glass in the region of the crystal front, which led to an increase in the growth rate.

Relatively less work has been done on the effect of vanadium additions. McMillan[12] has reported that V_2O_5 behaves similarly to P_2O_5 as a nucleating agent but is rather less effective. Williamson et al[16] found that small additions of V^{5+} increased the rate of crystal growth in a glass of composition $30CaO-2MgO-15Al_2O_3-53SiO_2$ (all in wt%). However the increase reached a maximum between 2 - 4 wt% V^{5+}, depending on the crystallization temperature, and further additions reduced the rate. The formation of vanadate complexes was suspected to account for this. Vanadium as V^{3+} also increased the growth rate but the effect was less than that for equivalent quantities of V^{5+}. The effect of V^{4+} was not investigated. Again the increase in growth rate was probably explained by a decrease in viscosity.

Chromium oxide (Cr_2O_3) is unusual amongst TM oxides in that

only a small proportion (< 1wt%) can be dissolved in aluminosilicate glasses. Keyworth[19] studied glasses with the same composition as above and found that additions of Cr_2O_3 (>0.3%) and MgO (>6.0 wt%) produced internal as well as surface nucleation and growth. The internal growth was in two stages: diopside dendrites were the first to grow, followed by anorthite formed by secondary nucleation on the diopside dendrites. An attempt was made to calculate the nucleation rate for diopside by the Johnson-Mehl-Avrami equation but this was not successful, probably because the composition of the crystallizing phase differed from that of the parent glass. The activation energy for nucleation was similar to that of viscous flow, indicating that the same rate controlling mechanism was involved.

The nucleation rate increased with increasing proportions of Cr^{6+} and electron probe microanalysis indicated that the nuclei were rich in chromium. As both Cr_2O_3 and MgO were necessary for nucleation, chromium spinel ($MgO.Cr_2O_3$) was suggested to be the nucleating phase. The actual effect of the Cr^{6+} ions was uncertain, but its high field strength was thought to have an ordering effect on non-bridging oxygen ions and cause a chromium rich phase to separate. Unlike other TM oxides, chromium oxide decreased the crystal growth rate. The effect was most pronounced for Cr^{3+} but was seen with Cr^{2+} and Cr^{6+} to a lesser extent.The effect is probably explained by an increase in the viscosity of the glass.

Shelestak et al[20,21] have investigated shale glasses with similar compositions to the glasses used in the various studies above. Even though these naturally occurring materials contained small proportions of TiO_2 (in an unspecified amount) and Fe_2O_3 (2wt%), no internal crystallization could be produced by heat treatment. Attempts were therefore made to achieve bulk crystallization by adding one of a number of common nucleating agents: P_2O_5, TiO_2,ZrO_2, CaF_2 and Cr_2O_3. Only additions of Cr_2O_3 were successful at a level of 1wt% and produced nuclei identified as an iron-chrome spinel. The authors expected ionic substitution of Mg^{2+} and Al^{3+} for Fe^{2+} and Cr^{3+} respectively and suggested the general formula: $(Mg,Fe)(Al,Fe,Cr)_2O_4$ i.e. of the same type found by Keyworth in iron free glasses. All these elements were detected within the spinel nuclei using energy dispersive X-ray analysis (EDAX). Again the activation energy for crystal growth was comparable to that for viscous flow.

Microstructural studies indicated that phase separation preceded the formation of a stable crystalline phase, thereby increasing the driving force for nucleation both by providing preferred sites as well as local enrichment of some component.

With regard to crystal growth, the spinel phase nucleated diopside as the major crystalline phase. As the degree of disregistry between diopside and iron-chrome spinel was only less than 15% in one direction, it was proposed that the dendritic structure produced gave rise to the least distortion of the crystal lattice.

Finally, several authors have attempted to relate the effectiveness of TM ions in promoting devitrification to parameters such as cation radius and field strength.

Williamson[18] showed that there was a rough correlation between the ionic potential of an ion (Z/r where Z is the atomic number and r the ionic radius) and its effect on the crystal growth rate, excluding chromium ions. For ions with the same oxidation state, higher ionic potentials exerted less influence on the growth rate. Using Dietzel's values for the cation field strength (Z/r^2), it was shown that the rate of crystal growth decreased as the cation field strength increased, although V^{5+} and V^{3+} did not follow this pattern. Tomozawa[22] has also proposed that the cation field strength parameter should describe nucleation phenomena in silicate systems generally.

MacKenzie and Brown[23] have compared their results with the conclusions of the above authors. They studied the effect of small additions of first row TM oxides on the devitrification temperature and 'heat of reaction' of a Al_2O_3-SiO_2 glass using differential thermal analysis. They could establish no simple relationship between these parameters and cation radius or field strength. The most effective cations in lowering the devitrification temperature were those with an octahedral site preference energy similar to that of Al^{3+}, for these interacted with both tetrahedral and octahedral regions of the structure. However these conclusions may be complicated by the presence of phase separation which occurred by spinodal decomposition assisted by the nucleating agents. This may explain the discrepancy with other workers.

1.2 Optical Absorption Spectroscopy

1.2.1 Introduction

The colouring of glasses by manganese and iron has long been of interest to glass-makers. Iron was usually introduced as an impurity in the sand in the batch, resulting in a yellowish-brown glass. Until comparatively recently, small quantities of manganese dioxide, or glass-makers soap, as it is known in the glass industry, were added to 'clean' or decolourise iron glasses.

The physical mechanisms of colour production have been unravelled in only the past thirty years with the development of ligand field theory. Ligand field theory considers the splitting of the degenerate electron orbitals of a metal ion when surrounded by ligands; electronic transitions between these levels are then responsible for light absorption in the near infra-red through visible to near ultra-violet region of the spectrum.

Ligand field theory is a development of the earlier crystal field theory which considered the ligands as point charges and assumed a purely electrostatic interaction between ligands and the central metal ion. Although it has great success in quantitatively explaining some spectra, the theory breaks down when the metal-ligand bond becomes partly covalent. Ligand field theory accounts for this covalency.

At the other extreme, all of the bonding electrons may be shared in covalent bonds. In this case molecular orbital theory is appropriate but again the ligand field approach can be derived from it, for some ions, as a special case.

Whichever model is applied, light absorption is caused by electronic transitions between ligand and metal ions, so the various possible transitions for the oxide glasses in this study will now be discussed.

1.2.2 Electronic Transitions

Electronic transitions may be classified as follows:

(a) Interionic
- (i) metal to metal e.g. $Fe^{2+} \rightarrow Fe^{3+}$
- (ii) ligand to metal
- (iii) metal to ligand
- (iv) ligand to ligand

(b) Intraionic (i) ligand: redistribution of p electrons
(ii) metal : redistribution of d electrons

Not all of the transitions listed above are allowed according to a quantum mechanical law known as Laporte's rule, which forbids transitions involving only a redistribution of electrons within a single quantum shell. Only transitions with $\Delta l = \pm 1$ are allowed (e.g. d→p, p→d, d→f etc., but not d→d, p→p or s→d), thus the d-d transitions responsible for colour in TM glasses are predicted not to occur. In practice, Laporte's rule is relaxed in one of two ways.

Firstly, for complexes without a centre of symmetry, some mixing of metal d orbitals with metal or ligand p orbitals can occur and transitions then take place between orbitals containing different amounts of 'p character'. The greater the mixing of orbitals, the more the rule is weakened and the greater the absorption becomes.

Secondly, those complexes with a centre of symmetry can have that centre momentarily displaced by thermal vibrations and mixing then takes place as above. For this reason non-centrosymmetric tetrahedral complexes have higher absorption intensities than centrosymmetric octahedral ones. Laporte's rule accounts for the large difference between the molar absorptivities of d-d spectra ($5 - 500$ l cm^{-1} mol^{-1}) and the $10^4 - 10^5$ cm^{-1} absorptivities of allowed transitions.

1.2.3 Interionic Transitions

1.2.3.1 Metal-Metal Charge Transfer Bands

This photon assisted electronic transfer is not to be confused with the phonon assisted transfer responsible for electronic conductivity and dealt with in section 1.4 below. Photon assisted transitions are not described by either ligand field or molecular orbital theories.

It will be shown in section 1.4 that during thermally activated hopping the energy of the electron, bound as a polaron, is raised by an energy equal to $\frac{1}{2}W_p$, where W_p is the polaron binding energy, by interaction with phonons. Simultaneously, the acceptor site is also at an energy of $\frac{1}{2}W_p$ below its previous position and therefore the hopping energy (W_H) is equal to $\frac{1}{2}W_p$. However, if the electron absorbs a photon, the hopping includes a Frank-Condon type process requiring an energy of:

$$h\nu = 2W_p \simeq 4W_H \qquad (1.2.1)$$

to excite the electron out of its polarization well. The energy requirement is greater because there is no 'prepared' acceptor site.

From small polaron theory this absorption should give a Gaussian absorption band centred at about $h\nu = 2W_p$, which in glasses will be broadened by disorder. The oscillator strength (f) of this transition is given approximately by[24]:

$$f \simeq z \left(\frac{m_o R^2}{\hbar^2}\right) \frac{(2J^2)}{h\nu} \qquad (1.2.2)$$

where z is the number of nearest neighbours, J the overlap integral between sites separated by distance R and m_0 is the effective polaron mass.

Therefore taking typical values; for example a crystal such as TiO_2 where R≈5 Å, hν≈1eV and J≈0.1eV gives an oscillator strength of 0.05. This compares with 10^{-4} - 10^{-5} expected for a spin forbidden ligand field band and $<10^{-3}$ for a parity forbidden and spin allowed band.

Various optical transitions observed in crystalline materials containing iron have been ascribed to metal-metal photon assisted electronic transfers. Examples include[24]:

(a) The strongly dichroic absorption band at 0.65eV (5250 cm^{-1}) in partially oxidised vivianite ($Fe_3(PO_4)_2.8H_2O$), presumably due to $Fe^{2+} \rightarrow Fe^{3+}$ electron transfer.

(b) In silicon doped yttrium iron garnet (YIG), Fe^{2+} ions are present in octahedral sites. Although the main absorption at 1.3 eV (10 500 cm^{-1}) is a ligand field transition of Fe^{2+}, it has been suggested that part of this band is a charge transfer process. This implies that $W_H \simeq 0.3$ eV in fair agreement with the hopping energy of 0.2 eV calculated from electrical measurements. The value of f was $\leq 10^{-2}$ but f values tend to be smaller when R is increased because J decreases. This observation also applies in the case of electronically conducting glasses.

Similar transitions in other materials have been described by Koffyberg[25] and Austin and Garbett[26].

Koffyberg[25] has reported measurements on TiO_2-SiO_2 glasses prepared by RF sputtering. Normal optical spectroscopy revealed only

ligand field bands of Ti^{3+} at 1.9 and 3.0 eV (15 325 and 24 200 cm^{-1}). However, a thermomodulated absorption spectrum gave a single band at 1.1 eV which, as W_H was measured as 0.38 eV for the same glass, is in the correct range for optical absorption by polarons. The theoretically calculated shape of the absorption band was in fair agreement with experimental data but the author thought that this was, in part, fortuitous.

Austin and Garbett[26] have reported studies on vanadium phosphate and manganese silicate glasses. For the vanadate glasses they found an absorption band at 1.8 eV, not immediately recognizable as a ligand field band of V^{4+}, which was proportional to the V^{4+} concentration. Since the dc conductivity hopping energy was 0.4 eV, there was reasonable agreement with theory, though the oscillator strength was again lower ($f \approx 4 \times 10^{-4}$) than that for 3d crystals.

The manganese silicate glasses (containing 12% MnO with a redox ratio of Mn^{3+}/total Mn = 25%) showed no unexpected absorptions within the range of 1 - 4 eV. The only band observed was the Mn^{3+} ligand field transition at 2.8 eV with $f \approx 10^{-4}$. This implies that any optical charge transfer either has a very low oscillator strength ($f < 10^{-5}$ and $J \leq 3 \times 10^{-3}$ eV) and is too weak to be observed, or it occurs at a photon energy of greater than 4 eV. The latter is quite possible since the authors reported a hopping activation energy of 1 eV, which is supported for similar glasses by the present study.

From the discussion above it is seen that the major difficulty in observing metal to metal charge transfer bands is that they are often obscured by ligand field or metal-ligand charge transfer bands.

1.2.3.2 Ligand-Metal Transitions

These may be one of two types; metal to ligand, involving oxidation of the metal ion, or ligand to metal. Transitions of the former kind require the ligand to be readily reducible and have low lying vacant orbitals. This is not the case for oxygen ligands therefore these transitions do not occur in oxide glasses; indeed they have not been studied generally in any detail.

The most important example of the second transition in this study is the Fe^{3+}-O charge transfer band, which gives a yellow-brown coloration to iron glasses. This results from the tail of the absorption, the peak of which lies in the near UV, encroaching on

the visible region of the spectrum.

The electronic transitions taking place can only be described with the aid of molecular orbital theory, but as these transitions are of little use in predicting the environment of the metal ion, only an outline of the theory will be given.

1.2.3.3 Molecular Orbital Theory

In the molecular orbital theory a set of molecular orbitals is constructed from the atomic orbitals of the metal ion and ligands. Once the molecular orbitals have been obtained, usually by the linear combination of atomic orbitals (LCAO) approximation, they are filled with the available electrons according to the same rules as for atomic orbitals.

From group theory, atomic orbitals can only overlap to form molecular orbitals if both have the same symmetry. For each pair of atomic orbitals, two new molecular orbitals are formed, one with lower energy and the other with higher energy, called bonding and antibonding orbitals respectively.

For TM ions of the first row only the 3d, 4s and 4p orbitals are considered, along with the ligand outer s and p orbitals. Only one of the ligand's three p orbitals is directed along the internuclear axis with the central metal ion. This and the s orbital can combine with metal orbitals to form σ bonds. These are cylindrically symmetrical about the internuclear axis. The other p orbitals can only form π bonds, which have equal electron density on either side of the plane containing the internuclear axis; π bonds are therefore not strongly bonding or antibonding so often they are considered as non-bonding orbitals. A typical molecular orbital energy level diagram for an octahedral complex is shown in Figure 1.8.

Charge transfer spectra arise from the transfer of an electron from a predominantly ligand orbital to one mainly on the metal ion. These are Laporte allowed (u → g) and are therefore very intense e.g.

$$\pi_{t_{2u}} \rightarrow d_{t_{2g}} \text{ or } d_{e_g}$$

This type of diagram can be used to account for two other transitions:

(a) Transitions between ligand orbitals and,

(b) High energy transitions within the metal ion e.g.

$$d_{t_{2g}} \rightarrow s_{a_{1g}}$$

but these will not be discussed further.

For TM ions the molecular orbitals are filled up to the $d_{t_{2g}}$ or d_{e_g} levels. By taking just these two levels and ignoring the rest of the diagram, the ligand field approach is obtained as a special case.

1.2.4 Intraionic Transitions

Internal d-d transitions are the most important mechanism of optical absorption within the visible spectrum. To describe these absorptions, ligand field theory is used, so the basis of the theory will now be summarized with special reference to the ions of interest in this study: Mn^{2+}, Mn^{3+}, Fe^{2+} and Fe^{3+}.

1.2.5 Ligand Field Theory

1.2.5.1 Ions with a Single d Electron

In a vacuum, the five d orbitals of a TM ion are degenerate. When the ion is removed from vacuum and placed in a medium, the electrical field around the ion is no longer uniform and as the d orbitals are directional in space, this non-uniform field results in the removal of degeneracy. The way in which the orbitals split depends upon the field symmetry. Octahedral and tetrahedral fields are the most common arrangements for TM ions in glass although distortions from these often occur. The details of typical splittings are shown in Figure 1.9.

In a d^1 octahedral complex, the electron resides in a t_{2g} orbital. As this orbital lies at an energy of $2/5\ \Delta_{oct}$ below the arbitrary zero, the electron has gained extra stability, which is known as the ligand field stabilization energy (LFSE). This is the case for all electrons added to the t_{2g} orbitals. Electrons in the e_g orbitals destabilise the system by $3/5\ \Delta_{oct}$. Note that after three electrons have been added to an octahedral complex, the next electron can either enter an e_g orbital according to Hund's rule, or pair with a t_{2g} electron. Which will occur will depend upon the relative values of the electron pairing energy and Δ_{oct}. For glasses, only high spin complexes are of interest.

For a single d electron in an octahedral field a single

absorption band is predicted corresponding to the $t_{2g} \rightarrow e_g$ transition. Although this is observed, for example for Ti^{3+} in glass, an extra feature is often seen, since a shoulder is present on the main band as a result of the Jahn-Teller effect.

This theorem predicts that any non-linear system with a degenerate electronic state will distort along a vibrational coordinate to remove the degeneracy and therefore lower its symmetry. In the example above, the distortion occurs in the excited state configuration e_g^1, so it is known as the dynamic Jahn-Teller splitting. Splitting of the ground state is known as the static Jahn-Teller effect. It would be expected to occur for partially filled t_{2g} orbitals, but the effect is predicted theoretically to be much smaller than for e_g states, because the orbitals lie away from the main axes. Splitting of the t_{2g} orbitals is not normally detected experimentally.

In this study, Mn^{3+}, a d^4 ion with the $t_{2g}^3 \; e_g^1$ ground state is expected to show static Jahn-Teller splitting of the e_g level and Fe^{2+}, a d^6 ion, dynamic Jahn-Teller splitting of the excited state $t_{2g}^3 \; e_g^3$ (ground state $t_{2g}^4 \; e_g^2$)

1.2.5.2 Ions with Several d Electrons

When more than one electron is present in the d shell, electron-electron interactions or couplings, must be taken into account.

For lighter elements, Russell-Saunders (or LS) coupling is assumed, which ignores the coupling of the spin of one electron with the orbital angular momentum of another. For other couplings it is assumed that:

spin - spin > orbital-orbital > spin-orbital (on the same electron)

With this assumption the vast number of permutations of electrons in the d orbitals, leading to different energies because of the various couplings, can be reduced into groups having nearly the same energy within each group. These groups of states are referred to as multiplet terms and are characterised by a particular value of the total orbital angular momentum quantum number (L) and total spin quantum number (S).

To deduce the terms for each d^n configuration is rather laborious so only the results are quoted below. The ground state is shown first in each case:

Configurations	Terms
d^1 d^9	^2D
d^2 d^8	^3F ^3P ^1G ^1D ^1S
d^3 d^7	^4F ^4P ^2H ^2F $^2D(x2)$ ^2P
d^4 d^6	^5D ^3H ^3G $^3F(x2)$ ^3D $^3P(x2)$ ^1I ^1G etc.
d^5	^6S ^4G ^4F ^4D ^4P ^2I ^2H etc.

where L = 0 1 2 3 4 5
S P D F G H

by analogy with atomic orbitals, and the superscript equals the spin multiplicity (2S + 1)

Note that the quantum numbers of states with n electrons are identical to those with 10 - n electrons (≡ n holes) because of the Pauli hole equivalence theorem.

The energies of the terms above the ground state can be expressed with two electron-repulsion parameters known as the Racah parameters, B and C. For d electrons the energy difference between states with different spin multiplicities are linear functions of multiples of both B and C, whilst if the spin multiplicities are equal, C does not enter the equation. In fact, transitions in which there is a change in the number of electron spins are forbidden by a quantum mechanical selection rule but this rule can be relaxed by the spin-orbit coupling ignored in the LS scheme.

Mn^{2+} ions show the weakest absorption of the first row TM complexes. Mn^{2+} is a d^5 ion and, like all d^4, d^5, d^6 and d^7 ions has low and high spin states. In glasses the oxygen ligands are weak-field and therefore the electron pairing energy is greater than Δ and the high spin state is stable. High spin Mn^{2+} has a ^6S ground state and all transitions are both spin and parity forbidden, therefore $\varepsilon \simeq 0.04$.

1.2.5.3 Effect of Ligand Fields

The discussion above has been concerned with free ion states. The effect of a ligand field is similar to the single d electron case and causes splitting of the Russell-Saunders terms as follows. The symbols used are of group theoretical origin: A and B represent orbital singlet states, E a doublet and T a triplet. The subscripts refer to the symmetry properties of the orbitals.

Free ion term	Terms arising in cubic fields
S	A_1
P	T_1
D	$E + T_2$
F	$A_2 + T_1 + T_2$
G	$A_1 + E + T_1 + T_2$

The variation in energy of the various levels with increasing ligand field strength has been calculated by Orgel for weak fields and Tanabe and Sugano for strong fields. An example of an Orgel diagram is shown in Figure 1.10.

Just as tetrahedral and octahedral fields are related for the d^1 system, so the relationship for d^n systems is as follows:

Octahedral d^n and tetrahedral d^{10-n} = reverse of octahedral d^{10-n} and tetrahedral d^n

where 'reverse' means that the order of levels coming from each free ion state is reversed; d^5 is identical for both coordinations.

The transitions observed in optical spectroscopy are those from the ground state to excited states as only the ground state is significantly populated at room temperature.

1.2.6 Literature Review

1.2.6.1 Glasses Containing Manganese

Originally the colouring species in glasses containing manganese was thought to be Mn^{7+}, because of the similarity in colour between manganese glasses and aqueous permanganate solutions. However, magnetic susceptibility measurements[28] have conclusively proved that Mn^{3+} is the oxidised species. Manganese is therefore present in glass as Mn^{2+} or Mn^{3+} or both.

The electronic structure of Mn^{2+} has been discussed above. The absorption bands are very feeble as electron transfer from the ^6S state is both parity and spin forbidden. The absorption spectrum of Mn^{2+} in glass can be studied, but great care must be taken to exclude Mn^{3+} for it will completely mask the Mn^{2+} spectrum. As Mn^{3+} is present in all of the manganese glasses in this study, the absorption of Mn^{2+} will not be discussed further as it is expected to be unobservable.

The absorption of Mn^{3+} in glass has been studied by various authors[29,30], usually in alkali borate base glasses to facilitate the dissolution of the glass for chemical analysis. Paul[29] made a systematic spectral assessment of Mn^{3+} in a series of alkali borate glasses containing each of the alkali metals. It has long been known that the shade of the Mn^{3+} colour depends on the alkali present; potash silicate glasses are bluish-pink and soda silicate glasses reddish-pink. The single absorption envelope obtained by Paul was resolved into the minimum number of Gaussian component bands, usually three: a 'main' peak at $\sim$20 000 cm^{-1}, with 'blue' and 'red' peaks at $\sim$24 000 cm^{-1} and $\sim$16 000 cm^{-1} respectively. The absorption became broad and assymmetric as the alkali content was decreased and this was accompanied by a marked reduction in the molar absorptivity. However, the molar absorptivity of Mn^{3+} in glass is still between 10 - 100 times higher than in a crystal.

From the portion of the main absorption band at $\sim$20 000 cm^{-1}, it was proposed that Mn^{3+} was in six-fold coordination. This absorption corresponds to the $^5E_g \rightarrow {}^5T_{2g}$ transition, which is the only spin-allowed transition expected for a high spin d^4 system. The enhancement of optical absorptivity was explained by an increase in the covalency of the TM-O bonds as the alkali content increased. In low alkali borate glasses the alkali ions are preferentially utilised by the anionic borate groups, which makes the TM-O bonds more ionic, but in high alkali glasses, TM ions form anionic complexes using alkali ions for local charge neutralisation.

The splitting of the bands was proposed to arise from any one, or combination of the following mechanisms:

(a) Two or three different octahedral (or lower than octahedral) species. If the symmetry was lower than octahedral the centre of symmetry would be destroyed thus increasing the intensity of the absorption, as observed.

(b) The Jahn-Teller effect. High spin octahedral Mn^{3+} has a ground state derived from the $t_{2g}^3\ e_g$ configuration and is expected to show a pronounced ground state Jahn-Teller distortion. However, the centre of symmetry is retained so the visible region d-d bands should not be enhanced with this mechanism.

(c) Spin-orbit coupling, though the spin-orbit coupling parameter was too small to account for the observed splitting.

(d) Five coordinated species of uncertain symmetry.

It was not possible to distinguish these mechanisms with the experimental analysis employed.

In the present study the optical absorption of Mn^{3+} has been treated as a single Gaussian band broadened by the Jahn-Teller effect.

1.2.6.2 Glasses Containing Iron

As discussed in the introduction to this section, the coloration of glass by iron has been, and still is, of the greatest importance in glass technology and therefore has received much study.

Iron is usually present in glass in the ionic state; as either ferrous or ferric ions or both, depending on the glass composition and melting conditions. However, other forms of iron such as atoms of metallic iron or colloidal Fe_2O_3 [31], have at different times been postulated for certain compositions, though the latter would only seem likely if the solubility limit has been exceeded.

Considering ferrous iron, both the ligand field stabilization energy and the radius ratio predict octahedral coordination when surrounded by oxygen ligands. The energy diagram for Fe^{2+}, a d^6 ion, in octahedral symmetry, predicts a single spin-allowed transition, $^5T_{2g} \rightarrow {}^5E_g$ together with several weak spin-forbidden transitions. A single band has been observed by a number of workers in both crystals [32] and glasses [33,34,35].

The absorption band of Fe^{2+} in crystal and solution is centered at about 10 400 cm^{-1} and is broad, though McClure [32] has reported two maxima with a separation of $\sim$2000 cm^{-1}. This was considered to be a consequence of Jahn-Teller splitting of the ^5E_g state. In glass the band is also broad, though it is shifted to 9100 cm^{-1} in soda-lime-silicate glass. This corresponds to a reduction in Δ of $\sim$12% compared to $6H_2O$ ligands as is commonly observed for ions in glasses when compared to the aquo ion.

Several authors have proposed that ferrous ion can also exist in tetrahedral coordination [36,37], in which case a single spin-allowed transition $^5E \rightarrow {}^5T_2$ would be expected. As Δ_{tet} is equal to $\sim 4/9\Delta_{oct}$ the band is predicted to occur at $\sim$4000 cm^{-1} (2.5 μm). Bishay [38] has reported the presence of such a band in phosphate glasses.

Edwards et al [39] have also observed two bands for the Fe^{2+} absorption at 10 000 and 5000 cm^{-1} in phosphate glasses. However, they do not agree that this indicates the presence of both tetrahedral

and octahedral Fe^{2+} and point out that Fe^{2+} complexes rarely show a single absorption band. This evidence has been gained from a study of iron bearing minerals where the Fe^{2+} site symmetry has been determined by X-ray crystallography. These minerals often show two bands separated by 2000 - 5000 cm^{-1}. The authors proposed a six-fold coordination that had been distorted from octahedral symmetry to some other symmetry of lower order that may lack an inversion centre.

Considering its commercial importance, the optical spectra of Fe^{3+} in glass is probably the least understood of all TM ions. The visible spectra of iron glasses is complicated by the ferrous ion absorption in the near infra-red and the intense ferric charge transfer band in the ultra-violet which mask the ligand field bands in the visible region. Fe^{3+} being a d^5 ion, has, of course, the same energy level diagram for both octahedral and tetrahedral coordination and even the radius ratio of Fe^{3+} with oxygen ligands cannot predict the coordination unequivocally. The differences in the spectra will be the result of differences in ligand field strength as well as possible differences in the Racah parameters B and C and in the molar absorptivity.

Bamford[34,40] studied both sodium phosphate and sodium silicate glasses containing iron. In the phosphate glasses absorption bands occurred at 415, 505, and 710 nm and octahedral coordination was proposed. In silicate glasses the bands were observed at 380, 425 and 440 nm and these were also ascribed to octahedral coordination, although according to Kurkjian and Sigety[41] this was erroneous.

These authors have also studied Fe^{3+} in phosphate and silicate glasses using optical absorption along with Mössbauer and EPR spectroscopy. Mössbauer measurements indicated that ferric ion preferred tetrahedral coordination in silicate glasses and octahedral coordination in phosphate glasses.

The optical spectra of the phosphate glasses generally showed three bands which were assigned to high spin octahedral Fe^{3+} as follows:

$$
\begin{aligned}
{}^6A_1 &\rightarrow {}^4T_1 && 720 - 760 \text{ nm} \\
&\rightarrow {}^4T_2 && 520 - 545 \text{ nm} \\
&\rightarrow {}^4E \; {}^4A_1 && 410 - 420 \text{ nm}
\end{aligned}
$$

The bands had low absorptivity values which is also consistent

with octahedral coordination.

The spectra of the silicate glasses was complicated by the ferrous ion absorption but the following assignment was possible:

$$^6A_1 \rightarrow {}^4T_1 \qquad 480 \text{ nm}$$
$$\rightarrow {}^4T_2 \qquad 448 \text{ nm}$$
$$\rightarrow {}^4E\ {}^4A_1 \qquad 425 \text{ nm}$$
$$\rightarrow {}^4T_2(D) \qquad 370 \text{ nm}$$

corresponding to tetrahedral ferric ion. The value of Δ_{tet} of 515 cm^{-1} was in reasonable agreement with that calculated from Δ_{oct} (1250 cm^{-1}) for which a value of 555 cm^{-1} was obtained.

A complication was observed for the $40Na_2O$-$60SiO_2$ glasses in which a weak band at ∿650 nm was also detected. It was thought possible that this was due to some octahedral Fe^{3+} in the glass.

Octahedral coordination of Fe^{3+} in phosphate glasses has also been reported by Edwards et al[39], whose results agreed well with those of Kurkjian and Sigety[41] and both octahedral and tetrahedral ferric ion have been identified in soda-lime-silicate glasses by Fenstermacher[42].

1.2.6.3 Glasses Containing Two or More TM Oxides

Compared to the work on single TM oxide glasses, very little work has been done on the optical properties of glasses containing more than one TM oxide.

One such study was carried out by van de Graaf[43], who found that after heat treatment of an alkali borosilicate glass containing iron and titanium ions, the optical absorption increased very strongly. Compared with glasses containing iron or titanium singly there was an additional absorption over the sum of the absorptions that iron and titanium displayed when they occurred separately in the glass. This was explained using a model which involved the formation of small areas rich in iron and titanium ions by phase separation. It was proposed that iron and titanium ions formed associates (e.g. Fe^{2+} (0) Ti^{4+} Fe^{3+} (0) Ti^{3+}) which exhibited strong interaction, resulting in enhanced absorptivity by a charge transfer process. It was not clear, however, if iron and titanium ions interacted in the quenched single phase glass, although the increase in absorption was very much less than in the cast glass. In the cast glass, clustering and associate

formation occurred due to phase separation as in the heat treated glass.

Paul[44] has attempted to explain the deep yellow coloration of glazes containing cerium and titanium oxides in terms of an interaction between the two elements. He investigated a sodium borosilicate glass with cerium and titanium oxides which was found by chemical analysis to contain only Ti^{4+}, Ce^{4+} and Ce^{3+} i.e. no Ti^{3+}. Additions of 1 - 5 wt% TiO_2 did not alter the cerium redox ratio. The differential absorption curve (equivalent to the extra absorption observed with both Ce and Ti present together), gave a broad maximum at around 30 000 cm^{-1}, the height of which increased with increasing TiO_2 concentration. A Ce^{3+}-O-Ti^{4+} associate was thought responsible for this extra absorption, with the ions in true solution as the glass showed no signs of phase separation. The author also suggested the way in which the intensity of such an absorption could be calculated theoretically. The photon absorption results in charge transfer from the low valency ion (electron donor) to the higher valency ion (electron acceptor) and the intensity depends upon the small delocalisation of the electron over the donor and acceptor sites. However, although the intensity can be estimated by calculating the valence delocalisation coefficients from the dipole length operator, which has been achieved for some materials, such an approach cannot be used for glasses at present as dipole length operators are not known.

Veinberg[45] has investigated the influence of titanium on the absorption spectra of various TM ions. The absorption spectra of the TM ions in lower valence states were strongly affected by Ti, though its effect on the higher states was weaker. The characteristic change was a shift in the TM ion UV absorption edge toward longer wavelengths, although bands in the visible or IR region of the spectrum were not greatly affected. Additions of titanium were found to shift the TM redox ratio to produce greater fractions of the lower states but since the additions were small (1-1.5%), no changes in glass structure were likely. Similarly, no evidence of changes in TM coordination were found. It was proposed that since Ti^{4+} is weakly acidic, as evidenced by the formation of titanates, and TM metals in lower redox states are weakly basic, then bonding between them is possible in a similar fashion to the titanates (i.e. TM -O- Ti^{4+}). This shifts the absorption edge of the TM ion. Since the higher TM oxidation states are weakly acidic, no complexes are formed so the

addition of Ti has little effect on the TM ion spectra.

Finally, Bandyopadhyay[46] has investigated the optical spectra of barium borate glasses containing vanadium, iron and copper oxides in mixed proportions. For each combination of two TM oxides, a single absorption band with a strong cut-off at high energy was observed. Comparison of these spectra with those of the single TM oxide glasses revealed that all the expected valence states of the two TM oxides were present. From the behaviour of the UV cut-off absorption edge, which moved to a different energy in the mixed glasses compared to what would be expected from the same concentrations of the individual ions acting independently, it was suggested that a strong interaction existed between the TM ions present. This interaction involved the formation of associates composed of two TM ions, one from each TM element, with one oxygen ligand. However, since the possibility of charge transfer processes involving the individual ions could not be eliminated, more detailed work was proposed.

1.3 Electron Paramagnetic Resonance

1.3.1 Introduction

Electron paramagnetic resonance (EPR) is a spectroscopic technique confined to the study of species containing one or more unpaired electrons i.e. those possessing a nonzero total angular momentum in their electronic systems. Paramagnetism is found in a wide range of species including:

(a) atoms, molecules and free radicals with an odd number of electrons,

(b) a small number of molecules with an even number of electrons which are not all spin-paired e.g. O_2,

(c) metals and semiconductors with conduction electrons,

(d) radiation induced centres in solids and solutions, and,

(e) ions with partially filled inner electron shells.

Group (e) includes, of course, the 3d TM ions, of which Mn^{2+} and Fe^{3+} are particularly amenable to study by EPR. However, the interpretation of EPR spectra is complex so a detailed analysis of the spectra obtained for selected glasses in this study is considered to be outside the scope of this thesis and only qualitative results will be reported. In view of this, only an outline of the theory behind the technique, together with a brief literature review, will be

presented.

In the absence of a magnetic field the free electron spin has no effect on the energy levels of the paramagnetic centre. However, when an external magnetic field is applied, the ground state of the centre is split and transitions by the unpaired electrons between these levels give rise to resonant absorption of electromagnetic radiation in the microwave frequency range. Therefore EPR can give a description of the ground state of TM ions and the effect of ligands on these energy levels.

Two approaches are available to interpret EPR spectra. The first is a fundamental approach concerned with the way that the unpaired electrons of a free ion behave when placed in a solid state environment. This is a complicated procedure so the second method using a 'spin Hamiltonian' is most often used.

1.3.2 The Spin Hamiltonian

The spin Hamiltonian is a quantum mechanical operator which is a function of empirical constants and electron and nuclear spin operators only. It can be used to describe resonance data without prerequisite knowledge of spin-orbit coupling, hyperfine interaction etc.. The operator is so derived that its eigenvalues are the energy levels of the system between which transitions are observed.

Generally only the lowest group of electronic states is involved in EPR which is characterized by an effective spin S'. This is defined by the number of electronic levels in the ground state, which is equal to (2S'+1). In some cases, S' can equal the free ion spin, S. From Kramer's theorem, ions with an odd number of unpaired electrons will always have at least a two-fold degenerate state irrespective of the strength of the ligand field; this gives S'= ½ even though S may be greater than ½. If the centre has an even number of unpaired electrons, strong ligand fields may lift the degeneracy before the external magnetic field is applied, therefore transitions may not be observable in the microwave region.

A general form of spin Hamiltonian for a paramagnetic ion is as follows:

$$\mathcal{H} = \underset{1}{\beta g_{ij} H_i S'_j} + \underset{2}{D_{ij} S'_i S'_j} + \underset{3}{A_{ij} S'_i I_j} + \underset{4}{Q'_{ij} I_i I_j} + \quad (1.3.1)$$

other terms describing direct nuclear spin and magnetic field interactions

where β is the Bohr Magneton (= $e\hbar/2mc$), I_j is the nuclear spin operator, H_i is the static magnetic field operator, S'_j is the electron spin operator and g_{ij}, D_{ij}, A_{ij} and Q'_{ij} are tensor quantities having the symmetry of the local ligand fields.

The four terms in equation 1.3.1 describe the following:

(1) Zeeman splitting of the lowest energy levels by the magnetic field. This will be discussed in greater detail below.

(2) Fine structure arising from zero magnetic field splitting by ligand fields or spin-spin interactions.

(3) Magnetic hyperfine interaction containing the nuclear spin coupling parameter A_{ij}, and,

(4) Nuclear quadrupole interaction.

The spin Hamiltonian therefore describes the way in which the spin is coupled to its surroundings and can be used to test models of local atomic structure.

1.3.3 The Resonance Condition

The magnetic moment of a free electron is associated with both its orbital motion around the nucleus and the spin about its own axis. The resultant magnetic moment $\underline{G}$ in the electronic system of a free atom or ion will give rise to a permanent magnetic dipole moment $\underline{\mu}$ related by:

$$\underline{\mu} = \gamma \underline{G} \tag{1.3.2}$$

where γ, the magnetogyric ratio = $-g(e/2mc)$ and g is the spectroscopic splitting factor, a pure number whose value depends on the relative contribution of orbital and spin motion to the total angular momentum. If the electron spin were absolutely free and had no coupling with any orbital motion, the 'g value' would be 2.0 (actually 2.0023 including the quantum electrodynamical correction).

If orbital and spin momenta are considered separately, then for each case respectively:

$$\begin{aligned} &\underline{G} = \hbar \underline{L}, \quad g = g_L = 1 \text{ and} \\ &\underline{G} = \hbar \underline{S}, \quad g = g_S \end{aligned} \tag{1.3.3}$$

where $\underline{L}$ and $\underline{S}$ are the total orbital and spin quantum numbers.

When both are present, the value of g depends upon orbital-spin coupling. Assuming Russell-Saunders (or L-S) coupling, the resultant

angular momentum is associated with a quantum number J = L+S and g becomes:

$$g_J = \frac{J(J+1)\ (g_L+g_S) + \{L(L+1)-S(S+1)\}\ (g_L-g_S)}{2\ J(J+1)} \quad (1.3.4)$$

The resultant electronic magnetic dipole moment is:

$$\underline{\mu}_J = -(g_J \frac{e}{2mc})\ \hbar\ \underline{J} = -g_j\ \beta\ \underline{J} \quad (1.3.5)$$

The Zeeman interaction between the electronic magnetic dipole and the field in the presence of a magnetic field H is:

$$E = -\underline{\mu}_J \cdot \underline{H} = g_J\ \beta\ H\ M_J \quad (1.3.6)$$

where M_J is the component of the electronic angular momentum $\underline{J}$ in the field direction.

When an alternating field of frequency ν is applied at right angles to $\underline{H}$, magnetic dipole transitions are induced according to the selection rule $\Delta M = \pm 1$ and a quantum of energy:

$$h\nu = g_J\ \beta\ H \quad (1.3.7)$$

will be absorbed thus flipping the spin of the electron from a parallel to an anti-parallel direction to the magnetic field. Induced emission is observed for the reverse process but as it is energetically more favourable for a system in thermal equilibrium to have more spins in a parallel direction, there will be a net absorption of power. Equation 1.3.6 may be compared with equation 1.3.1 for a free ion.

The transition between $M_S = -\frac{1}{2}$ and $M_S = +\frac{1}{2}$ is illustrated in Figure 1.11 for a field of value $\underline{H}'$ induced by radiation of frequency ν_1. Note that for zero field strength the energy of the system is equal to the free field value E_o and the spin levels ($M_S = \pm\frac{1}{2}$) are degenerate. The splitting of the M energy levels increases with increasing $\underline{H}$ according to:

$$E'_H - E''_H = \Delta E_H = h\nu = g\ \beta\ H \quad (1.3.8)$$

In general the electron is not free, thus g varies from g_e. Experimentally the g factor is calculated from $h\nu = g\beta H$, where H and ν are known, using the equation:

$$g = 21.418/ \lambda H \qquad (1.3.9)$$

where λ is the radiation wavelength in cm and H the magnetic field strength in kGauss.

For the 3d TM ions the paramagnetic 3d electrons are the outermost electrons and are exposed directly to the electrostatic field of the ligands. This interaction is large enough to quench the orbital motion, thus it is locked into the field of the ligands and no longer contributes to the magnetism. The magnetic behaviour is therefore essentially spin-only as the spin does not couple directly with the electrostatic field.

1.3.4 Features of the EPR Spectrum

The EPR spectrum is usually obtained using magnetic field modulation ensuring that the modulation frequency is very much less than the radiation frequency. This produces effectively the first derivative of the energy absorption curve.

The intensity of the absorption is proportional to the population difference of spins, which at constant microwave frequency and temperature is a constant fraction of the total number of unpaired spins. For the first derivative spectrum the product of the peak-peak intensity (I_{p-p}) and the linewidth (ΔH_{p-p}) can be used as a measure of the intensity of absorption and therefore of the number of unpaired spins.

The width of the absorption band may be very large in which case it may be necessary to reduce it if possible. Two interactions affect this width:

(a) Spin-lattice. When the spin is reversed, energy is exchanged with the lattice. The time needed for this process to occur and thermal equilibrium to be re-established is known as the spin-lattice relaxation time. If this is short the population difference can be maintained to high temperatures without saturation occurring. In general, systems with close orbital energy levels have short spin-lattice relaxation times which give wide absorption bands, though the width can be reduced by cooling the specimen.

(b) Spin-spin. The magnetic field experienced by a particular spin will be affected by the presence of neighbouring unpaired electrons. This causes a small variation in the value of the magnetic

field at which absorption occurs hence broadening the absorption maximum. This is important for materials with a high concentration of paramagnetic centres but can be reduced to some extent by diluting the sample with an isomorphous diamagnetic salt.

1.3.4.1 Hyperfine Structure

This is a useful feature of the EPR spectrum which arises from the interaction of the unpaired spin with the magnetic moments of neighbouring nuclei. The (2I+1) different orientations of the nucleus produce 2I+1 component levels in each electron state, the splitting between these being, to a first approximation, equal and independent of the external field. Since the total angular momentum must remain unchanged, a second selection rule $\Delta M_I = 0$ applies when nuclear magnetic moments are present. An example of nuclear splitting is shown in Figure 1.12(a) and (b) for constant and varying magnetic fields respectively.

1.3.5 Summary for TM Ions

The free ion is initially orbitally and spin degenerate but when placed in a ligand field environment some orbital degeneracy will be lifted, especially with tetragonal distortions of octahedral fields, e.g. the Jahn-Teller effect. If spin-orbit coupling becomes appreciable then all orbital degeneracy may be removed. However, each orbital is still two-fold spin degenerate which can be lifted by Zeeman splitting through the action of an external magnetic field. EPR spectroscopy observes transitions between the nondegenerate Zeeman levels of the orbital ground state (Figure 1.13).

The spin Hamiltonian describes the energy levels and resonance data, accounting for such factors as the symmetry and strength of the crystal field, spin-orbit coupling and the hyperfine interaction.

1.3.6 EPR Spectra of Glasses Containing Iron and Manganese

The first study of EPR in glassy solids was made by Sands [48] who investigated TM and rare earth ions in a number of soda-lime-silicate base glasses. All the glasses measured, including the undoped base glasses, produced resonances having apparent anisotropic g values of 4 and 6, which were ascribed to an unknown impurity. These high g values were subsequently identified as arising from Fe^{3+} which was present as an impurity in all of the glasses [49]. The work of Sands [48] also revealed resonances with $g \sim 2$ for all the doping ions, many of which exhibited characteristic hyperfine structure.

Of the redox states of iron and manganese usually found in glasses only Mn^{2+} and Fe^{3+} are of interest for EPR investigations. Both have the d^5 electronic configuration, which has a $^6S_{5/2}$ ground state in the free ion, and possesses zero orbital angular momentum. There is, therefore, no first order spin-orbit interaction so a resonance with $g \sim g_e$ is expected. The initial fine splitting of the level is 0.1 cm^{-1} and the spin-lattice time is long, both of which favour investigation by EPR.

In practice, however, g values higher than 2 are often observed and in particular an isotropic g at 30/7, though this is not a feature peculiar to S state ions[50]. The theory of these larger g values is usually based on a spin Hamiltonian of the form:

$$\mathcal{H} = \beta g_s H.S + D\{S_z^2 - \tfrac{1}{3}S(S+1)\} + E(S_x^2 - S_y^2) \qquad (1.3.10)$$

where the terms involving D and E are the axial and orthorhombic crystal field terms respectively. For the two limiting cases D>>0, E=0 and D=0, E>>0, the energy levels in zero magnetic field are three Kramers doublets. In the first case the lowest doublet has effective g values of $g_{\parallel} = 2$, $g_{\perp} = 6$ and in the second case (rhombic symmetry), the middle doublet has an isotropic g value of 4.29, the value seen for Fe^{3+} in glasses. Transitions arising from the other two Kramers doublets will yield a broad background with effective g values ranging from 1 to 10. Further discussion of this with more detailed references is given in reference 51.

1.3.6.1 Manganese Glasses

The EPR spectrum of divalent manganese has been investigated in a wide range of glass forming systems including silicates, borates, phosphates, chalcogenides, glasses based on BeF_2 and vitreous $ZnCl_2$, but only results from silicate and borate systems will be discussed here. A surprising feature is that the spectrum is almost identical in borate and silicate glasses in spite of the structural differences between them; fluorescence spectra indicate that Mn^{2+} is probably octahedrally coordinated in borate glasses and tetrahedrally coordinated in silicates.

The main features of the spectra obtained at X-band frequencies are:

(a) An absorption at $g \sim 4.3$ with a distinct shoulder at $g \sim 3.3$ and,

(b) Six hyperfine lines near g = 2.0 which are observed only if the manganese concentration is low. This is useful as the magnitude of the hyperfine coupling constant provides a measure of the covalency between the Mn^{2+} ion and its ligands.

Taylor and Bray[52] have explained this apparently universal Mn^{2+} response in various glass systems not in terms of a unique site found in all glasses but rather from singularities of powder patterns which remain invarient with changes in both D and E/D. This enables glass spectra resulting from random distributions of different primary sites to have similar envelopes. These authors investigated a series of polycrystalline compounds of strontium borate with different $SrO:B_2O_3$ molar ratios, as well as glasses containing between 20-43% SrO. The glass samples did not show such sharp spectra as the crystalline compounds but had a broader background response. The sharpness of the spectra of the crystalline compounds was attributed to the occupancy of a single site per compound, which is of interest considering that the compounds contained a range of three and four coordinated boron. A comparison of the sharper glassy spectra near g = 2.0, ∿3.3 and 4.3 with that of the compounds indicated that there were probably two primary Mn^{2+} sites in the glasses, both probably substitutional for Sr^{2+} ions. One had E/D ∿0.3 and the second ∿0.1. It was suggested that the manganese coordination number could change with doping level.

This assignment of two manganese sites agreed with the conclusions reached by Tucker[53]. Tucker ascribed one site, with a large value of E, (rhombic symmetry), to the g = 4.3 resonance and the second site with $|D,E| \ll g\beta H$ to the g = 2 resonance. This is similar to his conclusions on Fe^{3+} glasses which will be mentioned below.

A similar study to that of Taylor and Bray[52] on both glasses and crystalline compounds but in the lithium borate system was conducted in a classic paper by Griscom and Griscom[54]. The EPR spectra of the glasses was interpreted using a diagram of the resonance field constructed by the authors. The observed fine structure parameters, which had a range of ∿0 > 4 GHz with an apparent constraint favouring $|E/D| \sim 1/3$, resulted from the fact that in glasses the manganese ions experienced a wide spread of crystal fields. It was concluded that many of the Mn^{2+} sites in glasses were possibly distorted versions of the site occupied in the $Li_2O.4B_2O_3$ compound.

The ^{55}Mn hyperfine coupling constant ($A/g\beta \sim 93G$) was relatively large indicating that the manganese bonding was highly ionic, which would tend to support octahedral rather than tetrahedral coordination. Divalent manganese tends to be more covalently bonded in silicate systems though it has recently been pointed out by Griscom [55] that the coordination number cannot be determined by EPR measurements alone.

Investigations have also been made on potassium borate glasses with small concentrations of Mn^{2+} [56]. For very small amounts the central fine structure transitions ($M = +\frac{1}{2} \leftrightarrow -\frac{1}{2}$) were broadened by random orientations of small non-cubic crystalline fields, but the spectra showed a well resolved hyperfine structure. This was also broadened by the random orientation of the Mn^{2+} ions in the glassy structure. In addition to the $\Delta M_I = 0$ transitions, forbidden $\Delta M_I = \pm 1$ transitions were also observed. However, for larger manganese concentrations these were almost all washed out as the spectrum was inhomogeneously broadened by magnetic dipole-dipole interaction. It was concluded that the Mn^{2+} ions were situated in a slightly distorted cubic symmetry. The distortion varied from site to site and was estimated to range on average <5% in interatomic distance and 10^0 in angle. However, Griscom[55] has pointed out that the axial symmetry with a very small value of D_{av} as found in this work[56] cannot explain the frequency dependence of the spectra between 9 and 35 GHz.

Bandyopadhyay[57] has recently published work which included a study of Mn^{2+} in a soda-borate glass. The spectrum was described by a spin Hamiltonian appropriate for Mn^{2+} in a crystal field of axial symmetry as used by De Wijn and van Baldren[56]:

$$\mathcal{H} = g\beta_0 HS + D\{S_z^2 - \tfrac{1}{3}S(S+1)\} + ASI - g_I\beta_I I \qquad (1.3.11)$$

The results calculated from the spectrum indicated an overall deviation from cubic symmetry, however the high value of A suggested octahedral coordination.

Finally, the work done on silicate glasses will be briefly mentioned. Abrashitova[58] investigated both borate and silicate glasses. Low concentrations of Mn^{2+} in borate glasses were described by the spin Hamiltonian in equation 1.3.11. As the concentration of Mn^{2+} increased, first the forbidden lines were washed out and then

the hyperfine lines themselves. In the silicate glasses the forbidden lines were not observed which suggested a lesser splitting of the spin levels by the crystal fields than in the borates. Again two types of site were proposed: axial with g = 2.0 and rhombic with g = 4.3. The intensity of the g = 4.3 resonance depended on glass composition and manganese concentration but was stronger for silicate glasses. More recently Schreurs[59] demonstrated the presence of hyperfine structure at g = 4.3 and g = 9.4 in manganese silicate glasses whilst agreeing with the analysis of Griscom and Griscom[54].

1.3.6.2 Iron Glasses

Iron glasses have been studied by a number of authors since the pioneering work of Sands[48]. In general three distinct resonances at g = 6, 4.3 and 2.0 can be observed. The interpretation of these in terms of ferric ion coordination and site symmetry has, however, been a subject of great debate in the literature. Castner[49] interpreted the anisotropic line at g = 6 as due to a ferric site with axial distortion. The resonance arises from transitions between the bottom Kramers doublet in a weak magnetic field (i.e. $S_z = \pm\frac{1}{2}$ $g_{\parallel} = 2$ $g_{\perp} = 6$, the latter giving rise to g = 6 in a powder pattern). The intensity of the line at g = 4.3 was found to increase monotonically with the ferric concentration thus it was suggested that this might result from ferric ion in a tetrahedral (network forming) site.

A number of other authors including Bishay and Makar[38] and Hirayama[60] have supported the earlier work of Tucker[53] in which he ascribed the g = 4.3 resonance to tetrahedral ferric ion and the resonance at g = 2.0 to octahedral (network modifier) Fe^{3+}. These conclusions have been drawn using EPR in collaboration with other structure sensitive techniques such as optical[38] and Mössbauer spectroscopy[60]. However, this view has been challenged by Kurkjian and Sigety[41] and Loveridge and Parke[51]. The former authors used Mössbauer, optical and EPR spectroscopies to study the coordination of ferric ion in phosphate and silicate glasses. As stated in section 1.2.6.2 the Mössbauer spectra were interpreted as indicating four-fold coordination in silicate glasses and six-fold coordination in phosphate glasses. This was confirmed, though with some difficulty, for the silicate glasses, by the optical absorption spectra. It was demonstrated that the g = 4.3 resonance could be produced by low symmetry (rhombic) sites of either tetrahedral or octahedral

coordination when the ferric concentration is low. With an increase in the ferric concentration, a change from g = 4.3 to g = 2.0 was observed for both phosphate and silicate glasses. This was interpreted by the authors as a result of spin-spin interaction at either site, rather than a change from four to six-fold coordination.

Loveridge and Parke[51], in their work on soda-borate glasses, agreed with the results of Kurkjian and Sigety[41] and reaffirmed that it is not possible to use the resonance at g = 4.3 and g = 2.0 as indicators of four and six-fold coordination. This was based on the finding that the intensity of an absorption in a series of glasses changed very little with widely varying soda contents, contrary to expectation if only one type of coordination were contributing. A number of coordinations with associated low symmetry elements could be responsible for the g = 4.3 resonance.

More recent work[61,62] has confirmed the conclusions of Kurkjian and Sigety[41] and ascribed the g = 2.0 resonance to clusters of paramagnetic ions coupled by exchange interactions. The alternative to this explanation would be that the g = 2.0 resonance is solely due to weak crystal field terms. If this is so there should be a direct correlation between this and the g = 6 resonance, since they are the parallel and perpendicular effective g values of the same Kramers doublet. This direct correlation has not been observed. Moon et al[62] found that the g = 6 resonance decreased with increasing iron concentration, whilst that at g = 2 increased monotonically. Gupta et al[61] investigated a lead borate glass and found that the g = 6 resonance peaked at 0.3% Fe_2O_3 and had disappeared by 2% Fe_2O_3, whilst the g = 2 absorption commenced at 2% Fe_2O_3 and peaked at 7.7%. The g = 4.3 resonance increased up to 2% Fe_2O_3 and then decreased. Both of these papers[61,62] proposed the formation of iron clusters above a certain concentration.

In conclusion, therefore, the EPR resonances of iron glasses may be explained as follows:

(a) The resonance at g = 4.3 is due to isolated ferric ions which have undergone rhombic distortion from an octahedral or tetrahedral environment.

(b) A resonance at g = 2.0 corresponds to clusters of paramagnetic ions containing two or more ions coupled by exchange interactions, and,

(c) A resonance at g = 6.0 is observed only in dilute glasses and originates from ferric ions with an axially distorted configuration.

1.3.7 EPR Spectra of Mixed TM Oxide Glasses

The study by EPR of interactions between paramagnetic ions when more than one TM oxide is present in a glass has not received much attention. Indeed two recent and otherwise comprehensive surveys of EPR phenomena in glasses[50,55] do not include the simultaneous effect of two TM oxides. Of the little work that has been published, that of Bogomolova[63,64] appears to be the most extensive, with more recent studies by Bandyopadhyay and co-workers[46,57] reaching similar conclusions. Only a brief account of these works is included for completeness.

Bogomolova[63] was the first to notice that the addition of a second TM ion (Co^{2+} - spin 1) to a glass containing paramagnetic ions (Cu^{2+}, V^{4+}, Mn^{2+} and W^{5+} - spin 2) with a variety of host glass compositions, considerably attenuated the signal once a certain concentration had been exceeded. This could not be explained by the simple shift in redox ratio to produce diamagnetic ions but was attributed to cross relaxation processes between the two spin systems, one of which (Co^{2+}) has a very short spin-lattice relaxation time and the other, spin 2 ion , a long relaxation time. Spin diffusion within the spin 2 system was also thought to have an effect.

Considering V^{4+} and Cu^{2+} ions; when both are present, a chemical (electron) exchange is possible via the reaction: $V^{4+} + Cu^{2+} = V^{5+} + Cu^{+}$. This decreases the integrated intensity of the spectrum of a mixed glass compared with the sum of the individual integrated intensities of single TM glasses with identical V and Cu concentrations, because both V^{5+} and Cu^{+} are diamagnetic. In addition to this however, the hyperfine components of the lines were broadened due to an exchange interaction. Bogomolova[64] also reported results for a mixed glass with a high concentration of TM ions (20% V_2O_5 + 10% Cu_2O) which showed a sharp increase in resistivity compared to a vanadium only glass, while the integrated intensity of the spectrum decreased by a factor of ten and the g value changed from 1.96 to 2.06. The increase in resistivity was attributed to a decrease in the V^{4+} concentration not only because of chemical exchange, which would only account for the change in integrated intensity, but also an

exchange interaction between V^{4+}-Cu^{2+} ion pairs to explain the change in g factor. These ion pairs did not appear to take part in the conduction process. Further work on the copper-vanadium system will be discussed in section 1.4.5.3 below.

Bandyopadhyay[57] obtained EPR spectra for three soda-borate glasses each containing 0.5% Cu_2O and 0.6% MnO melted at different temperatures. Spectra obtained at room temperature and 77 K were similar but the latter were sharper indicating a spin-lattice relaxation effect. The Cu^{2+} hyperfine lines were observed but the Mn^{2+} hyperfine structure was washed out. This could not be a cross-relaxation effect, since both Cu^{2+} and Mn^{2+} have long spin-lattice relaxation times, though spin diffusion within the Mn^{2+} system or nuclear relaxation were suggested. The alternative and favoured proposal, however, was that exchange coupled Mn^{2+} - O - Cu^{2+} associates were formed.

In a separate study, Bandyopadhyay[46] investigated EPR spectra of glasses containing high concentrations of Fe, V and Cu singly and in mixed proportions, as part of his study of electronic conduction in such materials. Of the work on mixed TM glasses that on the Fe-V system was the most complete. For a series of glasses with Fe replaced by V, whilst keeping the total TM concentration at nominally 10%, the Fe^{3+} absorption at g = 4.3 was always observed but the V^{4+} hyperfine structure was only present for glasses with high fractions of vanadium. The behaviour of the spectra with changes in the iron:vanadium ratio suggested that an interaction was taking place which obscured the V^{4+} hyperfine lines. A number of possible explanations were mentioned. The calculated g values showed that interaction between nuclear and electronic spin moments should increase along both parallel and perpendicular orientations but both nuclear spin coupling parameters $A_{\parallel}$ and $A_{\perp}$ decreased, implying that a process of nuclear relaxation could be taking place as V_2O_5 was replaced by Fe_2O_3. Alternatively, since optical absorption spectroscopy indicated that Fe^{2+} was probably present in the glasses, a cross relaxation process similar to that described above, could be taking place between Fe^{2+}, which has a very short spin-lattice relaxation time and V^{4+}. Finally, spin diffusion within the V^{4+} spin system could account for the disappearance of the hyperfine structure.

As the concentration of iron increased, the intensity and linewidth of the g = 4.3 absorption decreased. This was interpreted as a decrease in the number of distorted (rhombic) Fe^{3+} sites. Often a decrease in the g = 4.3 resonance of Fe^{3+} is accompanied by an increase at g = 2.0, but this was not observed in this case. The absence of a g = 2.0 line could be due to coupling of less distorted Fe^{3+} ions with V^{4+} ions to form associates, but not spin-spin coupling since the linewidth was not increased. However, magnetic coupling as proposed by Moon et al[62] and Friebele[65] could not be ruled out. The behaviour of these and the other mixed glasses suggested that considerable interaction was present forming associates between two ions with different valency joined by an oxygen ligand, i.e. $A^{n+} - O - B^{(n-1)+}$.

Finally, it is noted that EPR investigations of TM ions in glasses are usually conducted with small concentration levels (< 1%) to obtain maximum resolution of the spectrum. Only in a few cases have results on glasses containing up to 20% TM oxide been reported and these were principally because of the interest in the electrical conductivity of such glasses. The information that can be gained from such spectra is more limited. In the present study very dilute glasses have been specially melted for EPR measurements in addition to the more concentrated glasses melted primarily for conductivity measurements.

1.4 Electrical Conduction Mechanisms in Glasses

The fact that most common alkali containing glasses conduct electricity at sufficiently high temperatures has been recognized for over a hundred years. Experiments at the turn of the 20th century established that the current was carried by mobile group IA alkali ions, whereas alkaline earth or network former ions do not migrate appreciably in an applied electric field. Although experimental investigations continue, no major theoretical advances concerning ionic conduction have been made and dc conductivity results are normally expressed in terms of semi-empirical laws.

1.4.1 Ionic Conductivity

A detailed review of the work on ionic conduction in glasses is beyond the scope of this thesis, since glasses containing a significant proportion of TM ions are expected to be electronic conductors.

Indeed, the relatively mobile alkali ions have been deliberately excluded from glass compositions used in this study. However, it has been found that an ionic conduction mechanism may be appropriate for glasses containing only a small proportion of TM ions, so a brief outline of the subject is included.

The usual model of dc ionic conduction pictures a thermally activated process involving the mobile ions migrating between interstices in a comparatively open glassy structure. Each cationic site is assumed to be surrounded by a number of similar sites of equivalent energy, separated by an energy barrier, and the conduction process is similar to ionic migration via point defects in crystalline materials. Application of an electric field alters the energy of the sites so that net movement of the carrier in the direction of the field is favoured.

The Rasch-Hinrichsen equation is usually invoked to explain the resistivity-temperature dependence found experimentally for a wide range of glass compositions and temperatures:

$$\log \sigma = A - B/T \qquad (1.4.1)$$

where σ is the conductivity, T the temperature and A and B are constants. This expression is obtained from the Arrhenius equation, therefore B is a measure of the activation energy of conduction.

A model with greater physical insight was developed by Stevels who derived an equation for the conductivity by considering the mobile ions to be vibrating in potential wells. Each ion is surrounded by a number of vacant sites (b) to which it can jump. The application of an electric field alters the height of the potential wells as described above. Consideration of this model leads to the following equation:

$$\ln \sigma = \ln (\nu b e^2 \lambda^2 n / 6kT) - \Delta H_{dc} / RT \qquad (1.4.2)$$

where n is the number of carriers, λ the distance between sites, ν the vibration frequency of the ions and R is the gas constant.

Therefore a plot of $\ln \sigma T$ against $1/T$ will be a straight line with gradient equal to ΔH_{dc}. In fact experimental data fit either $\ln \sigma$ or $\ln \sigma T$ against $1/T$ plots equally well. A detailed review of the theory and experimental results obtained for ionic conduction in glasses is given in reference 66.

1.4.2 Electronic Conductivity

In 1954, Denton, Rawson and Stanworth[1] announced the discovery of the first electronically conducting glasses. These were prepared from the vanadium phosphate system. Since then, electronic conduction in glasses has generated great experimental and theoretical interest for the following reasons:

(a) It is possible to study electronic transport in disordered systems and compare with processes in related crystalline materials where the band structure is often well understood.

(b) New and useful semiconducting materials might be developed and also the amorphous equivalents of conventional semiconductor devices e.g. p-n junctions.

(c) The phenomenon of switching found in many amorphous semiconductors can be investigated and perhaps exploited.

The result of this work has been to develop a large number of non-crystalline materials in which an electronic conduction mechanism is thought to operate. Three main groups can be identified:

(a) Tetrahedrally bonded amorphous semiconductors such as a-silicon and a-germanium. These provide the greatest comparison between conduction in crystalline and amorphous states of the same material.

(b) The chalcogenide glasses based on S, Se and Te combined with one or more of the following elements: Si, Ge, P, As, Sb and Bi. Vitreous selenium has also received considerable attention.

(c) Oxide glasses containing transition metal oxides. Phosphate glasses have been most extensively studied since they can form glasses containing large proportions of some TM oxides, though borate, silicate and tellurite glasses have also received attention. Those TM oxides studied include: V, Fe and Ti, and to a lesser extent: Mn, Cu, Mo and W.

Many of the concepts of electronic conduction in amorphous materials have been developed from studies of classes (a) and (b) above, though some apply equally to oxide glasses. Therefore for completeness, a brief review of these materials is presented, preceded by the basis of the conduction process in conventional crystalline semiconductors.

A complete survey of electronic processes in non-crystalline

materials is contained in reference 67, whilst references 68 and 69 deal with the electronic properties of a wide range of glasses and amorphous materials.

1.4.3 Tetrahedral Amorphous Materials and Chalcogenide Glasses

The electronic conductivity of crystalline materials is now well understood in terms of their electron band structures. From the basis of a crystal with a perfect periodic lattice it can be shown that electrons with certain energies would interact strongly with the atoms in the lattice and therefore cannot propogate through the crystal. This gives rise to the concept of allowed energy bands, separated by forbidden gaps. The arrangement and filling of the uppermost energy bands, the highest called the conduction band (CB) with the valence band (VB) below it, determine if the material is an insulator, semiconductor or conductor. Semiconductors such as crystalline silicon and germanium have an empty conduction band separated from a full valence band by an energy gap of $\sim$1 eV. A larger energy gap would give an insulator and partial filling of either the conduction band or the valence band, or overlap between these bands, a conductor.

Pure silicon, a group IV element, is an intrinsic semiconductor since conduction takes place by electrons excited across the forbidden gap from the valence to the conduction band, together with the electron holes that they leave behind in the valence band. This requires either thermal or optical excitation. The conductivity may be increased by controlled doping with elements of a different valency: group III e.g. boron, or group V e.g. arsenic. This increases the carrier concentration by providing sites within the forbidden gap. Donor states (group V atoms) lie at an energy just below the conduction band and ionise at temperatures above absolute zero to provide electrons for the CB, thus producing an n-type semiconductor. Acceptor states (group III atoms), lying just above the valence band in energy, remove electrons from the VB, allowing conduction by electron holes and producing a p-type semiconductor. At low temperatures, however, for an n-type semiconductor, the Fermi level lies close to the donor states so practically all of the excess electrons are condensed on these centres. Conduction is only possible, therefore, if the material is compensated by introducing acceptor states, which remove electrons from the donor states, thus

allowing the remaining electrons to hop from charged to uncharged donor atoms. The understanding of this impurity conduction in doped and compensated crystalline semiconductors has greatly aided the study of amorphous semiconductors and especially TM oxide glasses.

At higher temperatures when the CB or VB are partially filled, the carriers migrate by band conduction through the extended states until scattered by either structural imperfections, such as grain boundaries or impurity atoms, or thermal vibrations of the lattice (phonons). Thus a resistivity which increases with temperature at sufficiently high temperatures is a characteristic of crystalline conductors and semiconductors.

When considering amorphous semiconductors some of the ideas which lead to the electronic band structure must be modified, since the concept of a perfect periodic lattice is no longer valid. However, although long range order vanishes in the amorphous state, short range order is essentially unchanged. Since the density of states for a given material is mainly determined by the first coordination number, then, if short range order is unchanged in the amorphous state or varies only slightly, no major change in the density of states is likely except due to changes in specific volume. Mott[67] has emphasised that the density of states is a valid concept for amorphous materials. It is also possible to define extended states, although the band edges are no longer well defined.

Localized states at the band edge result as a consequence of the lack of long range order in amorphous materials. The theory of this localization is mainly due to Anderson[70] and this transition from extended to localized states is of such fundamental importance in the theory of conduction in the non-crystalline state, that Mott[67] regards this localization theorem as the key to the understanding of electronic behaviour in amorphous solids. Anderson[70] considered a three dimensional crystalline array of potential wells with site energies distributed in a random way over a range U_o. He showed that with increasing U_o, the ratio U_o/B, where B is the width of the band formed by the interaction of nearest neighbour states which is proportional to the overlap integral, approaches a critical value. At this value an electron placed on a given well at T = 0 K will no longer diffuse away, but becomes localized. This can be

applied to doped and compensated semiconductors where it arises from a random array of impurity atoms in a crystalline lattice. Disorder has a similar effect. It is assumed that the above condition is reached, for wideband semiconductors, at the energy E_c in Figure 1.14(b) and the band tail states below E_c are then localized. If the bandwidth of the system is small then disorder may localise all of the states.

This localization is a feature of an 'ideal glass'. In real glasses structural defects such as broken or dangling bonds, vacancies, nonbridging atoms or chain ends, give rise to deeper states within the gap. Figure 1.14(c) shows a more realistic gap state distribution typical of a-Si and other simple amorphous materials. The charge distribution in the defect states largely determines the position of the Fermi level, so the defect structure has a great influence on the electronic properties.

Cohen, Fritzsche and Ovshinsky[71] have proposed a different model, primarily for complex chalcogenide glasses with four or five components. This is shown in Figure 1.14(d). The valence and conduction band tails extend throughout the mobility gap in a featureless distribution and the overlap pins the Fermi level. More recent evidence, however,[68] suggests that model (c) is more appropriate for these materials.

Two conduction mechanisms are generally observed in amorphous semiconductors. Firstly, for electrons with energies just above E_c and for holes just below E_v, conduction occurs in the extended states. However, transport is not by band motion with occasional scattering since the effect of random potentials and fluctuations in atomic distance reduces the mean free path and the coherence length of the electron wave functions so that they approach the interatomic spacing. The motion therefore becomes diffusive[72] and is similar to Brownian motion; no thermal activation is involved. Estimates of the drift mobility in this region are $\sim 10\ cm^2\ V^{-1}\ s^{-1}$ and Cohen[72] regards $10^{-2}\ cm^2\ V^{-1}\ s^{-1}$ as a lower limit for the diffusive mobility in extended states. Secondly, below E_c or above E_v all the states are localized and carriers can only move by phonon assisted hopping through the tail or gap states. The mobility for this process is given by:

$$\mu(E) \simeq \left(\frac{eR^2(E)}{kT} \right) \nu_{ph} \left(\exp -2\alpha R \right) \exp \left(- \frac{W}{kT} \right) \qquad (1.4.3)$$

where R is the average hopping distance, which is a function of energy because it depends on the density of states distribution. The term exp $(-2\alpha R)$ describes the overlap of the wavefunctions on neighbouring hopping sites with α representing the spatial decay of a localized wave function and ν_{ph} exp $(-W/kT)$ represents the probability per second that the localized electron hops to a new site at an energy W above the original one. Equation 1.4.3 predicts hopping mobilities at room temperature of $<10^{-2}$ cm^2 V^{-1} s^{-1}. This change in drift mobility between diffusive band transport and hopping defines a mobility gap which is an important concept in amorphous semiconductor theory.

Therefore in addition to conduction through the extended states there are current paths through the localized states. In particular, a special case occurs at low temperature where it is more favourable for a carrier to hop to a site closer in energy to its original site rather than to its spatially nearest neighbour. This is known as variable range hopping and conduction occurs near the Fermi level.

Finally, the question of which mechanism operates in various materials is still a matter of controversy. For chalcogenide glasses three mechanisms have been proposed:

(a) Direct phonon-assisted hopping between localized states, perhaps also involving thermally-activated release from deeper traps. This is favoured for Se-As glasses including As_2Se_3.

(b) Polaron hopping

(c) Transport in the extended states with some trapping in shallow localized states. This is favoured for vitreous Se.

For tetrahedrally bonded materials, such as a-Si, transport is thought to occur in the extended states near E_c. It is possible, however, that these conclusions may be altered in the light of the considerable theoretical and experimental work that is being expended on these materials and that the evidence may need to be considered separately for each composition to define the mechanism operating.

1.4.4 Oxide Glasses Containing TM Ions

Compared to the materials described above, the knowledge of the band structure of oxide glasses is very primitive. It may be assumed that commercial soda-lime-silicate glasses must have a forbidden gap

of several electronvolts width between the full valence band and empty conduction band, to explain the fact that they are transparent to visible light. However, only a few attempts have been made to calculate the band structures of such complex materials.

When considering TM oxides, more progress has been made and band structures have been determined; see, for example, Catlow and Muxworthy[73]. A schematic illustration for a typical divalent TM oxide is given in Figure 1.15. The electrical properties of TM oxides have also received much attention with special emphasis on mixed valence oxides[74]. It has been established that charge transport occurs through the partially filled 3d orbitals. The overlap between 3d orbitals is small and the carriers are further trapped to form polarons, thus a hopping mechanism is appropriate rather than band conduction.

When TM oxides are introduced into an oxide base glass the 3d levels are likely to remain within the forbidden gap of the glass, thus giving rise to the optical absorption noted above. However, in the glass the 3d levels will form localized states in the Anderson sense, if the Anderson localization criterion is satisfied. For 3d semiconducting oxide glasses this may be expressed as[75]:

$$W_D \gtrsim 6\ (2Jz) \qquad (1.4.4)$$

where W_D is the disorder energy, J, the overlap integral and z the number of nearest neighbours with which the d wavefunction overlaps.

This condition is usually satisfied for TM oxide glasses so the carrier hopping energy is increased by the disorder term W_D. In addition to this a second kind of localization is also expected because of polaron formation. Polaron formation is the principal feature of conduction in glasses containing multivalent TM ions and will be discussed at length below. A crude schematic band structure of these glasses has been drawn in the spirit of Figure 1.15 and is shown in Figure 1.16.

1.4.4.1 Conduction Mechanism

An essential pre-requisite for conduction is that the TM ions are present in more than one oxidation state. Therefore, for many TM glasses either reducing or oxidising melting conditions are needed to promote the production of a second species, generally with an

oxidation state ±1 that of the oxidation state normally attained. Two common techniques used to achieve this are varying the oxygen partial pressure in the furnace during melting, or adding a reducing agent, such as dextrose, to the batch. The conduction mechanism is then due to the transfer of an electron from an ion with the lower valence state to one with the higher valence state, under the influence of an electric field (e.g. $V^{4+} \rightarrow V^{5+}$, $Fe^{2+} \rightarrow Fe^{3+}$). Conduction is therefore diffusion-like in nature. The transfer of two electrons, as might be expected in tin glasses ($Sn^{2+} \rightarrow Sn^{4+}$), has not been observed.

The drift mobility, μ, is defined by the usual equation:

$$\sigma = n e \mu \qquad (1.4.5)$$

However, even for glasses with the greatest conductivities the drift mobility is very low ($<10^{-4}$ $cm^2V^{-1}s^{-1}$). Therefore the electron moves slowly through the network and it is thought that it interacts strongly with the network to form a polaron.

1.4.4.2 Polaron Formation

Moving with such a low velocity, the electron remains on a site for a time interval longer than the typical period of vibration of the network ions and hence the surrounding ions are able to assume new equilibrium positions consistent with the presence of the additional charge. These ionic displacements produce a potential energy well which, if deep enough, effectively traps the electron and localizes it on the TM ion and it is unable to move without an alteration in the positions of the surrounding ions. The bound electron and its associated network deformation (or lattice deformation in crystalline solids) is termed a polaron. When the electron moves, the polarization cloud moves with it and so the two can be treated as a single particle.

1.4.4.3 Activation Energy for Conduction

The theory of polaronic conduction in glasses containing TM ions has mainly been developed by Mott[76] and Austin and Mott[77] and their work forms the basis of the following discussion.

The activation energy for polaron hopping from one ion to another may be calculated by considering two TM ions, e.g. Fe^{3+}, on adjacent crystallographically equivalent sites[76]. One ion, Fe^{2+}, carries an additional electron and produces a field which

polarizes the medium. This polarization gives rise to a potential well in which the energy of the electron is:

$$V(r) = - \frac{e^2}{4\pi\varepsilon_o r} \left(\frac{1}{\varepsilon_\infty} - \frac{1}{\varepsilon_s} \right) = \frac{- e^2}{4\pi\varepsilon_o r\, \varepsilon_p} \qquad (1.4.6)$$

where ε_p is an effective dielectric constant defined as $(\varepsilon^{-1} - \varepsilon_s^{-1})^{-1}$.

Following Austin and Mott[77], this equation is supposed to be valid up to a radius r_p. So if r is greater than r_p:

$$V(r) = - \frac{e^2}{4\pi\varepsilon_o \varepsilon_p r} \qquad (1.4.7)$$

and r is replaced by r_p if r is less than r_p.

The subsequent derivation depends upon the effective mass of the electron. If this is large then the small polaron case is applicable and the potential well is located at a single ionic site. The value of r_p is somewhat less than the interionic distance R. In the other case, the smaller effective mass means that the kinetic energy of the electron must be considered as well as its potential energy and this gives the large polaron case. However, this will not be considered further as it is not applicable to TM glasses.

For a small polaron, the total energy of the electron and the distortion is made up from:

(a) The energy required to polarize the medium, which is equal to $\frac{1}{2}(e^2/4\pi\varepsilon_o\varepsilon_p r_p)$, and,

(b) The lowering of the potential energy of the electron, which is equal to $-(e^2/4\pi\varepsilon_o\varepsilon_p r_p)$

Therefore the polaron binding energy $(-W_p)$ is given by:

$$-W_p = \tfrac{1}{2} \left(\frac{e^2}{4\pi\varepsilon_o\varepsilon_p r_p}\right) - \left(\frac{e^2}{4\pi\varepsilon_o\varepsilon_p r_p}\right) = - \tfrac{1}{2} \left(\frac{e^2}{4\pi\varepsilon_o\varepsilon_p r_p}\right) \qquad (1.4.8)$$

Transport at high temperatures occurs by hopping but transfer of the electron from one ion to the other can only occur when the energy levels of the two sites are brought into coincidence by thermal activation with longitudinal optical phonons. The energy required to achieve this situation, shown in Figure 1.17(b), is calculated by adding the following components:

(a) The energy to raise the level of the electron on site 1.
$= \frac{1}{2} (e^2/4\pi\varepsilon_o\varepsilon_p r_p) = W_p$

(b) The polarization energy released on site 1 by relaxing the displacements of the ions, which is equal to - 3/4 W_p [77].

(c) The energy required to form the well on site 2 = ¼ W_p.

Therefore the hopping energy is given by:

$$W_H = W_p - 3/4\ W_p + 1/4\ W_p = \tfrac{1}{2}\ W_p \qquad (1.4.9)$$

An alternative and more exact method of calculating the small polaron binding energy is by treating the interaction of the electron with the whole spectrum of the vibrational modes of the surrounding network. This was first considered in a classic paper by Holstein[78] of which only the result is quoted:

$$W_p = \frac{1}{2N} \sum_q |\zeta_q|^2\ \hbar\omega_q \qquad (1.4.10)$$

where N is the number of centres per unit volume, ω_q is the angular frequency of an optical phonon with wavenumber q and $|\zeta_q|^2$ is the electron-phonon coupling constant.

Therefore to calculate W_p a knowledge of the phonon spectrum is required. As this is rarely known, it is assumed that the optical phonon spectrum is narrow and dispersion can be ignored. Therefore $\omega_q = \omega_o$, the characteristic phonon frequency and:

$$W_p = \zeta\ \hbar\ \omega_o \qquad (1.4.11)$$

Calculations have shown that the coupling constant is always quite high for TM glasses. For example, Mansingh et al[79], assuming a phonon frequency (ν_o) of 10^{13} Hz, reported a value of 10 for a tungsten phosphate glass, which gives the effective polaron mass as about 200 times the mass of an electron.

Bogomolov et al[80] have shown that an equation of the same form as that derived above (1.4.8) can be obtained from Holstein's equation (1.4.10), assuming a non dispersive system. This gives the small polaron radius as:

$$r_p = \tfrac{1}{2}\ (\ \pi/6\ )^{1/3}.\ R \quad \text{where } R = N^{-1/3} \qquad (1.4.12)$$

For the small polaron model to apply, the polaron radius must be smaller than the intersite distance R and greater than the radius of the ion on which the electron is localized, as measured by the reciprocal of the electronic decay component α (i.e. α^{-1}). Therefore:

$$\alpha^{-1} < r_p < R \qquad (1.4.13)$$

Returning to the mechanism of polaron hopping, Killias[81] has suggested that if the centres are close together, the polarization clouds will overlap and give a partial reduction in W_H. This is only expected for high TM oxide concentrations. Killias[81] proved that W_H increases linearly with site separation. This may be written as:

$$W_H = W_H(R_o) + a\Delta R \qquad (1.4.14)$$

In view of this, Mott[76] has suggested a modification of equation 1.4.8 using simple electrostatics, to obtain:

$$W_H = \tfrac{1}{4} \left(\frac{e^2}{4\pi\varepsilon_o\varepsilon_p}\right) \left(\frac{1}{r_p} - \frac{1}{R}\right) \qquad (1.4.15)$$

So far in this section, only the hopping energy has been considered. However, it was suggested above that disorder of the glass will lead to the TM sites being spread over an energy equal to W_D, where $\frac{1}{2}W_D$ may be defined as the average energy between nearest neighbour sites at a distance R. Miller and Abrahams[82] have estimated W_D for impurity conduction in doped and compensated semiconductors as:

$$W_D = \left(e^2/4\pi\varepsilon_o\varepsilon_s R \right) . K \qquad (1.4.16)$$

where K is a constant tabulated by them, which is equal to $\sim$0.3 for glasses containing TM ions.

Typical values of W_D from this equation are $\leq$0.1 eV for vanadium phosphate glasses[83].

The total activation for hopping is therefore:

$$W = W_H + \tfrac{1}{2}W_D \qquad (1.4.17)$$

where the terms in W_D^2 have been ignored[77].

In fact this only applies at temperatures greater than $\theta_D/2$, where θ_D is the Debye characteristic temperature defined by the equation:

$$k\theta_D = \hbar\omega_o \qquad (1.4.18)$$

Since hopping at high temperatures is a multi-phonon process involving optical phonons, W_H decreases with temperature and at

$T < \theta_D/4$ single optical phonons dominate and W_H should approach $\hbar\omega_o$ (84,85). Emin[86] however, has suggested that W_H is constant down to $\theta_D/3$, especially if there is appreciable phonon dispersion, and then $W_H \rightarrow \hbar\omega_o$ rapidly as T drops further. At the lowest temperatures, $W_H \simeq 0$, and the polaron hops with one or more acoustic phonons making up the energy difference between sites[84] i.e. $W = \frac{1}{2}W_D$.

Mott[76], however, has proposed that at very low temperatures $W_D \rightarrow 0$, because the polaron will prefer to hop to more distant sites with a smaller energy difference. This behaviour gives rise to the Mott $T^{-\frac{1}{4}}$ rule for variable range hopping, which will not be discussed further since measurements in this study have only been made at ambient temperatures and above.

The discussion in this section has been based on the assumption that the two ions involved in the hopping process are in crystallographically identical sites. This can only be approximately true in a glass. However, in some cases it is known from optical absorption and EPR measurements that different environments are present e.g. octahedral and tetrahedral. Austin[75] has proposed the addition of another term (ΔU) to the total activation energy to account for these differences in structure. Therefore equation 1.4.17 becomes:

$$W = W_H + \tfrac{1}{2}W_D + \Delta U \qquad (1.4.19)$$

For barium borate glasses containing small concentrations of vanadium, ΔU probably reflects the energy that must be provided to equalise the centres before hopping can occur[87]. Austin[75], however, put forward an alternative explanation for iron glasses suggesting that if the iron ions are too far apart for hopping to occur, the polaron could hop indirectly via an extended state e.g. the 4s conduction band. It will be shown that it is necessary to invoke a ΔU term for some glasses in the present study.

1.4.4.4 The Mott Equation for D.C. Conductivity

The basic equation for the conductivity is as given above i.e.

$$\sigma = n e \mu \qquad (1.4.5)$$

The number of carriers (n) can be calculated from experimental data, assuming that all the TM ions take part in the conduction

process, which seems from recent evidence to be the case[88]. Therefore the mobility (μ) remains to be calculated.

A suitable expression for the mobility is:

$$\mu = (eR^2/kT) \cdot P_1 \cdot P_2 \qquad (1.4.20)$$

where P_1 is the probability of coincidence of the two sites and P_2 the probability of polaron transfer when the sites have equivalent energy.

The first probability is the product of the predominant phonon frequency (ν_o) and the Boltzmann factor involving the minimum energy for coincidence as derived above. Therefore:

$$P_1 = \nu_o \exp (- W/kT) \qquad (1.4.21)$$

The expression for P_2 depends if the electron transfer is adiabatic or non-adiabatic.

In the former case, the electron tunnels backwards and forwards many times during each excitation of the lattice, so the probability of transfer is unity ($P_2 = 1$). Therefore the mobility for adiabatic transfer is given by:

$$\mu = (\nu_o eR^2/kT) \exp (- W/kT) \qquad (1.4.22)$$

In the non-adiabatic case, the probability of transfer is small, since the time required for the electron to hop is large compared with the duration of a coincident event, therefore $P_2 << 1$ and at high temperatures ($T > \theta_D/2$) [77,95]:

$$P_2 = \tfrac{1}{2}\pi^{\frac{1}{2}} J^2 / \{\nu_o \hbar (W_H kT)^{\frac{1}{2}}\} \qquad (1.4.23)$$

For temperatures such that $kT \sim \hbar \omega_o$, the hopping will be non-adiabatic if $J < \hbar\omega_o$.

The electronic transfer integral J is a measure of the electronic wavefunction overlap of neighbouring sites separated by a distance R. If α is the electronic decay function i.e. the fall-off with distance, then the overlap integral between sites is:

$$J = J_o \exp - \alpha R \qquad (1.4.24)$$

Therefore the mobility is given by:

$$\mu = \left(\frac{eR^2}{kT}\right) \pi^{\frac{1}{2}} \left(\frac{J_o^2}{2\hbar}\right) (W_H kT)^{-\frac{1}{2}} \exp - \left(2\alpha R + \frac{W}{kT}\right) \qquad (1.4.25)$$

From a consideration of non-adiabatic hopping in TM oxide glasses, Mott[89] has proposed the following expression for the conductivity:

$$\sigma = \nu_{ph}\, c(1-c)\, (e^2/RkT) \exp(-2\alpha R) \exp(-W/kT)$$

$$\sigma = \nu_{ph}\, Nc(1-c)\, (e^2R^2/kT) \exp(-2\alpha R) \exp(-W/kT) \quad (1.4.26)$$

where N is the total number of TM ions per unit volume, c is the fraction of reduced ions and (1-c) is the fraction of oxidised TM ions.

The Mott equation may be written:

$$\sigma = Nc(1-c) \times e \times (\nu_{ph} eR^2/kT) \exp(-2\alpha R) \exp(-W/kT)$$

$$= N' \times e \times \mu$$

and the similarity of the mobility to the expression quoted above (equation 1.4.25) may be seen. It may also be compared to the Arrhenius equation: $\sigma = \sigma_o \exp(-E/kT)$.

The Mott equation is now almost exclusively used in the analysis of electronic conduction in glasses containing TM ions. It makes the following predictions:

(a) A plot of log σT against $1/T$ should be a straight line with a gradient of $(W_H + \frac{1}{2}W_D)/k$ at high temperatures, falling continuously to $\frac{1}{2}W_D/k$ as T approaches 0 K.

(b) The conductivity should increase as the TM ion spacing decreases, and,

(c) The conductivity should go through a broad maximum as the redox ratio is varied.

A test of these predictions is one of the aims of the present study.

Finally, it is noted that the Mott equation is mathematically very similar to the equation for ionic conductivity developed by Stevels (equation 1.4.2). The differences are the inclusion of a tunnelling term and the absence of the geometrical factor of 1/6 in the Mott equation, although Austin and Garbett[85] have included the geometrical term in some of their calculations of polaron hopping conductivities. This similarity is not surprising given that the situations are similar. This means, therefore, that ionic and electronic conduction cannot be distinguished by plots of either

log σT or log σ against 1/T.

1.4.5 Previous Investigations of Conduction in TM Ion Glasses

Although early studies of electronic conductivity, carried out before about 1968, analysed dc conductivity results in terms of a simple Arrhenius relationship and calculated the pre-exponential factor (σ_o) and activation energy (E), most work since that date has been discussed using the Mott equation outlined above. The principal aim has been to compare the theoretical predictions for a small polaron hopping mechanism with experimental data obtained over a wide range of TM oxides and glass compositions. The terms selected for comparison between different systems have been the intersite distance (R), redox ratio (c) and tunnelling term exp ($-2\alpha R$) of the pre-exponential factor and, of course, the activation energy.

Considering first the effect of the redox ratio, the Mott equation has been formulated on the basis of a diffusion-like conduction mechanism between a random distribution of TM ions. It is, therefore, not strictly applicable to glasses exhibiting some kind of structure on either a macroscopic or microscopic scale. Such structure, ordering or segregation has therefore been invoked to explain deviations from the predictions of the Mott equation on otherwise apparently homogeneous glasses. Some examples of this are quoted below. The description of the conduction process in systems which are obviously two phase i.e. glass/crystal or glass/glass phase separation, is a different matter and will be discussed in a following section (1.4.6). However, having noted these exceptions, the simple fact remains that the theoretical prediction of the Mott equation, that the conductivity should reach a maximum at a redox ratio of 0.5, is only observed in a limited number of systems and most notably in iron phosphate glasses.

The system that has received the greatest attention in the field of electronically conducting TM oxide glasses has been the vanadium phosphate system. In these glasses the conductivity maximum occurs at a V^{4+}/V_{total} ratio of between 0.1 and 0.2 and this maximum corresponds to a weak minimum in the activation energy[90]. This behaviour has also been found in other glasses containing vanadium[91]. Various theories have been put forward to explain these findings. One of the earliest was that a fraction of V^{5+} ions was rendered

inactive with respect to the conduction process by being trapped in polymeric complexes within the glass structure. However, this explanation has been challenged by Sayer and Mansingh[92], as little independent experimental evidence (e.g. spectroscopic) has been put forward in its support. The latter authors suggested that for a high concentration of TM oxide, and in particular with a high concentration of reduced ions, polaron-polaron interactions may be important. These interactions could be direct, via Coulombic repulsion, or indirect, by changing the network relaxation at a given site due to the presence of a polaron on an adjacent site. In the latter case it could be required that the n nearest neighbours of the acceptor site must also be unoccupied for a hop to take place. This requirement changes the total hopping probability from $c(1-c)$ to $c(1-c)^{n+1}$. Some evidence was found in support of this from their experimental results with a value of $n = 5$. A further theory is that phase separation is responsible, since homogeneous $BaO-B_2O_3-V_2O_5$ glasses exhibited a sharp minimum in the resistivity at $c = 0.46$ [87]. However, a problem still exists because this minimum was much sharper than that predicted by the Mott equation and was due mainly to a minimum in the activation energy; a point which will be discussed further below (section 1.4.5.3).

The behaviour of iron and vanadium glasses is similar in that a maximum in conductivity is usually found at some value of c. In contrast , copper glasses studied by Tsuchiya and Moriya[93] showed no maximum, a discrepancy explained as a consequence of a mixed conduction process involving both ionic and electronic components. This is a reasonable hypothesis as the reduced state of copper in glass (Cu^+, group IB) is singly charged and therefore can migrate in an electric field in an analogous way to group IA alkali ions. The conductivity was found to increase with Cu^+ content as would be expected with this mechanism.

Titanium borosilicate glasses also showed an increase in conductivity as the redox ratio varied from $c \approx 0.2 - 0.6$, but for a somewhat different reason. In this case it was proposed[94] that carriers move along relatively highly conductive chains of Ti-O-Ti groups, rather than diffusing through a random distribution of Ti ions (see also section 1.4.5.3).

The need for a tunnelling term in the conductivity expression has been questioned by Sayer and Mansingh[92]. They melted a series

of phosphate glasses comprising 50% of the following TM oxides: Ti, V, Fe, Mn, Co, Ni, Cu, Mo and W, together with additional glasses containing up to 90% V_2O_5. This forms one of the most complete works to study the effect of individual TM oxides. They found that the magnitude of the conductivity at any given temperature was smallest in the glasses having the highest thermal activation energy. This indicated that the effect of the tunnelling term was not great and a small polaron model assuming adiabatic hopping was more appropriate. A plot of log σ at 500 K against the activation energy for each glass showed that the relationship was linear, with a slope corresponding to a measurement temperature of 530 K. Therefore the pre-exponential term, inclusive of exp $(-2\alpha R)$, was virtually constant for the whole series of glasses. A somewhat more complete plot of this type has been compiled by Murawski et al[95] from published data incorporating more than one point for each glass system. Good agreement between the experimental temperature chosen and the temperature calculated from the slope of the line, was only found for the V_2O_5-P_2O_5 and WO_3-P_2O_5 systems. In the other cases the calculated 1/kT value was between 1.6 and 3.5 higher than the experimental value, if the tunnelling term was ignored. This applied to the V_2O_5-TeO_2, FeO-P_2O_5, MoO_3-P_2O_5, TiO_2-P_2O_5 and V_2O_5-BaO-B_2O_3 systems for which the non-adiabatic approximation was therefore proposed. The weakness of this analysis is that the effect of different carrier concentrations in different glasses is assumed to be small.

Several attempts to calculate the electron wavefunction decay constant α have been made. Usually N, R and c in the Mott equation are estimated from experimental data, a value for the phonon frequency ν_{ph} assumed and hence α can be calculated. Murawski and Gzowski (96) attempted to calculate α^{-1} from the slope of a plot of log $\sigma_o/c(1-c)$ against R for iron phosphate glasses at a constant temperature. The value they obtained was reasonable (1.5 Å) although the analysis is not strictly accurate as R appears twice in the expression for σ_o:

$$\sigma_o = \frac{\nu_o e^2 c(1-c)}{kT\ R} \exp(-2\alpha R) \qquad (1.4.27)$$

A similar approach has been attempted by Hirshima and Yoshida[97]. They substituted Killias' expression (equation 1.4.14) into the Mott equation and obtained:

$$\log (\sigma R) = \log\{\frac{\nu_o e^2}{kT} c(1-c)\} - \{\frac{W_H(R_o)+\frac{1}{2}W_D}{kT}\} - (2\alpha+\frac{a}{kT}) R \quad (1.4.28)$$

Log (σR) was then plotted against R, with σ normalised to a value of c of 0.1, at constant temperature. An approximately linear relationship was found for Fe_2O_3 in a variety of base glasses, yielding values of α^{-1} between 0.5 and 1.0 Å. However, linear relationships were not found for CuO or TiO_2 glasses. The reason for the failure in CuO glasses was thought to be the significant contribution of ionic conductivity but no reason for the TiO_2 glasses was given.

Examination of published literature shows that the high temperature activation energy has a pronounced effect on the magnitude of the conductivity and depends to a large extent on the proportion and nature of the TM ion. The data of Sayer and Mansingh[92] reflects the latter effect as the proportion of TM oxide was roughly constant at 50%:

Ni	1.32 eV	Cu	1.03 eV	Ti	0.76 eV
Mn	1.24 eV			Fe	0.60 eV
Co	1.23 eV			V	0.42 eV

In general, these values are typical of those found by other workers in a wide variety of glass systems with fairly high proportions of TM oxide. For lower proportions, <15% for example, the activation energy is high, >1.2 eV, and is less dependent on the nature of the TM ion. However, only a small number of studies have concentrated on glasses with such low proportions.

In the table above, three regions of high temperature activation energy have been distinguished:

(a) Above 1.2 eV. A value as high as this leads to an extremely small, usually unmeasurable, value of room temperature dc conductivity ($<10^{-16}\ \Omega^{-1}cm^{-1}$). A feature in common with these TM elements is the predominance of the reduced (M^{2+}) state over higher valence states.

(b) Between 0.8 and 1.2 eV. Copper glasses are the main representatives of this group, which may be associated with a mixed electronic and ionic conduction process.

(c) Less than 0.8 eV, as typically found for Ti, Fe and V containing glasses. Usually vanadium glasses have the smallest activation energies and are the least resistive of this group,

though exceptions do occur[98].

The basic problem is to separate the activation energy into its constituent parts i.e. W_H, W_D and any ΔU term. If the low temperature conductivity is measurable then this can be used to calculate a value of W_D if the temperature dependence is known, hence W_H can be calculated from the high temperature activation energy ($W = W_H + \frac{1}{2}W_D$). Alternatively W_D may be estimated from the temperature dependence of the thermoelectric power, if this can be measured. More indirect ways involve using small polaron theory to calculate W_H (equations 1.4.8 and 1.4.9) with $\varepsilon_p \simeq \varepsilon_\infty = n^2$ and the polaron radius calculated from Bogomolov's equation (1.4.12), and calculating W_D from the Miller-Abrahams equation (1.4.16). If W_D as calculated from $W - W_H$ is much greater than the Miller-Abrahams disorder energy then a structural differences term may also be involved. Typical values of W_H and W_D are $\sim$0.2-0.4 eV and <0.1 eV respectively for V_2O_5-P_2O_5 glasses. The high values found for Mn, Co and Ni oxide glasses have yet to be adequately explained.

With this broad background in mind, a survey of more detailed findings on some individual glass systems especially relevant to this study will now be presented.

1.4.5.1 Iron Glasses

Hansen[99] was among the first to systematically investigate oxide glasses containing iron. He measured the electrical resistivity and thermoelectric power of both a series of 55%(FeO+MgO)-45%P_2O_5 glasses with FeO increasing from 0 to 55% in 5% intervals, together with a series of 55%FeO-45%P_2O_5 glasses with differing redox ratios. The results were analysed in terms of a simple Arrhenius relationship and it was found that for most glasses there was a change in slope of the log ρ-1/T line at temperatures between 110 and 150°C. Several possibilities were put forward to explain this including: conduction in different phases above and below the break, a change from predominantly electronic conduction to ionic conduction, though no polarization effects were observed, and charge transfer between iron ions in a similar crystallographic position at low temperatures and different positions at higher temperatures.

The conductivity was proposed to be due to a thermally activated hopping process between Fe^{2+} and Fe^{3+} ions, similar to

crystalline TM oxides with the activation energy pertaining to mobility rather than carrier generation. The activation energy changed from 1.6 eV for glasses containing 0 and 5% FeO, to 0.7 eV for concentrations of greater than 25%. Above 25% FeO, log ρ was proportional to %FeO.

Further analysis of the temperature dependence of the conductivity was carried out using an expression for mobility equivalent to that for adiabatic hopping:

$$\mu = \frac{ne^2R^2\nu_o}{kT} \exp\left(-\frac{E}{kT}\right) \qquad (1.4.29)$$

with n calculated from thermoelectric power measurements. The mobilities ranged from 10^{-10} $cm^2V^{-1}s^{-1}$ at 400 K to 10^{-7} $cm^2V^{-1}s^{-1}$ at 600 K. Calculation of the values of ν_o, the lattice vibrational frequency, yielded satisfactory values (0.8×10^{13} and 1.7×10^{12} s^{-1}).

A plot of resistivity against redox ratio revealed a broad minimum between Fe^{2+}/Fe_{total} of 0.4 - 0.6 in the 55% FeO glass. Thermoelectric power measurements showed that the glass changed from n-type to p-type conduction as the Fe^{3+}/Fe_{total} ratio decreased below 0.38.

Consideration of these results in the light of the Mott equation indicates that only partial agreement is found. The tunnelling term may be ignored and the resistivity minimum with the redox ratio was deeper than that predicted by a c(1-c) factor. That the minimum even occurs for the 55% FeO glass is perhaps fortuitous considering the behaviour of the rest of the system which is discussed below.

Following on from this work, Hansen and Splann[100] were the first to observe dielectric dispersion in a series of three iron phosphate glasses with different redox ratios. The ac dispersion exhibited a temperature dependence equivalent to that of the dc conductivity, which was therefore attributed to the resonance of hopping electrons, or holes, between Fe^{2+} and Fe^{3+} as in the dc conduction process. However, this conclusion has been questioned by Kinser[101] who examined $55FeO-45P_2O_5$ glasses subjected to different heat treatments. The change of dc resistivity after thermal treatment will be discussed in section 1.4.6, but it was found that loss peaks appeared after heat treatment at 400 and 500 °C for 1 hour. Samples heat treated at 300, 600 and 700 °C gave no loss peaks in the 10^2-10^6 Hz frequency range. Correlation of these results with optical

and transmission electron microscopy showed that the dielectric dispersion was the result of a Maxwell-Wagner-Sillars heterogeneous loss mechanism arising from the production of a finely dispersed highly conductive crystalline phase after heat treatment at 400 and 500 °C. Thermal treatments at lower temperatures produced no resolvable crystals or any evidence of liquid-liquid phase separation and therefore no loss peaks. At higher temperatures only a few large crystals were produced which, because of their number, did not lead to observable losses. The results of Hansen et al[100] were therefore explained by Kinser[101] as not being the result of a Fe^{2+}-Fe^{3+} electronic resonance but rather arising from partial devitrification of the glass during annealing from between 475 and 500 °C. Further discussion between Splann and Kinser[102] has not provided any definite conclusion since in most cases the conduction losses could mask the peaks in question.

Dozier et al[103] have reported further studies relating changes in the ac and dc electrical properties of a glass with a nominal composition of $55FeO\text{-}45P_2O_5$ to the redox ratio and devitrification induced by heat treatment. The glass with a redox ratio (Fe^{3+}/Fe_{total}) of 0.76 showed no dispersion in the as-cast state, but a dispersion appeared after heat treatment at 600 °C. With further heat treatment a second dispersion appeared and both grew in magnitude. This two peak phenomenon was explained by the nucleation and growth of two conducting crystalline phases giving rise to a Maxwell-Wagner-Sillars inhomogeneous loss mechanism. The dispersion behaviour for the glass with a redox ratio of 0.31 was less well defined although in this case a loss peak was present for the as-cast specimen. A further specimen cast onto copper blocks cooled with liquid nitrogen, revealed no loss peaks. This shows clearly the effect of quenching rate on producing a truly homogeneous glass. An increase in quenching rate also decreased the density of the glass thereby increasing the separation of the iron ions, thus increasing the resistivity of the specimen. The final glass, which had a redox ratio of 0.44, showed no loss peaks after 2 hr at 600 °C even though X-ray diffraction analysis showed the presence of crystallites. This was attributed to their large size (0.5 - 1.0 mm in diameter). This work was inconclusive as to the origin of the dispersion i.e. whether it was due to the polaron hopping resonance or devitrification, though the latter was favoured.

Thurzo et al[104] have recently investigated the dielectric behaviour of FeO_x - P_2O_5 glasses using the method of thermally stimulated depolarizatiom (TSD). They claim the the TSD technique is more convenient than conventional ac dielectric loss measurements for investigating semiconducting glasses, since conduction losses are absent in the former case. The as-cast glass exhibited two TSD peaks, one at low temperature representing a Debye-type dielectric dispersion and the other,at a higher temperature, a space-charge (electrode) polarization. The low frequency permittivity dispersion, related to the low temperature peak, was not adequately described by a model involving electron hopping between Fe^{2+} and Fe^{3+} ions as proposed by Sayer and Mansingh[92] and Thurzo et al suggested that another model, based on the presence of clusters of at least one dispersed phase within the homogeneous matrix, was more appropriate. The authors also considered the effect of heat treatment on the TSD peaks and their conclusions agreed with those of Kinser[101]. No suggestion was given regarding the nature of the dispersed phase although its volume appeared to be controlled by the redox ratio.

Vaughan and Kinser[105] extended the work of Hansen[99] by looking at a series of glasses in the $FeO-Fe_2O_3-P_2O_5$ system. Glasses containing greater than 50% P_2O_5 were homogeneous whilst those with less than 40% P_2O_5 were phase separated. The authors suggested that a complete compositional and microstructural description is necessary to characterize the glasses and that a more informative way of presenting the resistivity-composition data for a three component system such as this, is achieved by using the Gibbs' triangle. This permits simultaneous examination of the effect of total TM ion concentration and redox ratio. It was found that in general the minimum resistivity of a glass with a given composition did not occur at c = 0.5, except for the $55\%(FeO/Fe_2O_3)$-$45\%P_2O_5$ composition as reported by Hansen[99]. In addition, the change of resistivity with TM ion spacing R, deviated from the expected behaviour at low values of R.

For glasses with high iron concentrations, the effect of the heterogeneous structure was considered in that Fe^{2+} ions may be segregated to islands which do not enter the conduction process. Alternatively, if the isolated phase is rich in Fe^{3+}, then magnetic coupling between Fe^{2+} ions in the matrix phase would effectively remove Fe^{2+} ions and push the minimum resistivity to a higher redox

ratio, as observed. Removal of one redox state from participating in conduction would explain the changes in resistivity with R. For high iron contents, hence low R spacings as calculated from the composition, the effective R is higher because of segregation, hence the resistivity rises.

The effect of segregation would reduce as the iron concentration is reduced leading to the apparent ideal behaviour for the 55% FeO_x composition. At lower iron concentrations, it was suggested that ferric ions acted as network formers, thus shifting the minimum resistivity to a lower redox ratio (i.e. higher in Fe^{3+}).

These arguments should be related to the activation energy as well but no relationship between resistivity and activation energy changes could be found. The change in c(1-c) was also too small to account for the large changes in resistivity observed. The authors therefore concluded that the resistivity behaviour of the system was not easily rationalised even with the microstructural and magnetic arguments advanced and was incompatable with first order theories.

Borate glasses containing iron have been investigated by Gawish and Saleh[106,107] and Ardelean[108].

The former authors studied calcium borate glasses containing between 10 and 23% Fe_2O_3 and measured ac and dc conductivities and thermoelectric power. The results were initially analysed using the Arrhenius relationship producing plots which were linear above ~400 K, but with a steadily decreasing gradient below that temperature. Compositions containing less than 20% Fe_2O_3 were vitreous, but higher iron concentrations promoted devitrification, which produced a marked decrease in the activation energy and resistivity, especially for temperatures below 300 K. The authors concluded from the variation of the dc conductivity with temperature, together with the frequency dependence of the ac conductivity, that conduction was due to electron or polaron hopping between ferrous and ferric ions and hence the Mott equation should apply. However, no attempt was made to analyse the results in terms of the polaron parameters, r_p, α^{-1}, W_H and W_D. The glasses all had a constant redox ratio so a test of the c(1-c) prediction was not possible.

The same authors have recently reported further studies on the same glass system concerning mainly ac properties[107]. For glasses

with an Fe_2O_3 concentration of less than 20%, a hopping mechanism was proposed. However, in the partially crystallized glasses with compositions between 20 - 30% Fe_2O_3, the predominant conduction mechanism was thought to be trap limited band conduction at frequencies below 5 kHz and hopping above this value. For even higher concentrations, the material was completely crystalline, with possibly a diffusive conduction mechanism operating, involving transport in non-localized states $>E_c$ with hopping in localized states only above 10 kHz.

Lead borate glasses containing iron were studied by Ardelean[108] with Fe_2O_3 contents varying from 2-50%. Glasses with greater than 15% Fe_2O_3 exhibited a change in slope in the log ρ - 1/T plot, though in this case the temperature of the change increased linearly with Fe_2O_3 concentration. The reason for this was ascribed to the coordination environment of both ferrous and ferric ions, both of which can have two types of site. Therefore, at low temperatures charge transfer was between Fe^{2+} and Fe^{3+} ions in similar environments, whilst ions in different environments could be involved at higher temperatures, therefore introducing a ΔU term (of $\sim$0.4 eV in magnitude) into the activation energy. By analysis of the polaron parameters it was found that the Mott equation was valid between 5 - 15% Fe_2O_3 whilst an adiabatic approximation, putting $\exp(-2\alpha R) = 1$, was more appropriate for higher iron concentrations. The activation energy for the 2% glass was 1.21 eV, which is high for a polaron hopping mechanism, suggesting that another mechanism was operating.

Silicate glasses containing iron have not received much study, though Anderson and MacCrone[109] have investigated equimolar $PbO-SiO_2$ glasses containing low concentrations of iron ions. This is one of only a few studies concentrating on the conduction mechanism in glasses with such a low TM level (<10%). They found that the dc conductivity was always lower than the ac conductivity, even at the highest temperatures. The dc activation energy was constant over a large temperature range and the dependence of the conductivity on the redox ratio predicted by the Mott equation was not observed. Finally, the activation energy for hopping was constant over the concentration range studied. Analysis of the dielectric data using both Cole-Cole and Grant plots revealed two distinct relaxation processes: the first at low temperatures and

high measuring frequencies with a relaxation time distribution apparently independent of temperature. The second, at high temperatures and low frequencies, with a high magnitude and a relaxation time distribution which varied randomly with temperature.

The discrepancies with small polaron theory promoted the development of a new conduction model in which a random distribution of TM ions was no longer assumed. Instead the new model proposed that charge carriers moved preferentially along paths of relatively high conductivity. These paths were thought to consist of three dimensional tree-like clusters of linear chains of Fe^{2+}-O-Fe^{3+} units, with the clusters connected at a limited number of points. The iron ions are electronically coupled through the oxygen ion by an exchange mechanism.

The various abnormal features of the conduction process were therefore explained as follows. The ac conductivity is dominated by carriers hopping between ferrous and ferric ion pairs within the chains. This gives rise to the first relaxation process noted above and also provides a reason for the constant value of W_H, independent of composition and redox ratio. The dc conductivity results from movement of carriers along the chains, producing the second relaxation process, but is dependent on connections between clusters. Thus as the iron concentration increases from zero, the clusters grow in size, with the dc conductivity remaining constant, or slowly increasing, as the clusters begin to overlap. At a critical composition, enough connections have been established for the conductivity to increase rapidly with composition. Further evidence for a model of this type was provided from magnetic susceptibility and EPR data. The carriers were proposed to be small polarons hopping adiabatically between sites.

Finally in this section, Munakata[110], Kennedy and MacKenzie[111] and Hirashima and Yoshida[97], have specifically investigated the effect of the base glass on the conductivity of TM oxide glasses.

The latter authors reported work on the dc conductivity of iron containing glasses with different network formers (SiO_2, B_2O_3, P_2O_5) and different basicities. The conductivity of the borate glasses increased with increasing PbO/B_2O_3 ratio, but this could not be accounted for by the change in either the Fe ion density, and hence in R, or the redox ratio. In the light of their previous work on

the behaviour of iron in glass melts, they attributed the increase in conductivity to an increase in the fraction of four-fold coordinated iron in the glass at the expense of six-fold coordinated iron. A similar explanation was advanced for the increase in conductivity of the phosphate glass. In contrast, the basicity of the silicate glass had very little effect on the conductivity, therefore it was assumed that there was a less significant change in the iron coordination state as the PbO/SiO_2 ratio was altered. The authors suggested that a non-adiabatic small polaron conduction mechanism was most appropriate for their results.

1.4.5.2 Manganese Glasses

To date there have been only a very few systematic investigations of the electrical properties of glasses containing manganese.

One early study was that of McMillan[112] who investigated manganese as well as some other TM ions in the system TM oxide/Al_2O_3/SiO_2. Compositions containing less than 35% MnO could not be produced as homogeneous melts, even after melting at 1450 °C for long periods of time, but glasses were formed containing between 35-55% MnO. From the colour of the glasses most of the manganese was thought to be present in the divalent state. The volume resistivity at room temperature was very high at 10^{14}- 10^{15} Ωcm. The surface resistivity likewise was between 10^{13}-10^{15} Ωcm, but this was reduced by 10^4 after suitable heat treatment, which led also to the appearance of a reflecting film on the surface of the glass. It was concluded that although the bulk glass was insulating, a semiconducting surface layer was formed by oxidation of some of the Mn^{2+} to Mn^{3+}. It was proposed that as the Mn^{3+} formed within the glass at 1450°C did not impart semiconducting properties, then Mn^{3+} formed by oxidation at 600°C must occupy a different site i.e. an energetically more favourable site for allowing electronic conduction to take place. This could be because the crystallographic site of the Mn^{2+} ion is unlikely to change during oxidation at 600°C, thus allowing conduction between Mn^{2+} and Mn^{3+} in equivalent sites. No mention of the temperature relationship of the bulk resistivity was given for these glasses.

Calcium manganese silicate glasses have also been investigated by Kuznetsova and Evstrop'ev[113] but the glasses were treated as insulating and no mention was made of electronic conduction. The

resistivity at 300°C was between 10^8-10^{13} Ω cm and glasses melted under reducing conditions were found to have a resistivity of half an order of magnitude greater than that of glasses synthesised in a weakly oxidising medium. It was stated that the resistivity did not depend greatly on the valency of manganese ions in the glass.

Ershov and Shul'ts[114] measured the conductivity of glasses with MnO concentrations from x = 10-55% in $30PbO-(70-x)SiO_2$ base glasses. An electronic conduction mechanism was indicated by the absence of polarization effects with p-type conductivity demonstrated by the thermopower. As the manganese concentration increased up to 55% MnO, the resistivity decreased from 10^{13}- 10^9 Ω cm at 200°C and the activation energy from 2.6 to ∿1.7 eV (see note on activation energy below), though the conductivity and activation energy were almost constant for MnO concentrations of greater than 40%. The redox ratio was determined by chemical analysis and also estimated from the thermopower with the two results being in fair agreement. The fraction of Mn^{3+} increased from 3.1% to 23.4% as MnO increased from 20-55%.

The same authors as part of a study of conductivity in the mixed $MnO(Mn_2O_3)$-$FeO(Fe_2O_3)$-SiO_2 system also reported measurements on some binary manganese silicate compositions containing between 40-70% MnO[115]. Only compositions containing between 40-50% MnO_2 were glassy, whilst higher MnO concentrations produced either partially or fully crystallized materials containing tephroite as the main crystalline phase. The glasses contained about 7% Mn in the trivalent state. A plot of log σ against 1/T was linear yielding activation energy values of 2.21-2.28 eV for the glasses, dropping to 1.30 eV for a crystallized glass. Only a very slight change in log σ and activation energy were noted as MnO increased from 40-50%. The dramatic change on crystallization was thought to be due to a higher electron mobility with the ordering of the structure.

(Note: Whilst not stated in these references[113,114,115] it is understood that Russian practice is to analyse conductivity using the equation: $\sigma = \sigma_o \exp(-E/2kT)$. The activation energies quoted must therefore be divided by 2 for comparison with others quoted in this thesis.)

Finally, the work of Sayer and Mansingh[92], which included

a $50Mn_3O_4$-$50P_2O_5$ glass is relevant. A low conductivity and high activation energy were found (1.24 eV) but the redox ratio was not stated. Infrared absorption studies separated the series of TM oxide glasses into two distinct groups. The first, including: Mn, Co, Ni and Cu oxides, showed features in the spectrum which were thought to be characteristic of phosphate tetrahedra. The second group, comprising such TM oxides as: Ti, V, Mo and W were found to show spectra dominated by groups of the form MO_n, where M is a TM ion. This suggestion of a fundamental difference in the glassy structure can be used to explain the much higher activation energy shown by glasses in the first group, including manganese, to those in the second group. However, it is not easy to extend this argument to glass systems based on other network formers, where the same differences in activation energy apply.

Some further work on binary manganese phosphate systems will also be discussed in the following section on mixed TM oxide glasses.

1.4.5.3 Mixed TM Oxide Glasses

Although interest in glasses containing more than one TM oxide began in the 1960's, when such glasses with high conductivities were developed[116], no detailed study of the conduction mechanism was made at that time. It is only in recent years that greater attention has been focussed on conduction mechanisms in these systems. Some work on mixed iron-manganese systems has been reported, which will be described first, though this does not directly identify the role of each TM element. Therefore this section concludes with a brief account of work on other mixed systems.

Tsuchiya and Moriya[117] studied electronic conductivity and dielectric relaxation in phosphate glasses containing Fe_2O_3 and MnO. For the glasses containing MnO singly, reduction of the glass with carbon during melting and increasing the concentration of MnO, both decreased the conductivity. Whilst the former finding can be explained easily, the latter is surprising. Although glasses were not analysed to determine the manganese redox ratio, it is reasonable to expect the fraction of Mn^{3+} to be small, as found in all other studies of manganese glasses. Further reduction during melting will therefore lower this fraction even further, thus decreasing the conductivity. It is possible that the redox ratio for the glass

with higher MnO content is very small, thus explaining the decrease in conductivity with increasing MnO, but this is contrary to most findings in which the fraction of Mn^{3+} increases as the MnO concentration increases. In contrast, the conductivity of the iron only glasses increased with the total iron content and as the redox ratio decreased from ∿0.8 to 0.5. The activation energy for the manganese glass was about twice that of the iron glass with similar TM oxide molar concentrations. The dc conductivity of the mixed glasses increased after replacing MnO by Fe_2O_3 but it appeared to be unaltered by the iron redox ratio and heat treatment. It was suggested that iron and manganese interacted with each other by oxidation and reduction, but the final redox state had very little effect on the conductivity. No explanation for this was offered.

Broadly similar results were found by the same authors in a later work on xFe_2O_3-(50-x)MnO-$50P_2O_5$ glasses[118]. In this work just one manganese only glass was investigated in both normal and 'reduced' redox states, although the exact ratios were not specified. The results for the reduced glass were, however, distinctly different to their earlier work on a glass with the same composition, though the redox ratios may be different. In this case the log σ - 1/T plot showed a change in slope at ∿373 K and the conductivity at higher temperatures was almost identical for normal and reduced glasses, rather than being nearly an order of magnitude lower as found previously. The high temperature activation energy for the reduced glass was also different in the two studies. In the mixed glasses, the conductivity increased linearly by replacing MnO with Fe_2O_3 and also increased in the reduced glasses. Some of the log σ - 1/T plots showed a slight change in gradient (2-3 kcal/mole) at about 373 K as had been observed in the previous work, but the change was very much less noticeable than that of the manganese glass. In both of these works the proportion of Mn^{3+} was not stated and no attempt was made to analyse the results in terms of small polaron theory.

Ershov and Shul'ts[115] measured the conductivity of glasses in the MnO(Mn_2O_3)-Fe_2O_3(FeO)-SiO_2 system. They considered that all four possible redox states: Fe^{2+}, Fe^{3+}, Mn^{2+} and Mn^{3+} were present simultaneously in the glasses, although their analysis technique could only measure the difference between Mn^{3+} and Fe^{2+} concentrations because of redox reactions on dissolving the glass for chemical analysis. For glasses with 5% Fe_2O_3, the concentration of MnO was

varied between 45-60%, but no systematic variation in activation energy or conductivity was found, though the activation energy was generally 0.2-0.3 eV lower than manganese only glasses. In a further series with 45% MnO, an increase in Fe_2O_3 up to 8% also had no systematic effect; the activation energy decreased by 0.2 eV in the 5% glass but returned to the manganese only value with 8% Fe_2O_3. It was only with the onset of crystallization that decreases in resistivity and activation energy were observed. Chemical analysis of this series showed that the concentration of Mn^{3+} was greater than Fe^{2+}, suggesting that the increase in the conductivity was largely due to crystallization, resulting in a heightened carrier mobility, rather than the effect of mixing two TM elements. These authors also considered the effect of the change in the ferrous content of the glasses. On going from Fe^{2+}/Fe_{total} = 0 to 0.5, the conductivity increased by two orders of magnitude and the activation energy decreased by 0.35-0.40 eV. This was attributed to an increase in the number of Fe^{2+} donors and possible structural arrangements in the glass, due to a change in the iron coordination number on going from Fe^{3+} to Fe^{2+}, to explain the change in activation energy.

Mixed iron-manganese glasses have also been studied by Pronkin et al[119], but these also contained an appreciable proportion of sodium ions. This paper also referenced some previous work on iron containing sodium glasses where mixed cationic-electronic conductivity was found, depending upon the iron concentration and measuring temperature. The authors determined that the transport number of the sodium ions was unity, as measured by Tubandt's method, and so proposed purely cationic conductivity in the experimental temperature range of 280-380°C. The log σ against 1/T relationship was linear for each of the three glasses, but the activation energy progressively decreased from 1.00 eV through 0.88 to 0.72 eV as MnO was replaced by Fe_2O_3, whilst keeping the sodium content constant. Such a change does not seem easy to reconcile with purely cationic conductivity, especially when the results of the present study are considered.

A systematic investigation of conduction in barium borate glasses containing mixed iron-vanadium, copper-vanadium and copper-iron oxides has been made by Bandyopadhyay[98]. Except for the copper-iron glasses, the resistivity of the mixed glasses was less than that of the single TM oxide glasses with the same concentrations

of TM ions. The reason why this was not observed for the copper-iron compositions was thought to be due to the low concentration of reduced states. The enhancement of conductivity in the mixed glasses could arise either from polaron hopping between ions of different TM elements, or a change in the redox ratio. However, it was demonstrated that the observed changes in redox ratio could not account for the increase in conductivity. It was therefore concluded that hopping between neighbouring ions of different TM elements is energetically more favourable than hopping between ions of the same element at greater average distances.

As well as his work on EPR outlined above, Bogomolova[120] has measured the resistivity of some mixed TM oxide glasses and attempted to relate the changes in the EPR spectra to the change in resistivity. As stated already, the effect of additions of a second TM oxide could either be to allow electron exchange between different TM elements, or simply change the redox ratio, thus producing a change in the conductivity. Thus during the melting of glasses containing vanadium and copper, the following reaction will take place:

$$V^{4+} + Cu^{2+} \rightarrow V^{5+} + Cu^{+}$$

possibly with an exchange interaction at sufficiently high concentrations leading to V^{4+}- Cu^{2+} associates. For a glass with composition $32CaO\text{-}25.3P_2O_5\text{-}42.7V_2O_5$, the addition of 3.3×10^{20} atoms of Cu per gram of glass increased the resistivity by $\sim 10^2$ Ω cm. The EPR spectrum changed as well: the width of the exchanged narrowed V^{4+} line increased, the integrated intensity fell by a factor of 1.6 but the g value remained approximately constant at 1.97. To explain these findings, Bogomolova assumed a chemical exchange between V^{4+} and Cu^{2+} which left 4×10^{20} V^{4+} ions g^{-1}, compared to the starting figure of 6.65×10^{20} V^{4+} g^{-1}, thus reducing the vanadium redox ratio to 0.095. Such a change could cause the observed increase in resistivity without the necessity of postulating that copper ions enter the conduction mechanism. For higher concentrations, 6.6×10^{20} Cu^{2+} g^{-1} and 10^{21} V^{4+} g^{-1}, the resistivity was slightly reduced and the EPR spectrum altered: the integrated intensity fell by 1.14, the linewidth increased and the g factor increased to 2.05. It was proposed that a chemical exchange with a similar reaction constant to that above took place, which reduced the concentration of both Cu^{2+} and V^{4+}, but the remaining V^{4+} ions

($\sim$7.4 x 10^{20} g^{-1}) interacted with Cu^{2+} ions to form associates producing an exchange broadened EPR line with average g factor. However, these associates were thought to have little influence on the charge transfer process, thus giving very little change in resistivity. Replacement of CaO by an equal weight of Cu_2O also increased the linewidth and integrated intensity of the EPR spectrum and changed g to 2.07, but reduced the resistivity. This was explained by a shift in the equilibrium to higher V^{4+}, together with the production of V^{4+} - Cu^{2+} pairs and more complex clusters of both types of ions. It was thought that the reduction in resistivity could be due to the presence of large clusters of associates.

Sayer and Lynch[121] investigated the electrical properties of two series of tungsten phosphate glasses with small additions of other TM ions: Series 1: 0.2 - 8.6% V_2O_5, MoO_3 and CuO, Series 2: 1.5% of other TM ions including Fe_2O_3 and MnO. EPR, NMR and optical spectroscopy were also utilised to investigate the impurity effects[122]. V_2O_5 and MoO_3 reduced the conductivity sharply, even for concentrations of less than 1%; V_2O_5 had its maximum effect at $\sim$1.5% after which the conductivity increased with further additions, whilst MoO_3 reduced the conductivity continuously. All the other TM ions had very little effect, especially at low concentrations. It was thought that the conductivity was affected partly by changes in the redox states of the ions, but mainly by a change in the probability of hopping. The activation energy was the dominant parameter and varied inversely with impurity spacing at low impurity concentrations, but it was not possible to account for this behaviour using a model of trap-controlled drift mobility. The fact that only V and Mo had a strong impurity effect indicated that structural considerations could be important. Isolated V and Mo ions both localized electrons in their vicinity with localization energies of 0.75 and 0.80 eV respectively, but for high vanadium impurity levels the results suggested direct electron transfer between vanadium sites. The conduction mechanism was thought to be similar to the Miller-Abrahams model for impurity conduction in semiconductors and the possibility of relatively long range interactions between impurity sites to overcome the localization energy (especially for vanadium) was mentioned. Thermopower and optical absorption measurements on undoped glasses were consistent with a small polaron hopping mechanism, with the correlation $W_{opt} \sim 4W_H$

being qualitatively observed even for doped glasses. EPR spectra indicated exchange interactions between the paramagnetic ions at mean spacings of <16 Å, whilst at high impurity concentrations a strongly exchanged narrowed resonance was observed.

In more recent work, Bogomolova[123] has both extended his previous work on the $CaO-CuO-V_2O_5-P_2O_5$ system and also investigated tungsten phosphate glasses containing copper, with the same composition as used by Sayer and Lynch[121]. The copper-vanadium glasses were found to be phase separated; one phase contained V^{4+} and was conducting. As the copper concentration increased to 5%, the resistivity first increased but then fell to just below the undoped value. The author proposed that copper ions entered the conducting phase forming V^{4+} - Cu^{2+} pairs which took part in the transport process, but as their concentration was very much less than that of V^{4+}, there was little effect on the resistivity. With an increase in copper over 5%, further phase separation took place producing a new conducting phase whose resistivity was practically independent of the copper concentration. EPR spectra of these glasses were highly sensitive to heat treatment and hence the degree and type of phase separation. For the tungsten glasses, Bogomolova[123] remarked that the small change in conductivity agreed poorly with the assumption about delocalization of unpaired electrons from W^{5+} ions as given by Sayer and Lynch[121]. EPR spectra indicated that the amount of W^{5+} decreased as copper increased but no signal from any Cu^{2+} - W^{5+} associates was observed. This was possibly because of the large differences in g between Cu^{2+} and W^{5+} which leads to smearing of the signal and hence difficulty in detection. It was proposed that copper would, in the absence of phase separation, have a similar effect on both vanadium and tungsten phosphate glasses. A model involving the structure of the glass was proposed in which the copper ions were located in the cation layers of the glass, whilst vanadium and tungsten were in the glass network through which electronic transport takes place. The process of charge transport was thought to be determined by either indirect exchange between V^{4+} (or W^{5+})- O - Cu^{2+} or direct delocalization between W^{5+} and Cu^{2+}.

Mansingh, Sayer et al[124] have recently measured the dc conductivity and dielectric properties of vanadium phosphate glasses containing 0-5% molybdenum 'impurity'. The conductivity of

the 1% MoO_3 glass was increased by two orders of magnitude and smaller changes were also seen in the activation energy and dielectric constant at this impurity level. It was thought that the Mo ions had only an indirect effect and conduction continued to take place between the vanadium ions. The results could be explained by the small polaron theory, with the change in conductivity due to doping being attributed primarily to a modification of the high frequency dielectric constant, which will affect the polaron hopping energy. The high frequency dielectric constant is determined by the electronic polarizability of the glass lattice, which in turn is a function of the local bonding. It was also found that the mean hopping distance was greater than the mean TM ion spacing, which allows percolation to a number of sites beyond the nearest neighbour. Percolation considerations could be of fundamental importance in TM oxide glasses if changes in the site energy, because of local bonding, exclude carrier transitions between adjacent sites.

1.4.6 Previous Investigations of Electronic Conduction in Crystallized Glasses Containing TM Oxides

Hamblen et al[125] were the first to try to correlate the electrical properties and thermal history of a glass, particularly after heat treatment between the liquidus temperature and the annealing range. Glasses prepared from V_2O_5 melted with various metaphosphates (those of Ba, Pb, Li, Na, K, Cd and V) were found to be electronically conducting with resistivities which decreased with increasing vanadium content. The metaphosphate cation also appeared to exert an effect on the resistivity with cadmium containing glasses exhibiting the lowest resistance. Resistivities could be altered considerably by using a suitable heat treatment. Generally the resistivity decreased after heat treatment, with the exception of Cd and Li glasses for which the opposite occurred. For some glasses it was observed that as the devitrification temperature was increased, the resistivity decreased. For isothermal heat treatments above the transformation range, the greatest decrease in resistivity occurred during the first half hour of treatment, after which a slight increase was observed. No attempt was made to explain any of these observations in terms of the phases produced on devitrification and their effect on the vanadium ion distribution or electron mobility.

A more complete examination of crystallized glasses in the $MgO-Al_2O_3-SiO_2-TiO_2$ system was made by Kumar and Nag[126]. For a composition containing 6.5% TiO_2, conduction in the vitreous state was thought to be by impurity Na^+ ions, possibly with some contribution from Mg^{2+} ions, because of the high dc activation energy (1.39 eV). The ac activation energy was 1.19 eV which suggested that the mechanism was similar to that of dc conduction. During crystallization in the range 900-1140°C, one of the earliest crystal phases to appear was magnesium aluminium titanate. Specimens crystallized at <900°C were deep blue in colour, probably resulting from partial reduction of Ti^{4+} to Ti^{3+}. This was accompanied by a decrease in the dc resistivity and activation energy (to 0.80 eV), along with a corresponding increase in dielectric loss. This was thought to be due to the presence of semiconducting crystals within the insulating glass matrix, which also gave rise to a high frequency dielectric relaxation band through Maxwell-Wagner loss. The ac activation energy at 0.50 eV, was significantly lower than the corresponding dc value and was probably associated with the electron mobility within the nonstoichiometric titanate crystals. The dc activation energy increased with increasing crystallization temperature as the degree of reduction of the titanate phase reduced and the fraction of insulating crystalline phases (cordierite, cristobalite and enstatite) increased.

Much of the work on the effect of crystallization on TM glasses has been done with iron as the TM ion. O'Horo and Stenitz[127] investigated a calcium alumino-borosilicate glass containing Fe_2O_3. The glass in the as-cast condition exhibited some signs of phase separation and had a fairly high room temperature conductivity, with a dc activation energy of 0.68 eV, which is typical of iron glasses. With a single stage heat treatment between 650 - 800°C, iron oxides were crystallized increasing both the resistivity and activation energy (to 1.2 eV). For heat treatment temperatures below 750°C, the resistivity continued to increase with time but above that temperature, a dramatic decrease in resistivity and activation energy (to 0.02 eV) was found. These changes were explained as follows. Growth of a crystalline iron oxide phase will increase the resistivity by removing iron ions from the conduction process. Segregation of ferrous and ferric ions will also result in changes in the redox ratio of the residual glass, the distance between

Fe^{2+} - Fe^{3+} ion pairs and hence a change in activation energy. However, at a certain crystallized fraction, a continuous crystal network can be formed through which conduction will take place, rather than through the residual glass. Consequently there is a reduction in resistivity and activation energy to values typical of the crystalline phase.

Schultz[128] was mainly interested in the devitrification behaviour of iron containing lead silicate glasses for the production of magnetic lead ferrite, but his results on the electrical properties of these glasses are of interest in the present work. Glass compositions included up to 3% ZrO_2 as a nucleating agent which, after heat treatment, produced semiconducting glass-ceramics with room temperature log resistivities between 1.5-4.8 Ω cm and activation energies between 0.09-0.22 eV. These should be compared with respective values of 10.22 Ω cm and 0.65 eV for the uncrystallized glass. These low values were thought to be the result of the formation of a nonstoichiometric lead ferrite phase along with tunnelling effects through the residual glass, because of the close proximity of neighbouring crystals.

Kinser[129] included the effect of devitrification in his study of an iron phosphate glass. The resistivity of the glass decreased slowly with one hour thermal treatments up to 500°C, but similar treatments at 600, 700 and 800°C caused pronounced increases in resistivity. It was suggested that the former finding could be explained in one of two ways. Firstly, by a decrease in the interionic distance arising from the decreasing volume of glass, because of higher annealing temperatures, or secondly by the fact that crystals observed by TEM after a low temperature heat treatment were preferentially formed from ferrous ions. This left the matrix richer in ferric ion, thus increasing the effective value of the redox ratio (Fe^{3+}/Fe_{total}). However, after heat treatment at higher temperatures the opposite effect was found with the dispersed phase preferentially incorporating ferric ion, hence reducing c and the resistivity. The dispersed phase was not thought to contribute to the dc conductivity as no high conductivity path was formed.

Following this work, Kinser[101] and Dozier et al[103] together investigated the effect of heat treatment at 600°C on three glasses with the same composition but with different redox ratios. The

effect of the change in sample volume was found to be small compared with the variation in redox ratio, depending on the stoichiometry of the precipitating phases and the redox ratio of the as-cast glass. The glass with c = 0.76 showed an initial decrease in resistivity resulting from segregation of Fe^{3+} ions into the crystalline phase ($FePO_4$). After a while, a phase incorporating Fe^{2+} was precipitated resulting in a subsequent increase in the resistivity. Similar explanations were advanced for the two glasses with c < 0.5, for which the resistivity initially increased after heat treatment. The overall change for the specimen with c = 0.44 was less than for the other two. This would be expected as the 'U' shape of the log ρ against c curve will result in relative insensitivity to segregation of either Fe^{3+} or Fe^{2+} ions for 0.4 < c < 0.6.

Tricker et al[130] carried out ^{57}Fe Mössbauer and X-ray photoelectron spectroscopic studies on a number of iron containing calcium borate glasses which showed large changes in dc conductivity upon annealing. For a 17% Fe_2O_3 glass, the resistivity in the unannealed condition was 10^{10} Ω cm, but after heat treatment at 750°C for 3 hr the resistivity rose to ∿5 x 10^{13} Ω cm. After longer annealing times the resistivity progressively decreased to a constant value of 3 x 10^3 Ω cm at 20 hr. Changes in the Mössbauer spectra correlated with these changes in resistivity. The spectrum of the unannealed glass was consistent with the presence of predominantly ferric ion in a distorted octahedral oxygen ion environment. Short heat treatment times produced a partial ordering of the glassy phase which reduced the linewidth, intensity and quadrupole splitting of the resonances and also the conductivity. Longer times led to precipitation of α-Fe_2O_3, which was identified by both Mössbauer spectroscopy and X-ray diffraction. The enhanced conductivity was, therefore, probably due to a continuous network of α-Fe_2O_3 crystals, though detailed mechanisms for changes in conductivity were not discussed in the paper.

A sodium boro-aluminosilicate glass containing iron was developed by Russak and McLaren[131] for use as a semiconducting glaze for porcelain insulators. It was stated that the as-melted glass was not semiconducting but was made so by the controlled devitrification of magnetite (Fe_3O_4). The degree of crystallinity and crystal size were dependent on the heat treatment time and temperature, and crystal growth was controlled by diffusion of iron ions with an

activation energy of 28 kcal/mole. Only surface resistivities were measured, yielding values which depended on the degree of crystallization. The activation energy was 7 kcal/mole but was independent of heat treatment temperature and hence the degree of crystallinity.

Tsuchiya and Moriya[118] studied the properties of crystallized manganese and mixed manganese-iron glasses. A $50MnO-50P_2O_5$ glass showed a dramatic increase in conductivity (greater than 5.5 orders of magnitude) after annealing at 534°C for 24 hr. The log σ - 1/T plot also showed a change in slope at about 80°C, with a higher activation energy above this temperature although it was still less than that of the uncrystallized glass. The changes in conductivity for the mixed glasses containing 10, 20 and 25% Fe_2O_3 were minor and could probably be accounted for by the error in measurement of log σ ($\sim\pm0.1-0.2$). However, the mixed, as well as the manganese glasses, gave X-ray diffraction patterns indicating that crystallization has occurred, although the phases were unspecified. The authors suggested for the manganese glass that preferential segregation of manganese, consisting of a particular oxidation state, could be assumed to explain the large increase in conductivity.

Ershov and Shul'ts[115] also measured a sharp decrease in resistivity and activation energy for manganese silicate glasses which crystallized on cooling, producing tephroite as the major crystalline phase. This was attributed to the heightened mobility of electrons with ordering of the structure. For the mixed iron-manganese compositions, crystallization also produced a decrease in resistivity (by 3-4 orders of magnitude) and activation energy ($\sim$0.7 eV), with the activation energy for the composition $13Fe_2O_3-45MnO-42SiO_2$ being just 0.08 eV. This again was ascribed to heightened carrier mobility during ordering of the structure as a result of the decrease in the energy of electron jumps between TM ions with different valencies. Because of the differences in conductivity and activation energy between manganese and the mixed glasses when crystallized, and bearing in mind the relative conductivities of MnO and Fe_2O_3, it was assumed that iron and manganese silicate structures were differentiated in the crystallized mixed glass resulting in conduction through iron rich regions.

Hench[132] investigated a number of glasses based on the vanadium phosphate system including some glasses previously studied

by Hamblen[125] reported above. He showed that during heat treatment an initial ordering of the glass was followed by detectable crystallization. These microstructural changes significantly increased the dc conductivity, probably by influencing the electronic transport mechanism. The electrical properties of some of the glasses, e.g. those based on K_2PO_3-V_2O_5, were strongly affected by fabrication variables such as quenching temperature and rate of cooling, since these determine the short range order of the glass. Chemical composition was also an important variable, especially the addition of alkali or alkaline earth ions, since these affected the tendencies towards phase separation and crystallization. They therefore produce variations in the material's sensitivity to thermal treatments. Some unusual dielectric behaviour was associated with the partially crystallized glass because of the presence of crystals, with different conductivities, in a glassy matrix and the resulting interfacial effects. Finally, this was one of the few studies to attempt to explain the findings in terms of a band theory and schematic representations of the electronic band structures were presented.

Finally in this section, two of the most recent works on the effect of crystallization on the properties of electronically conducting TM glasses, both dealing with the V_2O_5-P_2O_5 system, will be briefly mentioned. Limb and Davis[133] found that heat treatment of V_2O_5-P_2O_5 binary and V_2O_5-P_2O_5-B_2O_3 ternary compositions promoted phase separation of coalesced amorphous droplets of V_2O_5 at 220°C, and subsequent bulk crystallization at higher temperatures. The dc resistivity and activation energy both decreased after heat treatment at 290 and 410°C, as a result of the production of a continuous and highly conducting polycrystalline V_2O_5 phase, with individual crystals in point to point contact. After heating at 410°C, the samples were 83% crystalline with values of conductivity and activation energy very close to those of pure polycrystalline V_2O_5. The redox ratio was independent of annealing and crystallization temperatures and the value of σ_o from the analysis:

$$\sigma = \sigma_o \exp(-W/kT) \quad : \quad \sigma_o = kc(1-c)/T$$

was relatively unchanged, indicating that the conductivity was controlled principally by changes in activation energy.

Yoshida and Matsuno[134] studied heat treatment effects on

mixed Nb_2O_5-V_2O_5-P_2O_5 glasses. Two compositions were selected, one rich in V_2O_5 (A) and the other rich in Nb_2O_5 (B). Heat treatment increased the conductivity and decreased the activation energy of both compositions with the activation energies falling to that of crystalline V_2O_5 (0.23 eV). X-ray diffraction analysis showed that composition A produced V_2O_5 plus another unidentified phase or phases, whilst B produced $NbPO_5$ and V_2O_5. There was a reduction in the vanadium redox ratio (V^{4+}/V_{total}) for both compositions during crystallization, but the decrease could not account for the increase in conductivity. Electronic transport through a conductive crystalline phase was therefore suggested.

TABLE 1.1

PREPARATION OF AMORPHOUS MATERIALS FROM SOLID, LIQUID AND GASEOUS PHASES

Starting Phase	Technique	Examples of Materials Prepared by the Technique
Gas	Vapour Phase Hydrolysis	Synthetic high purity fused silica. Also used to control the refractive index gradient of optical fibres by ion doping
	Glow Discharge Decomposition	Amorphous films of Si and Ge from their respective hydrides. Can also be used to dope amorphous semiconductors.
	Thermal Evaporation	Most classes of amorphous semiconductors Si, Ge and chalcogenide glasses.
	Sputtering	Some chalcogenides. Amorphous V_2O_5.
Liquid	Splat Cooling	Glassy metals
	Chemical Reaction and Precipitation	Amorphous As_2S_3 by passing H_2S gas through a solution of As_2O_3 in HCl.
	Electrolytic Deposition	Ge from electrolysis of $GeCl_4$ in glycol
Solid	Neutron or Ion Bombardment	Silica
	Shock Wave Bombardment	Silica

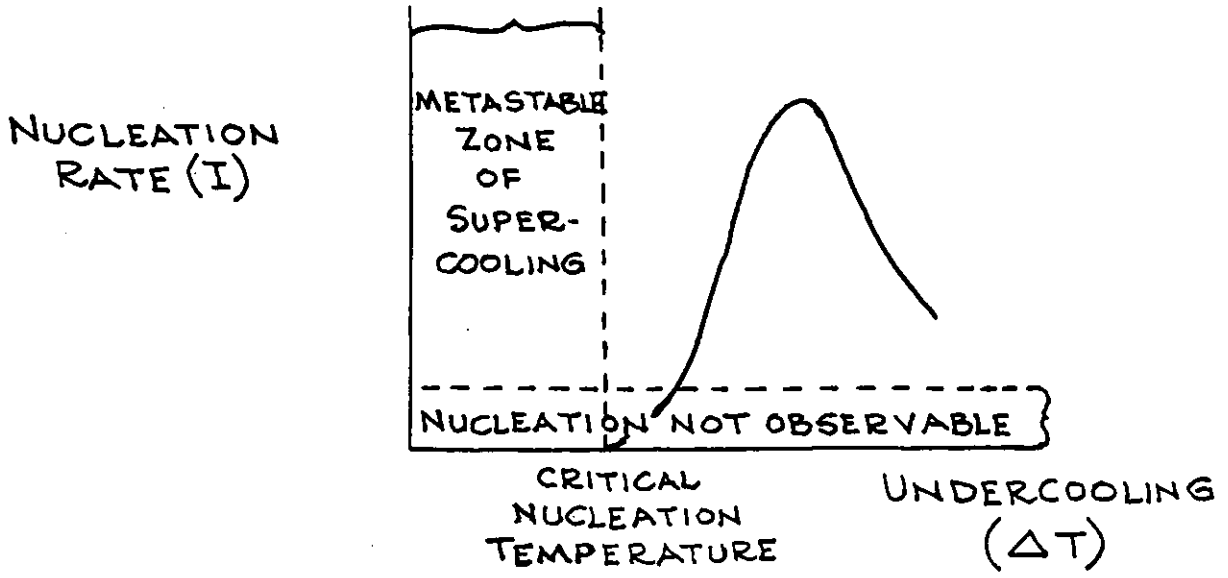

FIGURE 1.1 RELATION BETWEEN NUCLEATION RATE AND UNDERCOOLING.

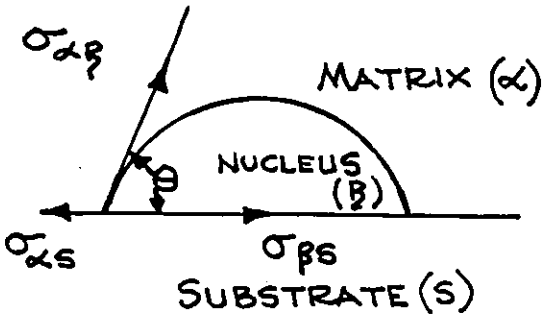

FIGURE 1.2 SPHERICAL CAP MODEL OF HETERO-GENEOUS NUCLEATION

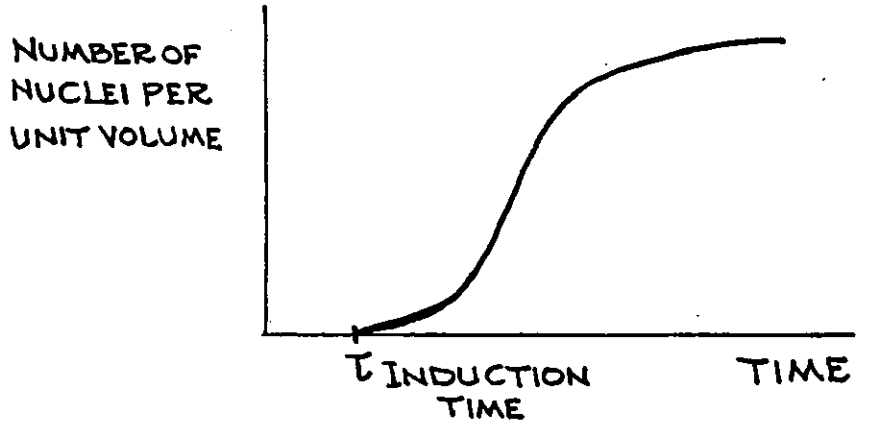

FIGURE 1.3 VARIATION OF THE NUMBER OF NUCLEI PER UNIT VOLUME WITH TIME

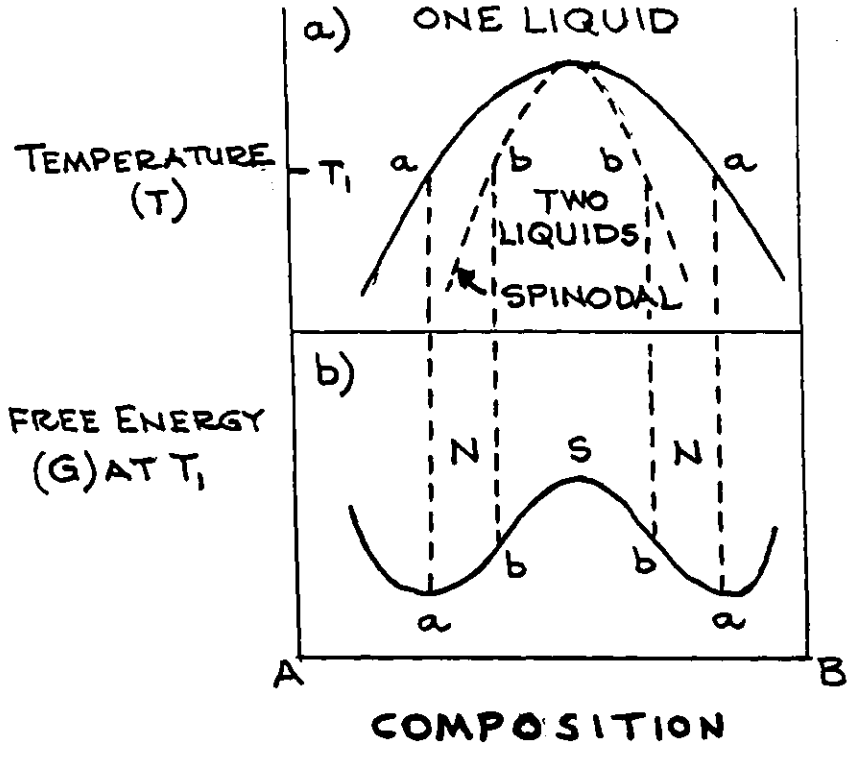

FIGURE 1.4a HYPOTHETICAL PHASE DIAGRAM SHOWING TWO-LIQUID & SPINODAL REGIONS

FIGURE 1.4b FREE ENERGY OF MIXING CORRESPONDING TO TEMPERATURE T_1

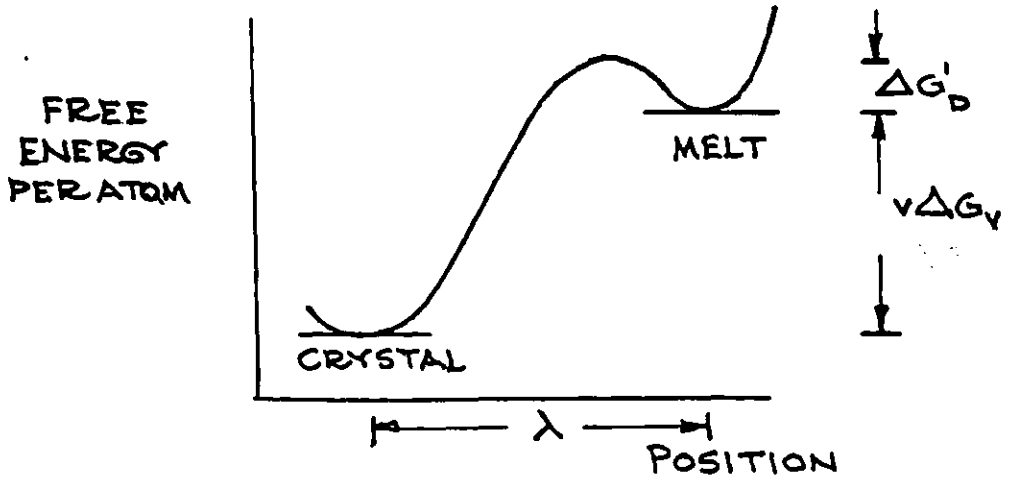

FIGURE 1.5 FREE ENERGY RELATIONSHIPS DURING THE ATTACHMENT PROCESS AT THE CRYSTAL-MELT INTERFACE

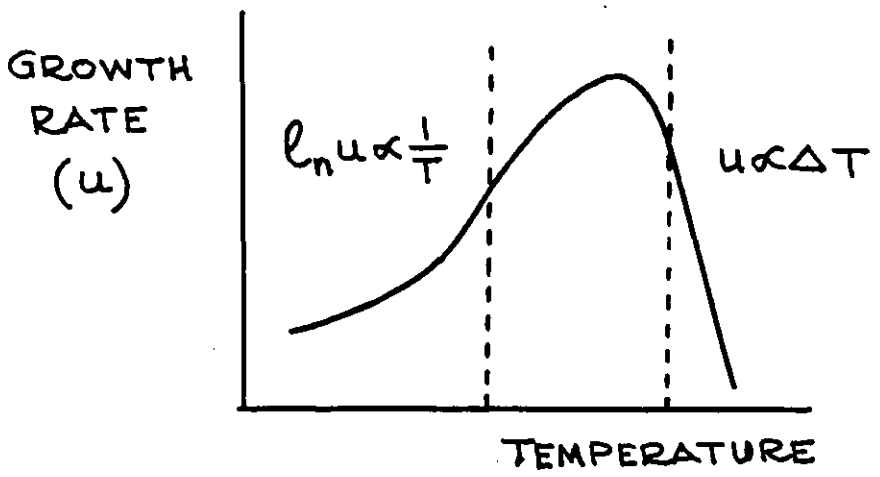

FIGURE 1.6 TYPICAL BEHAVIOUR OF GROWTH RATE WITH TEMPERATURE.

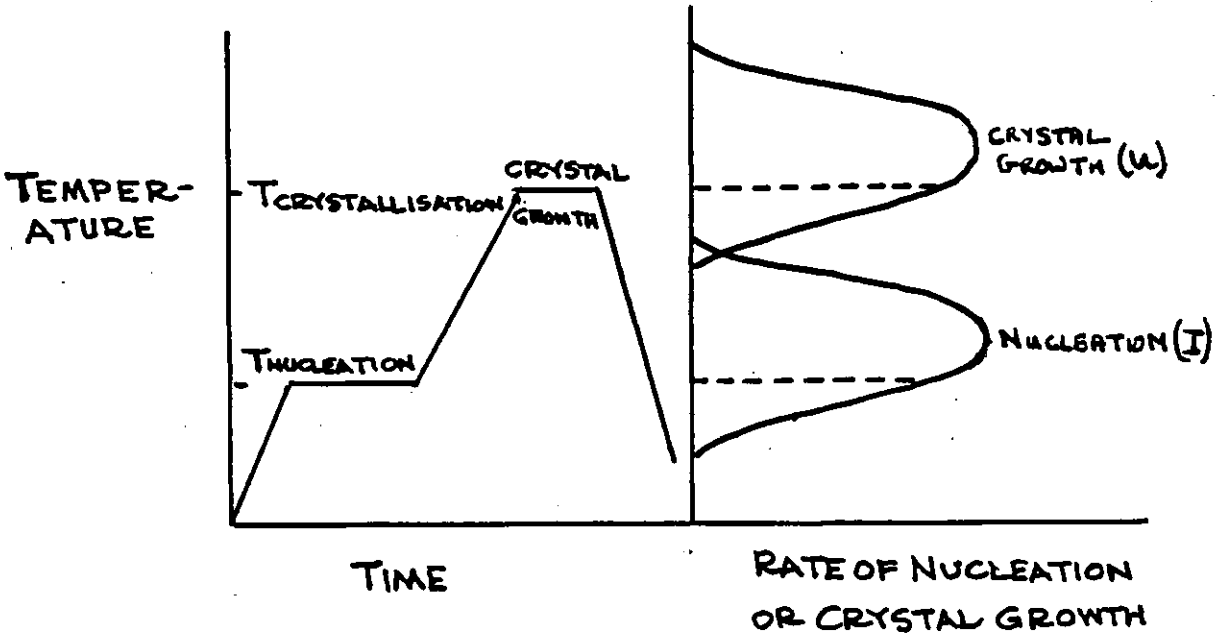

FIGURE 1.7 a) SCHEMATIC HEAT TREATMENT SCHEDULE USED FOR THE PRODUCTION OF GLASS-CERAMICS.

b) RATES OF NUCLEATION OR CRYSTAL GROWTH ASSOCIATED WITH THE HEAT TREATMENT SCHEDULE.

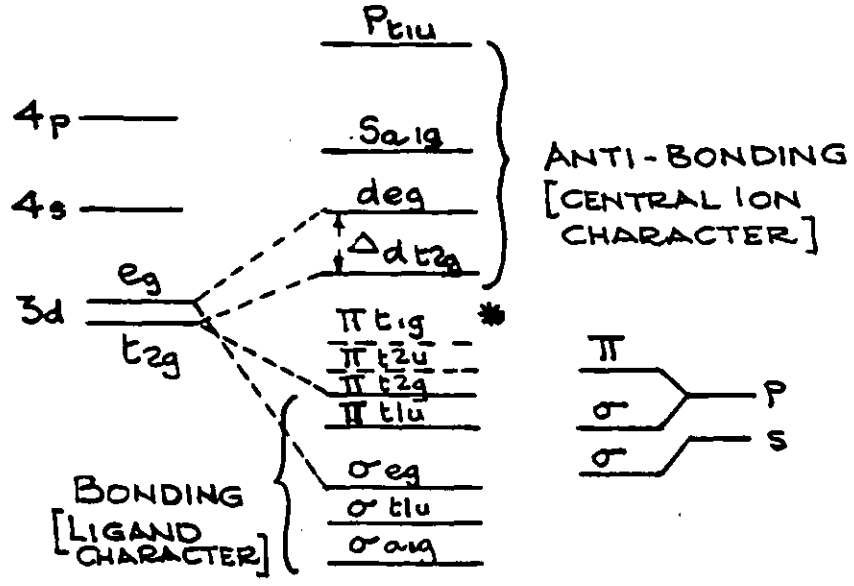

[* ---- INDICATES NON-BONDING LIGAND ORBITALS SINCE NO CENTRAL ION ORBITALS HAVE t_{1g} OR t_{1u} SYMMETRY.]

FIGURE 1.8 MOLECULAR ORBITAL ENERGY LEVEL DIAGRAM FOR AN OCTAHEDRAL COMPLEX [AFTER BATES (27)]

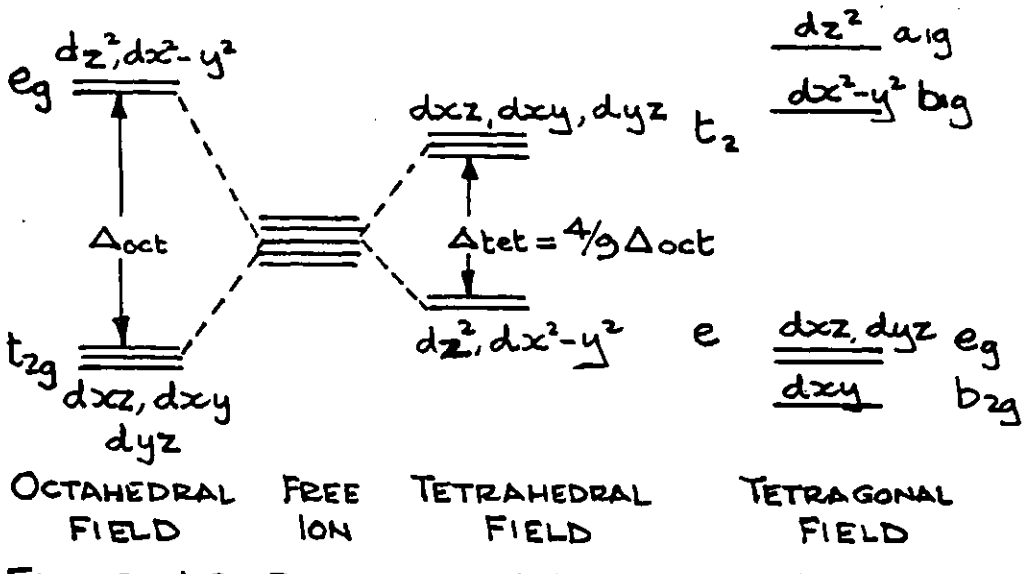

FIGURE 1.9 ENERGY LEVELS OF THE d-ORBITALS IN OCTAHEDRAL, TETRAHEDRAL AND TETRAGONAL FIELDS

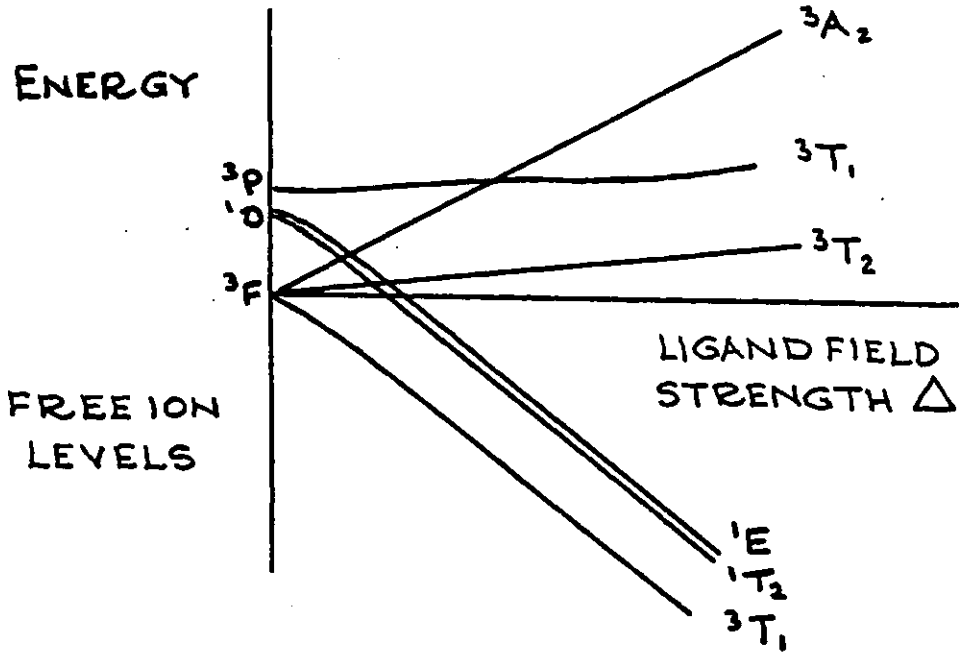

FIGURE 1.10 TYPICAL ORGEL DIAGRAM FOR THE d^2 - CONFIGURATION IN AN OCTAHEDRAL FIELD (AFTER BATES[27])

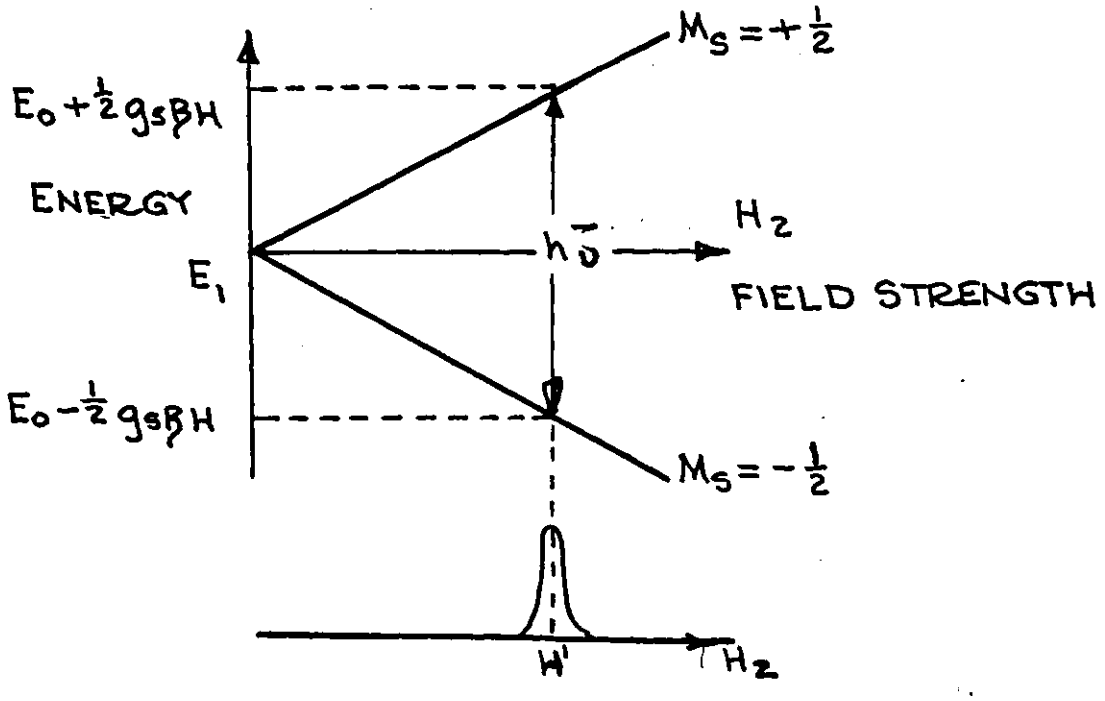

FIGURE 1.11 REPRESENTATION OF AN ELECTRON PARAMAGNETIC RESONANCE TRANSITION WITH CORRESPONDING ABSORPTION LINE (FROM REFERENCE 47)

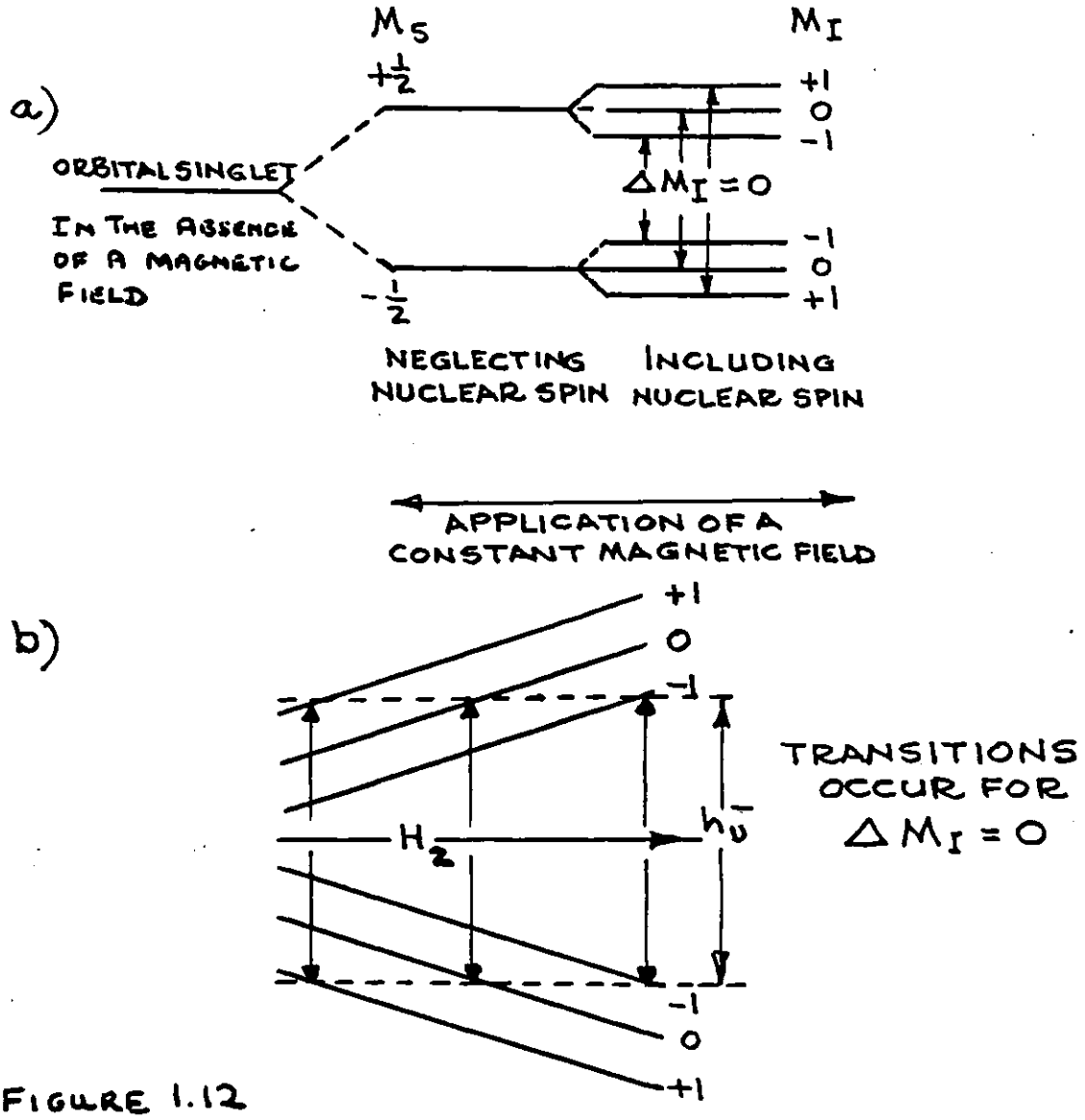

FIGURE 1.12

a) HYPERFINE SPLITTING OF THE ENERGY LEVELS AT CONSTANT MAGNETIC FIELD STRENGTH FOR $S = \frac{1}{2}$ $I = 1$.

b) ABSORPTION OF MICROWAVE RADIATION OF FIXED FREQUENCY AT DIFFERING MAGNETIC FIELD STRENGTHS.

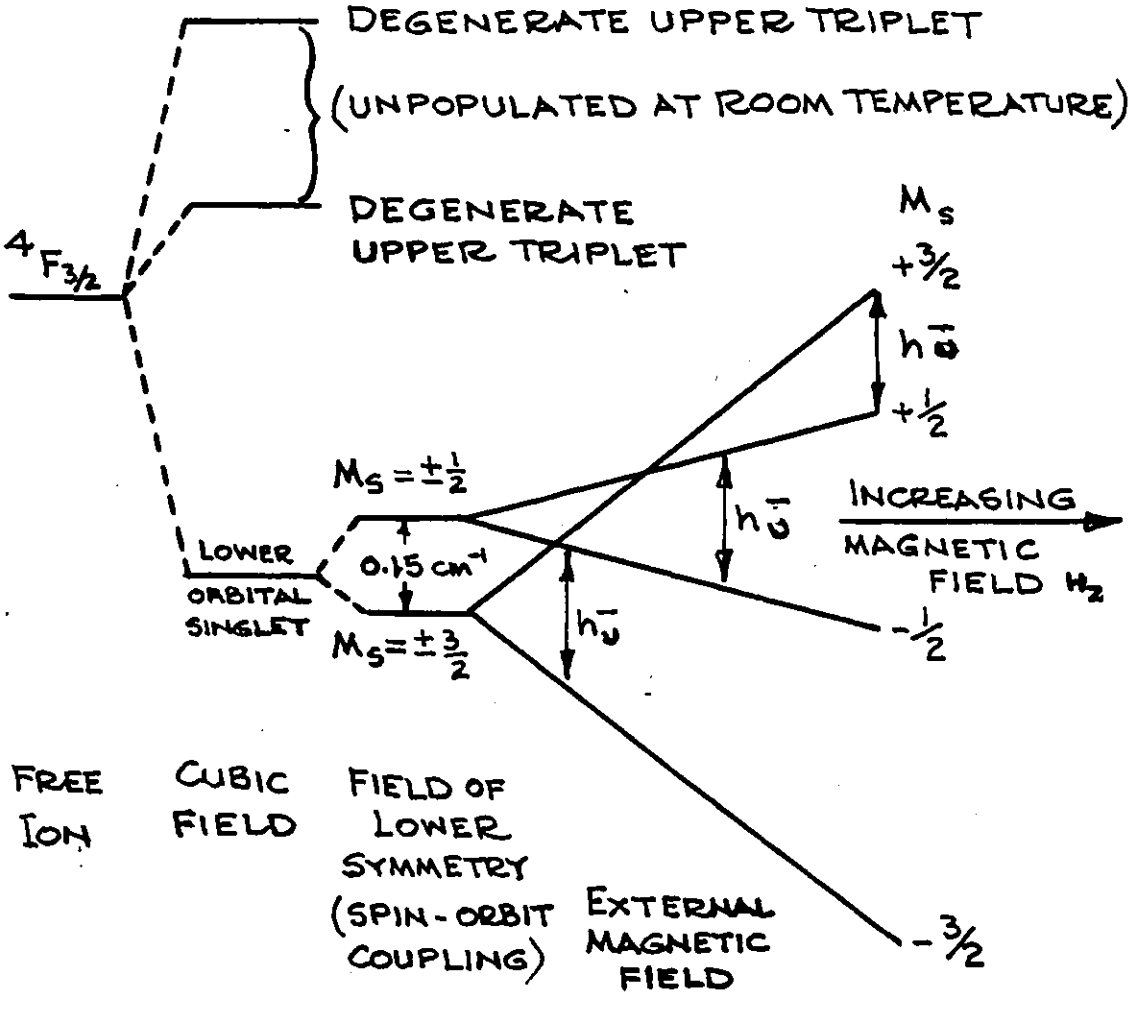

FIGURE 1.13 SPLITTING OF THE $^4F_{3/2}$ ENERGY LEVEL OF Cr^{3+} BY INTERNAL ELECTRIC FIELDS OF DIFFERENT SYMMETRY AND BY AN EXTERNAL MAGNETIC FIELD TO PRODUCE THREE RESONANCE LINES.

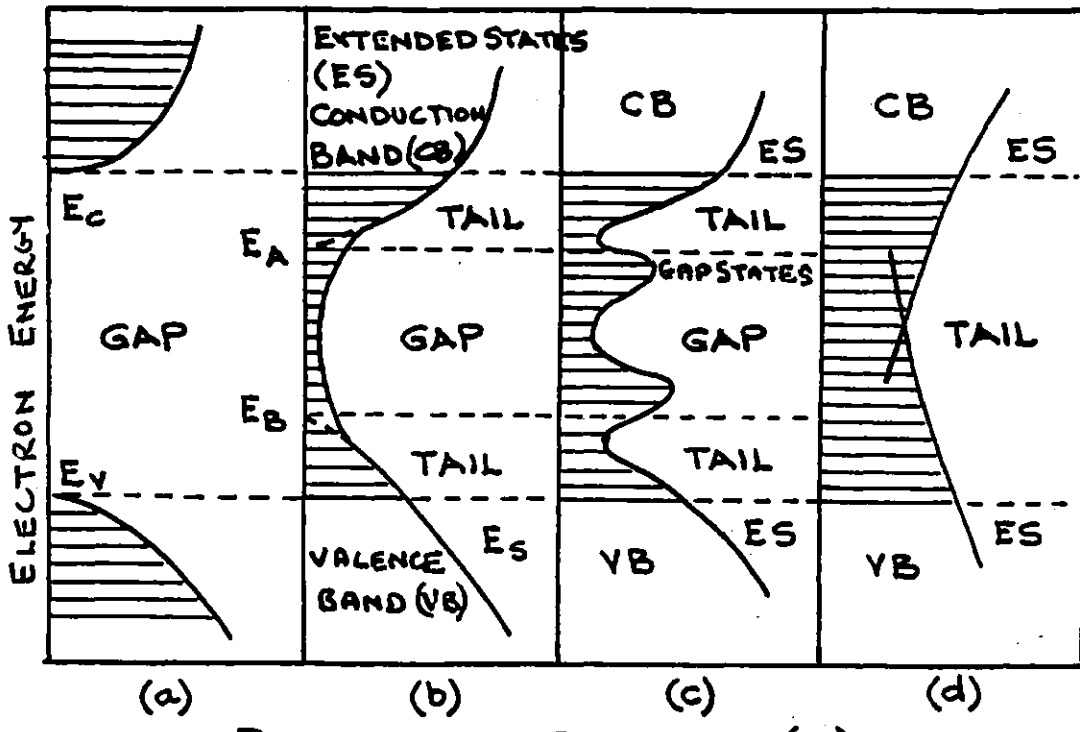

FIGURE 1.14 SCHEMATIC DENSITY-OF-STATES DIAGRAMS FOR SEMI-CONDUCTING GLASSES COMPARED WITH AN IDEAL CRYSTAL

(a) IDEAL CRYSTAL

(b) "IDEAL" GLASS

(c) GLASS WITH DEFECT STATES

(d) COHEN-FRITZSCHE-OVSHINSKY MODEL[71]

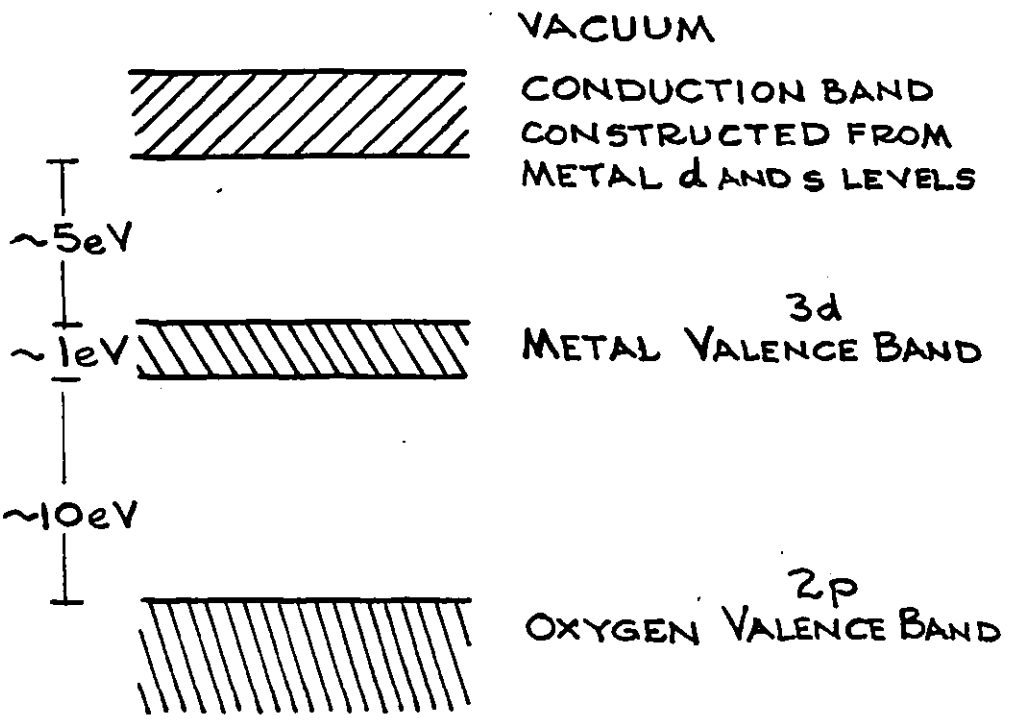

FIGURE 1.15 SCHEMATIC ILLUSTRATION OF THE BAND STRUCTURE OF A DIVALENT TRANSITION METAL OXIDE (AFTER CATLOW AND MUXWORTHY (73))

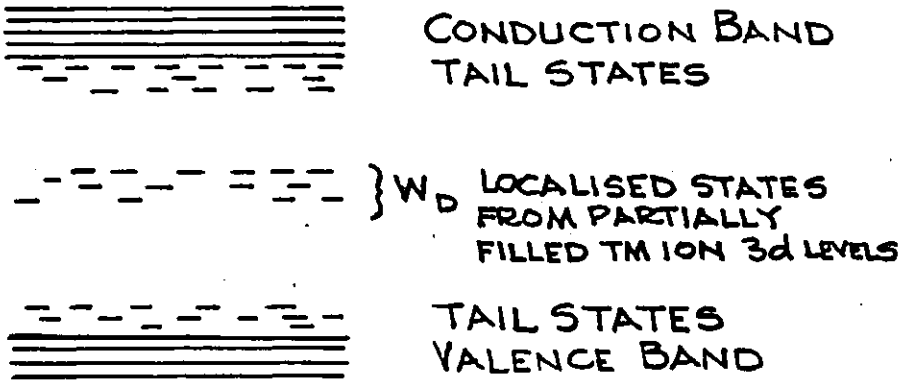

FIGURE 1.16 LOCALIZED ENERGY LEVELS OF THE TRANSITION METAL IONS IN A TRANSITION METAL OXIDE GLASS

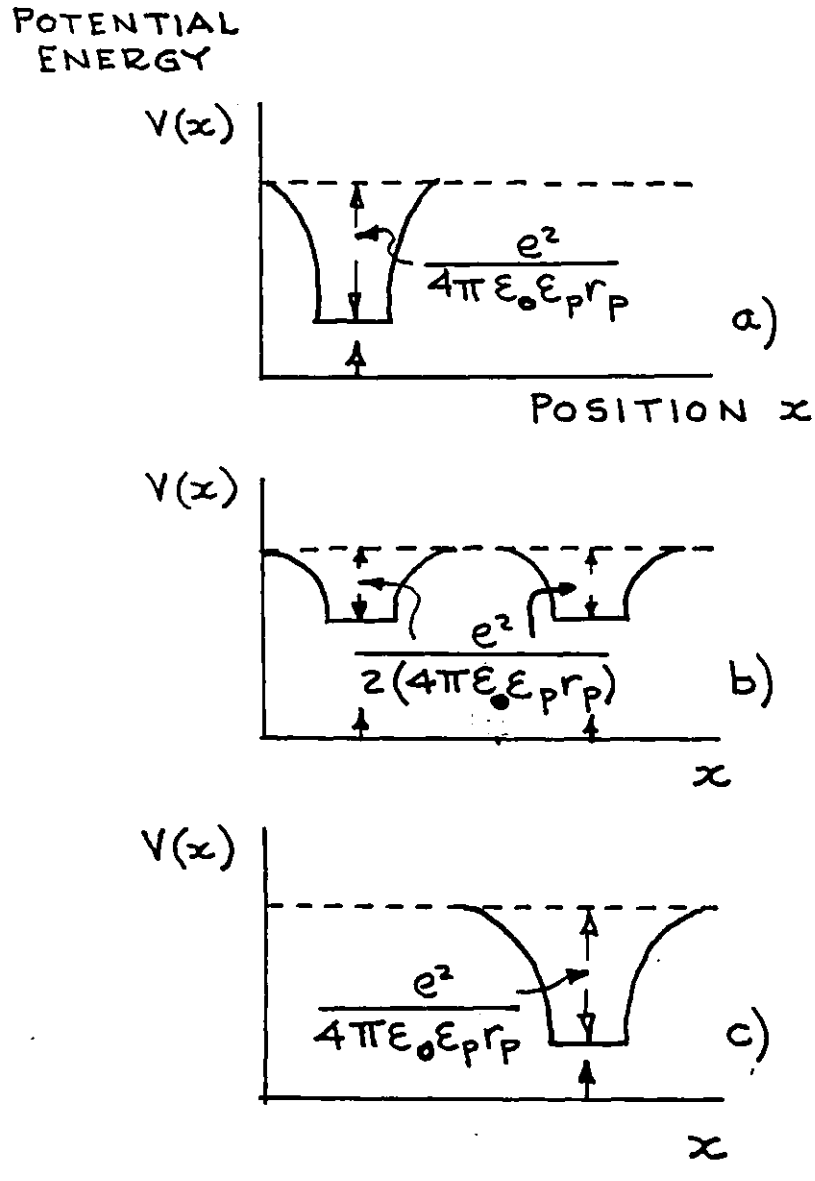

FIGURE 1.17. THE POLARIZATION WELLS FOR TWO TRANSITION METAL IONS IN GLASS
a) BEFORE HOPPING
b) THERMALLY ACTIVATED STATE WHEN ELECTRON CAN MOVE
c) AFTER HOPPING

[AFTER MOTT (76)]

CHAPTER 2

EXPERIMENTAL DETAILS

2.1 Glass melting

2.1.1 Choice of Base Glass Compositions

It has already been mentioned that most studies of electronic conductivity in oxide glass systems have been made on phosphate and borate glasses. It was therefore thought that a study of silicate glasses would be interesting and allow comparisons to be made. Most silicate glasses also possess superior chemical durability and mechanical properties to phosphate and borate glasses and are therefore more suitable for commercial applications, where such properties may be important.

Previous work at Imperial College had been concerned with the production of glass-ceramics (Slag-ceram) from blast furnace slags with the generic composition $CaO-MgO-Al_2O_3-SiO_2$. Such compositions are also excellent as base glasses for studies of electronic conductivity in vitreous systems, since they contain no mobile group IA alkali ions and will also dissolve appreciable concentrations of most TM oxides. It was natural therefore, that this study should commence with an investigation of a base glass with such a composition (base glass 1 in Table 2.1). A glass of this composition had also been used by Rouse[135] in his study of conduction in glass-ceramics containing vanadium and iron.

Manganese glasses were studied first since electronic conductivity in manganese glasses has received very little attention. However, it soon became apparent that the proportion of Mn^{3+} that could be retained in a glass with the composition of base glass 1 was limited. It was therefore decided to change the base glass composition to try and increase the Mn^{3+} concentration. This was achieved by increasing the basicity of the silicate glass by increasing the alkaline earth oxide concentration at the expense of silica and alumina. Magnesia was also replaced by lime to give a calcium aluminosilicate glass with the composition shown in Table 2.1 (base glass 2). To compare with this, another series of glasses was melted using base glass 3 which had alumina and silica increased at the expense of lime and hence had a lower basicity than base glass 2. The compositions of these glasses are shown on the $CaO-Al_2O_3-SiO_2$

phase diagram in Figure 2.1.

Even with base glass 2, the maximum proportion of Mn^{3+} attainable on melting in air was only 25%. It was thought desirable to try to produce some glasses with Mn^{3+} proportions of 40 - 50% to test the dependence of the conductivity on the redox ratio and to see if the conductivity became more typical of glasses which normally have an excess of the oxidised ion. Therefore a barium borate base glass was chosen, since glasses can be melted with high proportions of BaO to achieve a high basicity, and the author had had previous experience with this glass system. The melting temperatures of such glasses are also lower than the silicate glasses, which will favour the formation of Mn^{3+}. In any case, even if high proportions of Mn^{3+} were not achieved with these glasses, it was thought that the change in glass former would provide interesting results on the effect of glass former on the conductivity behaviour of a TM ion. This has also received little attention to date.

Later studies of iron and mixed iron-manganese glasses were made only with a silicate base glass and base glass 2 was chosen.

In the description which follows, the glasses and glass-ceramics have been coded according to the following general scheme. The first letter indicates the type of glass former: silicate (S) or borate (B), and the following letter(s) the TM ion: manganese (M), iron (F) or manganese and iron (MF). The letters are, in turn, followed by a number which indicates the order of melting and the letter C is appended if the particular sample had been heat treated to promote crystallization. All compositions are given in mole% unless otherwise stated.

2.1.2 Study of Redox Equilibrium in Glasses

It has been shown above that the electrical resistivity of an electronically conducting glass depends upon the ratio of redox states of the TM element. It is therefore important to be able to study the resistivity as a function of redox ratio to test the validity of the theoretical relationship described by the Mott equation (1.4.26).

The equilibrium redox ratio of a given multivalent ion in a glass will depend upon the following parameters:

(a) Concentration of the redox oxide

(b) Composition of the base glass i.e. basicity

(c) Melting temperature, and,

(d) Partial pressure (fugacity) of oxygen in the furnace atmosphere.

In some cases it can take many hours for equilibrium to be established within the melt and if equilibrium has not been established then obviously the period of melting will affect the redox ratio observed at any particular time. A final additional factor affecting the redox ratio is that if the glass is cooled slowly enough from the melting temperature, then the redox ratio may have time to partially adjust to the continually changing equilibrium conditions and so will not be representative of the true equilibrium at the melting temperature. This, however, should not apply in this study since glasses were rapidly quenched to a temperature at which oxygen diffusion rates were low.

Taking a particular redox oxide in a glass with a given concentration therefore leaves three independent means of controlling the equilibrium redox ratio: varying the melting temperature, furnace atmosphere or base glass composition. Generally the latter technique is inappropriate although, as mentioned already, it has been used in the present study where it was desired to both increase the yield of a particular redox state and investigate any effect of the base glass composition on the resistivity. Therefore melting temperature and the composition of the furnace atmosphere remain as variables.

Two methods can be used to investigate the range of redox ratios which can occur for a particular base glass composition:

(a) At equilibrium, by choosing a range of temperatures and oxygen partial pressures in the furnace atmosphere and allowing a series of melts to reach equilibrium at each combination;

(b) Following the path to equilibrium by sampling a single melt at different times at a given temperature. The redox state of the TM ion in the starting material can be varied to cover a wider range of redox ratios.

For the second method to be of use it must be assumed, or preferably shown by experiment, that the redox ratio is uniform throughout the whole volume of the melt i.e. that the sample is typical of the bulk melt and not just of the surface open to the

atmosphere. However, this technique has been used in the present study to gain information on the equilibrium redox ratios in various melts.

2.1.2.1 Calcium Magnesium Aluminosilicate Glasses Containing Manganese

Preliminary melts to study the approach to equilibrium in manganese glasses were made using base glass 1 with the composition shown in Table 2.1.

The dried raw materials to produce 100 g of glass were weighed to an accuracy of ±0.01 g, thoroughly mixed in a porcelain mortar and then melted in a 70 ml capacity Pt - 5% Au crucible at 1450°C in an electric furnace. After allowing sufficient time to produce a homogeneous, refined melt, typically a period of three hours, the glass was quenched, crushed and weighed.

From this weight, the weight of the manganese compound of the desired oxidation state to give the final glass composition was calculated. The manganese compound was weighed to an accuracy of ±0.0001 g, thoroughly mixed with the base glass and then the glass was remelted at the required temperature, with intermittent stirring using a platinum stirrer. Samples were poured at regular intervals for subsequent analysis.

In order to approach the equilibrium redox ratio from both sides, two glasses were prepared using manganese(II) carbonate (Analar grade), one containing 3wt% (SM1) and the other 6 wt% (SM3) manganese expressed as MnO, and attempts were made to produce compounds rich in Mn^{3+} which could be added to the batch.

Manganic oxide was prepared by heating β-MnO_2, a high purity pyrolusite ore supplied by Ever Ready Ltd., in air at 700°C for two hours. The conversion to Mn_2O_3 was confirmed by X-ray powder diffraction analysis. However, when this oxide was used as a batch material, a vigorous reaction occurred at the glass melting temperature of 1450°C which forced most of the batch over the top of the crucible. Analysis of the small quantity of glass remaining showed that only 9.6% of the total manganese was present as Mn^{3+}. In the light of this result a search was made for a compound rich in Mn^{3+} which might be stable at the glass melting temperature.

Glasser[136] has determined the CaO-Mn_2O_3 phase diagram and in

particular has reported X-ray diffraction data on calcium manganate ($Ca_2Mn_2O_4$). This was prepared by heating a mixture of 75wt% Mn_2O_3 and 25wt% CaO at 1430°C for 30 hr. It was stable up to its melting point of 1450°C, but the liquid rapidly lost oxygen at higher temperatures. Chemical analysis indicated an Mn^{3+} content of 85% of the total manganese.

Calcium manganate was prepared in the way described by Glasser and confirmed by X-ray powder diffraction analysis. Chemical analysis gave the Mn^{3+} content as 77% and 80% by two separate determinations. However, when the base glass and 6wt% calcium manganate were melted at 1400°C most of the glass was again lost because of vigorous frothing, with the remaining glass having just 9% of the total manganese as Mn^{3+}.

It is therefore very difficult to prepare glasses containing high proportions of Mn^{3+} by adding a compound rich in Mn^{3+} to the batch. At the glass melting temperature Mn_2O_3 must lose oxygen rapidly to produce MnO + Mn_3O_4 which dissolves in the glass. This is confirmed by the phase diagram for this system. Presumably calcium manganate also reacts, possibly with a component in the batch, when dissolving in the glass and yields oxygen, for when heated alone it is stable at 1400°C.

No attempt was made to melt in atmospheres other than air as the effect of increased p_{O_2} seems to be limited. Johnston[137] found that melting in pure oxygen did not significantly alter the Mn^{2+}/Mn^{3+} ratio in a soda-silicate glass.

2.1.2.2 Calcium Aluminosilicate Glasses Containing Iron

Base glass 2 (Table 2.1) was used for this and all the other iron glasses. The approach to equilibrium was studied from both sides by melting two glasses; the first containing initially only ferrous iron and the second, initially, only ferric iron.

Firstly, the calcium aluminosilicate base glass was prepared using dried raw materials as described above. After quenching, crushing and weighing, iron was added to the batch using either pure ferric oxide or reagent grade ferrous oxalate. Glasses were melted containing 0.1151 moles Fe per 100 g of base glass (equivalent to 6% FeO), at 1450°C and were sampled with time. At regular intervals a button of 30 mm diameter was poured, which was then annealed from 680°C. These samples were large enough to prepare a conductivity

specimen which was later sacrificed for chemical analysis and optical absorption spectroscopy. These two glasses are subsequently referred to as SF1 (prepared from Fe_2O_3) and SF3 (prepared from ferrous oxalate).

2.1.3 Details of Glass Melting for Conductivity Specimens

2.1.3.1 Calcium Aluminosilicate Glasses Containing Manganese: High Lime (Series SMH)

Base glass 2 with the composition given in Table 2.1 was used for this series since it was hoped that the higher basicity of this glass would increase the proportion of Mn^{3+} compared to the calcium magnesium aluminosilicate glass described above. Dilute glasses containing initially: 0.5% (SM15), 1.0% (SM16) and 2.0% (SM17) MnO_2 were prepared by melting 100 g of base glass followed by quenching, crushing and weighing. Manganese was then added as pure MnO_2 to obtain the desired composition, followed by melting at 1500°, 1450° and 1450°C respectively. Each glass was melted for at least five hours to attain equilibrium, with occasional stirring with a platinum blade stirrer to ensure homogeneity. The glass was then poured onto a large brass disc into circular buttons of 30 mm diameter, which were subsequently annealed by furnace cooling from 680°C.

Five more concentrated glasses containing approximately: 6% (SM11), 10% (SM18), 13% (SM12), 18% (SM13) and 23% (SM14) MnO_2, were prepared by thoroughly mixing the batch for 100 g of base glass with the appropriate weight of reagent grade MnO_2. These glasses were each melted at 1400°C for at least six hours with occasional stirring, then poured and annealed as above. In each case it was sought to keep the melting temperature as low as possible, consistent with the production of homogeneous glass, to encourage formation of Mn^{3+}. Attempts to produce glasses with concentrations of MnO_2 of greater than 23% were not successful as the solubility limit was exceeded.

2.1.3.2 Calcium Aluminosilicate Glasses Containing Manganese: Low Lime (Series SML)

Base glass 3 with the composition shown in Table 2.1 was used for this series since the lower basicity should yield lower proportions of Mn^{3+} compared to equivalent glasses in series SMH. The

crystallization behaviour would also be expected to be different to series SMH. Only concentrated glasses were prepared containing: 6% (SM7), 13% (SM8), 18% (SM9) and 23% (SM10) MnO_2, using techniques and melting conditions identical to those of the concentrated glasses in section 2.1.3.1. It is seen that these concentrations are equivalent to those in series SMH.

2.1.3.3 Barium Borate Glasses Containing Manganese (Series BM)

The phase diagram for the binary $BaO-B_2O_3$ system is shown in Figure 2.2. No information is thought to be available for the quaternary $MnO-Mn_2O_3-BaO-B_2O_3$ system. Binary barium borate glasses can be prepared easily in the region between 15-40% BaO, which corresponds to an area of low liquidus temperatures on the phase diagram. The range of glass formation may be extended, however, by a few per cent on either side by rapid quenching. The following glasses were melted:

(a) One glass with composition $18\%BaO-77\%B_2O_3-5\%MnO_2$, melted at 1100°C (BM7)

(b) Two glasses with composition $38\%BaO-57\%B_2O_3-5\%MnO_2$, one melted at 1050°C (BM5) and the other at 980°C (BM8), just above the liquidus temperature. This was to provide different redox ratios.

(c) Two glasses with composition $36\%BaO-54\%B_2O_3-10\%MnO_2$, again one at 1050°C and the other at 980°C (BM6 and BM9 respectively).

(d) Two glasses with a $BaO:B_2O_3$ ratio of 2:3 as in (b) and (c) above, containing 15% (BM10) and 20% (BM11) MnO_2. Both were melted at 1100°C.

Each of these seven glasses was melted in a Pt-5%Au crucible using Analar grade barium carbonate and boric acid, and reagent grade MnO_2 as source materials. Batches to produce 100 g of glass were weighed out and thoroughly mixed prior to melting and the melts stirred several times to ensure homogeneity. Blocks were poured as above which were annealed at temperatures ranging from 560° - 600°C depending on the manganese content.

Several attempts were made to produce glasses with higher BaO contents to further increase the basicity and hence the proportion of Mn^{3+}. A glass containing $50\%BaO-45\%B_2O_3-5\%Mn_2O_3$ showed extensive crystalline patches, both on the surface and in the bulk of the specimen and was therefore rejected.

One other area of low liquidus temperature occurs in the binary

system at 61%BaO-39%B_2O_3 at which it might be possible to produce glasses. A binary glass with the composition given above crystallized completely on cooling, but compositions with a similar BaO: B_2O_3 molar ratio containing 5% and 10% MnO_2 showed extensive glassy regions when quenched. The unannealed glasses, however, had little mechanical strength and tended to crystallize fully on annealing, therefore work with these compositions was abandoned.

2.1.3.4 Calcium Aluminosilicate Glasses Containing Iron (Series SF)

This series of glasses used base glass 2 and had equivalent iron ionic concentrations to those in manganese series SMH. Similar techniques for batch mixing and melting were used. Dilute glasses with: 0.25% (SF2), 0.5% (SF8) and 1.0% (SF7) Fe_2O_3, added as pure ferric oxide, were melted at 1500°, 1500° and 1450°C respectively. Samples were poured and then annealed from 680°C.

More concentrated glasses were melted at 1450°C with: 5% (SF6), 6.5% (SF4) and 9% (SF5) Fe_2O_3 again added as pure ferric oxide. The annealing temperature was again 680°C.

All these glasses were melted for at least six hours to approach equilibrium, with frequent stirring to ensure good homogeneity.

2.1.3.5 Mixed Manganese-Iron Glasses (Series SMF)

Five glasses were melted in this series with equal molar proportions of manganese and iron dissolved in the base glass.

The three dilute glasses containing 0.5% (SMF1), 1.0% (SMF4) and 2.0% (SMF5) total TM oxide, intended primarily for spectroscopic measurements to determine the effect of mixing the two TM oxides, were prepared as in section 2.1.3.1. Firstly, 100 g of base glass was melted, pure ferric oxide and manganese dioxide added as required, and the glasses melted at 1450°, 1450° and 1400°C respectively. To ensure a homogeneous distribution of TM ions throughout the glass, the glass was quenched during the latter melting period, finely crushed and remelted. The total melting time was four hours. These mixed TM glasses have nominally the same composition as the dilute iron and manganese glasses as follows: SMF1 ≡ SM15, SF2, SMF4 ≡ SM16, SF8 and SMF5 ≡ SM17,SF7.

The other two glasses with equal proportions of iron and manganese were more concentrated and contained 0.2302 and 0.3588 moles of TM ion in total added to 100 g of base glass (SMF2 and SMF3

respectively). These were effectively combinations of equivalent iron and manganese glasses: SMF2 ≡ SM11 + SF1, SMF3 ≡ SM18 + SF6. These glasses were prepared in a similar way to the concentrated manganese glasses described above and melted at 1450° and 1350°C respectively, with one intermediate quench and crush. The second glass (SMF3) produced a crystalline residue which settled on the bottom of the crucible indicating that the solubility limit had been exceeded, however, the glassy portion was used.

Two more glasses each with a total of 0.2302 moles of TM ion, but with iron : manganese ratios of 7 : 3 and 9 : 1, were melted to form a series with SMF2 (5:5 ratio) in which manganese was progressively replaced by iron whilst keeping the total TM ion content constant. These glasses, referred to as SMF2A and SMF2B respectively were melted by adding ferrous oxalate and manganese dioxide to 100 g of premelted base glass. Ferrous oxalate was used as the starting material, along with a short melting time of just 45 minutes at 1425° C, to retain a high proportion of ferrous ion in the glasses. Premelting of the base glass allowed homogeneous glasses to be produced in such a short time. All glasses in this section were annealed from 680°C.

2.2 Density Measurement

The densities of all the glasses were measured using the Archimedes method. One of the annealed blocks, weighing about 15 g, was suspended by a fine platinum wire on a single pan balance capable of reading to ±0.0001 g, and weighed in both air and distilled water. The density was calculated and values are quoted to ±0.001 g cm^{-3}. No change in weight could be detected for any of the glasses whilst immersed in water.

2.3 Chemical Analysis of the Glasses

One problem often encountered when attempting to chemically analyse silicate glasses is that the glass cannot usually be dissolved without the use of concentrated hydrofluoric acid. This acid frequently interferes with the chemical analysis, particularly if the redox ratio is being determined. For example, ferrous ion is rapidly oxidised in air in the presence of fluoride ions which renders redox titrations involving ferrous ion inaccurate. Cerium ions are also complexed with similar consequences. For this reason

borate and phosphate glasses are usually preferred for studies of redox equilibrium and also electronic conductivity. It was fortunate therefore, that the low silica content of the calcium aluminosilicate glasses (base glasses 2 and 3) allowed dissolution to be accomplished using strong sulphuric or hydrochloric acids, without the need for additions of hydrofluoric acid. However, the $CaO-MgO-Al_2O_3-SiO_2$ glasses containing manganese used for redox studies were more difficult to dissolve, making the use of HF unavoidable. Both dissolution and titration were performed under an oxygen free nitrogen atmosphere, further deoxygenated by passing the gas through a tube furnace containing copper wool heated to 450°C, to prevent oxidation of the reducing agent in the Mn^{3+} determination.

Following the recommendations of Hillebrand et al[138] only small quantities of HF were used and after the glass had dissolved, excess HF was removed by complexing with boric acid, to prevent fluoride ions complexing with the cerium sulphate used for back titration.

2.3.1 Manganese Glasses

It is reasonable to assume that with the melting conditions described above, manganese will only be present as Mn^{2+} or Mn^{3+}. Trivalent manganese may be conveniently estimated by redox titration and total manganese either colorimetrically or by atomic absorption spectroscopy. The following techniques were used for both borate and silicate glasses.

2.3.1.1 Estimation of Trivalent Manganese

Mn^{3+} is unstable in acidic solution and is therefore easily reduced by reducing agents such as ferrous ammonium sulphate. The analysis is based on one described by Paul[139].

For the determination, a quantity of 0.3-1.0 g of glass, depending upon the total manganese concentration, was finely ground in an agate mortar under methyl chloroform and accurately weighed into a glass beaker. To this was added 20 ml of 0.02N ferrous ammonium sulphate and 50 ml of 6N sulphuric acid to dissolve the glass. The dissolution was effected in a reaction vessel under an inert atmosphere of oxygen free nitrogen to prevent oxidation of ferrous ion by the air. In some cases, for the more dilute glasses, it was necessary to gently warm the vessel to completely dissolve

the glass. For SM1 , SM3 and other glasses with base glass 1, 4-5 ml of 40% HF was added to the sulphuric acid and the dissolution was carried out in a plastic beaker.

After dissolution, the excess HF, if present, was complexed with boric acid and the unreacted ferrous ion determined by back titration with 0.025M ceric sulphate solution, detecting the end point either potentiometrically or using ferroin as an indicator. The titration was also usually performed under an OFN atmosphere.

For potentiometric analysis, a platinum electrode and a standard calomel reference electrode were used and the solutions were bridged by a 3% agar saturated KCl gel in a flexible polyethylene tube. The electrochemical e.m.f was measured by a Keithley electrometer and the end point determined graphically using the second derivative method.

2.3.1.2 Total Manganese

This was performed either colorimetrically for glasses containing greater than 6% MnO, using the standard periodate method, or by atomic absorption spectroscopy (AA).

For the periodate method the weight of glass needed to give 24 mg Mn when dissolved in one litre was calculated from the batch composition. This weight of ground glass was dissolved in 100 ml of 2N H_2SO_4 and the solution made up to a litre using distilled water. A portion of 25 ml was transferred to a 50 ml flask to which was added 5 ml conc HNO_3 and 1 g KIO_4. The solution was boiled for two minutes and then kept in a water bath at above 90°C for a further 10 minutes to oxidise all of the manganese to Mn^{7+}, hence giving a purple coloration.

The flasks were allowed to cool, the solution made up to 50 ml with distilled water and the optical absorption measured in a 1 cm cell at 545nm using a Unicam SP600 Series II spectrophotometer. The optical absorption was compared with standards made from a 1000 ppm Mn solution treated as above, to estimate the manganese concentration.

For the more dilute glasses, the amount of glass that would need to be dissolved would produce an appreciable amount of $CaSO_4$ precipitate, which would interfere with the method above. Therefore the appropriate weight of ground glass to give 12-15 mg Mn per litre

of solution was dissolved in 50 ml 9N HCl, with additions of HF for base glass 1 compositions, and the solution diluted to 1 1 with distilled water. Standards were prepared containing 0-20 mg/1 of manganese from the 1000 ppm solution but diluted with a solution of the base glass treated as above. This was to provide a blank to guard against errors from any interfering ions. Manganese concentrations were determined using a Perkin Elmer 290B atomic absorption spectrometer with standard operating conditions. By also measuring some standards prepared with water it was determined that there were no interfering ions.

2.3.2 Iron Glasses

With the melting conditions used in this study, iron is only expected as Fe^{2+} and Fe^{3+}. Glasses have been analysed for Fe^{2+} and total iron and Fe^{3+} was calculated by difference.

2.3.2.1 Estimation of Divalent Iron

The analysis is based on the oxidation of Fe^{2+} by iodine monochloride as described by Hey[140].

A solution of iodine monochloride was prepared by dissolving 3.22 g potassium iodate in 37.5 ml water, then adding 5.00 g potassium iodide and making up to 100 ml with 9N HCl. A volume of 10 ml of this concentrated solution was diluted to 100 ml with 9N HCl to produce a working solution which was adjusted to just remove traces of free iodine, from a carbon tetrachloride layer, by adding dilute KIO_3 or KI solutions dropwise as required.

A suitable weight of glass, usually 0.1-0.3 g, was finely ground under methyl chloroform and accurately weighed into a 100 ml volumetric flask. To this was added 5 ml ICl with 2 ml CCl_4 to dissolve the liberated iodine and 50 ml 9N HCl to dissolve the glass. The flask was stoppered and shaken in a high speed shaker for 20 minutes to completely dissolve the glass and oxidise Fe^{2+}.

Free iodine was determined by titration against 0.004N KIO_3. The reactions are as follows:

$$2Fe^{2+} + 2ICl + 2H^{+} = 2Fe^{3+} + 2HCl + I_2$$

$$2I_2 + KIO_3 + 6HCl = KCl + 5ICl + 3H_2O$$

Therefore: 1 ml 0.025M KIO_3 ≡ 0.005585 g Fe^{2+}.

2.3.2.2 Total Iron

Total iron was measured exclusively by atomic absorption spectroscopy. Approximately 0.1-0.3 g of finely powdered glass, depending on the iron concentration, was accurately weighed and dissolved in 50 ml 9N HCl. The solution was diluted with distilled water to give a final iron concentration of 12-15 mg/l. Standards were prepared containing between 0-20 mg Fe/l from a 1000 ppm solution using a solution of base glass as described above. Iron concentrations were determined using a Perkin Elmer 290B AA spectrometer with standard operating conditions. No interference from other ions was observed.

2.3.3 Mixed Iron-Manganese Glasses

Generally speaking it is not possible to chemically analyse a glass with two or more TM elements for individual redox ion concentrations since the ions will react when the glass is dissolved hence changing the concentrations. The best that can be achieved is an estimate of the total concentration of oxidising or reducing ions. This was not performed in the present study since it was hoped that the individual Fe^{2+} and Mn^{3+} concentrations could be determined by optical absorption spectroscopy.

The only chemical analysis applied to these glasses was therefore total iron and manganese concentrations, both of which were performed by AA spectroscopy on the same sample. Samples containing suitable TM concentrations were prepared in a similar way to the single iron and manganese glasses described above. No interference between iron and manganese was observed.

2.4 Optical Absorption Spectroscopy

Optical absorption spectra were obtained for most of the glasses using a Perkin-Elmer 450 UV-VIS-NIR double beam recording spectrophotometer. In all cases air was used as reference. Two wavelength ranges were scanned: the near infra-red between 600 - 2700 nm for which the transmittance of the specimen was recorded and secondly, the visible- near ultraviolet region between 350 - 750 nm for which the absorbance of the specimen was recorded.

The measurements were performed on thin sections prepared by grinding a block of glass and diamond polishing to a 1 μm finish. For the dilute glasses the intensity of the colour was low enough

for thin discs of unsupported glass to be used, but for the more intensely coloured glasses the specimen was cemented onto a microscope slide with canada balsam after one side had been polished. The specimen was then thinned, polished and measured with the slide as a support. The absorption of the slide and canada balsam was subtracted from the total absorbance when the absorption curves were plotted.

In this study, optical absorption data are reported according to the current recommended spectrometry nomenclature as given by Angell and Wong[50]:

(a) % Transmission = $I/I_o \times 100$ (2.1)

where I = transmitted beam intensity

and I_o = incident beam intensity.

(b) Absorbance = $-\log (I/I_o)$. (2.2)

(c) Absorptivity (α) is defined by Beer's law:

$$dI = -I\,dl \tag{2.3}$$

$$\alpha = -\log (I/I_o) / l \tag{2.4}$$

where l is the thickness of the sample.

(d) At an absorption peak which can be assigned to a particular ionic species, the molar absorptivity is defined as:

$$\varepsilon = \alpha/c = -\log (I/I_o) / lc \tag{2.5}$$

with units of litre $mole^{-1}$ cm^{-1}, where c is the concentration of absorbing species in moles l^{-1}, which equals the concentration of absorbing species per gram of glass multiplied by the density of the glass in g l^{-1}.

The energy of the absorption in units of cm^{-1} or electronvolts has been used to report data, in preference to wavelength:

$$1 \text{ eV} = 8065.45 \text{ cm}^{-1} \equiv 1240 \text{ nm}.$$

2.5 Electron Paramagnetic Resonance

Several glasses and some glass-ceramics were selected for study by EPR spectroscopy. In each case the material was coarsely powdered, taking particular care to avoid contamination by metallic iron and the sample was held in a quartz tube purged with nitrogen. The EPR spectrum was recorded as the first derivative of the absorption using a Varian E12 EPR spectrometer. Measurements were

only made at X band frequency at room temperature.

2.6 Crystallization Studies

All of the silicate glasses, except the dilute mixed manganese-iron glasses SMF1, SMF4 and SMF5, were given a series of two stage heat treatments to see if bulk internal nucleation and growth could be produced. Small pieces of glass, approximately 1 cm cubed, cut from one of the annealed blocks were placed in an electric muffle furnace at the chosen nucleation temperature for a period of at least three hours and in some cases longer. After this nucleation heat treatment, the temperature of the muffle was raised to the selected temperature for crystal growth and samples were removed after one hour at this temperature. Polished thin sections were then prepared to measure the extent of crystallization.

Each glass received nucleation heat treatments at a range of temperatures between 710 - 830°C, followed by a standard crystal growth treatment at 930±10°C. If this temperature proved too low, as indicated by little observed surface crystallization, the growth temperature was raised progressively to as high as 1000°C and/or the time was increased.

Once heat treatment conditions for a particular composition had been established such that bulk internal crystallization was produced, further blocks of glass were crystallized for optical and electron microscopy, X-ray diffraction analysis and electrical measurements. Some glasses were heat treated at the growth temperature for various times, withdrawing a sample after each interval to observe the progress of crystallization.

2.7 Optical Microscopy

Optical examination using transmitted light was carried out on all of the glasses, to establish homogeneity and absence of crystalline phases, as well as on heat treated materials. In each case thin sections were prepared mounted on glass microscope slides with Lakeside cement. For preliminary crystallization experiments to establish heat treatment conditions the thin sections were prepared with 600 grade carborundum paper; however, sections for more detailed examination and photomicrography were polished to a 1 μm diamond finish. A Reichert polarising microscope fitted with a 35 mm camera was used for optical examination and photomicrography.

2.8 X-Ray Diffraction Analysis

X-ray diffraction analysis has been used both to examine glasses rich in TM oxide, to detect evidence of crystallinity and also to determine the crystal phases present in the glass-ceramics. Compositions containing iron were examined using a Gunier De Wolff focussing camera with cobalt K_α radiation.

Cobalt radiation is unsuitable for materials containing manganese because its characteristic wavelength is shorter than the manganese K absorption edge, therefore fluorescent radiation is produced which fogs the film and masks low intensity reflections. Therefore for manganese specimens copper radiation was used, with either a Debye-Scherrer camera or a Phillips diffractometer.

One sample (SM10C) was also analysed by the Natural History department of the British Museum using iron radiation.

2.9 Electron Microscopy

Transmission electron microscopy has been used on certain samples for the following reasons:

(a) To detect any phase separation (liquid-liquid) or fine scale crystallization of some concentrated glasses (SM13, SM14).

(b) To investigate crystallization behaviour within the microscope (SM10, SF4).

(c) To examine conventionally crystallized glass-ceramics (SM10C, SM12C, SM13C and SM14C).

The latter has been supplemented by scanning electron microscopy for both manganese and iron glasses.

2.9.1 Transmission Electron Microscopy

Samples were prepared by either mechanical thinning or blowing, followed by ion beam thinning.

The first method was based on that described by Clinton[141]. A small piece of the glass or glass-ceramic was polished on one side to a 1 μm finish and then cemented to a glass slide with Lakeside cement. The specimen was ground on a 600 grade carborundum disc until the edges began to disintegrate, when a final polish to a 1 μm finish was given. The thickness of the specimen at this stage was between 30-40 μm. A 3 mm single hole copper microscope grid was stuck onto the sample using a PVA adhesive and the sample released

from the glass slide by soaking in toluene.

The specimen was thinned further using a Technics Auto MIM ion beam thinner until a small hole appeared in the centre of the specimen. Generally the angle of incidence of the beams was 15^{o} although once a hole had appeared this was reduced to 10^{o} to remove surface irregularities. As the angle is reduced the thinning rate is also reduced, so a compromise must be reached between thinning time and surface smoothness. At angles of $10-15^{o}$ the removal rate was typically 1-2 μm/hr with an acceptable degree of surface irregularity.

The second method was used to prepare some glass specimens for crystallization studies in the microscope, by blowing down a silica glass tube onto which a small gob of molten glass had been gathered. The bubble formed disintegrated into a shower of small pieces with thicknesses down to 1 μm. For examination by the high voltage electron microscope these were just thin enough, although some were ion beam thinned further at an angle of incidence of 10^{o}. This method is of little use for investigating any microscopic structure that might be present in the glasses as cooling rates are so much higher than bulk quenched and annealed specimens.

Most of the specimens were examined using an AEI EM7 high voltage electron microscope (HVEM) operating at 1000 kV. At this voltage a thickness of up to 1 μm is sufficiently transparent to the electron beam. In-situ crystallization experiments were made using a platinum strip heater incorporated within the specimen holder surrounding the copper grid. It was not possible to incorporate a thermocouple alongside the specimen, so temperatures were therefore estimated from the power input to the heater and a previous calibration.

For some preliminary investigations of the glass-ceramics an AEI EM6G microscope operating at 100 kV was used. However, the reduced penetrating power of the beam allowed only small areas of the specimen to be examined compared to the HVEM.

Generally, charging of the specimen was not a problem, though some of the earlier observations were carried out on specimens coated with evaporated carbon.

2.9.2 Scanning Electron Microscopy

Routine investigations were made on the morphology of crystalline

phases in glass-ceramics SM10C, SM13C, SF4C and SF5C using a Cambridge 600 scanning electron microscope.

Freshly fractured surfaces were prepared and etched in 1% HF solution for five seconds to preferentially dissolve the glass between dendrites and therefore enhance the surface relief between glass and crystalline phases. The sample was cleaned in an ultrasonic bath to remove corrosion products and then fixed to an aluminium stub using Durofix adhesive. To prevent charging in the electron beam, samples were coated with a 100 Å thick layer of gold by dc sputtering. Some samples were examined without HF etching but were found to be featureless.

2.10 Electron Probe Microanalysis

It is of considerable importance to know the distribution of the TM ions in a glass-ceramic to be able to interpret the electrical properties of the specimen. TM ions may either be rejected by a growing crystal or may crystallize out, either as a single TM oxide or in combination with other oxides. Much of this information may be obtained from optical microscopy used in conjunction with X-ray diffraction analysis, but electron probe microanalysis (EPMA) is also an extremely valuable tool.

Two techniques have been used. In most cases polished specimens were scanned using a Joel EPMA. With this instrument the specimen can be moved while twin crystal spectrometers are set to monitor different elements. Thus a continuous measure of changes in Ca, Al, Si or Mn can be recorded as the beam moves from glassy to crystalline areas. Quantitative analysis can only be obtained after calibration against standards.

For further examination of SM10C a Microscan EPMA was used which enabled the composition of an area of about 5 μm in diameter to be determined. Thus various small areas of both glassy and crystalline phases could be analysed individually, which was impossible using bulk chemical analysis. However, for SM10C the crystallite size was of the order of the electron beam diameter hence analyses were subject to interference from surrounding matrix material.

Specimens for both instruments were made by embedding a small block of glass-ceramic in a cold setting resin, then grinding and

polishing the surface to a ¼ μm diamond finish. Carbon coating was used to reduce charging.

2.11 D.C. Resistivity Measurements

Specimens for dc resistivity measurements were ground to a thickness of between 1.5-3.5 mm from one of the annealed blocks and polished to a 6 μm finish. Gold contacts were applied by dc sputtering in a conventional three terminal guarded arrangement. The absence of electrode effects was confirmed for two specimens by measuring with both gold and silver electrodes, the latter applied as silver DAG. No significant difference in results between the two electrodes could be detected.

The resistance was measured by the V-I method. A stabilised dc voltage was applied to the specimen held in the apparatus shown in Figure 2.3 and the resulting current was measured by a Keithley 602 high impedence electrometer. To check for linear V-I plots, i.e. ohmic behaviour, a series of voltages between 5-500 V was applied. Two regulated power supplies were used: a Heathkit IP-20U for the range 5-50 V and an APT 501 from 201-500 V. Deviations from ohmic behaviour were found for some of the glass-ceramics but the reasons for this will be discussed in Chapter 4 below.

Occasionally during measurements, the voltage polarity applied to the specimen was reversed but no change in current (except in sign) was observed, indicating that there were no rectifying contacts. Some authors[142] have reported switching effects in some TM oxide glasses but no such effects could be found in these glasses or glass-ceramics.

The resistance was measured at 50°C intervals from room temperature to about 500°C, though for some glasses readings were extended to 700°C. For the dilute glasses, measurements at low temperatures were not possible so the specimen was heated until readings could be taken. Temperatures were accurately measured using a Pt - Pt/13%Rh thermocouple placed next to the specimen and the furnace temperature was controlled to ±1°C using a phase-angle Eurotherm controller with an independent thermocouple. To check for temperature stability and also the presence of any time dependence of the current, the thermocouple and electrometer outputs were displayed on a Linseis chart recorder.

The resistivity (ρ) of the glass or glass-ceramic was calculated using the standard expression:

$$\rho = \frac{V}{I} \times \frac{\pi(d/2)^2}{b} \quad \Omega \text{ cm} \qquad (2.6)$$

where V is the applied voltage, I the current, d the diameter of the smaller electrode and b the thickness of the specimen.

2.12 A.C. Resistivity and Dielectric Properties

Several of the glasses and glass-ceramics with relatively low dc resistivities were selected for ac resistivity measurements. Generally the same specimen as used for the dc measurements was used although for SF1.4 and SF3.5, thinner discs with a thickness of 0.16 mm were prepared.

The specimens again had a three terminal sputtered gold electrode arrangement and were placed in a similar rig to that used for dc resistivity after the measuring bridge had been trimmed. This was done with the leads connected to the sample holder, which was in position in the furnace. The conductance and capacitance of the specimen were measured in the frequency range between 0.1 - 40 kHz by balancing the output of a Wayne Kerr AF S121 signal generator applied to the specimen with a Wayne Kerr B221 (Mk III) universal bridge using a Dymar AF wave analyser type 771A as the detector.

The sample was heated using a dc powered Kanthal wound furnace and the temperature measured using a chromel-alumel thermocouple placed alongside the specimen. At each temperature, before ac measurements were made, the dc resistance of the sample was checked using either the V-I method as described above or with a Keithley 602 electrometer in the resistance mode.

2.13 Thermoelectric Power

An attempt was made to measure thermoelectric voltages on some of the more conducting glasses.

A purposely designed rig was built, of which an enlarged schematic diagram of the specimen holder is shown in Figure 2.4. The specimen was a piece of glass 30 -40 mm long and approximately 10 x 10 mm in section, cut from a specially poured block. The ends were ground and polished to be plane and parallel and sputtered

with gold to form the electrodes. The specimen was held between two platinum foil electrodes and was supported by two brass blocks, one of which was spring loaded. The brass and platinum were separated by alumina plates to prevent electrical contact.

The specimen and holder were heated in a small Kanthal wound furnace and a reversible temperature difference could be established at the chosen measuring temperature using the independently controlled heater associated with each end of the specimen. The temperature at each electrode was accurately measured using a chromel-alumel thermocouple embedded in a small recess in the alumina plate close to the platinum foil. Temperatures were displayed on a twin pen recorder for easy determination of the temperature difference across the specimen.

Once the temperature differential had been established, the thermoelectric voltage was measured by a Keithley 602 electrometer with its unity gain terminals connected to a Data Precision digital multimeter to give an accurate digital output.

TABLE 2.1

COMPOSITIONS OF THE SILICATE BASE GLASSES

Oxide	Raw Material	Drying Temp (^{o}C)	Composition (wt%)		
			Base Glass 1	Base Glass 2	Base Glass 3
SiO_2	Thermal Syndicate Crushed Quartz	1000	42	40	50
Al_2O_3	Analar Al_2O_3	1350	20	15	19
CaO	Analar $CaCO_3$	110	28	45	31
MgO	Analar MgO	1350	10	-	-

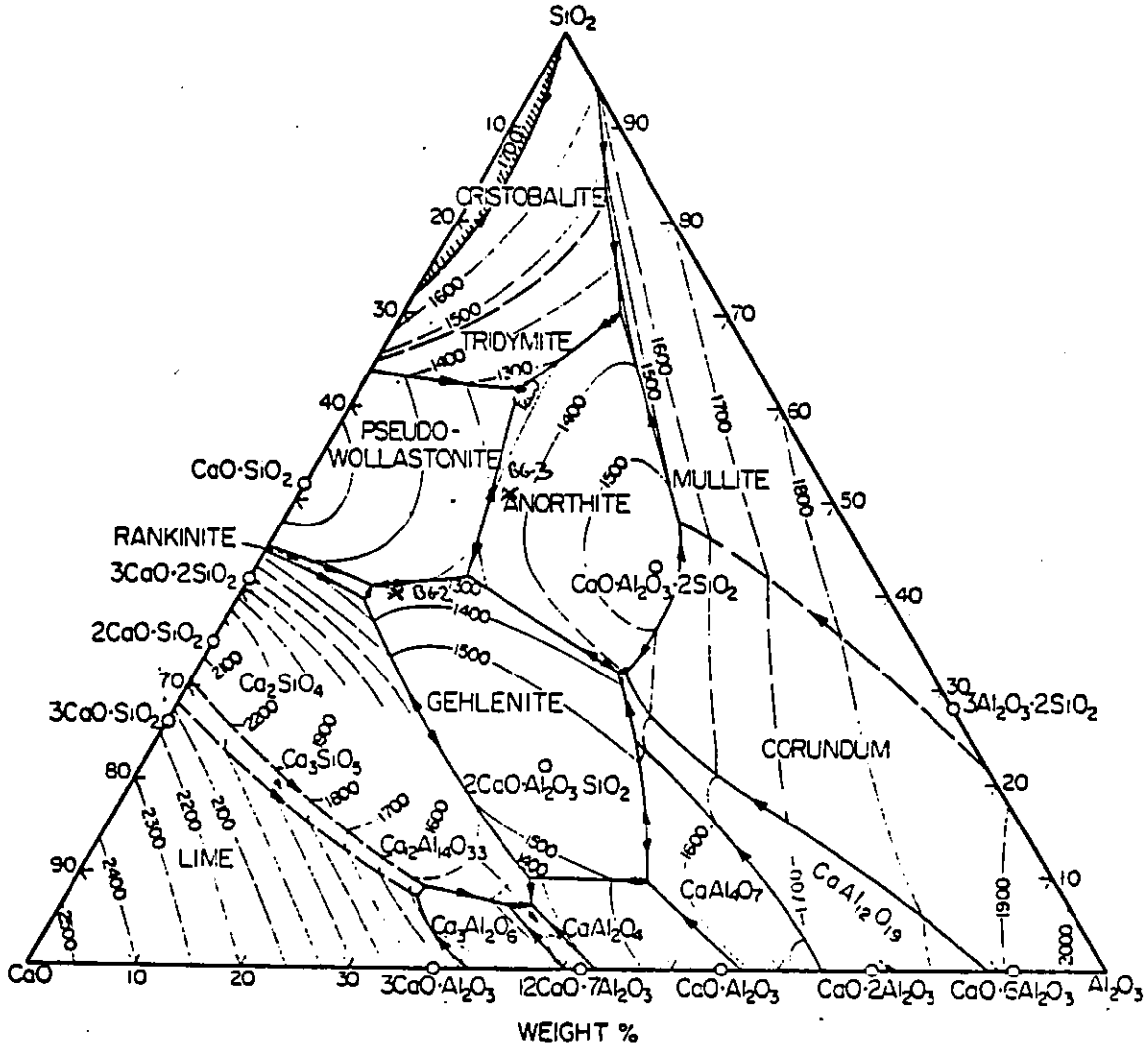

Figure 2.1 Phase Diagram of the $CaO-Al_2O_3-SiO_2$ System

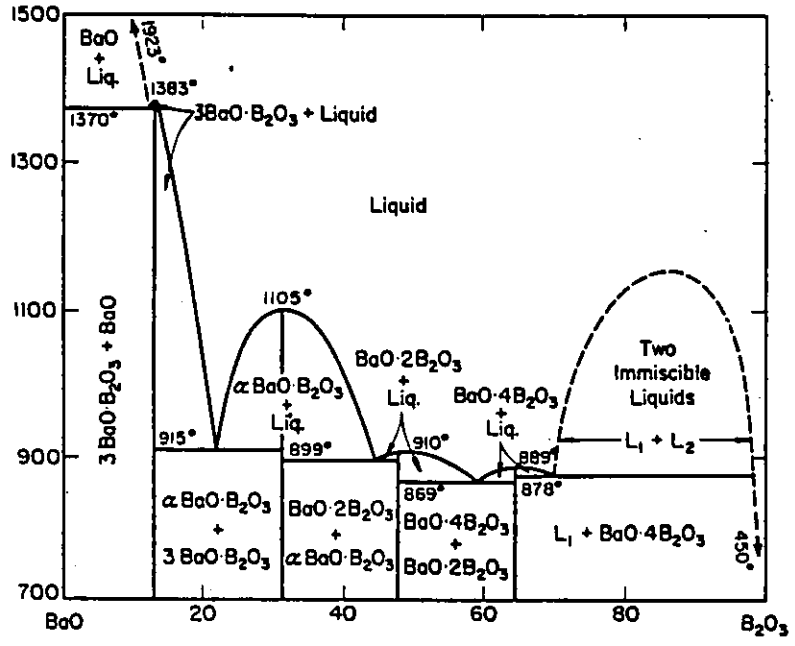

Figure 2.2 Phase Diagram of the $BaO-B_2O_3$ System

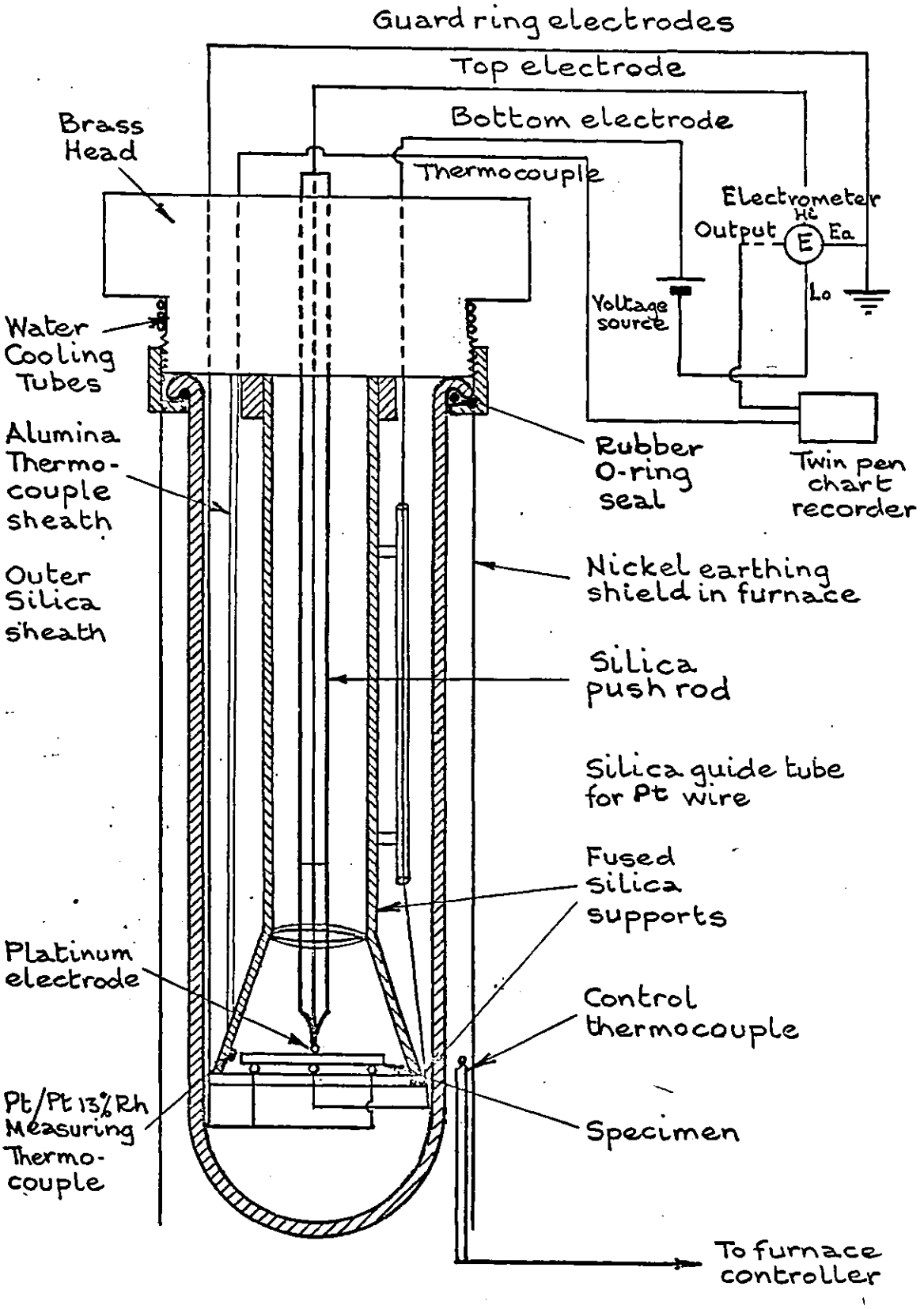

Fig 2.3 Schematic Diagram of Conductivity Measuring Apparatus [Furnace not shown.]

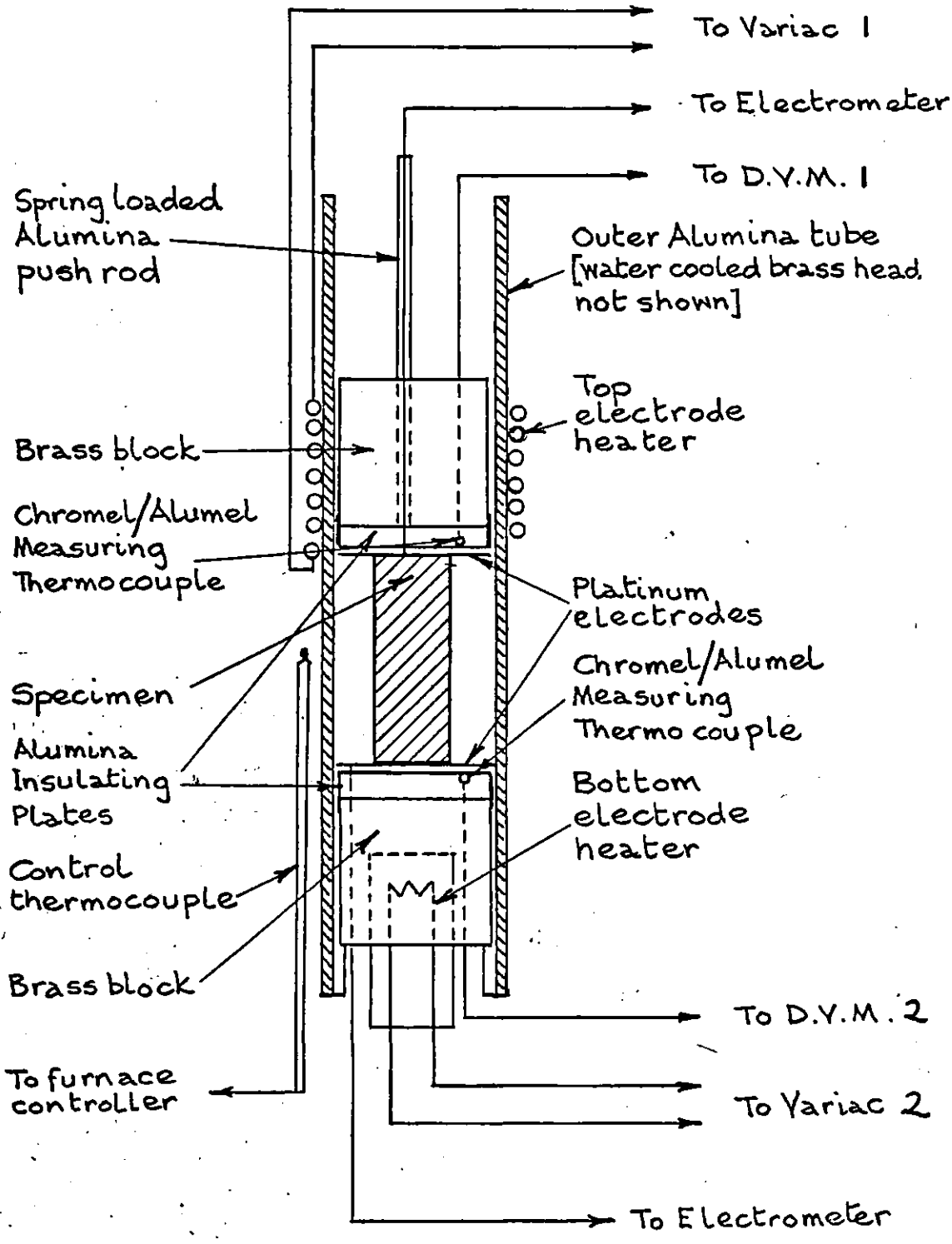

Fig 2.4 Schematic Diagram of Specimen Holder in Thermopower rig [Furnace not shown.]

CHAPTER 3

EXPERIMENTAL RESULTS

3.1 Composition of the Glasses

The results of the analysis of the total TM ion content of the glasses have been calculated in terms of the number of moles of TM ion contained in 100 g of glass. If the result is to be expressed in terms of the percentage of TM oxide then it must be recognized that all glasses contained a mixture of at least two TM ion valence states and therefore of two 'oxides'. In practice for manganese glasses, although the starting material was MnO_2, analysed glass compositions have been expressed with manganese as MnO because the Mn^{2+} ion was the predominant valence state in the glass.

All of the iron glasses, with the exception of those in the SF3 series, were melted with Fe_2O_3 as the starting material and as Fe^{3+} was the major valency state, compositions have been expressed in terms of Fe_2O_3. Glass SF3, however, was melted with ferrous oxalate and as it initially contained appreciable proportions of Fe^{2+}, the composition was calculated in terms of FeO.

The mixed iron-manganese glasses were calculated either as Fe_2O_3 + MnO or FeO + MnO depending upon the valency state of iron in the batch.

From the analysis of the total TM ion concentration in moles of TM ion per 100 g of glass, the weight percentage of the appropriate TM oxide, as discussed above, could be calculated. Since all additions of TM oxide were made to nominally 100 g of base glass, the weight of starting material necessary to obtain this composition could be deduced and compared with the actual weight added to the batch. This allowed an estimate of the losses during batch preparation and melting, and also as a result of possible batch material impurity. Generally these losses were between 5 and 7% for manganese glasses melted with reagent grade MnO_2 and less than 1% for iron glasses melted with pure Fe_2O_3.

Knowing the weight of starting material corresponding to the analysed total TM ion concentration and assuming this to be added to 100 g of base glass, made up of the appropriate number of moles of components to obtain the desired composition shown in Table 2.1, the

full molar composition of the glass could be calculated. These compositions are given in Tables 3.1.1 - 3.1.5 for series SMH, SML, EM, SF and SMF respectively.

This calculation assumes that little loss of base glass components occurred on melting but was necessary because the actual proportion of each individual oxide was not determined by a full chemical analysis of the glass. Losses on preparing and melting the base glasses were typically between 1 - 2% which provides some justification for the assumption above. Care was taken during weighing and mixing of the batch and while charging the crucible to minimise losses.

3.1.1 Vitrification and Homogeneity of the Glasses

A polished thin section from each glass composition was used to check that the glass was homogeneous and completely free of any crystalline phases, either from undissolved material or devitrification products. The examination was carried out using transmitted polarized light microscopy and it was found that all compositions which could be examined in this way were completely vitrified. For those glasses which were too highly coloured to be examined in transmitted light, X-ray powder diffraction analysis was undertaken.

None of the glasses containing high proportions of TM oxides produced any diffraction lines in the X-ray pattern once the surface layer (with a thickness of the order of a few μm) had been ground away. Surface crystallization was noted for SM14, SF4 and SF5. In the latter case the surface changed colour after heat treatment presumably due to oxidation of an iron oxide layer. The crystallization product was subsequently identified as magnetite (Fe_3O_4).

During melting it was noted that SMF3 was not fully in the liquid state but had a solid sediment on the bottom of the crucible. On casting, the liquid cooled to a glass with no evidence of devitrification, though the sediment in the crucible was crystalline. It was considered that the solubility limit of the TM oxides had been exceeded.

The homogeneity of the glasses was assessed by the uniformity of colour throughout the thin sections. It was satisfactory for all glasses, but with the following two exceptions:

(a) SM10: Dark reddish-brown coloured streaks were observed. This probably arose from inhomogeneity in the melt as the furnace failed during the melting schedule, resulting in the glass being melted and poured at 1200°C instead of 1400°C.

(b) SF3.1: This sample was the first to be cast from melt SF3 prepared for redox ratio studies. It was coloured green (i.e. rich in Fe^{2+}) in the centre of the thin section but yellowish-brown (i.e. rich in Fe^{3+}) throughout the remainder. This indicates that equilibrium had not been established within the melt and the surface layers were more oxidised than the bulk of the melt. The melt had not been stirred before the sample was taken because of the short melting time required to retain a high proportion of Fe^{2+}. For this reason the optical and electrical properties of this glass must be treated with caution. Such inhomogeneity was not noted for other glasses in this series or for glasses in series SF1.

3.2 Calculation of the Distance Between TM Ions

The number of, and distance between, TM ions in the glass are two important parameters in the Mott equation. These were calculated from the density and molar composition of each glass using the following equations:

(a) Molar volume (V_m) i.e. the volume containing one mole of glass:

$$V_m = \frac{W}{M\,D} \qquad (3.1)$$

where W is the total weight of glass, M the number of moles of glass in that weight and D the density.

(b) Number of TM ions per unit volume (N):

$$N = \frac{M_{TM}\,N}{V_m} \qquad (3.2)$$

where M_{TM} is the number of moles of TM ion in one mole of glass and N is Avogadro's number.

(c) Distance between TM ions (R):

$$R = \sqrt[3]{1/N} \qquad (3.3)$$

This is equivalent to calculating the cubic volume associated with a single TM ion and then taking the cube root to calculate the interatomic distance. It assumes a random distribution of ions in

the glass.

For the mixed manganese-iron glasses calculations (b) and (c) have been performed to find the average distances:

(a) between manganese ions,

(b) between iron ions, and,

(c) between adjacent ions whether they be iron or manganese.

Experimentally determined values of density and redox ratio, together with calculated values of molar volume, number of TM ions per unit volume and TM interionic distance are presented in Tables 3.2.1 - 3.2.5 for each glass series.

3.3 Optical Absorption Spectra

The recorded optical absorption spectra of the manganese, iron and mixed glasses have been replotted on a graph of absorptivity against wavenumber which are shown in Figures 3.1.1 - 3.1.6.

The spectra of the barium borate glasses containing manganese were measured for two different specimen thicknesses and the calculated absorptivities showed satisfactory agreement.

For glasses containing a single TM element the molar absorptivity was calculated at the absorption peak of Fe^{2+} or Mn^{3+} as appropriate. The accuracy of the calculation was variable because for dilute and highly concentrated glasses, large errors were introduced in the measurement of ionic concentration and specimen thickness respectively. The values obtained for the molar absorptivities will be discussed in greater detail in Chapter 4.

3.4 Crystallization Behaviour of the Glasses

The results of heat treatments which were successful in producing bulk crystallization in the glasses are recorded in Tables 3.3.1 - 3.3.4. As well as the heat treatment conditions, the results of optical examination by transmitted polarized light microscopy and also of X-ray diffraction analysis are also included.

3.4.1 Optical Photomicrography

Selected photomicrographs showing typical microstructures of some of the crystallized glasses are shown in Plates 3.1 - 3.9. Details of the microstructure of each glass-ceramic are given in

the accompanying notes. These are complementary to the observations noted in Tables 3.3.1 - 3.3.4.

3.4.2 Phase Determination - X-Ray Diffraction Analysis

In all cases surface devitrification preceded internal nucleation and growth. As the major interest of the study was the effect of TM oxides on nucleation phenomena within the glass, the surface growth on each specimen was removed by grinding on a diamond lapping wheel before X-ray analysis or electrical measurements were made.

Optical examination of many of the glass-ceramics indicated that several crystalline phases were often present simultaneously. In some cases only small proportions were present which gave only weak reflections in the X-ray powder pattern, thus making identification difficult. The following discussion indicates the likely minority phases present whilst a more general discussion of the crystallization processes is reserved for Chapter 4.

(a) SM7C: Comparing the diffraction pattern with standard ASTM patterns revealed that anorthite was the major crystal phase present. However, certain lines were more intense than predicted and other lines present were not accounted for by the anorthite pattern. This is indicative of a second phase, which was also just discernable in the thin sections and optical micrographs.

The best fit for these additional lines was provided by manganese metasilicate ($MnSiO_3$) but with the monoclinic structure. Usually $MnSiO_3$ (rhodonite) which is synthetized at 1 atm pressure has a triclinic structure. The synthesis of the monoclinic structure has only been reported at higher pressures, so the reason for its formation in a glass is not clear. It could be the result of the constraint of the surrounding glass during growth.

(b) SM10C: The major phase produced after short heat treatments was a pyroxene, the composition of which will be discussed in section 4.8 below. However, the dendritic phase which crystallized first appeared brown in transmitted light, thus it was inferred that it contained an appreciable quantity of Mn^{3+}. Of the possible phases, braunite ($MnO.3Mn_2O_3.SiO_2$) provided the best fit to the X-ray data, although the experimental powder pattern was not distinct enough for identification to be certain, therefore the identification is tentative.

(c) SM13C: As for SM10C the reddish-brown coloration of the dendrites indicated a high proportion of Mn^{3+}, although braunite could be ruled out in this case from a consideration of the X-ray data. The identification was mainly based on those lines of the major crystalline phase (gehlenite) which had greater intensity than that expected from the ASTM standard. Two likely phases were γ-Mn_2O_3 and Mn_3O_4 both of which have similar d-spacings so therefore the powder patterns differ only in the intensity of certain lines. The lines in these patterns are predicted to overlap some of the gehlenite lines, thus a measure of their intensity was difficult. However, it was felt that Mn_3O_4 provided better agreement with the experimentally determined powder pattern.

(d) SM14C: It was not certain from the optical examination how many phases were present. Unfortunately it has proved impossible to match the residual X-ray pattern, after the lines of the major phase (gehlenite) had been subtracted, to any one single phase. In addition, there were insufficient lines to be able to postulate a mixture of phases.

(e) Iron glasses: The powder diffraction patterns of SF4C, SF5C and SF6C were all similar and characteristic of a pyroxene phase. The likely compositions are discussed below. Whereas all of the manganese glass-ceramics in series SMH had produced gehlenite this was only detected in SF6C, though small amounts may have been present in the other glass-ceramics.

The optical examination revealed a fine dispersion of particles in SF4C which were not birefringent. This suggested a cubic crystal structure. X-ray analysis indicated that these particles were probably magnetite (Fe_3O_4), which has a spinel structure and is therefore cubic. However, the d-spacings of magnetite are very similar to those of maghemite (γ-Fe_2O_3) but the latter is reported to revert to haematite on heating and therefore it was felt that it would not be stable at the crystal growth temperature. SF6C and SF5C did not appear to have any other detectable crystalline phases in the internal nucleation and growth region although magnetite was detected on the surface of SF5C after heat treatment.

(f) Mixed glasses: All of the mixed glasses gave broadly similar X-ray powder patterns after crystallization. It has not been possible to exactly determine the phases present, although

compositions close to gehlenite and wollastonite seemed to be likely. The total number of phases could not be ascertained by optical examination.

3.4.3 Electron Microscopy

It was felt that because of the fine crystallite size of some of the glass-ceramics, electron optical techniques could be of value because of the increase in resolution offered. Both scanning and transmission electron microscopy were attempted.

3.4.3.1 Scanning electron Microscopy (SEM)

Selected SEM micrographs of SM13C after crystal growth for 1 hour are shown in Plate 3.10A - 3.10D. Although some debris from the chemical etching has been left on the crystal surface, it is just possible to detect a number of platelets running perpendicular to the direction of the dendrite arms. These will be referred to again below. Also evident is the shape of the dendrite arms from the section through the arm which comes out from the page.

The micrographs for SM10C and SM14C were less helpful. Plate 3.10E shows only the vague outline of a dendrite in SM10C giving no hint of the internal structure noted in the optical micrographs. The morphology of the crystalline phase(s) in SM14C is still unclear, so even the number of phases present is unknown (Plate 3.10F).

Plate 3.11 shows various features of the crystalline structure of SF4C, with Plate 3.11B being typical of the bulk of the specimen. Therefore as X-ray diffraction analysis indicated that a pyroxene was the major phase, this plate gives an indication of the pyroxene morphology and particle size. The dendritic structure shown in the other pictures was found towards the edge in just one part of the specimen. It is proposed that this phase may be gehlenite, judging by the shape of the dendrite arms shown in Plate 3.11D, but the quantity present was insufficient to be detected by X-ray diffraction analysis. The well defined crystal morphology probably indicates that the dendrites were surrounded by residual glass, which has been dissolved away, rather than the pyroxene phase.

The microstructure of SF5C as seen in the SEM was identical to that shown in Plate 3.11B. Careful searching of the specimen did not reveal any coarse dendritic structures as seen in SF4C. SF6C would be expected to show a similar microstructure to SF4C, though

with a larger proportion of gehlenite but a specimen has not been examined by SEM.

3.4.3.2 Transmission Electron Microscopy (TEM)

This section deals only with TEM studies of specimens heat treated in a furnace in the normal manner i.e. outside the microscope.

Plate 3.12 shows the microstructure of an area representative of SM12C together with the accompanying electron diffraction pattern. The picture shows part of a spherulite and the individual fibres can be distinguished. The electron diffraction pattern shows noticeable splitting of some of the spots indicating that the fibres are crystallographically related.

Plates 3.13 and 3.14 are of SM13C, the former of the early stages of crystallization showing the characteristic Mn_3O_4 dendrites in a glassy matrix and the latter of a completely crystalline specimen after a longer heat treatment. More information is gained in the second case because the thinning rate of the fully crystallized material was more even. Plate 3.13 shows that the glass was preferentially thinned away leaving the dendrites still relatively thick although some internal structure is visible in pictures B and C. The most striking effect in Plate 3.14 is the striping. The electron diffraction pattern shows a single crystal pattern (i.e. spots) superimposed on a polycrystalline background (spotted rings). The simplicity of the single crystal pattern indicates that the stripes are of the same material and it is proposed that they have probably been formed by a martensitic-type transformation. This is a diffusionless transformation, which occurs very rapidly and has been observed in other ceramic materials. It is suggested that Mn_3O_4 nucleates in the glass as a spinel ($MnO.Mn_2O_3$) and then grows with cubic symmetry. However, at low temperatures the tetragonal form is the most stable and so on cooling a cubic to tetragonal martensitic transformation takes place. A series of platelets are formed in the crystal with half the platelets in one orientation and the other half in a different orientation to minimise the strain energy. Thus two platelets with the same orientation are generally separated by one with the different orientation. This can be clearly seen in Plate 3.14E where certain bend contours run through alternate platelets and do not appear in the intermediate ones.

Plate 3.14D shows the existence of stacking faults on the 'bright' orientation of the platelets, running diagonally across the picture. The crystallographic relationship between the two regions is shown by the electron diffraction pattern in Plate 3.13D.

TEM studies were also made on samples of SM10C but the crystalline dendrites could not be thinned sufficiently for the electron beam to penetrate before the surrounding glass was completely thinned away and the specimen lost. Electron micrographs of the relatively thick dendrites were not very informative and so have not been included.

3.4.4 Electron Probe Microanalysis (EPMA)

It has been noted previously that identification of many of the crystalline phases was difficult and therefore it was not always possible to know the distribution of TM ions among the different phases. To help clarify this situation EPMA has been performed on selected crystallized manganese glasses.

(a) SM10C: Two backscattered electron images of large dendrites in the sample are shown in Plate 3.15. The core of each dendrite arm appears light, corresponding to a high mean atomic number, and therefore are probably rich in manganese. Conversely, the surrounding pyroxene phase has a similar manganese concentration to the remaining glass. However, between and around the pyroxene arms the picture is darker, which indicates a lower mean atomic number and therefore depletion of manganese. These changes in manganese concentration were confirmed by quantitatively scanning across the surface of the specimen to assess the distribution of selected elements (Mn, Si, Al and Ca).

(b) SM13C: The Mn_3O_4 dendrites clearly showed up as higher atomic number material on the backscattered electron image. Quantitative scanning revealed a depletion in manganese concentration in the glassy area surrounding the dendrite. The dendrite arms themselves were very high in manganese thus confirming the hypothesis that the phase was rich in manganese. However, all the other elements scanned were greatly reduced in the dendrite although the concentrations did not fall to zero. This was because the resolution of the electron beam was 4-5 μm compared with the dendrite arm width which was estimated to be 1-2 μm by optical microscopy. Thus the analysis was affected by the surrounding glass and the values

obtained represented a mean analysis of both glassy and crystalline material.

(c) SM14C: Unfortunately the fine particle size of the crystalline phases resulted in the specimen appearing to have a uniform distribution of elements in both the backscattered electron image and also the quantitative element scans across the specimen. Therefore there seems to be no appreciable partition of manganese between the different phases unless the particle size was much less than the resolution of the electron beam (5 μm).

3.4.5 In-Situ Crystallization in the High Voltage Electron Microscope

Only two glasses (SM10 and SF4) were studied using this technique. For SM10 two samples were examined; one being a blown glass film and the other an ion beam thinned foil prepared from a glass which had received a nucleation heat treatment.

Plates 3.16 A and C seem to show a two phase effect on a specimen coated with carbon. It was thought at first that this was indicative of some kind of phase separation, however, it could also be the result of a poorly applied coating. Comparison of Plates 3.16 A and D shows that some fine scale structure is present in the sample which had received a nucleation heat treatment. This cannot be the same effect as in the glass because the electron diffraction patterns in B and E are different. Plate 3.16B is typical of an amorphous material whilst the broad rings shown in Plate 3.16E are the result of the fine particle size. Therefore the nucleation heat treatment has produced either phase separation or crystalline nuclei. The latter possibility was confirmed as follows.

After heating to about 900°C in the microscope the dispersed second phase became more pronounced; occurring either as almost spherical particles with a range of diameter, or as rods. After continued heating the crystalline phase consumed the original glass (Plate 3.17A,C and E). Analysis of the electron diffraction patterns in Plates 3.17B, D and F showed that only one phase crystallized and that it had a cubic spinel type structure. However, it was not possible to identify the actual composition.

The crystallization of the blown glass film in the microscope was different. In this case the crystals were larger, more angular

and showed greater contrast (Plate 3.18). Some crystals had bands running across (Plate 3.18E) which could be faults in the crystal structure. In this case the electron diffraction patterns confirmed that braunite was the probable phase, as bulk nucleation and growth studies had indicated. Once again identification was tentative as the camera constant of the microscope, which is needed to calculate the d-spacings, could only be estimated. It should be noted that this film was not carbon coated and did not show any two phase effect before heating.

The reasons for these differences in crystallization behaviour are not obvious. Generally heat treatment temperatures in the microscope were higher for the latter sample which produced braunite, though the actual temperatures were not known. Therefore it is concluded that the first phase to nucleate at lower temperatures is a spinel type phase. At low growth temperatures this continues to grow but if the temperature is raised, braunite grows on the spinel nuclei. This is probably because the greater diffusion necessary to grow the more complicated crystal structure of braunite is possible at higher temperatures. One difference between this technique and conventional studies of crystallization is the short timescale involved. Growth occurs in minutes rather than hours.

The results of the study of SF4 are shown in Plate 3.19. In this case the growing phase had almost perfect spherical morphology. Whilst this is not unknown for crystalline phases, it is rare and it is thought that phase separation by a nucleation and growth process occurred at high temperatures. On cooling, the discrete phase crystallized, giving the electron diffraction pattern shown in picture E. Unfortunately this could not be indexed as lines with high d-spacings were masked by the centre spot because of an increase in the camera length.

Several interesting effects were noted for this specimen. Although the intersection between the two spheres appears darker as would be expected, some spheres have a dark hemisphere without a second overlapping sphere being apparent. Secondly the particles show a remarkable absence of internal structure in C and D, possibly indicating that they were amorphous. The specimen was held at the growth temperature when these micrographs were taken but it was not possible to record an electron diffraction pattern at temperature to confirm that they were amorphous because of movement of the specimen.

Finally, Plate 3.19F shows the boundary between a phase separated area and part of the foil with little separation. It is believed that separation only occurred when the electron beam was on the sample, probably because of the extra heating of the beam rather than any radiation damage effects.

To summarize, in-situ heat treatments in the HVEM can give some information about the early stages of crystallization. However, these mechanisms may not be applicable during conventional heat treatments because of the following effects:

(a) Uncertainty in the temperature distribution across the specimen and the effect of heating by the electron beam.

(b) The possibility of irradiation effects in the nucleation process. This could contribute to the short time-scale during which nucleation and growth occurs.

(c) The abnormally large surface to volume ratio of the specimen.

3.5 Electron Paramagnetic Resonance

All of the spectra were obtained with basically similar conditions. X band frequency (9.506 GHz) was used with a modulation frequency of 100 kHz and modulation amplitude of 5 G. However, the microwave power and receiver gain were varied to allow the wide variations in signal intensities between the glasses to be recorded. The first derivative of the intensity was recorded against the magnetic field strength and these are shown in Figures 3.2.1 - 3.2.5.

An attempt was made to measure the EPR spectra of the three dilute iron-manganese glasses SMF1, SMF4 and SMF5. Unfortunately the intensities were extremely low and with the high gain needed to detect the signal, the background noise swamped the TM ion absorption. These spectra are not reproduced but it was possible to distinguish two absorptions for each glass, the first at about 1.7 kG and the second at 3.4 kG, both of which increased as the TM ion concentration was increased. The derivative intensity approximately doubled as the TM ion concentration doubled. These effects will be discussed further in section 4.3.3.

Two crystallized glasses were examined. The spectra of SF6C is shown in Figure 3.2.4 but problems were experienced with SMF2AC. The signal obtained had high intensity and was very broad. Such

extreme broadness is indicative that ferromagnetic (or ferrimagnetic) resonance is involved rather than paramagnetic resonance. In ferromagnetism the magnetic ions are incorporated into well defined magnetically coupled structures and are no longer impurities in a non-magnetic host phase. Since ferromagnetic resonance (FMR) and the associated area of amorphous magnetism are beyond the scope of this study, no further measurements were attempted on either this sample or any other crystallized mixed TM glasses in the same series.

3.6 D.C. Resistivity Measurements

3.6.1 Glasses

The dc resistivity variation with temperature has been analysed using the Mott equation for small polaron hopping conduction (Equation 1.4.26). For convenience the equation has been rewritten in logarithmic form with conductivity replaced by resistivity as follows:

$$\log \frac{\rho}{T} = \log \frac{k}{\nu_{ph} N e^2 R^2 c(1-c)} + \frac{2\alpha R}{2.303} + \frac{W}{2.303kT} \qquad (3.4)$$

Mott's prediction of a polaron hopping mechanism is therefore validated if a plot of log ρ/T against $1/T$ is a straight line at high temperatures.

Many references, especially early ones in the field, have data plotted in terms of log ρ against $1/T$ and this is also the conventional method of presenting resistivity-temperature data for ionically conducting glasses. In recognition of this, the gradient and intercept of both log ρ/T and log ρ - $1/T$ plots have been calculated in this study. In practice the difference between these was small and the data may fit either relationship equally well, although the gradient was greater when log ρ/T - $1/T$ plots were used.

A computer programme was written to calculate the resistivity at each temperature from the experimentally determined parameters and also perform linear regression analysis to determine the best straight line through the data. In all cases the plot of log ρ/T - $1/T$ had a marginally higher correlation coefficient so only these results have been quoted subsequently.

For many of the glasses the experimental data were not best described by a linear relationship so the regression analysis was repeated for two intersecting straight lines. The temperature at which the lines intersect has been determined and will be referred

to as the transition temperature (T_I). This is not to be confused with the glass transition temperature (T_g).

Graphs showing the resistivity-temperature data together with the lines fitted by linear regression analysis are shown for each series of glasses in Figures 3.3.1 - 3.3.5. From the best fit lines the resistivities at 293,400, 500 and 600 K were calculated to facilitate comparison of the glasses in this study with those reported in the literature by other workers. (Values at 293K were usually extrapolated).

The gradient and intercept of the best fit lines have been used to evaluate various parameters for the glasses as follows. The Mott equation predicts the gradient of the log ρ/T - $1/T$ plot to be equal to $W/2.303k$, therefore the activation energy for conduction was easily calculated. The intercept has the value:

$$\text{Intercept} = \log\left(\left\{\frac{k}{Ne^2R^2c(1-c)}\right\}.\frac{1}{\nu_{ph}}\right) + \frac{2\alpha R}{2.303} \qquad (3.5)$$

The terms in the curly brackets are either universal constants or have been determined experimentally, therefore only the phonon frequency (ν_{ph}) and electron decay component (α) were unknown. Usually the phonon frequency for TM ion glasses is assumed to be of the order of 10^{13} s^{-1} (95), thus α and α^{-1} could be calculated.

For many of the glasses containing small proportions of TM oxides the value of α^{-1} calculated by this method were unrealistic, being either negative or large and positive. Now α^{-1} physically represents the rate of electronic wave decay on the TM ion and therefore negative values are meaningless, whilst positive values of large magnitude are unreasonable. This discovery points to a defect in the analysis and suggests that the tunnelling term involving α may not apply for these dilute glasses. It has been stated previously that Sayer and Mansingh(92) have postulated an adiabatic hopping model with $\alpha = 0$ for glasses containing a very high proportion of TM oxide though it is not suggested that the adiabatic model applies in the present case.

With the assumption that the tunnelling term does not enter equation 3.4, the phonon frequency can be calculated from the intercept of the log ρ/T -$1/T$ plot and this calculation has been performed for all glasses.

Finally, the size of the polaron has been estimated using Bogomolov's approximate equation:

$$r_p = \tfrac{1}{2} (\pi/6N)^{1/3} \qquad (1.4.12)$$

For the small polaron formalism to apply then the following condition must be satisfied:

$$\alpha^{-1} < r_p < R \qquad (1.4.13)$$

and an estimation of this has been made in each case.

The results of the calculations described in this section are presented in Tables 3.4.1 - 3.4.7. for each series of glasses.

3.6.2 Glass-Ceramics

The analysis of the temperature dependence of the resistivity of glasses following crystallization on heat treatment was more difficult. It has previously been noted that several crystalline phases may be present in addition to residual glass and the TM ions are distributed between these phases. The main problem is therefore defining the conduction path through these phases along which the current carriers move. In some cases the resistivity may be determined by the gaps between conducting crystals and in others conduction may occur exclusively through a residual glassy phase; it is often difficult to detect traces of glass which remain after crystallization.

This uncertainty in the nature of the conduction path results in the resistivity of the specimen, as calculated from the resistance, electrode surface area and specimen thickness, being a nominal value for that specimen alone. It may not always represent the resistivity of the conducting phase and is therefore not a 'material' property in such a way as the resistivity of a homogeneous material is. It may depend on specimen dimensions if the specimen is cut from a block of material with a non-uniform microstructure.

For this reason, a comparison of the activation energies in the glass-ceramic and original glass probably provides the best indication of a change in the conduction mechanism, rather than the change in resistivity taken alone.

However, in spite of this difficulty the resistivity-temperature relationship has been treated by the small polaron model. Values of interionic distance and redox ratio were assumed, as a first approximation, to be unchanged from those calculated for the parent glass and these have been used in the calculations.

Therefore straight lines have been fitted by computer to the log ρ/T - $1/T$ plots using linear regression analysis. From the computed gradient and intercept, the resistivity at 293, 400, 500 and 600 K, conduction activation energy, electron decay component (with $\nu_{ph} = 10^{13} s^{-1}$) and phonon frequency (assuming $\alpha = 0$) have been calculated. These are presented in Tables 3.4.1 - 3.4.7 along with the parent glasses to aid comparison. Graphs of log ρ against $1/T$ for both crystallized glass and parent glass are shown in Figures 3.4.1 - 3.4.11.

3.7 A.C. Resistivity of Glasses and Glass-Ceramics

The ac measurements were obtained as readings of conductance and capacitance at a range of frequencies for a range of temperature. The total conductivity measured at a particular frequency is defined as the sum of the ac and dc components:

$$\sigma_{total}(\omega) = \sigma_{dc} + \sigma_{ac}(\omega) \qquad (3.6)$$

Therefore to evaluate the true ac conductivity, the dc component must be calculated and subtracted from the total conductivity. For most glasses dc resistivities were measured on the sample before ac measurements were taken. These values proved to be in close agreement with the independently determined dc values. For glasses for which this was not done, dc values were calculated using values of gradient and intercept of the computer fitted lines obtained from dc resistivity measurements.

Reverting to resistivity equation 3.6 becomes:

$$\frac{1}{\rho_{total}(\omega)} = \frac{1}{\rho_{dc}} + \frac{1}{\rho_{ac}(\omega)} \qquad (3.6a)$$

Therefore:

$$\rho_{ac}(\omega) = \frac{\rho_{total}(\omega) \times \rho_{dc}}{\rho_{dc} - \rho_{total}(\omega)} \qquad (3.7)$$

Graphs have been plotted showing the relationship between the dc and total resistivities at various frequencies as a function of temperature and these are shown in Figures 3.5.1 - 3.5.9.

It is often found experimentally that the ac conductivity of a wide range of materials obeys the empirical relationship:

$$\sigma_{ac}(\omega) = k\,\omega^{n}$$

i.e. $$\log \rho_{ac}(\omega) = k' - n \log f \qquad (3.8)$$

where ω is the angular frequency ($= 2\pi f$) and k, k' and n are constants.

To test this relationship, $\log \rho_{ac}$ was plotted against log f and these graphs are shown in Figures 3.6.1 - 3.6.9. For plots which were linear, values of slope and correlation coefficient have been calculated by linear regression analysis and these have been tabulated on the graphs.

The dielectric properties of the glasses and glass-ceramics have been assessed by calculating both the real (ε') and the imaginary (ε'') parts of the complex dielectric constant ε using the following relationships:

$$\varepsilon = \varepsilon' - i\varepsilon'' \qquad (3.9)$$

where $$\varepsilon' = \frac{C}{\varepsilon_o (A/1)} \qquad (3.10)$$

$$\varepsilon'' = \frac{1}{\omega \varepsilon_o} \times \frac{1}{\rho_{ac}} \qquad (3.11)$$

and the loss tangent: $\tan \delta = \varepsilon''/\varepsilon'$.

In these equations C is the capacitance of the specimen with thickness 1, and A is the area of the electrodes.

Values of ε' and ε'' have been plotted against log f to determine the presence of loss peaks. These graphs are shown in Figures 3.7.1 - 3.7.9.

3.8 Thermoelectric Power

A number of glasses were investigated including SF5 which had one of the highest dc conductivities, but unfortunately in spite of considerable effort it was not possible to measure meaningful thermoelectric voltages.

Typically a temperature differential of 25 - 50°C was created across the specimen, which was accompanied by a measurable emf between the platinum electrodes. However, as the temperature gradient was reversed the emf did not change in sign as would be expected for a thermoelectric emf, hence no valid measurements

could be obtained.

The reason for the failure of these experiments could lie in the fairly high resistivity of the glasses, although the thermopower of iron glasses with similar Fe_2O_3 contents to SF5 has been measured before[106], but it seems more likely that the problem lies in the measuring apparatus. It was difficult to maintain a steady temperature gradient across the sample and the currents flowing in the various heating coils during measurement might have generated sufficient electrical noise to mask the small thermoelectric emf. Some improvements to the rig were made but with little success and it was decided that a more sophisticated rig would be required. Hence further work on thermoelectric power was discontinued.

TABLE 3.1.1.

COMPOSITIONS OF THE HIGH LIME MANGANESE ALUMINOSILICATE GLASSES (SERIES SMH)

Glass Code	Composition (Mole %)				Melting temperature (°C)
	SiO_2	Al_2O_3	CaO	MnO	
SM 15	41.02	9.06	49.43	0.49	1500
SM 16	40.79	9.01	49.16	1.04	1450
SM 17	40.39	8.92	48.67	2.02	1450
SM 11	38.66	8.54	46.58	6.22	1400
SM 18	37.32	8.24	44.97	9.46	1400
SM 12	36.11	7.98	43.51	12.41	1400
SM 13	34.46	7.61	41.53	16.40	1400
SM 14	32.67	7.22	39.37	20.75	1400

TABLE 3.1.2.

COMPOSITIONS OF THE LOW LIME MANGANESE ALUMINO SILICATE GLASSES (SERIES SML)

Glass Code	Composition (Mole %)				Melting temperature (°C)
	SiO_2	Al_2O_3	CaO	MnO	
SM 7	49.47	10.93	33.40	6.20	1500
SM 8	46.32	10.23	31.27	12.17	1400
SM 9	44.07	9.74	29.75	16.44	1400
SM 10	41.77	9.23	28.20	20.81	1400

TABLE 3.1.3.

COMPOSITIONS OF THE BARIUM BORATE GLASSES

CONTAINING MANGANESE (SERIES BM)

Glass Code	Composition (Mole %)			Melting temperature (^{o}C)
	BaO	B_2O_3	MnO	
BM 7	18.03	77.14	4.83	1100
BM 5	38.20	57.30	4.50	1050
BM 8	38.18	57.28	4.54	980
BM 6	36.33	54.49	9.18	1050
BM 9	36.47	54.70	8.83	980
BM 10	34.28	51.42	14.31	1100
BM 11	32.05	48.07	19.88	1100

TABLE 3.1.4.

COMPOSITIONS OF THE CALCIUM IRON ALUMINOSILICATE GLASSES (SERIES SF)

Glass Code	Composition (Mole %)				Melting temperature (^{o}C)
	SiO_2	Al_2O_3	CaO	Fe_2O_3	
SF 2	41.11	9.08	49.55	0.25(8)	1500
SF 8	41.01	9.06	49.42	0.50(4)	1500
SF 7	40.82	9.02	49.20	0.96(0)	1450
SF 1	39.79	8.79	47.95	3.47	1450
SF 6	39.08	8.63	47.09	5.20	1450
SF 4	38.32	8.46	46.18	7.04	1450
SF 5	37.11	8.20	44.73	9.96	1450

TABLE 3.1.5.

COMPOSITIONS OF THE MIXED IRON - MANGANESE GLASSES (SERIES SMF)

Glass Code	Compositions					Melting temperature (°C)
	SiO_2	Al_2O_3	CaO	Fe_2O_3	MnO	
SMF 1	41.06	9.07	49.48	0.14	0.26	1450
SMF 4	40.90	9.03	49.28	0.28	0.50	1450
SMF 5	40.64	8.98	48.97	0.49	0.93	1400
SMF 2	37.24	8.23	44.87	3.33	6.33	1450
SMF 2A	36.28	8.01	43.89	8.27 (FeO)	3.55	1425
SMF 2B	36.30	8.02	43.75	10.68 (FeO)	1.25	1425
SMF 3	35.36	7.81	42.61	4.80	9.43	1350

TABLE 3.2.1.

GLASS PARAMETERS FOR SERIES SMH

Glass Code	%MnO	Redox Ratio $\frac{Mn^{2+}}{Mn}_{total}$ (%)	Density (g cm^{-3})	Molar Volume (cm^3)	Number of Mn Ions per unit Volume (N) (x 10^{21}) (cm^{-3})	Mn-Mn Spacing (R) (Å)
SM 15	0.49	91.8	2.919	21.24	0.14	19.3
SM 16	1.04	90.1	2.928	21.19	0.29	15.0
SM 17	2.02	88.3	2.943	21.11	0.57	12.0
SM 11	6.22	85.8	2.993	20.87	1.80	8.23
SM 18	9.46	80.2	3.064	20.49	2.78	7.11
SM 12	12.41	81.5	3.101	20.32	3.68	6.48
SM 13	16.40	78.4	3.166	20.02	4.93	5.88
SM 14	20.75	74.2	3.236	19.71	6.34	5.40

TABLE 3.2.2.

GLASS PARAMETERS FOR SERIES SML

Glass Code	% MnO	Redox Ratio $\frac{Mn^{2+}}{Mn}$ (%) total	Density (g cm^{-3})	Molar Volume (cm^3)	Number of Mn Ions per unit Volume (N) (x 10^{21}) (cm^{-3})	Mn-Mn Spacing (R) (Å)
SM 7	6.20	93.4	2.882	22.20	1.68	8.41
SM 8	12.17	92.5	2.979	21.63	3.39	6.66
SM 9	16.44	90.9	3.051	21.22	4.66	5.99
SM10	20.81	88.4	3.129	20.80	6.02	5.50

TABLE 3.2.3.

GLASS PARAMETERS FOR SERIES BM

Glass Code	% MnO	Redox Ratio $\frac{Mn^{2+}}{Mn}$ (%) total	Density (g cm^{-3})	Molar Volume (cm^3)	Number of Mn Ions per unit Volume (N) (x 10^{-21}) (cm^{-3})	Mn-Mn Spacing (R) (Å)
BM 7	4.83	93.4	2.871	29.81	0.98	10.1
BM 5	4.50	83.5	3.776	26.93	1.01	9.98
BM 8	4.54	79.6	3.787	26.85	1.02	9.94
BM 6	9.18	84.8	3.960	25.30	2.18	7.71
BM 9	8.83	79.9	3.818	26.27	2.02	7.91
BM10	14.31	83.2	3.855	25.56	3.36	6.68
BM11	19.88	83.6	3.873	24.98	4.79	5.93

TABLE 3.2.4.

GLASS PARAMETERS FOR SERIES SF

Glass Code	% Fe_2O_3	Redox Ratio $\frac{Fe^{2+}}{Fe}$ (%) total	Density ($g\ cm^{-3}$)	Molar Volume (cm^3)	Number of Fe Ions per unit volume (N) ($\times 10^{-21}$) (cm^{-3})	Fe-Fe Spacing (R) (Å)
SF 2	0.258	15.8	2.918	21.30	0.15	19.0
SF 8	0.504	18.1	2.926	21.32	0.29	15.2
SF 7	0.960	14.9	2.941	21.37	0.54	12.3
SF 1 (.2)	3.47	10.7	3.014	21.66	1.93	8.03
SF 6	5.20	11.0	3.065	21.86	2.87	7.04
SF 4	7.04	11.2	3.116	22.07	3.84	6.39
SF 5	9.96	11.6	3.193	22.44	5.35	5.72

TABLE 3.2.5.

GLASS PARAMETERS FOR SERIES SMF

Glass Code	$\%Fe_2O_3$	% MnO	Redox Ratio $\frac{Fe^{2+}}{Fe\ total}$ (%)	Redox Ratio $\frac{Mn^{3+}}{Mn\ total}$ (%)	Density ($g\ cm^{-3}$)	Molar Volume (cm^3)	Number of TM Ions per unit Volume (N)	($\times 10^{-21}$) (cm^{-3})	TM-TM Spacing (R) (Å)
SMF1	0.140	0.255	0.0	--	2.919	21.26	Mn	0.072	24.0
							Fe	0.079	23.3
							TM	0.15	18.8
SMF4	0.285	0.502	0.0	< 8.2	2.925	21.27	Mn	0.14	19.2
							Fe	0.16	18.4
							TM	0.30	14.9
SMF5	0.487	0.930	0.0	< 9.9	2.944	21.22	Mn	0.26	15.6
							Fe	0.28	15.4
							TM	0.54	12.3
SMF2	3.329	6.332	0.0	< 14.2	3.087	21.29	Mn	1.79	8.23
							Fe	1.88	8.10
							TM	3.67	6.48
SMF2A	8.269(FeO)	3.550	18.5	0.0	3.091	20.36	Mn	1.05	9.84
							Fe	2.45	7.42
							TM	3.50	6.59
SMF2B	10.68 (FeO)	1.250	20.9	0.0	3.103	20.33	Mn	0.37	13.9
							Fe	3.17	6.81
							TM	3.54	6.56
SMF3	4.796	9.433	0.0	< 20.0	3.192	21.13	Mn	2.69	7.19
							Fe	2.73	7.15
							TM	5.42	5.69

TABLE 3.3.1

SUMMARY OF HEAT TREATMENTS FOR GLASSES IN SERIES SML

Glass Code	%MnO	Heat Treatment				Optical Examination	X-Ray Identification of Phases
		Nucleation		Crystal Growth			
		T (°C)	t (hr)	T (°C)	t (hr)		
SM7	6.2	800	15	980	6	Devitrified completely with growth starting at the surface. Some evidence of a second phase with small crystals between the dendrites. (Plate 3.1.1)	Main phase was anorthite. Extra lines may correspond to manganese silicate. See text.
SM8	12.2	740	15	910	15	Surface growth only.	-
SM9	16.4	800	15	980	6	Completely crystallized from the surface as above.	As above
SM10	20.8	740	15	920	3	Uneven distribution of crystals probably due to inhomogeneity in the sample. For most of the specimen the crystal size was too fine to be resolved. In the remaining glassy matrix small dendrites could be resolved into two phases. (3.2.1-3.2.5)	Major phase surrounding brown dendrite arms was a pyroxene. Dendrite arms could be braunite. See Text.
		730	7	950	25	Completely crystallized. Probably four phases present; one showing green-pink pleochroism.	Major phase was glaucochroite with some indications of bustamite.

TABLE 3.3.2

SUMMARY OF HEAT TREATMENTS FOR GLASSES IN SERIES SMH

Glass Code	%MnO	Heat Treatment				Optical Examination	X-Ray Identification of Phases
		Nucleation		Crystal Growth			
		T (°C)	t (hr)	T (°C)	t (hr)		
BG2	0.0	730	4	930	15	Two phases: surface growth and fine feathery dendritic growth from a few internal nuclei. Large proportion of glass remained uncrystallized.	Not certain: probably wollastonite and rankinite with some gehlenite.
SM15	0.5	650	18	980	1	Small surface crystallization. Little or no internal growth.	-
SM16	1.0	700	18	980	1		
SM17	2.0	750	18	980	1		
SM11	6.2	800	18	980	1		
SM18	9.5	700-850	3	980	1	Few large tabular crystals in a glassy matrix. (Plates 3.3.1 & 3.3.2)	gehlenite
		700-850	3	980	3	No increase in the number of nuclei. Crystal morphology now spherulitic. Crystals grow to 2-3mm in a glassy matrix. (Plates 3.3.3 & 3.3.4)	
SM12	12.4	710	15	930	6	Spherulites in a glassy matrix.	gehlenite
		710	15	930	15	Similar to above but spherulites larger. (Plate 3.4.1)	

TABLE 3.3.2 (contd)

SUMMARY OF HEAT TREATMENTS FOR GLASSES IN SERIES SMH

Glass Code	%MnO	Heat Treatment				Optical Examination	X-Ray Identification of Phases
		Nucleation		Crystal growth			
		T(°C)	t(hr)	T(°C)	t(hr)		
SM13	16.4	730	3	920	0.5	Small brown six-arm dendrites (Plate 3.5.1)	Spherulitic matrix phase is gehlenite. Dendrites are possibly Mn_3O_4. See text.
					1.0 1.5 2.5	Remaining glass starts spherulitic crystallization while dendrites continue to grow. (Plates 3.5.2 - 3.5.5)	
					19	Brown 'cross-shaped' dendrites in a fully crystalline matrix. (Plate 3.5.6)	
SM14	20.8	710	3	910	7.0	Small spherulites in a brown unresolved fully crystalline matrix. (Plates 3.6.1 & 3.6.2)	Spherulitic phase again gehlenite. Matrix phase unknown. See text.
		720	2	930	1.5	Spherulites much larger and more perfectly formed than above. (Plate 3.6.3)	

TABLE 3.3.3

SUMMARY OF HEAT TREATMENTS FOR GLASSES IN SERIES SF

Glass Code	%Fe_2O_3	Heat Treatment				Optical Examination	X-Ray Identification of Phases
		Nucleation		Crystal Growth			
		T (^oC)	t (hr)	T (^oC)	t (hr)		
SF2 SF8 SF7 SF1 SF3	0.25 0.50 0.96 3.47	700 to 800	3	980	1	Surface growth only. No bulk crystallization	-
SF6	5.20	700 800	3	980	1	Small dendrites in a glassy matrix (Plate 3.7.1)	Major phase was a pyroxene close in composition to augite. The second 'brown' phase was probably gehlenite with some ionic substitutions
		700 - 800	3	980	15	Completely crystallized: dendrites had grown and consumed the bulk of the specimen. The surface growth appeared brown in plane polarized light and there were some areas of the same phase in the bulk growth. (Plate 3.7.2)	

TABLE 3.3.3 (Contd)

SUMMARY OF HEAT TREATMENTS FOR GLASSES IN SERIES SF

Glass Code	$\%Fe_2O_3$	Heat Treatment				Optical Examination	X-Ray Identification of Phases
		Nucleation		Crystal Growth			
		T(°C)	t(hr)	T(°C)	t(hr)		
SF4	7.04	800	3	950	0.5	Completely crystallized. The crystal size of the major phase was too fine to be resolved. At high magnifications a high density of small non-birefringent particles was apparent.	Major phase was a pyroxene possibly related to fassaite or a ferro-augite. Some evidence of magnetite as the second phase.
SF5	9.96	800	3	950	0.5	Completely crystallized. The major phase was again too fine to be resolved but in this case there was no evidence of any second phase.	Major phase was a pyroxene possibly related to fassaite or a ferro-augite as in SF4 above. No evidence of any other phase.

TABLE 3.3.4

SUMMARY OF HEAT TREATMENTS FOR GLASSES IN SERIES SMF

Glass Code	%Fe_2O_3	%MnO	Heat Treatment				Optical Examination	X-Ray Identification of Phases
			Nucleation		Crystal Growth			
			T(°C)	t(hr)	T(°C)	t(hr)		
SMF1 SMF4 SMF5	0.14 0.29 0.49	0.26 0.50 0.93	-		-		Not Heat Treated	-
SMF2	3.33	6.33	700 - 850	3	980	1	A few isolated dendrites and some surface growth. (Plate 3.8.1)	Pattern was similar to gehlenite plus magnetite.
			700 - 850	3	980	15	Completely crystallized: probably three phases: (a) Dark brown dendritic phase (b) A pleochroic phase (c) Orange dendritic surface growth.	
SMF2A SMF2B	4.32 5.64	3.71 1.32	700 - 850	3	980	1	Completely crystallized. Scale of crystallization too fine to be able to determine the number of phases present (Plates 3.9.1 (SMF2A) & 3.9.2 (SMF2B))	gehlenite and wollastonite with some ionic substitutions
SMF3							Not Heat Treated	-

TABLE 3.4.1.

ELECTRICAL PROPERTIES OF GLASSES IN SERIES SMH

Glass Code	% MnO	LOG RESISTIVITY (ρ in Ω.cm)				Activation Energy (W) (eV)	α^{-1} (Å)	r_p (Å)	R (Å)	ν_{ph} with $\alpha = 0$ (s^{-1})	
		293K	400K	500K	600K						
SM15	0.49	31.08	21.84	16.81	13.46	2.036	-6.55	7.78	19.3	3.62×10^{15}	
SM16	1.04	26.82	19.31	15.22	12.51	1.661	-73.0	6.06	15.0	1.51×10^{13}	
SM17	2.02	24.60	18.15	14.64	12.32	1.431	6.06	4.85	12.0	1.88×10^{11}	
SM11	6.22	22.16	16.55	13.50	11.48	1.249	2.70	3.32	8.23	2.25×10^{10}	
SM18	9.46	20.11	14.87	12.02	10.14	1.169	2.87	2.87	7.11	6.99×10^{10}	
SM12	12.41	19.02	14.07	11.38	9.60	1.105	2.58	2.61	6.48	6.62×10^{10}	
SM13 T_I = 535 K	16.40	17.34	12.94	10.55	8.97	0.988	1.94	2.37	5.88	2.33×10^{10}	$T < T_I$
		18.28	13.31	10.61	8.83	1.109	3.48			3.41×10^{11}	$T > T_I$
SM14 T_I = 508 K	20.75	16.90	12.44	10.01	8.42	0.999	2.27	2.18	5.40	8.63×10^{10}	$T < T_I$
		17.73	12.76	10.06	8.28	1.110	4.72			1.01×10^{12}	$T > T_I$

TABLE 3.4.1(a)

ELECTRICAL PROPERTIES OF GLASS-CERAMICS IN SERIES SMH

Glass Code	% MnO	LOG RESISTIVITY (ρ in Ω.cm)				Activation Energy (W) (ev)	α^{-1} (Å)	r_p (Å)	R (Å)	ν ph with $\alpha = 0$ (s^{-1})	
		293K	400K	500K	600K						
SM18C	9.46	15.35	12.74	11.33	10.40	0.598	0.86	2.87	7.11	6.02×10^{5}	$T < T_I$
T_I = 535 K		20.28	14.79	11.81	9.84	1.222	4.36			3.82×10^{11}	$T > T_I$
SM12C	12.41	18.69	13.78	11.11	9.35	1.097	2.81	2.61	6.48	1.00×10^{11}	
SM13 C 1.5	16.40	17.91	13.42	10.99	9.39	1.004	1.76	2.37	5.88	1.24×10^{10}	$T < T_I$
T_I = 526 K		19.04	13.88	11.08	9.23	1.150	3.34			2.98×10^{11}	$T > T_I$
SM13 C 19	16.40	17.46	13.19	10.88	9.36	0.956	1.56	2.37	5.88	5.37×10^{9}	$T < T_I$
T_I = 546 K		19.59	14.14	11.18	9.22	1.214	5.22			1.05×10^{12}	$T > T_I$
SM14C	20.75	21.21	15.35	12.16	10.04	1.304	4.16	2.18	5.40	7.46×10^{11}	

TABLE 3.4.2.

ELECTRICAL PROPERTIES OF GLASSES AND GLASS-CERAMICS IN SERIES SML

Glass Code	% MnO	LOG RESISTIVITY (ρ in Ω.cm)				Activation Energy (W) (ev)	α^{-1} (Å)	r_p (Å)	R (Å)	ν ph with α =O (s^{-1})
		293K	400K	500K	600K					
SM 7	6.20	24.67	18.21	14.70	12.38	1.432	4.29	3.39	8.41	1.99×10^{11}
SM 8	12.17	20.48	15.21	12.35	10.45	1.174	2.75	2.68	6.66	7.91×10^{10}
SM 9	16.44	19.40	14.18	11.34	9.46	1.164	3.95	2.41	5.99	4.84×10^{11}
SM10	20.81	18.38	13.22	10.43	8.57	1.149	6.97	2.22	5.50	2.07×10^{12}
SM7C	6.20	21.80	16.20	13.16	11.15	1.245	3.56	3.39	8.41	8.92×10^{10}
SM10C	20.81	13.91	10.28	8.32	7.02	0.817	2.49	2.22	5.50	1.21×10^{11}

TABLE 3.4.3.

ELECTRICAL PROPERTIES OF GLASSES IN SERIES BM

Glass Code	% MnO	LOG RESISTIVITY (ρ in Ω.cm)				Activation Energy (W) (ev)	α^{-1} (A)	r_p (A)	R (A)	ν ph with α =O (s^{-1})
		293K	400K	500K	600K					
BM 7	4.83	27.95	20.32	16.16	13.41	1.688	17.4	4.06	10.1	3.14×10^{12}
BM 5	4.50	26.44	18.89	14.78	12.06	1.669	-26.2	4.02	9.98	2.14×10^{13}
BM 8	4.54	25.51	18.23	14.27	11.64	1.611	-45.5	4.01	9.94	1.55×10^{13}
BM 6	9.18	21.39	15.80	12.77	10.76	1.243	3.29	3.11	7.71	9.26×10^{10}
BM 9	8.83	20.61	15.42	12.61	10.75	1.156	2.42	3.19	7.91	1.46×10^{10}
BM10	14.31	19.26	14.17	11.40	9.57	1.135	3.14	2.69	6.68	1.42×10^{11}
BM11	19.88	17.59	12.89	10.33	8.65	1.052	3.09	2.39	5.93	2.16×10^{11}

TABLE 3.4.4.

ELECTRICAL PROPERTIES OF GLASSES IN SERIES SF

Glass Code	% Fe_2O_3	LOG RESISTIVITY (ρ in Ω.cm)				Activation Energy (W) (ev)	α^{-1} (A)	r_p (A)	R (A)	ν ph with $\alpha = 0$ (s^{-1})	
		293K	400K	500K	600K						
SF 2	0.258	25.55	18.49	14.65	12.11	1.623	-136	7.65	19.0	1.32×10^{13}	
SF 8	0.504	26.52	19.15	15.13	12.47	1.631	53.0	6.13	15.2	5.68×10^{13}	
SF 7	0.960	19.58	15.39	13.12	11.62	0.940	2.04	4.95	12.3	5.92×10^{7}	$T < T_I$
		23.47	17.32	13.97	11.75	1.368	6.05			1.73×10^{11}	$T > T_I$
SF1.2	3.47	15.54	11.85	9.86	8.54	0.830	2.23	3.24	8.03	7.37×10^{10}	
SF 6	5.20	13.74	10.77	9.17	8.12	0.674	1.50	2.84	7.04	8.15×10^{8}	$T < T_I$
		14.26	10.66	8.72	7.43	0.811	2.71			5.55×10^{10}	$T > T_I$
SF 4	7.04	12.05	9.14	7.58	6.55	0.660	2.06	2.57	6.39	2.05×10^{10}	$T < T_I$
		12.66	9.23	7.38	6.15	0.774	4.15			4.62×10^{11}	$T > T_I$
SF 5	9.96	11.40	8.74	7.31	6.37	0.607	1.65	2.31	5.72	9.59×10^{9}	$T < T_I$
		11.90	8.64	6.80	5.72	0.737	3.87			5.22×10^{11}	$T > T_I$

TABLE 3.4.4.(a)

ELECTRICAL PROPERTIES OF GLASS-CERAMICS IN SERIES SF

Glass Code	% Fe_2O_3	LOG RESISTIVITY (ρ in Ω.cm)				Activation Energy (W) (ev)	α^{-1} (Å)	r_p (Å)	R (Å)	ν ph with $\alpha = 0$ (s^{-1})	
		293K	400K	500K	600K						
SF6C	5.20	10.25	7.81	6.50	5.64	0.559	2.37	2.84	7.04	2.61×10^{10}	Low V
		9.95	7.59	6.32	5.49	0.542	2.38			2.71×10^{10}	High V
SF4C	7.04	12.56	9.70	8.16	7.14	0.650	1.65	2.57	6.39	4.30×10^{9}	Low V
		12.12	9.38	7.90	6.93	0.625	1.65			4.38×10^{9}	High V
SF5C	9.96	8.30	6.24	5.13	4.41	0.477	2.31	2.31	5.72	7.10×10^{10}	Low V
		8.25	6.10	4.95	4.19	0.496	2.81			1.70×10^{11}	High V

TABLE 3.4.5.

ELECTRICAL PROPERTIES OF SELECTED GLASSES AND GLASS-CERAMICS IN SERIES SMF

Glass Code	$\%Fe_2O_3$ (%FeO) / %MnO	LOG RESISTIVITY (ρ in Ω.cm) 293K	400K	500K	600K	Activation Energy (W) (ev)	α^{-1} (Å)	r_p (Å)	R (Å)	ν ph with α =O (s^{-1})	
SMF1	0.14 / 0.26	27.03	19.36	15.19	12.42	1.696	-ve	7.56	18.8	1.7×10^{13}	
SMF2	3.33 / 6.33	18.98	14.19	11.58	9.86	1.072	3.00	3.32	8.23	4.1×10^{10}	Mn
							1.92	2.61	6.48	1.2×10^{10}	TM
SMF2A	8.27 FeO / 3.55	13.73	10.34	8.51	7.38	0.766	2.33	2.99	7.42	1.7×10^{10}	Fe
							1.90	2.66	6.59	9.6×10^{9}	TM
SMF2B	10.68 FeO / 1.25	12.67	9.39	7.61	6.44	0.743	2.87	2.75	6.81	8.7×10^{10}	Fe
							2.50	2.65	6.56	5.6×10^{10}	TM
SMF3	4.80 / 9.43	16.91	12.62	10.29	8.76	0.961	2.75	2.90	7.19	5.4×10^{10}	Mn
							1.80	2.30	5.69	1.5×10^{10}	TM
SMF2AC	8.27 FeO / 3.55	10.83	8.32	6.97	6.09	0.573	2.04	2.99	7.42	3.0×10^{9}	Fe
							1.72	2.66	6.59	4.5×10^{9}	TM
SMF2BC	10.68 FeO / 1.25	5.85	5.23	4.91	4.72	0.165	1.10	2.75	6.81	6.9×10^{7}	Fe
							1.10	2.65	6.56	4.4×10^{7}	TM

TABLE 3.4.6.

ELECTRICAL PROPERTIES OF IRON GLASSES WITH DIFFERENT REDOX RATIOS

Glass Code	$\frac{Fe^{2+}}{Fe}_{total}$ (%)	LOG RESISTIVITY (ρ in Ω.cm)				Activation Energy (W) (ev)	α^{-1} (Å)	r_p (Å)	R (Å)	ν ph with $\alpha^{-1}=0$ (s^{-1})
		293K	400K	500K	600K					
SF1.1	9.3	16.09	12.28	10.22	8.87	0.856	2.19	3.24	8.03	6.45×10^9
SF1.2	10.7	15.62	11.88	9.86	8.52	0.841	2.31	3.24	8.03	9.45×10^9
SF1.3	13.8	15.34	11.71	9.75	8.45	0.819	2.16	3.24	8.03	5.84×10^9
SF1.4	14.9	15.56	11.84	9.82	8.50	0.838	2.22	3.24	8.03	7.22×10^9
SF1.5	15.8	15.36	11.73	9.77	8.47	0.818	2.11	3.24	8.03	4.86×10^9

TABLE 3.4.7.

ELECTRICAL PROPERTIES OF IRON GLASSES WITH DIFFERENT REDOX RATIOS

Glass Code	$\frac{Fe^{2+}}{Fe}_{total}$ (%)	LOG RESISTIVITY (ρ in Ω.cm)				Activation Energy (W) (ev)	α^{-1} (Å)	r_p (Å)	R (Å)	ν ph with $\alpha = 0$ (s^{-1})
		293K	400K	500K	600K					
SF3.1	44.5	15.14	11.53	9.57	8.28	0.815	2.18	3.42	8.49	4.12×10^9
SF3.2	44.4	14.88	11.40	9.52	8.29	0.784	2.02	3.42	8.49	2.22×10^9
SF3.3	32.1	15.31	11.66	9.69	8.39	0.822	2.18	3.42	8.49	4.12×10^9
SF3.4	22.2	15.12	11.54	9.60	8.33	0.807	2.21	3.42	8.49	4.52×10^9
SF3.5	15.0	15.69	11.98	9.97	8.65	0.836	2.24	3.42	8.49	5.08×10^9

Fig 3.1.1. OPTICAL ABSORPTION SPECTRA OF HIGH LIME MANGANESE ALUMINOSILICATE GLASSES (SERIES SMH)

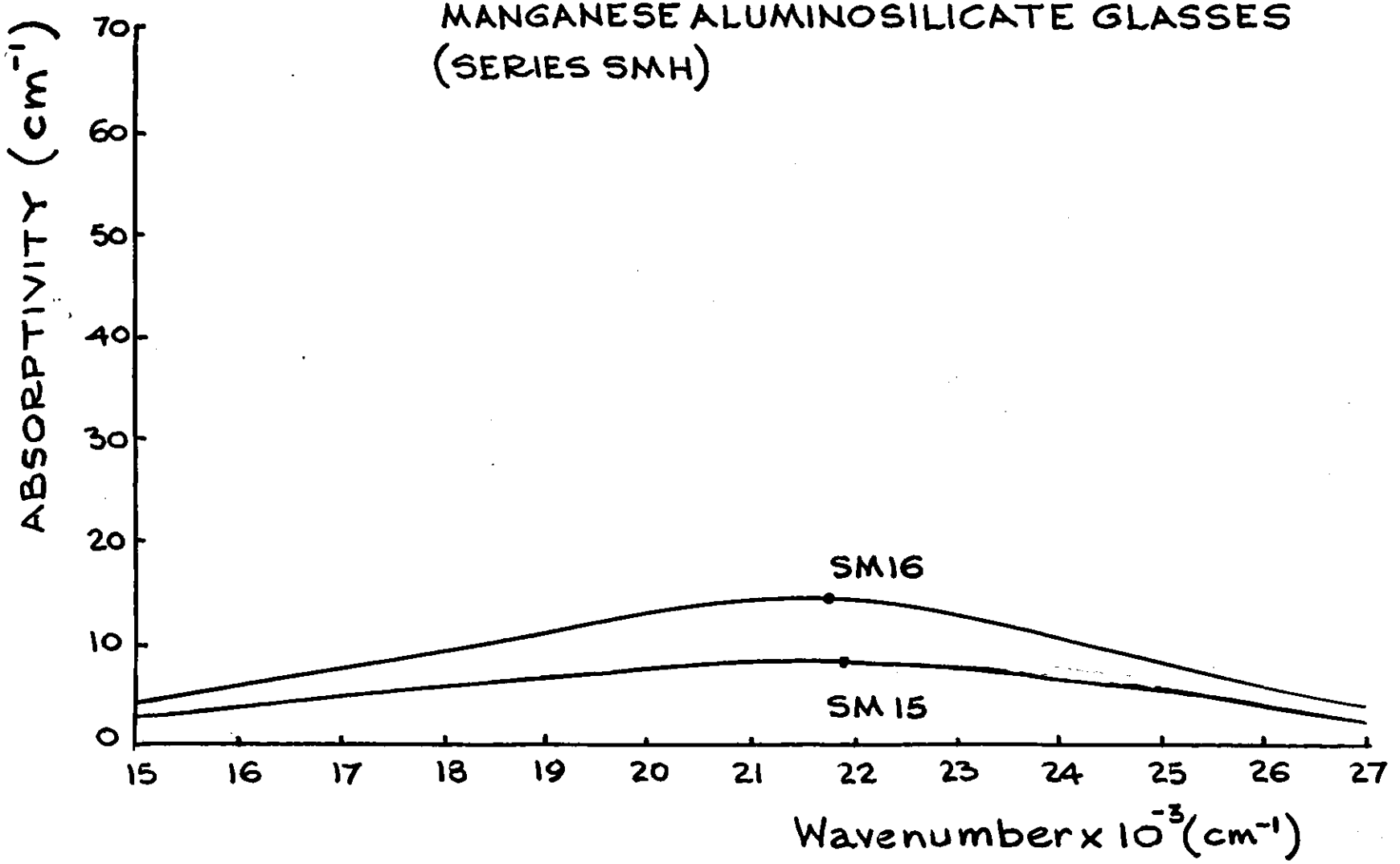

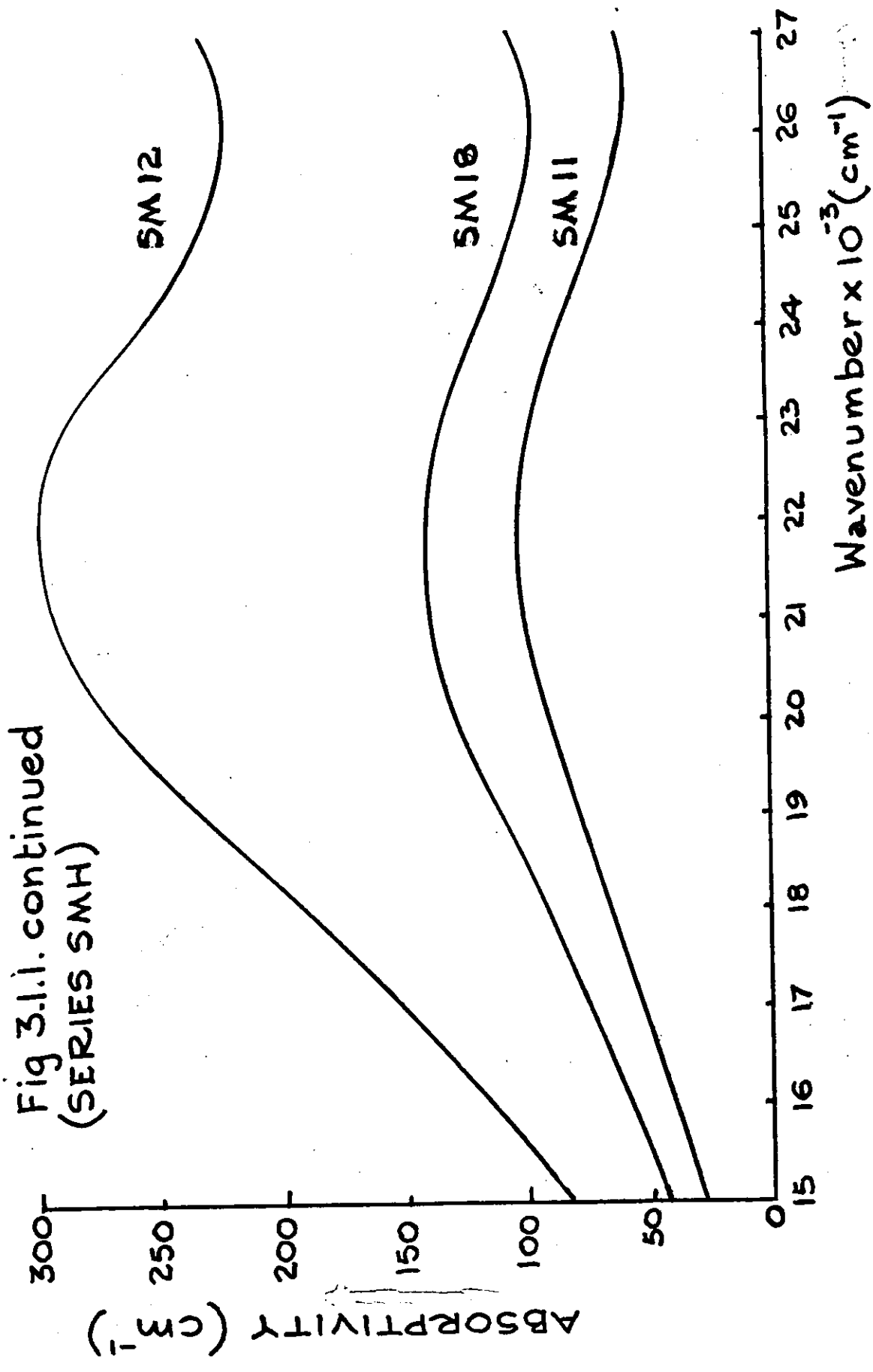

Fig 3.1.1. continued
(SERIES SMH)

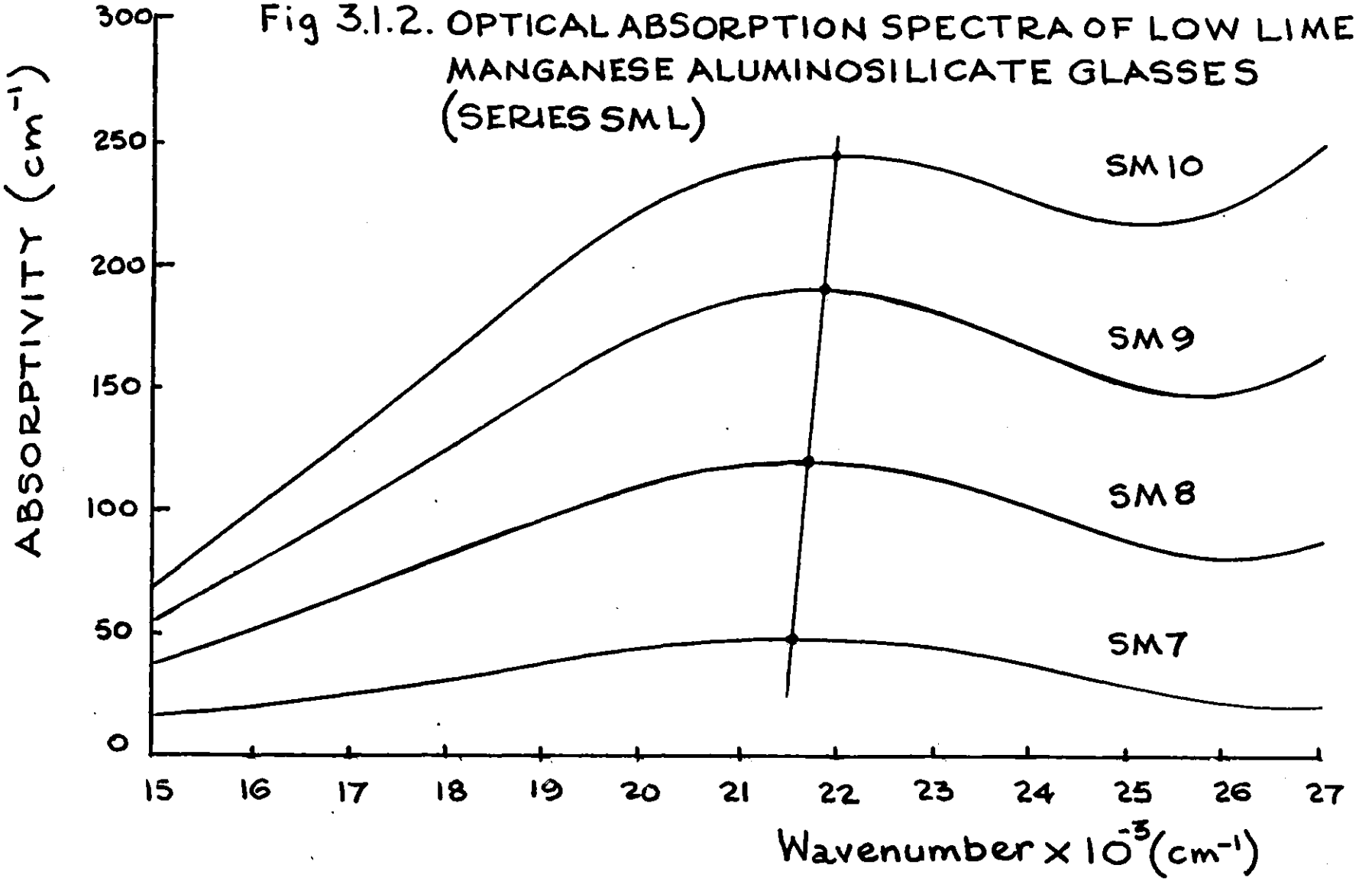
Fig 3.1.2. OPTICAL ABSORPTION SPECTRA OF LOW LIME MANGANESE ALUMINOSILICATE GLASSES (SERIES SML)
ABSORPTIVITY (cm⁻¹)
300
250
200
150
100
50
0
SM10
SM9
SM8
SM7
15
16
17
18
19
20
21
22
23
24
25
26
27
Wavenumber x 10⁻³ (cm⁻¹)

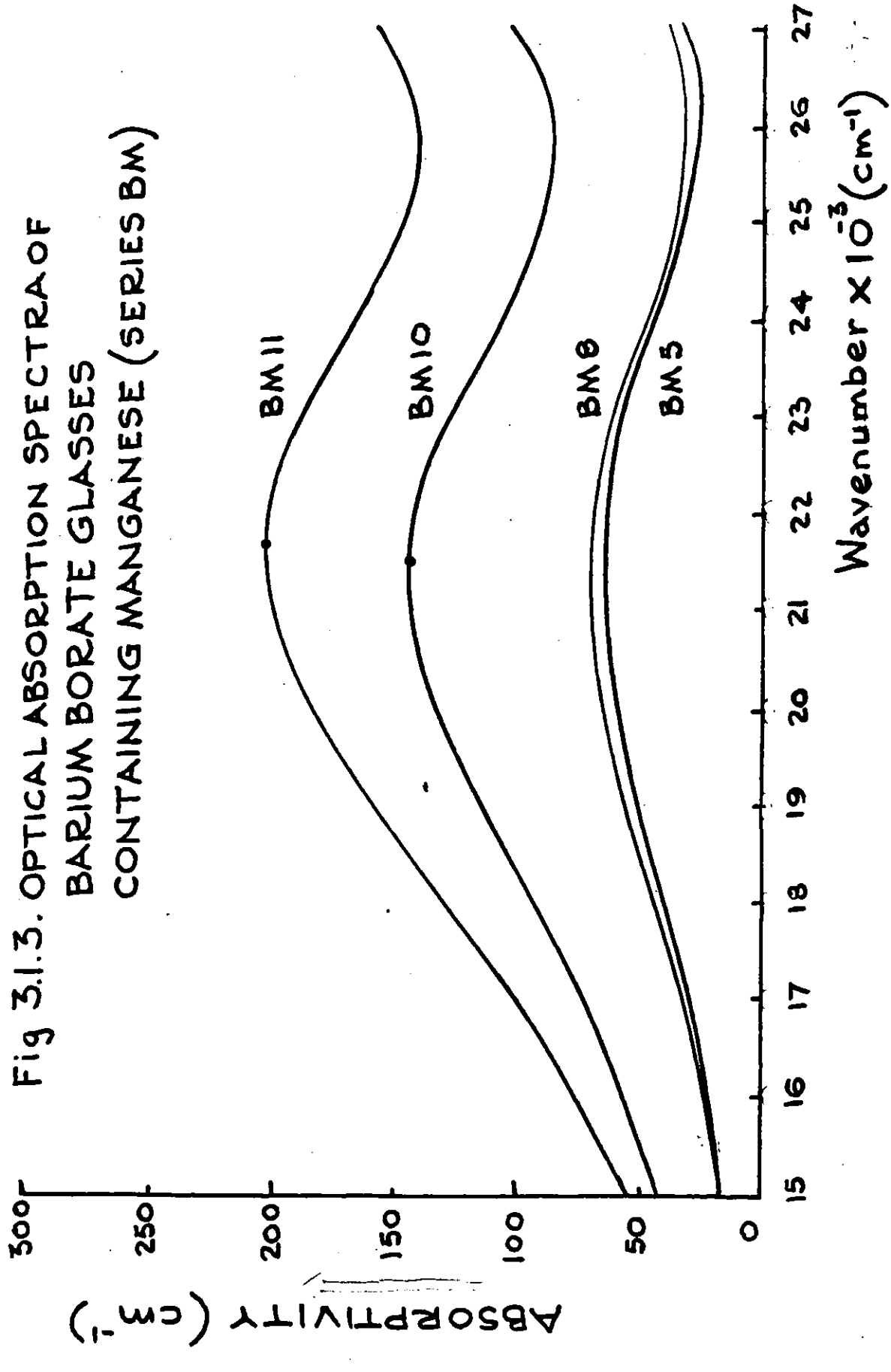

Fig 3.1.3. OPTICAL ABSORPTION SPECTRA OF BARIUM BORATE GLASSES CONTAINING MANGANESE (SERIES BM)

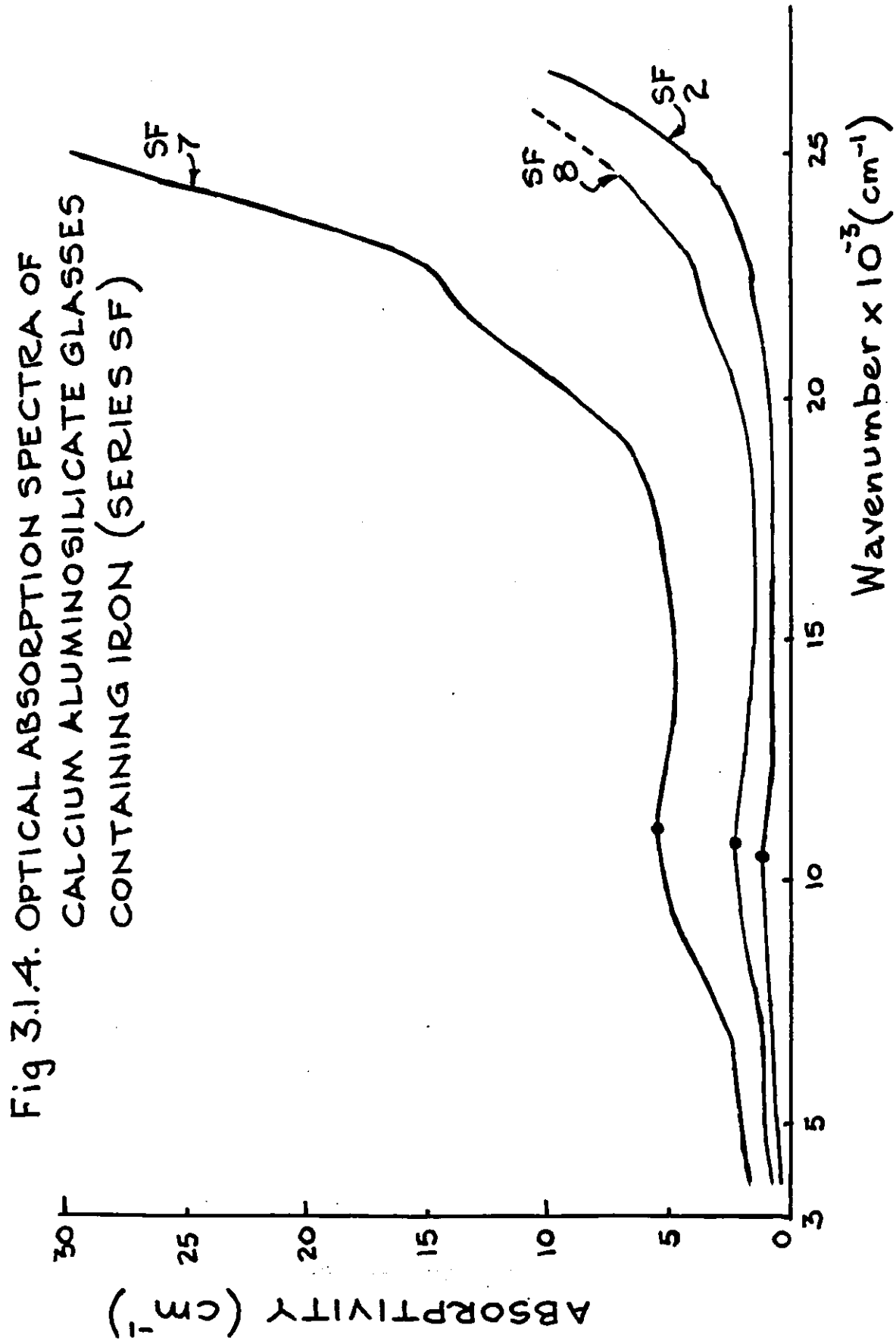

Fig 3.1.4. OPTICAL ABSORPTION SPECTRA OF CALCIUM ALUMINOSILICATE GLASSES CONTAINING IRON (SERIES SF)

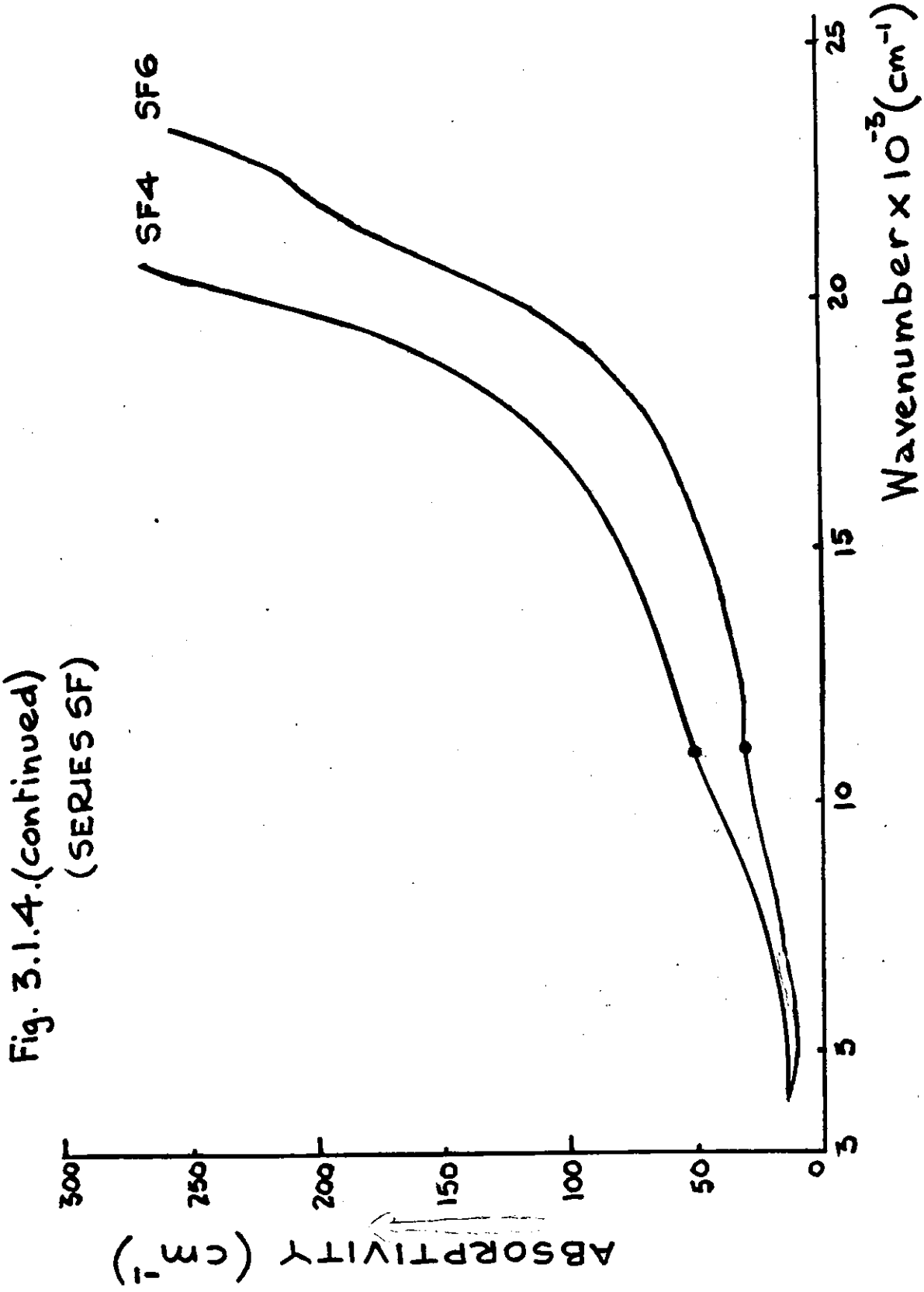

Fig. 3.1.4.(continued)
(SERIES SF)

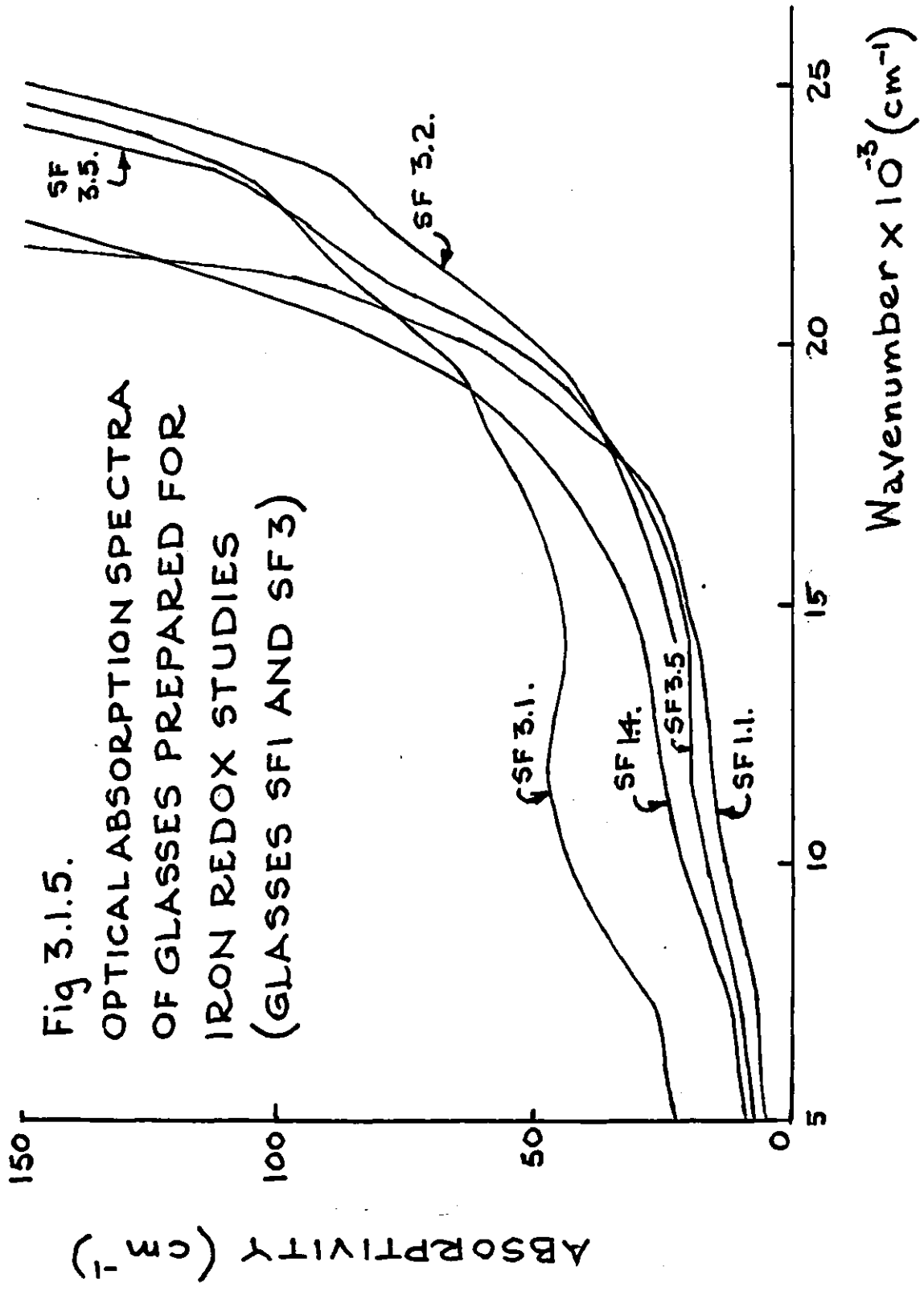

Fig 3.1.5.
OPTICAL ABSORPTION SPECTRA
OF GLASSES PREPARED FOR
IRON REDOX STUDIES
(GLASSES SF1 AND SF3)

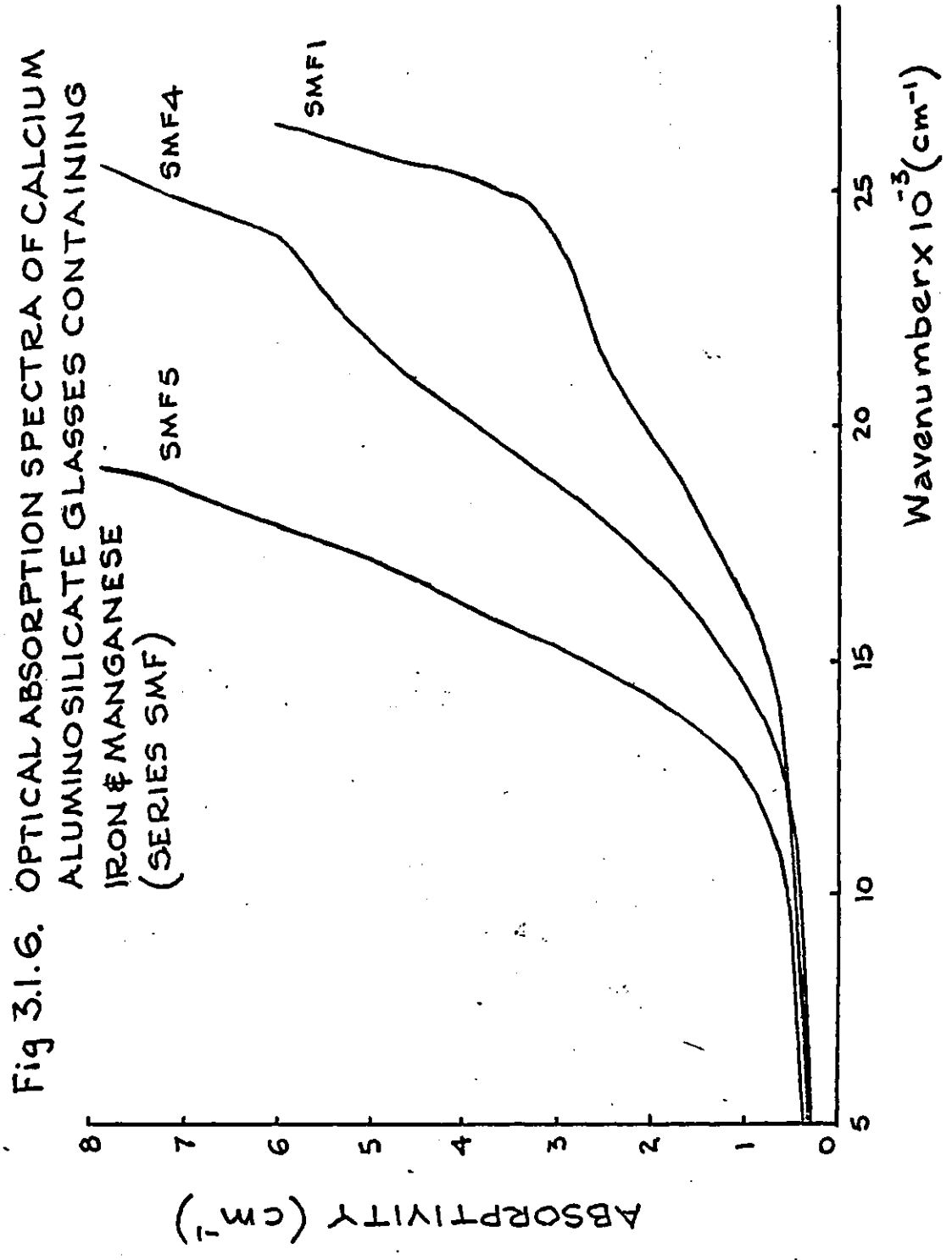

Fig 3.1.6. OPTICAL ABSORPTION SPECTRA OF CALCIUM ALUMINOSILICATE GLASSES CONTAINING IRON & MANGANESE (SERIES SMF)

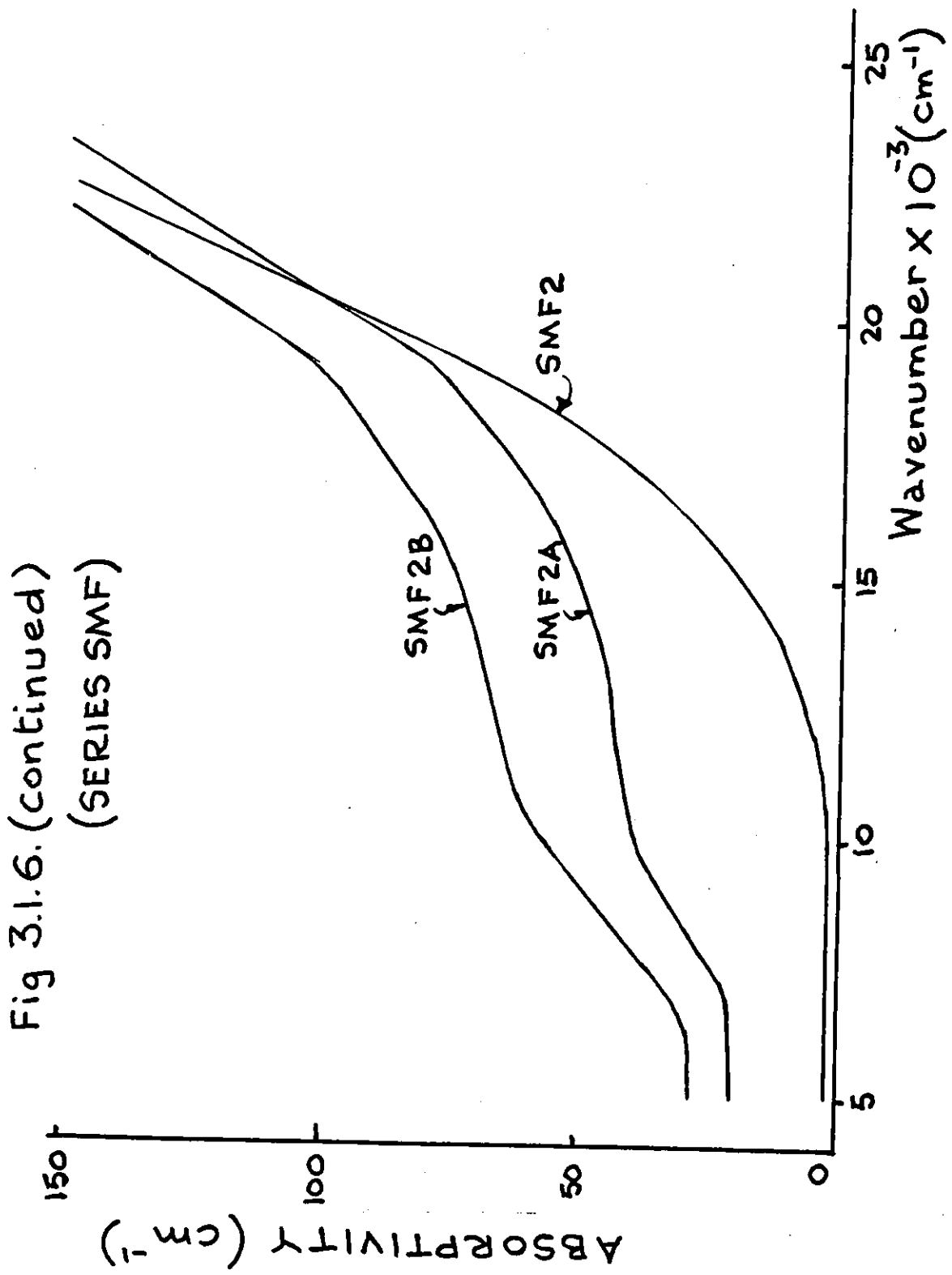

Fig 3.1.6. (continued)
(SERIES SMF)

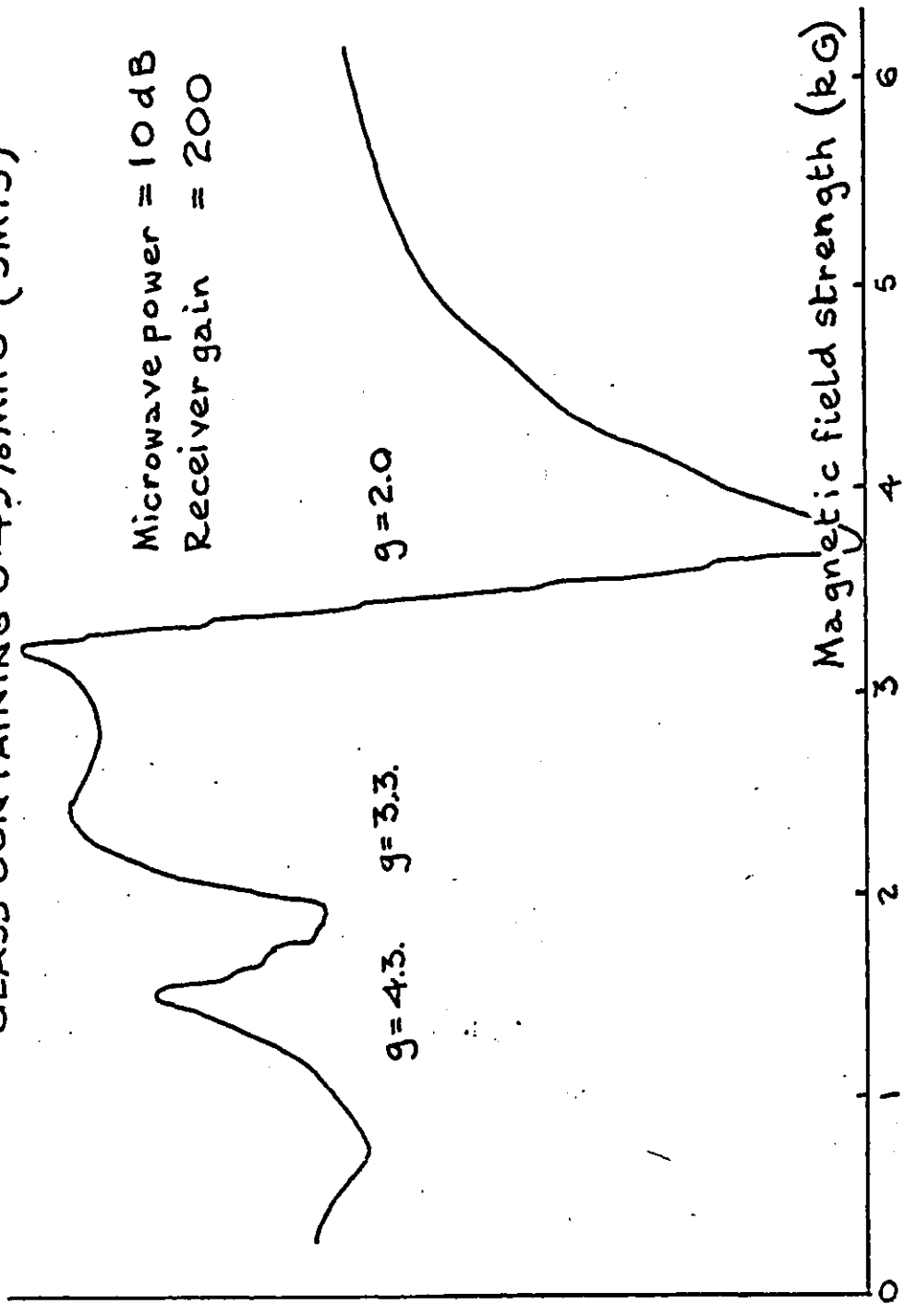

Fig 3.2.1. E.P.R. Spectrum of a calcium aluminosilicate glass containing 0.49% MnO (SM15)

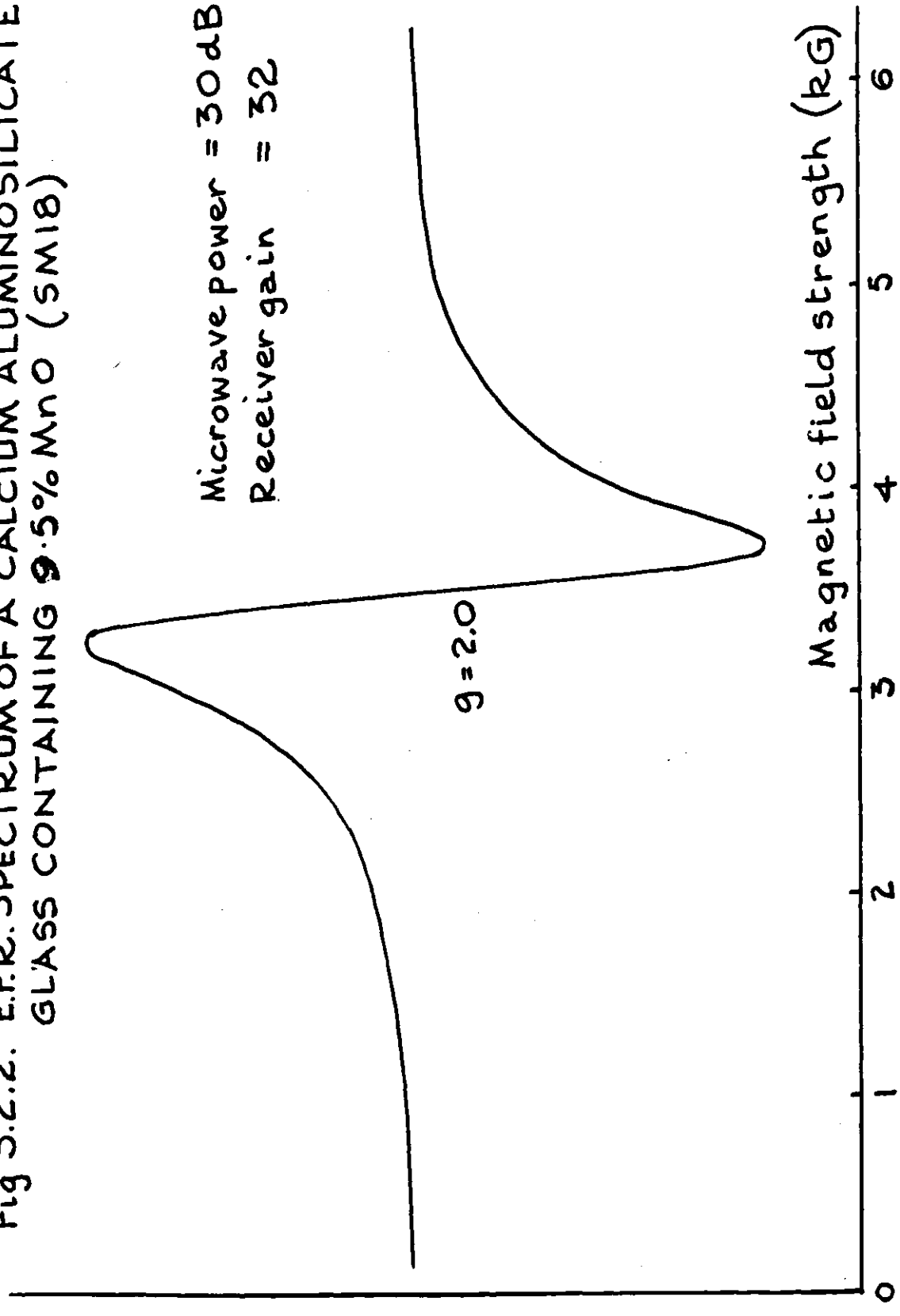

Fig 3.2.2. E.P.R. SPECTRUM OF A CALCIUM ALUMINOSILICATE GLASS CONTAINING 9·5% MnO (SM18)

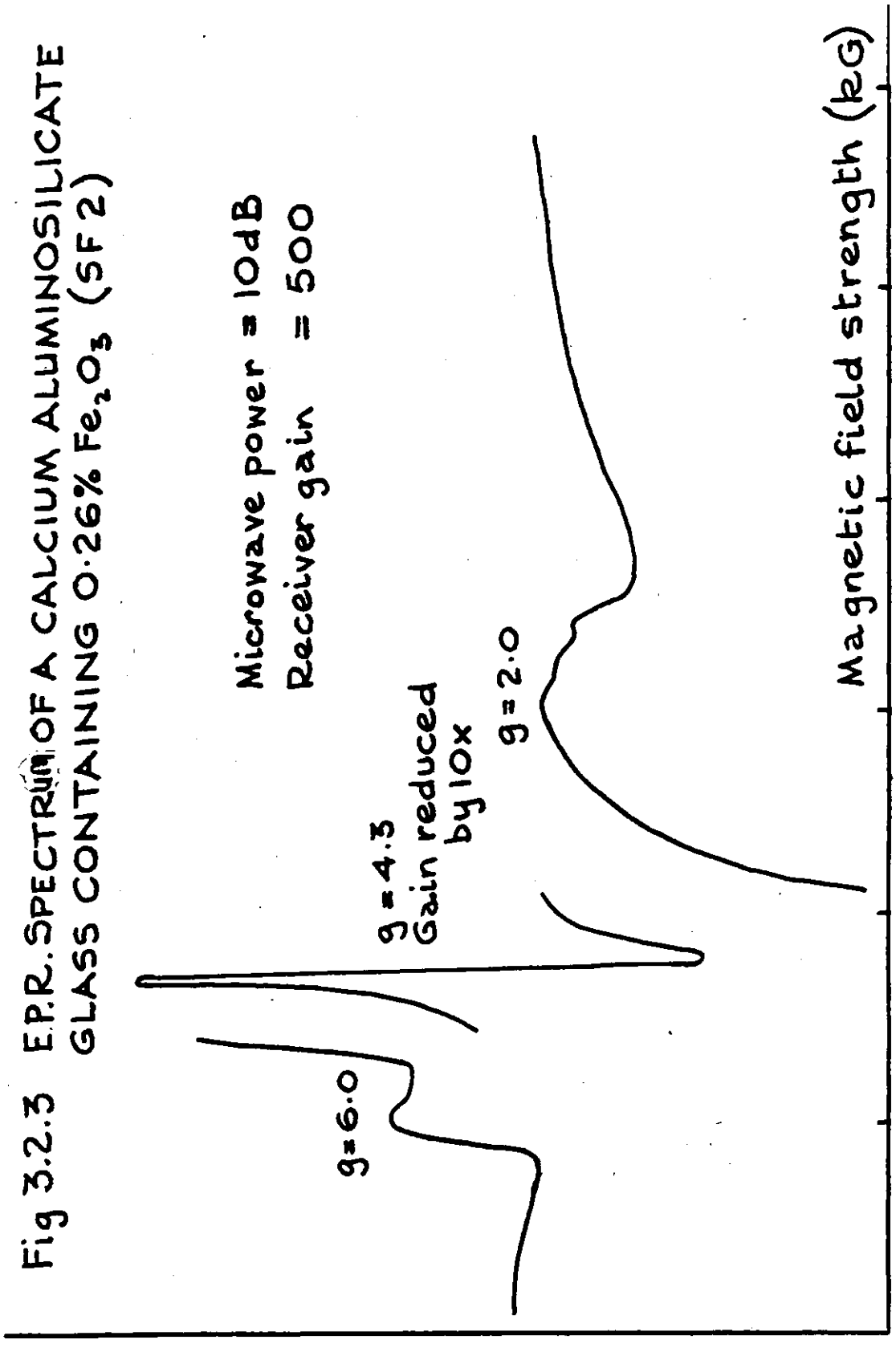

Fig 3.2.3 E.P.R. SPECTRUM OF A CALCIUM ALUMINOSILICATE GLASS CONTAINING 0·26% Fe_2O_3 (SF2)

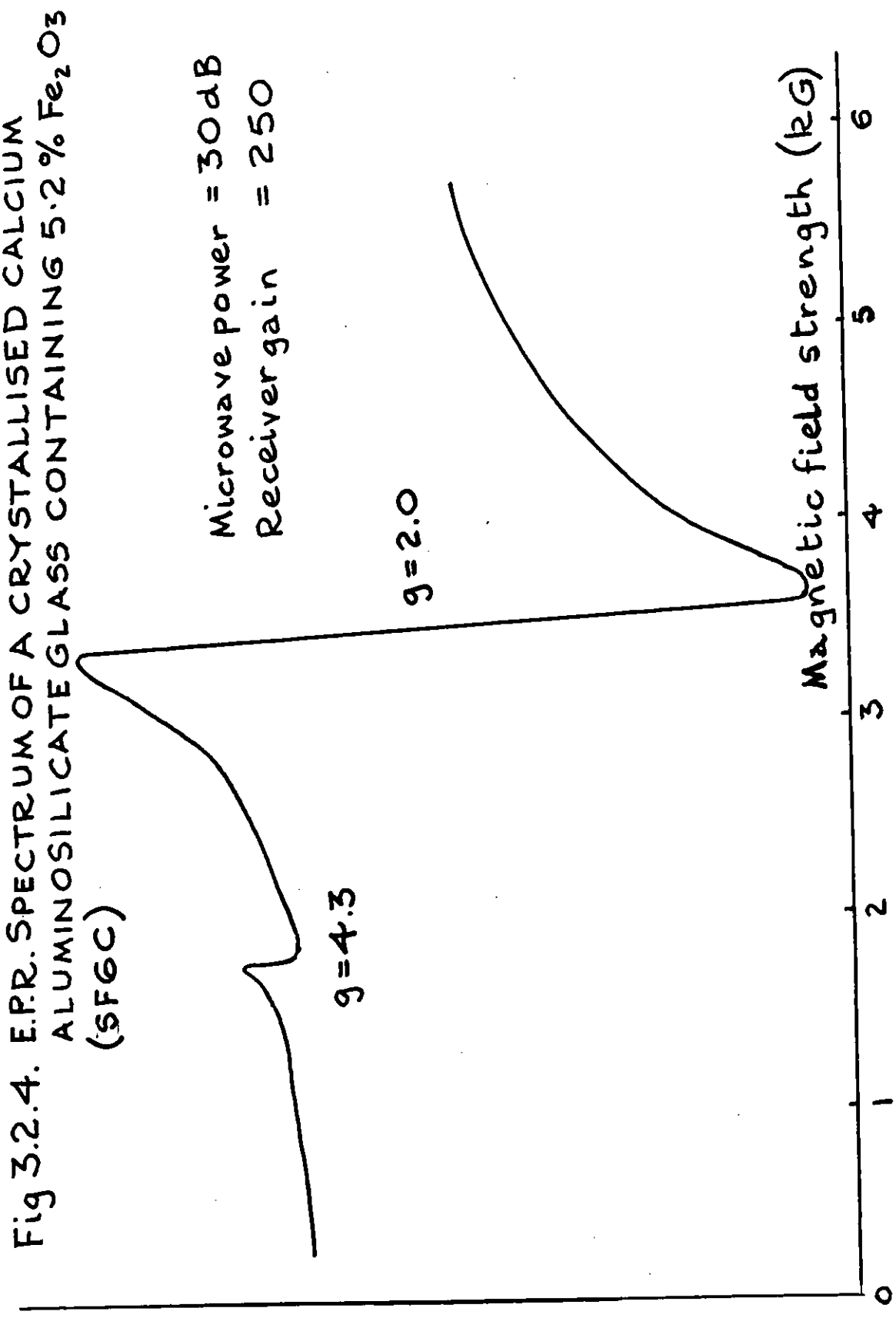

Fig 3.2.4. E.P.R. SPECTRUM OF A CRYSTALLISED CALCIUM ALUMINOSILICATE GLASS CONTAINING 5·2% Fe_2O_3 (SFGC)

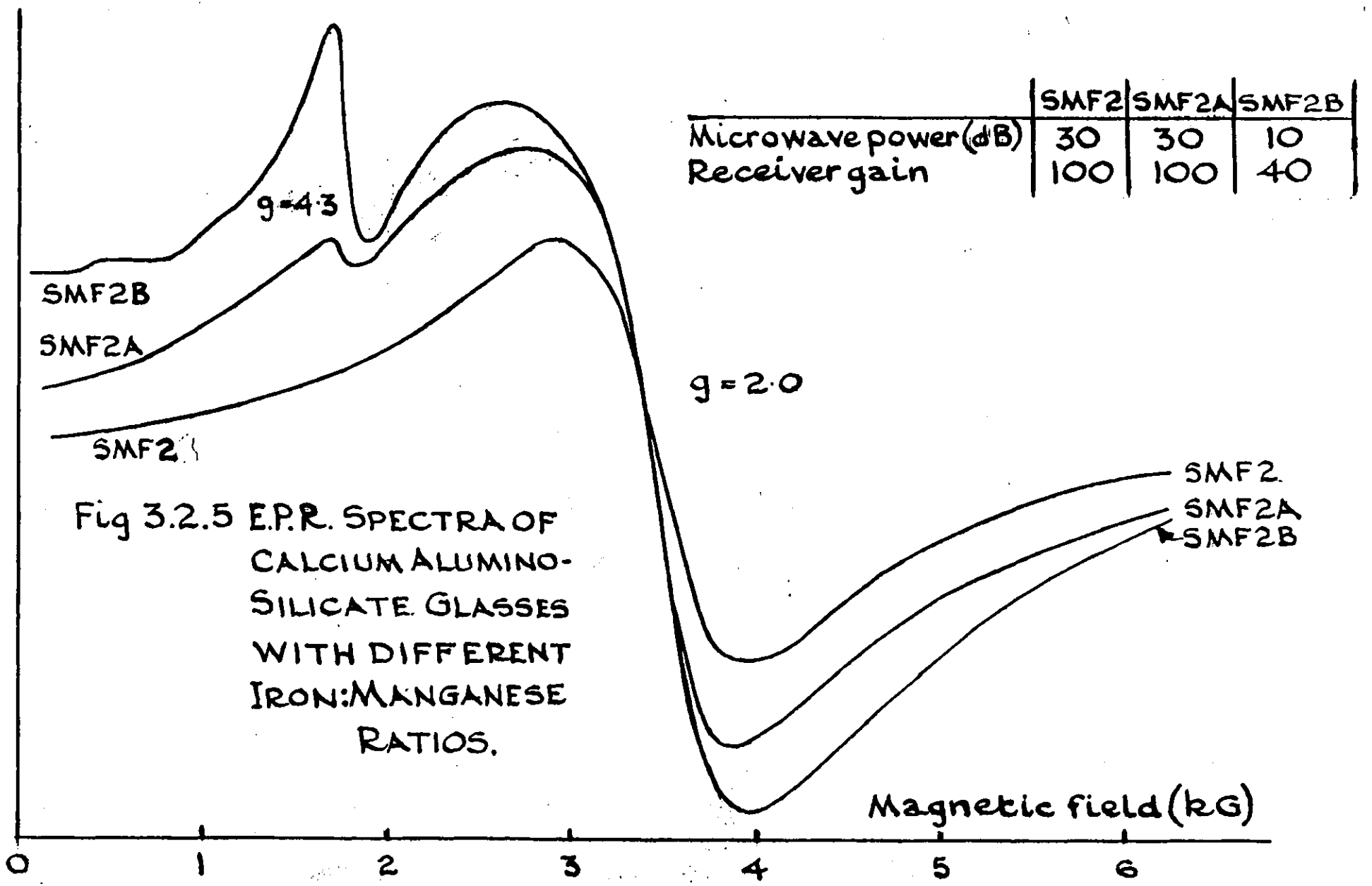

	SMF2	SMF2A	SMF2B
Microwave power (dB)	30	30	10
Receiver gain	100	100	40

Fig 3.2.5 E.P.R. SPECTRA OF CALCIUM ALUMINO-SILICATE GLASSES WITH DIFFERENT IRON:MANGANESE RATIOS.

Fig 3.3.1. Log e/T against $1/T$ for high lime manganese aluminosilicate glasses (Series SMH)

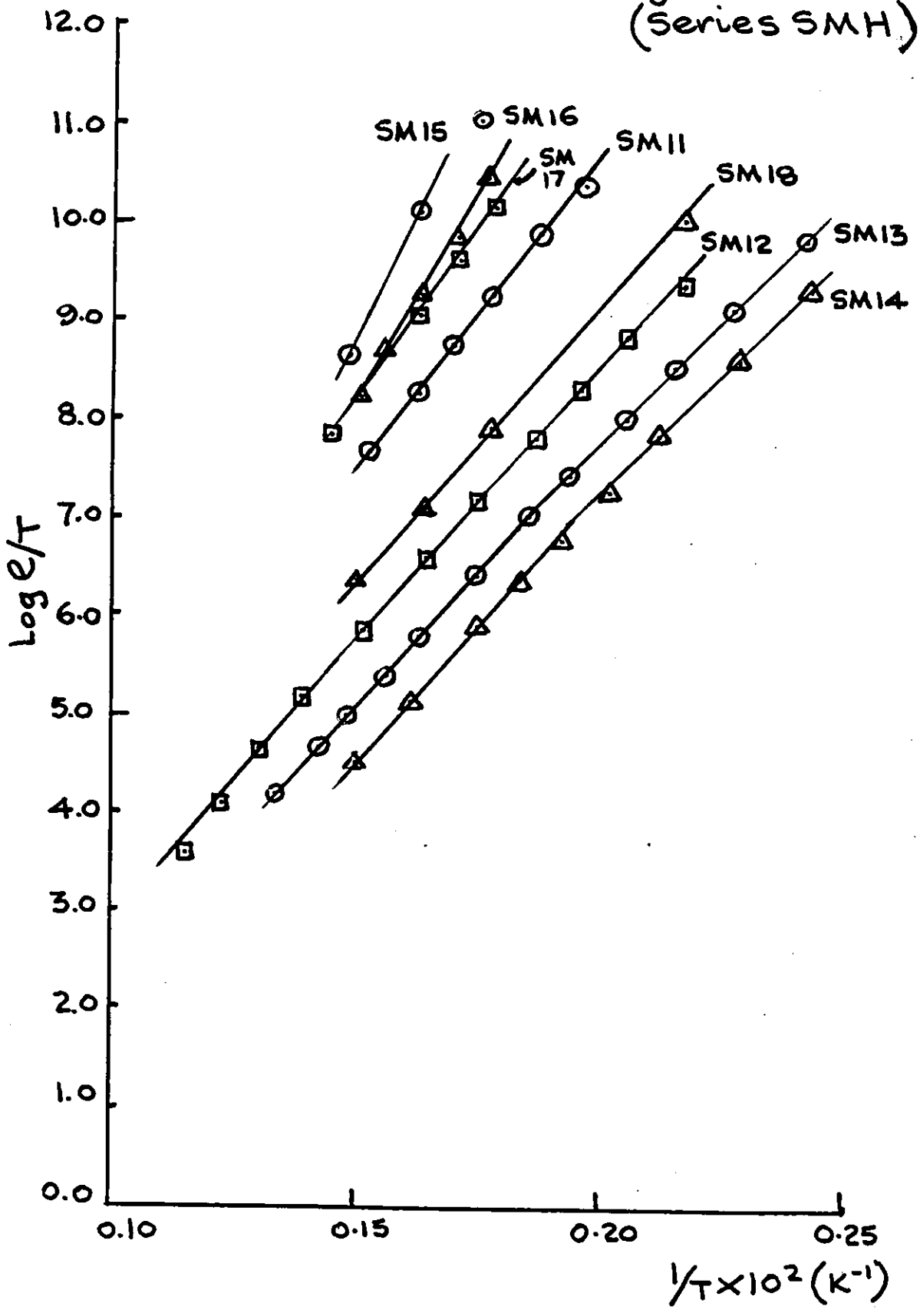

Fig. 3.3.2. Log ℓ/T against $1/T$ for low lime manganese aluminosilicate glasses (Series SML)

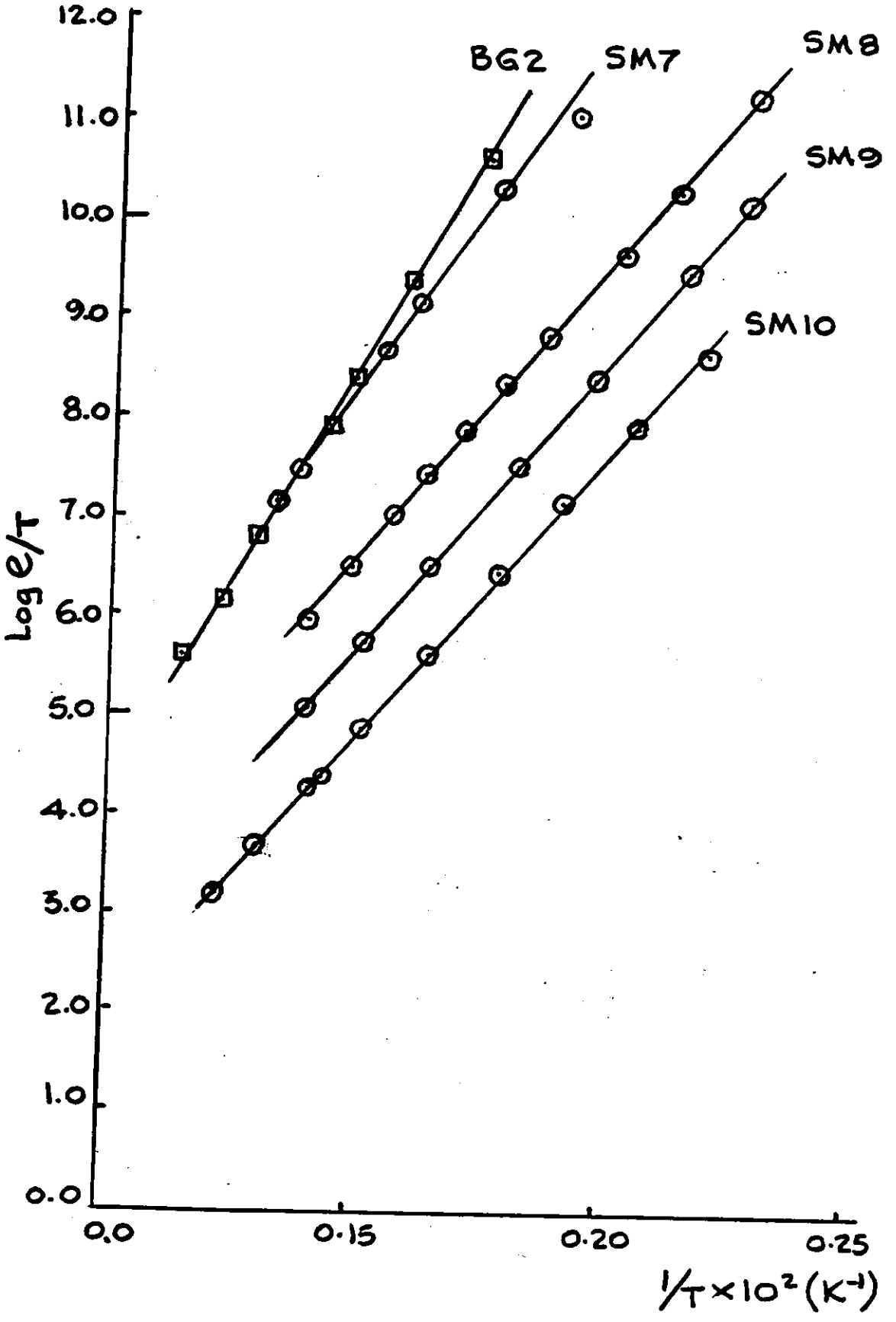

Fig 3.3.3. Log ℓ/T against $1/T$ for barium borate glasses containing manganese (series BM)

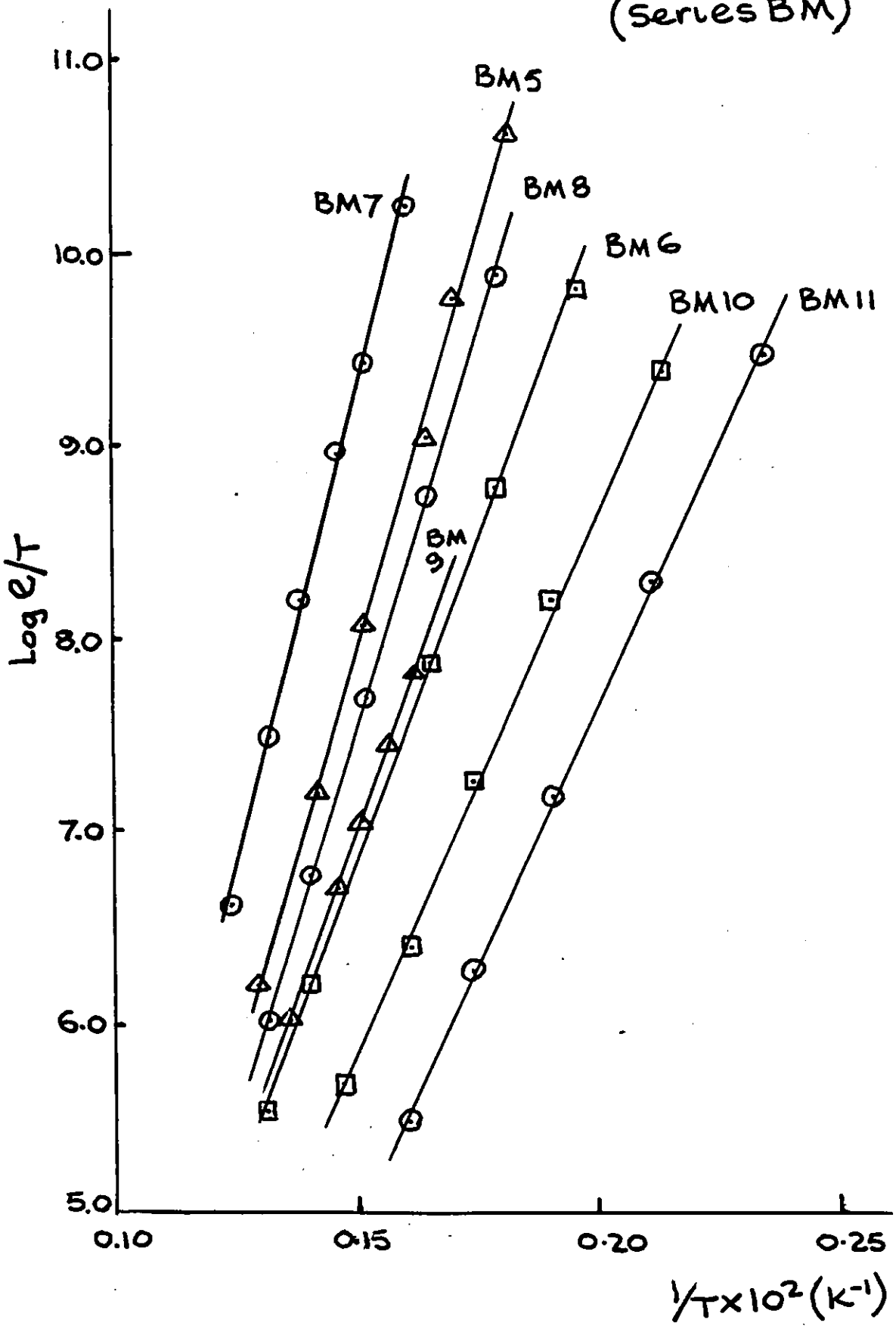

Fig 3.3.4. Log ρ/T against $1/T$ for Fe_2O_3-CaO-Al_2O_3-SiO_2 glasses

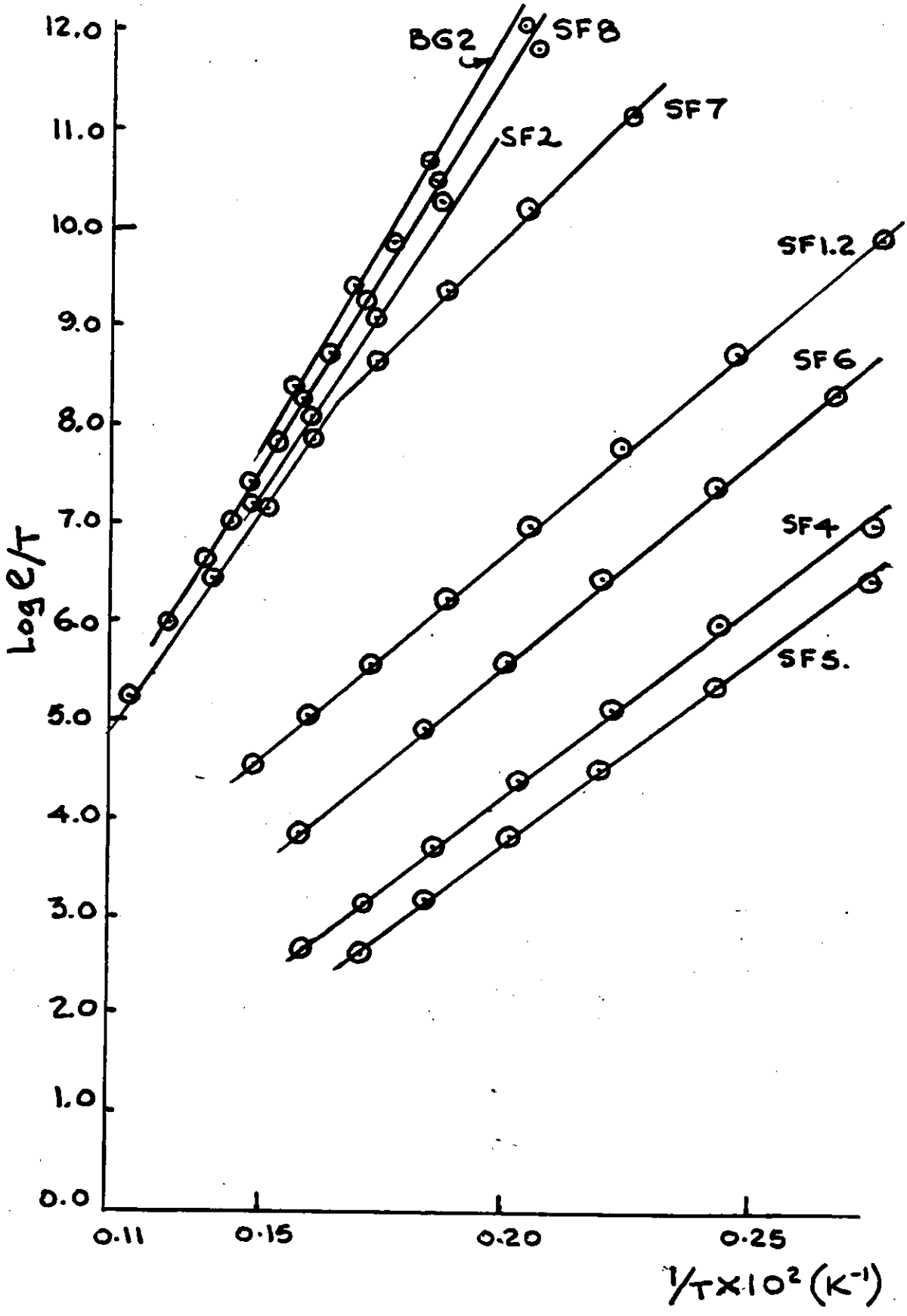

Fig 3.3.4 continued (Series SF)

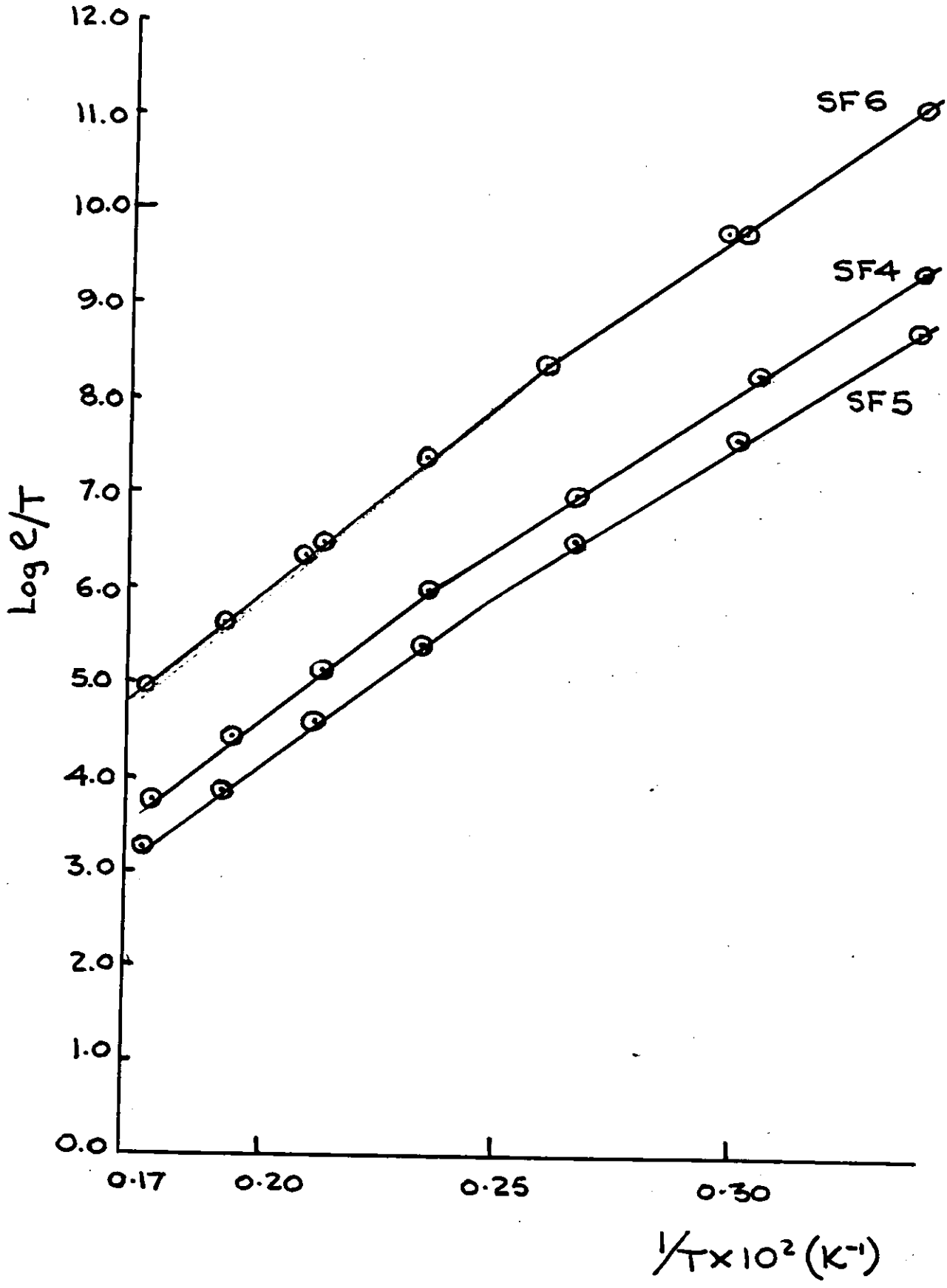

Fig 3.3.5. Log e/T against $1/T$ for $MnO-Fe_2O_3-CaO-Al_2O_3-SiO_2$ glasses

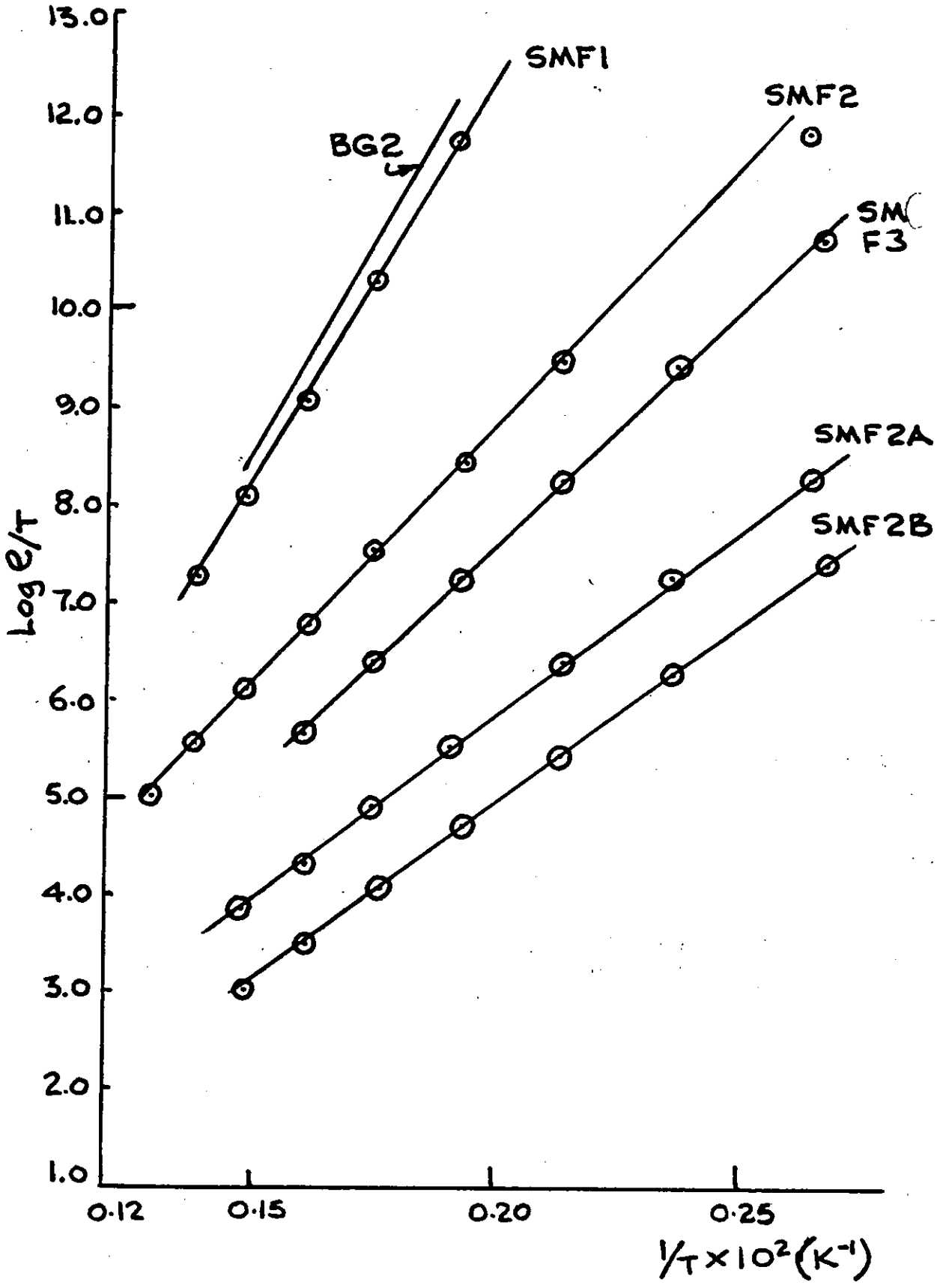

Figs 3.4.1 - 3.4.11.
Log ρ against $1/T$ for glasses and crystallised glasses.

Fig 3.4.1.

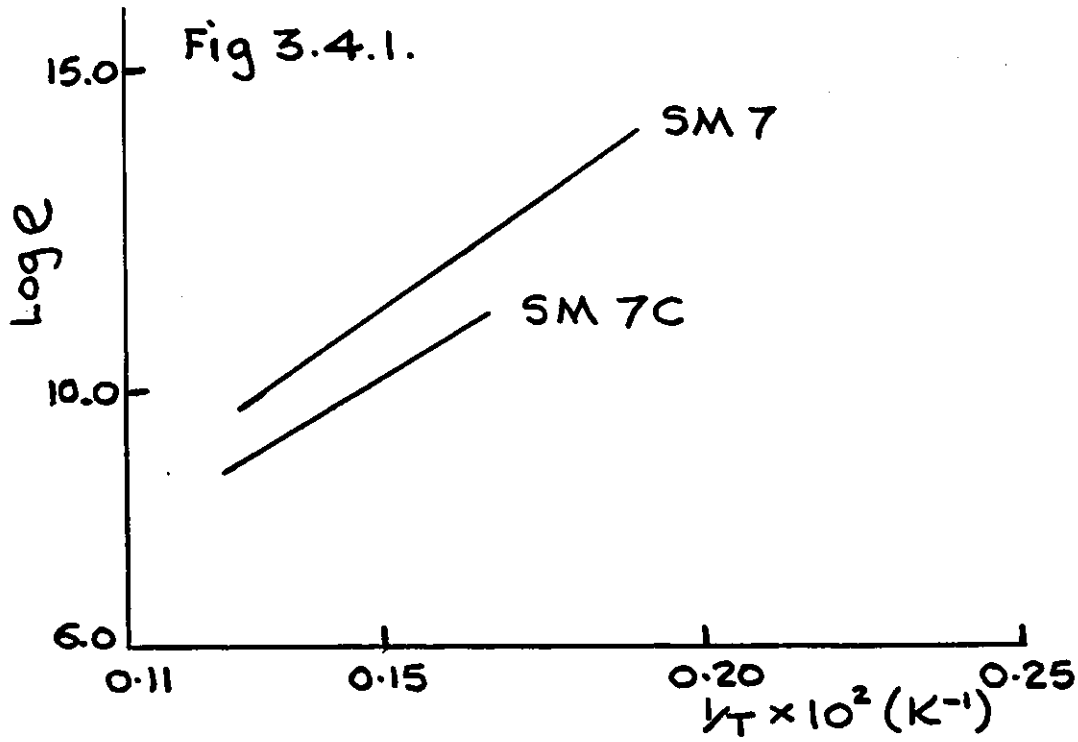

Fig 3.4.2.

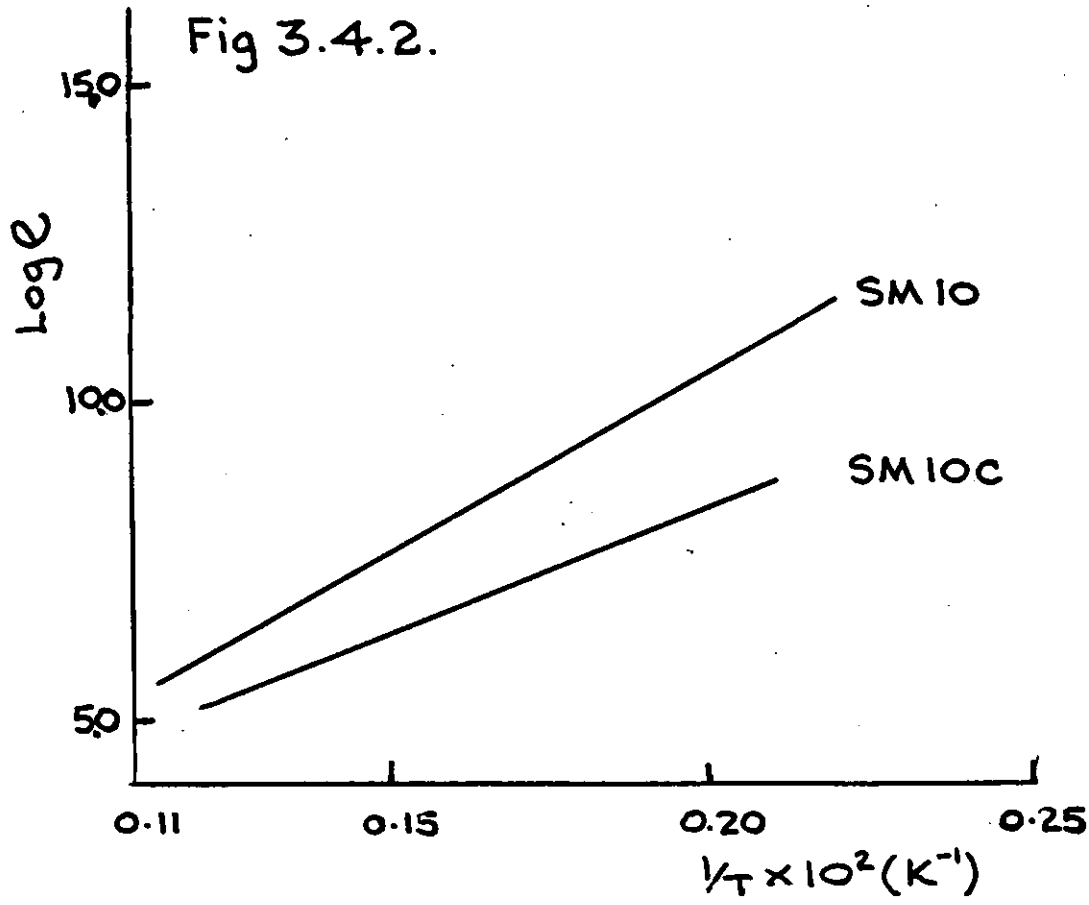

Log ℓ against 1/T for glasses and crystallised glasses

Fig 3.4.3.

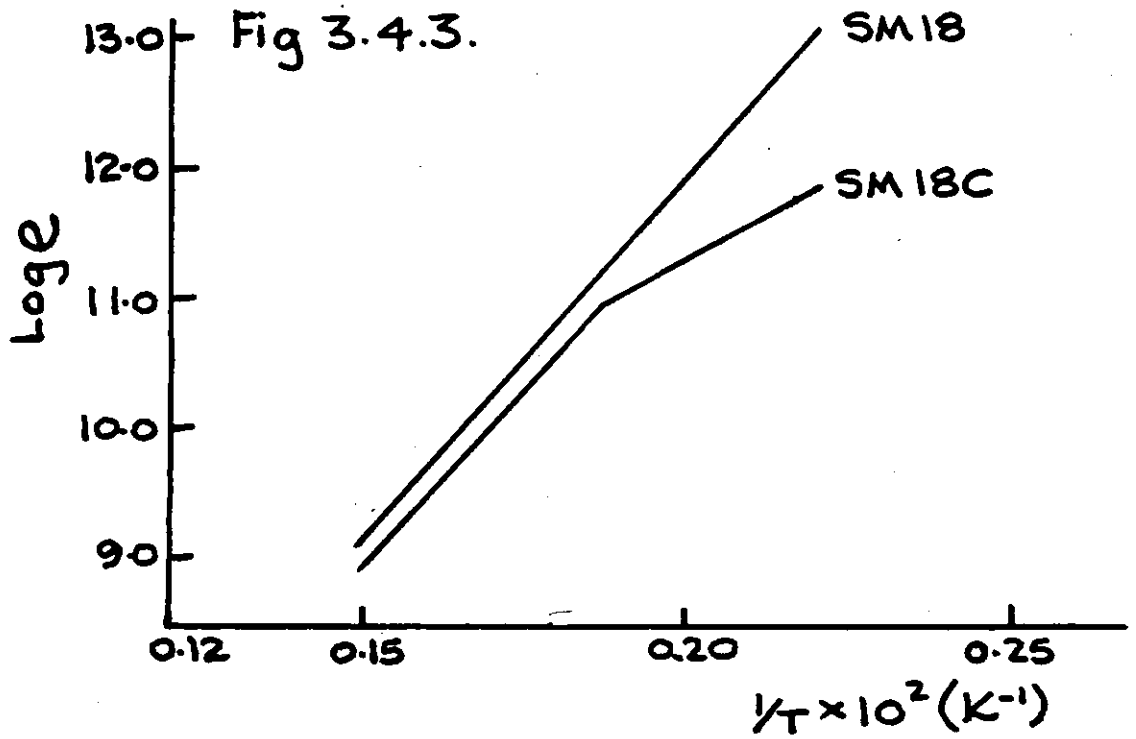

Fig 3.4.4.

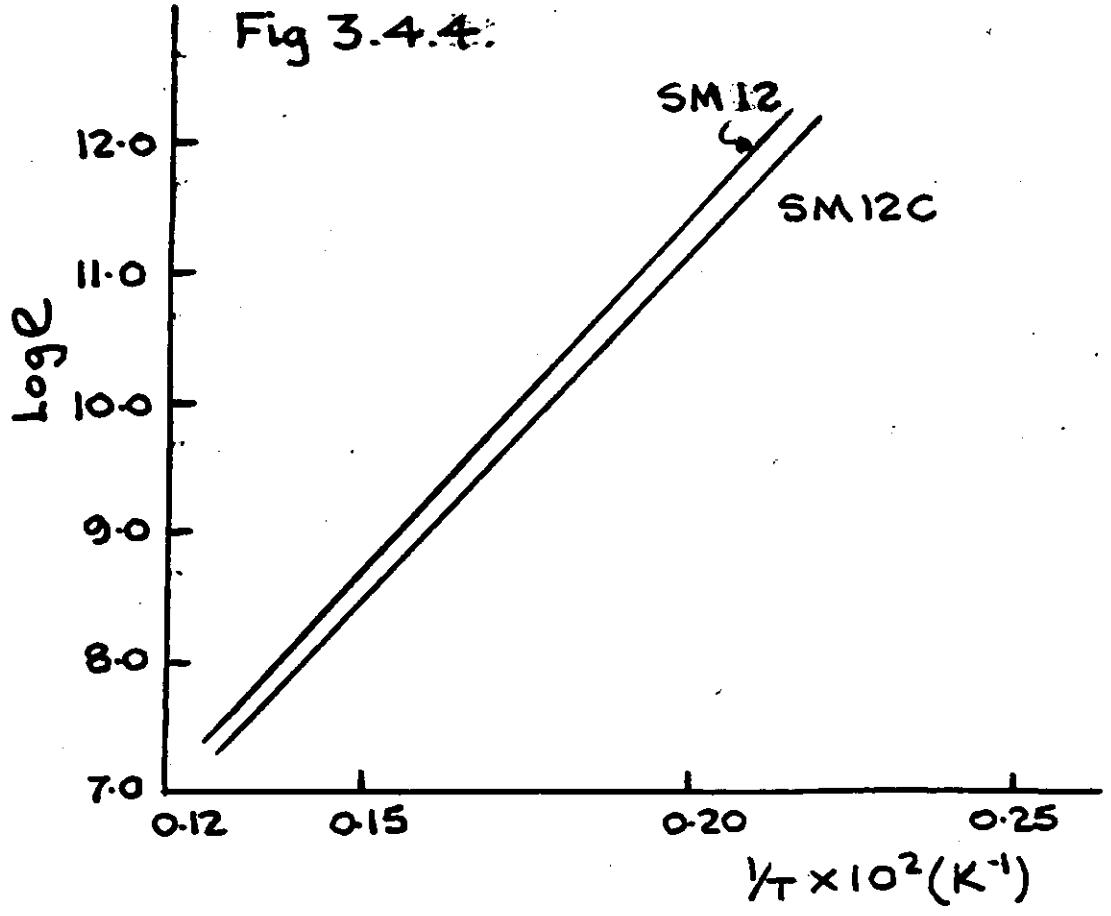

Log e against 1/T for glasses and crystallised glasses.

Fig 3.4.5.

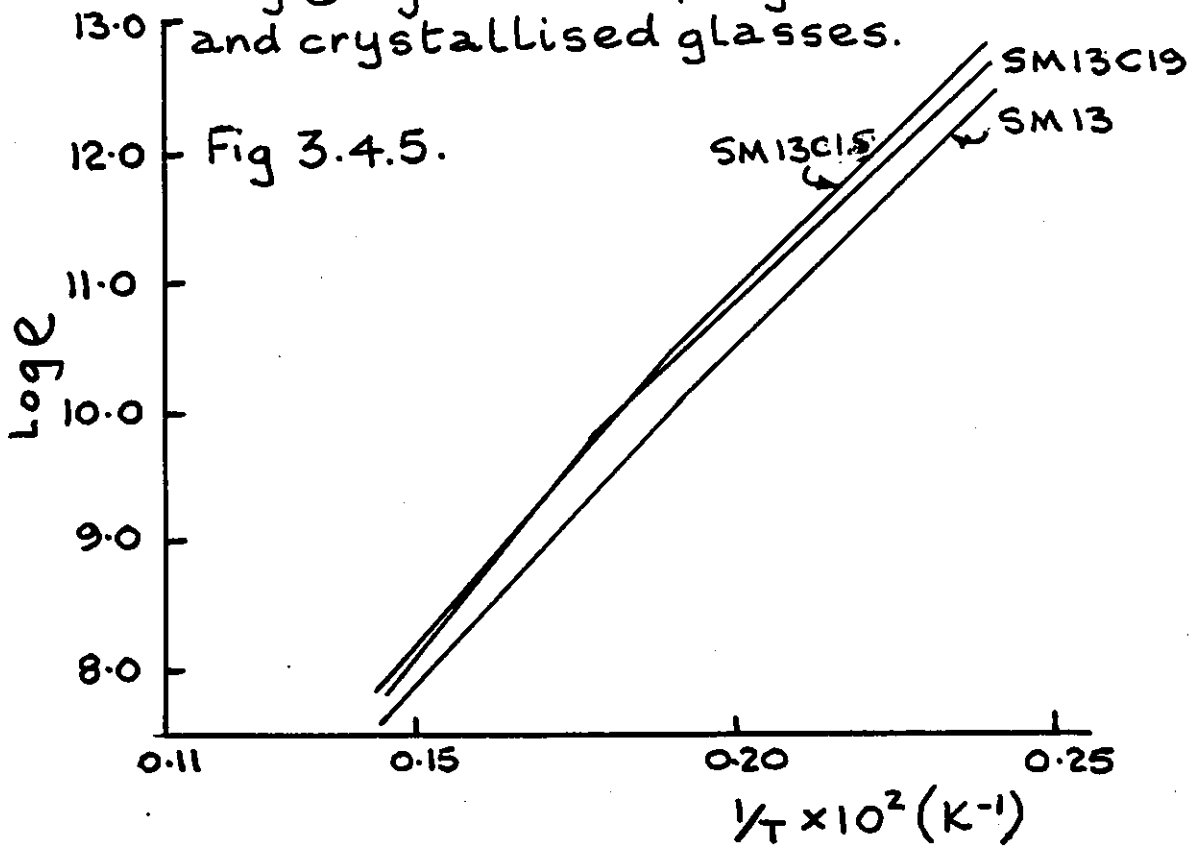

Fig 3.4.6.

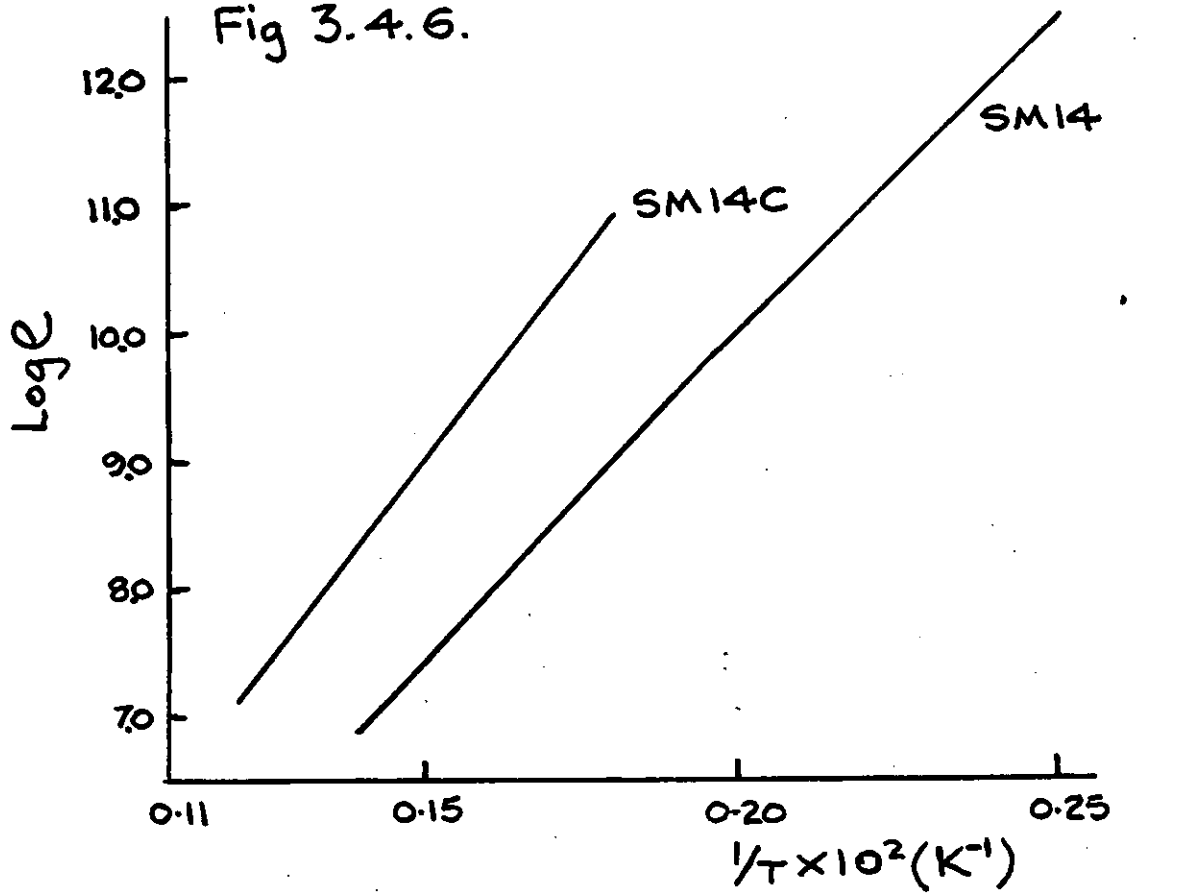

Log ℓ against 1/T for glasses and crystallised glasses.

Fig 3.4.7.

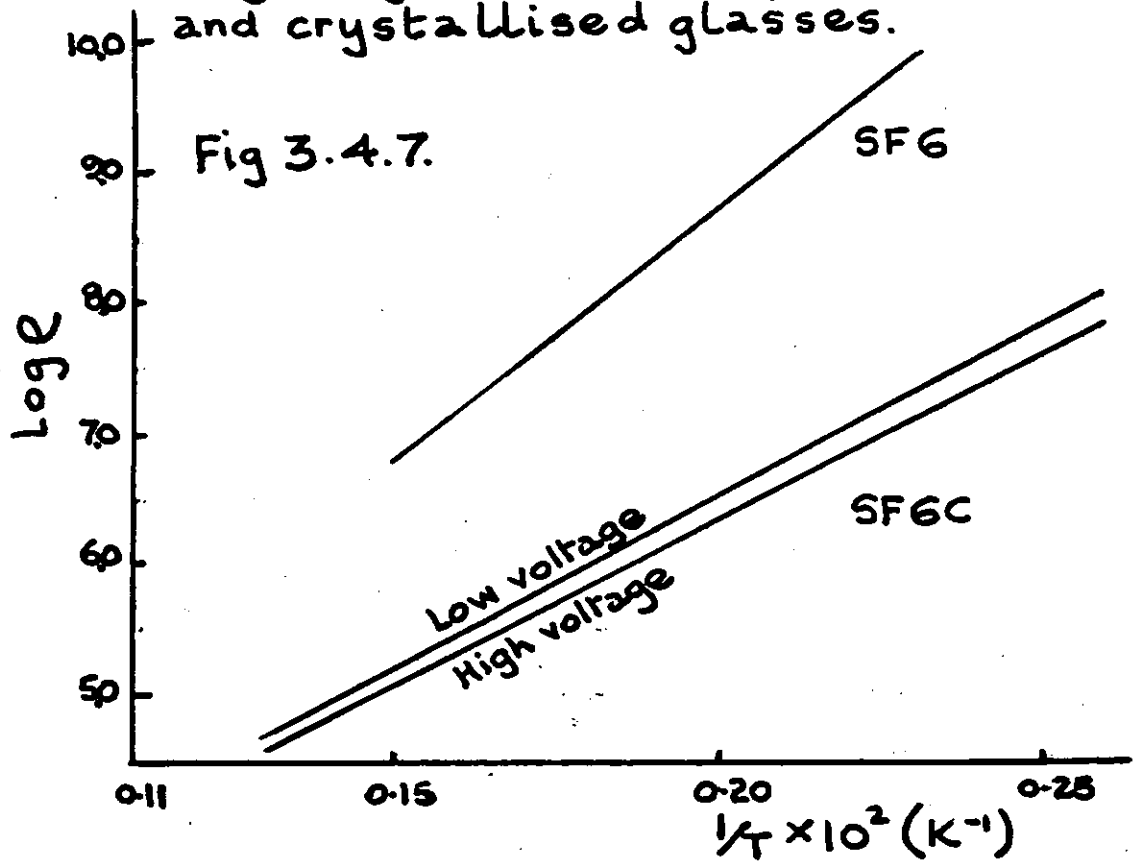

Fig 3.4.8.

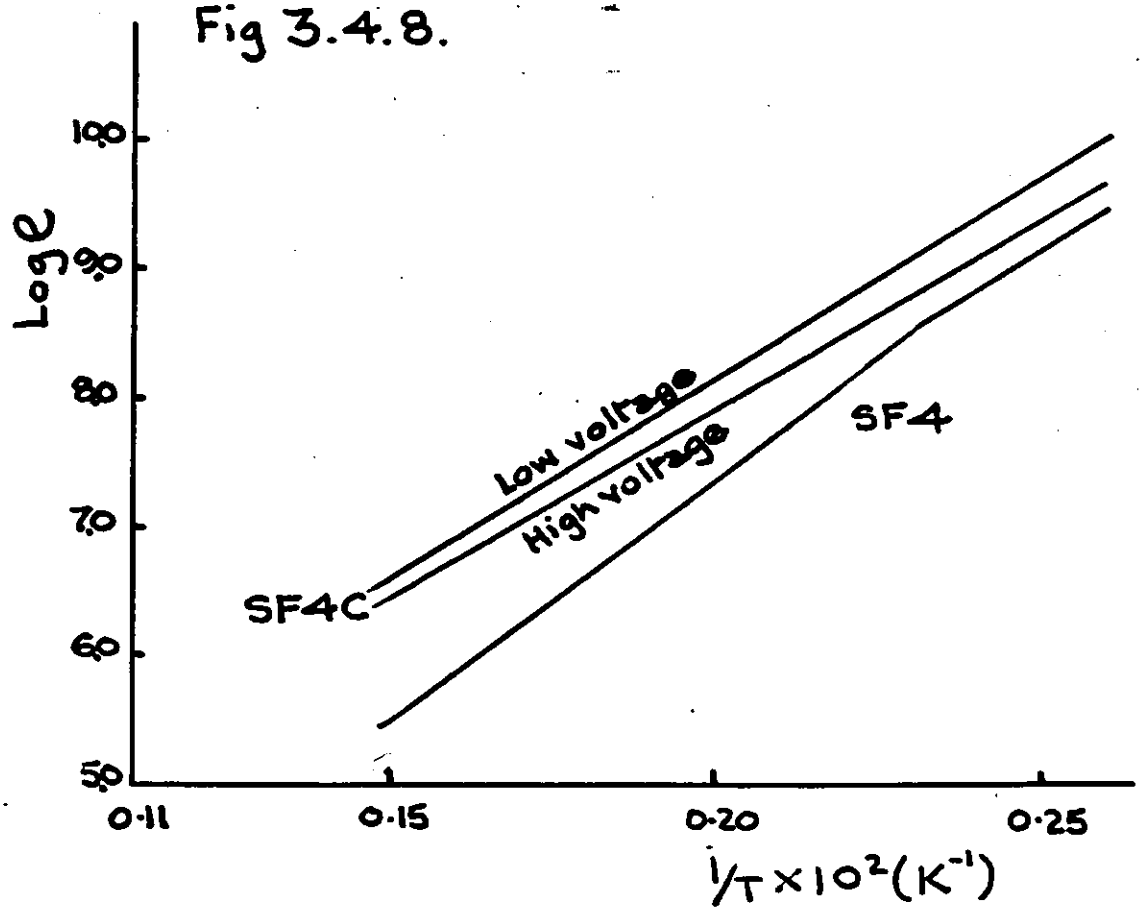

Log ℓ against 1/T for glasses and crystallised glasses.

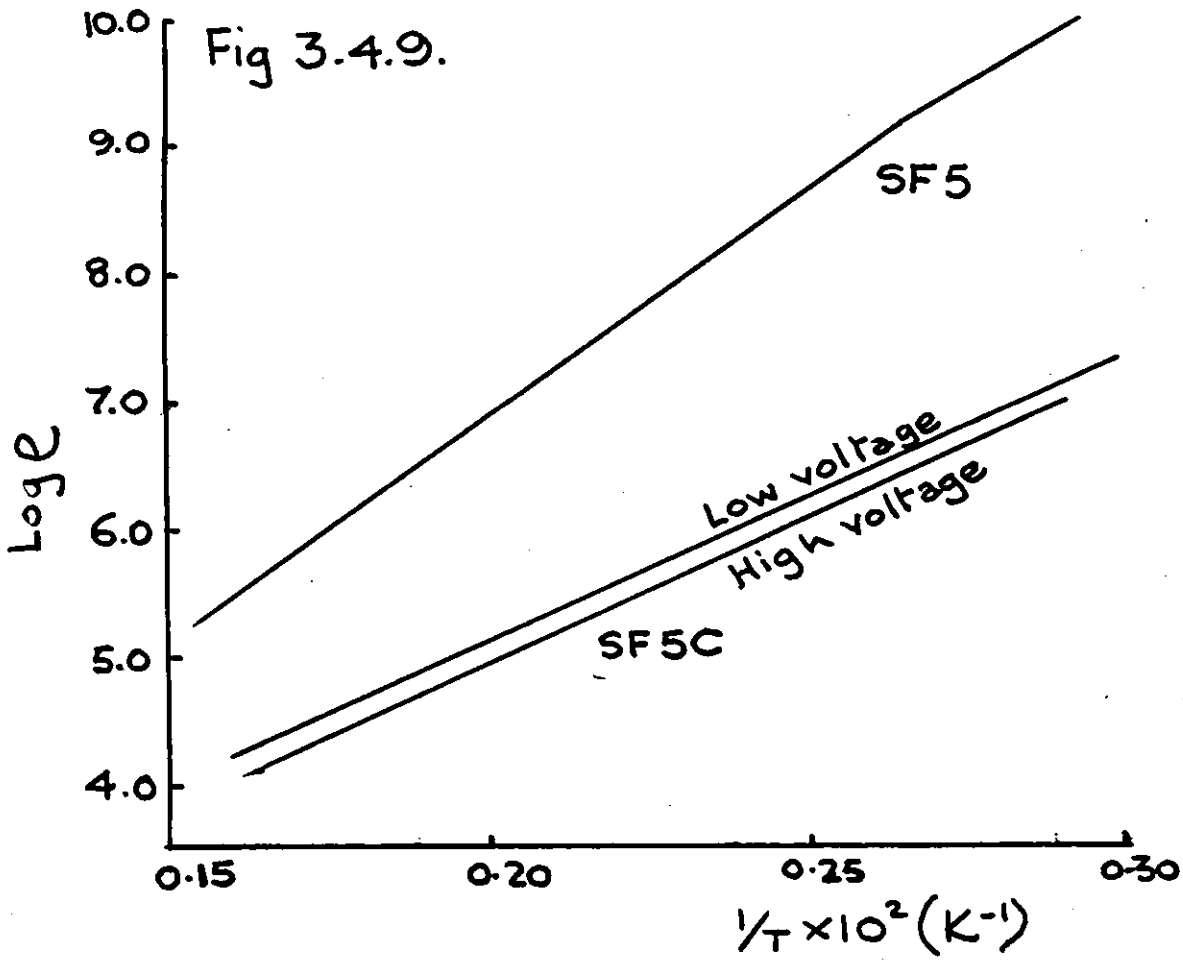

Log ρ against 1/T for glasses and crystallised glasses

Fig 3.4.10.

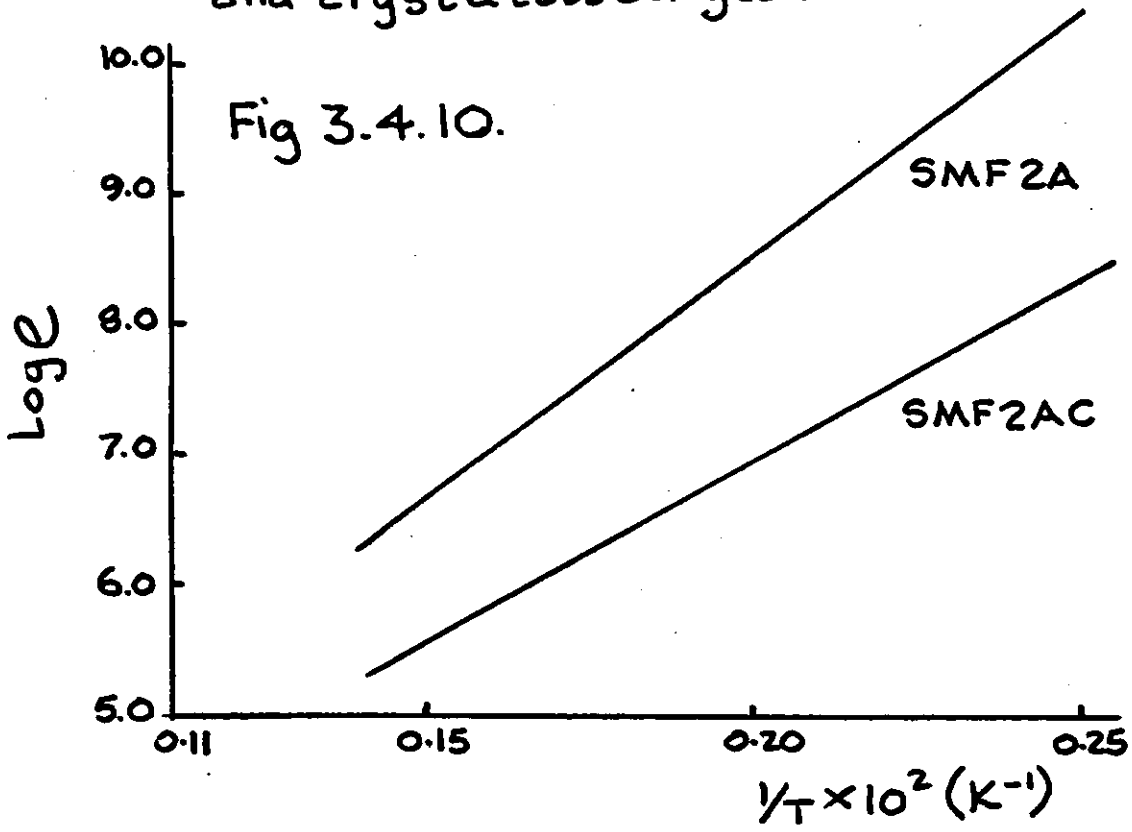

Fig 3.4.11.

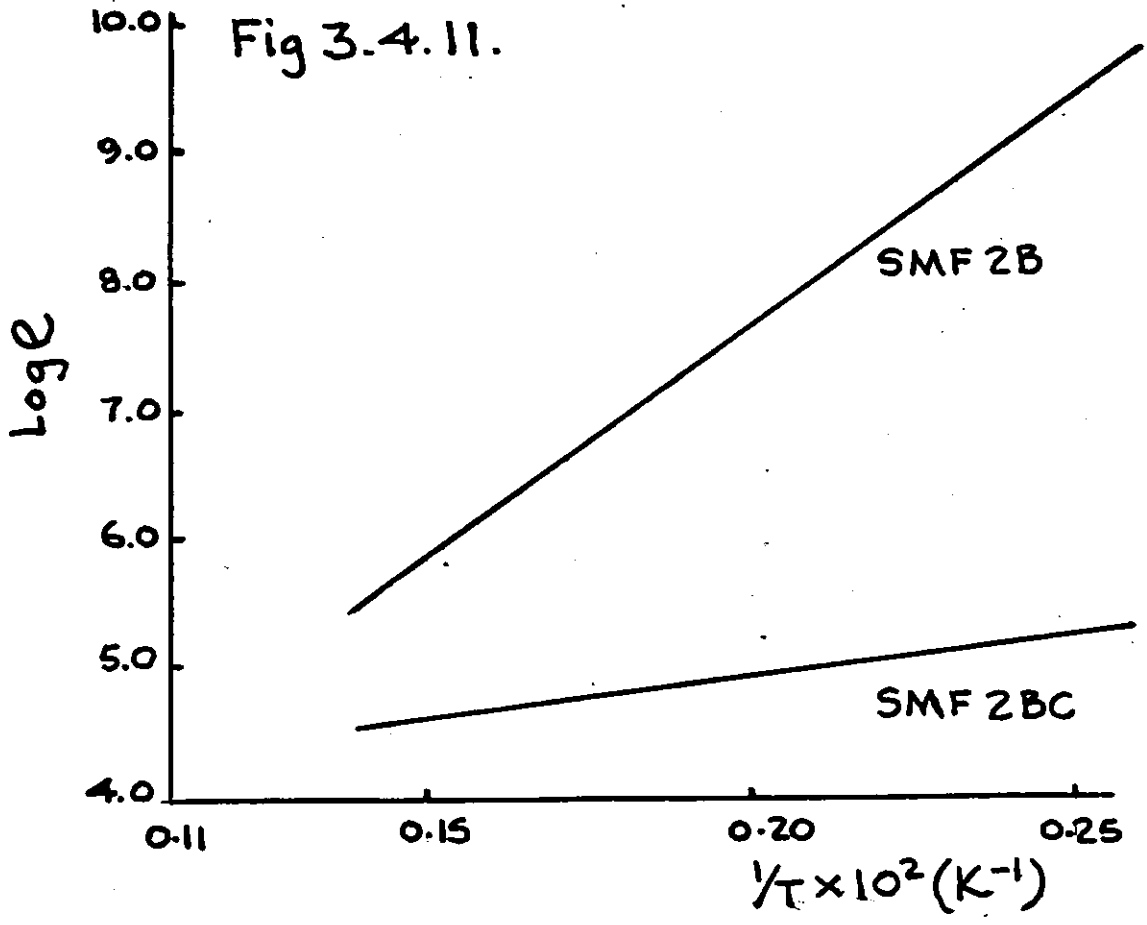

Fig. 3.5.1..

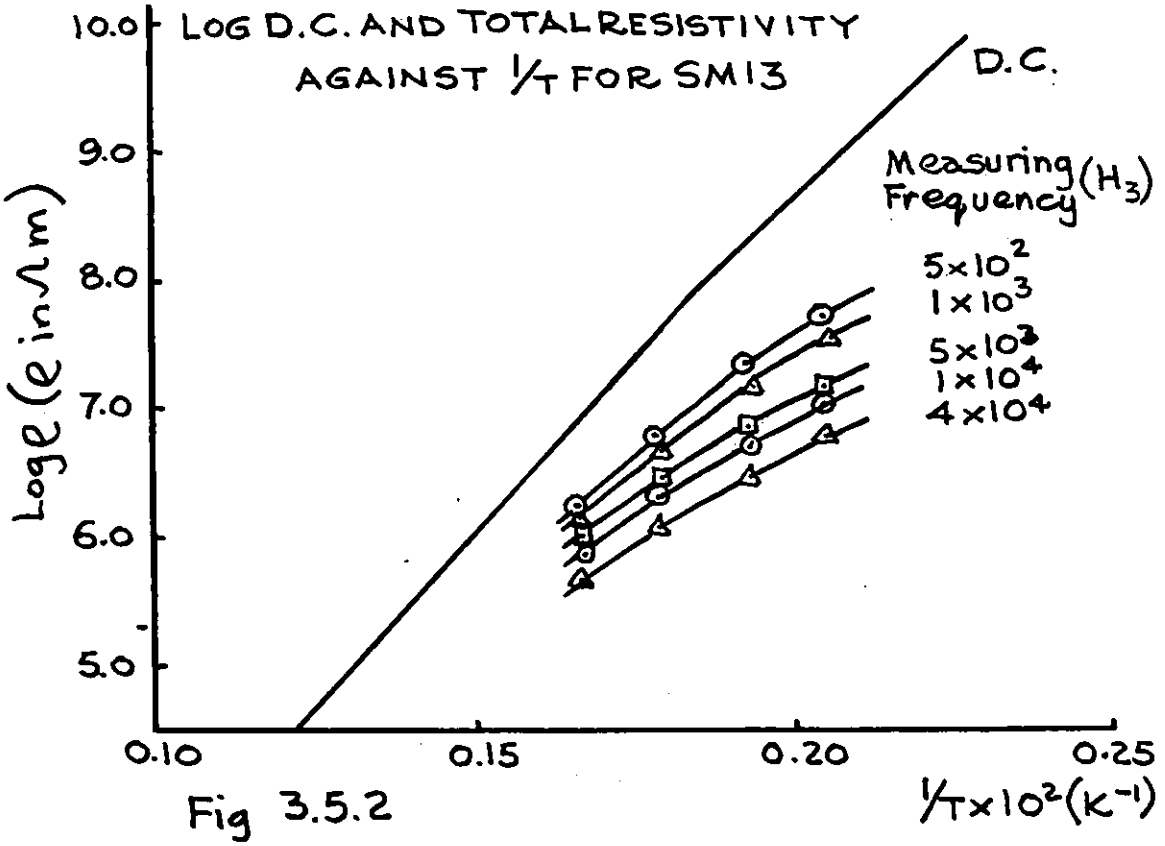

Fig 3.5.2

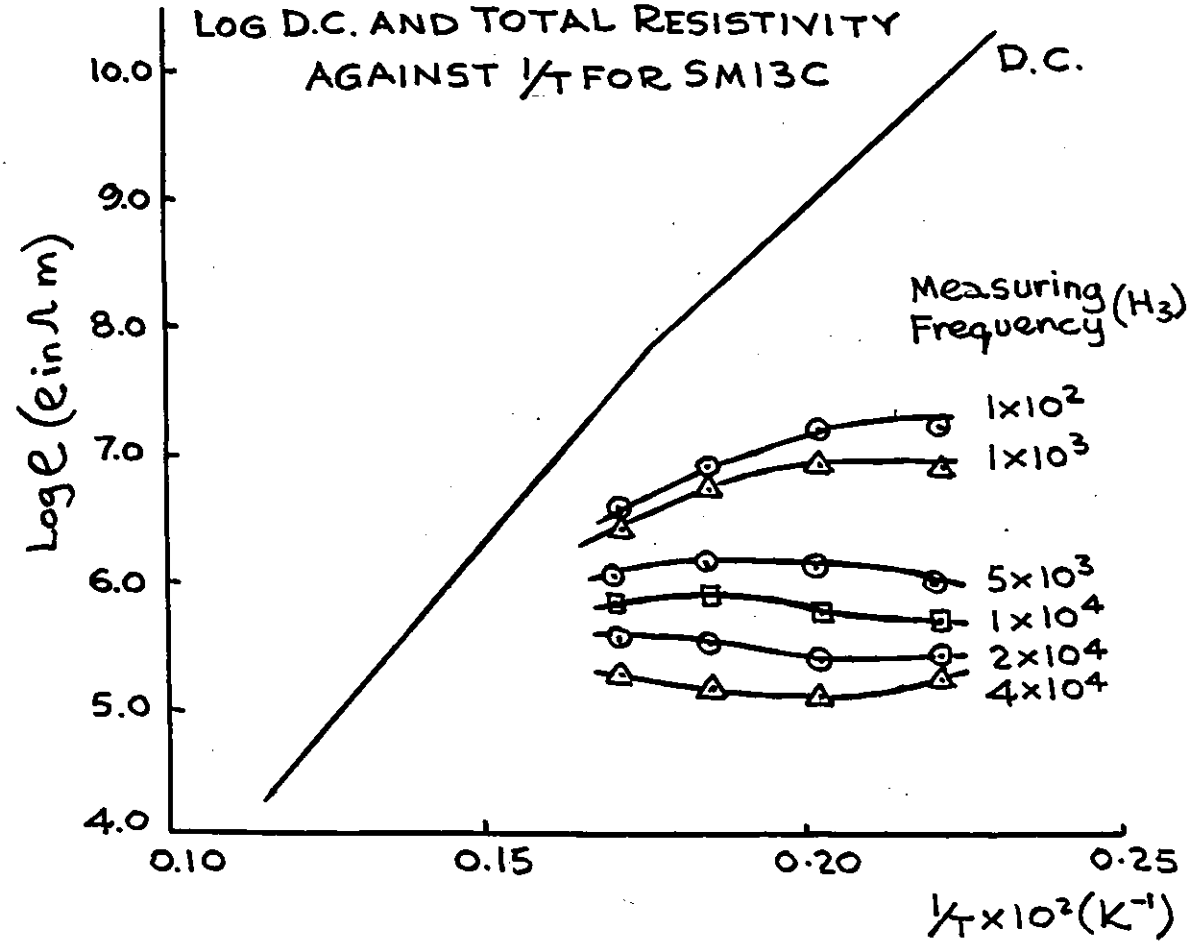

Fig. 3.5.3.

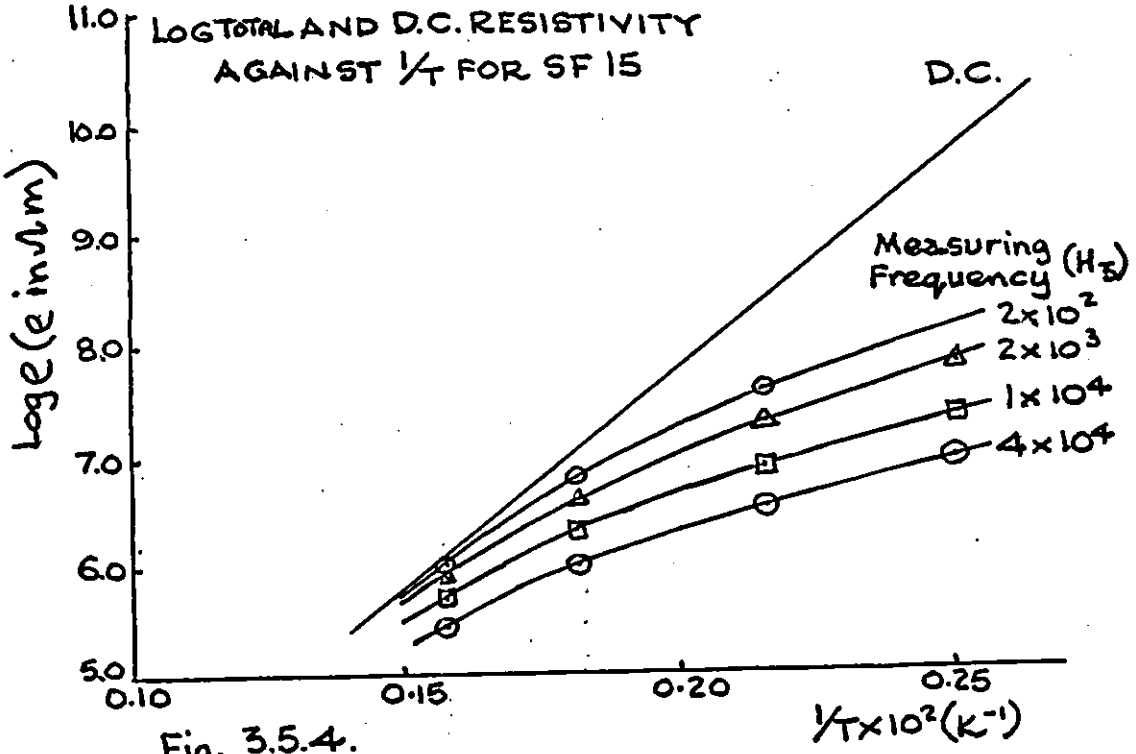

Fig. 3.5.4.

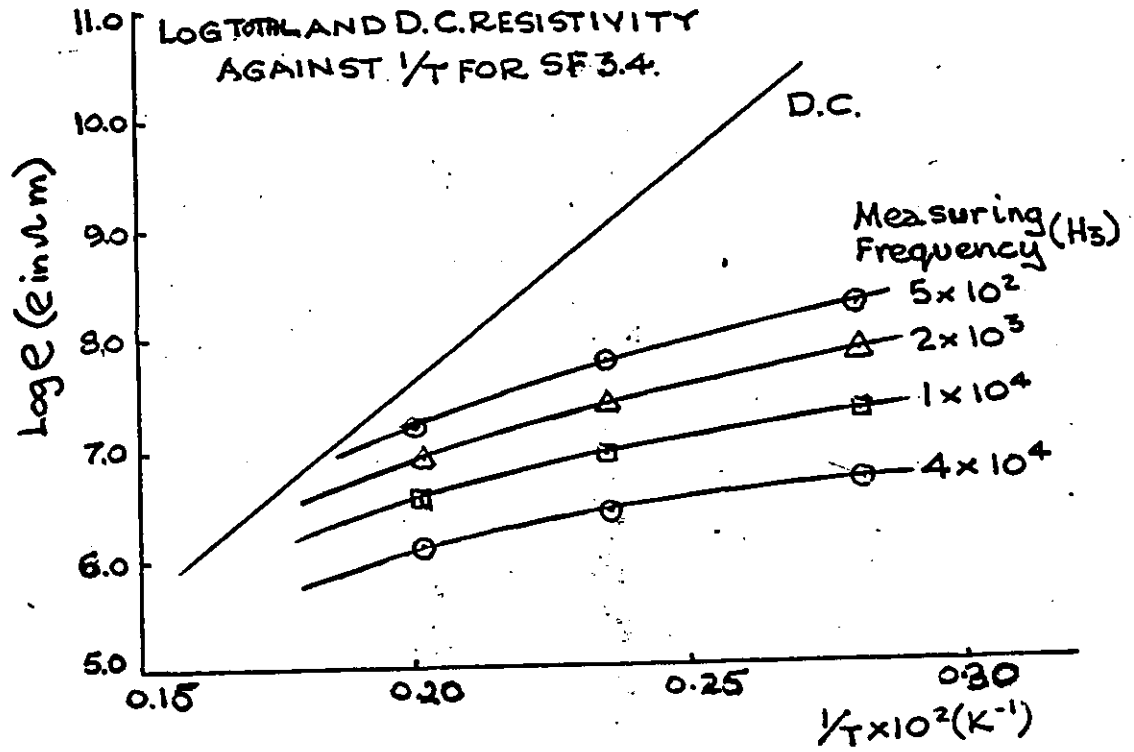

Fig. 3.5.5

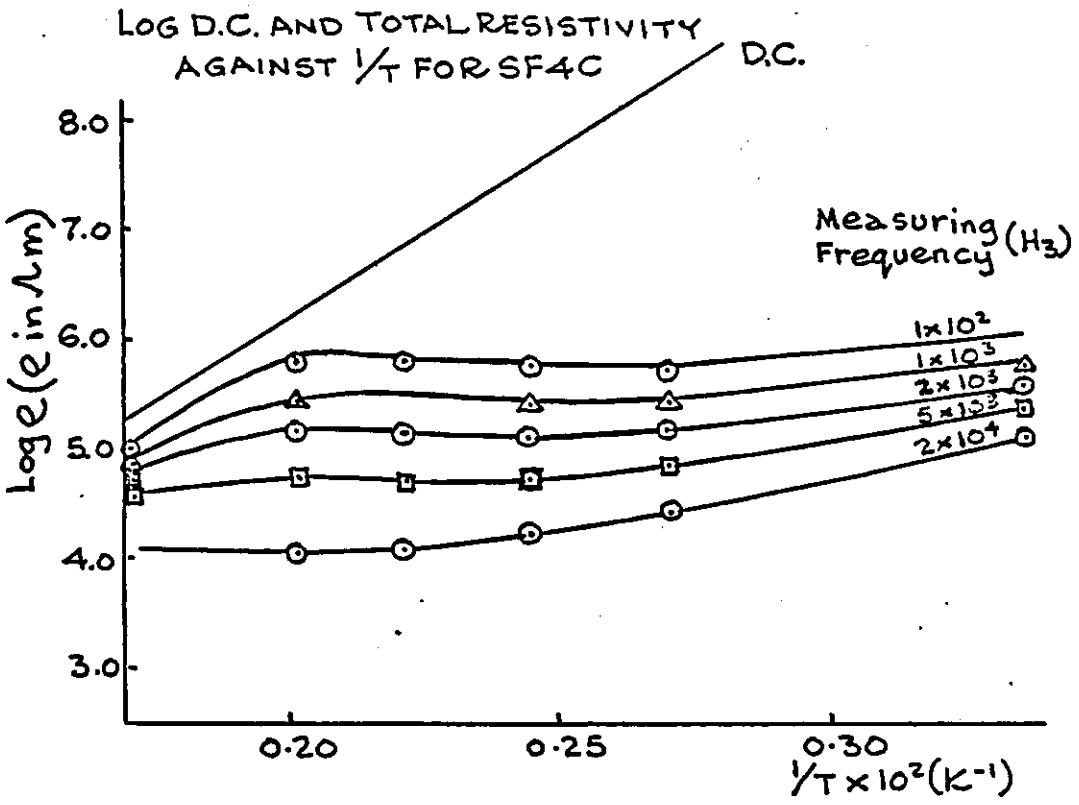

Fig. 3.5.6.

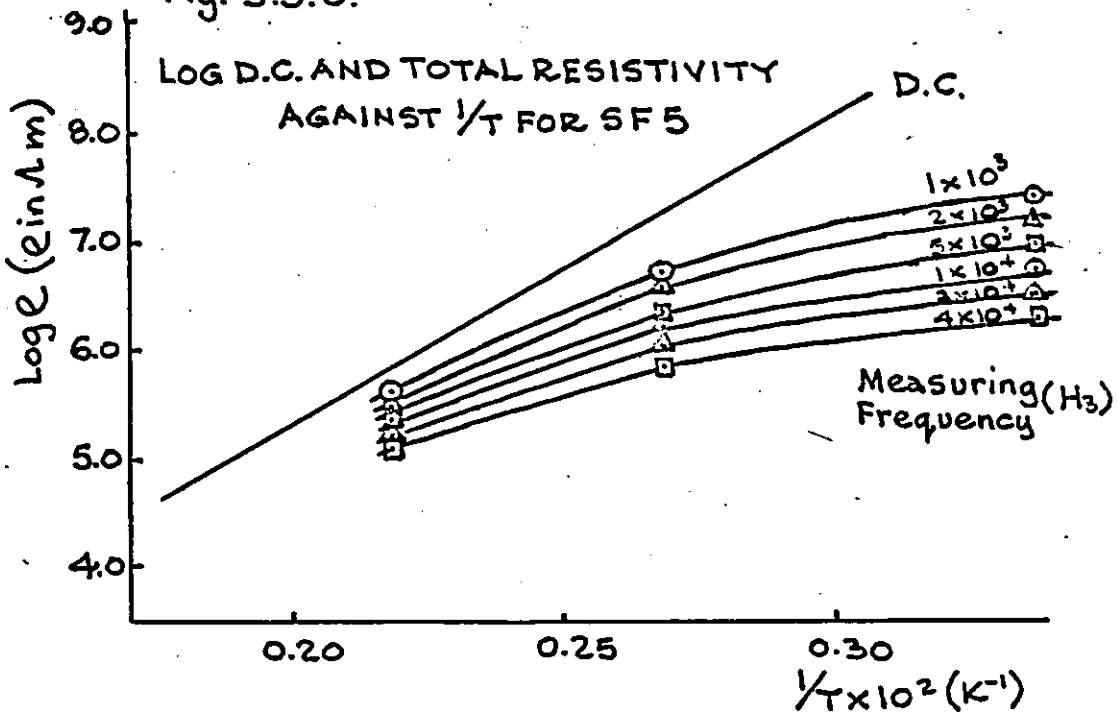

Fig. 3.5.7

LOG D.C. AND TOTAL RESISTIVITY AGAINST 1/T FOR SMF 2A

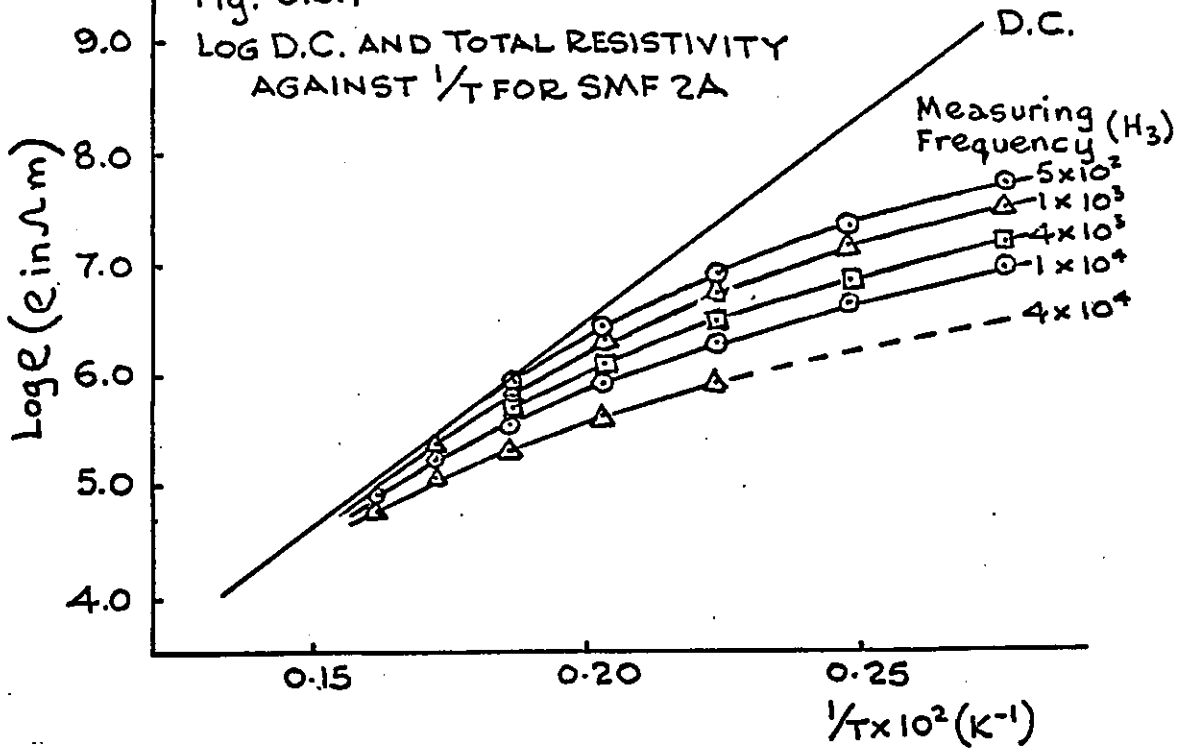

Fig. 3.5.8

LOG D.C. AND TOTAL RESISTIVITY AGAINST 1/T FOR SMF 2AC

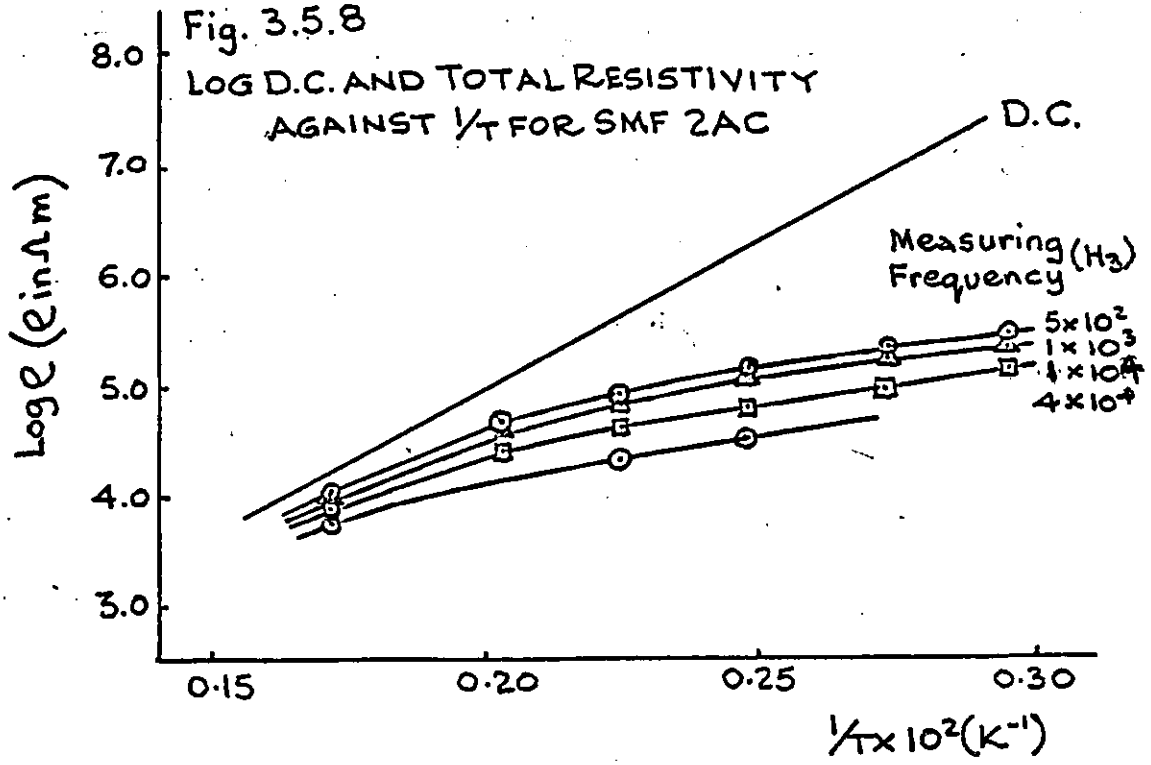

Fig 3.5.9

LOG TOTAL AND D.C. RESISTIVITY AGAINST 1/T FOR SMF 3

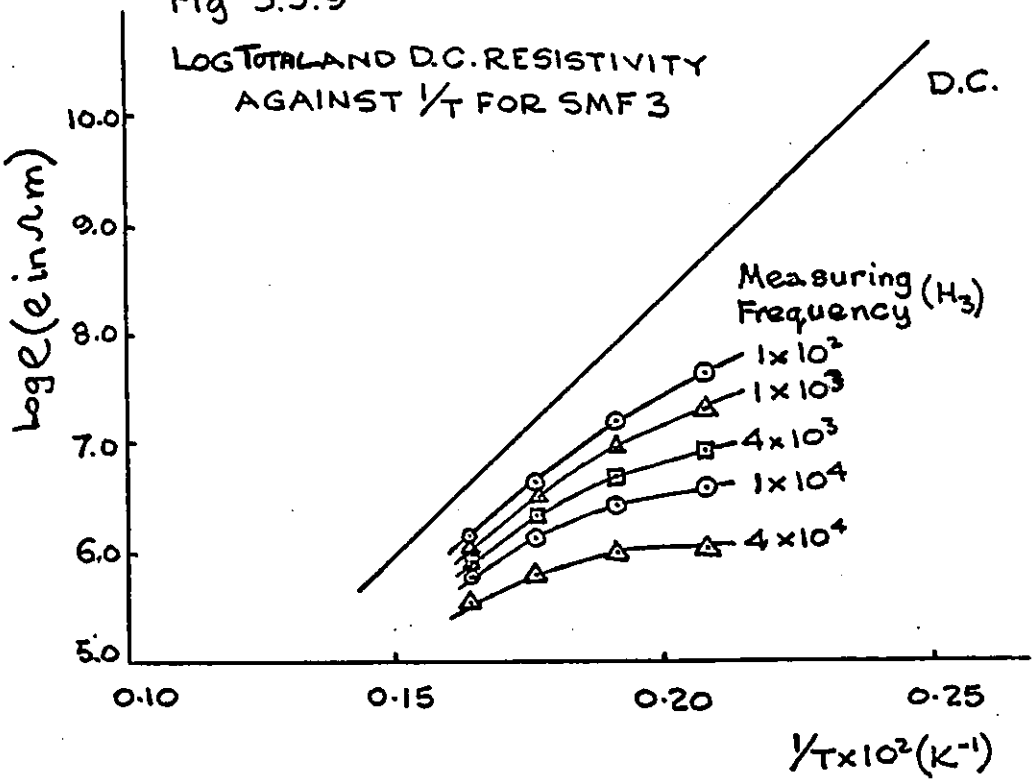

LOG A.C. RESISTIVITY AGAINST LOG FREQUENCY

Fig 3.6.1 SM13

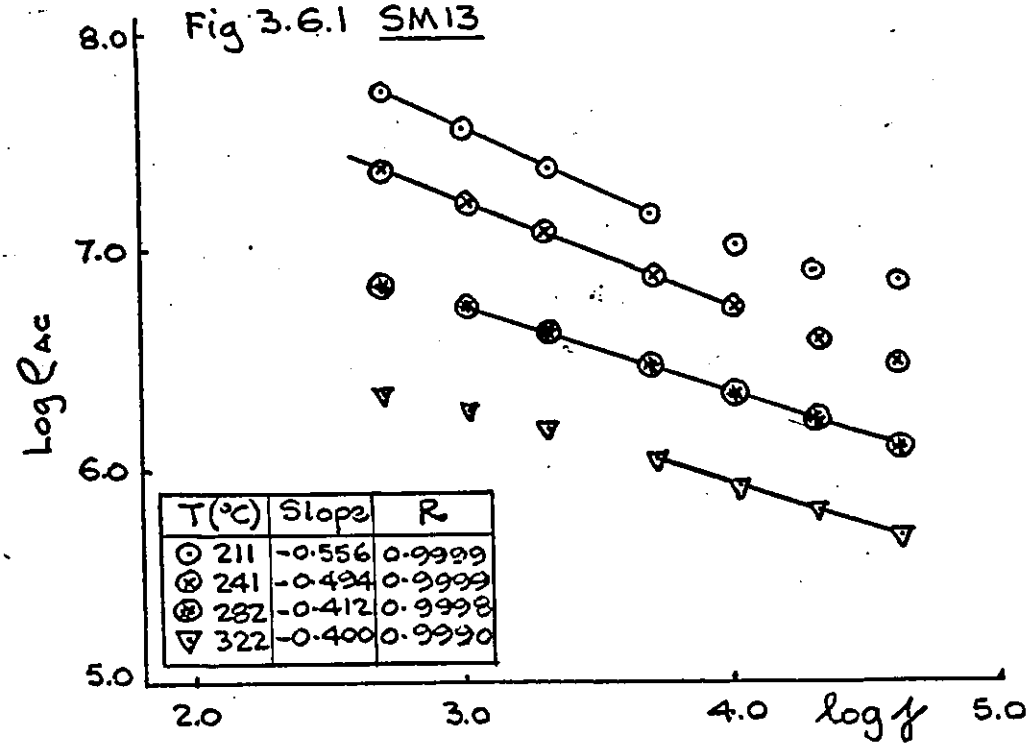

T(°C)	Slope	R
⊙ 211	-0.556	0.9999
⊗ 241	-0.494	0.9999
⊛ 282	-0.412	0.9998
▽ 322	-0.400	0.9990

LOG A.C. RESISTIVITY AGAINST LOG FREQUENCY

Fig 3.6.2. SM13C19

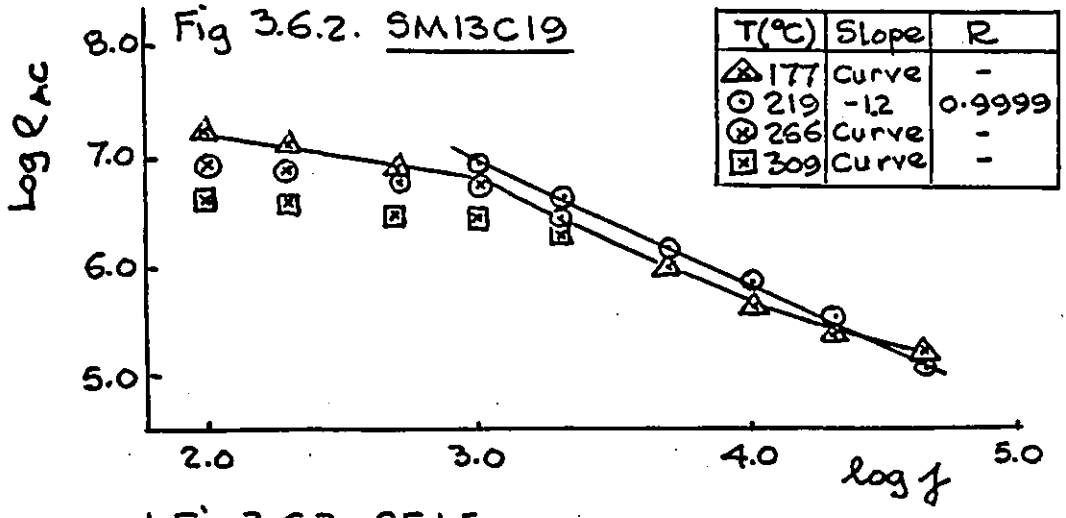

T(°C)	Slope	R
△ 177	Curve	-
⊙ 219	-1.2	0.9999
⊗ 266	Curve	-
⊠ 309	Curve	-

Fig 3.6.3 SF 1.5.

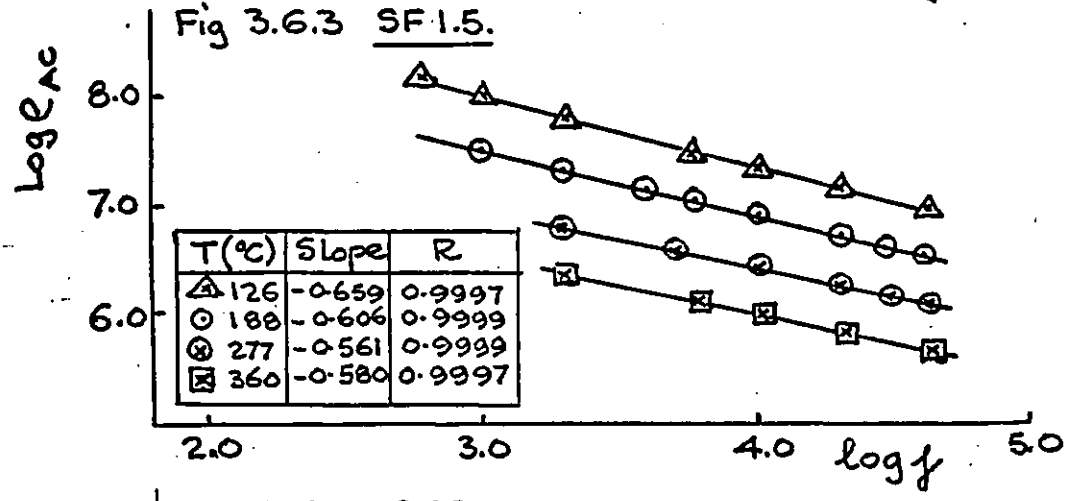

T(°C)	Slope	R
△ 126	-0.659	0.9997
⊙ 188	-0.606	0.9999
⊗ 277	-0.561	0.9999
⊠ 360	-0.580	0.9997

Fig 3.6.4 SF 3.4

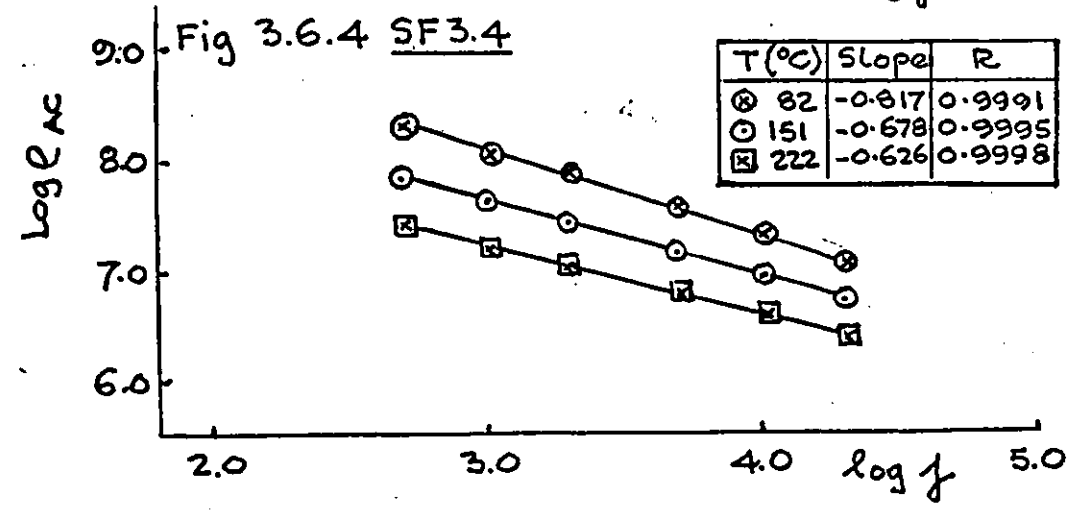

T(°C)	Slope	R
⊗ 82	-0.617	0.9991
⊙ 151	-0.678	0.9995
⊠ 222	-0.626	0.9998

LOG AC RESISTIVITY AGAINST LOG FREQUENCY

Fig 3.6.5 SF4C

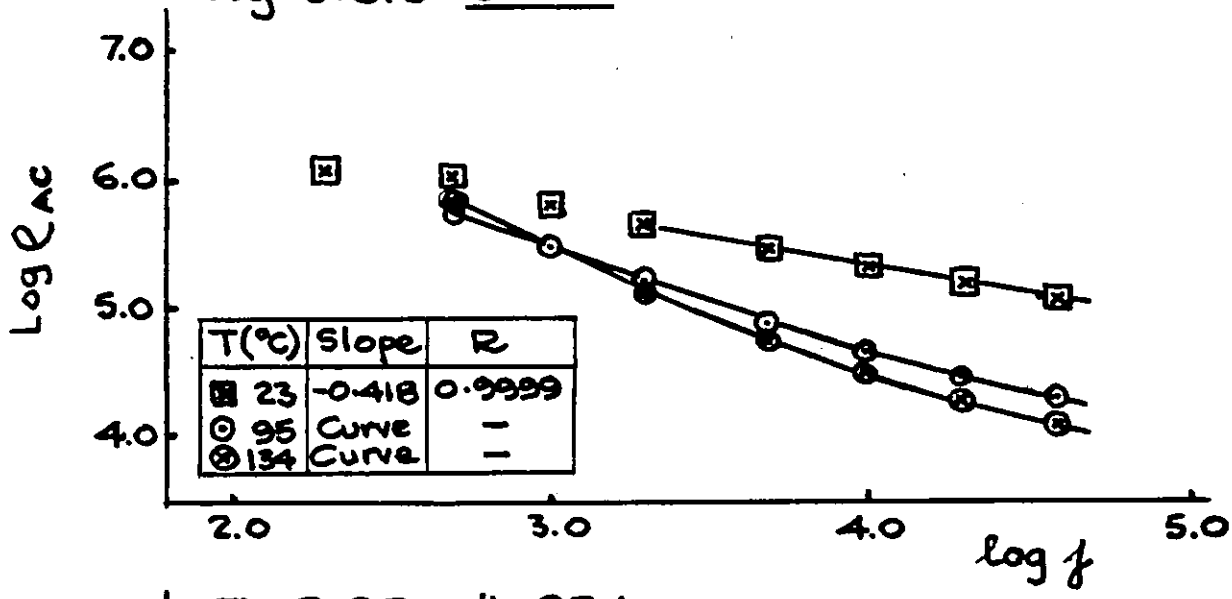

Fig 3.6.5 con't SF4C

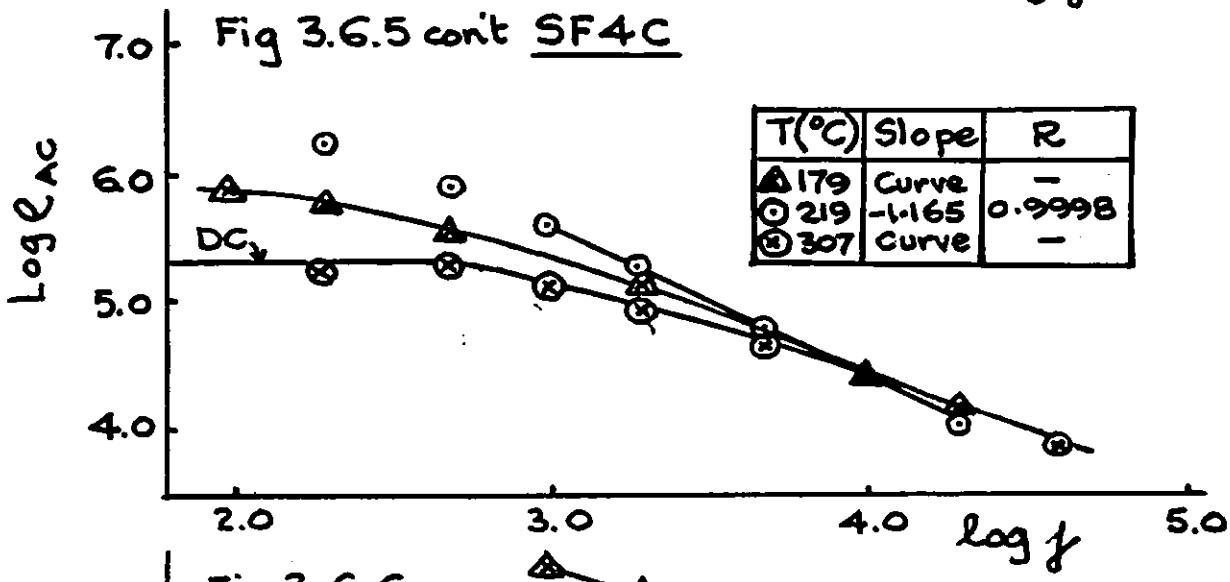

Fig 3.6.6
SF5

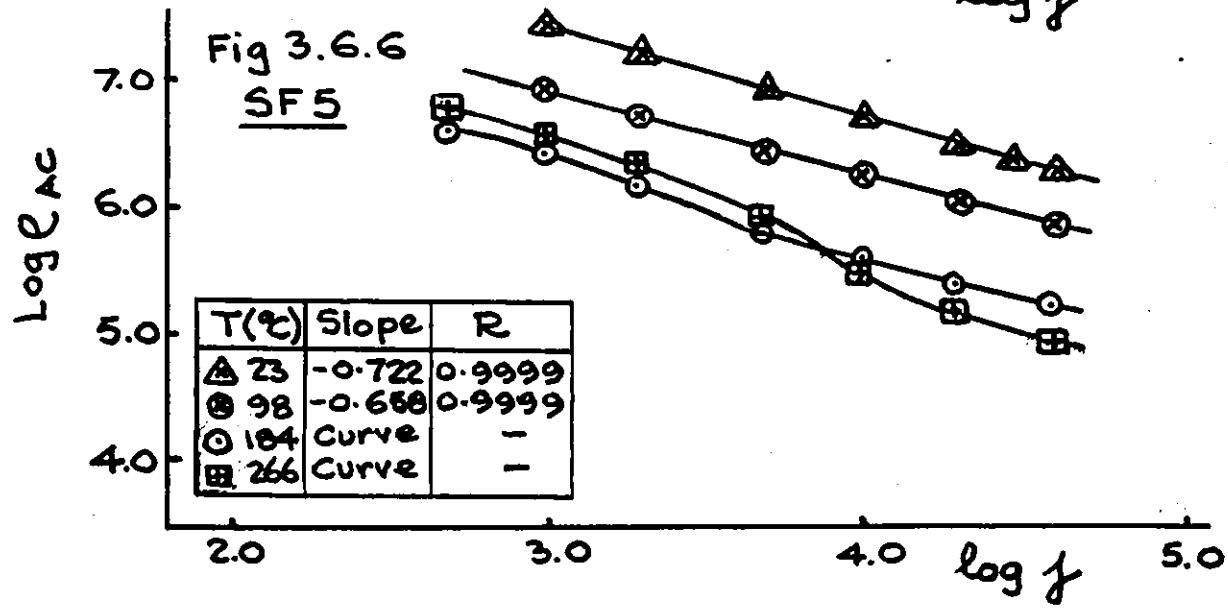

LOG A.C. RESISTIVITY AGAINST LOG FREQUENCY

Fig. 3.6.7. SMF2A

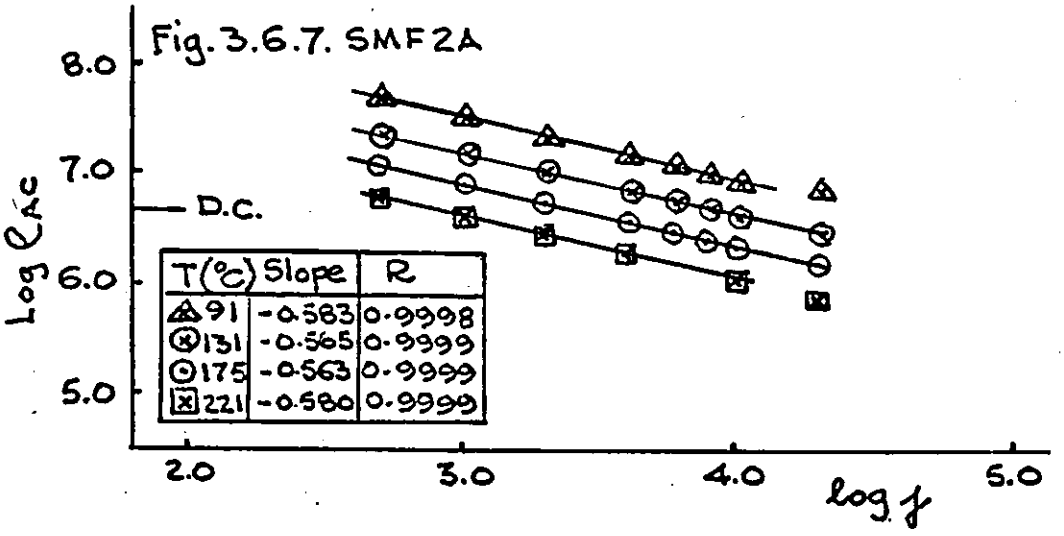

T(°C)	Slope	R
△ 91	-0.583	0.9998
⊗ 131	-0.565	0.9999
⊙ 175	-0.563	0.9999
⊠ 221	-0.580	0.9999

Fig. 3.6.7. SMF2A (cont.)

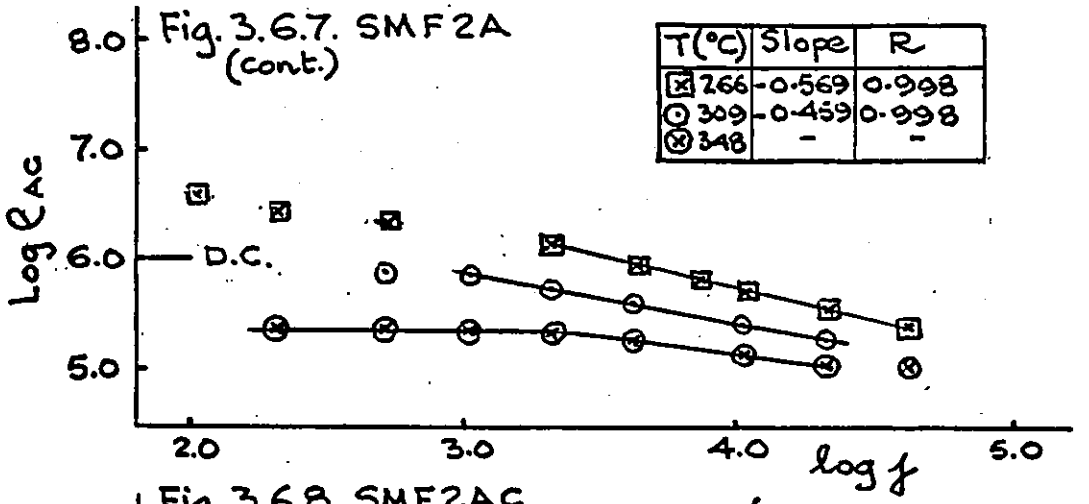

T(°C)	Slope	R
⊠ 266	-0.569	0.998
⊙ 309	-0.459	0.998
⊗ 348	-	-

Fig. 3.6.8. SMF2AC

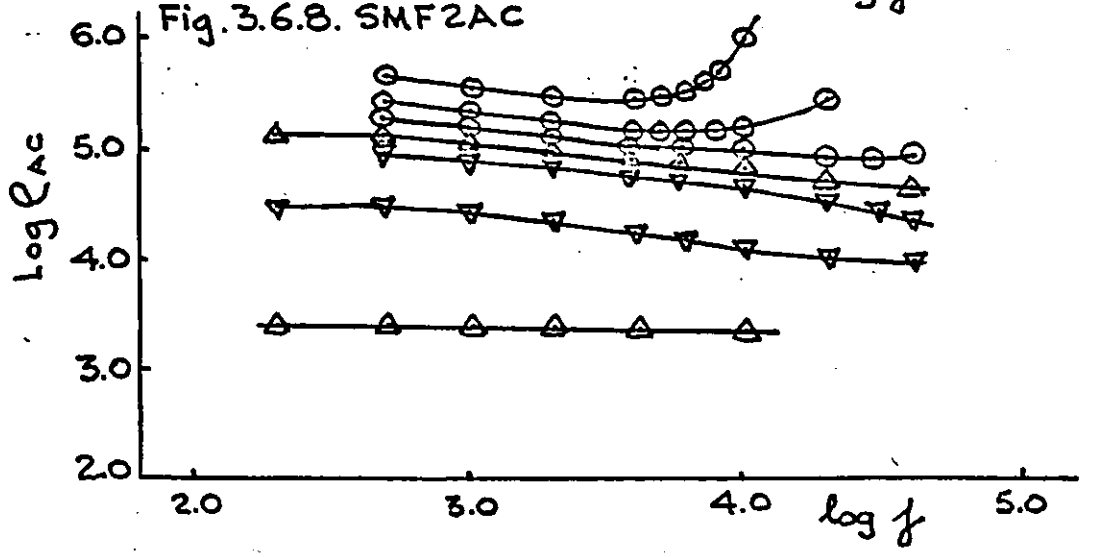

LOG A.C. RESISTIVITY AGAINST LOG FREQUENCY

Fig 3.6.9 SMF 3

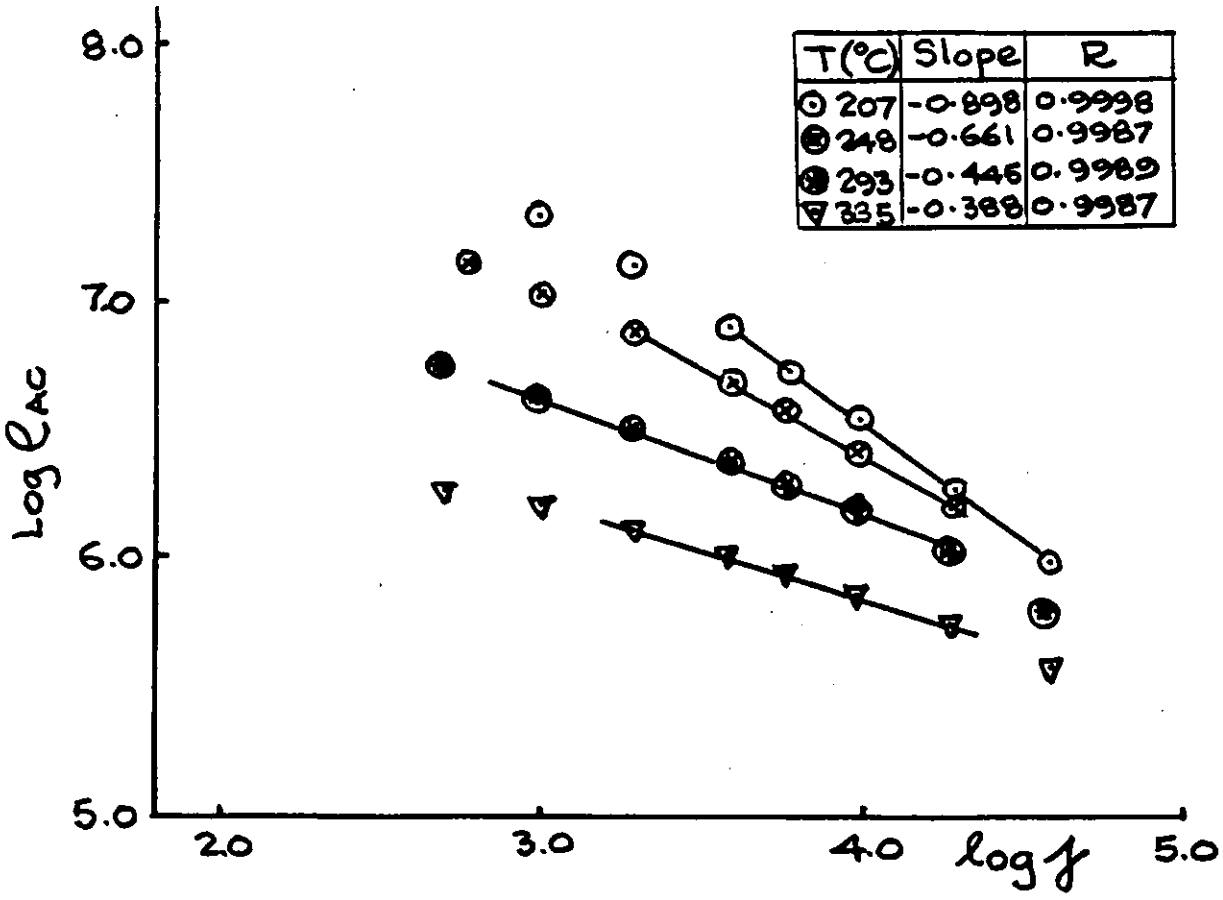

REAL AND IMAGINARY COMPONENTS OF THE DIELECTRIC CONSTANT AGAINST LOG FREQUENCY

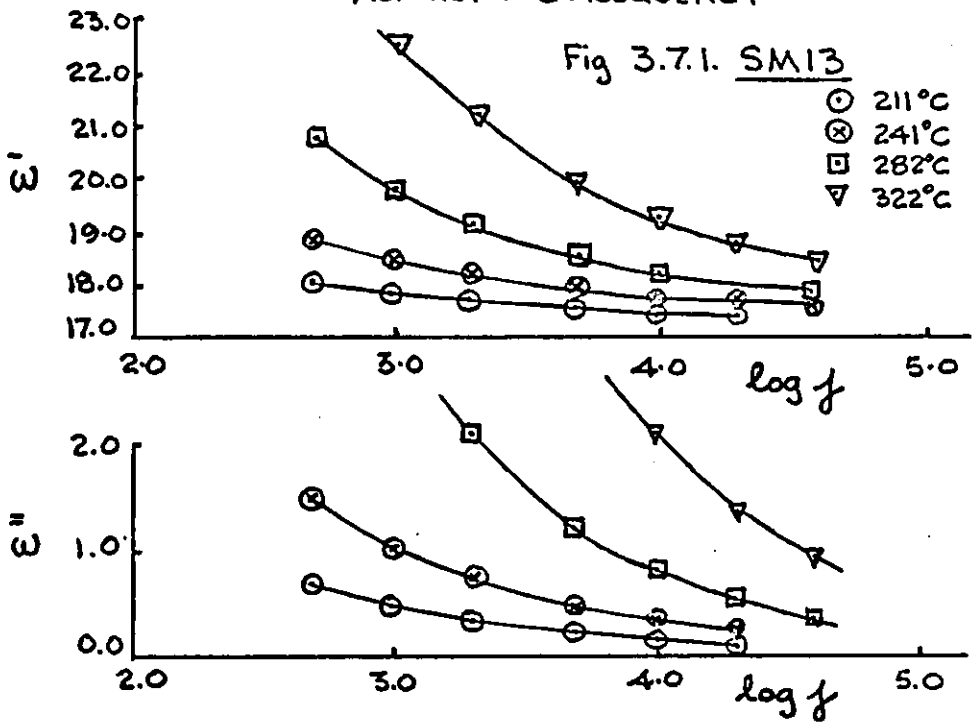

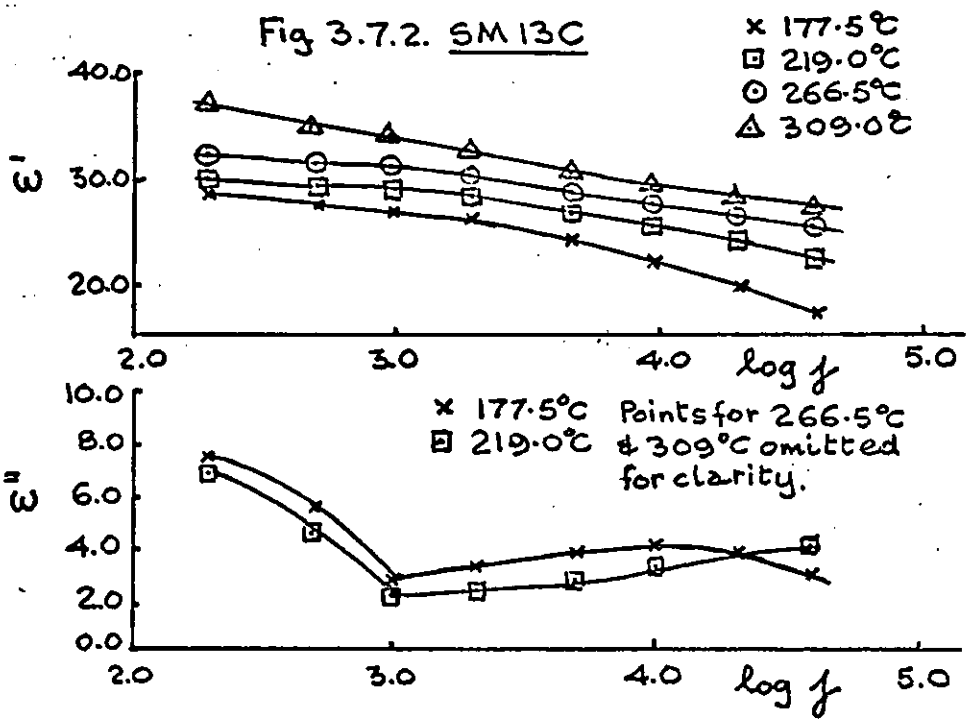

REAL AND IMAGINARY COMPONENTS OF THE DIELECTRIC CONSTANT AGAINST LOG FREQUENCY

Fig 3.7.3 SF 1.5

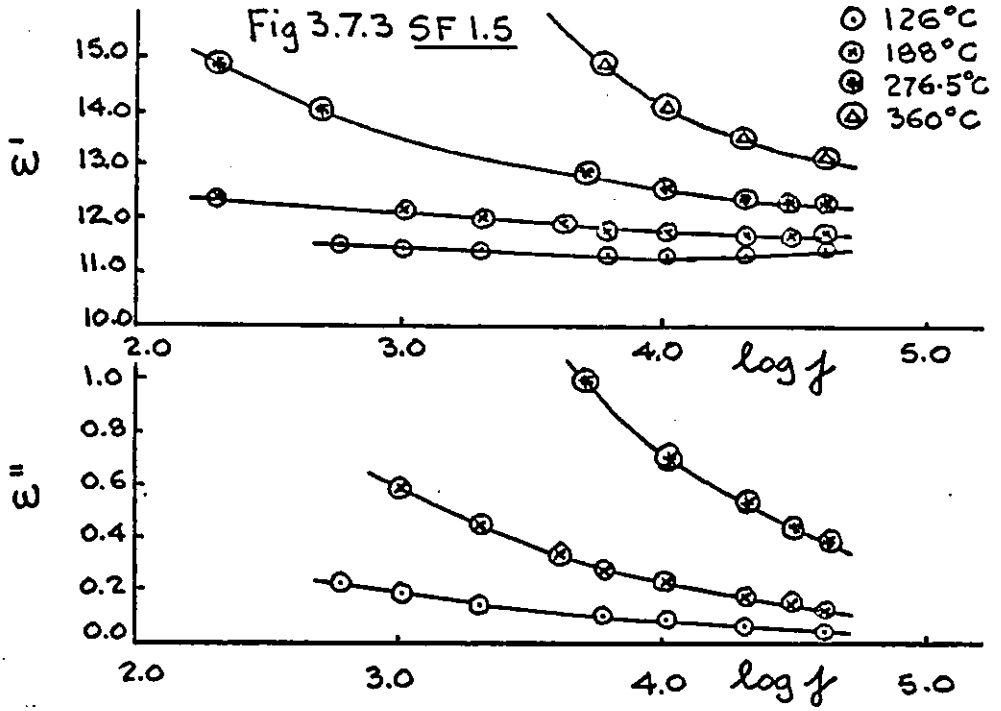

Fig 3.7.4 SF 3.4

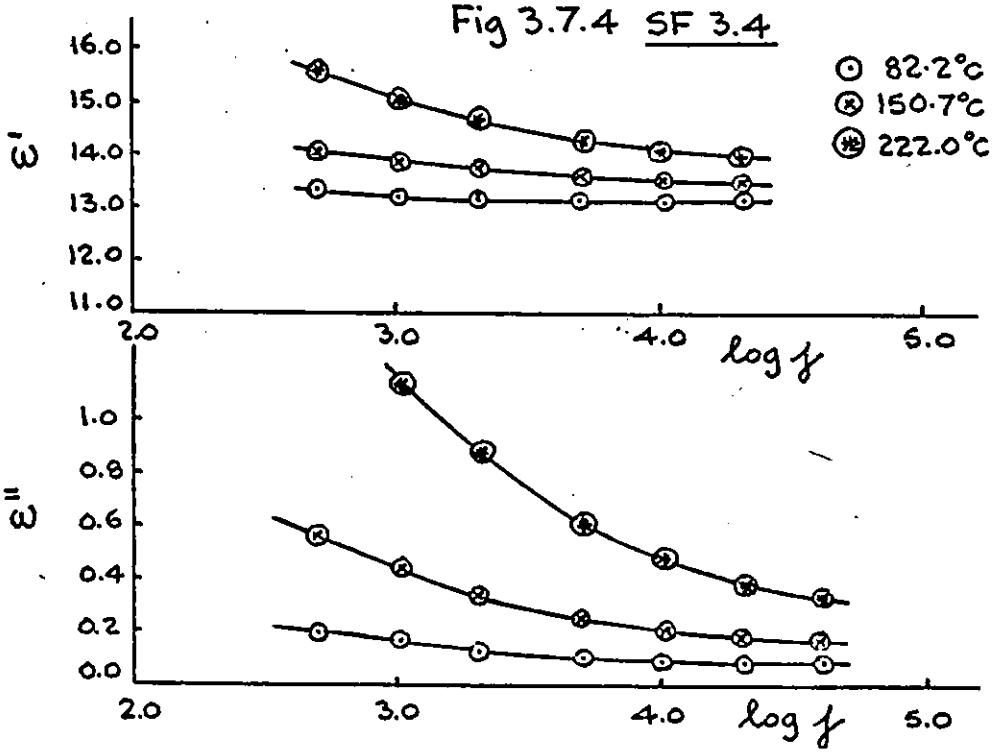

REAL AND IMAGINARY COMPONENTS OF THE DIELECTRIC CONSTANT AGAINST LOG FREQUENCY

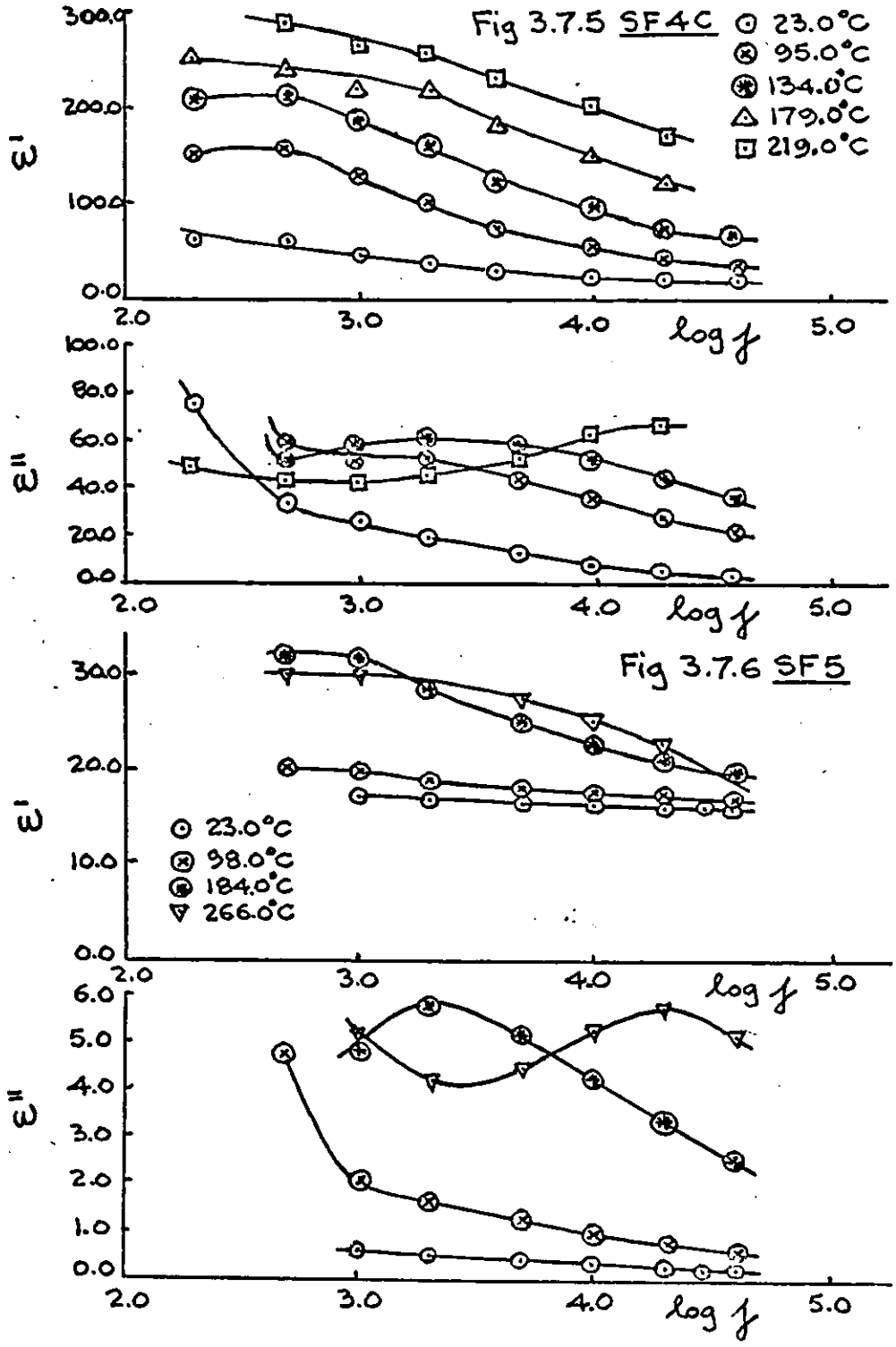

REAL AND IMAGINARY COMPONENTS OF THE DIELECTRIC CONSTANT AGAINST LOG FREQUENCY

Fig 3.7.7 SMF 2A

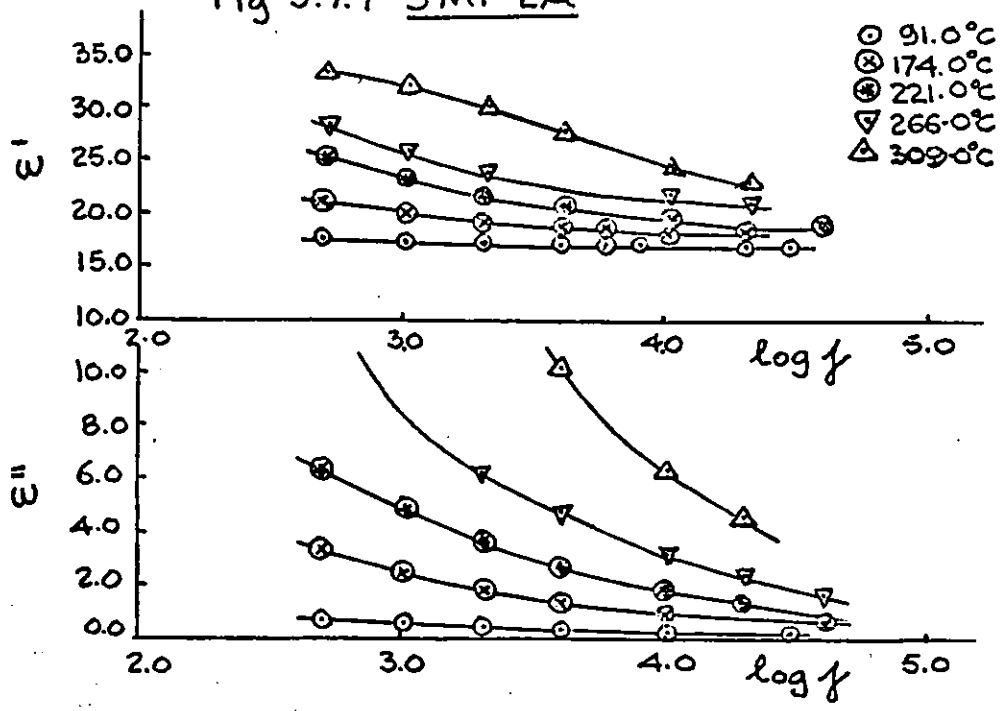

Fig 3.7.8 SMF 2A/C

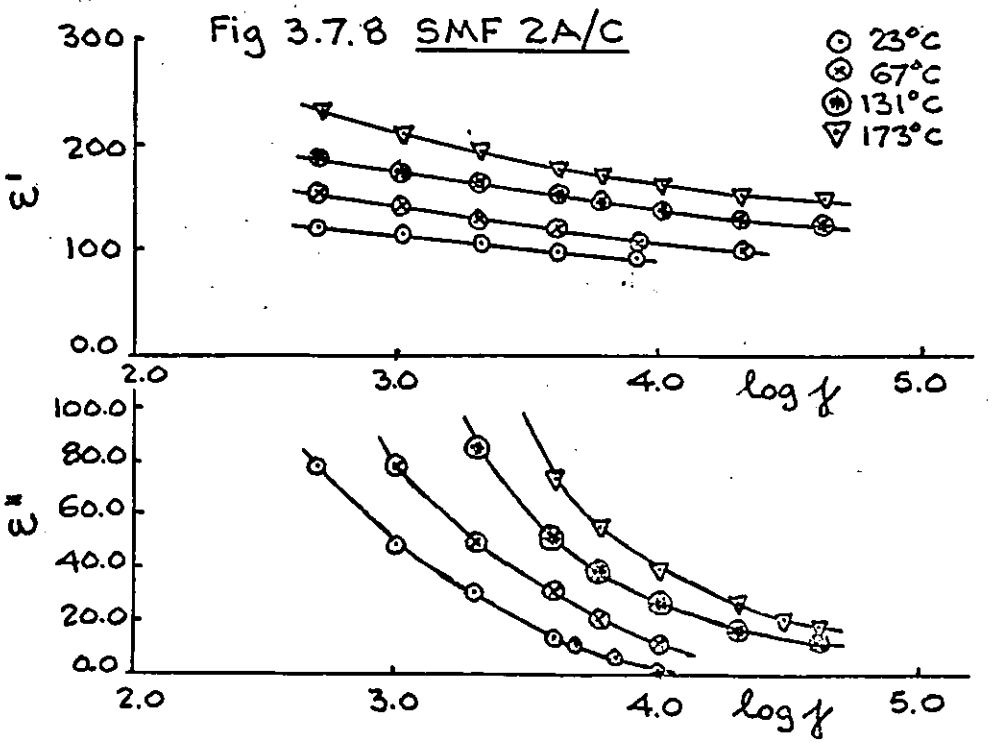

REAL AND IMAGINARY COMPONENTS OF THE DIELECTRIC CONSTANT AGAINST LOG FREQUENCY

Fig 3.7.9 SMF3

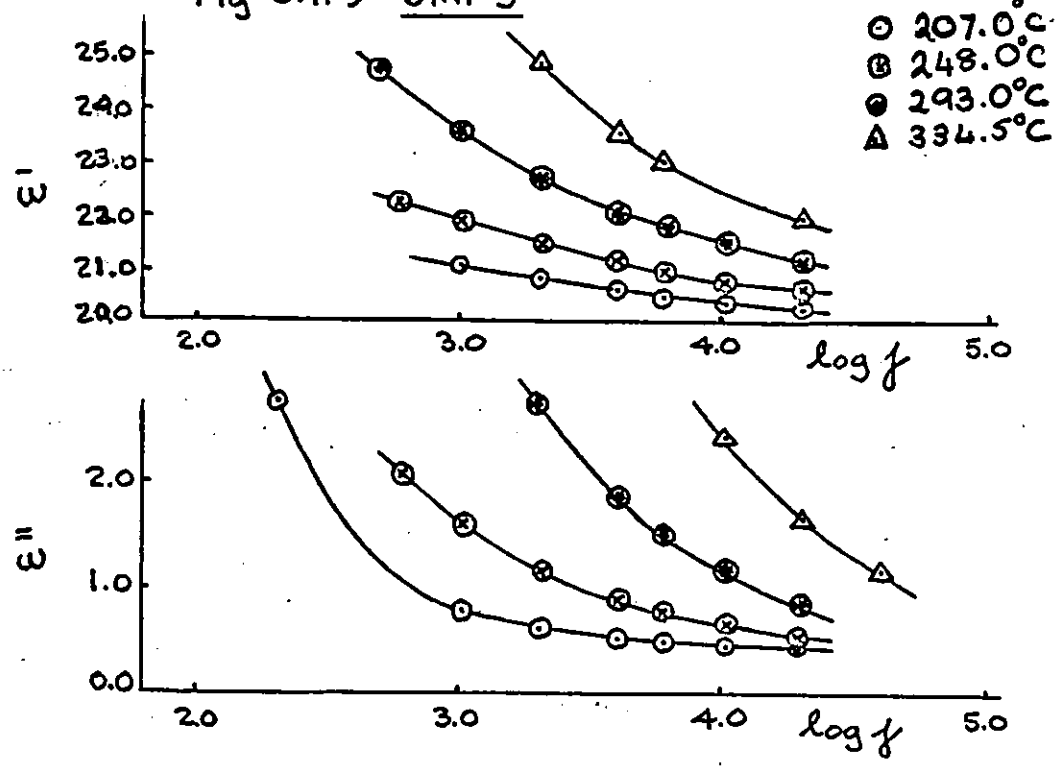

PLATE 3.1.1 SM7C

Section taken from the edge of the specimen showing dendritic growth of anorthite from the surface and transverse section through dendrites in bottom left hand corner. Small dark crystals between the dendrites thought to be $MnSiO_3$. x145 Observed with crossed polarizers.

PLATE 3.2.1 SM10C

Boundary between dense nucleation and residual glass with sparse nucleation in the sample used for conductivity measurement. This arose from inhomogeneity in the glass. x145 Plane polarized light.

PLATE 3.2.2 SM10C

Isolated dendrite clearly showing the two phase structure. A pyroxene phase has grown on the dendritic skeleton of a brown manganese-rich phase (probably braunite).

x575 Plane polarized light.

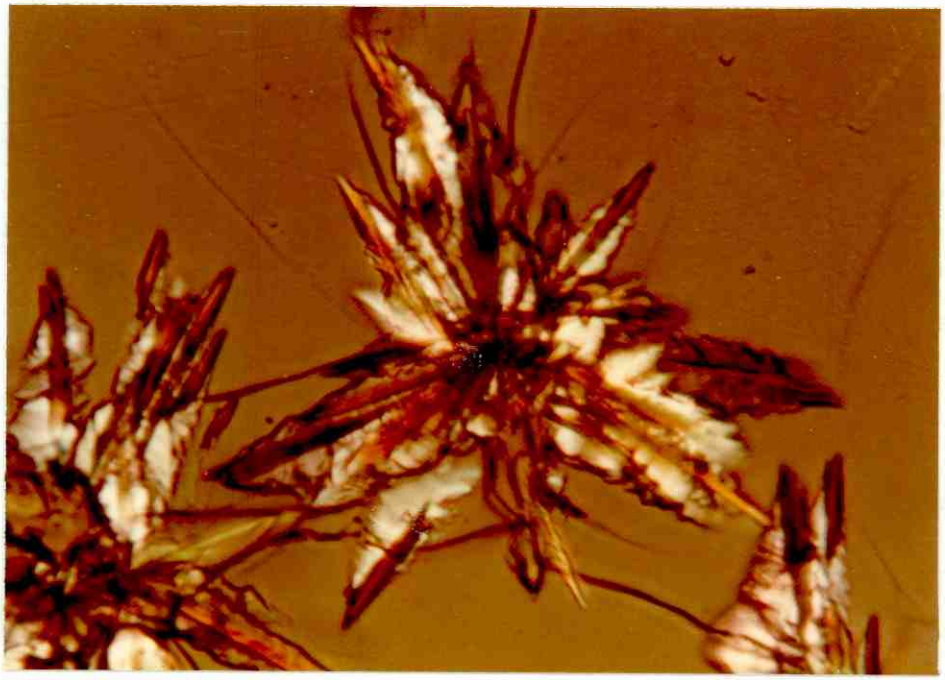

PLATE 3.2.3 SM10C

Another dendrite with a similar structure to that in Plate 3.2.2 observed with partially crossed polarizers.

x575

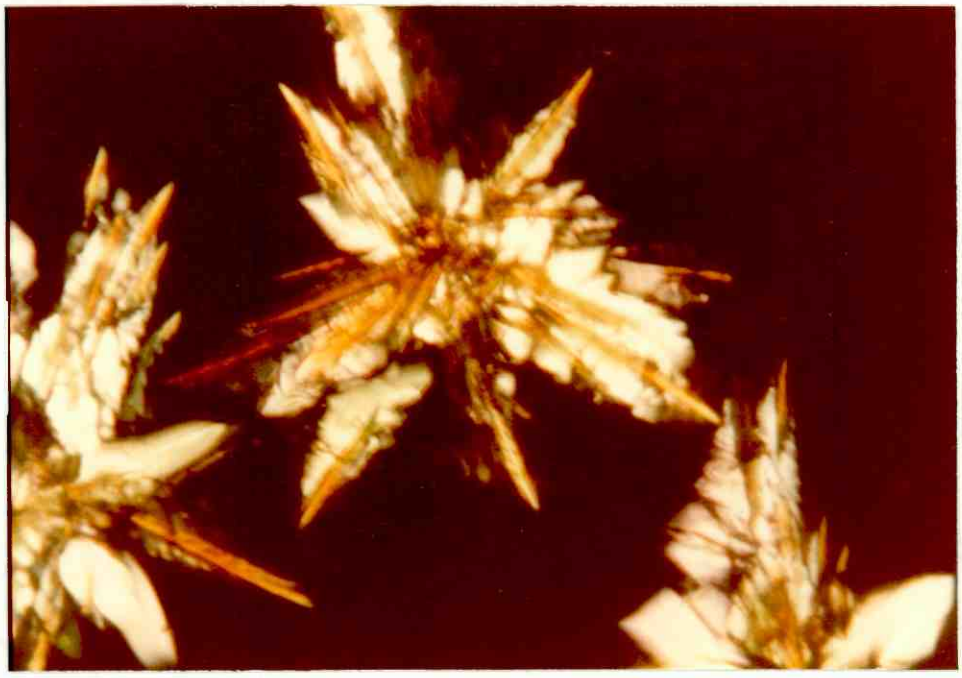

PLATE 3.2.4 SM10C

Same dendrite as for Plate 3.2.3 but now observed with polarizers fully crossed.

x575

PLATE 3.2.5 SM10C

Close-up of the structure of the dendrite arms.

x1450 Plane polarized light.

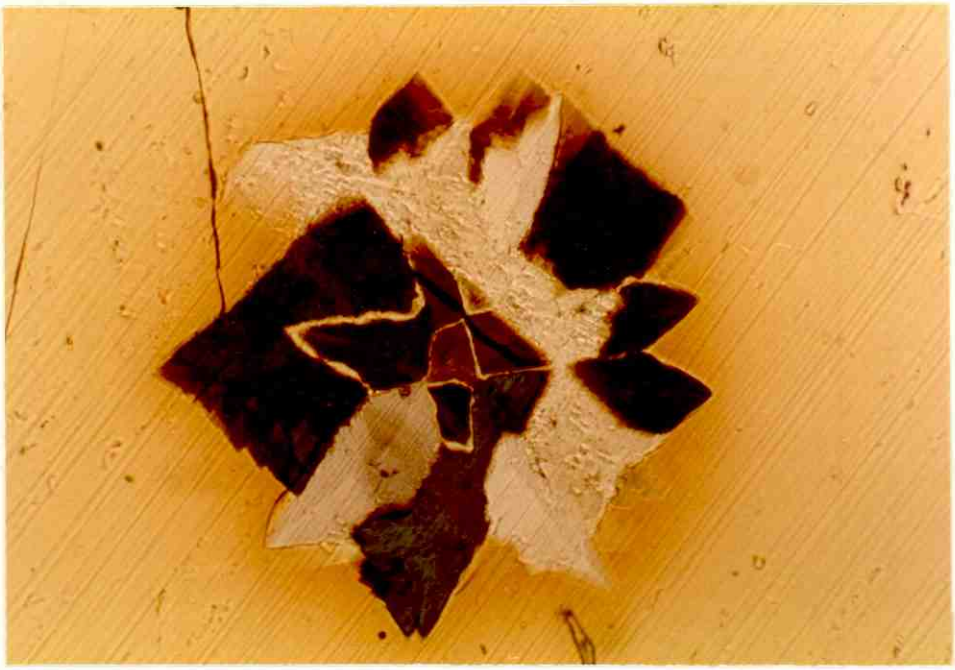

PLATE 3.3.1 SM18C Short growth time.

Large tabular crystals of gehlenite growing in a glassy matrix. The blue coloration is probably due to interference colours.

x145 Plane polarized light.

PLATE 3.3.2 SM18C Short growth time

Another crystal in the same sample as Plate 3.3.1. The actual size was over 1 mm across. Note spherulitic morphology developing to the right of the picture.

x145 Plane polarized light.

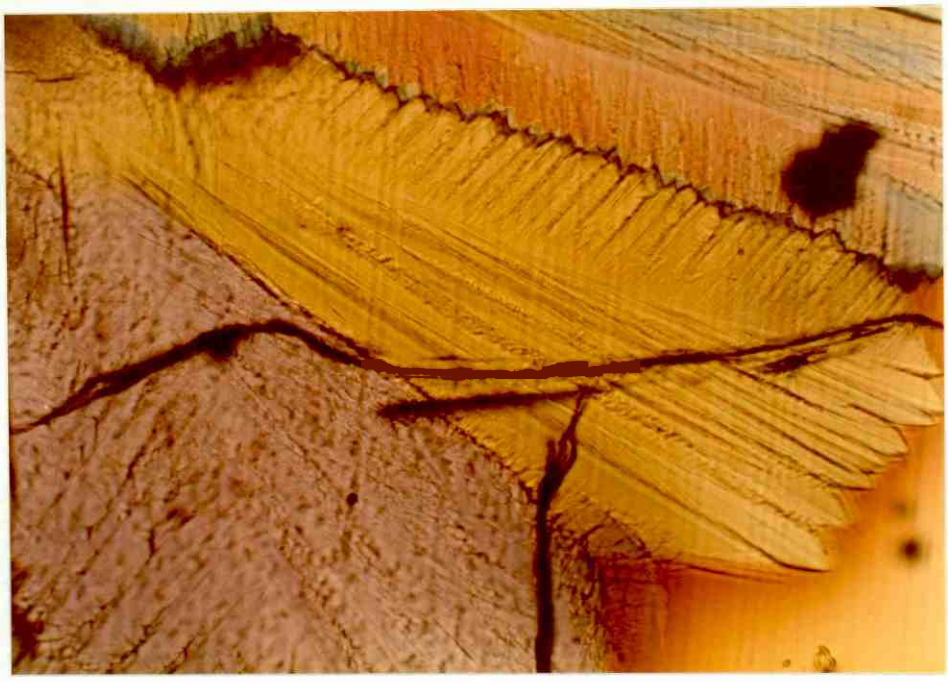

PLATE 3.3.3 SM18C Longer growth time.

The spherulites had a diameter of over 2 mm and were made up of a number of 'segments' distinguished by different interference colours. The micrograph shows a typical segment and boundary region.

x145 Plane polarized light

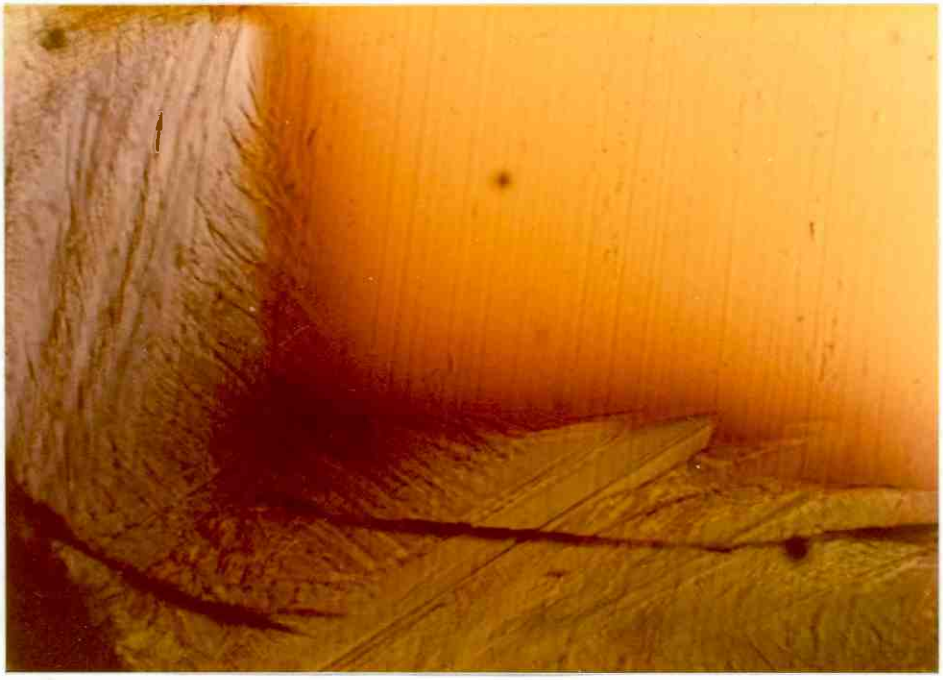

PLATE 3.3.4 SM18C Longer growth time.

As in Plate 3.3.3. Note the increase in density of colour near the edge of the spherulite as a result of rejection of Mn^{3+} into the residual glass.

x145 Plane polarized light.

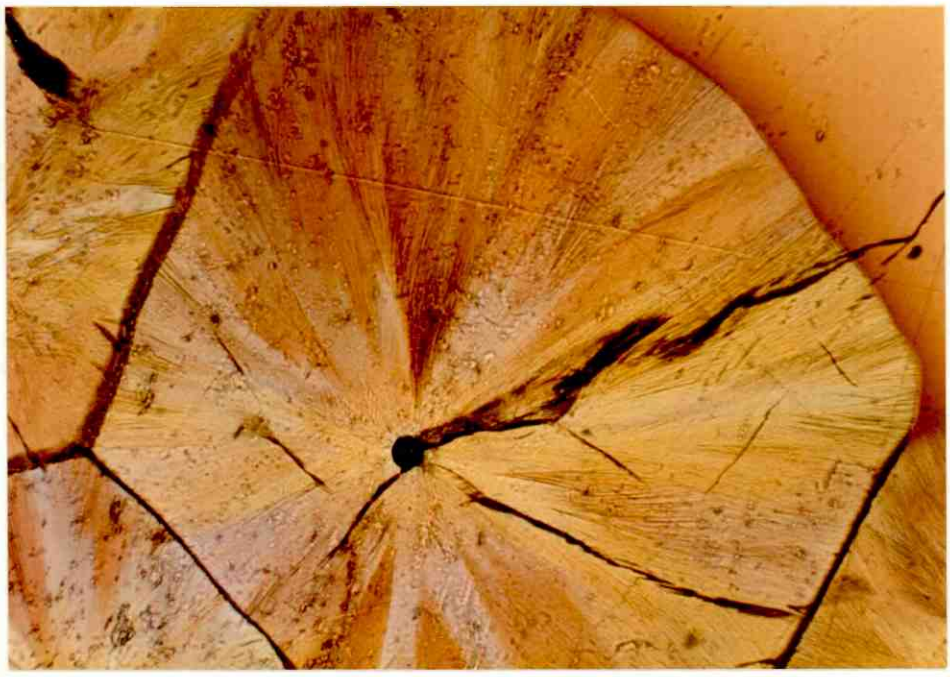

PLATE 3.4.1 SM12C

Spherulite of gehlenite in a glassy matrix; the intersection between three spherulites is shown. Interference colours are present and also a brown rim in the residual glass around the spherulite from build-up of rejected Mn^{3+}.

x145 Plane polarized light.

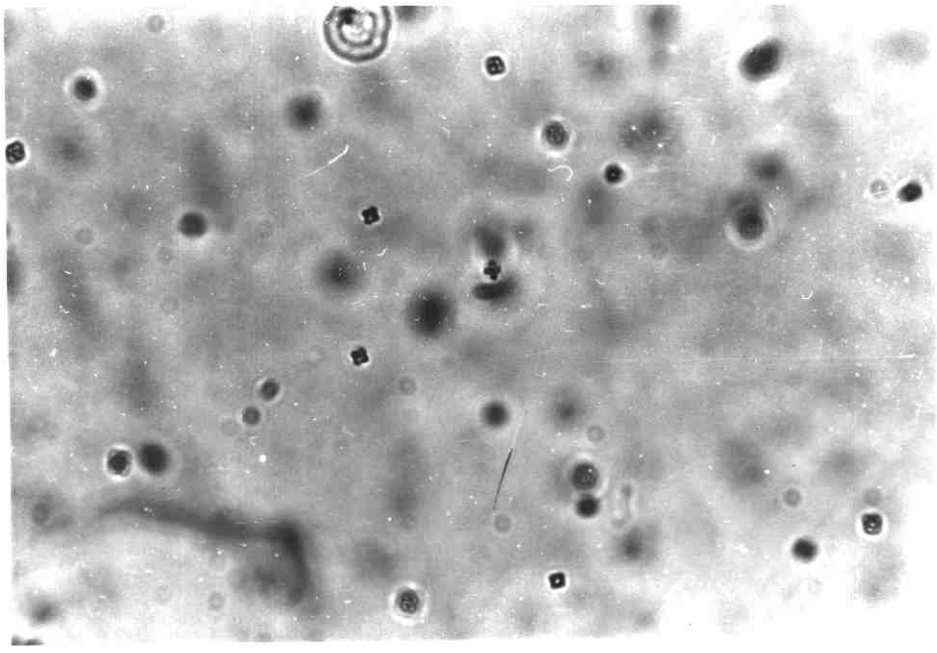

PLATE 3.5.1 SM13C 0.5 hr growth time.

This micrograph, obtained at high magnification, shows the early stages of growth of Mn^{3+} rich dendrites in a glassy matrix.

x1450 Plane polarized light.

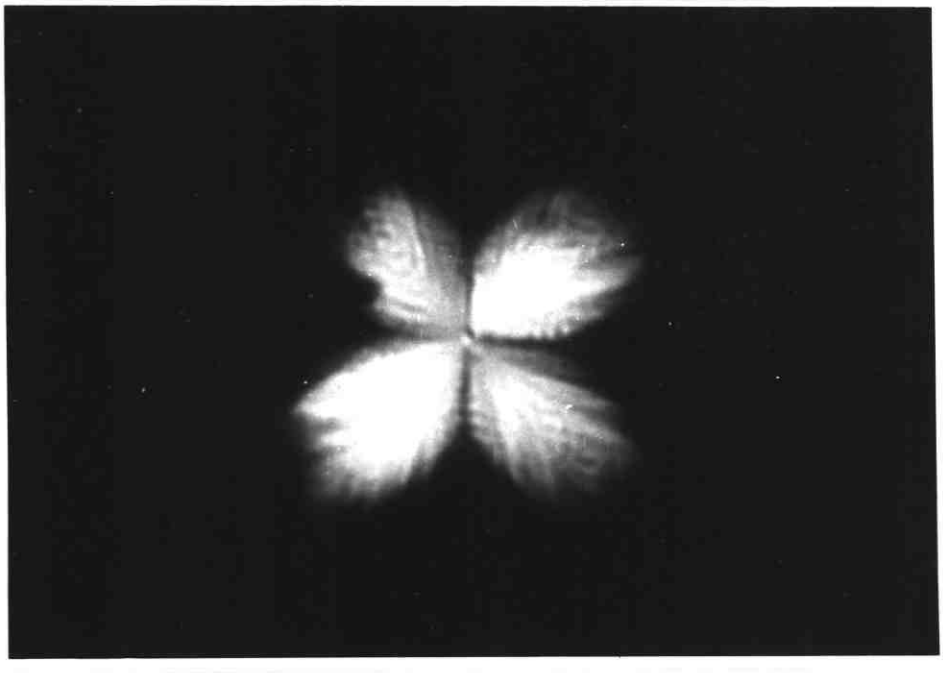

PLATE 3.5.2 SM13C 1.0 hr growth time.

The start of the crystallization of gehlenite from the residual glass observed between crossed polarizers. The extent of growth of the Mn^{3+} dendrites is also apparent.

x575

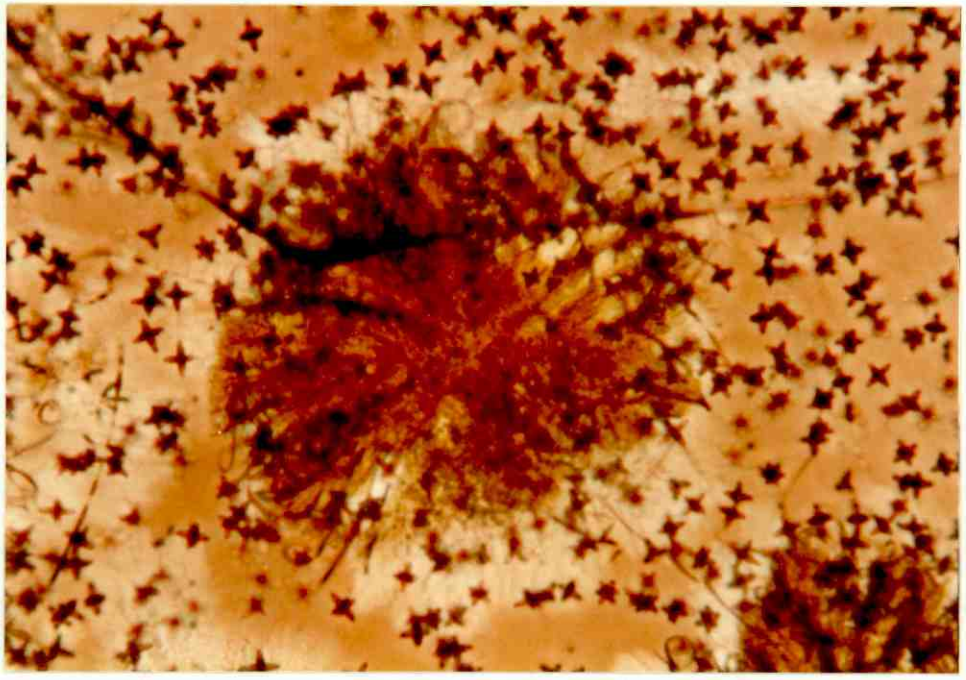

PLATE 3.5.3 SM13C 1.0 hr growth time.

A more highly developed spherulite of gehlenite in the same sample as that shown in Plate 3.5.2. The brown coloration may indicate either that Mn^{3+} is incorporated into the gehlenite or a residual glassy phase enriched in Mn^{3+} is present within the spherulite. x575 Plane polarized light.

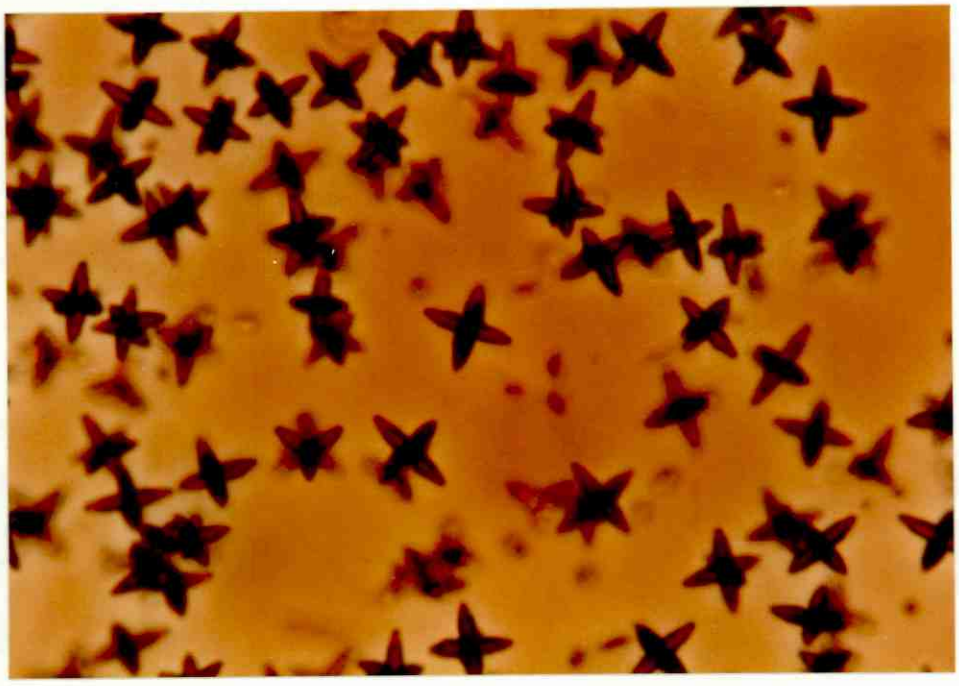

PLATE 3.5.4 SM13C 1.5 hr growth time.

The dendrites are now seen to have six arms which are mutually perpendicular. The glass in the immediate area of each dendrite is depleted in Mn^{3+} and appears a lighter brown. x900 Plane polarized light.

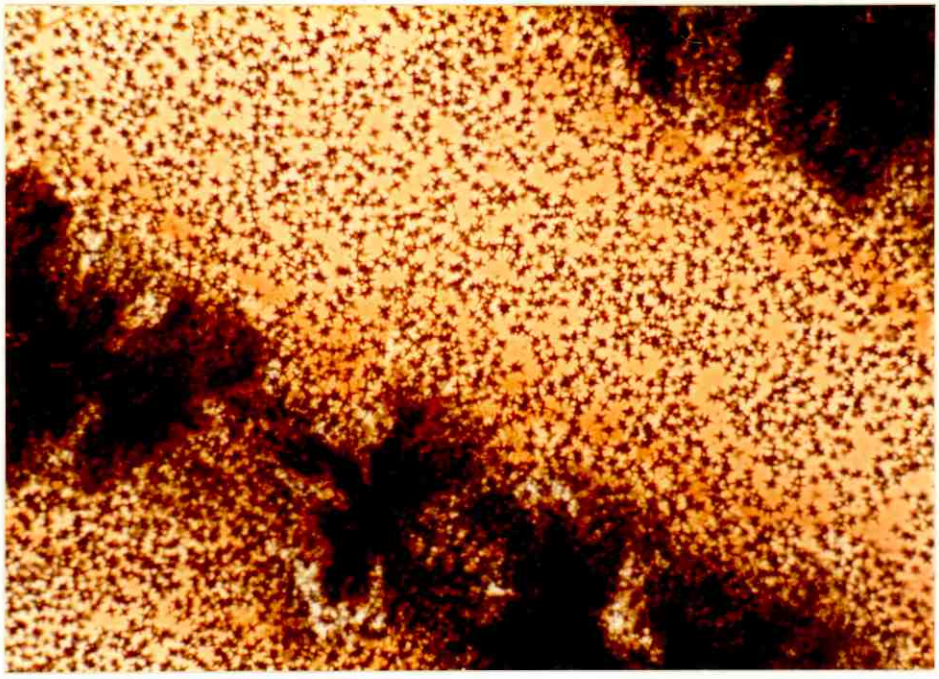

PLATE 3.5.5 SM13C 1.5 hr growth time.

A general low power view of both the manganese rich dendrites and the bulk growth.

x145 Plane polarized light.

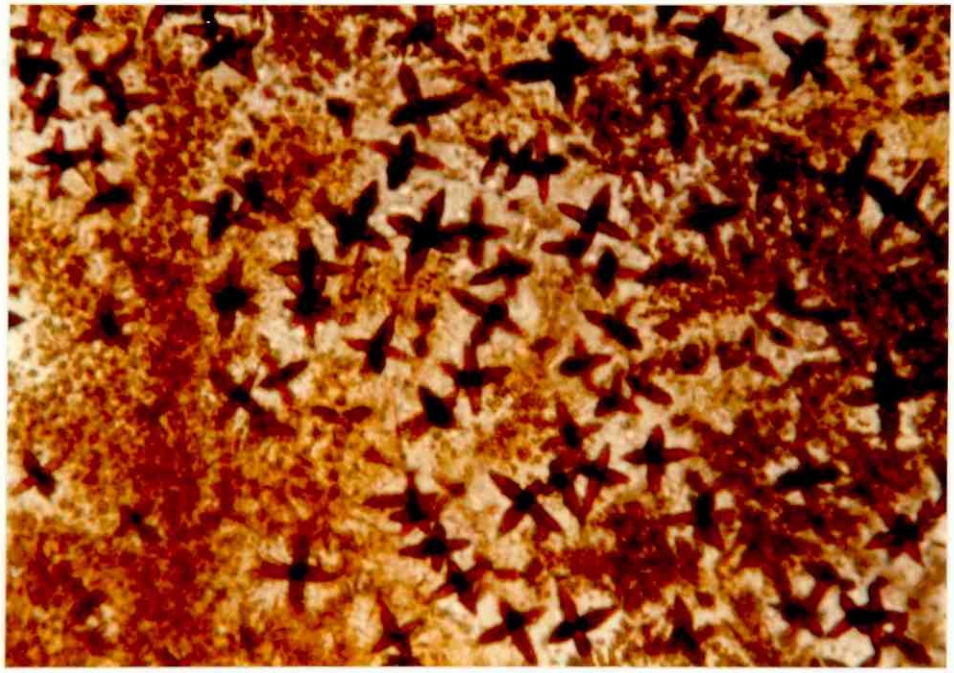

PLATE 3.5.6 SM13C 19 hr growth time.

The sample now appears completely crystalline. Three phases may be distinguished: brown dendrites, a white phase surrounding the dendrites which is probably gehlenite and a second brown phase in the bulk growth. The morphology of the third phase was impossible to determine.

x575 Plane polarized light.

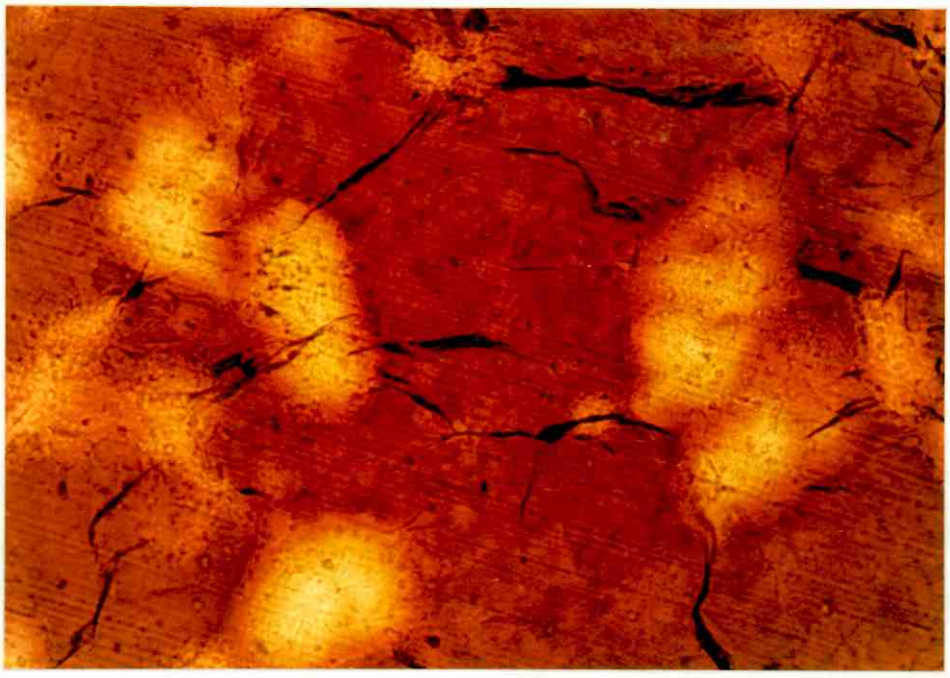

PLATE 3.6.1 SM14C Crystal growth at 910°C.

The yellow areas are probably incompletely formed spherulites of gehlenite in an unresolvable crystalline phase.

x145 Plane polarized light.

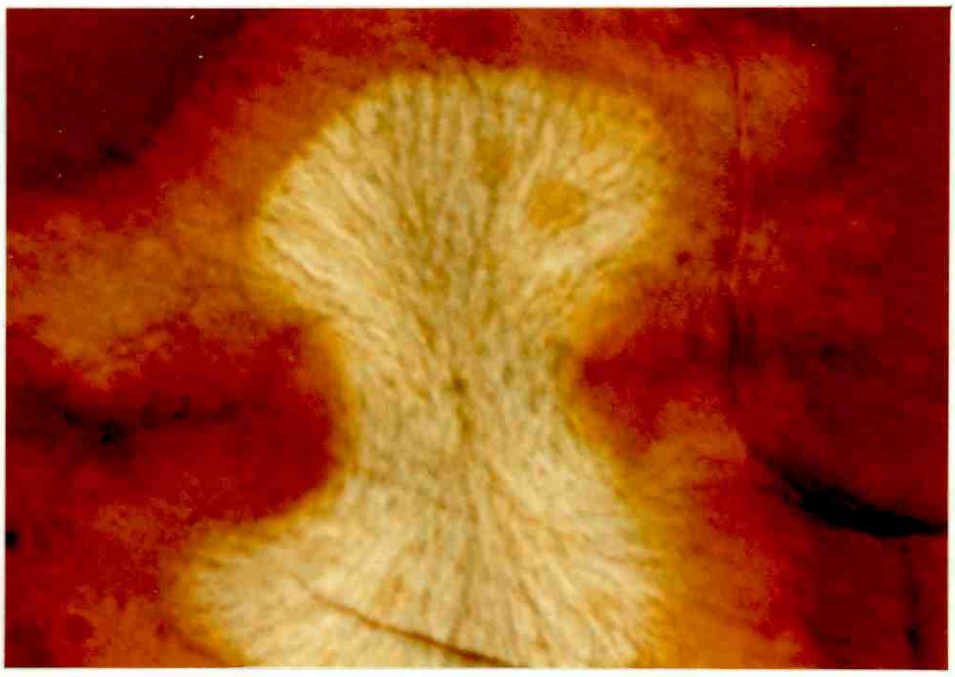

PLATE 3.6.2 SM14C Crystal growth at 910°C

Close up of an incompletely formed spherulite. The initial 'wheat-sheaf' shaped bundle of fibres is clearly seen. The phase surrounding the sheaf may be of a different composition to the matrix because of the difference in colour. x1440 Plane polarized light.

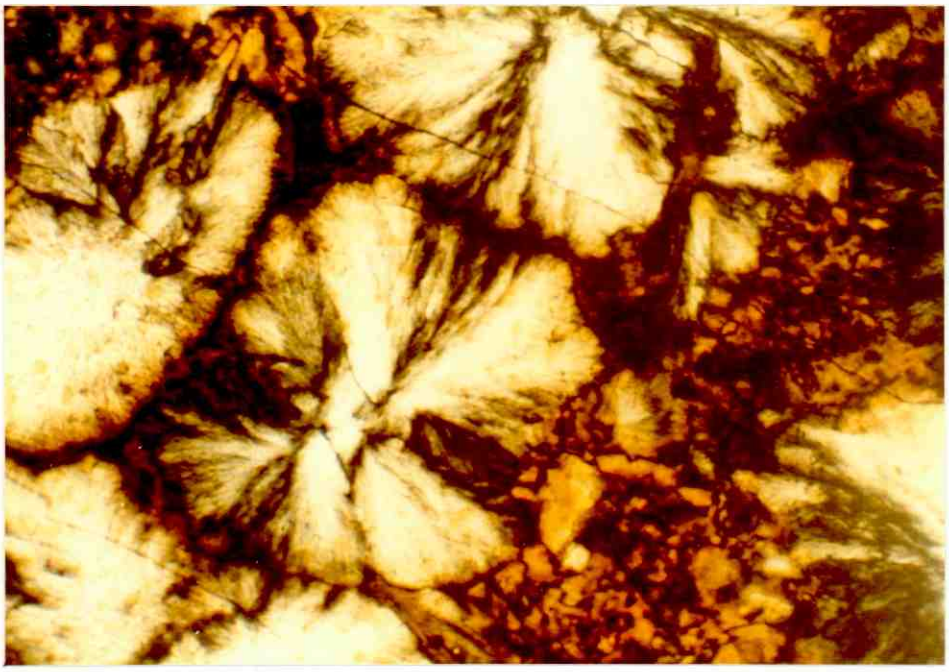

PLATE 3.6.3 SM14C Crystal growth at 930°C

The increased crystal growth temperature has resulted in the growth of more perfect spherulites which under crossed polarizers show the characteristic 'Maltese Cross' effect. The matrix was still not resolvable even at the highest magnification.

x145

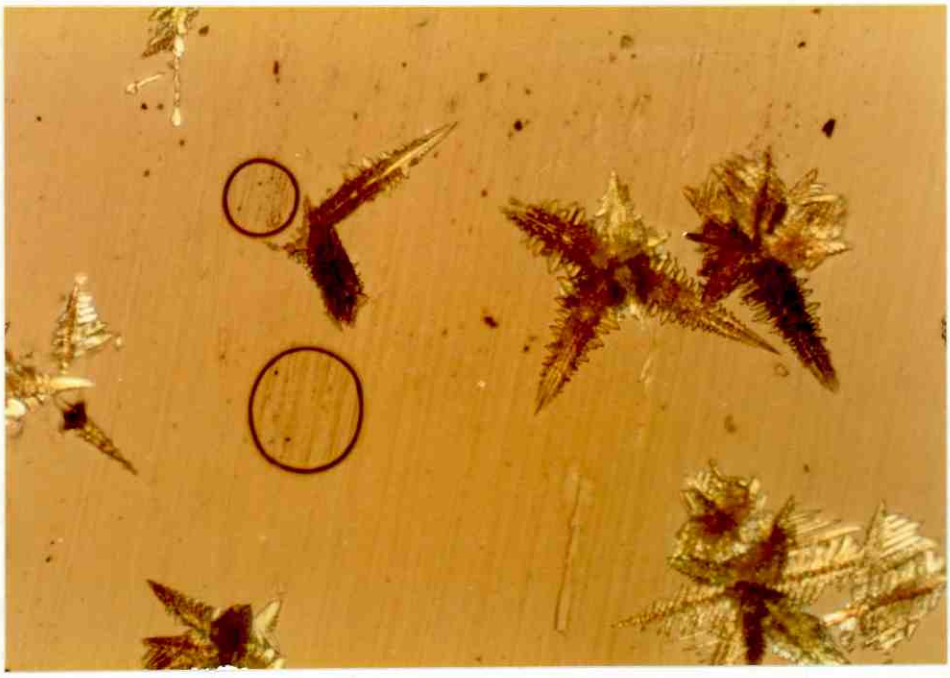

PLATE 3.7.1 SF6C Short crystal growth heat treatment.

Individual dendrites of a pyroxene phase growing in a glassy matrix observed with partially crossed polarizers.

x145

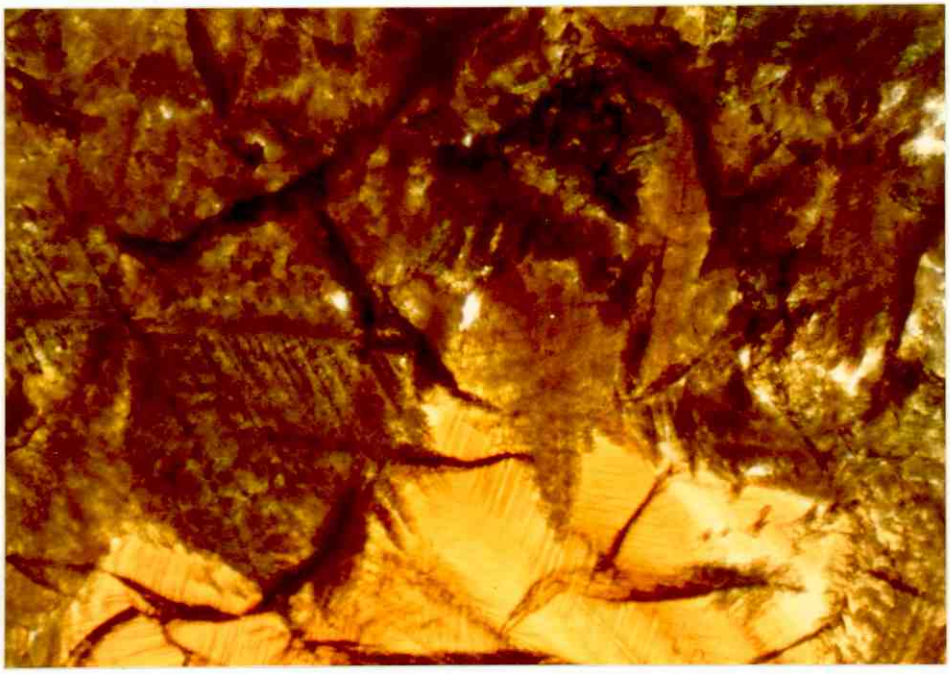

PLATE 3.7.2 SF6C Long crystal growth heat treatment.

This sample is fully crystalline. The bulk crystallization appears green and is the same pyroxene phase as in Plate 3.7.1. The orange phase is surface growth possibly of gehlenite. The change in density on crystallization has produced some micro-porosity.

x145 Plane polarized light.

PLATE 3.8.1 SMF2C Short heat treatment.

Isolated dendrites growing in a glassy matrix. The growth on the left is from the surface. Observation with partially crossed polarizers. With longer growth times the crystallization was complete and the microstructure resembled that of SF6 (Plate 3.7.2). The bulk phase was brown and the surface growth orange in plane polarized light. In isolated areas a third phase could be seen which exhibited green-pink pleochroism.

x145

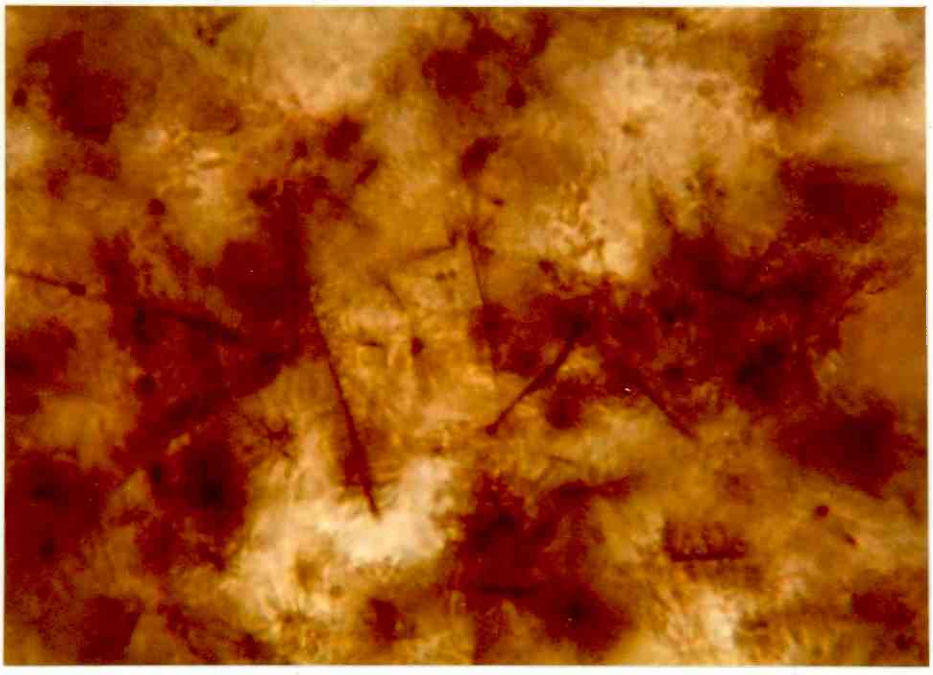

PLATE 3.9.1 SMF2AC

High magnification micrograph of the bulk internal growth of a completely crystallized specimen.

x1440 Plane polarized light.

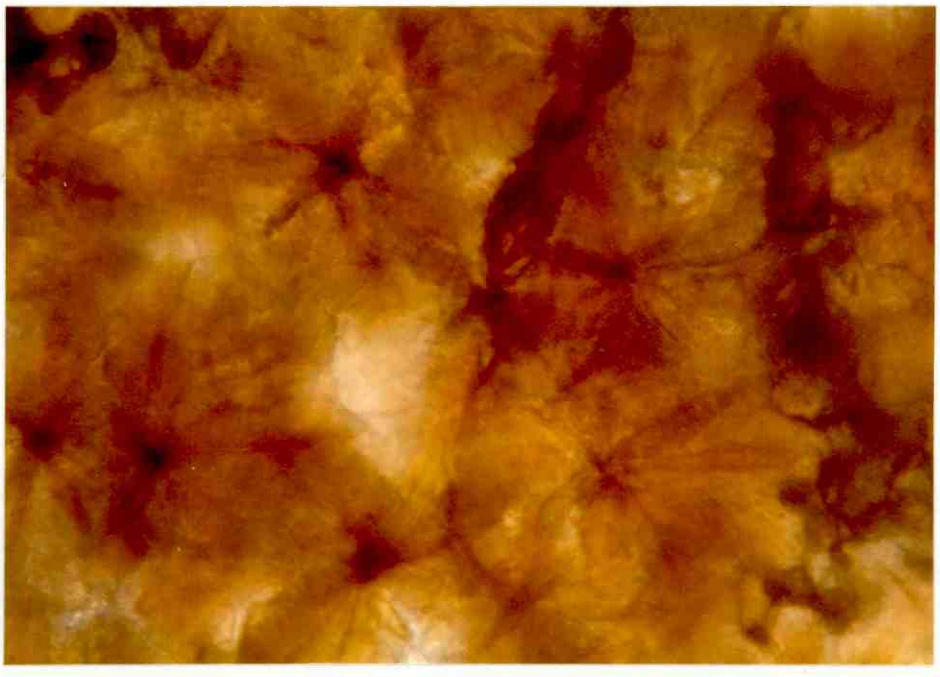

PLATE 3.9.2 SMF2BC

Medium magnification micrograph of the internally nucleated growth in a completely crystallized specimen.

x575 Plane polarized light.

A) SM13C x 1,000

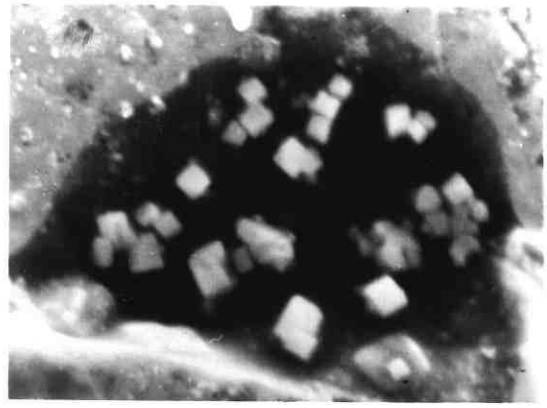

B) SM13C x 5,000

C) SM13C x 10,000

D) SM13C x 10,000

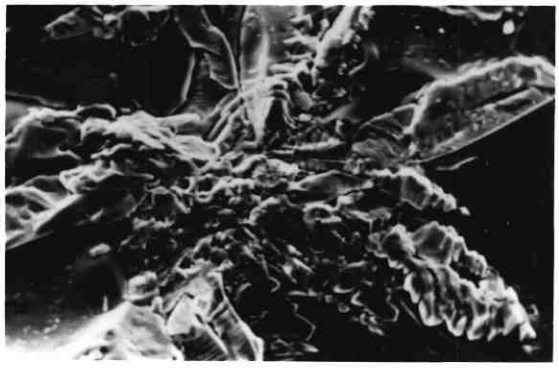

E) SM10C x 1,000

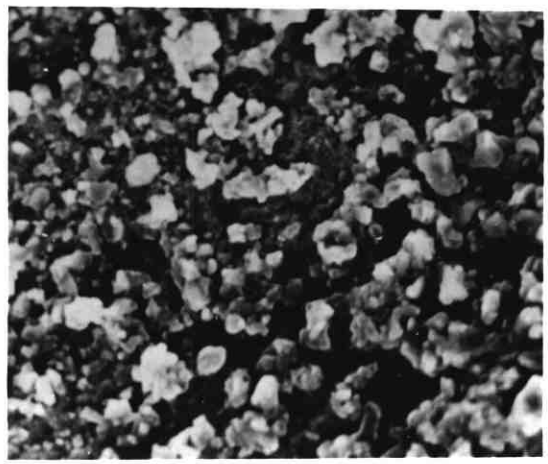

F) SM14C x 2,000

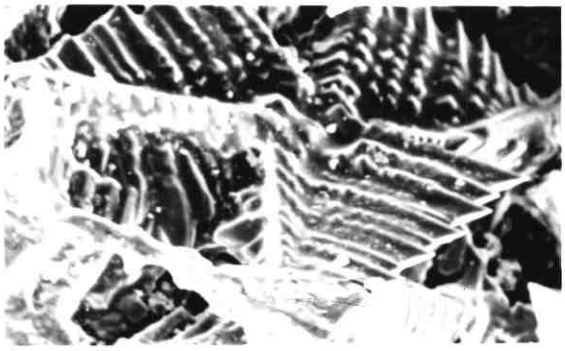

A) SF4C x 1,000

B) SF4C x 5,000

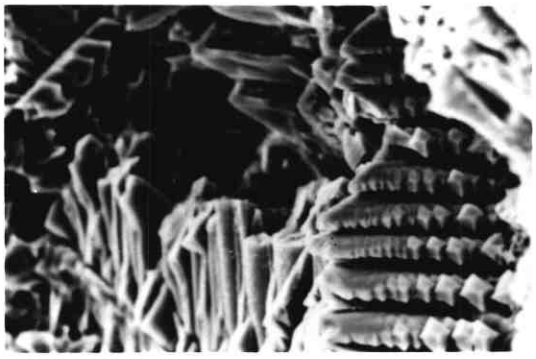

C) SF4C x 2,000

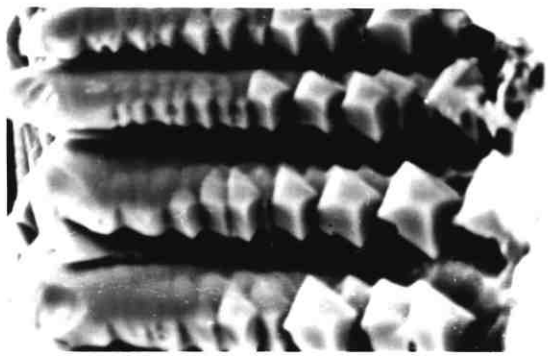

D) SF4C x 5,000

E) SF4C x 2,000

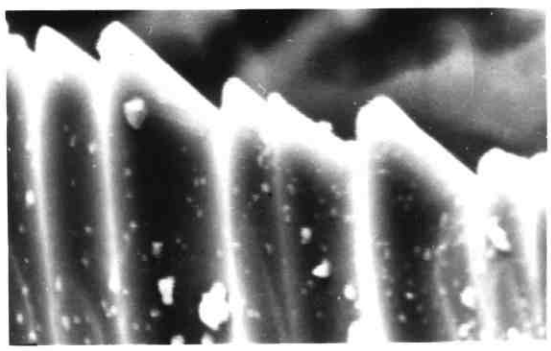

F) SF4C x 10,000

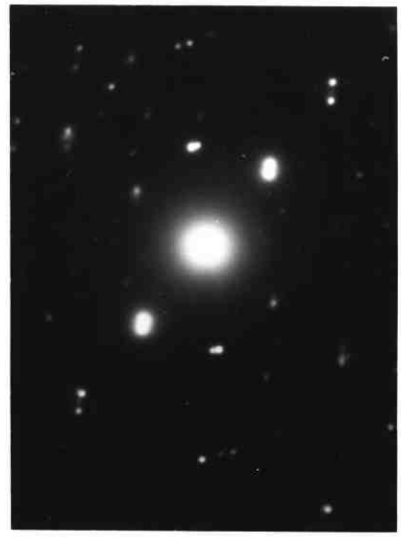

A) SM12C
Diffraction pattern of B)

B) SM12C x 25,000

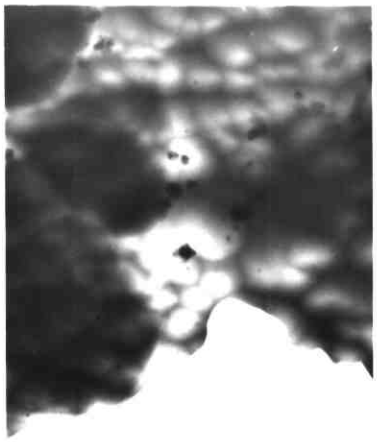

A) SM13C x 1,600

B) SM13C x 6,300

C) SM13C x 25,000

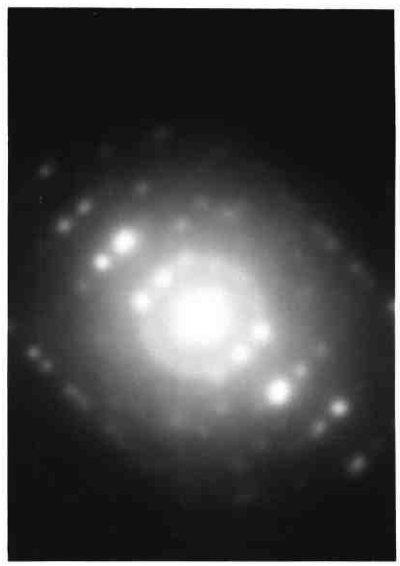

D) SM13C
Diffraction pattern of C

E) SM13C x 6,300

F) SM13C x 6,300

PLATE 3.14

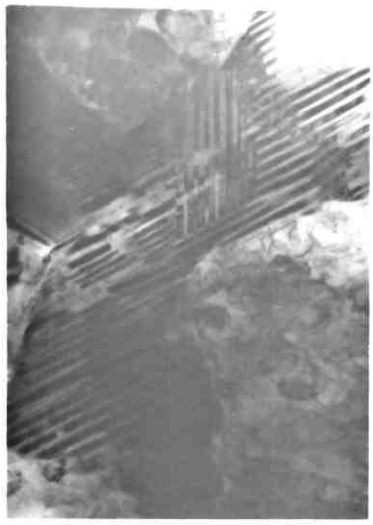

A) SM13C x 10,000

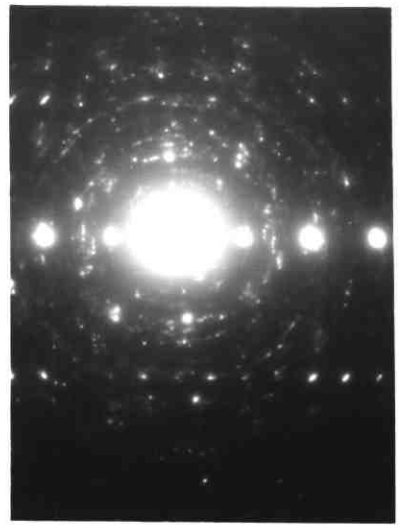

B) SM13C
Diffraction pattern of A)

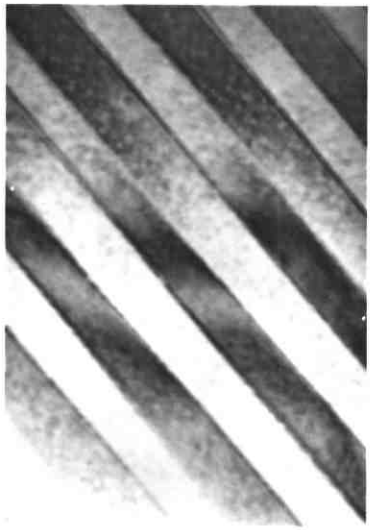

C) SM13C x 100,000

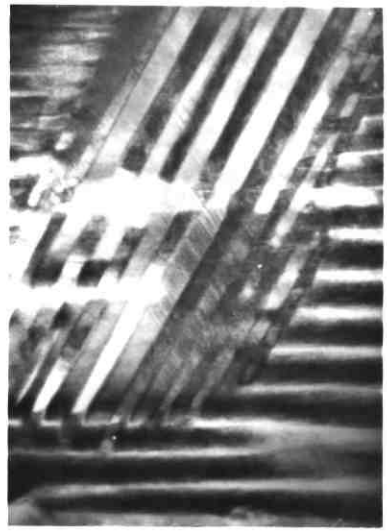

D) SM13C x 40,000

E) SM13C x 40,000

F) SM13C x 40,000

PLATE 3.15A SM10C

Backscattered electron image obtained by electron probe microanalysis of a large dendrite in a glassy matrix. x 800 approx.

PLATE 3.15B SM10C

EPMA micrograph of another dendrite as above. x 600 approx.

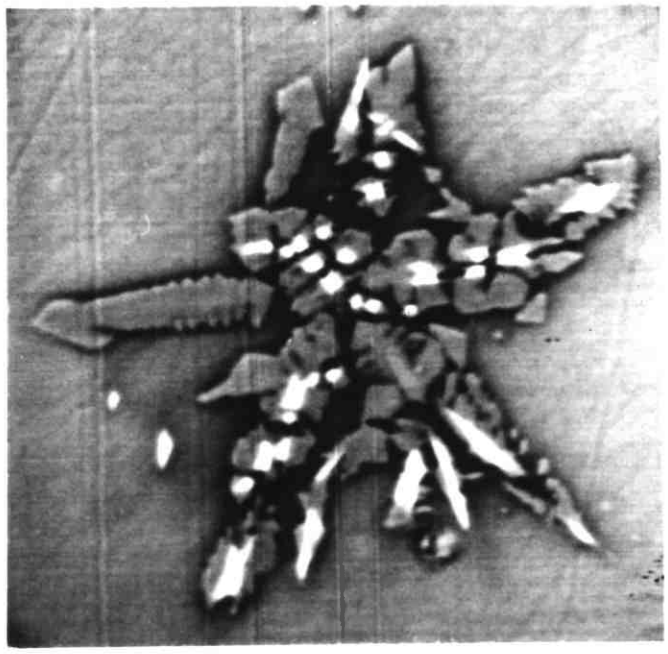

PLATE
3.15A

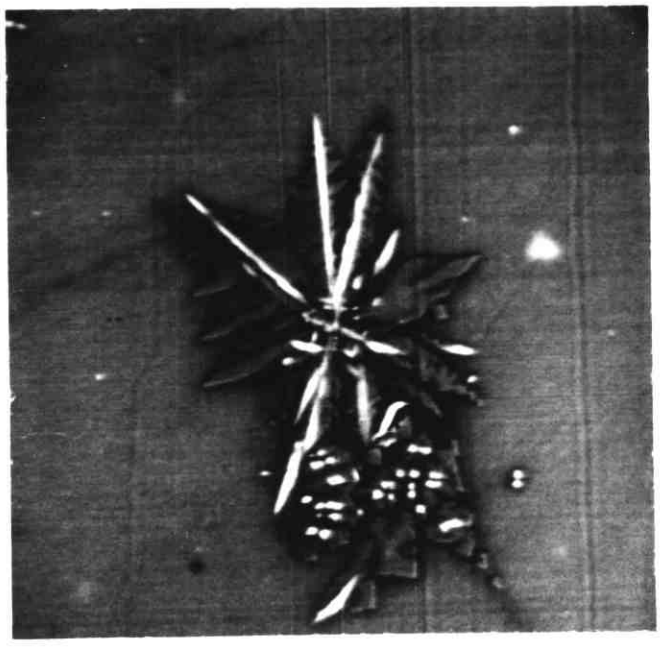

PLATE
3.15B

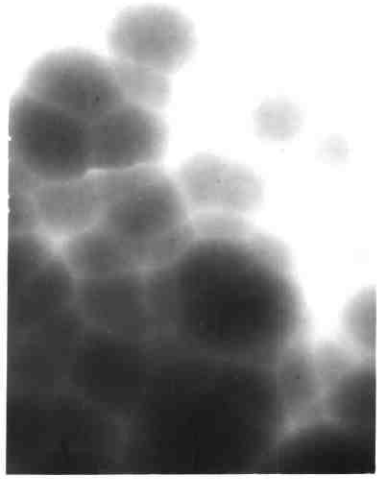

A)SM10a x 4,000

B) SM10a
Diffraction pattern of A)

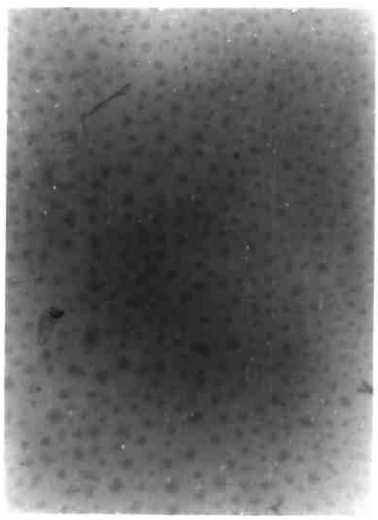

C) SM10b x 10,000

D) SM10N x 4,000

E) Diffraction pattern of D)

F) SM10N x 25,000

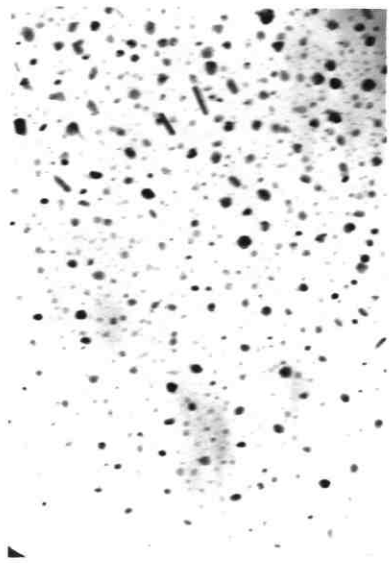

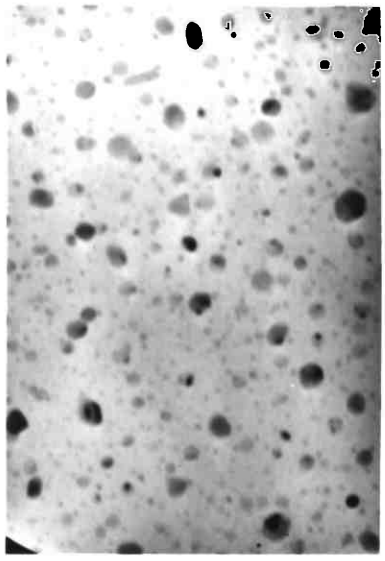

A) SM1ON x 63,000

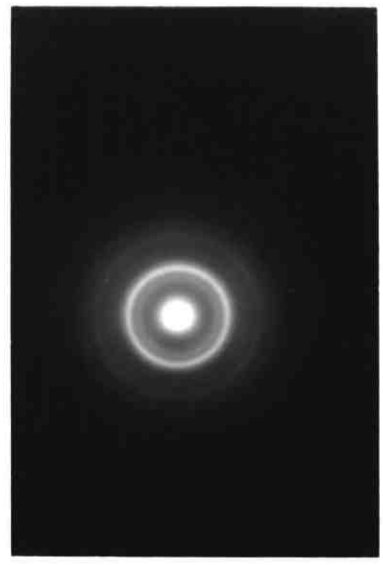

B) Diffraction pattern of A

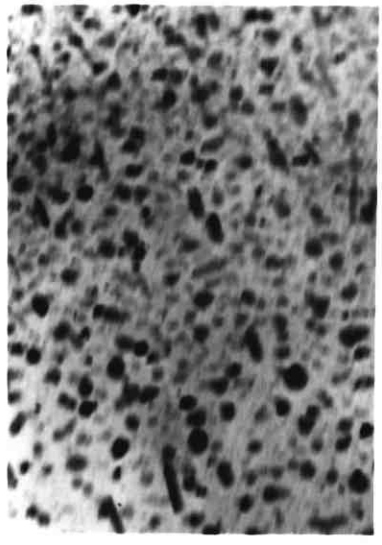

C) SM1ON x 40,000

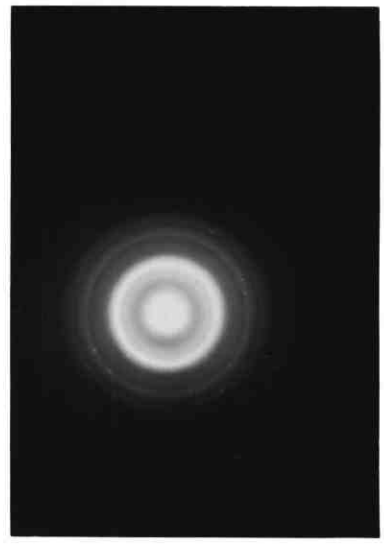

D) Diffraction pattern of C

E) SM1ON x 25,000

F) Diffraction pattern of E

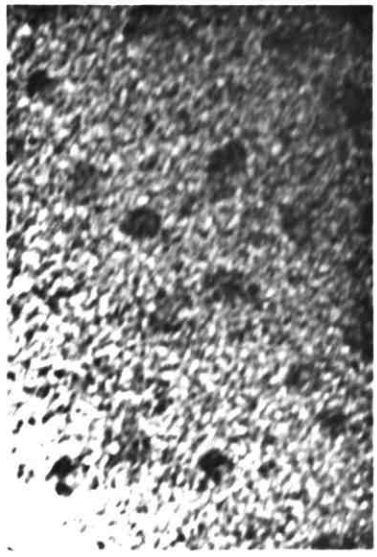

A) SM1Oc
Diffraction pattern of glass

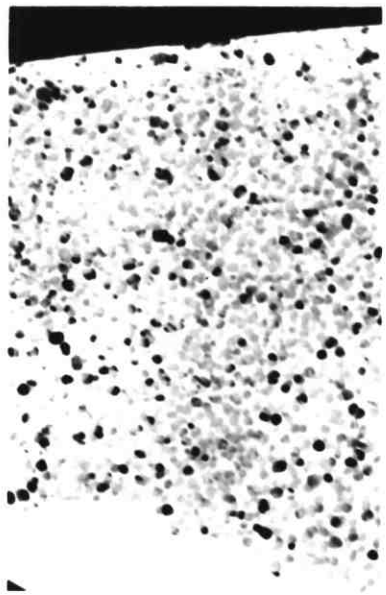

B) SM1Oc x 25,000

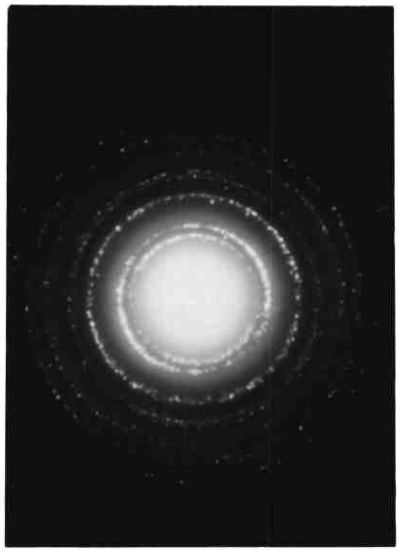

C) SM1Oc
Diffraction pattern of B

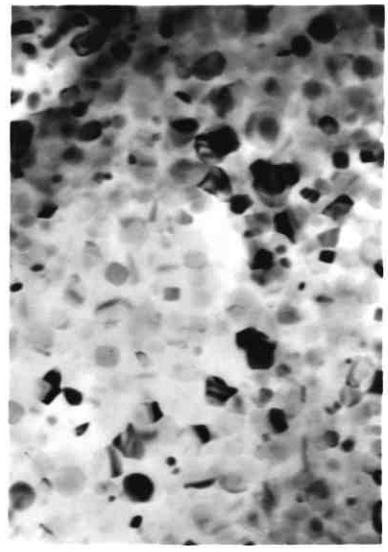

D) SM1Oc x 40,000

E) SM1Oc x 25,000

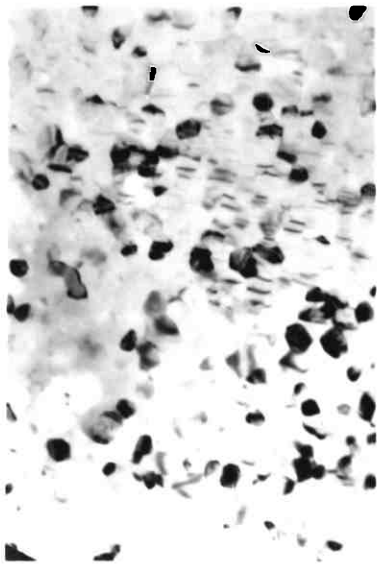

F) SM1Oc
Diffraction pattern of E

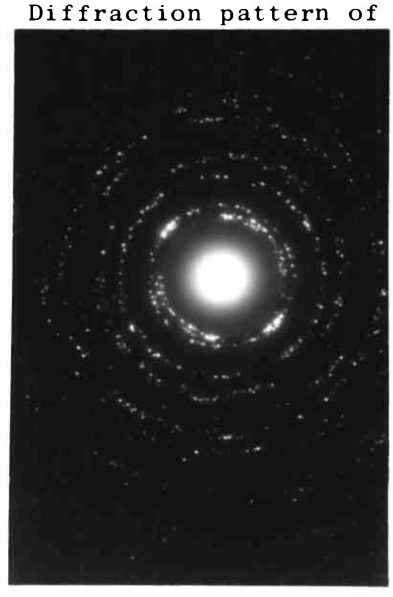

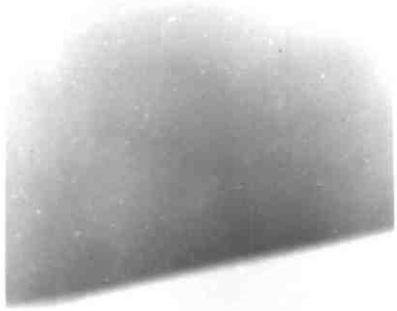

A) SF4 x 25,000

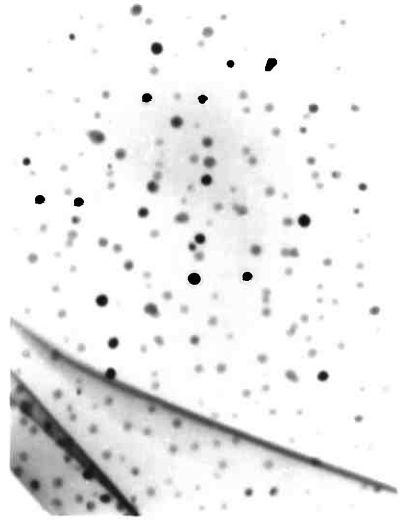

B) SF4 x 40,000

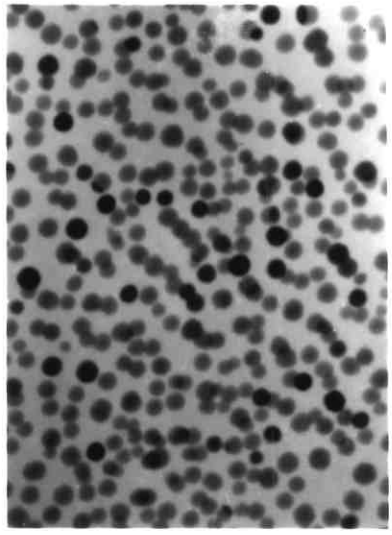

C) SF4 x 40,000

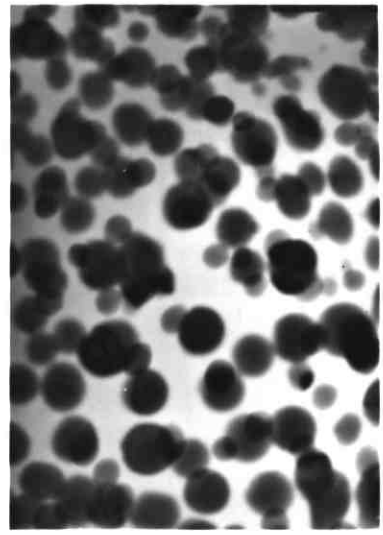

D) SF4 x 40,000

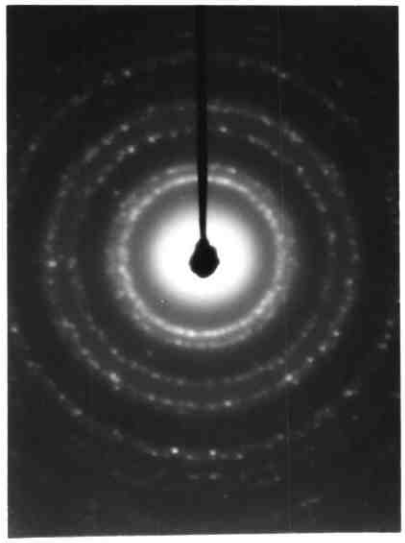

E) SF4
Diffraction pattern of D

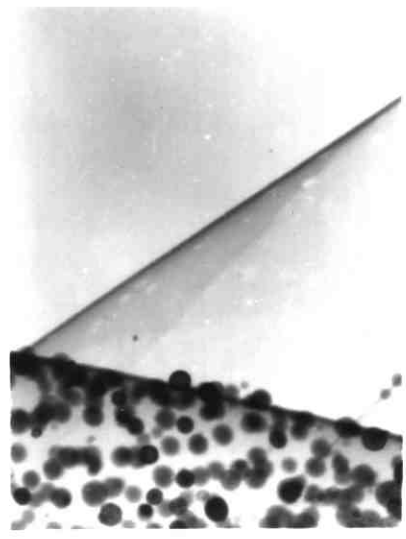

F) SF4 x 25,000

CHAPTER 4

DISCUSSION

4.1 Redox Ratios in the Glasses

4.1.1 Manganese

The attempts to produce glasses with a high proportion of Mn^{3+} have been described in Chapter 2, where it was concluded that the presence of manganese with an oxidation state of greater than +2 in the batch material had a negligible effect on the redox ratio attained in the glass, even after very short melting times. Evidently higher manganese oxides such as MnO_2, Mn_2O_3 and compounds thereof will rapidly dissociate or react at glass melting temperatures, losing oxygen and leaving only about 10% of the total manganese as Mn^{3+}, the balance being Mn^{2+}. This behaviour of the manganese-oxygen phase diagram[143] which predicts the following sequence of changes to occur in air with increasing temperature:

$$MnO_2 \xrightarrow{535^\circ C} Mn_2O_3 \xrightarrow{1080^\circ C} Mn_3O_4 + MnO$$

$$MnO \nearrow$$

Therefore at 1400°C in air a mixture of Mn_3O_4 ($\equiv Mn_2O_3 + MnO$) and MnO is expected, but because of the rapid rate of the reaction it was not possible to follow the approach to equilibrium.

The oxidation of manganese in glasses initially containing Mn^{2+} was much slower, as would be expected, since diffusion of oxygen into the melt is probably the rate determining step. The change of redox ratio could therefore be followed with time and the results for several glasses are shown in Figure 4.1(a).

Although the starting material did not affect the manganese redox ratio, this was affected by the glass composition and melting temperature as follows:

(a) In both silicate glass series SML and SMH, an increase in the total amount of manganese in the glass gave rise to a higher proportion of Mn^{3+}.

(b) Comparison between glasses in the SML and SMH series with nominally equivalent manganese concentrations reveals that the

higher the basicity of the glass, as measured by the amount of alkaline earth oxide, the higher the proportion of Mn^{3+}, and,

(c) Mn^{3+} was favoured by low melting temperatures as shown by the pairs BM5/BM8 and BM6/BM9.

The equilibrium between the ions and the furnace atmosphere may be expressed by the equation:

$$4Mn^{2+} + O_2 \rightleftarrows 4Mn^{3+} + 2O^{2-} \qquad (4.1)$$

and the equilibrium constant for the reaction is given by:

$$K = \frac{a^4_{Mn^{3+}}}{a^4_{Mn^{2+}}} \times \frac{a^2_{O^{2-}}}{p_{O_2}} \qquad (4.2)$$

where a_x represents the activity of species x and p_{O_2} is the partial pressure (or fugacity) of oxygen in the furnace atmosphere.

For small proportions of TM ions in a glass it is reasonable to assume that activity is proportional to concentration. Also the oxygen ion activity may be assumed constant for a given temperature and glass composition. Therefore a plot of $\log p_{O_2}$ against $\log Mn^{3+}/Mn^{2+}$ should have a slope of 4 if equation 4.1 is valid. The work of Johnston[137] shows that such an equation applies for manganese (and iron) in soda-silicate glasses. Johnston[137] also investigated the temperature dependence of the equilibrium constants for the same glasses, finding that an increase in melting temperature favoured the reduced state, as observed above, and log K decreased linearly with 1/T. It is difficult, however, to interpret this temperature dependence in thermodynamic terms since the temperature dependence of the oxygen ion activity is not known.

A problem arises when trying to explain finding (b) above in the light of equation 4.1, since an increase in the amount of basic oxide, such as CaO, would be expected to increase the oxygen ion activity and hence decrease the proportion of Mn^{3+}, at constant temperature and p_{O_2}, by favouring the reverse reaction. This is opposite to what was found experimentally. This has been observed quite generally and has generated considerable debate in the literature, from which there appears two possible explanations. The first suggests that the equilibrium constant changes with composition, which is not unexpected since concentration has been

used instead of activity, which is only permitted from a thermodynamic viewpoint for substances showing ideal behaviour. Activity and concentration are linked by an activity coefficient ($a_{Mn^{2+}} = \gamma\{Mn^{2+}\}$) and it is possible that this changes with the basicity of the glass. The second explanation is perhaps more understandable in terms of a physical model and recognizes that the higher valence state is the stronger Lewis acid and therefore has a greater affinity for electrons from available Lewis bases, which in this case are the oxygen anions. This effectively allows for the formation of TM ion-oxide ionic complexes and so the transfer of a solvent oxide ion from the melt to the coordination shell of the oxidised ion is included in the redox reaction:

$$Mn^{2+} + \tfrac{1}{4}O_2 + (x - \tfrac{1}{2})O^{2-} \rightleftarrows \{Mn^{(3+)}O_x\}^{(2x-3)-} \qquad (4.3)$$

The equilibrium constant for this reaction now requires that the Mn^{3+}/Mn^{2+} ratio must increase as the basicity is increased at constant temperature and oxygen fugacity, as found experimentally. This situation is analagous to the oxide transfers incorporated in the Mn^{2+}/Mn^{7+} redox process in aqueous solutions i.e. the production of the permanganate ion MnO_4^-. Further discussion and references can be found in reference 50.

Finally, it will be noted from Figure 4.1(a) that the redox ratios were almost constant after 3 - 4 hours melting, therefore the typical melting time of 5 - 6 hours was sufficient to produce an equilibrium redox ratio in the glass.

4.1.2 Iron

For the iron glasses, the process of reduction of Fe^{3+} or oxidation of Fe^{2+} when added to the melt was slow enough to allow the approach to equilibrium to be studied. Results obtained for the two glasses SF1 and SF3 used to show the change of redox ratio with time at constant temperature are presented in Figure 4.1(b).

In contrast to the identical base glass containing a similar proportion of manganese (SM11), iron was present at equilibrium largely in the oxidised state Fe^{3+}. Glasses containing ferric ion were slowly reduced and reached equilibrium within 24 hours. The rest of the iron series were melted for about 5 hours and it can be seen that although the glasses may not quite be at equilibrium, they are within 1 - 2%. Homogeneity of redox ratio throughout the

melt was ensured by occasional stirring. Glasses could be prepared with an appreciable proportion of Fe^{2+} by adding iron to the batch as ferrous oxalate. Furthermore, melting times were long enough to enable a homogeneous glass to be produced, consistent with high Fe^{2+} content. Uniformity of redox ratio was again ensured by stirring. The results depicted in Figure 4.1(b) are similar to those found by other workers on similar glass systems[135].

From the analysis of the redox ratios of the other iron glasses (Table 3.2.4) it is seen that:

(a) An increase in the melting temperature favoured the reduced state as discussed in the previous section, and,

(b) The redox ratio (Fe^{2+}/Fe_{total}) decreased as the total concentration of iron increased to 3.5% Fe_2O_3 but was then approximately constant with further increases (Figure 4.2(a)).

Once again the equilibrium between the ions may be expressed as either:

$$4Fe^{2+} + O_2 \rightleftarrows 4Fe^{3+} + 2O^{2-} \qquad (4.4)$$

or in the preferred form including the possible transfer of oxygen solvent ions:

$$Fe^{2+} + \tfrac{1}{4}O_2 + (x - \tfrac{1}{2})O^{2-} \rightleftarrows \{Fe^{3+}O_x\}^{(2x-3)-} \qquad (4.5)$$

There is some evidence for the existence of FeO_2^-, as in aqueous solutions but which of either Fe^{3+} or FeO_2^- is favoured will depend on the basicity of the glass. It was observed by Budd[144] that replacing Na_2O by CaO in a soda-lime-silicate glass i.e. decreasing the basicity, caused an increase in the ferric: ferrous ratio as predicted by equation 4.4, whereas the ratio increased with an increase in basicity in alkali silicate glasses. The situation for iron (and manganese) is not as clear as, for example, Cr^{6+} which is nearly always present as the negative complex chromate ion (CrO_4^{2-}) in glasses.

The variation of redox ratio with temperature was exactly equivalent to that for the manganese glasses discussed above, but the effect of increasing the total TM oxide concentration was different for the two elements. This is difficult to explain and in the literature generally the effect of the redox oxide concentration has not received such wide attention as that of melting

atmosphere, temperature and the compositional dependence.

Weyl[145] has reported the work of Densem and Turner and also Fuwa for iron in soda-lime-silicate glasses and these results are reproduced in Figure 4.2(a). The agreement of the present study is excellent in spite of the widely different base glasses. In contrast, the results for the manganese glasses in series SMH when plotted in the same way in Figure 4.2(b), show no signs of levelling off to a plateau, at least below 20% MnO. Other authors[146] have observed a similar effect at lower concentrations of Fe_2O_3 (<0.5%) but the reason for this behaviour is not known. The explanation may be linked with a change in the basicity of the glass as more TM oxide is added.

4.1.3 Mixed Manganese-Iron Glasses

The redox ratios discussed above were determined by chemical analysis but as yet no technique has been developed to chemically analyse the individual Fe^{2+}/Fe^{3+} and Mn^{2+}/Mn^{3+} ratios in glasses containing iron and manganese together. Physical methods must therefore be used to estimate at least one of the redox states (Mn^{3+} or Fe^{2+}) which, along with a chemical estimation of the remaining Mn^{3+} or Fe^{2+} when the glass has been dissolved and knowledge of the total TM oxide concentrations, will allow an estimation of both redox ratios. The technique used in this study was optical absorption spectroscopy, the results of which will be discussed in greater detail in Section 4.2.3, however, the conclusion of that work is relevant here; that Fe^{2+} and Mn^{3+} have not been observed simultaneously in any glass. Glasses containing equal proportions of iron and manganese contained small concentrations of Mn^{3+} but no evidence of Fe^{2+} could be detected. Conversely, those glasses melted with an excess of iron over manganese retained Fe^{2+}, but no Mn^{3+} was formed. As the stable states of iron and manganese in these glasses are Fe^{3+} and Mn^{2+} it is logical to assume that these constitute the balance. Therefore only three of the possible four valence states are observed.

A number of authors have attempted to describe the interaction between two redox couples in glass. Weyl[145] used the results of qualitative experiments to tabulate some of the commonly used redox oxides in order of their increasing 'inner oxygen pressure'. Any oxide will be oxidised by one placed above it in the table.

Tress[147] has plotted the Ellingham diagram for the pure oxides and obtained results similar to those of Weyl. Both are shown in Figure 4.3. These approaches are rather primitive and changes in glass composition, TM oxide concentration or melting temperature can result in the interchange of two couples. Both, however, would predict the following result for iron and manganese:

$$Mn^{3+} + Fe^{2+} = Fe^{3+} + Mn^{2+}$$

and it would appear from the present results that the ions react stoichiometrically in the glasses as they would in water. Therefore Mn^{3+} and Fe^{2+} do not appear to coexist in these silicate glasses.

This conclusion has been recognized for a long time, since MnO_2 has been used to decolorize green ferrous glasses. Only in the work of Ershov and Shul'ts[115] has it been reported that Mn^{2+}, Mn^{3+}, Fe^{2+} and Fe^{3+} could be present simultaneously in a glass. However, little justification was given for this statement and their analysis technique could not determine absolute Mn^{3+} and Fe^{3+} concentrations, therefore their claim would appear to be doubtful.

4.2 Optical Absorption Spectroscopy

4.2.1 Manganese Glasses

The main feature of the absorption spectra of manganese in both borate and silicate glasses was the single broad absorption band centred between 21 500 - 22 000 cm^{-1} (465 - 455 nm). There was no evidence of the asymmetric absorption noted by Paul[29] in glasses with low alkali content. The wavenumber at maximum absorption depended upon both the base glass composition and more particularly, the manganese ion concentration. The movement of the peak to higher energy with increasing manganese concentration was most clearly noted for series SML (Figure 3.1.2). This absorption band is produced by the only spin-allowed transition of Mn^{3+} in octahedral coordination: $^5E_g \rightarrow {}^5T_{2g}$.

The position of the band gives an apparent Δ_{oct} of ~22 000 cm^{-1}, which is high for an octahedral complex as a result of the strong Jahn-Teller distortion. It is slightly higher than that of the $\{Mn(H_2O)_6\}^{3+}$ ion (21 000 cm^{-1}). Octahedral coordination is

expected since the octahedral site preference energy is high for a d^4 ion and so tetrahedral Mn^{3+} has not been observed in glasses.

For each series of glasses the absorptivity increased as the proportion of manganese increased. The calculated molar absorptivities were constant within each series of silicate glasses for manganese concentrations of greater than 6% giving values of 274 ± 3 l mol^{-1} cm^{-1} and 260 ± 3 l mol^{-1} cm^{-1} for low (SML) and high (SMH) lime glasses respectively. For concentrations of less than 6%, the molar absorptivities were outside these ranges but this was probably due to inaccuracies in the redox ratio analysis. In contrast, calculation of molar absorptivity in the borate glasses did not produce a unique value. For glasses containing 5% manganese oxide the value was about 270 l mol^{-1} cm^{-1} but for higher concentrations the molar absorptivity decreased to about 150 l mol^{-1} cm^{-1}. However, all these values are 30 - 50 times higher than the molar absorptivity of the $\{Mn(H_2O)_6\}^{3+}$ ion in crystalline $CsMn(SO_4)_2.12H_2O$[29].

No conclusive explanation for this can be offered although other authors[145] have also found that the molar absorptivity changes with concentration and base glass composition. Paul[29] explained the increase in intensity of Mn^{3+} with increasing alkali content in terms of increasing covalency of the metal-oxygen bonds and also invoked the idea of five-fold coordinated species, though it is not clear if such ideas can be applied here. Certainly it is not obvious why a 5% increase in MnO in the borate glasses should bring about such a large change in molar absorptivity whilst the same change in silicate glasses had no such effect.

No other bands were observed, which is not surprising since the Mn^{3+} absorption will completely obscure the spin-forbidden bands of Mn^{2+}, the strongest of which should be at $\sim$23 000 cm^{-1}. Therefore it is not possible to speculate on the coordination of the Mn^{2+} ions from the optical absorption data.

4.2.2 Iron Glasses

The principal features of the spectra of the iron glasses were most clearly shown by those with small iron concentrations: SF2, SF8 and SF7. These features were:

(a) A broad absorption in the near infrared between 10 500 cm^{-1} and 11 000 cm^{-1} (950 - 910 nm).

(b) An ultraviolet absorption edge below 25 000 cm^{-1} for SF7 (400 nm), where the absorptivity increased rapidly with wavenumber.

(c) A relatively broad band (shoulder) at the edge of the cut-off at about 22 000 cm^{-1} (455 nm) becoming more pronounced as the iron concentration increased.

All were essentially unchanged as the concentration of iron increased although the wavelength at which they each appeared varied slightly. Most notable was the absorption cut-off which moved to longer wavelengths i.e. into the visible region, reaching about 21 000 cm^{-1} (476 nm) for glass SF4. In this case the absorption at 11 000 cm^{-1} (910 nm) appeared almost as a shoulder to the cut-off edge, making estimates of molar absorptivity very difficult. The broad absorption shoulder previously noted at 22 000 cm^{-1} (455 nm) was completely obscured. Glass SF5, with the highest iron concentration was too intensely coloured for any meaningful measurements to be made. Each of these three features will now be discussed in turn.

The broad infrared absorption can be assigned to Fe^{2+} ions in octahedral coordination. The ground state of the d^6 configuration (^5D) is split by the ligand field into $^5T_2$ and ^5E states and only one spin-allowed transition can occur. The absorption is therefore due to the $^5T_{2g}$ to ^5E_g transition of the high spin ion in an octahedral field. The position is similar to that of the $\{Fe(H_2O)_6\}^{2+}$ ion, found at about 10 400 cm^{-1} (962 nm) in crystals and solution[27]. The broadness of the absorption has been attributed to dynamic Jahn-Teller splitting of the $t_{2g}^3\ e_g^3$ configuration by McClure[32]; indeed, as was reported in section 1.2.6.2, two maxima may be observed.

The centre of the absorption moved to higher wavenumbers as the concentration of iron increased. The wavelengths of the absorption were less than usually found for Fe^{2+} in glasses. For example, Bates[27] quoted the band for Fe^{2+} in a soda-lime-silicate glass at 9100 cm^{-1} (1100 nm) and more recently Danielson and Schreurs[148] found values of 1080 - 1120 nm (8930 - 9260 cm^{-1}) for Fe^{2+} in a range of alkaline earth aluminosilicates. They found that the shorter wavelength was favoured by high ratios of

CaO/Al_2O_3. In the present study this ratio was much higher than any studied by Danielson and Schreurs[148] and the silica content was also much lower, thus the greater basicity of these glasses could be the reason for the lower absorption wavelengths. The change in the absorption peak with increasing Fe_2O_3 can also be explained by an increase in the basicity.

Unlike some investigations of Fe^{2+} in glasses, a second absorption band between 5000 - 10 000 cm^{-1} was not observed in the present study. The presence of the second band has been attributed to either Jahn-Teller splitting or Fe^{2+} in tetrahedral coordination depending on the magnitude of the splitting (2000 cm^{-1} for the former and $\sim$5000 cm^{-1} for the latter). It is now generally agreed, however, that Fe^{2+} in octahedral symmetry may give rise to a second band particularly if distortion is present. The actual wavelength of this extra band will depend upon the size of site, increasing as the site becomes larger. It is clear, however, that tetrahedral Fe^{2+} was not present in the glasses studied.

The absorptivity of the peak increased as the ferrous content of the glasses increased but it was impossible to obtain a single value for the molar absorptivity of ferrous ion. For glasses SF2 and SF7 the calculated value was 29.1 $\pm$ 0.5 1 mol^{-1} cm^{-1}, which is in good agreement with the work of Steele and Douglas[35] who reported a value of 28.9 1 mol^{-1} cm^{-1} for a $30Na_2O$-$70SiO_2$ glass containing 0.5% Fe_2O_3. However, the molar absorptivity of Fe^{2+} in silicate glasses is much greater than that of the $\{Fe(H_2O)_6\}^{2+}$ ion ($\varepsilon \sim 1.8$ 1 mol^{-1} cm^{-1}) and also Fe^{2+} in sodium borate glasses studied by Steele and Douglas[35] for which $\varepsilon \sim 3$ 1 mol^{-1} cm^{-1}.

For the more concentrated iron glasses, the present study has shown that the ferrous molar absorptivity rises to as high as 60 1 mol^{-1} cm^{-1} and the value is dependent on the ferric content of the glass. For example, the molar absorptivities of glasses SF1.1 and SF1.4 were between 51 - 53 1 mol^{-1} cm^{-1} but for glass SF3.1, with approximately the same total iron concentration but with a lower ferric content, the value was about 39 1 mol^{-1} cm^{-1}. This phenomenon, which is found in certain glasses, resulting in a high ferrous molar absorptivity which increases as the ferric content increases, may be the result of an interaction between Fe^{2+} and Fe^{3+} as suggested by Weyl and Bates[27, 145], but there is little independent evidence for this. An alternative explanation

is that the increase is due to the breakdown of the Laporte selection rule arising from structural changes which cause static distortion of the octahedral environment. Dunn et al[149] explained the change in $\varepsilon(Fe^{2+})$ in sodium borosilicate glasses as resulting from distortion arising from the conversion of boron from three- to four-fold coordination. Although a chemical interaction or structural change may be occurring as the concentration of iron is increased, the increase in molar absorptivity could be due solely to the additional intensity of the absorption contributed by the charge transfer edge as it moves to longer wavelengths. Certainly for SF6 and SF4 it was difficult to separate the two contributions and so define the ferrous absorptivity exactly.

The second feature, the UV absorption edge, arises mainly from the ferric charge transfer band centred at about 210 nm ($\sim$48 000 cm^{-1}). The transition is Laporte allowed and thus the intensity is very high ($\varepsilon \sim 3 \times 10^3$ 1 mol^{-1} cm^{-1}). This band could not be observed directly with the experimental equipment used, but as the ferric concentration increased, the cut-off edge moved further into the visible spectrum because of the increase in the absorption at 210 nm. A plot of the wavenumber at a given absorptivity against $\%Fe^{3+}$ is shown in Figure 4.4, from which it can be seen that the relationship is approximately linear indicating that the absorption edge is mainly determined by the Fe^{3+} content.

The third feature was the shoulder in the ferric charge transfer band at about 22 000 cm^{-1} (455 nm). As the only spin-allowed transitions for either Fe^{2+} or Fe^{3+} have already been accounted for, this must be due either to a spin-forbidden transition with high intensity or possibly an interionic charge transfer transition.

The former explanation must be favoured at this stage and the absorption is therefore assigned to ferric ion. As Fe^{3+} is a d^5 ion, only spin-forbidden bands are predicted. These are likely to be transitions to the quartet terms since those to the doublet terms are doubly spin-forbidden and therefore probably not observable. As there is no LFSE for a d^5 ion, neither octahedral or tetrahedral coordination is preferred. Therefore, following Bates[27] and assuming a value of Δ_{oct} equal to 12 300 cm^{-1}, which is 12% smaller than that observed experimentally for $\{Fe(H_2O)_6\}^{3+}$, and a Racah parameter B equal to 720 cm^{-1}, gives the following

transitions for octahedral coordination and also for tetrahedral coordination assuming $\Delta_{tet} = 4/9\Delta_{oct}$:

	Octahedral	Tetrahedral
$^6A_1 \rightarrow {}^4T_1$	13 600 cm^{-1} (735 nm)	20 000 cm^{-1} (500 nm)
$^6A_1 \rightarrow {}^4T_2(G)$	17 600 cm^{-1} (568 nm)	22 400 cm^{-1} (446 nm)
$^6A_1 \rightarrow {}^4E\ {}^4A_1$	23 400 cm^{-1} (427 nm)	23 400 cm^{-1} (427 nm)
$^6A_1 \rightarrow {}^4T_2(D)$	26 300 cm^{-1} (380 nm)	26 300 cm^{-1} (380 nm)

These values have also been quoted by Steele and Douglas[35] and are similar to those calculated by Kurkjian and Sigety[41] (see section 1.2.6.2), whose work was, in turn, confirmed by Edwards et al[39].

Examination of the optical spectra found in this study shows that for all glasses with iron contents up to ∿5% Fe_2O_3, a more or less pronounced absorption band was observed at ∿22 000 cm^{-1}. For the other iron glasses, including also SF1.4, any band at this frequency was obscured by the UV cut-off. This absorption can tentatively be assigned to the $^6A_1 \rightarrow {}^4T_2(G)$ transition of Fe^{3+} in a tetrahedral site. However, this is difficult to confirm since in most cases the other bands expected were not observed. In each case it was not possible to observe any absorption bands at 23 400 or 26 300 cm^{-1}, though this is not so important since an absorption at these frequencies can result from either tetrahedral or octahedral ferric ion and therefore cannot be used as evidence for one or the other. Also in most cases, no absorption band at or below 20 000 cm^{-1} could be distinguished, with the exception of SF3.1 and perhaps SF1.1, for which there was another band at ∿18 000 cm^{-1}. This can be assigned to the $^6A_1 \rightarrow {}^4T_1$ transition of tetrahedral Fe^{3+}, but could also be the $^6A_1 \rightarrow {}^4T_2(G)$ transition of octahedral Fe^{3+}. No band could be observed at 13 600 cm^{-1} which would be further indication of octahedral ferric ion though this is near enough to the Fe^{2+} absorption to be masked if the absorptivity is small.

Consideration of this evidence leads to the conclusion that some, if not all, of the Fe^{3+} are in tetrahedral sites. The spectra found were very similar to those found by Kurkjian and Sigety[41]

in a soda-silicate glass containing Fe_2O_3, where the absorption band at ∿22 000 cm^{-1} was the only prominent one, particularly at Fe_2O_3 concentrations of ∿5%. In that work also, tetrahedral Fe^{3+} was suggested. Similarly the results may also be compared with the reflection spectra of soda-lead-silicate glasses containing iron measured by Edwards et al[39], where below 25 000 cm^{-1} two bands were found, one at 18 500 cm^{-1} and the other at 22 000 cm^{-1}. Again it was concluded that ferric ion was tetrahedrally coordinated.

It was not possible to calculate the absorptivity of the ferric ligand field bands since the contribution of the UV edge was not known. Steele and Douglas[35] found that the two contributions could be separated, at least for the 380 nm band, by using Urbach's rule, which they noted was obeyed over the range 370 - 300 nm. However, in the present study, measurements of absorption could not be made accurately below ∿380 nm, thus this procedure cannot be used. It is obvious though, even without quantitative calculations, that the absorptivity of these spin-forbidden bands is high. Certainly, tetrahedral coordination will increase the absorptivity for the reason discussed previously, but an increase could also be due to a phenomenon known as 'intensity stealing'. This allows the intensity of a spin-forbidden ligand field transition to increase when it occurs close to a charge transfer band because of mixing of the electronic wavefunctions of the forbidden excited term with the allowed level, resulting in transitions to the excited term becoming more allowed.

The presence of octahedral ferric ion cannot be ruled out completely since its transitions may not be observable for three main reasons. Firstly, octahedral spin-forbidden transitions are less intense than tetrahedral because, being centrosymmetric complexes, relaxation of Laporte's rule is less likely to occur. Secondly, the positions of the octahedral absorption bands (568 and 735 nm) are further away from the charge transfer band, therefore 'intensity stealing', if operating, would be much less and thirdly, the band at 735 nm could be masked by the high absorptivity of Fe^{2+} in these glasses. Evidence of octahedral Fe^{3+} from other sources will be briefly considered below.

The final effect that must be considered for the 22 000 cm^{-1} band is that an interionic charge transfer process is operating. This initially would seem attractive for glasses with high iron

contents for if $h\nu = 22\ 000\ cm^{-1}$ for the $Fe^{2+} \rightarrow Fe^{3+}$ photon assisted transfer, then W_H is calculated to be $\sim$0.68 eV. This is approximately the value of the total activation energy for these glasses. However, this is probably fortuitous since the absorption remains invarient with widely differing iron concentrations for which the activation energy varies markedly. Also it has not been possible to prepare the most concentrated iron glasses thin enough for the band to be observed to see if its position changes at high iron concentrations.

4.2.3 Mixed Manganese-Iron Glasses

4.2.3.1 Glasses With Equal Proportions of Iron and Manganese

These glasses were melted for a sufficient period of time to be at or near equilibrium. By comparison with the spectra obtained for glasses containing iron or manganese separately, one of the obvious features of these glasses was the absence of any absorption band between 5000 - 11 000 cm^{-1}. The high value of $\varepsilon(Fe^{2+})$ in the iron glasses discussed above would result in appreciable absorption if any Fe^{2+} were present, therefore it must be concluded that Fe^{2+} is absent from these glasses.

SMF1 and SMF4 showed evidence of a single band at about 22 000 cm^{-1}, below the ultraviolet edge, for which several explanations can be advanced: a ligand field band of Fe^{3+} or Mn^{3+} or some kind of interionic absorption. The presence of any absorption due to Mn^{2+} will, of course, be completely masked.

SMF4 is, in effect, a combination of SM15 and SF2. The absorptivity at 22 000 cm^{-1} is less than the sum of those for SM15 and SF2, therefore the sum of the oxidised species contributing to this absorption, namely Fe^{3+} and Mn^{3+}, must be less in the mixed glass. It has already been stated that Fe^{2+} is absent, therefore, the amount of Fe^{3+} is greater than in SF2 which should result in a larger absorption if the peak is solely due to Fe^{3+}. Therefore to explain the curve for SMF4 it must be concluded that this glass contains less Mn^{3+} than SM15. The glass was reddish-brown in colour which confirms that this band is mainly due to the single spin-allowed transition of Mn^{3+}. Interionic charge transfer, although a possibility, is very unlikely. A similar argument can be applied to SMF5 which is in effect a combination of SM16 and SF8,

although in this case the absorptivity of the sample could not be measured below 19 000 cm^{-1} because of the sample thickness. However, the absorptivity of SMF5 at 19 000 cm^{-1} was less than the sum of that due to SM16 and SF8 independently, which means that it must contain less Mn^{3+} than SM16. The presence of Mn^{3+} was again confirmed by the characteristic colour. Finally, SMF2 (≡SF1 + SM11) also did not show a distinct band though it was measured to much higher absorptivities, because of the cut-off. This absorption cut-off will now be examined.

As it is proposed that all of the iron is present in the ferric state, the absorption edge, which is mainly the result of the ferric charge transfer band, should move to lower energies i.e. into the visible region, compared with the iron only glasses. Mn^{2+} and Mn^{3+} also have charge transfer bands in the UV but by examining the manganese only spectra it can be seen that the effect of these is small below 25 000 cm^{-1}, even for the most concentrated glasses.

Meaningful measurements could only be made for SMF4 and SMF2 since the absorption edge was included in these spectra. For SMF4 the absorptivity at 25 000 cm^{-1} was ∿8 cm^{-1} and the sum of that due to SM15 and SF2 at the same wavenumber was ∿9 cm^{-1}. However, at that wavelength the Mn^{3+} absorption was appreciable and as there was less Mn^{3+} in SMF4 than in SM15, the manganese component should be lower, whilst that of Fe^{3+} should be higher. It is probably best to conclude from optical spectroscopy that the behaviour of SMF4 is entirely due to the addition of the Mn^{3+} and Fe^{3+} absorptions and that no interaction is occurring. EPR results which support the opposite view will be discussed below.

The situation for SMF2 was a little clearer, the absorptivity reached 150 cm^{-1} at ∿22 500 cm^{-1}. Now this glass contained iron only as Fe^{3+}, therefore it should contain more Fe^{3+} than SF1.1, which had ∿9% Fe^{2+} and a nominally equivalent Fe_2O_3 content. SF1.1 reached an absorptivity of 150 cm^{-1} at ∿21 500/cm. Now whilst this may not seem a great difference it must be remembered that SMF2 contained some Mn^{3+}, which has a high molar absorptivity. Therefore it is concluded that the absorption edge for SMF2, once the Mn^{3+} contribution has been subtracted, has moved to higher energy, even though the proportion of Fe^{3+} has increased. This is possibly indicative of some kind of interaction taking place to form associates of the type $Mn^{2+} - O - Fe^{3+}$. Further evidence

for this will be considered subsequently.

It had been hoped that the optical absorption spectra would give a quantitative estimate of the proportion of Mn^{3+}, however, this does not now seem to be possible for the following reasons. Firstly, it is difficult to separate the relative contributions of the Mn^{3+} and Fe^{3+} ligand field transitions and the Fe^{3+} charge transfer band at 22 000 cm^{-1} to determine the absorption due to manganese alone. Secondly, even if this could be achieved, it is difficult to calculate a reliable value for the Mn^{3+} molar absorptivity from the single TM ion glasses as discussed above.

4.2.3.2 Glasses with an Excess of Iron Over Manganese

These glasses were melted for a short time to retain an appreciable quantity of ferrous ion.

The presence of ferrous ion is clearly indicated in Figure 3.1.6 with the characteristic absorption around 11 000 cm^{-1}. This again can be attributed to Fe^{2+} in octahedral coordination. The high proportion of iron in these glasses has brought the cut-off edge to ∿22 000 cm^{-1} therefore it was not possible to see any band due to Mn^{3+} or Fe^{3+}. The colour of the glasses, however, was typical of ferrous glasses and no reddish tint due to Mn^{3+} could be discerned, therefore it is proposed that Mn^{3+} is absent, having been completely reduced by Fe^{2+}.

The actual proportion of Fe^{2+} can be estimated from the spectra. Since Mn^{3+} is not thought to be present and Mn^{2+} has weak bands, the absorption at 11 000 cm^{-1} must be due to Fe^{2+} with some contribution from the cut-off edge as for the iron glasses SF6 and SF4. The molar absorptivity of Fe^{2+} in SF6 was calculated as 57 1 mol^{-1} cm^{-1} and using this value the redox ratio for SMF2A and SMF2B is calculated as 18.5% and 20.9% respectively. Of course these are only estimates as the value of $\varepsilon(Fe^{2+})$ is not exact, but it is hoped that by using a value typical of the same iron concentration as in the mixed glass, this error will be minimised.

The absence of Mn^{3+} allows the position of the absorption edge to be correlated with the proportion of ferric ion, using the plot in Figure 4.4. The percentage of Fe^{3+} has been calculated from the analysed total iron content and the redox ratio determined above and this has been plotted on the graph against the wavelength at an absorptivity of 150 cm^{-1}. It is seen that both glasses

have a cut-off at a higher energy than would be expected from the proportion of Fe^{3+} alone, indicating again the possibility of interaction and associate formation. However, the scatter in the plot is appreciable, as are the errors in the $\%Fe^{3+}$ estimation, therefore this cannot be used as conclusive proof for associate formation.

4.3 Electron Paramagnetic Resonance Spectroscopy

4.3.1 Manganese Glasses

The EPR spectrum of the dilute manganese silicate glass SM15 showed each of the three characteristic features usually associated with Mn^{2+} in glass. The principal absorption was centred at $g \sim 2.0$ with six inflexions corresponding to the six hyperfine lines of ^{55}Mn. A second absorption appeared at $g \sim 4.3$ and finally a 'shoulder' to the $g \sim 2.0$ line at $g \sim 3.0$. This final absorption was shifted from its usual position in manganese glasses at $g \sim 3.3$. The hyperfine lines were also less well resolved than in the work of other authors, using a similar doping concentration, as a result of the greater inhomogeneous broadening by magnetic dipole-dipole interactions.

The spectrum may be described by a spin Hamiltonian of the form:

$$\mathcal{H} = g\beta HS + D\{S_z^2 - \tfrac{1}{3} S(S+1)\} + E(S_x^2 - S_y^2) + ASI \qquad (4.6)$$

but the EPR parameters have not been calculated. It is not possible therefore, to estimate the ionicity of the Mn^{2+} - oxygen bond from the hyperfine coupling constant (A). However, even this information would be insufficient to infer the Mn^{2+} coordination number.

With a much greater concentration of manganese, as found in SM18, the only feature which remained was a symmetric intense absorption at $g \sim 2.0$, though in this case the hyperfine lines were completely washed out. The peak-peak bandwidth was, however, slightly less than that for SM15 at ~450 G. This information is not complete enough for a description of the Mn^{2+} site in these glasses to be advanced.

4.3.2 Iron Glasses

The spectrum of the dilute iron glass SF2 showed each of the resonances expected for a glass containing a small proportion of Fe^{3+}; weak signals at $g \sim 6.0$ and 2.0, with the main signal at $g \sim 4.3$. This indicates that the Fe^{3+} ions are isolated in the glass. The $g \sim 4.3$ resonance may be assigned to isolated Fe^{3+} ions in a rhombically

distorted octahedral or tetrahedral oxygen environment (D large and E/D $\sim$ 1/3). However, the presence of a g $\sim$ 6.0 resonance indicates that some of the Fe^{3+} is present in axially distorted sites (D large and E $\sim$ 0). The g $\sim$ 2.0 resonance is probably related to that at g $\sim$ 6.0, since they are the perpendicular and parallel g values of the Kramers doublets where E/D = 0. As discussed above, it is not possible to use the g $\sim$ 4.3 and 2.0 resonances as a measure of the tetrahedral/ octahedral ferric ratio.

It was not possible, unfortunately, to measure the whole series of iron glasses to follow the changes in the spectra with increasing iron concentration. However, glass SF6 was measured after heat treatment and this yielded the main resonance at g $\sim$ 2.0 with only a small signal at g $\sim$ 4.3. The resonance at g $\sim$ 6.0 had disappeared completely. There are two effects here; firstly the increase in ferric ion concentration and secondly, the effect of crystallization.

Examination of the literature reveals that as the ferric ion concentration is increased, the g = 6.0 resonance usually disappears for glasses containing over 2% Fe_2O_3 and the g = 2.0 resonance intensity increases at the expense of that at g = 4.3. The appearance of the g = 2.0 resonance is no longer connected with weak crystal field terms but may be attributed to clusters of paramagnetic ions containing two or more ions coupled by exchange interactions. However, the resonance centred on g = 2.0 is usually very broad; Kurkjian and Sigety[41] found a peak to peak linewidth of $\sim$1.5 kG at g = 2.0 for a 5% Fe^{3+} glass and an even greater value was found by Loveridge and Parke[51] for a 10% Fe_2O_3 glass. A broad resonance at g $\sim$ 2.0 is therefore typical of spin-spin interactions as the Fe^{3+} interionic separation decreases.

Examination of the EPR spectrum for SF6C reveals the the g $\sim$ 2.0 absorption is narrow with a peak-peak linewidth of only 250 G. This narrow resonance with a high intensity shows that spin-spin interaction forming exchange coupled Fe^{3+} or Fe^{3+} - Fe^{2+} pairs or clusters has not occurred. It is, however, indicative of the formation of a crystalline phase. A similar sharp resonance (ΔH_{pp} $\sim$ 200 G) was found by Friebele et al[65] for iron phosphate glasses following heat treatment. Phases rich in Fe^{3+}, including magnetite, were identified by X-ray diffraction analysis. Other authors have identified similar phases which are often ferrimagnetic. X-ray diffraction analysis of SF6C suggested that fassaite, an iron containing pyroxene, was the

major crystalline phase and is therefore reponsible for the EPR signal. The g ∿ 2.0 resonance shows strong exchange narrowing and is similar to the spectra of systems which show superparamagnetic behaviour. Superparamagnetism occurs when clusters of magnetic ions become very strongly coupled through exchange forces to give a large magnetic moment, whose energy is independent of orientation in space. More extensive work would need to be performed to establish the physical effects responsible for this resonance.

The presence of a pronounced resonance at g ∿ 4.3 in the spectrum of SF6C suggests that some of the Fe^{3+} ions are not incorporated into the crystalline phase and are still isolated, possibly in a residual glassy phase. EPR can therefore be used to give evidence that Fe^{3+} is contained in the crystalline phase, since any build up in the residual glassy phase should result in a broad signal at g ∿ 2.0 with reduced intensity because of exchange interactions. A high intensity (1 - 2 orders of magnitude) is certainly indicative of the presence of crystalline phases.

4.3.3 Mixed Iron-Manganese Glasses

The signals from the three dilute mixed glasses SMF1, SMF4 and SMF5 suffered severe attenuation. The receiver gain was so high that the signals were very noisy and affected by the background resonance of the quartz tube in the cavity, making the signal even harder to recognize. Therefore these signals have not been reproduced and will only be described.

For SMF1 there was only a very small resonance at g ∿ 4.3 but this increased in intensity for SMF4 and again for SMF5. No resonance at g ∿ 2.0 was obvious for SMF1 but it appeared for the other two glasses and was greatest for SMF5. It was quite impossible to identify the 'fingerprint' hyperfine lines of Mn^{2+} because of the noise in the signal, therefore it is not clear if the g ∿ 2.0 signal is due to Fe^{3+} or Mn^{2+}. If it is the result of Fe^{3+} then the continued increase in intensity of the g ∿ 4.3 signal is surprising in the light of previous work on iron only glasses.

The reason for the attenuation of the signal compared to the pronounced signals of the single iron and manganese dilute glasses is uncertain but several possibilities can be advanced. It cannot be the result of chemical interaction i.e. $Fe^{2+} + Mn^{3+} = Fe^{3+} + Mn^{2+}$, since

although this has undoubtably occurred, both Mn^{2+} and Fe^{3+} exhibit paramagnetic resonance and therefore the total signal of the mixed glasses should increase. Cross relaxation processes between Fe^{3+} and Mn^{2+} also cannot be expected since both have long spin-lattice relaxation times; Fe^{2+} has a short spin-lattice relaxation time but of course is not present in this series of glasses. This leaves spin diffusion within the Mn^{2+} system or nuclear relaxation as two possible mechanisms. The third alternative, and one which must be favoured at this stage, is that interaction between Fe^{3+} and Mn^{2+} has occurred possibly to form associates. Since the proportion of Fe^{3+} is considered to be greater than Mn^{2+} in this series, then some Fe^{3+} may remain unaffected by Mn^{2+} and the $g \sim 4.3$ resonance probably results from these free (unpaired) isolated Fe^{3+} ions. The resonance at $g \sim 2.0$ therefore corresponds to the paired $Mn^{2+} - Fe^{3+}$ associates. This is also supported by the fact that the g value had changed slightly in the mixed glass, by falling to 1.94 compared to 2 for the single iron glass. Similar changes in g were explained by Bogomolova[63,64] in terms of exchange interactions and associate formation.

The series of mixed glasses comprising SMF2, SMF2A and SMF2B was also investigated. SMF2 had nominally equal iron and manganese concentrations and showed a broad resonance at $g \sim 2.0$ with a linewidth of 1000 G. There was only a very slight inflexion in the signal at $g \sim 4.3$. The intensity of the $g \sim 2.0$ signal was high, though less than the signal of SM18 which had a greater manganese concentration. However, the linewidth was greater than that of SM18 indicating that the resonance could not be due solely to Mn^{2+} but either $Fe^{3+} - Fe^{3+}$ or $Fe^{3+} - Mn^{2+}$ interactions, or possibly all three.

As manganese was replaced by iron through the series SMF2, SMF2A and SMF2B, the intensity of the $g \sim 2.0$ resonance decreased but the peak-peak linewidth increased. The $g \sim 4.3$ signal also increased in intensity. These changes can only be explained once the species in SMF2 has been identified. The $g \sim 2.0$ resonance cannot be associated entirely with isolated Mn^{2+} ions because of the broad linewidth, therefore there must be a contribution from $Mn^{2+} - Fe^{3+}$ or $Fe^{3+} - Fe^{3+}$ pairs. If mixed pairs are responsible then there arises an anomaly in that mixed $Mn^{2+} - Fe^{3+}$ pairs were proposed to be the cause of the decrease in intensity of the dilute glasses, whereas for SMF2 they produce a considerable increase. It could be that the $g \sim 2.0$ signal is a mixture of isolated Mn^{2+} ions and $Fe^{3+} - Fe^{3+}$ clusters which are

non-interacting, or if some mixed associates are present they cannot be detected by EPR because of the low intensity of their signal. As manganese is replaced by iron the intensity would then decrease because of a reduction in the number of Mn^{2+} ions. This is reasonable since Mn^{2+} would appear to give a more intense signal than Fe^{3+}. Accompanying this is an increase in Fe^{3+} clusters which although not affecting the signal intensity, increases the linewidth by exchange coupling (spin-spin interactions). Unfortunately it is not easy to explain why the $g \sim 4.3$ resonance also increases except by assuming that the proportion of isolated Fe^{3+} ions increases.

The absence of any manganese hyperfine lines in these glasses may result from spin diffusion, nuclear relaxation or associate formation. However, it should be remembered that the hyperfine lines are normally washed out at high concentrations by dipole-dipole interactions (e.g. SM18). The absence cannot, therefore, be used as direct evidence for associate formation. Unfortunately the actual g values around 2 could not be measured with sufficient accuracy to observe any variation which would support associate formation.

In conclusion, therefore, although the idea of Fe^{3+} - Mn^{2+} associates would appear attractive for the dilute glasses, there is little positive evidence to suggest their presence in the more concentrated glasses. More work would be needed to clarify this situation.

4.3.4 Conclusions Regarding Ionic Coordinations

Results from optical spectroscopy have indicated conclusively that Mn^{3+} in these silicate and borate glasses is in octahedral coordination. However, no information has been gained on the coordination of Mn^{2+} either from optical or EPR spectroscopy. Previous work by other authors using fluorescence spectroscopy [150,151] has suggested that Mn^{2+} is six-fold coordinated in borate glasses and four-fold coordinated in silicate glasses. However, more recent work on $MnO-Al_2O_3-SiO_2$ glasses [152] has indicated that Mn^{2+} in an octahedral environment is possible in certain silicate compositions. More work is therefore needed to clarify the Mn^{2+} coordination since it cannot be stated with any certainty.

The situation is similar for iron glasses, for whilst it can be definitely stated from optical absorption spectroscopy that Fe^{2+} is in octahedral coordination, the situation for Fe^{3+} is unclear. It can be concluded that tetrahedral Fe^{3+} is present, as usually observed in

silicate systems[41], but it is difficult to confirm if octahedral Fe^{3+} is present as well. The evidence of some other recent work suggests that it may indeed be present. Fenstermacher[42] observed both six-fold and four-fold coordinated Fe^{3+} in soda-lime-silicate glasses though the identification of octahedral Fe^{3+} was difficult for the reasons discussed above. Octahedral Fe^{3+} was also observed in alkaline earth aluminosilicate glasses by Danielson and Schreurs[148] when the ratio of alkaline earth/alumina was less than one, since there were not enough alkaline earth ions remaining, after being used by Al^{3+} ions, to provide the necessary charge compensation for tetrahedral ferric ion. In both of these studies, however, the proportion of iron was small (<0.5% Fe_2O_3).

More pertinent results have been provided by Mössbauer analysis of Fe^{3+} in soda-lime-silicate glasses containing 35 wt% Fe_2O_3[153]. It was found that a large fraction of ferric cations were octahedrally coordinated even when the ratio of Fe_2O_3 to modifying oxides (FeO, Na_2O, CaO) was less than unity and there were sufficient oxygen anions to form tetrahedra around the ferric cations. In the analagous case of Al_2O_3, this situation would not be found and all of the Al^{3+} would be four-fold coordinated.

Further work, possibly using Mössbauer spectroscopy, would need to be undertaken to confirm the presence of octahedrally coordinated ferric ion in glasses in series SF, however, its presence cannot be completely ruled out at this stage.

4.4 Effect of Composition on the Distance Between TM Ions and the Polaron Radius

Values of the mean TM interionic spacing (R) and polaron radius (r_p) have been plotted against % TM oxide for each series of glasses in Figures 4.5.1 - 4.5.4.

The behaviour of each series was similar. As the concentration of TM oxide increased from 0.5%, the mean TM spacing initially decreased rapidly, but then the rate of decrease was reduced. In the range of measurement for series SMH and SF the change in R was approximately a factor of three.

The small polaron radius behaved in an identical manner, which is not surprising considering that it is related to R by Bogomolov's equation:

$$r_p = \tfrac{1}{2} (\pi/6). R \qquad (1.4.12)$$

By comparing the values of R (and r_p) for different glass series, it is found that the values for the two silicate series containing manganese are very close, reflecting only the small change in density between the two base glasses. This similarity is also seen for iron and manganese glasses with equivalent compositions (SMH amd SF).

It should be noted at this point that the calculation of R assumes a random distribution of ions throughout the volume of the glass. The absence of long range order and variations in short range order inherent in the glassy structure indicate that a value of R calculated using such an assumption represents, at best, a mean of the actual distribution of interionic spacings. A further possibility that should be considered is that the TM ions are grouped in clusters, as suggested by MacCrone and coworkers[94,109], in certain glass systems. The results from the present study have been examined with this possibility in view but no evidence from spectroscopic or electrical measurements for such clusters has been found. Finally, no signs of phase separation have been detected in any of the glasses; therefore all glasses are assumed to have a random distribution of TM ions.

4.5 D.C. Resistivity Measurements of Glasses

Before considering the details of the dc resistivity results it is necessary to mention some of the problems encountered in performing the resistance measurements.

Generally it was impossible to obtain time independent resistivity values for glasses or glass-ceramics with a resistance of greater than about 10^{13} Ω. Measurements of the current flowing soon after the voltage was applied were much higher than after a few minutes had passed. The reason for this is thought to be the 'anomalous current' effect arising from a slow dielectric relaxation within the glass. The anomalous current which flowed initially was 1 - 2 orders of magnitude higher than the final dc value and decreased almost exponentially with time. The time needed to establish the steady state dc value depended upon the resistivity and hence the temperature. It is likely that local movement of the current carriers, which charges the specimen, is responsible for this effect.

For the highly resistive glasses at lower temperatures (20 - 200°C) the anomalous current could take many minutes or even hours to decay, therefore time dependent readings in this region have been ignored. Failure to do this would result in a misleading change in the gradient of the log ρ/T against 1/T line, depending upon how soon the current was measured after the voltage had been applied.

For some glasses the current changed with time at higher temperatures at constant voltage. This may result from one of two mechanisms:

(a) Electrode Polarization; the current decreases with time. This can only occur for ionically conducting glasses. It is the result of ions becoming depleted at one electrode and piling up at the other, which leads to the formation of blocking layers. Generally this electrolytic effect is difficult to observe for glasses having resistivities of greater than 10^{7} Ω cm because an excessive time is required to pass sufficient charge to observe the decrease in the current.

(b) Joule heating; the current increases with time. When an appreciable current flows through the specimen, the heat generated by resistance heating can cause a temperature increase if not dissipated away quickly. The condition can become self-propagating as the resistance decreases and the current consequently increases, until the available current of the power supply is exceeded or the specimen melts.

4.5.1 Series SMH

The log ρ/T verses 1/T relationship for glasses containing between 1.0 - 12.4% MnO has been shown to be linear with correlation coefficients of greater than 0.9999. However, for glasses containing less than 1% MnO

or greater than 12.4% MnO, the points obtained on the plot were best described by two intersecting straight lines with different slopes.

The glass with the smallest concentration of MnO (SM15 0.5%) had a very high resistivity and all measurements of resistance increased with time, even at the highest temperatures of measurement. The best fit line was drawn through the two measurements made at the highest temperatures as inclusion of data obtained at lower temperatures produced a large decrease in gradient. This is a result of the anomalous current discussed above. However, because of this, the errors involved in calculating the activation energy are large. The actual value obtained of 2.04 eV is therefore subject to a larger error than is normally associated with these measurements.

The data for glasses containing MnO concentrations of greater than 12.4% (i.e. SM13, 16.4% and SM14, 20.8%) were better described by two intersecting straight lines, each fitted with a correlation coefficient of 0.99998. The temperature of the intersection was 262^{o}C for SM13 and 235^{o}C for SM14. The situation was marginal for SM12, so a single line has been fitted by ignoring the points at the highest temperature of measurement.

The series can be conveniently divided into two groups:

(a) Glasses containing up to 7% MnO, which exhibited a decrease in activation energy and an increase in intercept on the log ρ/T axis as the concentration of MnO increased.

(b) Glasses containing more than 7% MnO, which were characterized by an almost constant activation energy at temperatures higher than the intersection temperature, if present. The values were 1.17 eV for SM18 and 1.11 eV for SM12, SM13 and SM14. Ignoring any change in gradient at low temperatures for the moment, the change in resistivity in this group was entirely due to the change of the intercept, which decreased steadily with increasing MnO.

This behaviour is clearly shown by the graph in Figure 4.6. It should be noted that the figure of 7% MnO has been arbitrarily chosen at present, since the change in intercept behaviour could lie anywhere between 3 - 8% MnO with the experimental data available.

This change in the behaviour of the intercept does not seem to have a pronounced effect on the resistivity as calculated at three different temperatures (Figure 4.7). Smooth curves could be drawn through the points if an experimental error in the SM11 data is assumed. Alterna-

tively a discontinuity may be present between 6 and 9% MnO, thus recognizing the two groups above.

The effect of this difference in behaviour between the two groups is more clearly observed by plotting both log ρ at various temperatures and the activation energy against the mean separation of manganese ions. This is shown in Figure 4.8. Considering the resistivity, the data can be described by two straight lines which intersect at R spacings of between 8 - 9 Å. These values correspond to concentrations of 7% and 5% MnO respectively i.e. within the range separating the two groups.

The electron wavefunction decay constant (α) was calculated by interpreting the intercept of the log ρ/T - $1/T$ plot using the Mott equation. This too shows interesting effects (Table 3.4.1). For glasses SM15 and SM16 containing 0.5% and 1.0% MnO, α^{-1} values were large and negative. As such values are meaningless, α was set equal to zero and values of the phonon frequency were calculated from:

$$\text{Intercept} = \log \left(\left\{ \frac{k}{Ne^2R^2c(1-c)} \right\} \cdot \frac{1}{\nu_{ph}} \right) \qquad (4.7)$$

This gave values of 4×10^{15} and 2×10^{13} s^{-1} for SM15 and SM16 respectively. The former is greater than the value of 1×10^{13} s^{-1} usually accepted for this parameter but with the errors in fitting a straight line to the data this is not surprising. The latter value is in good agreement with the expected value suggesting that the tunnelling term (exp $-2\alpha R$) in the Mott equation should be neglected. Therefore a model of small polaron hopping may not be appropriate for these glasses.

For the remainder of series SMH, values of α^{-1} were of the expected magnitude and sign. However, if small polaron formalism applies, α^{-1} is expected to decrease to a value which is less than the polaron radius at a particular composition to satisfy the $\alpha^{-1} < r_p < R$ criterion and then remain less than r_p at higher TM concentrations. For series SMH, α^{-1} was less than r_p for SM18 (9.4% MnO) but then increased to above r_p with increasing MnO concentration. However, if values were calculated for SM13 and SM14 using the data from regression analysis of the low slope line (i.e. $T < T_I$), then the agreement with the above criterion was more satisfactory (Figure 4.5.1).

It is concluded, therefore, that a number of different conduction

mechanisms may be operating for glasses in series SMH depending on the composition and measuring temperature. Their precise nature will be discussed in greater detail in section 4.7.

4.5.2 Series SML

In most respects this series exhibited similar behaviour to that of SMH but with the important difference that even for the glasses with the highest MnO concentrations (equivalent to SM13 and SM14), there was no evidence of two slope behaviour of the log ρ/T - $1/T$ plot (Figure 3.2.2). For each composition a single line could be fitted to the data using linear regression analysis, again with correlation coefficients of greater than 0.9999.

The activation energy for each glass has been plotted against the MnO concentration in Figure 4.9. As for glasses in series SMH, the three most concentrated glasses had an almost constant activation energy: 1.17 eV (SM8), 1.16 eV (SM9) and 1.15 eV (SM10). These values may be compared with 1.11 eV for SM12, SM13 and SM14. However, the activation energy for SM7 was substantially higher than its counterpart in the SMH series (SM11). Figure 4.10 shows that the resistivity at 500 K decreased steadily with increasing manganese concentration.

Plots of W and log ρ_{500} against the mean separation of manganese ions, shown in Figure 4.11, are not as informative as those for series SMH because there are fewer data points. Although the activation energy starts to rise rapidly as R increases above 7 Å, the effect of this on log ρ_{500} is not so apparent.

Calculation of α^{-1} from the intercepts shows that the $\alpha^{-1} < r_p < R$ criterion is never satisfied (Figure 4.5.2). The value of α^{-1} decreased initially but then increased as the intercept became more negative while the gradient remained constant. If α was set equal to zero then the calculated phonon frequencies were 1 - 2 orders of magnitude below 1×10^{13} s^{-1} (Table 3.4.2), therefore the tunnelling term cannot be neglected completely and small polaron hopping with abnormally high values of α^{-1} may be operating.

4.5.3 Series EM

Correlation coefficients for the log ρ/T - $1/T$ plots fitted by linear regression analysis were 0.9998 or better. Two glasses (EM6 and EM7) showed evidence of a change in slope for temperatures above 450°C, possibly because of Joule heating, so this has been ignored in

subsequent calculations and regression analysis was only applied to the lower temperature part of the line.

Figure 4.9 shows that the decrease of activation energy with increasing amounts of MnO for borate glasses melted between 1050°-1100°C was identical to series SML up to about 12% MnO. Thereafter, however, the values for the borate glasses did not become constant but decreased to 1.05 eV for BM11. The resistivity at 500 K also changed in a similar way to the SML series but the resistivity of the borate glasses was always less than that of glasses in series SML with equivalent manganese concentrations. This implies that the carrier mobility is higher in the borate glasses (Figure 4.10)

The effect of the change in the mean separation of manganese ions is shown in Figure 4.11. Both W and log ρ_{500} are linear below 7.7 Å (∿9.5% MnO), but appear to show a change of slope at higher concentrations, although more data would be needed to clarify this.

Additional points have been entered on these plots representing the two glasses (BM8 and BM9) melted at lower temperatures, both of which contained higher fractions of Mn^{3+}. In both cases the activation energy was different from the glass melted at a higher temperature and the difference was too large to be accounted for by density differences, leading to a change in R. Since all the other parameters for these pairs should be constant, the activation energy would appear to depend on the redox ratio, which is not accounted for by the Mott equation. This aspect will be discussed in greater detail below.

Finally, calculation of α^{-1} for the 5% MnO glasses again gave unrealistic values, but ν_{ph} was calculated as ∿2 x 10^{13} s^{-1} when α was set equal to zero. This again suggests that the tunnelling term is not applicable to these glasses. Higher concentrations of MnO gave reasonable values of α^{-1} (Table 3.4.3) but in most cases α^{-1} was greater than r_p (Figure 4.5.3). A small polaron conduction mechanism may not therefore be applicable in the dilute glasses (BM5 and BM8).

4.5.4 Series SF

Dilute glasses SF2 and SF8, containing 0.5 and 1.0% Fe_2O_3, showed a linear log ρ/T - $1/T$ plot (Figure 3.3.4). An interesting feature of these two glasses is that SF2 had a lower resistivity than SF8 at all temperatures, which implies that iron ions may not play a significant role in the conduction process at this doping level.

The most pronounced change in gradient of the 'two slope' glasses was that shown by SF7 (2% Fe_2O_3). At temperatures below the transition temperature (T_I = 368°C) the gradient, and hence the activation energy, was slightly less than that of SF2 and SF8. For lower temperatures, the activation energy fell by 0.43 eV to a value which was typical of glasses with higher iron concentrations.

Each of the remaining glasses, with one exception, showed two slope behaviour. The transition temperatures were in the range 124° - 156°C (much less than for SF7), but did not vary systematically with iron concentration. The change in activation energy was 0.11 - 0.13 eV. The exceptions were the glasses in series SF1 and SF3 (3.5% Fe_2O_3) but it is believed that readings were not continued to low enough temperatures to observe the transition because of the high resistivity.

As for the manganese glasses, the data have been presented in two ways, by plotting activation energy and log ρ_{500} against both the iron concentration and the mean separation of iron ions. Figures 4.9 and 4.12 show the changes in activation energy, which decreased rapidly with iron concentrations up to 3.5% Fe_2O_3, which corresponds to a mean iron separation of 8 Å, and then decreased linearly with both iron concentration and R. Considering the low temperature activation energy of the two slope lines, Figure 4.12 shows that this also varied linearly with R up to at least 12.3 Å for SF7. This is surprising since the intersection temperature was quite different between SF7 and the other glasses, indicating that the mechanism responsible for the change in slope could be different. Also no change in slope could be detected for SF1.2, whereas it,could for the lower iron containing glass.

The log resistivity at 500 K also decreased steadily with increasing amounts of Fe_2O_3 above 1 - 2%. Figure 4.13 shows this behaviour compared to the manganese glass series SMH. The resistivities of the iron glasses were always less than the manganese glasses by up to three orders of magnitude. This must mean that the mobility of the carriers is greater in iron glasses as the difference in the number of carriers, because of the redox ratio, cannot account for such a large change. The log resistivity at 400 and 600 K appears to decrease linearly with R below 9 - 10 Å (Figure 4.14).

The electron wavefunction decay constant α showed similar behaviour in the iron glasses to that in series SMH. For SF2 and SF8,

calculations of α^{-1} gave unreasonable values and when the tunnelling term was neglected, the calculated values for the optical phonon frequency were 1×10^{13} and 6×10^{13} s^{-1} respectively (Table 3.4.4). For glasses containing above 2% Fe_2O_3, calculated α^{-1} values were of the same order as the small polaron radii; however, for the $\alpha^{-1} < r_p$ condition to apply, values had to be calculated from the lower temperature slope for SF7, SF4 and SF5 though not for SF1.2 or SF6. For SF4 and SF5 the decrease in intercept at approximately the same activation energy for the lower temperature slope gave rise to an increase in α^{-1}. These changes are shown in Figure 4.5.4. A small polaron conduction mechanism would appear to be operating for glasses with $\geq$3.5% Fe_2O_3.

4.5.5 Variation of Resistivity with Redox Ratio in Series SF

Figure 4.15 shows the variation of resistivity at 500 K and 600 K with the fraction of total iron present as Fe^{2+}. The individual points are the experimental data for glasses SF1 and SF3, but the lines are not the best fit lines to describe these data. Instead these lines have been calculated from the theoretical relationship of log ρ and redox ratio as predicted by the Mott equation.

For a series of glasses with identical compositions but varying redox ratio, the resistivity at a given temperature may be written as:

$$\rho = \frac{1}{c(1-c)} \rho_o \qquad (4.8)$$

where $$\rho_o = \frac{kT}{\nu_{ph} N e^2 R^2} \exp(2\alpha R) \exp\left(-\frac{W}{kT}\right) = \text{constant} \qquad (4.9)$$

provided that the activation energy does not vary with the redox ratio. If an arbitrary value of ρ_o is assumed then it can be shown that the log ρ against c plot gives a flat minimum between c = 0.3 and 0.7. Therefore glass SF3.2 with c = 0.44 was chosen to calculate a value of ρ_o characteristic of glasses SF1 and SF3; since ρ_o will be less sensitive to errors in log ρ and c for $0.3 < c < 0.7$ because of the shape of the curve. SF3.1 also had a c value of 0.44 but was not chosen because of the inhomogeneity already noted. Using this value of ρ_o the expected log ρ - c relationship has been calculated and is shown plotted in Figure 4.15. The individual points have an error band corresponding to $\pm$0.1 of the log ρ value which is probably a reasonable estimate of the reproducibility of these measurements between different glasses. It is seen that there is reasonable agreement with the

theoretical curve for all glasses except SF1.1. This indicates that the broad minimum predicted by the Mott equation is valid for these glasses. Other workers have also found a minimum at c = 0.5 for iron glasses[99].

Unfortunately only one data point exists for c < 0.1, that of SF 1.1. It was not possible, therefore, to check on the increase of resistivity below c = 0.1 which may be steeper than predicted. Finally, it is noted that SF1.2 - SF1.5 all have a lower resistivity than is expected from the analysis. This is probably a result of the slight increase in the iron concentration of the SF1 series compared to SF3 which has not been included in the calculation.

Figure 4.16 shows that there is a dependence of the activation energy on the redox ratio and the minimum in resistivity observed in Figure 4.15 is also seen for the activation energy. Discussion of this finding will be reserved for section 4.7.

Calculated values of α^{-1} are given in Tables 3.4.6 and 3.4.7. Considering the scatter in the resistivity and activation energy for these glasses α^{-1} values are surprisingly constant at 2.2 ± 0.1 Å. In all cases $\alpha^{-1} < r_p$, which is good evidence for a small polaron conduction mechanism.

4.5.6 Series SMF

The data for each glass in this series could be described by a single line using linear regression analysis. No evidence of any two slope behaviour was found and correlation coefficients were better than 0.9999. Figure 3.3.5 shows that the glasses in this series can be divided into three groups according to their behaviour:

(a) SMF1: This glass stands apart from the other glasses in this series because of its high resistivity and activation energy. The values were typical of those of the dilute manganese and iron glasses SM15 and SF2. Figure 3.3.5 shows that the resistivity of SMF1 was only slightly less than that of the undoped base glass BG2, therefore the contribution of TM ions to the conduction process is small. Optical spectroscopy revealed that Mn^{3+}, Mn^{2+} and Fe^{3+} were the likely oxidation states of the ions, but the manganese redox ratio has not been established. The small polaron hopping parameters have been calculated, assuming a range of likely c values, but α^{-1} was always negative. Calculations of phonon frequency assuming $\alpha = 0$ gave values

in the range $2 \times 10^{13} - 1 \times 10^{14}$ s^{-1} depending on the value of c assumed. Electrical properties of the other dilute mixed glasses SMF4 and SMF5 were not measured but are not expected to be different to the other dilute single TM glasses.

(b) SMF2 and 3: These were the only other glasses investigated containing nominally equivalent concentrations of manganese and iron (5:5 ratio). Again Mn^{3+}, Mn^{2+} and Fe^{3+} were the likely TM oxidation states. Any polaron formation therefore must be localised on the Mn^{2+} ion as this is the only ion in a reduced oxidation state. However, once an electric field has been applied a polaron site is surrounded by two kinds of acceptor site, Mn^{3+} and Fe^{3+}, to which it can hop. It should be possible to determine which of these is dominant in the conduction process.

Supposing initially that only hops between manganese ions are favourable; the mean separation between manganese ions expected for glasses with these compositions is recorded in Table 3.4.5. By using Figure 4.8 it is possible to interpolate the log resistivity at 400, 500 and 600 K and also the activation energy for manganese glasses with these R spacings. It is assumed that the iron ions do not interfere. These values are tabulated with the data for SMF2 and SMF3 in Table 4.1. It is immediately obvious that the activation energy is reduced by $\sim$0.2 eV from that expected for manganese only conduction and the resistivity values are also correspondingly reduced. Conduction by manganese ions alone does not seem sufficient to explain the results, and the changes are certainly too great to be explained by differences in redox ratio. Therefore it is likely that ferric ions enter the conduction process in some way.

The mean spacing of TM ions (whether Fe or Mn) is also given in Table 3.4.5. Using these values for SMF2 and SMF3 with Figure 4.8 gives values of both resistivities and activation energies which are very near to those found for the mixed glasses. This suggests that the mean TM ion spacing is the important parameter.

This is a simplistic approach, but the use of manganese conduction data can be defended in that it is basically hops between manganese ions that are of interest, since Fe^{2+} is not an energetically stable oxidation state in these glasses. The ferric ions may be thought of as providing a'bridge' between manganese donor and acceptor sites, thereby lowering the interionic spacing R. The activation energy barrier is

also reduced by such a bridge.

(c) SMF2A and SMF2B: This is a similar case to (b) above but in this case, bearing in mind the optical absorption spectroscopy results, there are two donor sites but only one acceptor site. The same arguments have been applied and the relevant data are listed in Table 4.1: compiled from Table 3.4.5 with Figures 4.12, 4.13 and 4.14. In this case iron glass data have been used since iron conduction will be dominant because Mn^{3+} is not an energetically stable oxidation state in these glasses. The two glasses will be treated separately, remembering that the total TM oxide concentration is nominally identical.

For SMF2A the resistivity and activation energy were lower than for the equivalent iron containing glass; however, the differences were less than in the manganese case above and the possibility of redox ratio changes may be important. The likely iron redox ratio was estimated from optical spectroscopy yielding a value of 18.5% for SMF2A (section 4.2.3.2). The corresponding value from which data have been taken for the single iron glass is 11%. With the information from the previous section that the c(1-c) relationship appears to be obeyed for the iron glasses, the resistivities of the single iron glass have been recalculated to that appropriate for c = 18.5% and these are shown in Table 4.1. The resistivity of the mixed glass is still lower than the equivalent glass containing iron alone, even having compensated for the differing redox ratios.

Calculation of the expected conduction parameters for $Fe^{2+} - Fe^{3+}$ conduction with mean TM separations equivalent to that in the mixed glass reveals that in practice the resistivity of the mixed glass is higher than would be predicted, although the activation energy is lower. This probably means that although $Fe^{2+} - Fe^{3+}$ conduction is predominant in this glass, there is some effect of Mn^{2+} on the conduction process, mainly in lowering the activation energy rather than increasing the number of carriers. Its role is therefore more indirect than the effect of Fe^{3+} in the mixed glasses in (b), which is probably explained in that Mn^{2+} is a donor and Fe^{3+} an acceptor.

SMF2B had the smallest proportion of manganese in the mixed glasses but again the resistivity and activation energy were lower than that expected for iron only conduction after taking the changes in redox ratio into account. However, in this case, these values were also lower than those calculated for $Fe^{2+} - Fe^{3+}$ conduction with a value of

R typical of the TM - TM interionic spacing. Therefore once again Mn^{2+} ions must be affecting the conduction process and lowering the activation energy. Further discussion of the conduction process in mixed glasses will be given in section 4.7.4.

In conclusion therefore, for each of the mixed glasses the conduction process is predominantly that of the TM ion present in two oxidation states and the observed activation energies are typical of that process (i.e. >1 eV for Mn in two redox states and ∿0.7 eV for Fe in two states). However, in each case the resistivity and activation energy are lower than that expected for conduction between the two redox states in a single TM oxide glass, even when redox ratio changes have been taken into account. The dominant parameter seems to be the mean TM spacing which means that the mobility of the carriers, rather than their number, is most affected by the presence of a second donor or acceptor site, hence the change in activation energy. A change in the number of donors or acceptors alone would not be expected to have such a great effect on the activation energy

Finally, values of α^{-1} are presented in Table 3.4.5. The results have been calculated in two ways; firstly just for the element present in two oxidation states, assuming that the second element does not interfere, and secondly for both elements together. The values of c used for these calculations have been chosen as follows:

$$\frac{Mn^{3+}}{Mn_{total}} \simeq 0.1 \text{ for SMF2 and SMF3}$$

$$\frac{Fe^{2+}}{Fe_{total}} \simeq 0.2 \text{ for SMF2A and SMF2B}$$

$$\frac{TM^{2+}}{TM_{total}} \simeq 0.5 \text{ for all glasses except SMF2B and,}$$

$$\frac{TM^{2+}}{TM_{total}} \simeq 0.4 \text{ for SMF2B}$$

In practice, the variation in α^{-1} for TM^{2+}/TM_{total} ratios between 0.3 and 0.5 was small. It may be concluded from Table 3.4.5 that the $\alpha^{-1} < r_p$ condition is satisfied for the concentrated glasses, therefore a small polaron hopping conduction mechanism is likely to be operating.

4.6 A.C. Conductivity of the Glasses

A.C. conductivity and dielectric properties have been measured for manganese glass SM13, iron glasses SF1.5, SF3.4 and SF5 and mixed glasses SMF2A and SMF3. Similar measurements have also been made on selected crystallized glasses but these results will be discussed in section 4.10 below. The total resistivity (ac + dc) at a range of frequencies has been plotted as a function of 1/T in Figures 3.5.1 - 3.5.9. The behaviour of each of the glasses was similar.

For lower temperatures in the range of measurement, the dc conductivity was always lower than the ac conductivity. The actual difference between the two values depended greatly on the measuring frequency and temperature: the lower the temperature and the higher the frequency then the greater the difference. Typically, at low temperatures, an increase in frequency from 100 Hz to 40 kHz decreased the resistivity by 1 - 2 orders of magnitude. As the temperature increased, the dc component became the greater part of the conductivity until at high enough temperatures the total conductivity and dc plots tended to join. At high temperatures the effect of an increase in frequency on the conductivity was reduced and eventually the total measured conductivity at a given frequency became equal to the dc value. It is seen from the curves in Figures 3.5.1 - 3.5.9 that the slope of the log total resistivity - 1/T curve was slightly less than the dc plot and decreased at any particular temperature as the frequency increased. Similarly at any fixed frequency, the slope decreased as the temperature decreased.

Room temperature resistivity measurements were limited and subambient measurements impossible because of the high resistivity of these glasses. It is apparent, however, that the ac conductivity at sufficiently low temperatures is tending to become temperature independent. This is most evident for the iron glasses measured down to room temperature (SF3.4 and SF5: Figures 3.5.4 and 3.5.6); however, it is expected that the manganese and mixed glasses would show the same behaviour, but the higher resistivity prevented measurements at low enough temperatures. For each of the glasses the slope of the log ρ_{tot} - 1/T curve increased steadily with increasing temperature unlike some of the crystallized glasses to be discussed below.

Values of the real and imaginary parts of the dielectric constant (ε' and ε'') have been calculated and both have been plotted against log frequency in Figures 3.7.1 - 3.7.9. Measurements were not made below 100 Hz but it is seen for most glasses, at the lowest measuring

temperatures, that ε' is almost independent of frequency and does not tend to increase rapidly in the low frequency range. It is found that ε' does increase rapidly with decreasing frequency in ionically conducting glasses. Values of ε' and ε'' were lowest for SF1.5 and SF3.4, but increased with iron content up to SF5. Values for SMF2A, in which mainly Fe^{2+} - Fe^{3+} pairs are responsible for conduction, were similar to SF5 whilst the other mixed glass SMF3, with mainly Mn^{2+} - Mn^{3+} conduction, had lower values of ε', in the same temperature range, which were similar to those of SM13.

The results for SF5 (Figure 3.7.6) showed the most interesting behaviour amongst these glasses. At 23° and 98°C the dielectric loss increased smoothly as the frequency decreased but for higher temperatures a loss peak was observed which shifted to a higher frequency as the temperature increased. Below the frequency corresponding to the loss peak, the real part of the dielectric constant was constant and can be taken as the static dielectric constant (ε_s). This result is similar to the dielectric dispersion noted by Hansen and Splann[100] in iron phosphate glasses.

The nature of the relaxation giving rise to this absorption has been discussed above (section 1.4.5.1). Two possibilities have been suggested: electron hopping between Fe^{2+} - Fe^{3+} pairs or Maxwell-Wagner-Sillars polarization because of heterogeneity within the glass, usually arising from micro-crystallization during annealing. No secondary phase could be detected in SF5 by either X-ray diffraction analysis or optical microscopy, therefore unless it is proposed that any secondary phase is below the detection limits of these techniques, the absorption peaks must be assigned to Fe^{2+} - Fe^{3+} electron (or polaron) hopping. The peaks therefore arise from a Debye-type dielectric dispersion characterized by a particular relaxation frequency and occur at a temperature at which the measuring frequency equals the relaxation frequency.

No loss peaks were observed for the other glasses studied, though in each case the magnitude of the dielectric loss increased with increasing temperature. This probably indicates that a loss peak was present at a lower frequency than measurements were made at and the frequency of the peak increased with temperature, thereby increasing the loss at measured frequencies. Similar dielectric relaxations were noted by Tsuchiya and Moriya[117,118] for phosphate glasses containing MnO and Fe_2O_3 but at much higher concentration levels (~40% TM oxide).

The loss peaks observed between 20 - 100°C were at lower frequencies for the manganese glass (log f_{max}:-3.5 to -1.5) than for the iron glass (log f_{max}:1 to 3) with the mixed glass lying inbetween (-1.5 to +0.5). The behaviour of the glasses in the present study is in general agreement with this, but the much lower concentrations prevented the actual peaks being observed. It is usually found that the smaller the dc conductivity of the glass then the lower the relaxation frequency, if the same hopping process determines both the ac and dc conductivities.

Apart from this apparent low frequency relaxation peak, the ac data for TM oxide glasses at higher frequencies is often described by the equation:

$$\sigma(\omega) = A\omega^n \qquad (4.10)$$

where n is usually a constant with values between 0.5 - 1.0. Plots of log ρ_{ac} against log frequency are shown in Figures 3.6.1 - 3.6.9 to examine this relationship.

For SM13 (Figure 3.6.1), the relationship was only obeyed over a small frequency range. Calculated values of n from linear regression analysis over the linear portions of the plots were in the range from 0.56 decreasing to 0.40 as the temperature increased. The decrease with temperature is usually observed but values of less than 0.5 have not been reported by other workers. The agreement for iron glasses SF1.5 and SF3.4 (Figures 3.6.3 and 3.6.4) was more satisfactory with n values between 0.82 - 0.58, over nearly two decades of frequency, in the temperature range 82° - 360°C. For SF5 the relationship was obeyed at 23° and 98°C with n $\sim$ 0.7 but not at higher temperatures at which the loss peaks were observed. Finally, agreement was good for the mixed glass SMF2A but with n constant between 91° - 221°C, though not so good for SMF3, which was only linear over a small frequency range with n values which were extremely temperature dependent.

The key to whether a linear relationship was found appeared to be the behaviour of the dielectric loss with frequency. For temperatures at which the loss was almost independent of frequency, log ρ_{ac} was proportional to log f with n values between 0.6 - 0.8. The more strongly dependent the loss on frequency then a linear log ρ_{ac} - log f plot was not observed over the whole frequency range and n values were outside the range above.

The ac response of these glasses may therefore be subdivided, as

proposed by Owen[69], into a low frequency loss peak having a similar activation energy to the dc conductivity, seen fully only for SF5, and secondly a power law ac conductivity at higher frequencies as a frequency independent loss is approached. The temperature dependence of the loss peaks for SF5 could only be estimated because the precise frequencies of the peaks were not known and only two data points were available. However, the activation energy calculated by applying the equation:

$$f_{max} \propto \exp(-\Delta H_{ac}/kT) \qquad (4.11)$$

was similar in magnitude to the dc activation energy.

The ac conductivity in an alternating field of frequency ω arising from the hopping of carriers between pairs of isolated centres is given by:

$$\sigma(\omega) = \frac{(\varepsilon_s - \varepsilon_\infty)\,\omega^2\tau}{1 + \omega^2\tau^2} \qquad (4.12)$$

and the dielectric loss by:

$$\varepsilon'' = \frac{(\varepsilon_s - \varepsilon_\infty)\,\omega\tau}{1 + \omega^2\tau^2} \qquad (4.12a)$$

where ε_s and ε_∞ are the static and high frequency dielectric constants and τ the relaxation time characterizing the delayed response. These equations are examples of the Debye equations and seem to apply equally well to both electronic and ionic conduction in glasses, with different equations governing τ depending if the carrier moves by phonon-assisted quantum mechanical tunnelling between sites or is thermally activated over the barrier.

In practice, both TM oxide glasses and glasses displaying ionic conduction show a broader peak in ε'' than predicted by the Debye equation. This is because sites in a glass are expected to be distributed with regard to spacing and energy, therefore the system must be characterized by a distribution of relaxation times rather than the single time applied above.

The nature of this distribution of relaxation times has received great attention. Hansen and Splann[100] suggested a Gaussian distribution for iron phosphate glasses and Mansingh et al[154,155] have also used a symmetric distribution. The latter authors have analysed the ac conductivity results of several TM phosphate glass compositions in terms of two components:

$$\sigma(\omega)_{total} = \sigma_1(\omega) + \sigma_2(\omega)$$

where $\sigma_1(\omega)$ is dominant at low temperatures and is described in terms of a Debye type process involving a distribution of relaxation times and $\sigma_2(\omega)$, dominant at higher temperatures, is of the form $\sigma \sim \omega^n$ and can be described in terms of hopping conduction in a disordered matrix. The physical interpretation of these mechanisms is that $\sigma_1(\omega)$ at low temperatures results from electron hopping near the Fermi level, whilst $\sigma_2(\omega)$ is due to carriers hopping near the mobility edge and hence is temperature dependent.

Other authors (see Owen[69] for detailed references) have put forward different ideas to explain the broad loss peaks observed for glasses, which do not involve a distribution of relaxation times because of the problem of physically interpreting such large distributions often spanning many decades of frequency.

Mott and Davis[67] and other authors, especially Pollak[156] have interpreted the power law ac conductivity in terms of hopping between pairs of isolated sites situated close to the Fermi level, with a random distribution of separation distances R. They show that for phonon-assisted quantum mechanical tunnelling:

$$\sigma(\omega) = Ce^2\{N(E_F)\}^2 \, kT \, \alpha^{-5} \, \omega \, (\ln \nu_{ph}/\omega)^4 \qquad (4.13)$$

where C is a constant = $\pi/3$ (Mott and Davis) or $\pi^3/96$ (Pollak)

It can be shown that $\sigma \propto \omega^{0.8}$ with this model, but n values >0.8 or that decrease with increasing temperature cannot be explained. Some authors[87,157] have used this equation to estimate the density of states at the Fermi level for TM oxide glasses whilst Mansingh[124] has used the same equation to calculate the total density of states active in ac conductivity.

This equation has been evaluated for iron glasses SF3.4 and SF5 together with mixed glass SMF2A, using values of ac conductivity calculated at 1×10^4 Hz, α^{-1} values from the dc conductivity calculations and assuming $\nu_o = 10^{13}$ s^{-1}. The values were:

3.1×10^{19} cm^{-3} eV^{-1} for SF3.4 at 355 K

2.0×10^{20} cm^{-3} eV^{-1} for SF5 at 371 K and,

6.7×10^{19} cm^{-3} eV^{-1} for SMF2A at 364K

It is possible to use this information to estimate the carrier

concentration:

$$N_{eff} = N(E) \cdot kT$$

At 300 K calculated values were as follows. In each case the carrier density calculated from cN (i.e. the number of Fe^{2+} ions determined by chemical analysis) is included in parenthesis for comparison:

SF3.4 8.0×10^{17} cm^{-3} (4×10^{20} cm^{-3})

SF5 5.0×10^{18} cm^{-3} (6×10^{20} cm^{-3})

SMF2A 2.0×10^{18} cm^{-3} (7×10^{20} cm^{-3})

In each case it is clearly seen that the above equation yields an effective carrier concentration which is 2 - 3 orders of magnitude too small. Calculated carrier concentrations such as these could indicate that only a small proportion of sites are involved in the ac conduction process but it is more likely that the above equation is not applicable to polaronic semiconductors in this temperature range (300 - 400 K). In terms of the two component behaviour of the vanadates noted by Mansingh[154] it could be said that in the present study only the high temperature component is measured corresponding to conduction at the band edge. The temperature dependent loss peaks may also result from this process.

Finally, the similarity between the ac response of ionic and polaronic oxide glasses has suggested to some workers[69] that some kind of common fine-scale heterogeneity in structure is responsible for this 'universal response' especially the low frequency dielectric loss peak. An alternative suggestion is that the glass network rather than the mobile carriers may give part of the response.

4.7 Possible Conduction Mechanisms

4.7.1 Glasses Containing Small Concentrations of TM Ions

The conductivity of the glasses containing less than 2% TM oxide (SM15, SM16, SM17, SF2, SF8, SF7 and SMF1) was small and appeared to be insensitive to both the type of TM element and the amount present. It was therefore decided to compare the resistivity of these glasses with that of the base glass of this series (BG2) which had the following molar composition: 41.2% CaO-9.1% Al_2O_3-49.7% SiO_2.

The resistance measurements of BG2 did not show any obvious increase with time which would be indicative of an ionic conduction

mechanism. However, the high resistivity of this glass probably makes polarization, due to electrolysis, unobservable because of the long periods required to pass sufficient current. The log ρ/T - $1/T$ plot has been included on Figure 3.3.4 to compare with the iron containing glasses. It is seen that the base glass has only a marginally higher resistivity than the dilute iron glasses and also that SF8 had a higher resistivity than SF2 even though it had a higher iron content. A plot of the data for BG2 on the manganese SMH plot would show that the resistivity values lie between those of the 0.5% and 1.0% glasses. By this it must be inferred that conduction in these glasses, except SF7 at low temperatures, is not due to electron or polaron hopping between TM ions but arises from the same mechanism responsible for conduction in the calcium aluminosilicate base glass. The similarity of the activation energy of the dilute TM glasses (1.4 - 1.6 eV) with that of the base glass (1.66 eV) also leads to this conclusion. Figure 3.3.5 shows that the mixed glass SMF1 is also behaving in a similar manner.

A theory of this sort was also suggested by the attempt to apply the Mott equation to these results. The non-adiabatic polaron equation was inappropriate and reasonable values of the optical phonon frequency were calculated by ignoring the tunnelling term. Clearly any notion of adiabatic hopping at these concentration levels is nonsensical and the data are best described by the classical Arrhenius relationship usually applied to ionic conduction in glasses. In fact the equation due to Stevels given above (1.4.2) is similar mathematically to the adiabatic hopping equation and would appear to apply to these glasses.

The nature of the conduction process operating in alkali free calcium aluminosilicate glasses has still not been properly elucidated. The obvious possibility is that Ca^{2+} ions are responsible; Schwartz and MacKenzie[158] observed an activation energy of 1.45 eV in a $40CaO$-$60SiO_2$ glass and suggested that Ca^{2+} ions were the current carriers. Terai and Ohkawa[159], however, measured the self-diffusion coefficients of Ca^{2+} in a calcium aluminosilicate glass with a similar composition to that in the present study and found a diffusion activation energy of 2.6 eV, which seems to suggest that Ca^{2+} is not responsible. Owen[160] has concluded that oxygen anions are the carriers in calcium aluminoborate (CABAL) glasses though this has been disputed by Hagel and MacKenzie[161] even though their values for dc activation energy

and oxygen diffusivity activation energy were very similar, indicating a common mechanism. The latter authors also included a slag glass with composition $45CaO-13Al_2O_3-42SiO_2$ in their study which had a similar activation energy for electrical conduction (1.59 eV) to the CABAL glasses. The oxygen diffusivity, however, had an activation energy which was much higher (2.6 eV) indicating that oxygen diffusion was not responsible for electrical conduction. This has also been confirmed by the work of Terai and Ohkawa[159] mentioned previously, who found that the self-diffusion coefficients of both calcium and oxygen anions were similar in the solid slag glass; therefore it was inferred that oxygen ion conduction was as unlikely as that due to calcium ions. Owen[162] has also suggested that a mechanism other than oxygen ion conduction must be operating in calcium aluminosilicate glasses.

Considering the remaining ions in these glasses it seems quite impossible for either Al^{3+} or Si^{4+} ions to migrate and therefore conduction must result from impurity ions introduced unintentionally into the glass. Mobile alkali ions from the batch materials are a possibility even though care was taken to use pure materials. Alternatively, hydroxyl ions or protonic conduction produced by the dissociation of water may be responsible. There is no evidence from the present study to indicate which, if any, is most likely.

The important conclusion drawn from the behaviour of these dilute TM glasses is that the TM ions have very little influence on the conduction mechanism at such low concentrations. This is not surprising since mean TM interionic distances are greater than than 12 Å in these glasses which probably makes polaron or electron hopping impossible. Some kind of impurity is probably responsible for the conductivity.

The dramatic change in slope of SF7 (1% Fe_2O_3) at low temperatures may suggest, however, that electronic processes cannot be ruled out completely, particularly at temperatures for which insufficient thermal energy is available for ionic movement. The activation energy determined for this glass (0.94 eV) is certainly within the range observed for polaronic conduction in TM oxide glasses, though it is high for an iron glass. The surprising fact that the activation energy of the low slope portion of the plot varies linearly with interionic separation up to 12 Å has already been noted, though the satisfaction of the $\alpha^{-1} < r_p < R$ criterion is perhaps fortuitous. This probably arises because the intercept on the log ρ/T - $1/T$ is high because of the high

resistivity. The data, however, would seem to clearly indicate that a classical model of polaron hopping is operating at low temperatures until it becomes masked by ionic effects at higher temperatures.

Few other authors have investigated conduction in iron glasses with such low concentrations and the present data are at variance with most of that published. Hansen[99] found an activation energy of 1.6 eV over an equivalent temperature range for a 5% FeO glass which was the same as his base glass. Similarly, Ardelean[108] reported a value of 1.21 eV for a $2Fe_2O_3$-$98(3B_2O_3.PbO)$ glass with no two slope behaviour. Anderson and MacCrone (109) noted that electronic conduction was observed in lead silicate glasses containing greater than 1.5% Fe_2O_3, but as a result of conduction along chains of iron ions rather than random hopping. The only work to which this study is comparable is that of Bandyopadhyay et al[98] who measured an activation energy of 0.97 eV for a $5Fe_2O_3$-BaO-B_2O_3 glass. No two slope behaviour was noted however.

The behaviour of the equivalent manganese glass SM17 was similar in some ways since although the resistivity was comparable to that of SM16, the activation energy was reduced by 0.23 eV. However, an activation energy of 1.4 eV is probably much too high for electronic conduction. Therefore although the conduction mechanism may be different to SM15 and SM16 it is unlikely to be the result of electronic conduction and a basically ionic mechanism is proposed.

4.7.2 Manganese glasses

4.7.2.1 Series SMH

The discussion in section 4.5.1 divided the manganese glasses in this series into two groups depending on the manganese concentration. The difference between them is most clearly seen by plotting log ρ and W against R (Figure 4.8). It is obvious that SM11 is intermediate in behaviour between the dilute glasses discussed in the previous section and those with higher MnO concentrations. The latter group was characterized by log ρ decreasing steeply and linearly with decreasing R. This variation with R is strong evidence for an electronic or polaronic conduction mechanism, since the decrease of three orders of magnitude in ρ cannot be explained by only a five-fold increase in the number of manganese ions. Hence it is the increase in the mobility of the carriers, rather than their number, which is responsible for the increase in conductivity. It would appear that R has a dominant effect on the mobility.

The behaviour of SM11 may be intermediate with regard to its resistivity but the decrease in activation energy compared with the dilute glasses indicates that another conduction mechanism is operating, possibly electronic. Electronic or polaronic hopping would therefore seem to dominate below mean manganese ion spacings of ~8 Å with log $\rho \propto R$. Such a cut-off is not significant from any structural viewpoint because the density changes smoothly with increasing MnO, hence there is no evidence for a change in structure at this concentration which might heighten the mobility. The value of 8 Å probably reflects the distance at which electron hops between manganese ions become unfavourable. Any clustering of Mn ions in the glass will reduce the effective value of R within the cluster and would be expected to permit electronic conductivity in glasses with apparent mean R spacings of >8 Å. Such a situation may be occurring in SM11. Alternatively, when the ions are too far apart for direct hopping, then indirect hopping via an excited state (e.g. the 4s conduction band) may take place[75], which will have a higher activation energy.

Values of α^{-1} seem to support a polaron hopping mechanism for SM18, SM12 and SM13 (low slope) since the condition $\alpha^{-1} < r_p < R$ was satisfied. Calculated values of α^{-1} were in the range 2 - 3 Å which is only slightly higher than the range of 1 - 2 Å expected from small polaron theory. The agreement is therefore good, considering the relatively low concentration of MnO in these glasses. The fact that this condition was not satisfied for SM14 (low or high slope) does not necessarily mean that the small polaron model is not applicable, since it is due to a high value of α^{-1} as a result of the high activation energy leading to a high (negative) intercept. It is not expected that α^{-1} should increase with the manganese concentration as was observed (Figure 4.5.1). For SM11, however, $\alpha^{-1} > r_p$ gives a good indication that the small polaron mechanism may not be operating.

Bandyopadhyay et al[87] have argued that high values of α^{-1} observed for barium borate glasses containing < 20% V_2O_5 might be explained by a non-random distribution of vanadium ions. The effective R is therefore altered and as α^{-1} is sensitive to the value of R assumed, high values of α^{-1} calculated using the mean R might not contradict the theory of polaron conduction. Such an explanation would seem reasonable to explain their results for which $\alpha^{-1} > r_p$ for glasses containing up to 20% V_2O_5 (corresponding to $R \geq 5.5$ Å). In the present case, however, high α^{-1} values were only found for R > 8 Å where the

ions were probably far enough apart so that polaron hopping would be expected to become difficult. The only exception was SM14 which is a result of the high activation energy.

The activation energies of these glasses showed three main features:

(a) The most concentrated glasses in series SMH (SM13 and SM14), though not in series SML or EM, exhibited two slope behaviour.

(b) Values of W derived from the high slope portion of the line for SM13 and SM14, along with that for SM12, were almost constant. Consequently the change in resistivity between these glasses was almost entirely due to changes in the pre-exponential factor. Usually both have an effect in TM oxide glasses.

(c) The values of W for all the manganese glasses were greater than the range usually found for electronic conduction in TM oxide glasses containing Ti, Fe and V ions.

Isard[163] has discussed the variation of W with N (and hence R) and shown that W_H should rise with increasing R to an asymptotic value at $R = \infty$. For vanadium glasses with only one other oxide, the variation of W_H with R was as predicted. However, for glasses containing a network modifier, the increase in W was much steeper. Iron glasses conversely, did not show this pronounced effect of network modifier.

For the manganese glasses a description of the relationship between W and R is affected by the two slope behaviour. Such behaviour at high temperatures has only previously been noted for certain iron glasses as discussed in section 1.4.5.1, although most glasses show the continuous decrease of activation energy expected at low temperatures as multi-phonon processes are frozen out. Of the possibilities advanced to explain this effect in iron glasses, that involving a difference in co-ordination of the ions involved in the conduction process in different temperature ranges would seem the most attractive; only ions in identical coordinations can transfer electrons at lower temperatures, whilst at higher temperatures, when more thermal energy is available, electron transfer between ions in different coordinations is possible. This introduces an additional term ΔU into the activation energy. Ardelean[108] used this concept to explain a difference of 0.4 eV between high and low slope portions of his iron glasses. However, Isard[163] has argued that because of the high activation energy of the high slope line, together with the fact that satisfactory values of α^{-1} could only be calculated from the low slope line, polaron hopping may

not be operating at high temperatures.

In the present study, the similarity of the high slope activation energy of SM13 and SM14 with the activation energy of SM12 for which polaron conduction is thought responsible, probably indicates that the same mechanism is operating. This is in spite of the fact that $\alpha^{-1} > r_p$ because of the value of the intercept with high W. The difference in activation energy between the two slopes ($\sim$0.1 eV) is much smaller than that noted by Ardelean[108] which also gives support to the idea that the conduction process is basically the same in both ranges.

Ardelean[108] also found that the high slope portion was best described by the equation for adiabatic hopping. The high values of α^{-1} mean that exp $(-2\alpha R)$ tends to unity and calculations for SM13 and SM14 with $\alpha = 0$ yield values for ν_{ph} of 3×10^{11} and 1×10^{12} s^{-1} respectively in the high slope portion. It is tempting to interpret this in terms of adiabatic hopping in these glasses at high temperatures with non-adiabatic hopping at lower temperatures, however, adiabatic hopping is not expected for $R > 5$ Å. Also there seems no theoretical evidence for mixed adiabatic/non-adiabatic mechanisms.

The reason for the two slope behaviour cannot be stated conclusively with the available data. Conduction in different phases above and below T_I does not seem likely since no evidence of any second phase could be detected, unless the scale of separation was too fine to be observed with the techniques used. A more attractive hypothesis involves coordination differences. Conduction has been assumed to result from polaron hopping between tetrahedral Mn^{2+} ions and octahedral Mn^{3+} ions and therefore incorporates a change in coordination, which could explain the high activation energy. Other coordinations of Mn^{3+} are very unlikely because of the large octahedral site preference energy for a d^4 ion. Also the absorptivities at the Mn^{3+} peak were consistent with all of the Mn^{3+} in SM13 and SM14 present in octahedral coordination. However, octahedral coordination of Mn^{2+} is more likely as there is no LFSE for a d^5 ion. Therefore some octahedral Mn^{2+} may be present in these glasses which would allow polaron hopping between ions which are both in similar environments. This would occur at lower temperatures with a reduction in activation energy. The coordination of the Mn^{2+} could not be established by the techniques used in the present study, therefore a more detailed spectroscopic analysis would be needed to substantiate this hypothesis. The

possibility of different structural arrangements around different manganese ions with different hopping probabilities will also affect the calculation of α^{-1} and might explain the high values of α^{-1} for SM13 and SM14 high slope lines.

It is interesting to note that glasses in series SML did not show two slope behaviour even at the highest MnO concentration and activation energies were a little higher (by 0.04 - 0.06 eV) than equivalent glasses in series SMH (high slope portion). Therefore any change in coordination does not seem to occur in these glasses possibly because of the different base glass composition or redox ratio. The difference in activation energy between the two series may be explained by redox ratio effects since the concentration of Mn^{3+} in series SML was always less than in SMH.

Returning to the variation of W with N and R, the almost constant activation energy at high MnO concentrations is contrary to theoretical predictions. Using equation 1.4.15 and following Isard's[163] argument by ignoring the contribution of the electrostatic disorder energy W_D then:

$$W = W_H = \frac{e^2}{16\pi\varepsilon_o} \left(\frac{1}{\varepsilon_\infty} - \frac{1}{\varepsilon_s}\right) \left(\frac{1}{r} - \frac{1}{R}\right) \qquad (4.14)$$

It has been customary to derive ε_∞ and ε_s from electrical measurements but this usually gives W_H values which are too small. Therefore Isard[163] has suggested that it is more appropriate to regard ε_∞ and ε_s as limiting values at frequencies above and below the optical phonon frequency of 10^{13} s^{-1}; ε_∞ is therefore taken as the square of the optical refractive index and ε_s from high frequency electrical measurements. Assuming the field strengths of the TM ions are similar to the other cations in the glass, then ε_∞ and ε_s should be independent of N and c and equation 4.14 becomes:

$$W = A \left(\frac{1}{r} - \frac{1}{R}\right) \qquad (4.15)$$

where $A = e^2/(16\pi\varepsilon_o\varepsilon_p)$

which is a constant for a particular system

In principle, the value of r could be equated with the polaron radius derived from Bogomolov's equation[80], therefore:

$$W = \frac{A}{R}\left(\frac{2}{(\pi/6)^{1/3}} - 1\right) \qquad (4.16)$$

but this requires that W is inversely proportional to R which is not found in practice. Isard[163] has therefore suggested that r should be taken as a constant and hence the W against R curve as described above was derived. A constant value of r does seem physically realistic since r defines the volume surrounding a TM ion within which electronic polarization occurs, which should be constant for a given glass system.

Equation 4.15 may therefore be written:

$$W \simeq (\text{const} - \frac{1}{R}) \qquad (4.17)$$

where the constant = 1/r and assuming $\varepsilon_\infty = 2.5$, $\varepsilon_s = 8$. The value of W is in eV and R and r in Å.

Such an equation does not describe the behaviour of series SMH but provides an excellent fit for SM8, SM9 and SM10 in the SML series, yielding r = 0.75 Å. Series EM may be described with r ≃ 0.78 Å but the fit is not as good as for SML. These values of r seem rather small but it should be remembered that the analysis is relatively unsophisticated; the total activation energy has been used instead of W_H, though W_D and ΔU could be appreciable for manganese glasses which would increase the value of r. Also, typical values have been used for ε_∞ and ε_s which will be slightly different for these particular compositions.

The anomalous behaviour of series SMH may simply be the result of experimental error which masks the slow decrease of W with R. The alternative explanation is that r increases slowly with R according to the expression:

$$r = (A' + \frac{1}{R})^{-1} \qquad (4.18)$$

where A' = W/A is a constant for glasses with constant W.

In practice the increase in r would be small if this equation applies; r changes from 0.84 to 0.88 Å as R increases from 5.4 Å to 7.1 Å with A' ≃ 1. Such a change also seems physically acceptable, although the difference between SMH and SML would be a problem if this explanation were accepted.

The high activation energy found for these glasses is in common

with other studies of phosphate and silicate glasses containing manganese, even with manganese present in high proportions. All values quoted are above 1 eV. This seems to be a general feature of TM oxide glasses in which the lower oxidation state ion, usually TM^{2+}, is predominant. Other examples include cobalt and nickel glasses which also have high activation energies (>1.2 eV) and very low room temperature conductivities ($<10^{-16}\ \Omega^{-1}\ cm^{-1}$). In these cases the conduction is controlled by vacant polaron sites and the conduction process can be thought of as the movement of positive polaron holes based on the oxidised TM ions.

No satisfactory explanation of these high activation energies has yet been put forward. Murawski[95] suggested that it is the result of an absence of higher valence states, however, this cannot be the case in the present study since proportions of up to 25% of the oxidised ion were observed. It may be true for Co and Ni glasses though since Co^{3+} and Ni^{3+} are very rarely found in glass systems. Therefore the reason for the high activation energy of manganese glasses may be different.

One assumption often made when attempting to explain such large values of W is that a structural differences term ΔU forms a significant part of the activation energy. An estimate of ΔU requires a knowledge of both W_H and W_D. In principle W_D can be calculated from the Miller-Abrahams equation (1.4.16), in the absence of low temperature conductivity data, taking ε_s as the limiting low frequency dielectric constant from ac electrical measurements. For SM13, ε' at the lowest frequency of measurement was 17 hence a value of 0.04 eV is calculated for W_D. Such a value is reasonable for a TM oxide glass but probably represents an upper value since ε_s estimated from readings at ∿500 Hz is probably low. The disorder energy is therefore a minor part of the total dc activation energy. The hopping energy is usually estimated from the most concentrated glass of a series with TM oxide levels of over 20%, since the magnitude of W_D or ΔU is expected to be small for such a glass. This approach may not be applicable for these manganese glasses since W did not fall below 1 eV which seems too high for W_H. This means therefore that either the most concentrated glass has an appreciable ΔU component or W_H is uncommonly high for manganese glasses. This latter explanation is favoured if the assignment of the change in activation energy between the two slopes in SM13 and SM14 to a ΔU term is correct. This gives $\Delta U \sim 0.1$ eV and hence $W_H \sim 0.9$ for the most

concentrated glasses.

Finally, it is suggested that such a high value of W_H may be realistic. From the analysis of W_H outlined above it is clear that as r increases, the value of W_H decreases. Therefore the smaller the 'volume' that the polaron is spread over, the higher the activation energy for conduction. The value of r calculated above was 0.8 - 1.0 Å which is smaller than values calculated for Fe, V and Ti oxide glasses. In the latter glasses r is in the range 1 - 2 Å and hence the polaron is less 'localized'. This is a feature of the lower hopping energy in these glasses. It is difficult to speculate why Mn and Fe, though neighbours in the periodic table, should behave so differently but the answer may lie not with the preponderance of the reduced state in manganese glasses but rather the electronic configuration of the redox states. For V, Ti, W and Mo, all of which have activation energies of typically less than 0.8 eV in glass when present in appreciable concentrations, the oxidised state has a d^0 electronic configuration whilst the reduced state is d^1. Similarly for iron the oxidised state is d^5 and the reduced state d^6. Generally speaking, the d^0 or d^5 configurations would be expected to be more stable since the 5 d orbitals are either empty or half full. The polaron therefore resides on a d^1 or d^6 ion on which the extra electron is not so strongly bonded and would be expected to move more easily in an electric field. Contrast this with manganese glasses for which the polaron resides on the 'stable' d^5 state. It would therefore be expected that the 'extra' electron which forms part of the d^5 configuration would be more strongly held than for a d^1 or d^6 state and hence the loss of an electron through polaron motion to form a less stable d^4 would be more difficult. This may explain the higher polaron binding energy and hence hopping energy of manganese glasses. If such a theory is correct then the discrepancy between r_p calculated from Bogomolov's equation and r calculated from the activation energy must be explained. A similar discrepancy was also found for manganese glasses by Sayer and Mansingh[92] who suggested that Bogomolov's equation might not be applicable because of a large dispersion in the phonon spectrum. Also it is difficult to see how low enough values of α^{-1} could be calculated to satisfy the $\alpha^{-1} < r_p$ criterion bearing in mind the high value of the gradient of the log ρ/T - $1/T$ line which leads to a low value of log ρ_o. Polaron theory requires values of α^{-1} typically in the range 1 - 2 Å but it could be that higher values are acceptable when the activation energy is high.

4.7.2.2 Series SML

Much of the behaviour of glasses in series SML has already been discussed as it is similar to series SMH (high slope). The high, almost constant, activation energy led to a sharply decreasing intercept at $1/T = 0$ from which calculated α^{-1} values increased with increasing MnO. The $\alpha^{-1} < r_p$ condition was never satisfied although $\alpha^{-1} \simeq r_p$ for SM8 (Figure 4.5.2). In view of the similarity of the behaviour of SM8, SM9 and SM10 with their counterparts in series SMH, it is believed that the conduction mechanism is basically by polaron hopping although with abnormally high values of α^{-1}. However, the high activation energy and resistivity of SM7 probably indicate that polaron conduction is not operating because of the large separation of Mn ions. The suggestion, as for glasses in series SMH, that high α^{-1} values are indicative of adiabatic hopping may be ruled out on the grounds that R in these glasses is too high to observe this.

The variation of ρ and W with R (Figure 4.11) is as expected. Log ρ decreases almost linearly with R for manganese spacings below 7 Å and the activation energy changes slowly with R as predicted by the analysis outlined above. The increase in W for $R > 7$ Å is a result of a change in the conduction process and eventually ionic processes will dominate.

4.7.2.3 Series BM

The three glasses containing 5% MnO (BM5, BM7 and BM8) behaved like the dilute manganese silicate glasses SM15 and SM16 discussed above. Activation energies were very high (1.62 - 1.69 eV) and a simple Arrhenius relationship was more appropriate to describe the data than the non-adiabatic polaron hopping equation. An ionic conduction mechanism was therefore suspected. The resistivity of the base glass of this series was not measured but Gough et al[164] have investigated a similar glass with composition $37BaO\text{-}3Al_2O_3\text{-}60B_2O_3$. The activation energy of a log ρ - $1/T$ plot for that glass was 1.69 eV compared to 1.62 eV for a similar plot of BM5, suggesting that the conduction mechanism is the same for both. Gough et al[164] suggested conduction by oxygen ion migration, since the activation energy decreased as the proportion of non-bridging oxygen ions increased for a range of alkaline earth aluminoborate glasses and was not dependent on the type of cation. Residual hydroxyl ions were also thought to affect the conductivity.

For the remainder of the borate glasses a polaronic conduction mechanism is expected even though the $\alpha^{-1} < r_p$ condition was not obeyed, with the single exception of BM9. Values of α^{-1} did not rise as high as those for series SML because the activation energy decreased as the resistivity decreased, hence the intercept behaved differently to SML; α^{-1} values were only a little greater than r_p calculated using Bogomolov's equation (Figure 4.5.3).

One unexpected result in this series was the dependence of the activation energy on the redox ratio. The analysis of the relationship between W and R may be extended to include the effect of c as follows. For $c > \frac{1}{2}$, R will be determined by half the mean separation of the oxidised TM ions, which, if they are uniformly distributed, leads to: (163)

$$R = \frac{\frac{1}{2}}{\sqrt[3]{(1-c)N}} = R_o / (2(1-c)^{1/3}) \qquad (4.19)$$

where R_o is the mean TM ion spacing. The activation energy may therefore be written:

$$W_H \simeq \left(\frac{1}{r} - \frac{2(1-c)^{1/3}}{R_o} \right) \qquad (4.20)$$

Values for BM6 and BM9 substituted into this equation did not yield consistent values for r, hence the change in W_H is too great to be explained simply by changes in c and R. This is difficult to understand remembering the close similarity of these glasses and may reflect experimental errors in the data rather than any difference in structure.

4.7.2.4 Effect of Base Glass Composition

Comparison of these three glass series can be used to gain information on the effect of base glass composition on the conductivity of a given TM ion. A comparison of Figure 4.7 with 4.10 reveals that the conductivity was highest for a given concentration of MnO in series SMH and lowest in series SML, with borate glasses showing intermediate behaviour. The difference between SMH and SML glasses was over an order of magnitude for MnO concentrations less than 15% which is too high to be the result solely of differences in redox ratio. Therefore it is the different mobility of the carriers in these silicate glasses rather than the small difference in carrier concentration that is responsible for the change in conductivity. Equation 1.4.26 shows that R and W are mainly responsible for altering the mobility, whilst changes in the optical phonon frequency and α^{-1} will have only a minor

effect for glasses with similar compositions. A comparison of Figures 4.8 and 4.11 shows that the difference in mobility between SML and SMH is mainly due to changes in activation energy since the R spacings are similar because the densities are nearly equal. Conversely, R has a major effect in determining differences between series SMH and BM, since when the resistivity is plotted against R, series BM lies below SMH because of the difference in density. Finally, the effect of base glass on the activation energy is shown in Figure 4.9. The common curve for SML and BM for MnO concentrations of less than 12% is surprising considering the different structures of these glasses but Figure 4.11 shows that for a given R spacing borate glasses have a lower activation energy than glasses in series SML. SMH glasses always had a lower activation energy than those in SML which cannot be explained simply in terms of R and c, and the difference in behaviour of the borate glasses is clearly seen.

The effect of base glass composition on TM oxide glasses has not received a great amount of attention. Munakata[110] investigated the effect of the network modifier ion on the conductivity of V_2O_5 glasses and explained differences in terms of the ionic field strength of the modifier ion. Kennedy and MacKenzie[111] studied the effect of the network former also on V_2O_5 glasses and concluded that it too had a real effect. They found that changes arose from differences in carrier mobility rather than concentration but could not explain their findings in detail.

The present study has shown that the base glass will affect the conductivity by varying a number of parameters in the equations describing small polaron hopping conduction. For different glasses with constant TM oxide concentration the conductivity is first affected by changes in redox ratio since this alters the number of carriers. Changes in carrier mobility are brought about through the density, which affects R, and also the activation energy. The activation energy itself comprises several components (W_H, W_D and possibly ΔU); W_H will depend on R and c as described above whilst any changes in the structure of the glass would be expected to alter W_D and ΔU. W_H will also be affected by changes in ε_∞ and, to a lesser extent ε_s, both of which depend on the polarizability of the oxygen ions and of the oxygen-cation bonds. A complete description of the effect of the base glass is therefore very complicated and requires detailed knowledge of the glass structure, TM ionic environment and bonding, as well as macroscopic properties.

4.7.3 Iron Glasses

The iron glasses could be divided into two groups in a similar way to the manganese glasses; those with low iron concentrations discussed above and those with higher concentrations for which the decrease in log ρ with R was linear. For the latter group, with Fe_2O_3 concentrations of greater than 3.5%, a non-adiabatic small polaron hopping conduction model is thought appropriate since the data were described by the Mott equation, although some modification is necessary to account for the two slope behaviour.

Polaronic conduction seems to occur at higher temperatures for R spacings of less than 9 Å, whilst at lower temperatures it seems to operate up to R spacings of 12 Å (for SF7). The former value may be compared to 8 Å found for manganese glasses. Once again this probably signifies the distance above which direct polaron hops become unfavourable. At lower temperatures the longer hops may be accomplished indirectly, possibly via the band edge, although further evidence, such as thermopower measurements, would be needed to verify this.

Support for a classical form of small polaron hopping is given by the behaviour of the resistivity with the redox ratio. This showed a broad minimum apparently centred on c = 0.5 as predicted by the Mott equation and found by other workers on iron glasses[99]. Unfortunately it was not possible to melt glasses in air to produce c > 0.5 or < 0.09 therefore only a portion of the curve could be studied.

Further support for small polaron conduction was given by the magnitude and behaviour of α^{-1}. Values derived from the low slope lines for all the glasses showing polaronic conduction were in the range 1 - 3 Å and in each case were less than r_p calculated using Bogomolov's equation.

As for the manganese glasses the major feature of the dc resistivity results requiring explanation was the two slope behaviour. The difference in activation energy of 0.12 eV between the slopes was less than that observed by Ardelean[108] although about the same as that found by Hansen[99]. Ardelean[108] noted that both Fe^{2+} and Fe^{3+} were in octahedral and tetrahedral sites in his glasses and explained the change in slope in terms of these different coordinations. For $T > T_I$ the data were better described by an adiabatic hopping equation.

Once again it is argued for the present glasses that the similarity

of the high slope activation energy with those of SF1 and SF3 glasses, for which small polaron conduction has been shown to be operating, means that the mechanism is the same. This is in spite of the fact that α^{-1} values for this portion were $\sim$4 Å and hence greater than r_p. The activation energy was, however, $\leq$ 0.8 eV which is reasonable for electronic conduction. There is no evidence of an adiabatic mechanism for $T > T_I$, since calculations of ν_{ph} with $\alpha = 0$ gave values of 5×10^{11} s^{-1} which is lower than that usually accepted. Also R was always greater than 5 Å and adiabatic hopping is only expected at smaller distances.

The difference in activation energy, therefore, may be equal to a ΔU term required to equalise centres with different coordinations before hopping can occur at $T > T_I$, whilst for $T < T_I$ for the most concentrated glasses, conduction takes place between ions in similar environments. Optical absorption spectroscopy of the iron glasses revealed that Fe^{2+} was present only in octahedral coordination. Fe^{3+} was thought to be in mainly tetrahedral coordination though in this case octahedral coordination is possible and could not be ruled out. It is therefore suggested that Fe^{3+} is present in octahedral sites for higher concentrations of Fe_2O_3 thus hopping between identical or different coordinations is possible depending on the temperature range. The different structural arrangements might lead to difficulties in calculating α^{-1} using the Mott equation which could explain the high values for the high slope lines.

It is possible to separate the total activation energy of SF1.5, SF3.4 and SF5 into the separate contributions since dielectric constants are available from the ac conductivity measurements. The disorder energy may be estimated from the Miller-Abrahams equation (1.4.16) taking a value of 19 for the static dielectric constant measured at 200 Hz for SF5. This gives $W_D \sim 0.04$ eV which seems reasonable since W_D is expected to be small for iron glasses. Assuming that there is no ΔU contribution to the lower temperature slope then W_H $(=W-\frac{1}{2}W_D) = 0.587$ eV. This compares with values determined by other workers for a similar R spacing on widely differing glass systems.

Austin[75] has argued that only a small part of the activation energy of this magnitude can be due to hopping since optical data on ferrites indicated that W_H for $Fe^{2+} - Fe^{3+}$ transport was $\leq$ 0.2 eV. The difference between this and the activation energy of an iron

phosphate glass was suggested to be accounted for by a ΔU term of the order of 0.5 eV, which is much higher than the value quoted above. It is therefore pertinent to enquire if a value of 0.6 eV for the hopping energy is realistic.

Using equation 4.15 and putting $\varepsilon_p \simeq \varepsilon_\infty = n^2$ with the optical refractive index n = 1.53, gave a value of 1.8 Å for r which is smaller than that calculated from Bogomolov's equation (2.3 Å). Alternatively, using this latter value to estimate W_H from the same equation gave $W \sim 0.4$ eV which is nearer Austin's estimate. A value of 1.8 Å for r, although subject to some error because the value of ε_∞ is uncertain and ε_s has been ignored, is similar to that found by Sayer and Mansingh [92] for an iron phosphate glass with an identical activation energy. Their glass, however, was richer in Fe_2O_3 and no discrepancy with r_p calculated using Bogomolov's equation was found. It must be concluded that either Bogomolov's equation overestimates the true value of r_p because of some dispersion in the phonon spectrum or, more unlikely, an additional ΔU term of $\sim$0.2 eV is required to equalise the centres before hopping can take place.

The variation of W_H with R can now be examined. W_D may be assumed constant for the iron glasses since values for SF1.5 and SF3.4 were 0.05 and 0.04 eV respectively, which indicate with the result for SF5 that the spread of site energies is not great in this composition range. Using r = 1.8 Å, values of W_H have been calculated using equation 4.15 and added to the other relevant components to compare with the total activation energy measured experimentally. All values are given in eV:

Glass	W_H	$W_H + \frac{1}{2}W_D$	$W_H + \frac{1}{2}W_D + \Delta U$	W_{expt} (low slope)
SF7	0.729	0.749	0.879	0.940
SF1.2	0.663	0.683	0.813	0.830
SF6	0.636	0.656	-	0.674
SF4	0.614	0.634	-	0.660
SF5	0.586	0.606	-	0.607

Fair agreement is therefore obtained for all glasses except SF7. Therefore W_H varies with R as predicted by equation 4.15 with constant r, which is further proof of a small polaron conduction mechanism.

Finally, the apparent variation of the activation energy with

redox ratio shown in Figure 4.16 requires explanation. The redox ratio was not included in the analysis above since it was almost constant for all of the glasses.

For $c < 0.5$, R will be determined by half of the mean separation of the reduced TM ions. Therefore, if they are uniformly distributed then:[163]

$$R = \frac{1}{2\sqrt[3]{cN}} = R_o/2c^{1/3} \qquad (4.21)$$

and

$$W_H = \frac{e^2}{16\pi\varepsilon_o\varepsilon_p}\left(\frac{1}{r} - \frac{2c^{1/3}}{R_o}\right) \qquad (4.22)$$

The total measured activation energy for glasses in series SF1 and SF3 should be equal to $W_H + \frac{1}{2}W_D + \Delta U$ and these are compared below with the experimental value in parenthesis:

SF1.1	0.831 eV	(0.856 eV)	SF3.1	0.728 eV	(0.815 eV)
SF1.2	0.823 eV	(0.841 eV)	SF3.2	0.728 eV	(0.784 eV)
SF1.3	0.807 eV	(0.819 eV)	SF3.3	0.766 eV	(0.822 eV)
SF1.4	0.802 eV	(0.838 eV)	SF3.4	0.785 eV	(0.807 eV)
SF1.5	0.798 eV	(0.818 eV)	SF3.5	0.812 eV	(0.836 eV)

Agreement for series SF1, with the exception of SF1.4, seems reasonable especially if the trend, rather than the absolute values, is considered. It is not so good for SF3, even ignoring the results for SF3.1 and 3.3 which seem much too high. It would appear that the decrease in W observed for c values between 0.2 and 0.5 is less than is predicted using the equation above. This is unusual since the reverse is usually found with a deeper minimum than predicted, hence a decrease in ΔU as well as W_H is postulated. In the present case it can only be suggested that either the decrease in W_H with c is less than predicted or ΔU values increase with c, which seems most unlikely. More glasses with $c \sim 0.5$ would need to be melted to study the relationship more closely to explain this discrepancy.

4.7.4 Mixed Glasses

The analysis of the results of the mixed glasses in section 4.5.6 has given clear evidence that although the conductivity is typical in magnitude and has a similar activation energy to that expected for the element present in two oxidation states, the second element, present in only one oxidation state, does exert a real effect. The important parameter in determining the resistivity appeared to be the

mean TM ionic spacing, assuming a random distribution of the two elements. The actual mechanism whereby this is achieved depends on whether the ion of the second element is a donor or acceptor. In the latter case the ion acts as a bridge between the donor and acceptor sites of the element present in two states hence effectively reducing the distance R. This explanation is applicable to SMF2 and SMF3 in which manganese was present in two states, hence the transfer process is:

$$Mn^{2+} + Fe^{3+} + Mn^{3+} \rightarrow Mn^{3+} + Fe^{2+} + Mn^{3+} \rightarrow Mn^{3+} + Fe^{3+} + Mn^{2+}$$

along with some contribution from direct $Mn^{2+} \rightarrow Mn^{3+}$ transfers.

Since Fe^{2+} is not a stable oxidation state in these glasses, the extra electron cannot reside on the ferric 'bridging' ions for any more than a few atomic vibrations before transfer to a Mn^{3+} ion. It is possible that these three ions are grouped by exchange interactions which may also include oxygen ligands. The groups may be formed during cooling of the melt by rapid hopping between the ions, hence the environment of each individual ion is similar. This explanation may be compared to that advanced by Drake[165] for copper glasses. If this is so then it is possible that not all of the TM ions may be involved in conduction, therefore a change in the c(1-c) term may result. The presence of some kind of interaction is supported by the optical absorption spectroscopy results discussed above, although the precise nature of the group or associate is not clear.

In the former case when the second element ion acts as a donor, as found for SMF2A and SMF2B, there may be some direct $Mn^{2+} - Fe^{3+}$ hops although these are not very likely because of the high polaron binding energy on the Mn^{2+} site. It should also be remembered that as Mn^{3+} is not a stable oxidation state in these glasses then the Mn^{3+} state formed by any direct hopping would have to accept an electron immediately. Therefore the main conduction process is still $Fe^{2+} - Fe^{3+}$ and it is possible that Mn^{2+} only acts in an indirect way.

From the previous analysis of conduction mechanisms in mixed TM ion glasses, two distinct types of explanation seem to emerge; either the second TM element participates directly in the conduction process or only exerts an indirect effect on the structure of the glass.

Perhaps one of the best examples of the direct mechanism is the study of Bandyopadhyay[98] whose results differ from those found in this study since both TM elements were present in substantial

proportions of both the oxidised and reduced states. Polaron hopping between ions of different TM elements paired as associates was proposed to explain the lower resistivities and activation energies of the mixed glasses. It was also suggested subsequently that the reduction in activation energy of the mixed glass could be due chiefly to changes in ΔU since only those compositions with an appreciable ΔU component showed a large decrease. Other authors such as Bogomolova[120] have also suggested hopping through mixed TM ion associates.

Mansingh et al[124], however, have proposed that the effect of Mo ions on conduction in V_2O_5 glasses is indirect since Mo ions do not act as polaron donor or acceptor sites. Instead, the changes in conductivity could be attributed primarily to a modification of ε_∞ through a change in the local bonding. This will, of course, affect the hopping energy. Structural considerations were also thought to be important by Sayer and Lynch[121,122].

In the present study it is therefore possible that both effects might be operating. The direct role of Fe^{3+} in decreasing the value of R by acting as an acceptor site in SMF2 and SMF3 has already been discussed. The decrease in W for these glasses was, however, greater than that predicted solely by the change in R which might be explained by an indirect effect on W_H via ε_∞. For SMF2A the resistivity predicted assuming ferrous-ferric conduction with the mean TM ionic spacing was lower than the experimental value, hence the contribution of Mn^{2+} ions as donors was small and $Fe^{2+} - Fe^{3+}$ hops were energetically more favourable. The decrease in W, however, could again be effected by a change in ε_∞. Similarly for SMF2B, although the fraction of Mn^{2+} ions was quite small and its direct role as a donor probably negligible, it could still exert an influence to produce the decrease in W observed.

It has not been possible to investigate any changes in ε_∞ via the optical refractive index since measurements as a function of composition could not be made with any accuracy using a refractometer because the glasses were too highly absorbing. It must be noted, however, that the changes in local bonding which will affect the polarizability and hence ε_∞ of a glass might also change other properties. For example, changes in site energy might introduce or affect a ΔU term. This may be sufficient to exclude carrier transitions between adjacent sites, hence altering the $c(1-c)$ term and introducing percolation effects. It could be that a full description of the effect of mixing TM ions is more complicated than the explanations put forward to date.

4.8 Crystallization Behaviour of the Glasses

The compositions of the two calcium aluminosilicate base glasses (SMH and SML) are indicated on the $CaO-Al_2O_3-SiO_2$ phase diagram shown in Figure 2.1. From this the primary phase fields can be seen to be gehlenite ($Ca_2Al_2SiO_7$) for SMH and anorthite ($CaAl_2Si_2O_8$) for SML.

Only the crystallization behaviour of base glass 2 (SMH) was studied. The X-ray diffraction pattern showed a large number of reflections, not all of which could be accounted for. However, gehlenite and wollastonite ($CaSiO_3$) were present with possibly a trace of rankinite ($Ca_3Si_2O_7$), as would be predicted from the crystallization path on the phase diagram. The nucleation rate was very low and only a few internal crystals were observed; these had probably nucleated exclusively on heterogeneities within the glass. Much of the crystallization had been nucleated at the surface. The crystals which had nucleated internally were very large and feathery in appearance.

Unfortunately the phase diagrams of the iron and manganese containing glasses have not been widely studied since in an atmosphere of air they are five component systems. Therefore it has not been possible to predict the equilibrium phases expected on crystallization from any phase diagrams of these systems.

4.8.1 Manganese Glasses

4.8.1.1 Series SMH

For glasses containing less than 6.2% MnO, gehlenite was the only phase crystallized after short heat treatments. Crystal growth was mainly from the surface though a few random internal crystals were also observed. These internal crystals changed morphology slightly as the manganese concentration increased, from being feathery dendrites for BG2, to relatively coarser dendrites. For SM18 (9.5% MnO), gehlenite was observed again though this time in the form of large tabular crystals. For longer growth times at the same temperature, the crystal growth became spherulitic and crystals grew to 2 - 3 mm diameter in a glassy matrix (Plates 3.3.1 - 3.3.4). This change in morphology as MnO was increased is probably associated with decreasing undercooling as the liquidus temperature decreased. SM12 also produced relatively few crystals of gehlenite but as the growth temperature was lower, the morphology was spherulitic (Plate 3.4.1).

For each of the glasses with less than 12.4% MnO since the

nucleation rate was so low, even though the nucleation temperature was varied between 650 - 800°C, it is postulated that manganese ions do not contribute to the nucleation process. Therefore the crystals must nucleate on heterogeneities as for the base glass.

When larger proportions of manganese oxide were present a manganese rich phase was the first to nucleate and grow. In the case of SM13C the large number of nuclei per unit volume indicated that either Mn^{2+} or Mn^{3+} was acting as a nucleating agent. Williamson et al[16] showed that a spinel was the nucleating phase in glasses containing iron with a similar composition to the present study. By analogy, these manganese glasses may be nucleated by Mn_3O_4 ($\equiv MnMn_2O_4$). However, a difference exists in that for this manganese glass (SM13C) the manganese oxide phase continued to grow to form the six-arm dendrites observed by optical microscopy (Plate 3.5.1) and SEM, rather than just acting as a nucleus for the major silicate phase. After about an hour at the growth temperature, a second phase started to crystallize. This was again gehlenite which showed spherulitic growth (Plate 3.5.2) but the nucleation may once more have been heterogeneous since no growth from the Mn_3O_4 dendrites was observed. Eventually the spherulites grew and consumed the glass matrix leaving very little, if any, residual glass. A second brown coloured phase was also formed, which again was also Mn_3O_4 (Plate 3.5.6).

SM14 contained the highest proportion of MnO (and Mn^{3+}) of all the manganese glasses. As was mentioned above it has not been possible to identify the brown matrix phase (Plate 3.6.1) by X-ray diffraction analysis. It would be expected that Mn^{2+} would behave in a similar manner to Fe^{2+} and Fe^{3+} in allowing ionic substitutions of Ca^{2+} and Al^{3+}. Little information, however, is available concerning manganese analogues of calcium aluminosilicate phases, especially with substitution of Mn^{3+} for Al^{3+} since the majority of geological systems do not contain appreciable quantities of manganese. Therefore it is thought that the Mn^{3+} rich phase which crystallized from SM14 is probably rare or even unknown in geological or synthetic systems. Again for this glass a relatively small number of gehlenite spherulites were produced, the diameter of which increased with increasing growth temperature. There is evidence at the lower growth temperature that crystallization of gehlenite and the matrix phase were competing since 'sheaf-like' incomplete spherulites were observed (Plate 3.6.2). A third phase, again unidentified, surrounding the gehlenite spherulites

was shown only by the difference in colour.

To summarise, it is postulated that quantities of Mn^{3+} of greater than 2.3% lead to internal homogeneous nucleation by the formation of Mn_3O_4 spinel. This either continues to grow dendritically (SM13C) or nucleates a second Mn^{3+} rich phase (SM14C). The only silicate phase to grow in this series was gehlenite which was nucleated heterogeneously, though probably not by the Mn^{3+} rich phases.

4.8.1.2 Series SML

These glasses contained smaller proportions of Mn^{3+} than the equivalent high lime glasses. Once again the major crystalline phase for all glasses, except SM10 with the highest manganese content, was that predicted by the phase diagram for the base glass, in this case anorthite. Thus the effect of adding MnO was to keep the composition in the anorthite primary phase field. For SM7, SM8 and SM9 only surface nucleation was observed which at high crystal growth temperatures (980 - 1000°C) completely consumed the glass. For slightly lower temperatures the surface growth was more limited. The absence of internal nucleation in these glasses gives further evidence that Mn^{3+} rather than Mn^{2+} is essential for bulk internal nucleation. Crystallization of anorthite enriched the residual glass in both manganese and silica and after long heat treatment times manganese silicate crystallized between the primary dendrites as the second phase (Plate 3.1.1).

The situation for SM10 was similar to that of the high Mn glasses in series SMH in that an Mn^{3+} rich phase nucleated and grew dendritically. However, X-ray diffraction analysis showed that the phase in SM10 was different to that in SM13C or SM14C and possibly the higher proportion of silica allowed the formation of braunite ($3Mn_2O_3.MnSiO_3$) as the first phase to crystallize, although this identification was not definite.

The second phase to crystallize was not anorthite as might have been expected but rather a pyroxene. The closest standard X-ray pattern to that obtained experimentally was that of an augite. However, the simplest formula for an augite is $Ca(Fe,Mg)(SiO_3)_2$ i.e. no manganese, therefore the phase in SM10C cannot strictly be called an augite. However, a wide variety of ionic substitutions can occur in pyroxenes and there is complete replacement between some of the group components. Augites are related to compositions between diopside ($CaMg(SiO_3)_2$) and hedenbergite ($CaFe(SiO_3)_2$) both of which have similar

X-ray powder patterns, and form a continuous solid solution series along with ferroaugite. The greater ionic size of Fe^{2+} compared to Mg^{2+} leads to an increase in d-spacings as Mg^{2+} is replaced by Fe^{2+} along the series.

The manganese equivalent of diopside and hedenbergite is johannsenite ($CaMn^{2+}(SiO_3)_2$) but as Mn^{2+} is larger than either Mg^{2+} or Fe^{2+} the d-spacings are even greater. In practice johannsenite provided the worst fit of these pyroxenes to the experimental patterns for SM10C. A continuous solid solution series between hedenbergite and johannsenite is also found.

For iron containing materials it has been suggested[166] that because there is a continuous chemical variation between diopside, hedenbergite and augite, the single name augite should be used with prefixes to describe the whole series. In view of the likely replacement of Ca^{2+}, Fe^{2+} and Mg^{2+} by Mn^{2+}, and Al^{3+} by Mn^{3+} it is proposed that the pyroxene in SM10C is a manganoan-augite with composition of the form $((Ca,Mn^{2+},Mn^{3+},Al)_2\{(Si,Al)_2O_6\})$ probably not found in nature. This formula is considerably more complex than the simple augite formula given above since it has been derived from the generic formula for augites $((Ca,Mg,Fe^{2+},Fe^{3+},Ti,Al)_2\{(Si,Al)_2O_6\})$.

A composition of this type has been justified by the analysis of Bevan et al[167]. They proposed that the most similar material occurring in nature was fassaite $((Ca(Mg,Fe^{3+},Al)\{(Si,Al)_2O_6\})$. Therefore for the phase in SM10C, Mg^{2+} is replaced by Mn^{2+} and Fe^{3+} by Mn^{3+}.

After longer crystallization at higher temperatures for SM10C, glaucochroite ($(Ca,Mn)_2SiO_4$), a rare member of the olivine family, was the major phase. The only indication from X-ray analysis of a manganese rich phase was bustamite ($(Mn^{2+},Ca)SiO_3$), although optical examination revealed that braunite and the manganoan-augite were still present.

In conclusion, therefore, Mn^{2+} may act as an effective nucleating agent when present in quantities greater than about 2.3% for either base glass composition. For low lime glasses with lower concentrations, anorthite nucleated at the surface and grew rapidly. For SM10C with Mn^{3+} > 2.3%, braunite dendrites grew initially which then acted as the nuclei for the augite phase giving the characteristic two phase dendrites (Plates 3.2.1 - 3.2.5). However, from TEM studies Mn_3O_4

probably acted as the nucleus for the braunite dendrites just as it nucleated and grew in the SMH series. The inhomogeneity in the sample of SM10 resulted in the non-uniform nucleation behaviour. The areas of high nucleation density corresponded to areas of the glass which were browner than the rest i.e. had higher Mn^{3+} contents, which confirms the effect of Mn^{3+} as a nucleating agent.

4.8.2 Iron Glasses

Only glasses containing above 5% Fe_2O_3 showed any tendency to nucleate and crystallize internally, a fact also noted by Rogers and Williamson[15]. Glasses containing less than this concentration produced only surface crystallization even after a wide range of nucleation heat treatments. For SF6 after a short crystal growth time only a small number of dendrites formed (Plate 3.7.1), but these subsequently grew to consume nearly all of the glass. These dendrites were again a pyroxene type material, probably related to augite, and the interdendrite matrix was largely gehlenite, although residual glass could not be ruled out completely. The exact identification of the pyroxene dendrites was again difficult with similar problems to those described above, because of the similarity of the powder X-ray diffraction patterns between hedenbergite, augite and fassaite.

In addition, the presence of a third phase such as magnetite was difficult to identify since the principal reflections from magnetite overlapped those from the pyroxene. For SF6C, after accounting for the lines resulting from gehlenite, the X-ray pattern was best described by an augite phase and since the dendrites had a characteristic 'ferrous green' coloration, the best description of the phase would be a ferroaugite with the generic formula $(Ca,Fe^{2+},Fe^{3+},Al)_2\{(Si,Al)_2O_6\}$.

Glass-ceramics derived from SF4 and SF5 exhibited very different dc conductivity behaviour to each other after similar heat treatments but their X-ray powder diffraction patterns were almost identical. The major phase was therefore the same in both: again an augite with a similar composition to that in SF6C, though in this case gehlenite was not detected in either. It was impossible to detect any magnetite from the X-ray diffraction analysis although optical microscopy did suggest that SF4C had a fine dispersion of crystals which were not seen for SF5C. It could be that magnetite crystals are present in SF4C but not in SF5C and this will be further considered when discussing the conductivity results below.

In conclusion, concentrations of 5%Fe_2O_3 or greater promote extremely fine grained glass-ceramics with a pyroxene as the major phase. Gehlenite was only detected optically and by X-ray diffraction analysis for SF6C, though it may have been present in very small amounts for SF4C as suggested by the SEM examination. The possible appearance of magnetite for only one glass is not understood but could have resulted from the crystallization of residual glass. No other phase, such as a spinel, which could have nucleated the pyroxene phase was detected although it is possible from the TEM studies of SF4 that phase separation could have preceded crystallization.

4.8.3 Mixed Iron-Manganese Glasses

The three dilute mixed glasses (SMF1, SMF4 and SMF5) melted primarily for spectroscopic studies were not heat treated and neither was the most concentrated glass SMF3.

Only one phase (gehlenite) could be identified by X-ray diffraction analysis for SMF2C although there were unaccounted lines for which magnetite provided the best fit. Optical microscopy indicated at least three phases. It is surprising that magnetite should be present in a glass of this composition since it had the smallest iron content of the series SMF2, SMF2A and SMF2B. It is possible therefore that this assignment is incorrect. The major phase seen optically appeared brown in transmitted light. This could be the result of substitution of Mn^{3+} for Al^{3+} in the gehlenite structure to give a phase of the form $Ca_2(Mn^{3+},Al)_2SiO_7$, however, manganese analogues of the melilite series have not been reported.

The X-ray powder diffraction patterns obtained for SMF2A and SMF2B were almost identical and could be described by a mixture of gehlenite and wollastonite. In both cases crystallization had produced extremely fine grained products. Optical examination indicated that TM ions were probably incorporated into the crystals to give the observed coloration (Plates 3.9.1 & 3.9.2).

Gehlenite is one end member of the melilite solid solution series and forms a continuous range of solid solutions with akermanite ($Ca_2(MgSi_2O_7)$). The X-ray powder patterns for both are very similar with only small intensity differences distinguishing end members, therefore identification of an exact composition was difficult.

The melilite series can contain appreciable amounts of iron and

both iron-gehlenite ($Ca_2\{Fe^{3+}AlSiO_7\}$) and iron-akermanite ($Ca_2\{Fe^{2+}Si_2O_7\}$) can be synthesised: both occur in blast furnace slags for example. Nurse and Midgley[168] have reported X-ray data for these compositions but the patterns for these phases do not match those determined experimentially for SMF2A and SMF2B. Therefore to explain the coloration of the dendrites it is suggested that their composition is probably intermediate between gehlenite and iron-gehlenite with possibly some substitution by Fe^{2+}. Iron-akermanite might seem more plausible since it does contain Fe^{2+} but it is not expected in these glasses since it is not stable above 775°C, but decomposes as follows:

$$Ca_2Fe^{2+}Si_2O_7 \rightarrow \underset{\text{wollastonite}}{CaSiO_3} + \underset{\text{kirscheinite}}{CaFe^{2+}SiO_4}$$

Kirscheinite has not been detected in either iron or mixed glasses.

The second crystallization product appeared to be wollastonite however this could also form solid solutions with iron to give ferroan-wollastonite which could also explain the green coloration of the phases in SMF2A and SMF2B.

Finally, it was noted that as the iron concentration increased in this series, the nucleation rate also increased. The rate of crystal growth was very much higher in SMF2A and SMF2B presumably because of the presence of Fe^{2+} which leads to an increase in the growth rate by the mechanism proposed by Williamson[18].

4.9 D.C. Resistivity of the Crystallized Glasses

4.9.1 Series SML

In this series only SM10C nucleated crystals internally which was the major interest of this study. However, considering that the surface growth of SM7C, SM8C and SM9C was so extensive, such that crystallization of the sample was nearly complete, it was decided to study the electrical properties of one of them and SM7C was chosen.

The major crystalline phase, anorthite, appeared from the optical analysis not to incorporate manganese ions, therefore all the manganese must have been rejected to the phase, glassy or crystalline, between the anorthite crystals. The conduction path is therefore between the crystals, since anorthite is not electrically conductive. This effective concentration of manganese ions will decrease the mean interionic spacing, which should result in a decrease in the resistivity.

Experimentally (Figure 3.4.1) it was found that both the resistivity and activation energy decreased. Using Figure 4.10, the decrease in activation energy from 1.43 to 1.25 eV could be explained by a reduction in the mean TM interionic spacing from 8.4 Å to about 7.2 Å. From the same figure the resistivity at 500 K corresponding to such an activation energy should be log ρ = 13.2, which is in excellent agreement with the experimentally determined value of 13.16. Therefore it is suggested that identical conduction mechanisms are operating in both the glass and crystallized glass and the overall increase in conductivity is the result of enrichment of manganese in a continuous glassy phase. It was remarked above that manganese silicate was detected in this glass but this does not seem to have a great effect on the conductivity behaviour, although it will slightly alter the carrier concentration.

In section 4.7.2.2 it was concluded that conduction in SM7 may not be the result of polaron hopping because of the high activation energy and value of α^{-1}. Alternatively, indirect hopping could be occurring. Although the value of α^{-1} for SM7C was nearer that of r_p, it is unlikely that this is a true value since no account of the exact conduction path has been taken. The value of W of SM7C is, however, only slightly higher than would be predicted by extrapolating W for the series SM8, SM9 and SM10 to the value of R for SM7C, which tends to give additional support to the mechanism of polaron hopping. This in turn supports polaron hopping for SM7 since the mechanisms in the glass and glass-ceramic are very similar.

The behaviour of SM10C was fundamentally different to SM7C since the activation energy decreased by 0.33 eV to a value of 0.82 eV which was one of the lowest observed for any manganese composition. The resistivity was also reduced. This corresponds to an enrichment of the residual glass such that R would need to be of the order of 2 Å; however, from the X-ray diffraction and optical examination it is known that manganese rich phases were crystallized. If these dendrites were separated from each other by a residual layer of glass then depletion of the manganese from this glass rim should increase the resistivity of this composite. Therefore it is postulated that in the dense region of dendritic growth the manganese rich spines of the dendrites are in loose contact and close enough for electrons to pass from one to another by either hopping or tunnelling. Conduction is therefore mainly along a continuous path formed by the mixed valency crystals of braunite.

Outside of the dense continuous growth the glass becomes the continuous phase and some conduction will occur through it. This contributes very little to the overall conductivity because the conductivity of the crystalline phase is so much higher.

As far as is known the electrical properties of braunite have not been measured therefore a comparison of the activation energy of SM10C with that of braunite is not possible. However, the decrease in W compared to the glass probably reflects the crystallographically ordered environment of the ions, which will reduce the W_D term, as well as the reduction in R in the crystal. Once again an exact calculation of α^{-1} does not seem possible because of the complexity of the conduction path.

4.9.2 Series SMH

D.C. resistivity was measured for glass-ceramics containing $\geq$ 9.5% MnO.

SM18C produced only a few large discrete tabular/spherulitic crystals of gehlenite on crystallization. The situation is therefore similar to that of SM7C in that manganese is rejected from the crystals although because of the small extent of the crystal growth, very little enrichment of manganese in the residual glass is expected. The electrical properties of the crystallized glass follow such an explanation since, at high temperatures, the resistivity was only a little lower than that of the parent glass, representing a decrease in R from 7.1 Å to 6.8 Å. This of course neglects any differences due to inter-sample reproducibility.

This decrease in R is averaged out over the whole sample which is not physically realistic since crystals will be surrounded by a rim of glass with higher Mn concentration, whilst outside this rim R will be almost unchanged. The decrease in resistivity was not mirrored by a decrease in activation energy as would be expected if R had been reduced. Instead an increase of 0.05 eV was observed though it is possible that this is the result of sample variability. The greater value of W also meant that α^{-1} increased compared to the glass and α^{-1} became greater than r_p, although the calculation may be affected by the presence of the crystalline phase.

The most unusual behaviour shown by SM18C was that it exhibited two slope behaviour in a manner quite unlike any of the other manganese glasses since the decrease in W was 0.6 eV (Figure 3.4.3). The low

slope activation energy was ∿0.6 eV which was the lowest observed for the manganese glasses. Similar behaviour was noted by Tsuchiya and Moriya[118] after crystallizing a manganese phosphate glass though the resistivity of their glass was also greatly lowered. For this reason their explanation (see section 1.4.6) does not seem applicable to SM18C since in this case no great change in resistivity was observed.

It does not seem possible to explain this dramatic change in slope in terms of any macroscopic parameter, but the answer could lie in the possibility of microscopic changes in the residual glass as a result of heat treatment. The nature of these and why they only affect the low temperature conductivity is however unknown.

The behaviour of SM12C was similar to SM18C, though it did not exhibit two slope behaviour. Both the resistivity and activation energy were slightly reduced and the change in resistivity could be explained by a decrease in R from 6.5 Å to 6.3 Å. The microstructure was similar to SM18C in that large discrete spherulites of gehlenite crystallized, which again produced rims of manganese enriched residual glass. It would seem that as these rims are well separated, the conduction path is relatively unaltered by them and polaron hopping operates in the continuous glassy phase. The value of α^{-1} was greater than in SM12 and also greater than r_p which may be a result of the presence of crystallites and the fact that parent glass parameters have been used which may not be appropriate. The absence of any two slope behaviour may be a result of crystallization at a lower temperature than SM18C.

In contrast to the two glass-ceramics in series SMH described above, the behaviour of SM13C and SM14C was different in that the resistivity increased after crystallization. Two conductivity samples were prepared for SM13C, one crystallized for 1½ hours, which was composed of discrete Mn_3O_4 dendrites in a glassy matrix and the second crystallized for 19 hours in which the matrix was crystalline. In fact the two showed remarkably similar dc conductivity behaviour (Figure 3.4.5); both showed two slope behaviour as in the parent glass although the intersection temperature was different in each case and higher than for SM13.

For the low slope line the resistivity rose by about half an order of magnitude after 1½ hrs but then dropped slightly after 19 hrs crystallization. The activation energy derived from this line first

increased (0.988 to 1.004 eV) but then fell in a similar way (to 0.956 eV). At the higher temperatures the increase in resistivity was about the same after both times, although the activation energy showed an increase (1.11 - 1.15 - 1.21 eV after 19 hours).

These changes may be interpreted as follows. Since the first crystalline product is rich in manganese the matrix must be depleted in manganese and as the conductivity is determined by the continuous phase, the resistivity increases. Evidently conduction between the dispersed Mn_3O_4 dendrites is impossible at these separations. This depletion is equivalent to an increase in R from 5.9 to 6.1 Å or expressed in another way, a decrease in the effective MnO concentration from 16.4 to 14.9% which is equivalent to 10% of the total manganese crystallizing as Mn_3O_4. This analysis ascribes the whole of the change in resistivity to a change in R which is only partially true since the redox ratio of the glass will also change. Two Mn^{3+} ions are required for every Mn^{2+} ion and hence the redox ratio (Mn^{2+}/Mn_{total}) will rise. The effect of this on the resistivity should be small since the redox ratio is 0.78 in the glass. This increase in R should increase the activation energy slightly which was also observed.

On continued crystallization after 1½ hrs, two opposing effects occur which are difficult to separate quantitatively. The dendrites continue to grow, consuming manganese, to a limiting size until gehlenite crystallizes and consumes most of the remaining glass. In doing so, manganese is rejected from the silicate phase and concentrates in the residual glass. The effective interionic spacing therefore first increases but then a reversal takes place such that a net decrease occurs. This is therefore a different case to SM7C above in which all the manganese was concentrated by the growth of a silicate phase.

This sequence of events is similar to that observed by some authors[130] particularly in iron glasses. A difference exists with the study of Tricker[130], for example, since in the present system a continuous path of crystals was never formed. The explanation is also different to that of Dozier[103] who ignored the decrease in R by the precipitation of iron rich phases and assigned the changes in resistivity solely to changes in redox ratio brought about by segregation of the two redox states during crystallization.

One anomaly noted for these glass-ceramics was the increase in the difference between the high and low temperature activation energies derived from the two slopes. Whereas the low temperature activation

energy was the lowest after 19 hrs crystallization, the high temperature value was highest after that time. It could be the result of site differences becoming accentuated in the residual glass thus increasing the ΔU term to $\sim$0.25 eV. This is difficult to prove without more data on the residual glass e.g. ion spacing, redox ratio and coordination of the Mn ions, which seems almost impossible to obtain.

Finally, the increase in resistivity of SM14C was very marked and contrasted strongly with the equivalent low lime glass SM10C. The increase in resistivity was $1\frac{1}{2}$ - 2 orders of magnitude and the activation energy also showed a marked increase of 0.2 eV. Since detailed information on the phases produced and their microstructure could not be obtained, it is difficult to speculate on the reasons for this increase. Evidently the crystalline phase incorporates some manganese since enrichment of any residual glass does not occur, unless this glass does not form a continuous phase. Also the crystals cannot be of mixed valency or else conduction would probably take place along them since point to point contact is almost certainly established. The reason for the increase could be that Mn^{2+} and Mn^{3+} have been almost completely segregated by crystal growth. A more complete microstructural and mineralogical analysis would be needed to confirm this.

4.9.3 Series SF

Conductivity measurements were performed on the three crystallized glasses with the highest iron concentrations: SF6C, SF4C and SF5C.

The behaviour shown by SF6C and SF5C was very different to that of SF4C. However, one feature in common for all the glass-ceramics was that the measured resistivity depended on the applied voltage and had a value that was lower at high voltages compared to low voltages. This effect of the field became less as the temperature increased.

Field dependent i.e. non-ohmic behaviour can occur in amorphous materials for a number of reasons. It may be associated with the electrodes, temperature rises in the sample (Joule heating) or may be a true bulk effect. Electrode effects could be important for heterogeneous materials such as these glass-ceramics although non-ohmic behaviour was not noted for the crystallized manganese glasses except SM13C. Also the V-I relationship at lower voltages was ohmic with deviations occurring only above 10^2 - 10^3 V cm^{-1} (Figure 4.17). It is possible therefore that this field enhanced conductivity may be a true bulk

effect.

Non-ohmic behaviour is often observed for TM and other glasses at sufficiently high fields. There are two basic mechanisms: firstly an increase in the free carrier density by field emission from traps (e.g. the Poole-Frenkel effect) or secondly, a field dependent mobility. Usually the second mechanism is observed for TM oxide glasses and it can be shown for simple hopping between adjacent sites that the field dependent conductivity is of the form:

$$\sigma(F) = \sigma(0) \frac{\sinh(eaF/2kT)}{(eaF/2kT)} \qquad (4.23)$$

where a is the jump distance and F is the field.

It would be expected from the sinh term that non-ohmic behaviour should begin when $eaF \simeq kT$ which, at room temperature with $a = R \simeq 5$ Å, requires a field of 5×10^5 V cm^{-1}. Values of 'a' between 15 - 40 Å are often calculated for TM glasses but clearly values of 'a' calculated for these glass-ceramics, for which deviations from Ohms law were found for fields of 150 V cm^{-1} or greater, are very large (2×10^4 Å) and probably unrealistic.

The origin of this behaviour in these glass-ceramics must lie within the microstructure and is possibly the result of a highly conducting crystalline phase separated by glass through which limited conduction is also possible. Some carriers may therefore be trapped within the conducting crystalline phase until a high enough field allows them to enter the conduction process by altering the height of the energy barrier (Schottky barrier) at the crystal/glass interface, where the band structure is not continuous. Such an explanation is more akin to the first mechanism given above i.e. field emission from traps, rather than a field dependent mobility, although the latter cannot be ruled out completely. For glass-ceramics in which the major crystalline phases were insulating (SM7C, SM12C and SM18C), this effect was not seen.

A detailed analysis of high field conduction in heterogeneous multiphase materials like these would be complex. Since the non-ohmic behaviour cannot be explained satisfactorily at present, the conductivity data to be discussed below will include only that obtained at low voltages i.e. within the ohmic range.

Returning to the effect of crystallization, the resistivity of SF6C was reduced by 2½ orders of magnitude after heat treatment with a

corresponding decrease of 0.25 eV in the activation energy to 0.56 eV, compared to the high slope value. It is thought that the crystal phase incorporated iron ions but the change in resistivity seemed too large to be accounted for by a change in redox ratio of the residual glass because of preferential segregation of a particular ion during crystallization. The crystal phase was tentatively described as a ferro-augite and it was suggested that it may contain Fe^{2+} and Fe^{3+}. Therefore there could be two possible conduction mechanisms: firstly through the crystalline phase and secondly through a residual glassy phase. It is believed that conduction is controlled by the residual glass since the activation energy is rather high for a crystalline mixed valence semiconductor containing iron. Typical values for ferrites, for example, are in the range 0.2 - 0.3 eV.

The residual glass probably forms a continuous path and contains an appreciable proportion of iron ions even though some iron appears to have been incorporated into the crystal phase. The interionic spacing to achieve the observed activation energy (from Figure 4.12) is 4.6 Å, assuming the absence of a ΔU term. The resistivity of SF6C was higher than would be predicted with this spacing (from Figure 4.14) but, of course, the total number of carriers was reduced by crystallization of a phase containing iron.

The idea of conduction through a residual glassy phase receives additional support when the behaviour of SF4C is considered. Although the major crystal phase appeared to be the same as in SF6C and SF5C, the resistivity of SF4C increased after crystallization unlike the other two. Therefore, provided the phases were the same, the conduction cannot be solely through the crystals since similar behaviour for all three should have been observed.

The behaviour of SF4C is undoubtably explained by the appearance of Fe_3O_4 crystals which, although semiconducting, were unconnected hence conduction was still through the continuous glassy phase which had been effectively denuded of iron ions and so the resistivity increased. One interesting feature was that the plot of log ρ/T - $1/T$ no longer exhibited two slope behaviour and the gradient was typical of the low slope portion of the parent glass throughout the temperature range. The same was also true of SF6C and SF5C. The reduction of conductivity on crystallization for SF4C was between $\frac{1}{2}$ - 1 order of magnitude depending on the temperature.

Finally, the decrease in resistivity of SF5C was similar in magnitude to SF6C. The activation energy was also reduced by 0.26 eV compared to the high temperature slope and 0.13 eV compared to the low temperature slope. Once again conduction through a mixed valence crystalline phase could be postulated but this is not as likely as a conduction path through, or controlled by, a residual glassy phase enriched in iron. Because of iron entering the crystals, the redox ratio of the continuous phase will also change but this is expected to have a small effect compared to the decrease in R.

4.9.4 Series SMF

Only two glass-ceramics were studied in this series: SMF2AC and SMF2BC.

SMF2AC behaved in a similar manner to the iron containing glass-ceramics SF6C and SF5C. A decrease in resistivity of $1\frac{1}{2}$ - 2 orders of magnitude was observed accompanied by a decrease in activation energy of $\sim$0.2 eV. A slight deviation from Ohm's law at higher fields was apparent but not to the same extent as in the iron glass-ceramics.

SMF2BC however, showed a much more remarkable decrease in resistivity of nearly four orders of magnitude at 400 K with a decrease in activation energy to just 0.17 eV. The resistivity and activation energy of this glass-ceramic were the lowest observed in this study since it had a room temperature resistivity of $<10^6$ Ω cm. An activation energy of this magnitude can only be explained by conduction through the crystal phase since it is of the same order as that found in crystalline FeO, Fe_2O_3 and Fe_3O_4. Since the manganese concentration of this glass was small, conduction is likely to be between Fe^{2+} - Fe^{3+} pairs in the crystal and the activation energy probably represents the hopping energy only, since there should be no contribution from W_D or ΔU.

The dramatic difference between these two glasses is surprising considering that the microstructures appeared very similar and the major crystalline phases were thought to be the same. The only difference is that SMF2AC contains slightly less iron and more manganese. One explanation, which is difficult to prove, is that the crystals in SMF2AC do not actually touch but are separated by a rim of residual glass which controls the conductivity. This is similar to the explanation for the iron glass-ceramics to which SMF2AC does show similar

behaviour, especially SF6C which has a nearly equivalent iron concentration. If this is the case then there must still be considerable enrichment of the residual glass in SMF2AC to decrease the resistivity to the extent seen. The crystals in SMF2BC are therefore assumed to be touching and a complete conduction path between the electrodes is formed. One anomaly at low temperature was that non-ohmic behaviour was noted for very small fields. This effect was very much less above 140°C hence it could have been an electrode effect which was removed by heating.

4.10 A.C. Resistivity of Crystallized Glasses

A.C. resistivity measurements were made on only three of the crystallized glasses: SM13C, SF4C and SMF2AC. Of these the behaviour of SM13C and SMF2AC may be compared with the dielectric behaviour of the parent glass on which measurements were also made.

Plots of the logarithm of the total resistivity against reciprocal temperature for a range of frequencies for SM13C and SF4C (Figures 3.5.2 and 3.5.5) showed different behaviour to that of most of the glasses since the resistivity at a given frequency did not always decrease smoothly with increasing temperature. Particularly at higher measuring frequencies an increase in resistivity with temperature was observed. This is indicative of the occurrence of discrete dielectric relaxation processes.

At lower temperatures the total resistivity at any given frequency was significantly lower than the dc value. Although the difference became less at higher temperatures, Figure 3.5.5 seems to indicate that unlike the glasses, the total and dc plots may not join and the total resistivity always remains smaller than the dc value. In contrast, the behaviour shown by SMF2AC was similar to that of the parent glass with little evidence of any relaxation processes since the total resistivity decreased smoothly with increasing temperature.

These differences between SMF2AC and the other glass-ceramics measured are also shown by the behaviour of the real and imaginary components of the dielectric constant. SM13C behaved in a very different way to SM13 as comparison of Figures 3.7.1 and 3.7.2 clearly shows. Both ε' and ε'' were appreciably higher for the glass-ceramic and a peak in ε'' against log f was apparent which moved to higher frequencies as the temperature increased.

The behaviour of SF4C was similar to SM13C but the increases in ε'

and ε'' were much greater, up to a factor of ten. The dielectric loss of this glass-ceramic also showed a peak when plotted against log f which again shifted to higher frequencies as the temperature increased. Although the appearance of the plots of ε' and ε'' against log f for SMF2AC were similar to the parent glass, once again the values were up to ten times greater. No loss peaks were observed in the measuring frequency range but may have occurred at lower frequencies.

An attempt was made to plot log ρ_{ac} against log f for each of the glass-ceramics but linear plots over a reasonable frequency range could not be obtained for most temperatures. In the few cases for which a linear plot was appropriate the gradient was either lower (<0.5) or higher (≈ 1.2) than the value of 0.5 - 0.8 expected for such a plot.

The two major effects of crystallization on the dielectric properties of the glass-ceramics are therefore a large increase in both the dielectric constant and loss, and the appearance of dielectric loss peaks. These arise because the glass-ceramic is effectively a polyphase aggregate consisting of two or more materials, each with a different conductivity, arranged in a particular microstructure. This gives rise to interfacial or space charge polarization. The dc conductivity results were explained either in terms of conduction through a layer of residual glass enriched in TM ions or in some cases by conduction through a contiguous crystal phase. In the first case motion of the polarons is interrupted when a glass/crystal boundary is encountered thus causing a build-up of charge at the interface. This corresponds to a large polarization and high dielectric constant.

Inhomogeneous dielectrics such as these have been studied by Sillars[169] who showed that even a few needles of conducting material in an insulating matrix would increase the dielectric loss, which is known as the Maxwell-Wagner loss. The magnitude of the loss depends critically on the conductivity, shape, size and amount of the dispersed phase but can only be analysed mathematically for relatively simple shapes, where it is found that the Maxwell-Wagner loss will produce a peak similar to the Debye relaxation peak. Such a loss was probably responsible for the peaks observed for SM13C and SF4C.

More detailed analysis of the dielectric properties of these materials was hampered by the lack of knowledge of the microstructure, therefore only qualitative conclusions could be drawn. For SM13C, although the dc resistivity of the glass-ceramic was higher than the

glass at any particular temperature, the ac resistivity was lower than SM13 for a given frequency, particularly at low temperatures and high frequencies. This could be the result of conduction within the small manganese-rich dendrites at high frequencies which can make no contribution to the dc conductivity. The cause of the loss peaks, however, is probably due both to the dendrite and the residual glass interfaces with the major silicate phase. Unfortunately it was not possible to calculate an activation energy corresponding to this relaxation process to compare with the dc value because there were insufficient data.

SF4C also had two crystalline phases both of which were probably semiconducting though only a single relaxation peak was found at higher temperatures in the range of frequencies measured. Dozier et al[103] found two relaxation peaks for a glass which produced two crystalline phases after heat treatment but it is not known if this is to be expected generally.

Finally, the behaviour of SMF2AC for which no loss peaks were seen cannot be interpreted as the result of no crystallization within the sample since, as has already been observed, the magnitude of ε' and ε'' showed very marked increases. The loss peaks may be occurring at lower frequencies. Comparison of SMF2AC with its parent glass (Figures 3.7.7 and 3.7.8) shows that for equivalent temperatures the apparent position of the loss peak has increased in frequency on crystallization. Other authors[101,103] have also noted the absence of loss peaks in some crystallized glasses which has been explained by the small number and large size of the crystallites. Such an explanation is not appropriate in this case since Plate 3.9.1 shows a substantial number of small crystallites. The relaxation time, and hence the frequency of the loss peak, is critically dependent upon the microstructure of the composite but a complex analysis would have to be taken to show the mathematical relationship for SMF2AC and the other glass-ceramics. The presence of these relaxation processes dominates the ac conductivity to the extent that the linear relationship of $\log \rho_{ac} \propto \log f$ expected for simple hopping between nearest neighbour sites is no longer observed.

4.11 Conclusions Regarding the Conduction Processes in Crystallized Glasses

The previous sections have given some indication of the complexity of the conduction process in glass-ceramic systems. Four possible

changes on heat treatment have been described each of which has a different effect on the resultant dc conductivity. These are:

(a) Growth of an insulating crystalline phase. This rejects TM ions into a residual glassy phase which causes an effective increase in TM concentration and hence in mobility since R is decreased with N and c unchanged. The change in conductivity observed depends upon the volume fraction of the crystalline phase. This is the appropriate mechanism for some of the manganese glass-ceramics (SM7C, SM12C and SM18C).

(b) Segregation of one TM oxidation state to the crystalline phase. The major effect of this is on the redox ratio although changes in R will also result, depending upon the degree of crystallization. In the limit the two TM redox states could become completely isolated, with one in a crystalline phase and the other in the residual glass or second crystalline phase. This will greatly decrease the mobility and hence the conductivity. Such a mechanism has been tentatively suggested only for SM14C.

(c) Growth of discrete crystallites of a mixed valence crystalline phase. Different effects are possible depending upon the volume fraction of the crystalline phase and the amount of TM ion that is incorporated. A small volume fraction will only have a small effect in reducing the TM ion concentration in the residual glass. Larger fractions can increase or decrease the conductivity of the residual glass depending upon the enrichment of the crystal. It is the residual glass that is the continuous phase and hence controls the overall conductivity even though its volume fraction may be small. This mechanism has been suggested for SM13C, with a contribution also from mechanism (a) since two crystalline phases were observed and also SF4C, SF5C, SF6C and SMF2AC.

(d) Growth of a mixed valence crystalline phase with a continuous path through the sample, as suggested for for SM10C and SMF2BC. In this case the mixed valence crystalline phase is continuous and controls the conductivity of the composite, usually producing a marked increase in conductivity.

This list is not exhaustive and other effects may also be possible. In fact SM10C does not conform entirely to mechanism (d) because the crystalline phase formed only a small part of the sample; conduction was therefore also occurring through the continuous glassy phase in

other parts of the specimen.

The effective conductivity of a multiphase medium is determined by the conductivities and morphologies of the component phases. In the simplest case, that of alternating layers of differing materials, the effective conductivity is given by the rule of mixtures with similar arguments applying also to the dielectric constant and loss. For example, taking the case of layers of material lying normal to the electrodes such that the same field is applied across each one, the mean conductivity (σ_m) is given by:

$$\sigma_m = v_1\sigma_1 + v_2\sigma_2 + \ldots = \sum_i v_i\sigma_i \qquad (4.24)$$

where v_i is the volume fraction of phase i with conductivity σ_i. The conductivity of the composite in this case is dominated by the better conductor. If the layers lie parallel to the electrodes then the resistances of the different layers are effectively in series and the mean conductivity is given by:

$$\frac{1}{\sigma_m} = \frac{v_1}{\sigma_1} + \frac{v_2}{\sigma_2} + \ldots = \sum_i \frac{v_i}{\sigma_i} \qquad (4.25)$$

Conduction is therefore dominated by the poorer conductor.

Equations 4.24 and 4.25 are special cases of a general empirical expression:

$$\sigma_m^n = \sum_i v_i\sigma_i^n \qquad (4.26)$$

where n is a constant with values between -1 and +1. For small n the logarithmic mixture rule is obtained:

$$\ln \sigma_m = \sum_i v_i \ln \sigma_i \qquad (4.27)$$

Expressions of the form above may be developed for more complex composites. One example which is more appropriate for some of the glass-ceramics studied is that of a random mixture of a continuous phase with a dispersed phase of spherical particles. By analogy to the Maxwell equation for the permittivity of such a system the conductivity is given by:

$$\sigma_m = \frac{\sigma_c\{1 + 2v_d(\frac{1 - \sigma_c/\sigma_d}{2\sigma_c/\sigma_d + 1})\}}{\{1 - v_d(\frac{1 - \sigma_c/\sigma_d}{2\sigma_c/\sigma_d + 1})\}} \qquad (4.28)$$

where the subscript c refers to the continuous phase and d to the dispersed phase. Taking the two limiting cases gives:

$$\text{(a)} \quad \sigma_c >> \sigma_d \qquad \sigma_m \simeq \frac{\sigma_c (1 - v_d)}{(1 + v_d/2)} \qquad (4.28a)$$

$$\text{(b)} \quad \sigma_c << \sigma_d \qquad \sigma_m \simeq \frac{\sigma_c (1 + 2v_d)}{(1 - v_d)} \qquad (4.28b)$$

The latter equations are most applicable to SM12C and SM18C which had spherulites of an insulating phase growing in the glass, hence equation 4.28a is appropriate. They may also be extended, possibly with the introduction of shape factors, to SM14C, SF6C, SF5C and SMF2AC. More complex expressions would be needed for SM13C and SF4C which had two crystal phases in addition to residual glass. On the other hand the more highly conducting materials SM10C and SMF2BC with continuous crystal paths can be described by expressions of the form of equations 4.26 and 4.27. As mentioned above, similar formulae may be used to describe the dielectric behaviour of multiphase materials in terms of ε' and ε''.

The conduction processes outlined above will contribute to the ac as well as the dc conductivity though there may also be contributions to the ac conductivity through conduction in any dispersed conducting crystalline phases. This causes an enhancement of the ac conductivity. The other important phenomena which have been discussed already are interfacial effects between the different phases which give rise to Maxwell-Wagner-Sillars inhomogeneous losses.

Finally, the nature of the charge carriers in these materials has not been discussed except for the manganese glass-ceramics where the volume fraction of crystalline phase was small. For those systems in which conduction is postulated to be through the residual glass it seems likely that polarons will be the carriers. Unfortunately it is difficult to estimate the polaron parameters (α^{-1}, r_p) as was achieved for the glasses, because of the lack of quantitative knowledge of the microstructure. Only for those glass-ceramics with the simplest microstructures (e.g. SM12C, SM18C) can factors such as R, N and c, calculated for the parent glass, be used to estimate α^{-1} and r_p for the glass-ceramic. For more complex glass-ceramics still involving conduction through a residual glass polaron conduction may be operating while for conduction through a crystalline phase an electronic mechanism is probably more appropriate.

TABLE 4.1

COMPARISON BETWEEN MIXED GLASSES AND EQUIVALENT SINGLE TM GLASSES

	SMF2	Manganese Glass		SMF3	Manganese Glass		SMF2A	Equivalent Iron Glass			SMF2B	Equivalent Iron Glass		
		R=8.23Å	R=6.48Å		R=7.19Å	R=5.69Å		c=11.0 R=7.42Å	c=18.5 R=7.42Å	c=11.0 R=6.59Å		c=11.0 R=6.81Å	c=20.9 R=6.81Å	c=11.0 R=6.56Å
% Fe_2O_3	3.33	-	-	4.80	-	-	4.32	4.43	4.43	≡6.45	5.64	5.71	5.71	≡6.45
% MnO	6.33	6.23	≡12.50	9.43	9.05	≡17.90	3.71	-	-	-	1.32	-	-	-
Mn - Mn Distance (Å)	8.23	8.23	-	7.19	7.19	-	9.84	-	-	-	13.94	-	-	-
re - Fe Distance (Å)	8.10	-	-	7.15	-	-	7.42	7.42	7.42	-	6.81	6.81	6.81	-
TM - TM Distance (Å)	6.48	-	6.48	5.69	-	5.69	6.59	-	-	6.59	6.56	-	-	6.56
$\frac{Fe^{2+}}{Fe_{total}}$ (%)	0.00	0.00	0.00	0.00	0.00	0.00	18.5	11.0	18.5	11.0	20.9	11.0	20.9	11.0
$\frac{Mn^{2+}}{Mn_{total}}$ (%)	90.0	85.8	81.5	90.0	81.0	78.0	00.0	00.0	00.0	00.0	00.0	00.0	00.0	00.0
Log ρ_{400K}	14.2	16.5	14.1	12.6	15.1	12.9	10.3	11.0	10.8	9.90	9.39	10.0	9.87	9.96
Log ρ_{500K}	11.6	13.4	11.4	10.3	12.2	10.5	8.51	9.12	8.93	7.85	7.61	8.30	8.07	7.85
Log ρ_{600K}	9.86	11.4	9.60	8.76	10.3	8.80	7.38	7.70	7.51	6.70	6.44	6.97	6.74	6.70
Activation Energy (eV)	1.07	1.25	1.11	.961	1.17	1.10	.766	.830	-	.785	.743	.795	-	.785

FIG. 4.1. REDOX RATIO AGAINST TIME SHOWING APPROACH TO EQUILIBRIUM OF a) MANGANESE AND b) IRON GLASSES

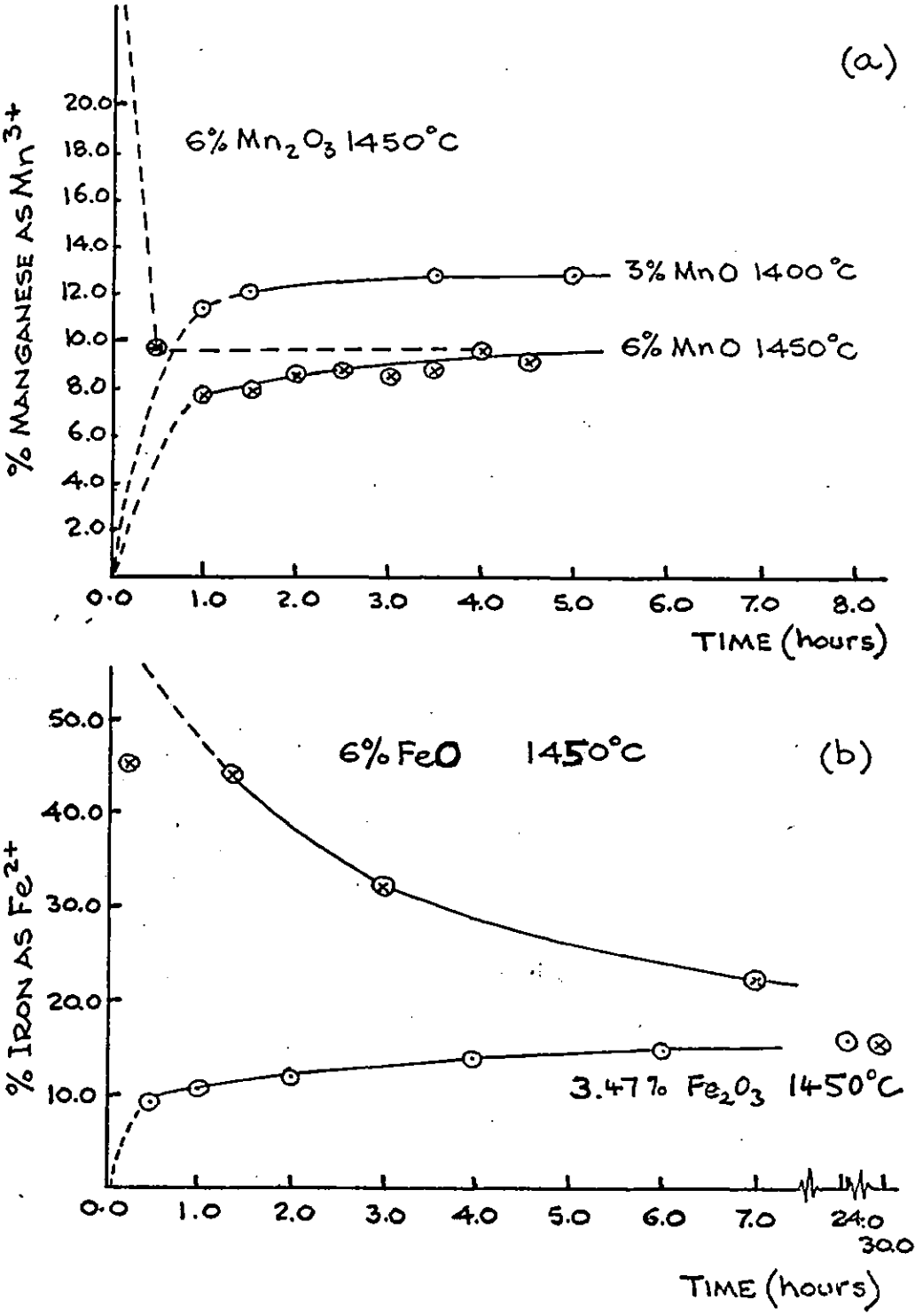

Fig 4.2 EFFECT OF THE TOTAL TM ION CONCENTRATION ON THE REDOX RATIO

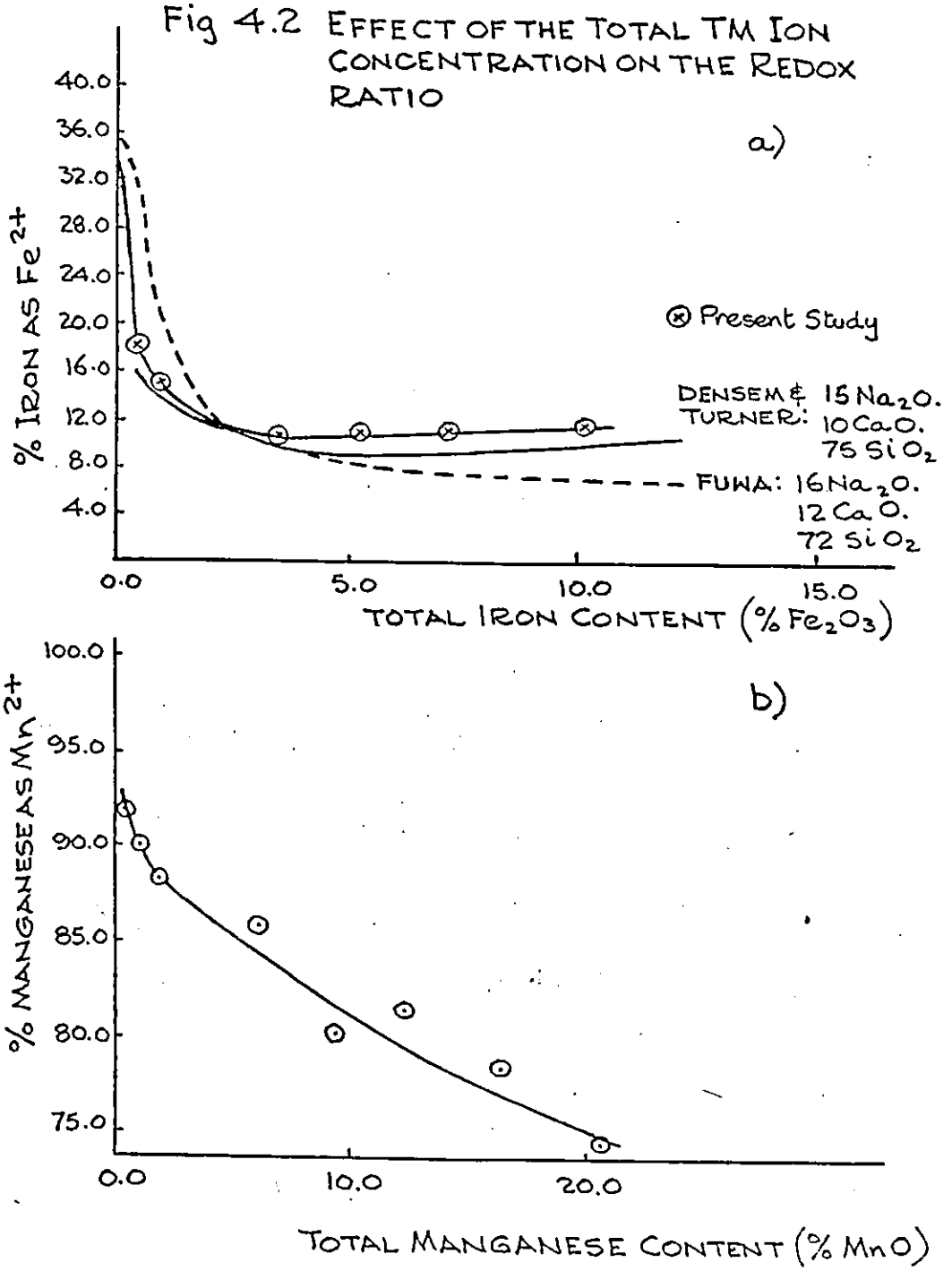

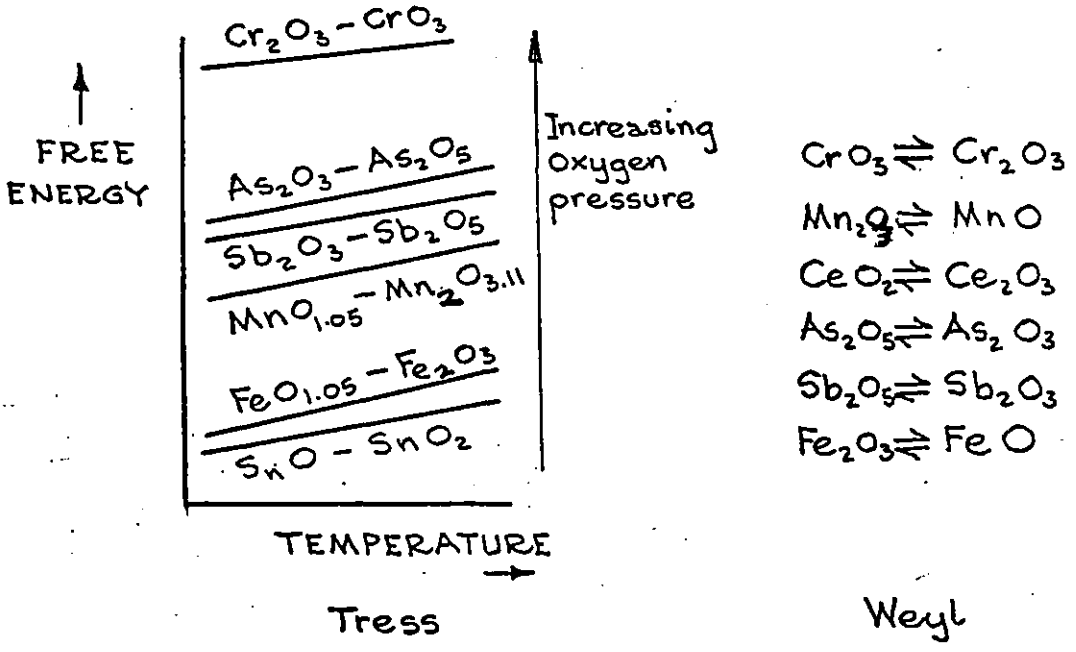

FIGURE 4.3 REDOX TABLES OF TRESS AND WEYL

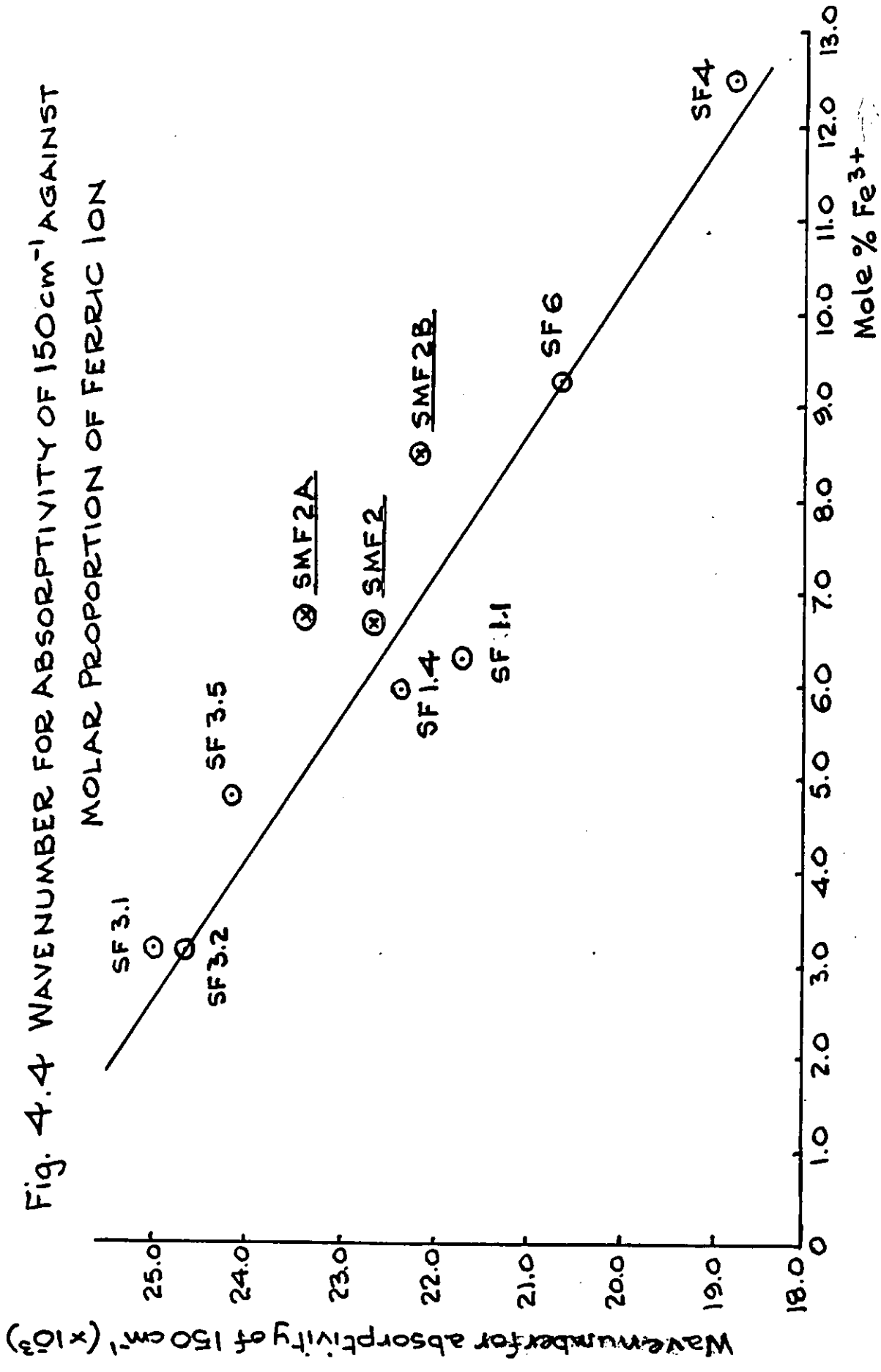

Fig. 4.4 WAVENUMBER FOR ABSORPTIVITY OF 150 cm^{-1} AGAINST MOLAR PROPORTION OF FERRIC ION

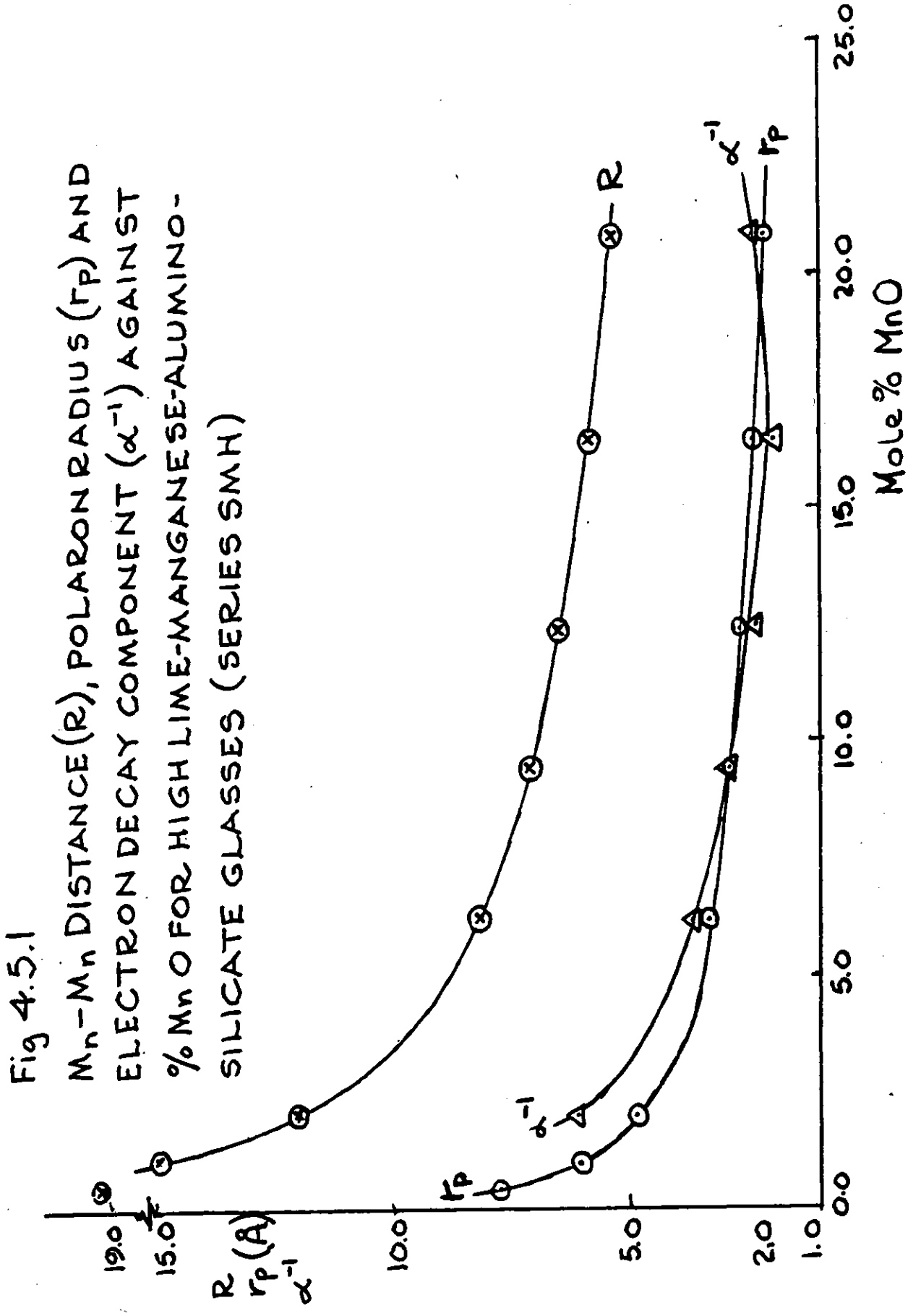
Fig 4.5.1
M_n-M_n DISTANCE (R), POLARON RADIUS (r_p) AND
ELECTRON DECAY COMPONENT (α^{-1}) AGAINST
% Mn O FOR HIGH LIME-MANGANESE-ALUMINO-
SILICATE GLASSES (SERIES SMH)
R
r_p
α^{-1}
R (Å)
r_p
α^{-1}
19.0
15.0
10.0
5.0
2.0
1.0
0.0
5.0
10.0
15.0
20.0
25.0
Mole % MnO

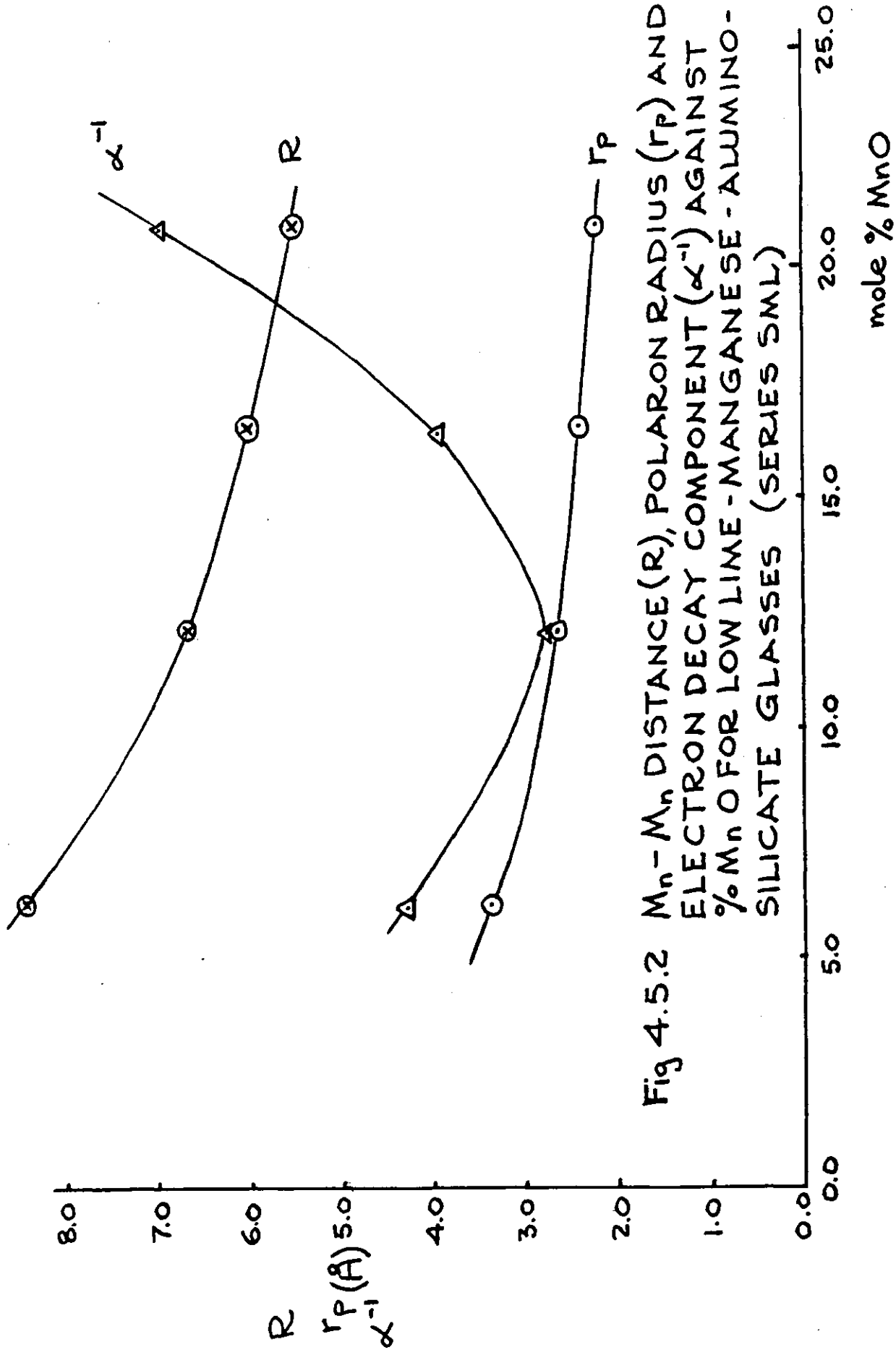

Fig 4.5.2 $M_n - M_n$ DISTANCE (R), POLARON RADIUS (r_p) AND ELECTRON DECAY COMPONENT (α^{-1}) AGAINST % Mn O FOR LOW LIME - MANGANESE - ALUMINO - SILICATE GLASSES (SERIES SML)

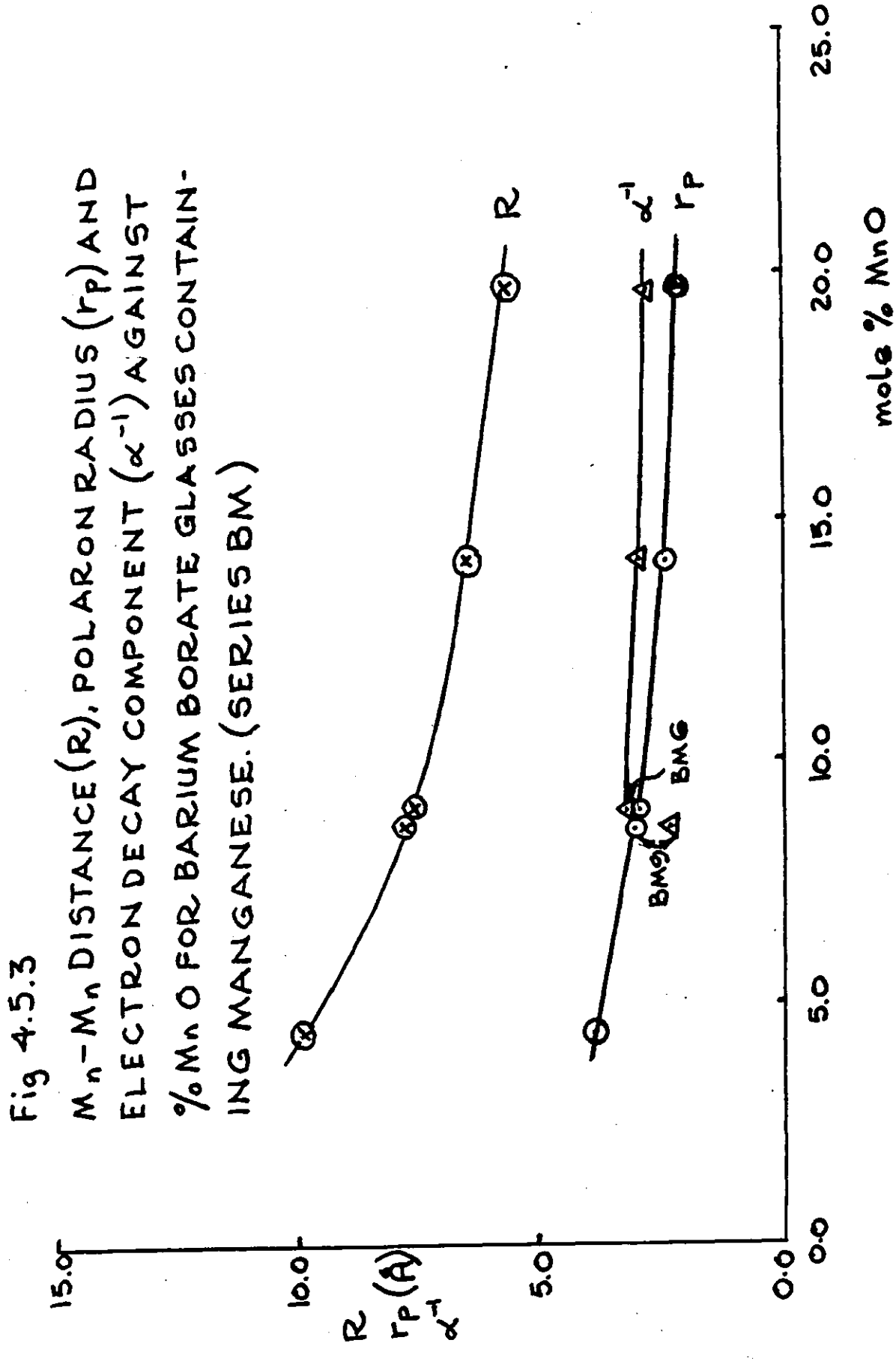

Fig 4.5.3
$M_n - M_n$ DISTANCE (R), POLARON RADIUS (r_p) AND ELECTRON DECAY COMPONENT (α^{-1}) AGAINST % $M_n O$ FOR BARIUM BORATE GLASSES CONTAINING MANGANESE. (SERIES BM)

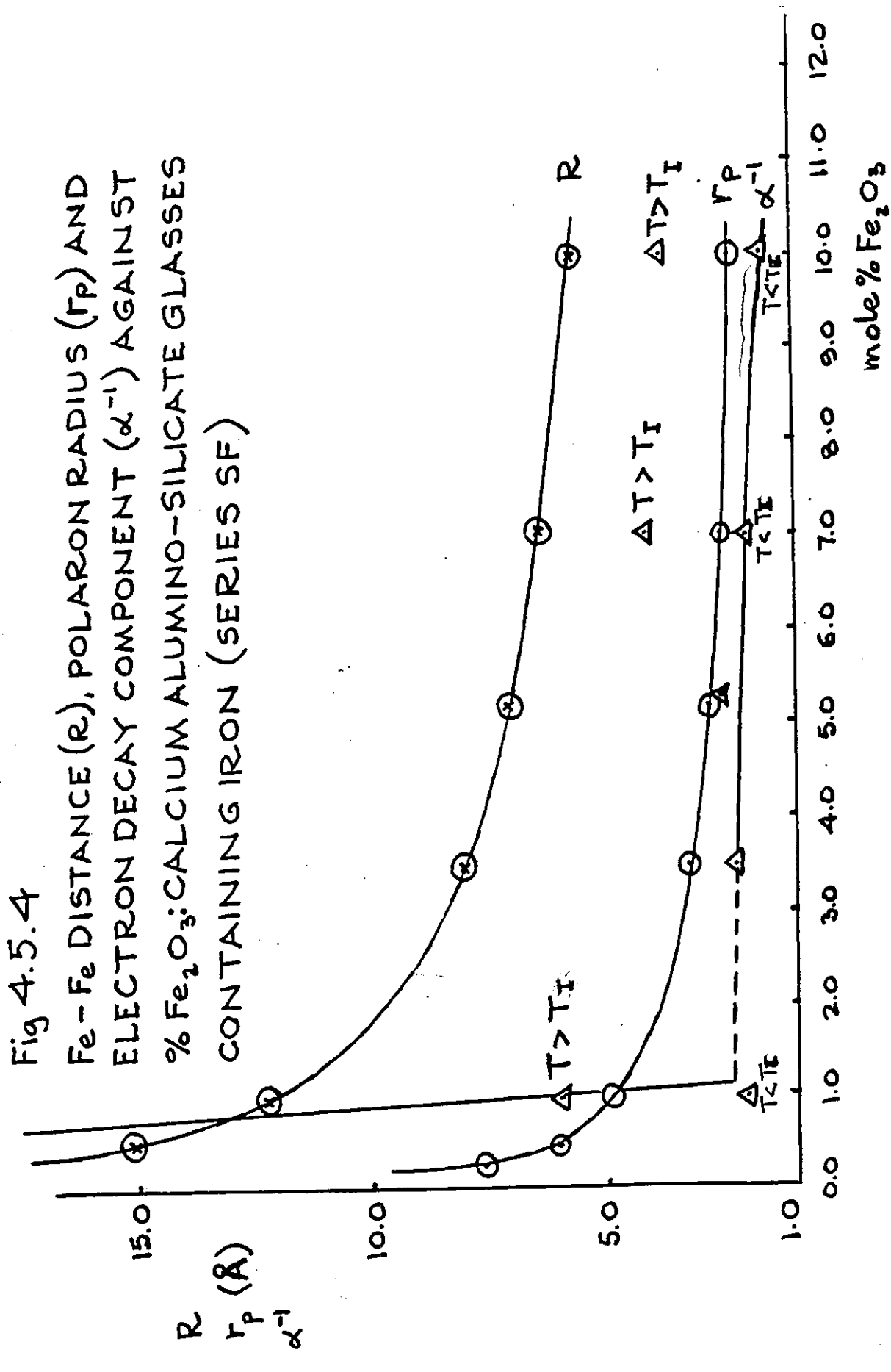
Fig 4.5.4
Fe - Fe DISTANCE (R), POLARON RADIUS (r_p) AND
ELECTRON DECAY COMPONENT (α^{-1}) AGAINST
% Fe_2O_3: CALCIUM ALUMINO-SILICATE GLASSES
CONTAINING IRON (SERIES SF)
R
r_p
α^{-1}
(Å)
15.0
10.0
5.0
1.0
0.0
1.0
2.0
3.0
4.0
5.0
6.0
7.0
8.0
9.0
10.0
11.0
12.0
mole % Fe_2O_3
R
r_p
α^{-1}
$\Delta T > T_I$
$\Delta T > T_I$
$T > T_I$
$T < T_I$
$T < T_I$
$T < T_I$

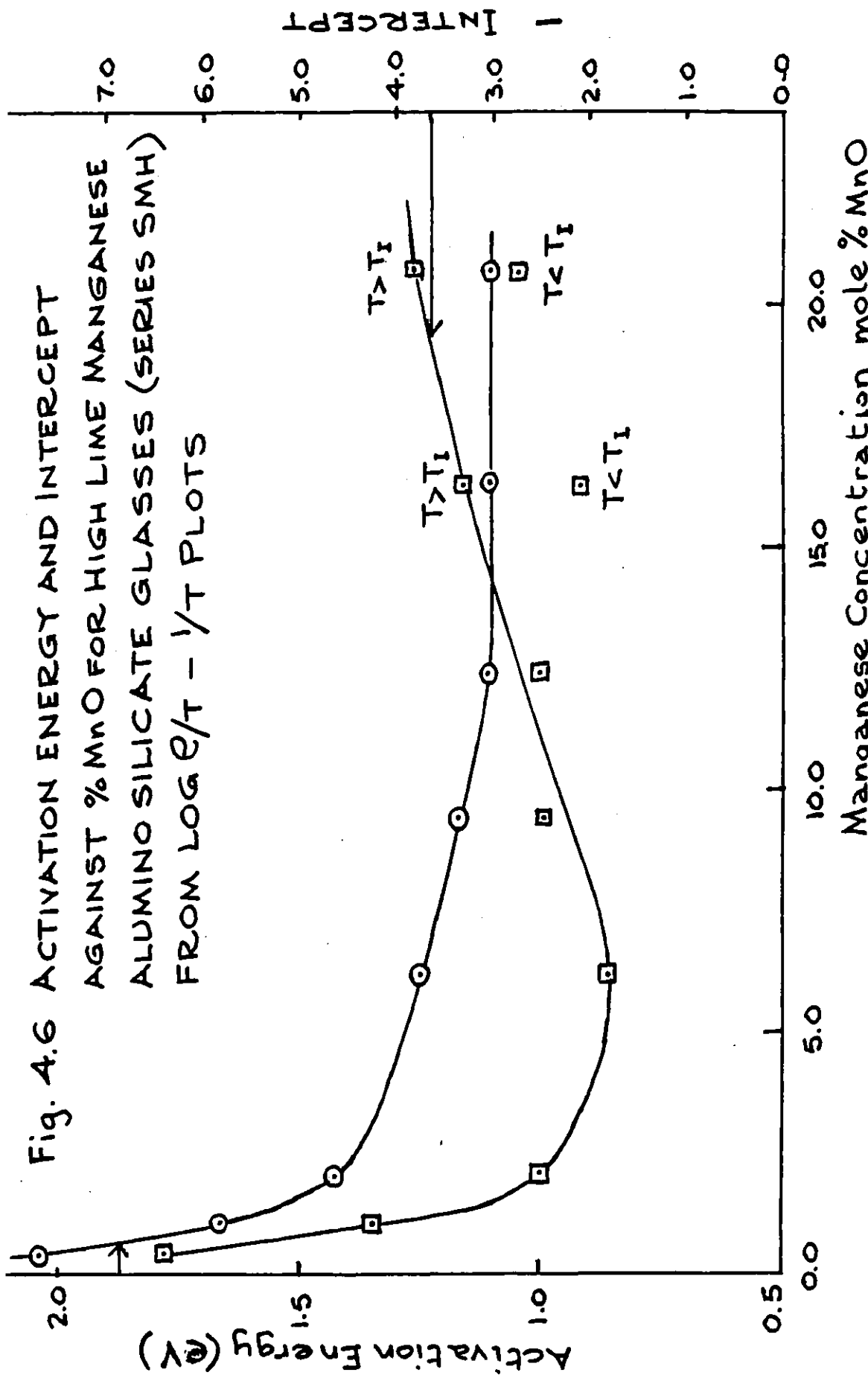

Fig. 4.6 ACTIVATION ENERGY AND INTERCEPT AGAINST % MnO FOR HIGH LIME MANGANESE ALUMINO SILICATE GLASSES (SERIES SMH) FROM LOG $\rho/T - 1/T$ PLOTS

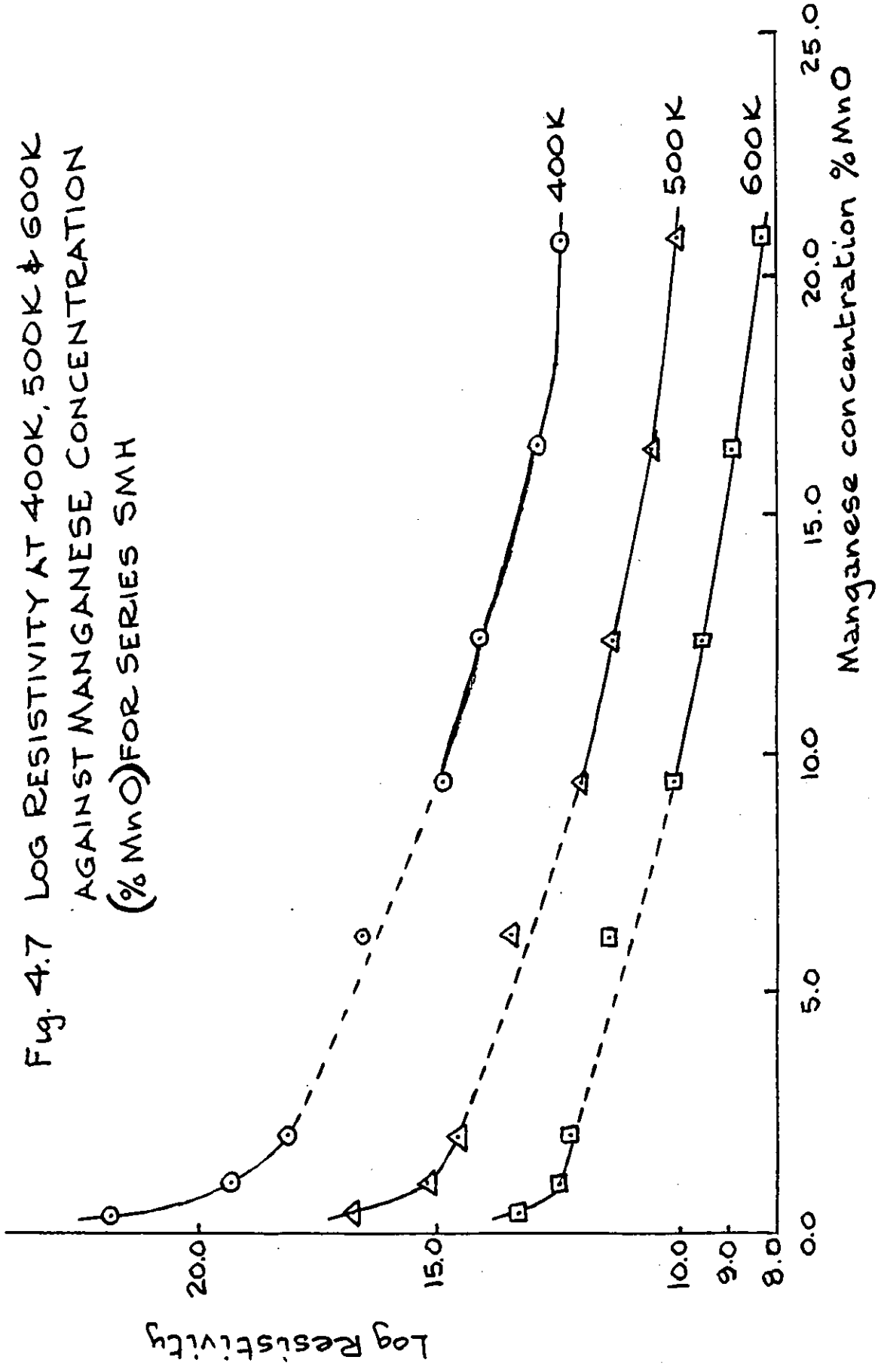

Fig. 4.7 LOG RESISTIVITY AT 400K, 500K & 600K AGAINST MANGANESE CONCENTRATION (% MnO) FOR SERIES SMH

Fig 4.8 ACTIVATION ENERGY AND LOG RESISTIVITY AT 400K, 500K AND 600K AGAINST MEAN SEPARATION OF MANGANESE IONS. (SERIES SMH)

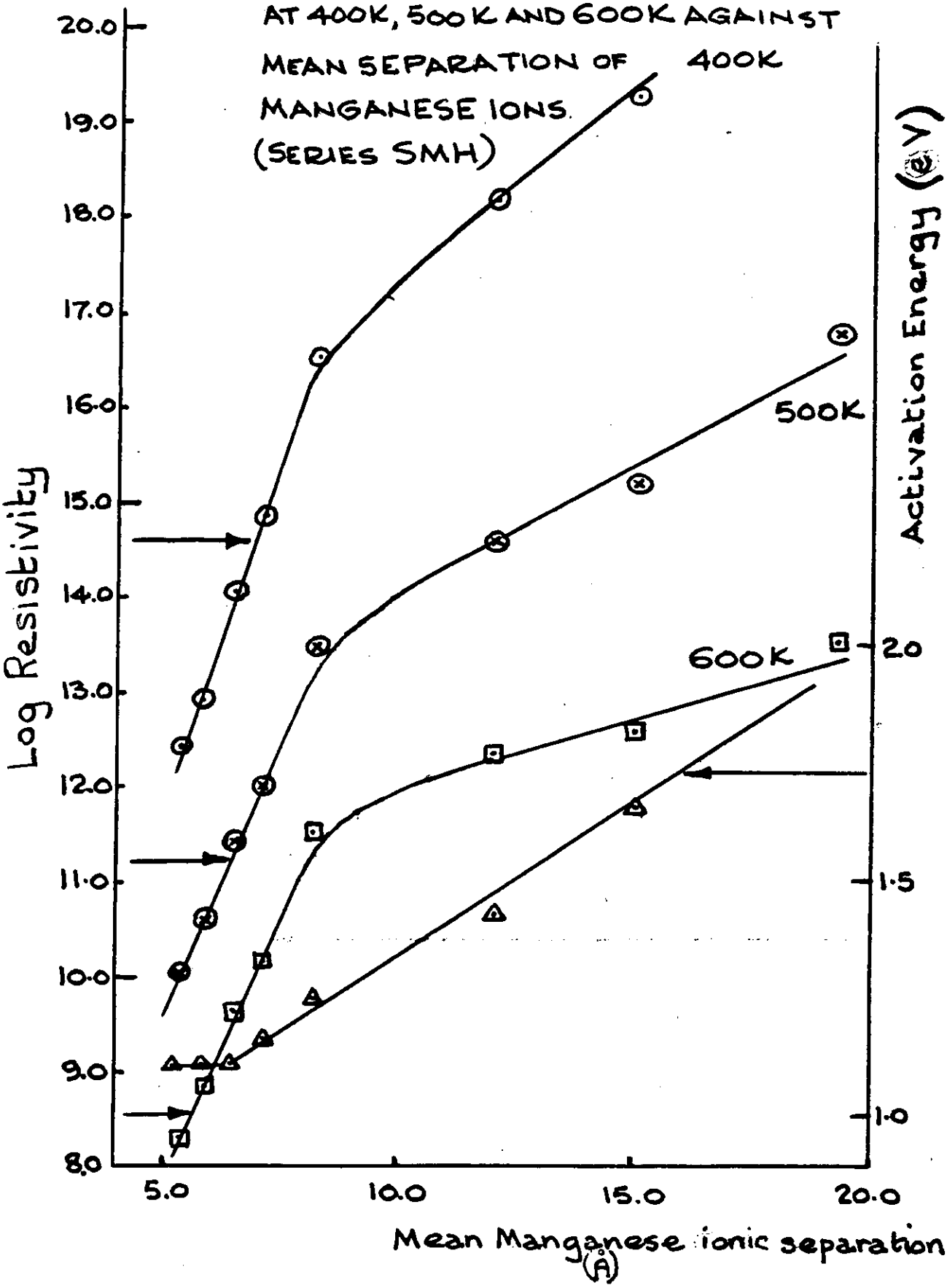

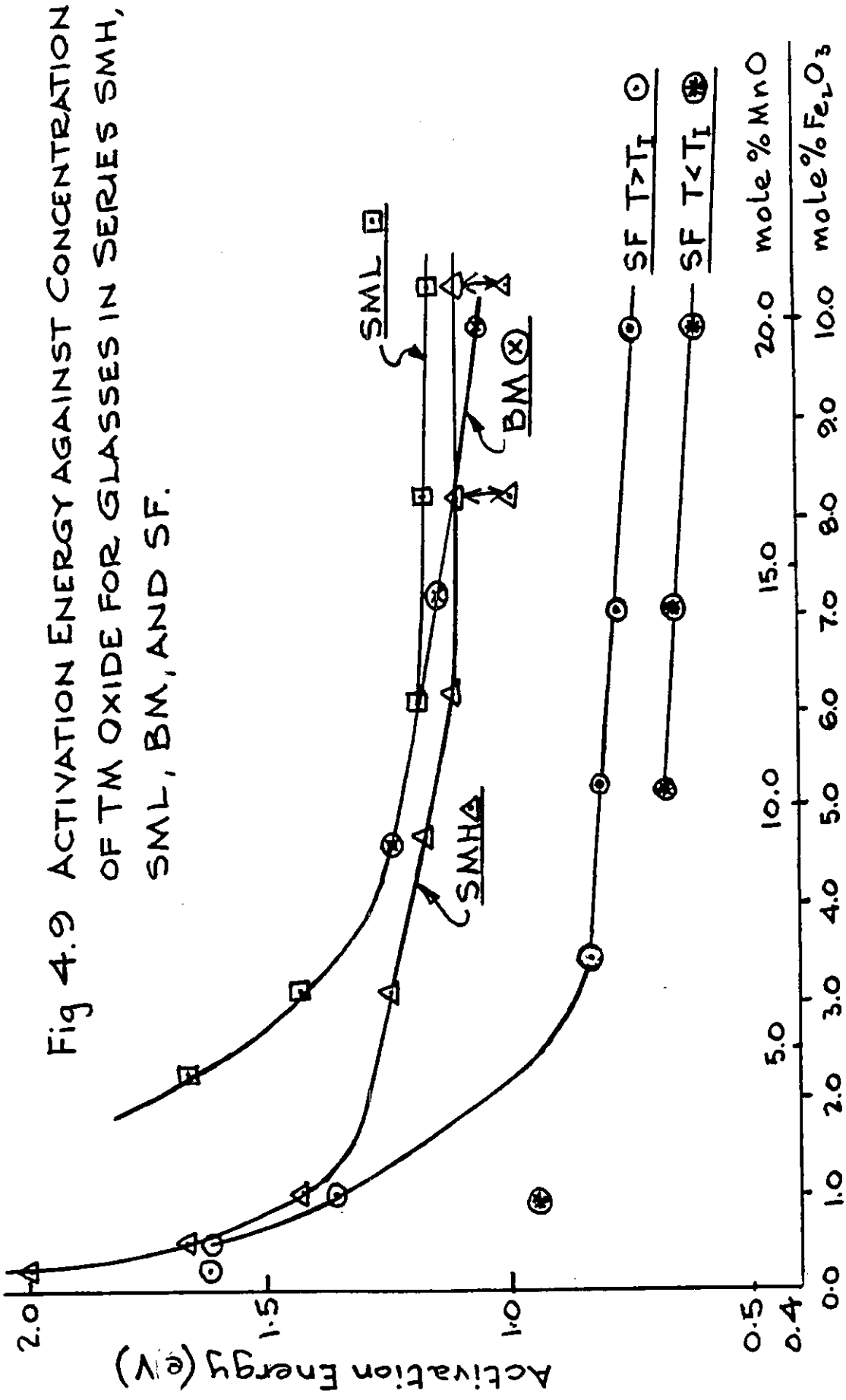

Fig 4.9 Activation Energy against Concentration of TM Oxide for Glasses in Series SMH, SML, BM, and SF.

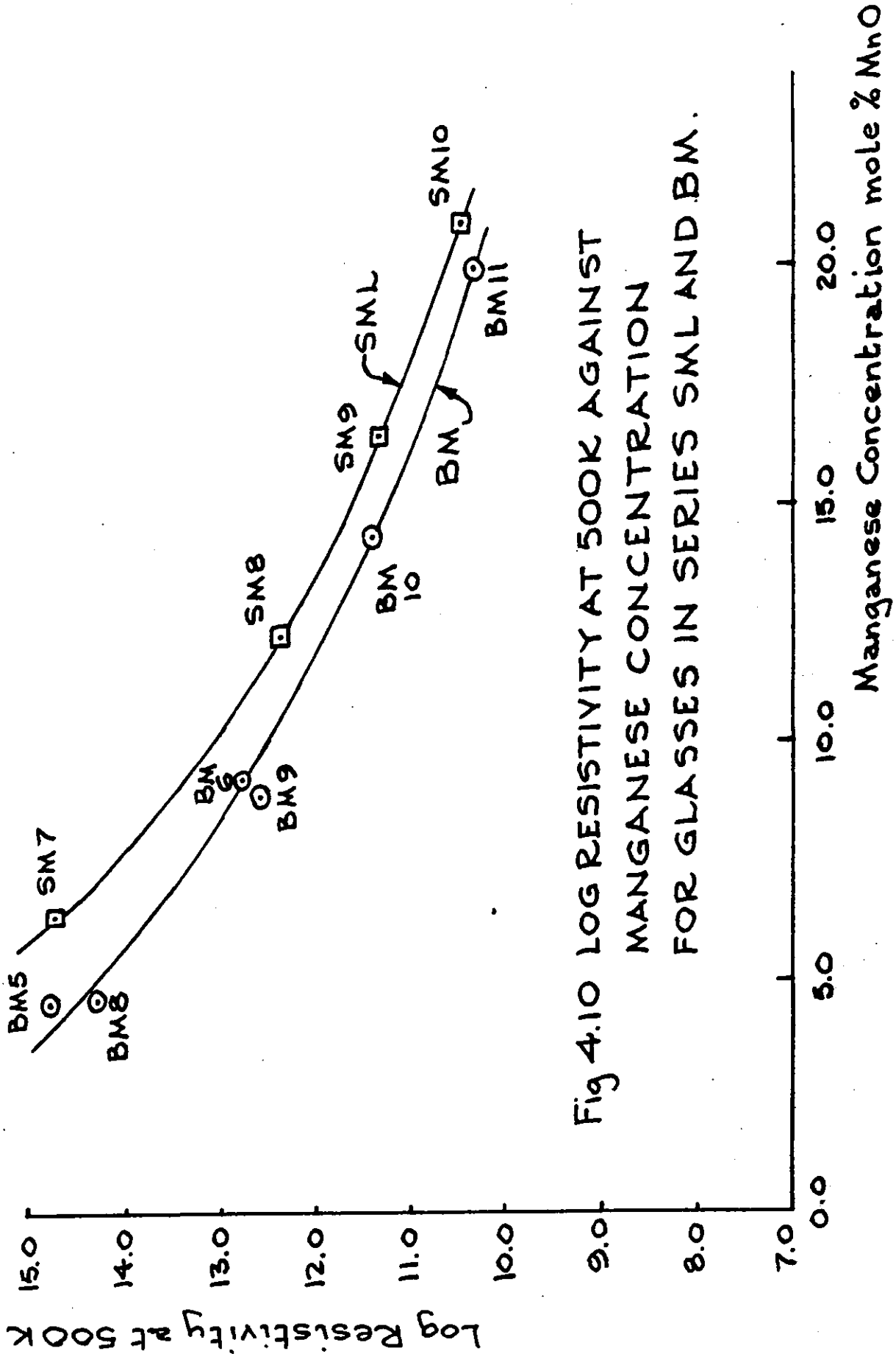

Fig 4.10 LOG RESISTIVITY AT 500K AGAINST MANGANESE CONCENTRATION FOR GLASSES IN SERIES SML AND BM.

Fig 4.11 ACTIVATION ENERGY AND LOG ρ_{500K} AGAINST MEAN SEPARATION OF MANGANESE IONS; SERIES SML AND BM

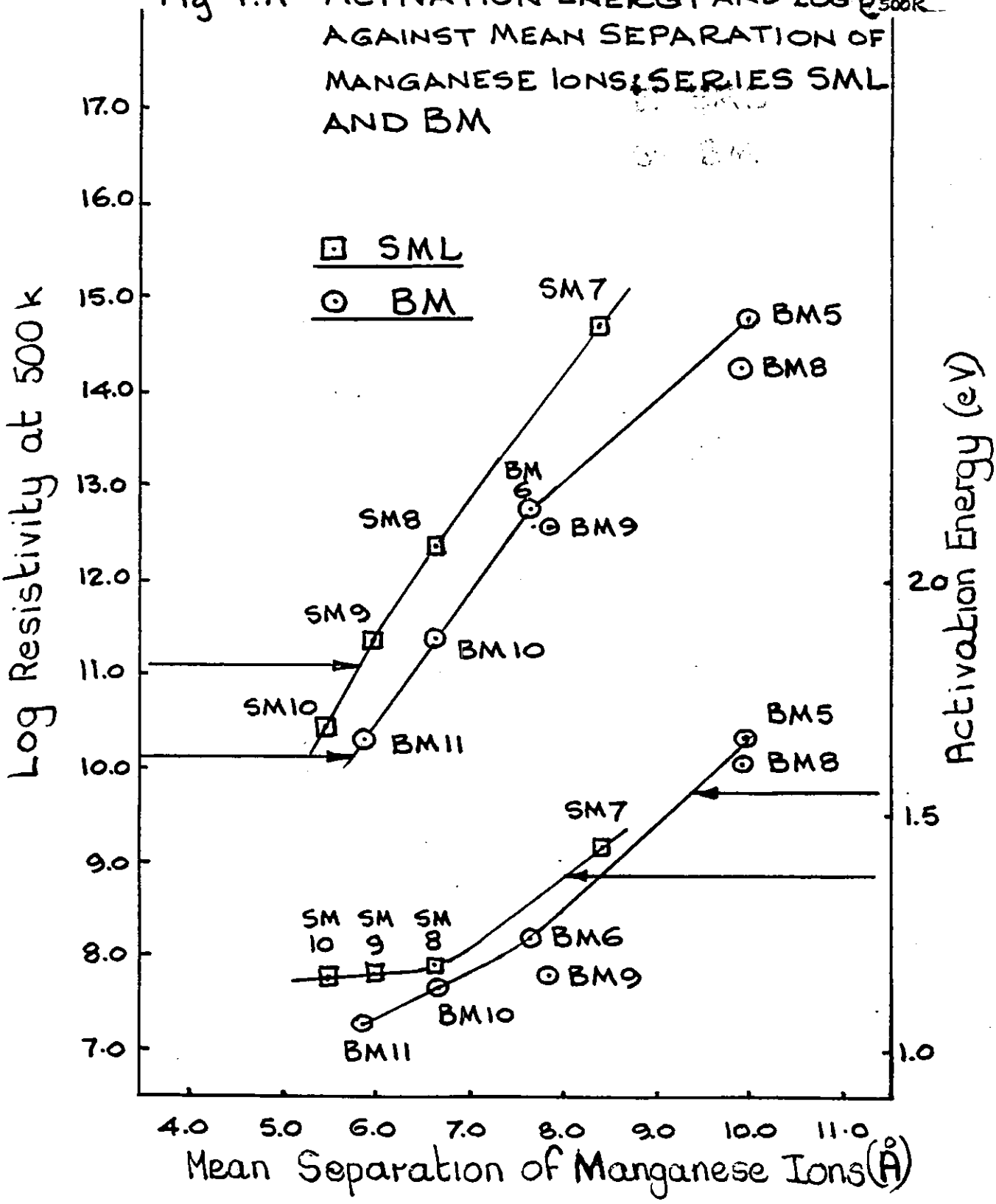

Fig 4.12 ACTIVATION ENERGY AGAINST MEAN SEPARATION OF IRON IONS (SERIES SF)

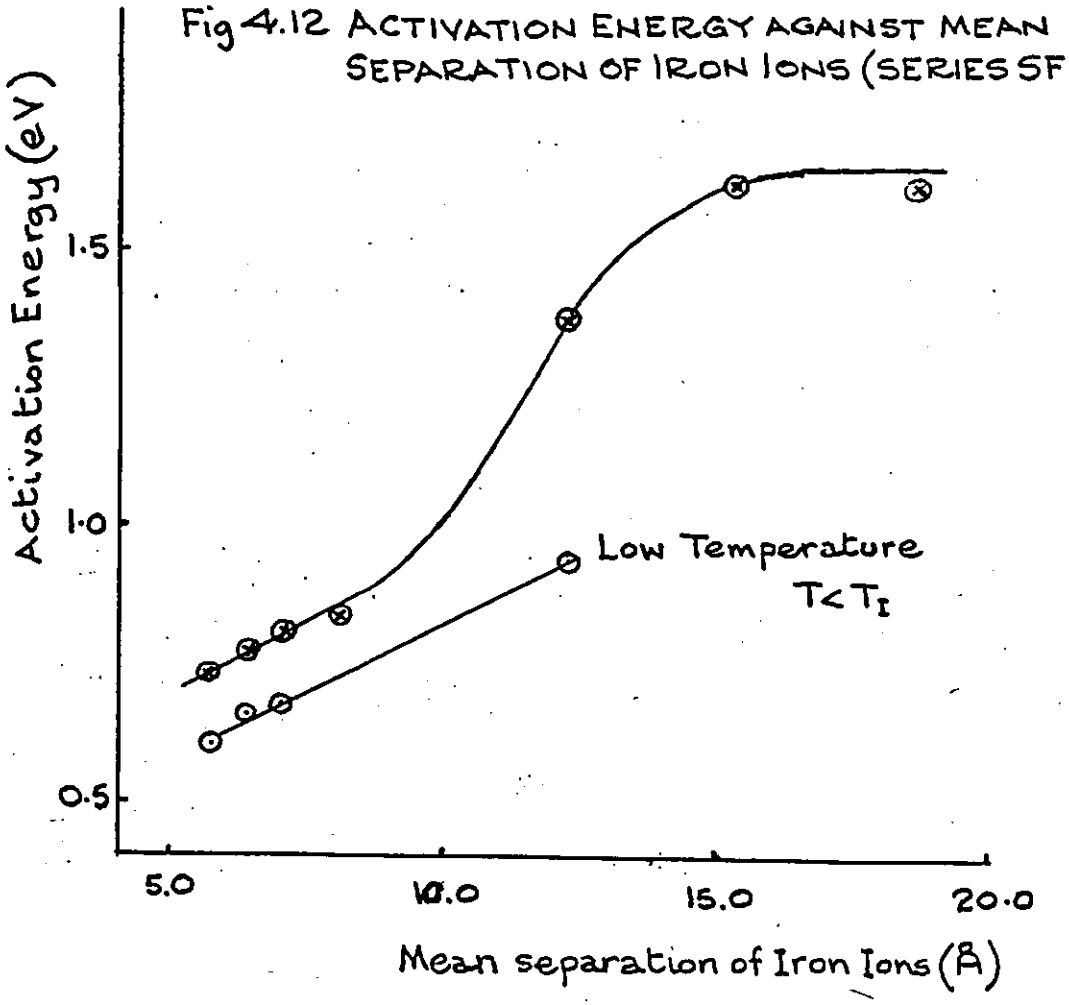

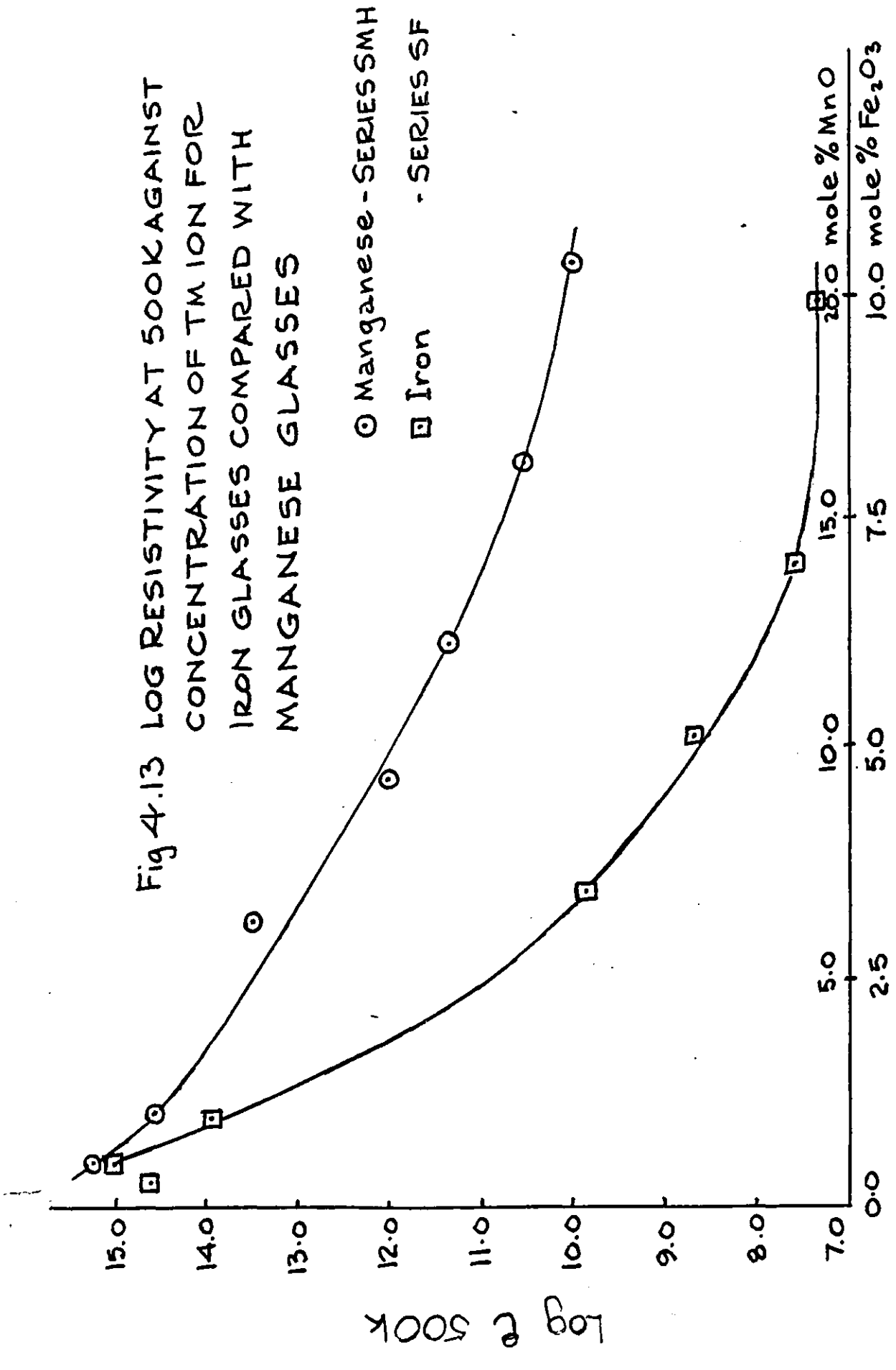
Fig 4.13 LOG RESISTIVITY AT 500K AGAINST CONCENTRATION OF TM ION FOR IRON GLASSES COMPARED WITH MANGANESE GLASSES
⊙ Manganese - SERIES SMH
⊡ Iron - SERIES SF
log ρ 500K
15.0
14.0
13.0
12.0
11.0
10.0
9.0
8.0
7.0
0.0
5.0
10.0
15.0
20.0 mole % MnO
2.5
5.0
7.5
10.0 mole % Fe2O3

Fig 4.14 LOG ρ AT 400K AND 600K AGAINST MEAN SEPARATION OF IRON IONS (SERIES SF)

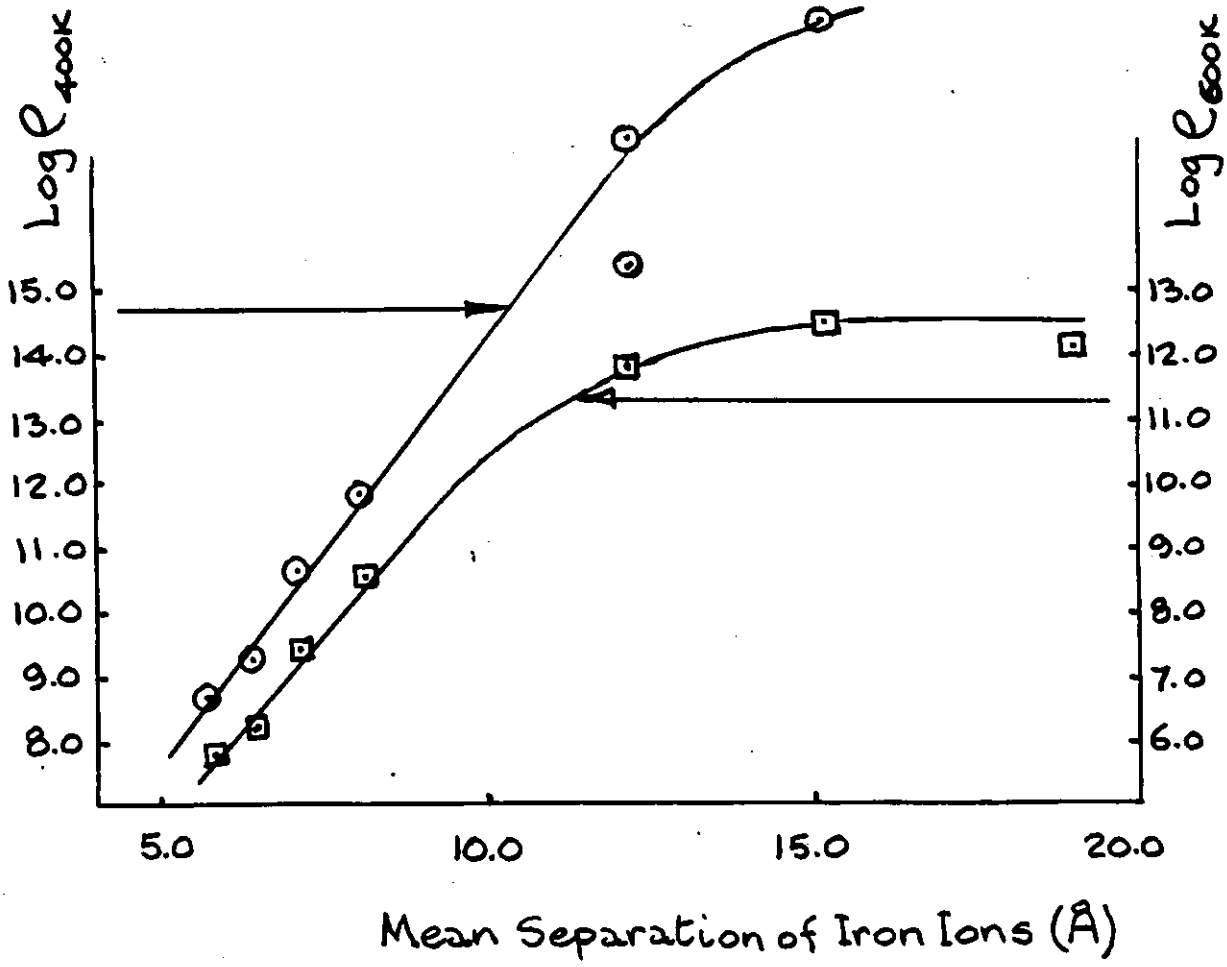

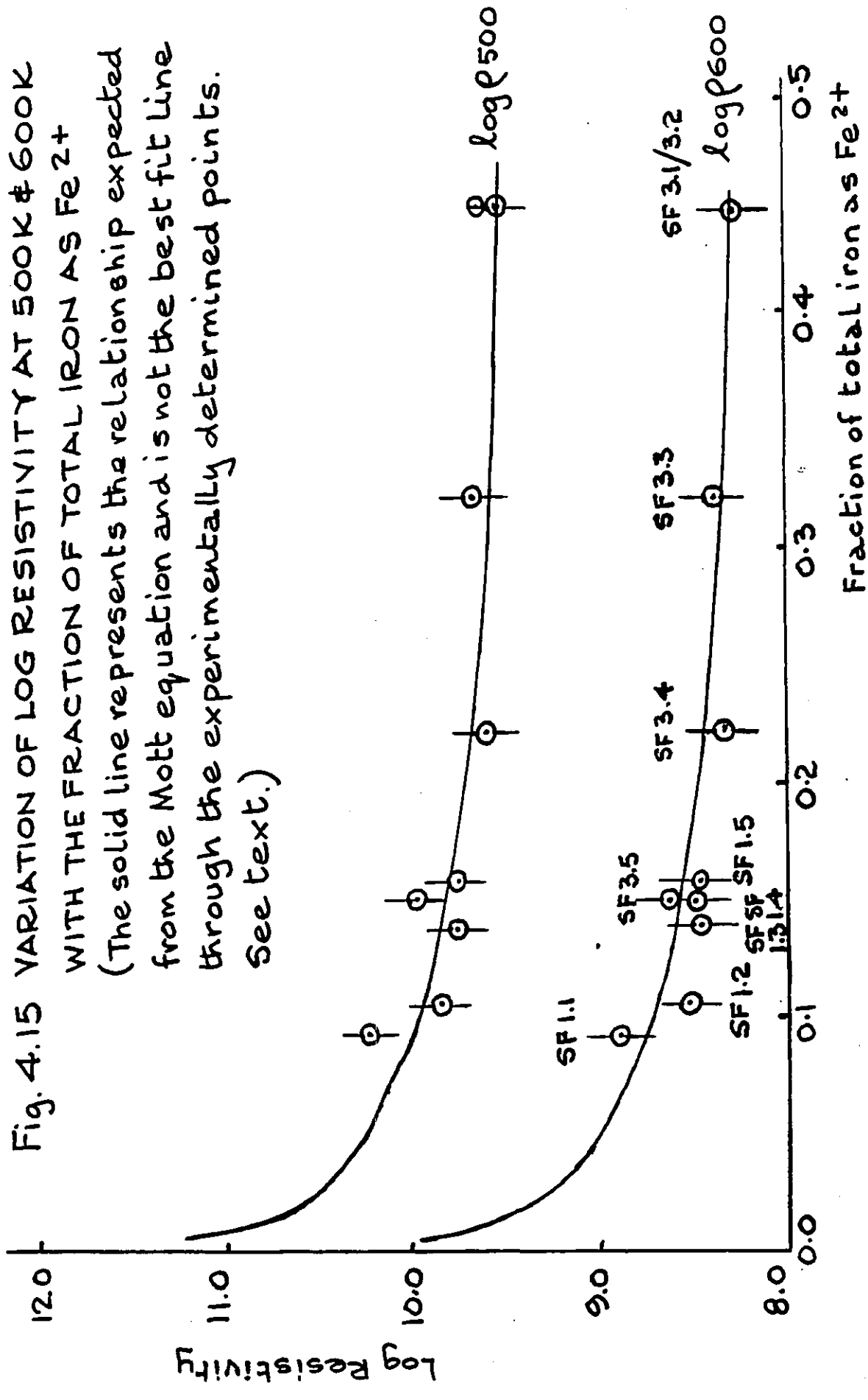

Fig. 4.15 VARIATION OF LOG RESISTIVITY AT 500K & 600K WITH THE FRACTION OF TOTAL IRON AS Fe^{2+}
(The solid line represents the relationship expected from the Mott equation and is not the best fit line through the experimentally determined points. See text.)

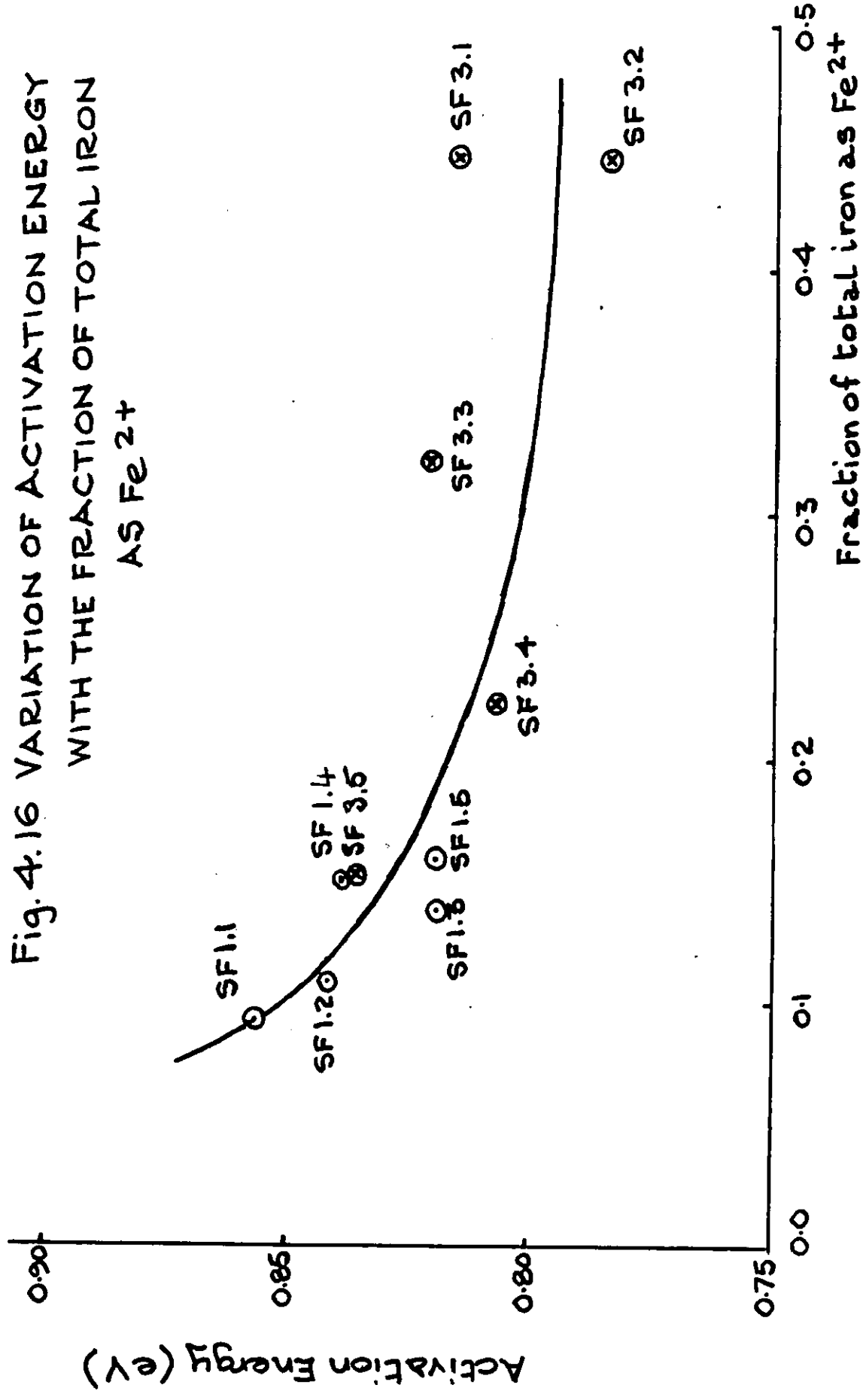

Fig. 4.16 VARIATION OF ACTIVATION ENERGY WITH THE FRACTION OF TOTAL IRON AS Fe^{2+}

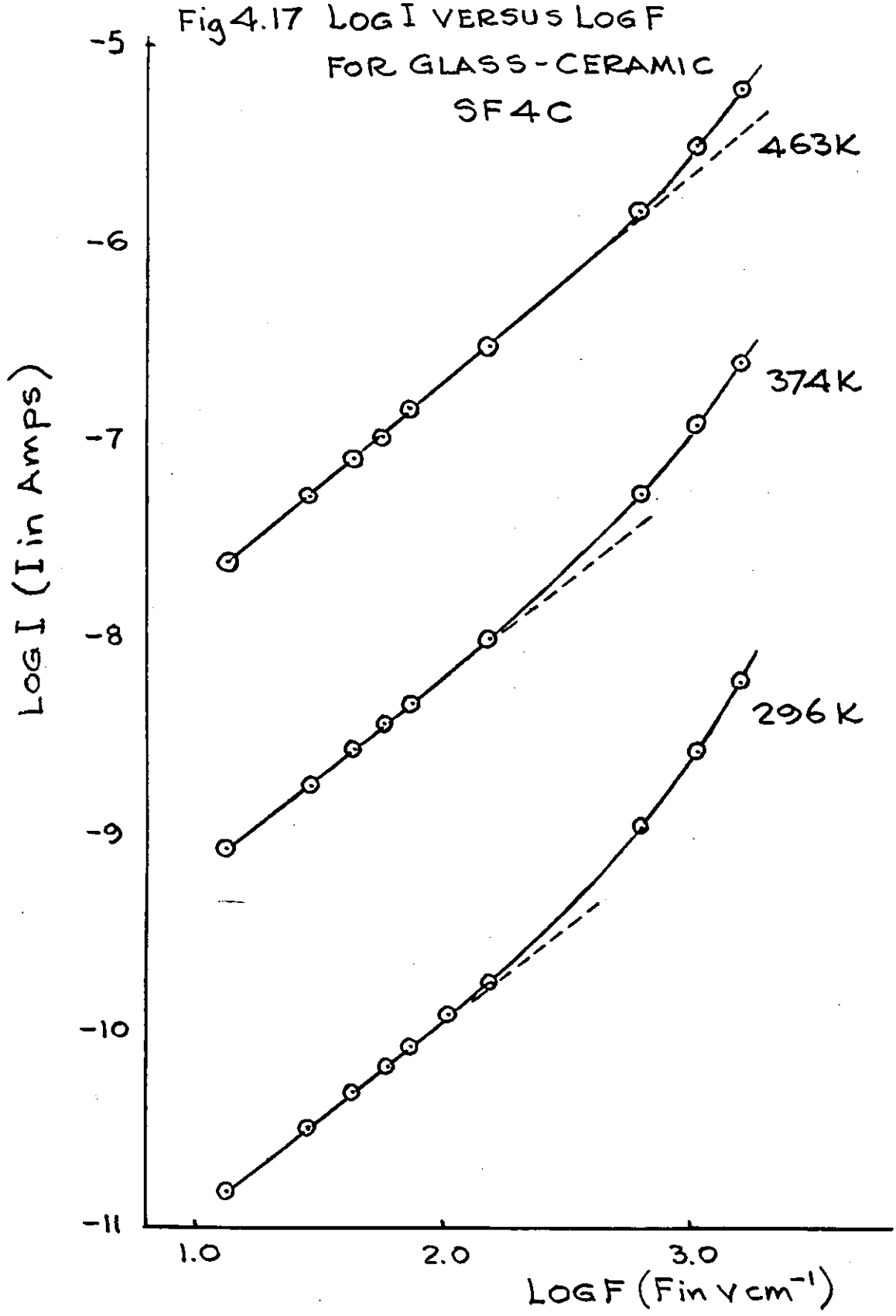
Fig 4.17 LOG I VERSUS LOG F
FOR GLASS-CERAMIC
SF4C
463K
374K
296K
-5
-6
-7
-8
-9
-10
-11
LOG I (I in Amps)
1.0
2.0
3.0
LOG F (F in V cm⁻¹)

CHAPTER 5

CONCLUSIONS AND SUGGESTIONS FOR FURTHER WORK

5.1 Conclusions

Two series of calcium aluminosilicate and one series of barium borate glasses have been prepared containing up to 20% MnO. In all of these glasses the divalent redox state predominated and it was difficult to obtain high proportions of Mn^{3+} (>20%). It was found that production of Mn^{3+} was favoured by: high total manganese concentrations, high glass basicity and lower melting temperatures.

Studies of dc conductivity in these glasses revealed that the log ρ/T - $1/T$ plots for concentrated glasses in one silicate series (SMH) showed two slope behaviour, whereas the other glasses were characterised by a single gradient. The conductivity behaviour in the lower temperature range for the 'two slope' glasses was well described by the Mott equation and a small polaron hopping conduction mechanism in the non-adiabatic regime was therefore appropriate. The condition for small polaron formation ($\alpha^{-1} < r_p < R$) was generally obeyed for these glasses in this temperature range. At higher temperatures the values of α^{-1} calculated from the intercept of the above plot at $1/T = 0$ were generally greater than the polaron radius calculated by Bogomolov's equation. This was also the case for the other glasses containing greater than 7% MnO and which showed a single slope in the log ρ/T - $1/T$ plot. However, in view of the similarity in behaviour of all these glasses and the small difference between 'high' and 'low' temperature activation energies, a small polaron conduction mechanism with abnormally high values of α^{-1} has been suggested. Such high values of α^{-1} are a direct consequence of the high activation energy of these glasses. The difference between the two slopes corresponded to a change in activation energy of $\sim$0.1 eV and this behaviour has been explained by introducing a structural differences term (ΔU) into the activation energy, to account for coordination differences between donor and acceptor sites. Conduction in all cases, except at low temperatures for glasses for which 'two slope' behaviour was observed, was between tetrahedrally coordinated Mn^{2+} and octahedrally coordinated Mn^{3+} ions. For concentrated glasses in series SMH it is proposed that some octahedrally coordinated Mn^{2+} was also present which dominated the conduction process at lower temperatures since the activation energy is lower for $Mn^{2+} \rightarrow Mn^{3+}$

transfers with both ions in octahedral sites. However, it has not been possible to confirm the coordination of Mn^{2+} with the spectroscopic techniques used. The presence of different sites with different hopping probabilities could also give rise to difficulties in the calculation of α^{-1} which might therefore also explain the high values observed.

Comparison of results between these three different glass systems has been used to provide information on the effect of base glass composition and glass former. These effects are complicated and changes in conductivity between different glass systems with identical proportions of TM ions are brought about by changes in both macroscopic and microscopic parameters. The macroscopic parameters identified included the redox ratio and density, since these affect the number of carriers and interionic spacing respectively, with the latter having a pronounced effect on the activation energy. Microscopic changes in glass structure and also in the polarizability of the oxygen ions and oxygen-cation bonding are also important since they affect the activation energy by altering the high frequency dielectric constant.

One series of calcium aluminosilicate glasses containing iron has also been prepared to compare with the manganese glasses. In these glasses iron was present mainly in the oxidised state. In a similar way to glasses in series SMH, glasses with high iron concentrations showed two slope behaviour which has been explained in an analogous way by proposing the existence of octahedrally coordinated Fe^{3+} in these glasses. In all of the glasses the presence of octahedrally coordinated Fe^{2+} and some tetrahedral Fe^{3+} was concluded from optical absorption spectroscopy. A small polaron hopping conduction mechanism was appropriate for glasses containing $\geq 3.5\%$ Fe_2O_3 and this was further confirmed by plotting log ρ against the redox ratio. A broad minimum was observed at $c \sim 0.5$ as predicted by the Mott equation; however, the activation energy also showed a minimum which was only poorly described by the theoretical dependence of W_H on c derived by Isard[163] using small polaron theory. Experimental error could possibly account for this.

Comparison of manganese and iron glasses revealed that the conductivity was higher in the iron glasses chiefly because of the lower activation energy. The activation energies of the manganese glasses were high (> 1 eV) even for the highest proportions of total manganese and Mn^{3+}. This has been tentatively explained in terms of tighter bonding of the 'extra' electron to the reduced Mn^{2+} ion since this ion has a

stable d^5 configuration compared to d^6 for Fe^{2+}. The polaron is therefore much more localized on the reduced ion in manganese glasses as a result of the greater polaron binding energy and this has been confirmed by simple calculations.

The dependence of the activation energy on the interionic spacing was analysed by the method described by Isard[163] assuming the polaron localization (r) was a constant in any series. Agreement for series SF, SML and BM was good but series SMH showed an almost constant activation energy energy at higher concentrations which required that r increased slowly with R. Such a change does seem physically reasonable although it was concluded that this was probably the result of experimental uncertainties to reconcile the behaviour of series SMH with the other manganese glasses.

The conductivity showed a marked dependence on R as predicted by the Mott equation but as the magnitude of R increased above 8 - 9 Å this dependence became less and the activation energy increased. The Mott equation was no longer applicable in this region and it would seem that such a distance reflects the limit at which polaron hopping between TM ions becomes unfavourable. At this and slightly greater distances some indirect hopping via an intermediate state, such as the band edge, may occur although this would need to be proved by further work. Eventually electronic or polaronic processes died out completely and conduction was by impurity alkali ions, hydroxyl ions or protons with the TM concentration having no effect on the conductivity. Activation energies in this compositional range ($\leq$2% MnO, $\leq$1% Fe_2O_3) were in the range of 1.4 - 1.7 eV which is typical of ionic mechanisms and similar to the value of the undoped base glass.

Some mixed iron-manganese glasses were also prepared and it was concluded from optical absorption spectroscopy that Mn^{3+} and Fe^{2+} did not coexist in these glasses. Hence only three of the possible four states were observed. The electrical conductivity was typical in magnitude to that expected for the element present in two oxidation states. The single oxidation state of the second TM element seemed to exert a real effect since the resistivity and activation energy were lower than would be predicted by only considering conduction involving the element present in two states. The TM-TM distance was the dominant parameter, hence it is suggested that the ion of the second element can reduce the conductivity by some kind of interaction which may differ in glasses containing Mn^{3+}, Mn^{2+} and Fe^{3+} to those containing Mn^{2+}, Fe^{2+} and Fe^{3+}.

In the former case some Fe^{3+} ions acted as acceptor sites and it was thought that $Mn^{2+} - Fe^{3+} - Mn^{3+}$ associates were formed which reduced R. In the second case it did not seem energetically favourable for Mn^{2+} ions to act as donor sites because of the higher polaron binding energy compared to Fe^{2+}. Therefore an indirect interaction via changes in the glass structure and hence in the dielectric constant, has been proposed. The presence of some interaction between ions of the two elements was also suggested by the behaviour of the cut-off edge in the optical absorption spectra which shifted to lower wavelengths than would have been expected from the individual ionic concentrations. Changes in the EPR spectra for these glasses could also be attributed to such an interaction.

In addition to dc resistivity measurements, ac measurements have also been made which, in most cases, were in support of polaron hopping between adjacent sites.

The crystallization behaviour of the glasses revealed that Mn^{3+} concentrations of greater than 2.3% acted as effective nucleating agents and in most cases a manganese rich phase developed along with the major silicate crystalline phase: gehlenite for series SMH and anorthite for series SML. Iron concentrations of greater than 5% promoted the production of fine grained glass-ceramics with a pyroxene as the major phase. In the mixed glasses identification of the major phases was uncertain although compositions were related to gehlenite and wollastonite with possible substitutions of iron and manganese for Ca^{2+} and Al^{3+}.

Analysis of the dielectric properties of the glass-ceramics revealed the presence of peaks in the dielectric loss which have been attributed to Maxwell-Wagner-Sillars loss of these inhomogeneous dielectrics. Some of the iron glass-ceramics also showed non-ohmic dc conductivity behaviour possibly because of the presence of small conducting crystals in an insulating matrix. In each case the changes in dc conductivity on crystallization have been correlated with the microstructure of the glass-ceramics and four main effects have been identified; growth of an insulating crystalline phase which caused an increase in conductivity; segregation of one TM oxidation state into a crystalline phase which caused a decrease in conductivity; growth of discrete crystallites of a mixed valence phase which decreased the dc conductivity but increased the ac conductivity and finally, growth of a contiguous mixed valence phase which produced the most dramatic decreases in both resistivity and activation energy.

5.2 Suggestions for Further Work

Two categories of further work should be considered; that intended primarily to confirm the conclusions of the present study by supplying additional information and more general work to extend the study into new areas.

In the first category, considerable uncertainty exists concerning the coordination of the Mn^{2+} and Fe^{3+} ions and further spectroscopic measurements are required to resolve this. Mössbauer spectroscopy would be the most appropriate for iron glasses although other techniques may also be applicable. More work is also needed to identify some of the crystalline phases produced in the glass-ceramics since it is possible that some of these phases may not have been observed in glass-ceramics before.

When considering extension of the work it should be remembered that although a considerable amount of information now exists on electronic conduction in various glass systems, this has been obtained on a relatively small number of systems compared to the wide range of TM oxide glasses possible. Of the first row TM elements only Cr, Co and Ni have not received much attention and a study of these ions would prove valuable. Attempts to produce larger fractions of the oxidised redox states in Co and Ni glasses by novel glass-forming techniques would be worthwhile for comparison with manganese glasses.

The conduction processes in mixed TM systems have still not been resolved and a number of different effects may be operating. Further study of a variety of mixed glass systems would be of interest to clarify this area particularly with regard to ionic interactions.

Finally, the effect of crystallization on conductivity is a vast subject which has received little attention and more work is required. The growth of semiconducting crystalline phases in glass-ceramics is an area which could produce useful materials and should be pursued.

ACKNOWLEDGEMENTS

The author would like to express his thanks to all the members of the academic and technical staff of the department of Metallurgy and Materials Science at Imperial College who have assisted in various ways with this project; especially Dr J. Humphreys for his advice on high voltage electron microscopy and Dr J.F. Gibson, of the Chemistry department, for his assistance with the EPR measurements. In particular the author wishes to thank his supervisor, Dr J. Williamson, for his continual help, guidance and encouragement throughout the period of this work.

Of his friends and relatives who have assisted in various ways the author is especially grateful to Mr Phil Williams for reading and commenting on the text of this thesis and also his father-in-law, Mr Paul Barker, for carefully drawing the figures. Thanks are also due to his parents and parents-in-law for their encouragement and to his wife, Jenny, for her love, patience and practical help during the period of writing up.

Finally, the provision of a research studentship by the Science Research Council is gratefully acknowledged.

REFERENCES

1 E.P. Denton, H. Rawson and J.E. Stanworth, Nature 173 (1954) 1030.

2 As this section is a general review individual references have not always been given. A good survey paper containing these references is:
D.R. Uhlmann, Survey Papers: XIth Int. Congress on Glass, (1977).

3 C.R. Masson, XIth Int. Congress on Glass, (1977).

4 A summary and criticism of these theories along with the original references is given in:
H. Rawson, Inorganic Glass-Forming Materials, Academic Press, (1967).

5 D. Turnbull and J.C. Fisher, J. chem. Phys. 17 (1949) 71.

6 A good review of this topic is given in:
D.R. Uhlmann and A.G. Kolbeck, Physics Chem. Glasses 17 (1976) 146.

7 W.B. Hillig and D. Turnbull, J. phys. Chem. 24 (1956) 914.

8 F.E. Wagstaff, J. Am. Ceram. Soc. 52 (1969) 650.

9 R.J. Kirkpatrick, Am. Miner. 60 (1975) 798.

10 H.D. Keith and J.G. Padden, J. appl. Phys. 34 (1963) 2409.

11 P.S. Rogers, Mineralog. Mag. 37 (1970) 3.

12 P.W. McMillan, Glass-Ceramics, Academic Press, (1979), 2nd Edn. and references therein.

13 R.D. Maurer, J. appl. Phys. 33 (1962) 2132.

14 T.I. Barry, J. Mater. Sci. 4 (1969) 596 and 5 (1970) 117.

15 P.S. Rogers and J. Williamson, Glass Technol. 10 (1969) 128.

16 J. Williamson, A.J. Tipple and P.S. Rogers, J. Iron Steel Inst. 206 (1968) 898.

17 P.S. Rogers, Mineralog Mag. 37 (1970) 741.

18 J. Williamson, Mineralog Mag. 37 (1970) 760.

19 B. Keyworth, Ph.D. Thesis, University of London, (1969).

20 L.J. Shelestak, R.A. Chavez, J.D. Mackenzie and B. Dunn, J. Non-cryst. Solids 27 (1978) 75.

21 L.J. Shelestak, R.A. Chavez, J.D. Mackenzie and B. Dunn, J. Non-cryst. Solids 27 (1978) 83.

22 M. Tomozawa, Advances in Nucleation and Crystallization in Glasses, Ed. L.L. Hench and S.W. Freimann, American Ceramic Society, (1971).

23 K.J.D. MacKenzie and I.W.M. Brown, Physics Chem. Glasses 16 (1975) 17.

24 I.G. Austin and R. Gamble, Eilat Conference on Conduction in Low Mobility Materials, Taylor and Francis, (1971).

25 F.P. Koffyberg, J. Non-cryst. Solids 28 (1978) 231.

26 I.G. Austin and E.S. Garbett, Electronic and Structural Properties of Amorphous Semiconductors, Eds. P.G. LeComber and J. Mort, London, Academic Press, (1973), 393.

27 T. Bates, Modern Aspects of the Vitreous State, Butterworths, Volume 2, (1962), 195.

28 A. Ram, S. Kumar and P. Nath, Cent. Glass Ceram. Res. Inst. Bull. 4 (1957) 182.

29 A. Paul, Physics Chem. Glasses 11 (1970) 168.

30 N.A. Ghoneim and H.A. El Batal, J. Non-cryst. Solids 12 (1973) 189.

31 C.R. Bamford, Physics Chem. Glasses 1 (1960) 159 & 165.

32 D.S. McClure, Solid State Physics 9 (1959) 399.

33 V.V. Varguine and T.I. Weinberg, Glass Ceram. 5 (1958) 255.

34 C.R. Bamford, Physics Chem. Glasses 2 (1961) 163.

35 F.N. Steele and R.W. Douglas, Physics Chem. Glasses 6 (1965) 246.

36 J. de Jong, J. Soc. Glass Technol. 38 (1954) 57.

37 A.M. Bishay, J. Am. Ceram. Soc. 42 (1959) 403.

38 A.M. Bishay and L.J. Makar, J. Am. Ceram. Soc. 52 (1969) 605.

39 R.J. Edwards, A. Paul and R.W. Douglas, Physics Chem. Glasses 13 (1972) 137.

40 C.R. Bamford, Physics Chem. Glasses 3 (1962) 54.

41 C.R. Kurkjian and E.A. Sigety, Physics Chem. Glasses 9 (1968) 73.

42 J.E. Fenstermacher, J. Non-cryst. Solids 38-39 (1980) 239.

43 M.A.C.G. Van de Graaf, K.J. de Vries and A.J. Burggraaf, Physics Chem. Glasses 14 (1973) 53.

44 A. Paul, Physics Chem. Glasses 17 (1976) 7.

45 T.I. Veinberg, Inorg. Mater. 11 (1975) 440.

46 A.K. Bandyopadhyay, J. Mater. Sci. 16 (1981) 189.

47 S. Walker and H. Straw, Spectroscopy, Vol 1, Chapman and Hall (London), (1961), Chapter 4.

48 R.H. Sands, Phys. Rev. 99 (1955) 1222.

49 T. Castner, G.S. Newell, W.C. Holton and C.P. Slichter, J. chem. Phys. 32 (1960) 668.

50 J. Wong and C.A. Angell, Glass Structure by Spectroscopy, Maurice Dekker Inc., New York, (1976), Chapter 9.

51 D. Loveridge and S. Parke, Physics Chem. Glasses 12 (1971) 19.

52 P.C. Taylor and P.J. Bray, J. phys. Chem. Solids 33 (1972) 43.

53 R.F. Tucker, Advances in Glass Technology, Plenum Press New York, Vol. 1, (1962), 103.

54 D.L. Griscom and R.E. Griscom, J. chem. Phys 47 (1967) 2711.

55 D.L. Griscom, J. Non-cryst. Solids 40 (1980) 211.

56 H.W. De Wijn and R.F. van Balderen, J. chem. Phys. 46 (1967) 1381.

57 A.K. Bandyopadhyay, J. Mater. Sci. 15 (1980) 1605.

58 E.I. Abrashitova and N.R. Yafaev, Soviet Phys. solid St. 9 (1968) 2500.

59 J.H.W. Scheurs, J. chem. Phys. 61 (1978) 2151.

60 C. Hirayama, J.G. Castle Jnr. and M. Kuriyama, Physics Chem. Glasses 9 (1968) 109.

61 R.G. Gupta et al., J. Non-cryst. Solids 33 (1979) 121.

62 D.W. Moon, J.M. Aitken, R.K. MacCrone and G.S. Cieloszyk, Physics Chem. Glasses 16 (1975) 91.

63 L.D. Bogomolova et al., Soviet Phys. Dokl. 14 (1969) 243.

64 L.D. Bogomolova et al., Soviet Phys. Dokl. 18 (1973) 61.

65 E.J. Friebele, L.K. Wilson, A.W. Dozier and D.L. Kinser, Phys. stat. Solidi B 45 (1971) 323.

66 K. Hughes and J.O. Isard, Physics of Electrolytes, Volume 1, Ed. J.H. Hladik, Academic Press, London, (1972), 351.

67 N.F. Mott and E.A. Davis, Electronic Processes in Non-Crystalline Materials, Oxford University Press, (1978), 2nd Edn.

68 A.E. Owen and W.E. Spear, Physics Chem. Glasses 17 (1976) 174.

69 A.E. Owen, XIth Int. Congress on Glass, (1977), 372.

70 P.W. Anderson, Phys. Rev. 109 (1958) 1492.

71 M.H. Cohen, H. Fritzsche and S.R. Ovshinsky, Phys. Rev. Lett. 22 (1969) 1065.

72 M.H. Cohen, J. Non-cryst. Solids 4 (1970) 391.

73 C.R.A. Catlow and D.G. Muxworthy, Phil. Mag. B 37 (1978) 63.

74 A.J. Bosman and H.J. van Daal, Adv. Phys. 19 (1970) 1.

75 I.G. Austin, J. Non-cryst. Solids 2 (1970) 474.

76 N.F. Mott, J. Non-cryst. Solids 1 (1968) 1.

77 I.G. Austin and N.F. Mott, Adv. Phys. 18 (1969) 41.

78 T. Holstein, Ann. Phys. (N.Y.) 8 (1959) 325.

79 A. Mansingh, A. Dhawan, R.P. Tandon and J.K.Vaid, J. Non-cryst. Solids 27 (1978) 309.

80 V.N. Bogomolov, E.K. Kudinov and Y.A. Firsov, Soviet Phys. solid St. 9 (1968) 2502.

81 H.R. Killias, Phys. Lett. 20 (1966) 5.

82 A. Miller and E. Abrahams, Phys. Rev. 120 (1969) 745.

83 M. Sayer, A. Mansingh, J.M. Reyes and G. Rosenblatt, J. appl. Phys. 42 (1971) 2857.

84 J. Schnakenberg, Phys. stat. Solidi 28 (1968) 623.

85 I.G. Austin and E.S. Garbett, Electronic and Structural Properties of Amorphous Semiconductors, Eds P.G. LeComber and J. Mort, London, Academic Press, (1973), Chapter 11.

86 D. Emin, Electronic and Structural Properties of Amorphous Semiconductors, Eds. P.G. LeComber and J. Mort, London, Academic Press, (1973), Chapter 7.

87 A.K. Bandyopadhyay, J.O. Isard and S. Parke, J. Phys. D 11 (1978) 2559.

88 M. Sayer and E. Prasad, J. Non-cryst. Solids 33 (1979) 345.

89 N.F. Mott, Adv. Phys. 16 (1967) 49.

90 G.S. Linsey, A.E. Owen and F.M. Hayatee, J. Non-cryst. Solids 4 (1970) 208.

91 B.W. Flynn, A.E. Owen and J.M. Robertson, Proc. 7th Int. Conf. on Amorphous and Liquid Semiconductors, Ed. W.E. Spear, Edinburgh, (1977), 678.

92 M. Sayer and A. Mansingh, Phys. Rev. B 6 (1972) 4629.

93 T. Tsuchiya and T. Moriya, Glass and Ceram. Bull. 22 (1975) 55.

94 B.S. Rawal and R.K. MacCrone, J. Non-cryst. Solids 28 (1978) 347.

95 L. Murawski, C.H. Chung and J.D. Mackenzie, J. Non-cryst. Solids 32 (1979) 91.

96 L. Murawski and O.Gzowski, Phys. stat. Solidi A 19 (1973) K125.

97 H. Hrashima and T. Yoshida, XIth Int. Congress on Glass, (1977), 365.

98 A.K. Bandyopadhyay and J.O. Isard, J. Phys. D 10 (1977) L99.

99 K.W. Hansen, J. electrochem. Soc. 112 (1965) 994.

100 K.W. Hansen and M.T. Splann, J. electrochem. Soc. 113 (1966) 895.

101 D.L. Kinser, J. electrochem. Soc. 117 (1970) 546.

102 D.L. Kinser, J. electrochem. Soc. 117 (1970) 1586.

103 A.W. Dozier, L.K. Wilson, E.J. Friebele and D.L. Kinser, J. Am. Ceram. Soc. 55 (1972) 373.

104 I. Thurzo, J. Doupovec and J. Kákoš, J. Non-cryst. Solids 33 (1979) 335.

105 J.G. Vaughan and D.L. Kinser, J. Am. Ceram. Soc. 58 (1975) 326.

106 M. Gawish and M.H. Saleh, J. appl. Phys. 47 (1976) 5349.

107 M.H. Saleh and M. Gawish, J. appl. Phys. 51 (1980) 459.

108 I. Ardelean, Solid St. Commun. 27 (1978) 697.

109 R.A. Anderson and R.K. MacCrone, J. Non-cryst. Solids 14 (1974) 112.

110 M. Munakata, Solid-St. Electron. 1 (1960) 159.

111 T.N. Kennedy and J.D. Mackenzie, Physics Chem. Glasses 8 (1967) 169.

112 P.W. McMillan, Advances in Glass Technology, Plenum Press New York, Vol.1, (1962), 335.

113 M.G. Kuznetsova and K.S. Evstrop'ev, Inorg. Mater. 8 (1972) 302.

114 O.S. Ershov and M.M. Shul'ts, Inorg. Mater. 9 (1973) 1025.

115 O.S. Ershov and M.M. Shul'ts, Inorg. Mater. 11 (1975) 266.

116 H.J.L. Trap and J.M. Stevels, Physics Chem. Glasses 4 (1963) 193.

117 T. Tsuchiya and T. Moriya, J. Ceram. Ass. Japan 81 (1973) 303.

118 T. Tsuchiya and T. Moriya, J. Ceram. Ass. Japan 83 (1975) 419.

119 A.A. Pronkin, V.E. Kogan and R.D. Verulashidi, J. appl. chem. USSR 50 (1977) 53.

120 L.D. Bogomolova, Soviet Phys. solid St. 15 (1974) 2477.

121 M. Sayer and G.F. Lynch, J. Phys. C 6 (1973) 3674.

122 G.F. Lynch and M. Sayer, J. Phys. C 6 (1973) 3661.

123 L.D. Bogomolova, J. Non-cryst. Solids 30 (1979) 379.

124 A. Mansingh, A. Dhawan and M. Sayer, J. Non-cryst. Solids 33 (1979) 351.

125 D.P. Hamblen, R.A. Weidel and G.E. Blair, J. Am. Ceram. Soc. 46 (1963) 499.

126 S. Kumar and B.B. Nag, J. Am. Ceram. Soc. 49 (1966) 10.

127 M. O'Horo and M. Steinitz, Mater. Res. Bull. 3 (1968) 117.

128 P.C. Schultz, Annual Meeting of the Int. Glass Commission, Toronto, (1969), 35.

129 D.L. Kinser, L.K. Wilson, G.J. Friebele and A.W. Dozier, IXth Int. Congress on Glass, 357.

130 M.J. Tricker, J.M. Thomas, M.H. Omar, A. Osman and A. Bishay, J. Mater. Sci. 9 (1974) 1115.

131 M.A. Russak and M.G. McLaren, Bull. Am. Ceram. Soc. 52 (1973) 271.

132 L.L. Hench, J. Non-cryst. Solids 2 (1970) 250.

133 Y. Limb and R.F. Davis, J. Am. Ceram. Soc. 62 (1979) 403.

134 T. Yoshida and Y. Matsuno, J. Non-cryst. Solids 38-39 (1980) 341.

135 C. Rouse, Ph.D. Thesis, University of London, (1975).

136 F.P. Glasser, Am. J. Sci. 259 (1961) 46.

137 W.D. Johnston, J. Am. Ceram. Soc. 48 (1965) 184.

138 W.F. Hillebrand et al., Applied Inorganic Analysis 2nd. Edn. John Wiley and Sons.

139 A. Paul and R.W. Douglas, Physics Chem. Glasses 7 (1966) 1.

140 M.H. Hey, Mineralog. Mag. 26 (1941) 116.

141 D.J. Clinton, Micron 3 (1971-2) 363.

142 M.H. Omar, M. El-Hamamsy and A. Bishay, IX th Int. Congress on Glass, 521.

143 E.M. Levin, H.F. McMurdie and F.P. Hall, Phase Diagrams for Ceramists, The American Ceramic Society.

144 S.M. Budd, Physics Chem. Glasses 7 (1966) 210.

145 W.A. Weyl, Coloured Glasses 2nd. Edn., The Society of Glass Technology, Sheffield.

146 A. Paul and R.W. Douglas, Physics Chem. Glasses 6 (1965) 212.

147 H.J. Tress, Physics Chem. Glasses 1 (1960) 196.

148 P.S. Danielson and J.H.W. Schreurs, J. Non-cryst. Solids 38-39 (1980) 177.

149 A.G. Dunn, K.J. Beales, G.R. Newns and J.L. Wilson, Physics Chem. Glasses 19 (1978) 1.

150 K. Bingham and S. Parke, Physics Chem. Glasses 6 (1965) 224.

151 S. Parke, K. Bingham and A.I. Watson, Physics Chem. Glasses 11 (1970) 223.

152 Y.H. Wong, D. Thomas, R.L. Thomas and P.S. Danielson, J. appl. Phys. 49 (1978) 1640.

153 R.A. Levy, C.H.P. Lupis and P.A. Flinn, Physics Chem. Glasses 17 (1976) 94.

154 A. Mansingh, R.P. Tandon and J.K. Vaid, J. Phys C 8 (1975) 1023.

155 A. Mansingh, R.P. Tandon and J.K. Vaid, J. Phys C 9 (1976) 1809.

156 M Pollak, Phil. Mag. 23 (1971) 519.

157 L. Murawski and O. Gzowski, Phys. stat. Solidi A 24 (1974) K115.

158 M. Schwartz and J.D. Mackenzie, J. Am. Ceram. Soc. 49 (1966) 582.

159 R. Terai and E. Ohkawa, Yogyo-Kyokai-Shi 85 (1977) 294.

160 A.E. Owen, Physics Chem. Glasses 2 (1961) 87.

161 W.C. Hagel and J.D. Mackenzie, Physics Chem. Glasses 5 (1964) 113.

162 A.E. Owen, Physics Chem. Glasses 6 (1965) 253.

163 J.O. Isard, J. Non-cryst. Solids 42 (1980) 371.

164 E. Gough, J.O. Isard and J.A. Topping, Physics Chem. Glasses 10 (1969) 77.

165 C.F. Drake, I.F. Scanlan and A. Engel, Phys. stat. Solidi 32 (1969) 193.

166 W.A. Deer et al., Introduction to Rock Forming Minerals, Longmans , (1966).

167 J. Bevan et al, Personal Communication.

168 R.W. Nurse and H.G. Midgley, J. Iron Steel Inst. 174 (1953) 121.

169 R.W. Sillars, J. Instn. elect. Engrs 80 (1937) 378.